CIVIL ENGINEERING STUDIES
Illinois Center for Transportation Series No. 17-024
UILU-ENG-2017-2024
ISSN: 0197-9191

MODIFIED STANDARD PENETRATION TEST–BASED DRILLED SHAFT DESIGN METHOD FOR WEAK ROCKS

Prepared By
Timothy D. Stark
James H. Long
Ahmed K. Baghdady
University of Illinois at Urbana–Champaign

&
Abdolreza Osouli
Southern Illinois University at Edwardsville

Research Report No. FHWA-ICT-17-018

A report of the findings of

ICT PROJECT R27-145
Modified Standard Penetration Test–based Drilled Shaft Design Method for Weak Rocks (Phase 2 Study)

Illinois Center for Transportation

December 2017

TECHNICAL REPORT DOCUMENTATION PAGE

1. Report No. FHWA-ICT-17-018	**2. Government Accession No.** N/A	**3. Recipient's Catalog No.** N/A
4. Title and Subtitle Modified Standard Penetration Test–based Drilled Shaft Design Method for Weak Rocks (Phase 2 Study)		**5. Report Date** December 2017 **6. Performing Organization Code** N/A
7. Author(s) Timothy D. Stark, James H. Long, Abdolrzea Osouli, and Ahmed K. Baghdady		**8. Performing Organization Report No.** ICT-17-024 UILU-ENG-2017-2024
9. Performing Organization Name and Address Illinois Center for Transportation Department of Civil and Environmental Engineering University of Illinois at Urbana–Champaign 205 North Mathews Avenue, MC-250 Urbana, IL 61801		**10. Work Unit No.** N/A **11. Contract or Grant No.** R27-145
12. Sponsoring Agency Name and Address Illinois Department of Transportation (SPR) Bureau of Research 126 East Ash Street Springfield, IL 62704		**13. Type of Report and Period Covered** Final Report: 1/1/2014 – 12/16/2017 **14. Sponsoring Agency Code** FHWA

15. Supplementary Notes

Conducted in cooperation with the U.S. Department of Transportation, Federal Highway Administration.

16. Abstract

In this project, Illinois-specific design procedures were developed for drilled shafts founded in weak shale or rock. In particular, a modified standard penetration test was developed and verified to characterize the in situ condition of weak shales or rocks in Illinois for drilled shaft design. For this project, *weak shale or rock* is defined as an intermediate geologic material (IGM) with an unconfined compressive strength of 10 to 100 ksf. These investigation and design improvements are anticipated to lead to safer deep-foundation design and reduced costs for IDOT.

17. Key Words drilled shaft, weak IGMs, axial capacity rock, shale, side and tip resistance, predictive method, resistance factor, standard penetration test, penetration rate	**18. Distribution Statement** No restrictions. This document is available through the National Technical Information Service, Springfield, VA 22161.

19. Security Classif. (of this report) Unclassified	**20. Security Classif. (of this page)** Unclassified	**21. No. of Pages** 78 pp + appendices	**22. Price** N/A

Form DOT F 1700.7 (8-72) **Reproduction of completed page authorized**

ACKNOWLEDGMENT, DISCLAIMER, MANUFACTURERS' NAMES

This publication is based on the results of **ICT Project R27-145, Modified Standard Penetration Test-based Drilled Shaft Design Method for Weak Rocks (Phase 2 Study).** ICT-R27-145 was conducted in cooperation with the Illinois Center for Transportation; the Illinois Department of Transportation; and the U.S. Department of Transportation, Federal Highway Administration.

Research team members would like to thank the Technical Review Panel (TRP) members and TRP chair, William Kramer, for his valuable inputs and organizational capabilities that facilitated completion of this research and preparation of the final report for this project. Research team members also want to thank Mike Short of IDOT District 3 and Dave Miller of IDOT District 7 for their valuable assistance with and contributions to the drilled shaft load test and field exploration at IL 89 over the Illinois River and IL 133 over the Embarras River, respectively. We also want to thank the members of the Technical Review Panel and interested participants for their support and many review comments:

William Kramer, TRP Chair, IDOT Bureau of Bridges and Structures

Bradly Hessing, IDOT Bureau of Bridges and Structures

Brian Laningham, IDOT District 6 Geotechnical Engineer

Chad Hodel, WHKS & Co.

Dan Tobias, IDOT Bureau of Materials

Greg Heckel, IDOT District 6 Geotechnical Engineer

Heather Shoup, IDOT Bureau of Materials

Luke Murphy, IDOT Bureau of Bridges and Structures

Megan Swanson, IDOT Bureau Materials

Michah Loesch, U.S. Department of Transportation (FHWA)

Mike Short, IDOT District 3 Geotechnical Engineer

Naser Abu-Hejleh, U.S. Department of Transportation (FHWA)

Rob Graeff, IDOT District 9 Geotechnical Engineer

Terry McCleary, McCleary Engineering

EXECUTIVE SUMMARY

Results are presented for the research project titled "Modified Standard Penetration Test–based Drilled Shaft Design Method for Weak Rocks (Phase 2 study)." In this phase of the project, the research team focused on the load-transfer mechanism of axially loaded drilled shafts socketed into weak, fine-grained rocks (e.g., weak shales). We also enhanced and verified the method of characterization of weak shales and the design procedure developed during Phase 1 of this study (Stark et al. 2013). The new design procedure will improve safety and reduce the Illinois Department of Transportation's (IDOT's) deep-foundation costs for future bridge structures.

The main objectives of this study were to: (1) improve the Modified Standard Penetration Test (MSPT) method developed during Phase 1 of this study; (2) improve the reliability of the empirical correlation between the unconfined compressive strength and MSPT penetration rate; (3) drill and test at 16 additional IDOT bridge sites and by including the influence of SPT hammer energy on the measured MSPT penetration rate; (4) conduct two full-scale, drilled shaft load tests to investigate the load-transfer mechanism in weak, fine-grained rocks and to evaluate the proposed predictive methods; (5) improve and verify Phase 1 drilled shaft side- and tip resistance predictive methods by including more drilled shaft load tests; (6) develop appropriate reliability-based resistance factors for drilled shaft design using the load and resistance factors design (LRFD) framework; (7) develop and calibrate a numerical model using the load test results to study the load-transfer mechanism of weak, fine-grained, socketed drilled shafts; and (8) conduct a parametric study to investigate the main factors controlling drilled shaft design. The major findings from this project are summarized below.

FIELD EXPLORATION AND LABORATORY TESTING

Field exploration was conducted at 16 additional IDOT bridge sites where weak shales are present. The main objective of this exploration was to augment and refine the relationship proposed in Phase 1 of this study regarding MSPT penetration rate (N_{Rate}) versus unconfined compressive strength (UCS) of weak shales and to investigate the strength and compressibility properties of weak shale in Illinois. The following is a summary of the major findings of this research phase:

- Undrained Young's modulus can be correlated with the in situ water content and the unconfined compressive strength of weak shales. These correlations can be used for estimating the modulus of shales for preliminary settlement analysis of bridge piers when site-specific data are not available or to evaluate site-specific data and laboratory testing.
- SPT hammer energy measurement for all IDOT drill rigs used in the MSPT penetration rate measurement imparted an average of 90% of the theoretical maximum hammer energy. A normalized penetration rate, $(N_{Rate})_{90}$, was developed herein to improve the reliability of the proposed correlation between unconfined compressive strength and MSPT penetration rates so that future MSPTs could be corrected to an energy rate of 90%.
- An energy-based correlation between unconfined compressive strength (UCS) and normalized MSPT penetration rate (N_{Rate}) was developed and verified using field load tests for Illinois weak shales or rocks. This correlation can be used with the MSPT penetration rate for drilled shaft

design, especially when obtaining high-quality shale samples for triaxial compression testing is difficult or impossible. The use of MSPT penetration rates for drilled shaft design should reduce the design time and costs by reducing or eliminating shale coring and laboratory triaxial compression testing by IDOT.

IMPROVEMENTS OF THE ILLINOIS-SPECIFIC DESIGN PROCEDURE

Additional drilled shaft load test data was developed herein and located in the literature and incorporated in the Phase 1 database to refine the proposed side- and tip resistance design methods. This updated load test database was used for more detailed statistical analysis and development of reliability-based resistance factors for the design method of drilled shafts in weak, clay-based rock. This larger database allowed identification of outlying data points in the original database and a refinement of the resistance factors, increasing the efficiency of the design correlations and reducing uncertainty in the design procedure.

Unit Side Resistance

Findings related to drilled shaft unit side resistance include the following:

- This study recommends a linear function to predict unit side resistance in weak shales—instead of the power functions commonly used to correlate rock undrained compressive strength to measured unit side resistance in a drilled shaft load test.
- Side resistance does not change significantly with changes in shaft diameter.
- After the ultimate unit side resistance is mobilized, additional drilled shaft displacement along the drilled shaft/weak rock interface does not decrease unit side resistance significantly.

Unit Tip Resistance

Findings related to drilled shaft unit tip resistance include the following:

- Available predictive methods (with the exception of the methods of Abu-Hejleh et al. [2003] and Abu-Hejleh and Attwooll [2005], and the *Canadian Foundation Engineering Manual,* [Canadian Geotechnical Society 2006]) correlate only the measured tip resistance in load tests to the unconfined compressive strength of weak rock.
- Analysis of load test data herein indicates that mobilized tip resistance is governed by the undrained compressive strength of weak rock, by drilled shaft movement at the tip elevation, and by depth of embedment of the drilled shaft in the weak shale or rock. Therefore, predictive methods for tip resistance should account for all of these factors, not just unconfined compressive strength.
- The load test database developed herein was used to develop a design method that can account for all of these tip resistance factors. The new method uses tip settlement, embedment depth, and strength criteria to predict unit tip resistance.

CONTENTS

CHAPTER 1: INTRODUCTION

1.1 PROBLEM STATEMENT

Use of drilled shafts as foundations for Illinois bridge structures is increasing. For example, over a 5-year period (i.e., 2007−2012), the Illinois Department of Transportation's (IDOT's) annual budget for driven-pile foundation systems was approximately constant at $12 million per year, while drilled shafts increased significantly. For the same 5-year period, use of drilled shafts increased from less than $0.5 million per year to almost $6.5 million per year because of a lower unit cost; flexibility during construction; widely available material, equipment, and contractors to construct the shafts; increased steel costs; and some additional scour resistance.

Drilled shafts are traditionally designed using predictive methods that are developed based on results of field load tests in similar soils or rocks. There is uncertainty in these methods due to assumptions involved in their development. Major projects can support axial field load tests and reduce the uncertainty associated with these predictive measures. The results of these load tests can be beneficial for satisfying design requirements for both bearing capacity and settlement. However, drilled shaft field load tests may or may not be justifiable for smaller projects, including bridge pier construction or replacement, because the cost of a load test can be a significant percentage of the total cost of the project. As a result, drilled shafts are traditionally designed using empirical predictive methods that were developed based on load tests in similar soils or rocks. These methods often have a degree of uncertainty due to their empirical nature and different subsurface conditions. Resistance factors developed for a given target reliability are used to compensate for these uncertainties.

Other state departments of transportation (DOTs) (e.g., Colorado and Missouri) have addressed this knowledge gap by conducting a number of field load tests on drilled shafts in weak, clay-based rocks (e.g., shale, mudstone, and claystone) and developed state-specific predictive methods for such foundations. These state-specific correlations have resulted in more refined and reliable drilled shaft designs and considerable cost savings for the corresponding state DOTs. Currently, IDOT uses correlations developed in other states or design methods developed for stronger rocks, which could result in conservative designs, as shown herein.

Considerable research has been devoted to improvement of drilled shaft design in various types of soils and rocks but not in weak, fine-grained rocks such as shale. During this study, *weak, fine-grained rock* is defined as a cohesive intermediate geomaterial (IGM) with unconfined compressive strengths between 10 and 100 ksf. Phase 1 of this study (i.e., Stark et al. 2013) developed an empirical design method and resistance factors for prediction of side and tip resistance of drilled shafts in weak rock, based on unconfined compressive strength (UCS). A preliminary modified standard penetration test method (MSPT) was also developed to predict the UCS of weak rock for the empirical design method via the measured penetration rate (N_{rate}), using only five IDOT bridge sites. The MSPT provides a convenient means for obtaining the UCS required for drilled shaft tip resistance design by eliminating or reducing the need for rock coring and laboratory undrained triaxial compression testing by correlating MSPT penetration rate directly to UCS of weak rock, e.g., Illinois shales. The standard penetration test (SPT) had to be modified because 18 in. (0.45-m)-penetration of the split-spoon sampler cannot be obtained in weak rock or shales.

This Phase 2 study was undertaken to refine, augment, and verify the methods for characterization of weak rock and predictive methods for side and tip resistance developed in the 18 months of the Phase 1 project. MSPTs were conducted at 16 additional locations in weak rock in Illinois. Rock cores were obtained at these sites, and undrained triaxial compression and unconfined compression tests were performed on the weak rock core samples to augment and refine the correlation between MSPT N_{rate} and the UCS of weak rock proposed in Phase 1. The laboratory values of UCS for weak rock were calibrated using the mobilized shear strength of weak rock estimated from an inverse analysis of the two drilled shaft load tests conducted herein to assess the effects of sample disturbance, mode of shear, progressive failure, time to failure, and presence of joints and fissures in the laboratory specimens. The resulting mobilized UCSs were correlated to MSPT penetration rate to develop a predictive method for estimating the in situ undrained strength parameters for drilled shaft design in Illinois weak rocks. One of the full-scale load tests was performed by IDOT at the IL 89 bridge over the Illinois River, and the other full-scale load test was performed by this research team at the IL 133 bridge over the Embarras River to refine and verify the proposed predictive methods for side and tip resistance of drilled shafts in weak rock and to study the load-transfer mechanisms in drilled shafts in Illinois weak rock.

Additional drilled shaft load test data were located in the literature and incorporated in the limited Phase 1 database to refine the proposed side- and tip resistance design methods. This updated load test database was used for more detailed statistical analysis and development of reliability-based resistance factors for the design method for drilled shafts in weak, clay-based rock. This larger database allowed identification of outlier data points in the original load test database, increasing the efficiency of the design correlations and reducing uncertainty in the design procedure; and it was used to justify the larger resistance factors for side and tip resistance developed herein.

1.2 SCOPE OF THIS RESEARCH

The following paragraphs provide a brief description of the main tasks and outcomes of this research project.

- The modified standard penetration test method was improved to reduce the need for shale coring and laboratory triaxial compression testing for IDOT drilled shaft design. MSPTs were performed; and rock cores were obtained at 16 additional IDOT bridge sites where weak shales were present, to augment the empirical correlation between the MSPT penetration rate and the unconfined compressive strength of weak shales outlined in Phase 1. Furthermore, SPT hammer energies for all drill rigs used in this study (Phases 1 and 2) were measured and/or obtained to improve reliability of the N_{Rate} v. UCS correlation. This correlation will allow IDOT engineers to utilize MSPT penetration rate for future drilled shaft design and verification of laboratory undrained shear strength values. This approach is recommended where shale is weathered, so blow counts can be measured; and obtaining shale cores is either difficult or involves sample disturbance levels that are not acceptable.

- Phase 1 predictive methods for drilled shaft side and tip resistance were modified based on the additional drilled shaft load tests collected during this phase of the study. This method allows the design engineer to account for mobilization of both tip and side resistance in the drilled shaft design instead of using only one of these resistances because of strain incompatibility between side and tip resistances. The proposed method accounts for this strain incompatibility between the tip and side resistances. The new design criteria ensure settlement or serviceability limits will be met even though axial movement of the drilled shaft occurs, mobilizing both tip and side resistance.
- The first order second moment (FOSM) method, as defined in NCHRP-507 (Paikowsky et al. 2004) with the modification proposed by Bloomquist et al. (2007), is used herein to calculate the resistance factor for the design method developed in this study. The resistance factor allows geotechnical engineers to adopt a load and resistance factor design procedure to be consistent with the structural design of bridge superstructures (Brown et al. 2010).
- A numerical model was developed in Phase 2 to investigate the factors influencing the axial capacity of drilled shafts socketed into weak, fine-grained rocks. Some of the factors investigated with this calibrated numerical model are drilled shaft socket roughness, relative stiffness between the drilled shaft and weak rock, mechanical properties of the weak rock, socket length, and socket diameter.
- Two Osterberg load-cell (O-cell) field load tests were conducted during this phase of the study on drilled shafts socketed into weak clay shales in Illinois. These two load tests were conducted at the IL 89 over the Illinois River and IL 133 over the Embarras River bridge sites. Results of these field load tests were used to understand the load-transfer mechanism of axially loaded drilled shafts and evaluate and update the side- and tip resistance design equations proposed in Phase 1.

CHAPTER 2: FIELD EXPLORATION AND TESTING

2.1 INTRODUCTION

In Phase 1 of this study (i.e.ICT-R27-99), the modified procedure for conducting and interpreting the standard penetration test (SPT) was proposed to improve its performance in weak, fine-grained rock (e.g., shales). An empirical correlation was also proposed that relates the split-spoon sampler penetration rate (N_{Rate}) to the laboratory-measured UCS, using only five IDOT bridge sites.

In Phase 2, MSPTs were conducted at 16 additional IDOT bridge sites where weak shales are present. Rock cores were obtained, and undrained triaxial compression tests and unconfined compressive tests were performed on shale cores to refine estimation of N_{Rate} and augment the proposed correlation between N_{Rate} and UCS of weak shales. Furthermore, SPT hammer energies were measured and/or obtained for all of the drill rigs used in this study (Phases 1 and 2) and an energy-based correlation between the N_{Rate} and UCS for weak shales that exhibits UCS between 10 and 100 ksf was developed. This Chapter summarizes the major finding of the field exploration and laboratory testing efforts conducted during this phase of the research.

2.2 SUBSURFACE INVESTIGATION

Two borings were drilled at each IDOT bridge site. The first boring was used to obtain shale core samples for determination of the UCS and undrained Young's modulus for the weak shales. Shale cores were retrieved using a 5-ft-long NQ2 or NWD4 size (2-in. internal diameter) core bit with a split double tube, swivel type core barrel to decrease sample disturbance during core removal. This type of core barrel is preferred and/or required because it minimizes exposure of the cored shale to the drilling fluid; and it allows easy examination and extraction of the shale cores, which improves the quality and integrity of the shale for laboratory strength testing. Shale cores were first examined in the field to calculate the rock quality designation (RQD) (Deere and Deere 1988) of the core, total core recovery (TCR) of the rock mass, and vertical spacing of joints and fractures. The shale cores were placed in a piece of half-circle, white PVC plastic pipe after extrusion from the double-core barrel, to support the cores and minimize mechanical breakage during handling and transportation of the cores. A piece of thick, nonwoven geotextile was placed on the PVC pipe to provide some cushioning to the bottom of the core. After placing the cores on the PVC pipe, the cores and plastic trays were wrapped with several layers of plastic wrap and duct tape to maintain the field-moisture content and condition. The sealed cores were transported to the University of Illinois at Urbana–Champaign (UIUC) at the end of drilling that day and tested within 24 hours of arrival to measure the UCS at or near the field-moisture content and condition.

A second boring was drilled, usually 10 to 15 ft from the first boring at each site, to obtain MSPT penetration rates at various depths. These MSPTs were performed in accordance with the procedure outlined in Appendix Q. Measurement of the MSPT penetration rate was performed using automatic hammers, to be consistent with Phase 1. Split-spoon samplers without liners were used to eliminate overestimation of the measured penetration rate, which could be as large as 30% due to the additional friction. Table 2.1 summarizes the weak rock formations, shale type, and a brief description of the shales that were encountered at each of the 21 IDOT bridge sites investigated in Phases 1 and 2 of this study. Figure 2.1 shows a state of Illinois map that illustrates the areas of weak shales and the location of the 21 shale sites drilled during both phases of this project. Each color code presents the percentage of weak shales in the sedimentary rock formation shown on the map. The shale map is based on the distribution and extent of geologic units within the state of Illinois (Willman et al, 1967; and ISGS 1996). In situ and laboratory results for the 16 IDOT bridge sites are presented in Appendices A through P.

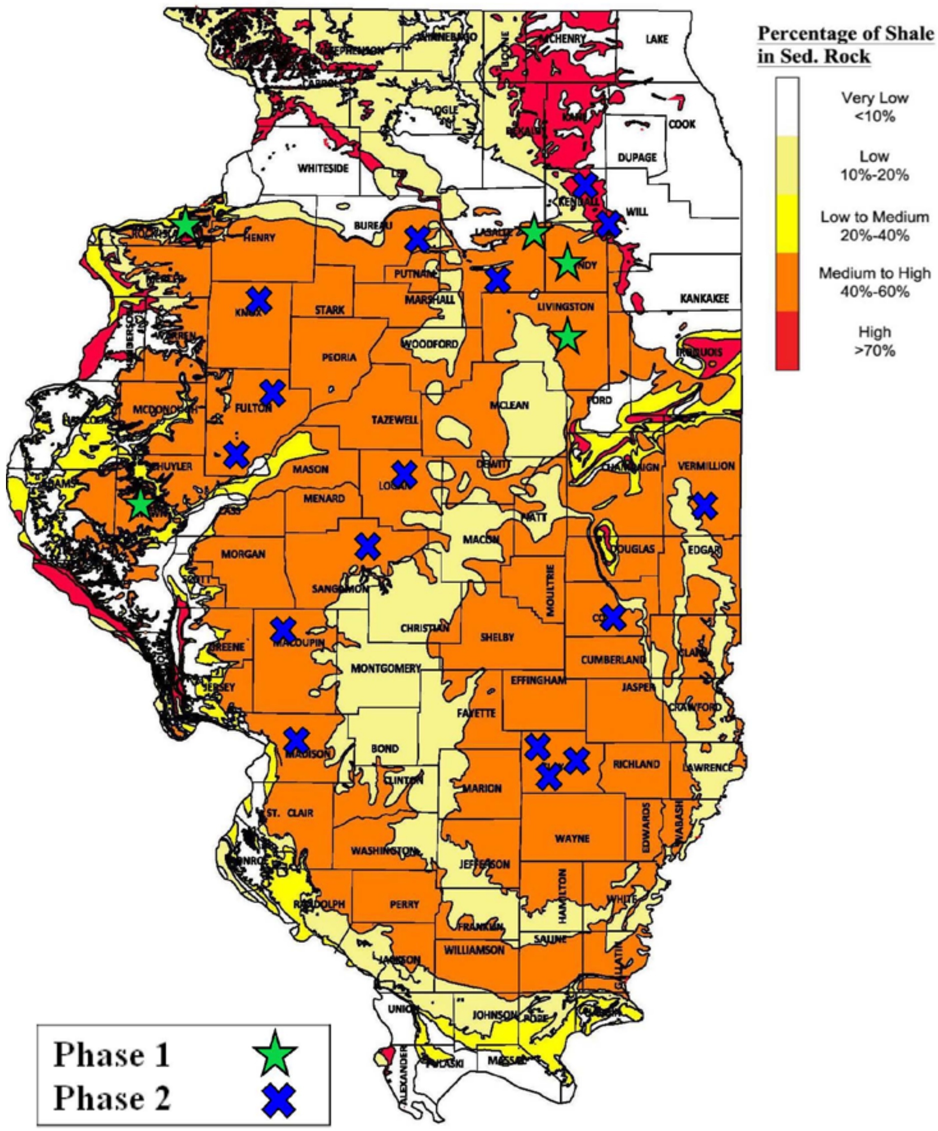

Figure 2.1 State of Illinois map showing areas of weak shales and the location of the 21 shale sites drilled during this project.

2.3 LABORATORY TESTING

2.3.1 Unconfined compression tests

Unconfined compression tests were performed on the obtained shale cores in accordance with ASTM D7012–14 (method D). An axial strain rate of 1% per minute was used in all of the unconfined compression tests to create an undrained shear condition and equal distribution of excess pore-water pressure. The peak deviator stress from each triaxial compression test was used to calculate the unconfined compressive strength for each test. A height-to-diameter ratio of 2 to 1 was used for the rock cores to minimize end effects. Because the shale cores were fractured and weathered, techniques to minimize or eliminate sample trimming were developed, as sample trimming usually results in specimen breakage along existing joints or fractures. To eliminate sample trimming, new base and top platens for the triaxial compression apparatus were fabricated so they matched the exact diameter of the shale cores obtained from the various core barrels. Therefore, only the ends of the triaxial specimens had to be trimmed or mitered to create a triaxial compression specimen. This end-trimming usually coincided with the direction of the joints or fissures, reducing additional disturbance. This mitering of the specimen ends was initially accomplished using a circular table saw, and then a 6-in. (15.2 cm)- long surgical razor blade.

2.3.2 Young's Modulus and In situ Water Content

The unconfined and confined triaxial compression test results (i.e., stress–axial strain relationship) were used to calculate the undrained Young's modulus (E_u) in accordance with ASTM D7012 (method D). In short, the modulus was calculated from the slope of the stress–strain relationship that corresponds to 50% of mobilized undrained compressive strength. In situ water content of the weak shale specimens was measured in accordance with ASTM D2216-10, using trimmings from the mitering. These data were used to develop the undrained Young's modulus versus in situ water content relationship proposed in Phase 1 of this study. Figure 2.2 shows results of unconfined and confined triaxial compression tests on Illinois shale specimens tested in both phases of this study. Figure 2.2 shows the Young's modulus increases rapidly with deceasing in situ water content, which is in agreement with the proposed Phase 1 relationship. The proposed relationship can be used to estimate the undrained Young's moduli of weak shales when site-specific triaxial compression test results are not available. This relationship can be used for preliminary settlement analyses of bridge piers founded on weak shales.

Young's modulus and the undrained compressive strength of shales are sensitive to moisture content, as shown in Figure 2.2. Therefore, it is important to preserve the shale cores at the in situ moisture content and test the cores as soon as possible for a reliable measurement of unconfined compressive strength, for correlations with the MSPT penetration rate.

2.3.3 Young's Modulus and Unconfined Compressive Strength

The results of the unconfined and confined compression tests were used to update the relationship between the undrained Young's modulus and the unconfined compressive strength of weak shales proposed in Phase 1 of this study.

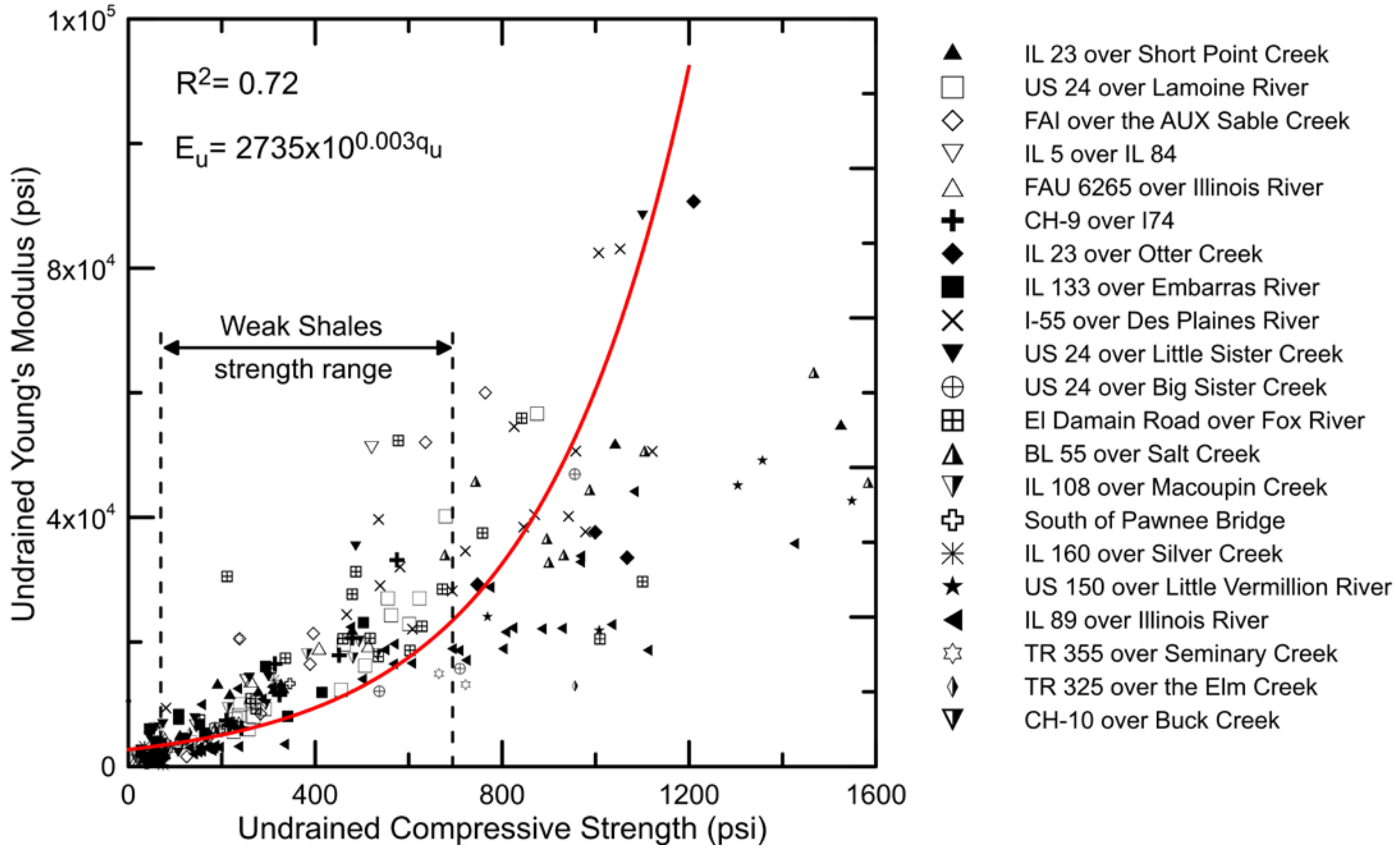

Figure 2.3. Undrained strength and modulus of weak shales are strongly related, which agrees with the Phase 1 observations and previous studies on shales (e.g., Mesri and Gibala 1972).

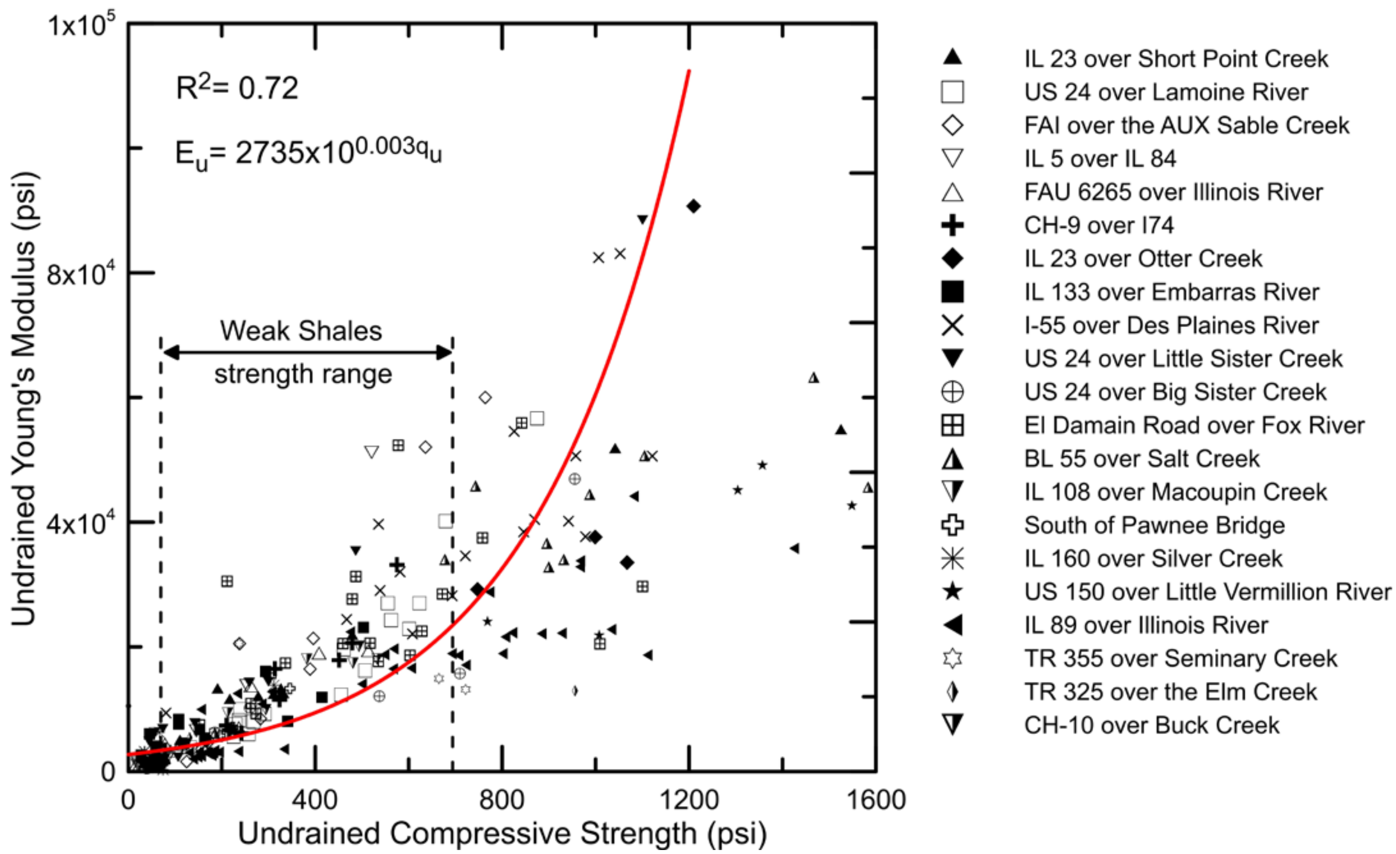

Figure 2.3. Undrained Young's modulus increases rapidly as the unconfined compressive strength increases.

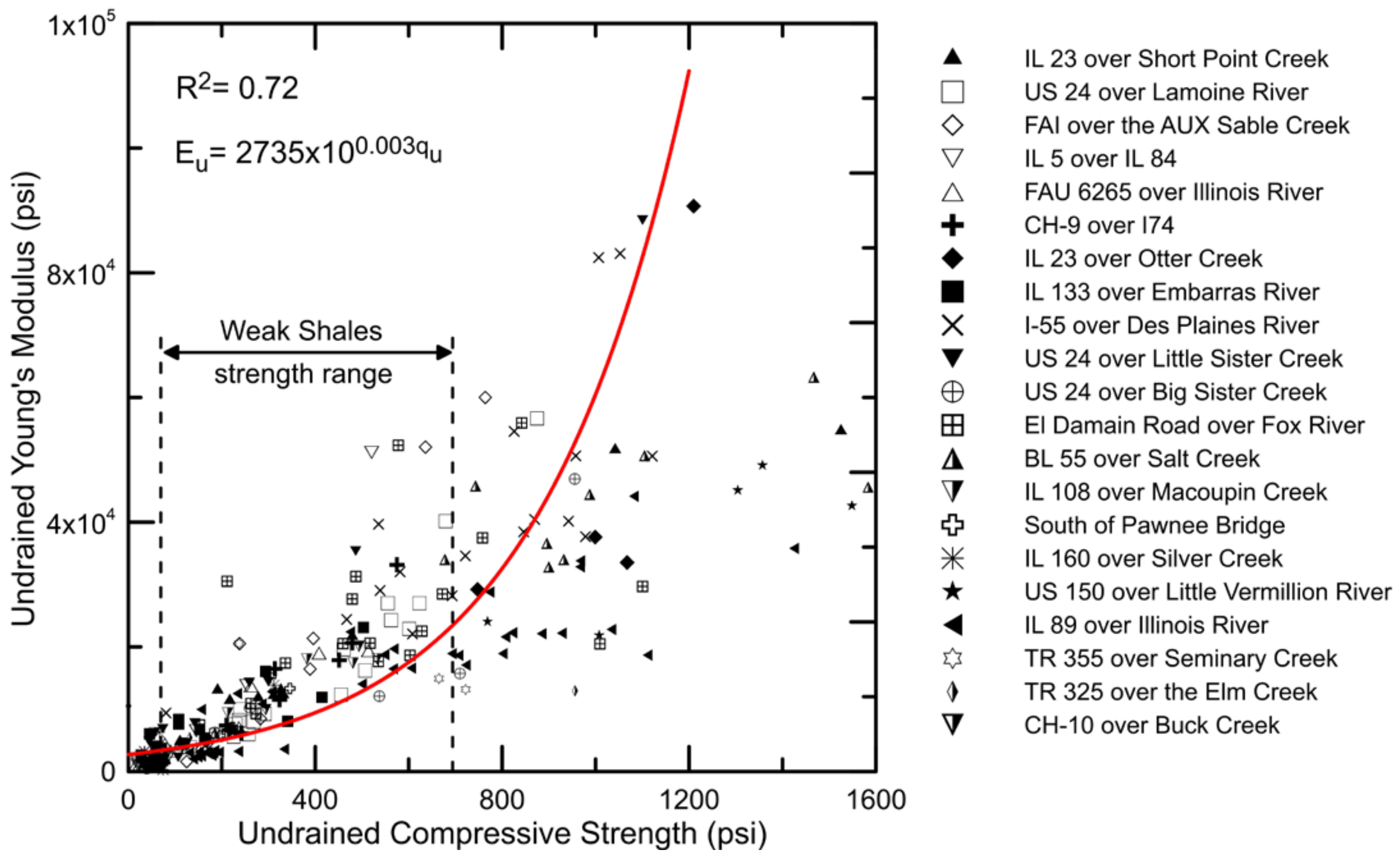

Figure 2.3. Preliminary elastic-settlement analysis of bridge piers resting on weak shales.

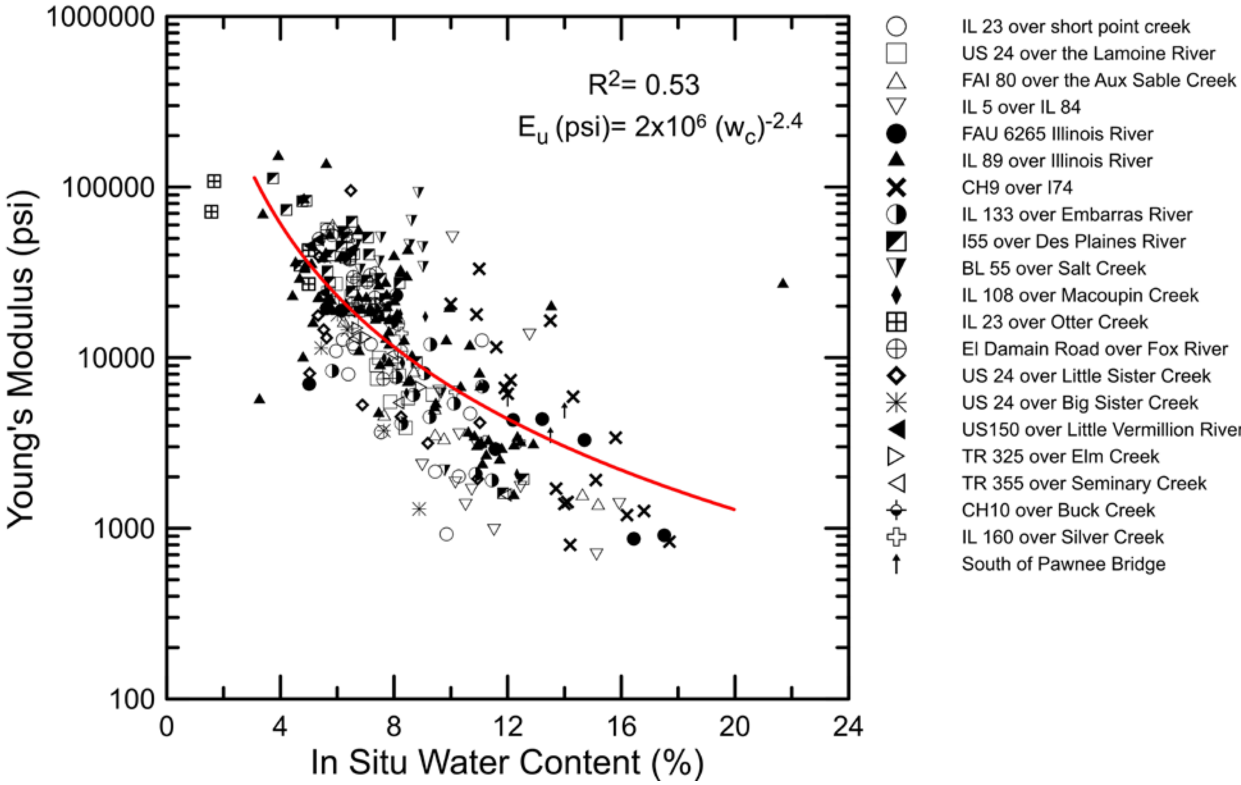

Figure 2.2. Relationship between in situ water content and undrained Young's modulus for shales in Illinois.

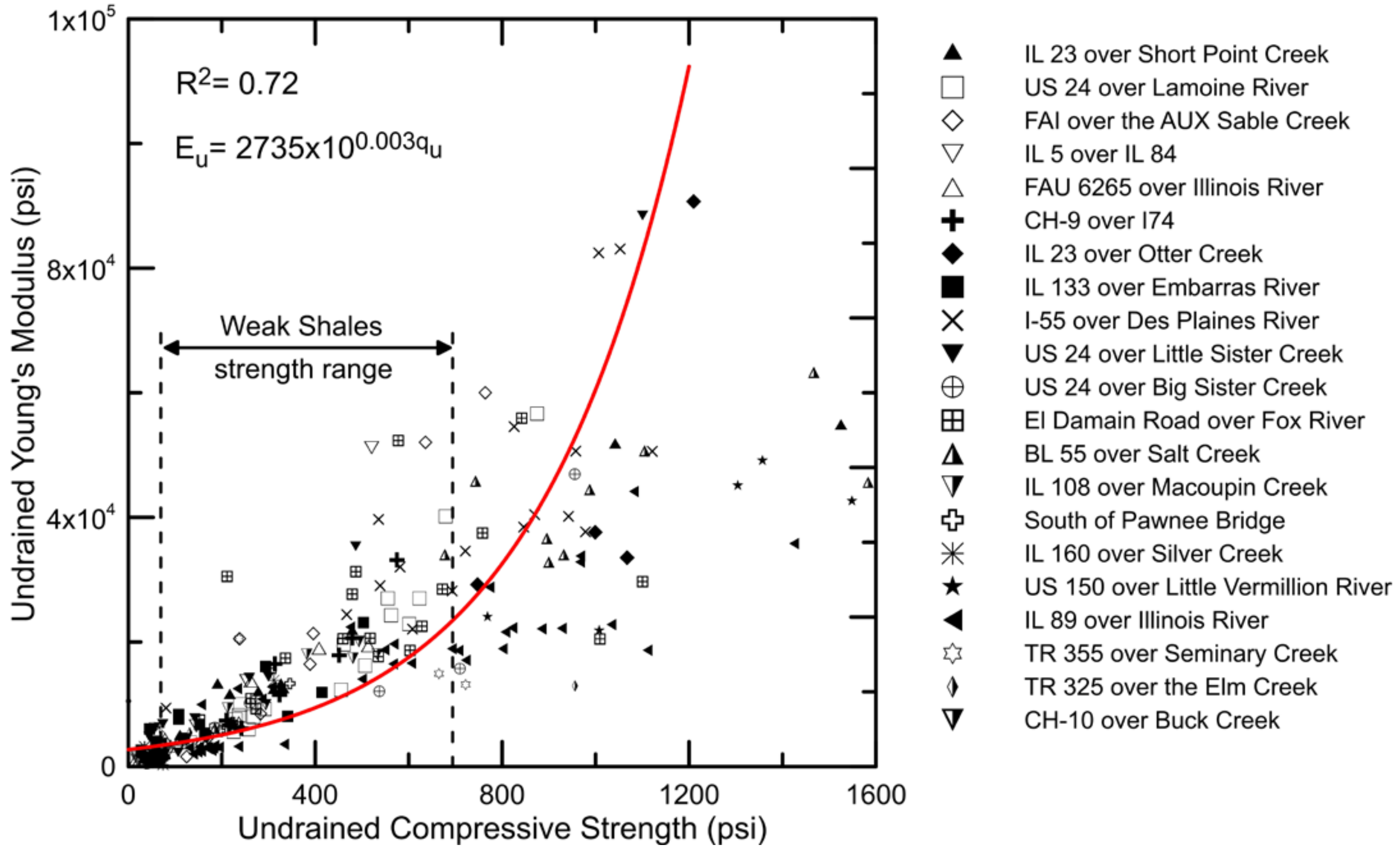

Figure 2.3 Relationship between unconfined compressive strength and undrained Young's modulus for shales in Illinois.

Table 2.1 Geology of IDOT Bridge Sites Used for MSPTs

Bridge Site	Location	Major Rock Formation	Rock Type	Rock Description
IL 23 over Short Point Creek	Cornell	Modesto	Pennsylvanian Shale	Gray-to-green shale with occasional limestone and coal inclusions
US 24 over the Lamoine River	Ripley	Carbondale	Pennsylvanian Shale	Hard gray shales
FAI80 over Aux Sable Creek	Minooka	Carbondale	Pennsylvanian Shale	Dark gray shale with sandstone
FAU 6265 over Illinois	Marseilles	Carbondale	Pennsylvanian Shale	Dark gray shale and mudstones
IL 5 over IL 84	Silvis	Abbott and Middle Devonian	Pennsylvanian Shale	Dark gray shale with lamination of sandstone
IL 89 over Illinois River	Spring Valley	Modesto	Pennsylvanian Shale	Dark gray shales with occasional limestone inclusions
CH-9 over I-74	Knoxville	Carbondale	Pennsylvanian Shale	Dark gray shales with traces of oxidized sand
IL 133 over Embarras River	Oakland	Modesto	Pennsylvanian Shale	Light to dark gray sandy shale
I-55 over Des Plaines River	Channahon	Spoon	Pennsylvanian Shale	Gray argillaceous shale
Eldamain Road over Fox River	Yorkville	Maquoketa	Pennsylvanian Shale	Gray, sandy, slightly argillaceous shale
TR 355 over Seminary Creek	Flora	Mattoon	Pennsylvanian Shale	Weathered, gray argillaceous shale
TR 325 over Elm Creek	Flora	Mattoon	Pennsylvanian Shale	Gray calcareous shale
CH 10 over Buck Creek	Flora	Mattoon	Pennsylvanian Shale	Weathered, gray argillaceous shale

Bridge Site	Location	Major Rock Formation	Rock Type	Rock Description
US 24 over Big Sister Creek	Little America	Spoon	Pennsylvanian Shale	Gray, silty shale with occasional coal inclusions
US 24 over Little Sister Creek	Little America	Spoon	Pennsylvanian Shale	Gray, silty shale with occasional coal inclusions
US 150 over Little Vermillion River	George town	Modesto	Pennsylvanian Shale	Gray, slightly micaceous, silty shale
BL55 over Salt Creek	Lincoln	Modesto	Pennsylvanian Shale	Light gray argillaceous shale
IL 108 over Macoupin Creek	Carlinville	Bond	Pennsylvanian Shale	Dark gray argillaceous shale interbedded with seams of poorly indurated limestone
IL 160 over Silver Creek	Grant fork	Modesto	Pennsylvanian Shale	,,,,,,,,
IL 23 over Otter Creek	Streator	Carbondale	Pennsylvanian Shale	Gray calcareous shale

2.4 MODIFIED STANDARD PENETRATION TEST (MSPT)

The standard penetration test (SPT) has been used to estimate strength parameters for soils and weak rock when it is difficult to obtain high-quality/undisturbed samples for laboratory testing (Peck et al., 1974). SPTs require 18-in.-penetration of the split-spoon sampler, which can be difficult to impossible to obtain in weak rocks or shales. In Phase 1 of this study, the procedure for conducting and interpreting the standard penetration test was modified to provide results in penetration per 10 blows increments where the penetration is less than 18 in. in weak shales. This new procedure is termed the modified standard penetration test (MSPT) and utilizes the concept of the split-spoon sampler penetration rate (N_{Rate}), not the sum of the penetration blow counts, to estimate the undrained strength parameters of weak shales. The penetration rate is the inverse of the linear slope of the penetration depth versus cumulative blow count relationship. This proposed test and recommended test procedure are discussed in detail in Appendix Q.

During this phase of the study, 16 IDOT bridge sites where weak shales are present were investigated. Modified standard penetration tests were conducted, and penetration rates were determined at various depths in weak shales in accordance with the MSPT procedure and recommendations developed herein and outlined in Appendix Q. MSPT results from the 16 sites investigated herein are presented in Appendices A through P. The results of the MSPT penetration rates (NRate), together with the laboratory-measured unconfined compressive strength for weak shales tested during both phases of the study were used to develop a useable empirical correlation between N_{Rate} and UCS (see Section 2.5.1).

2.5 SPT HAMMER ENERGY MEASUREMENTS

The SPT hammer energy used to measure penetration rate can vary from 40 to 100% of the maximum theoretical energy of a 140-lb weight falling 30 in. The wide variation in the transferred energy can cause inconsistent measurements of the MSPT penetration rate, which can undermine the targeted correlation. This inconsistency can lead to inaccurate values of UCS. Therefore, an energy correction must be developed and applied to the MSPT penetration rate to improve the reliability of the correlation, as is done for blow counts in soils where they are corrected to 60% of the maximum theoretical energy. In general, a higher energy results in a lower MSPT penetration rate, a lower UCS, and thus a more conservative drilled shaft design. Thus, it was important that the energy used to measure penetration rate be measured and/or obtained for each drill rig used in this study, to develop this energy-based correlation between UCS and penetration rate so designers can enter the correlation with a similar magnitude of MSPT energy to obtain an accurate estimate of UCS.

The research team measured the SPT hammer energy for all IDOT drill rigs used in this study. The tests were performed using an instrumented AW-J rod and a dynamic pile analyzer. Dynamic measurements were obtained using pairs of strain transducers and accelerometers mounted about 1 ft from the top of the drill rod. Measurements from the gauges were processed using the pile-driving analyzer (PDA), manufactured by Pile Dynamics, Inc. Table 2.2 summarizes the SPT hammer energy efficiencies for all of the operational IDOT drill rigs, together with the reported energies of the private drilling companies' drill rigs used in this study. Detailed SPT hammer energy measurements and results for all of the IDOT drill rigs are presented in Appendix S.

Table 2.2 Summary of the SPT Hammer Energies for all Drill Rigs Used in this Study

IDOT District/Drilling Company	Drill Rig	Hammer Energy Efficiency (%)
District 3	CME-75	93.2
	CME-45c	85.8
District 5	CME-75	91.3
District 6	CME-75	96.4
	CME-550x	80.4
District 7	CME-55	97.5
Wang Engineering	Mobile B-57	100
	D-50 TMR	78
Bulldog Drilling	CME-550x	94
Geocon	D-120	77
TSi Engineering	CME-550x	92

The results from this study indicate that 75 to 100% of the theoretical maximum hammer energy was delivered to the drill rod by the automatic hammers used herein. Because automatic hammers are now being widely used, an energy ratio of 90% shall be used to correct N_{Rate} for all of the drill rigs used during this study. In short, all of the drill rigs used during this study utilized an automatic trip hammer that imparted an average of 90% of the theoretical maximum hammer energy. Thus, MSPT N_{Rate} values obtained using an automatic trip hammer, which is the hammer most commonly used by IDOT, do not require significant corrections, in comparison to the previously suggested energy correction factor for soils, i.e., 60% of the theoretical maximum hammer energy, which is primarily based on a rope-and-pulley system. A normalized penetration rate, $(N_{Rate})_{90}$, was developed herein and is defined as follows for hammers that deliver 90% of theoretical maximum energy:

$$(N_{rate})_{90} = \frac{N_{rate} \times E_M \times C_B \times C_S \times C_R}{90}$$

where:

$(N_{Rate})_{90}$ = Nrate corrected for 90% of the theoretical energy and various field procedures

E_M = hammer efficiency, %

C_B = borehole diameter correction

C_S = sampler correction

C_R = rod length correction, and

N_{Rate} = measured penetration rate, bpf

Table Q.1 in appendix Q shows the recommended borehole diameter, rod length, and sampler correction factors from Skempton (1986). If the hammer does not yield 90% of the theoretical maximum hammer energy, the measured hammer energy should be inserted for E_M in the equation above to normalize the measured N_{Rate} to 90% of the theoretical maximum hammer energy. The sampler correction assumes that liners will be installed in the split-spoon sampler to be consistent with Skempton (1986) even though the practice now is to not use liners.

2.5.1 Proposed Correlation

The MSPT provides a convenient means for estimating the in situ strength properties of weak, fine-grained rocks, e.g., weak shales. Figure 2.4 presented the refined and calibrated correlation of MSPT penetration rate, corrected for 90% of the theoretical energy and various field procedures $(N_{Rate})_{90}$, and UCS of the weak shales tested herein. Figure 2.4 shows a linear relationship between $(N_{Rate})_{90}$ and the UCS of weak shales that can be used for future drilled

shaft design. This correlation for estimating the UCS of weak rocks reduces or eliminates the need for rock coring and subsequent laboratory testing that may be expensive, time-consuming, and problematic because of the fractured nature of weak rocks or shales.

Figure 2.4 shows the current line of best fit of the MSPT penetration rate and UCS data for the of Illinois weak shales tested herein. The following equation is recommended to estimate the UCS of weak shales, using the normalized MSPT penetration rate:

$$\text{UCS (ksf)} = 0.092 * (N_{rate})_{90} \quad (2.2)$$

where

UCS = Unconfined compressive strength, ksf

$(N_{Rate})_{90}$ = MSPT penetration rate corrected for 90% of the theoretical energy and various field procedures, bpf. (see appendix Q)

Figure 2.4 also presents upper and lower bounds of the empirical correlation, which can be used to investigate the range of UCS and thus drilled shaft design. For less critical structures, it may be possible to use the upper bound; while for vital structures, the lower bound may be relevant. This correlation should only be used to estimate the UCS values for geomaterials that have a UCS of 10 to 100 ksf. For fine-grained soils with UCS values lower than 10 ksf, previously published correlations (e.g. Stroud 1974) should be used. Differences in the compressive strength of the geomaterials and the procedures used to measure the blow count or penetration rate (N_{spt} and N_{rate}) are the reasons for the significant difference between previous correlations (e.g., Stroud 1974) and the correlation presented herein to estimate the UCS.

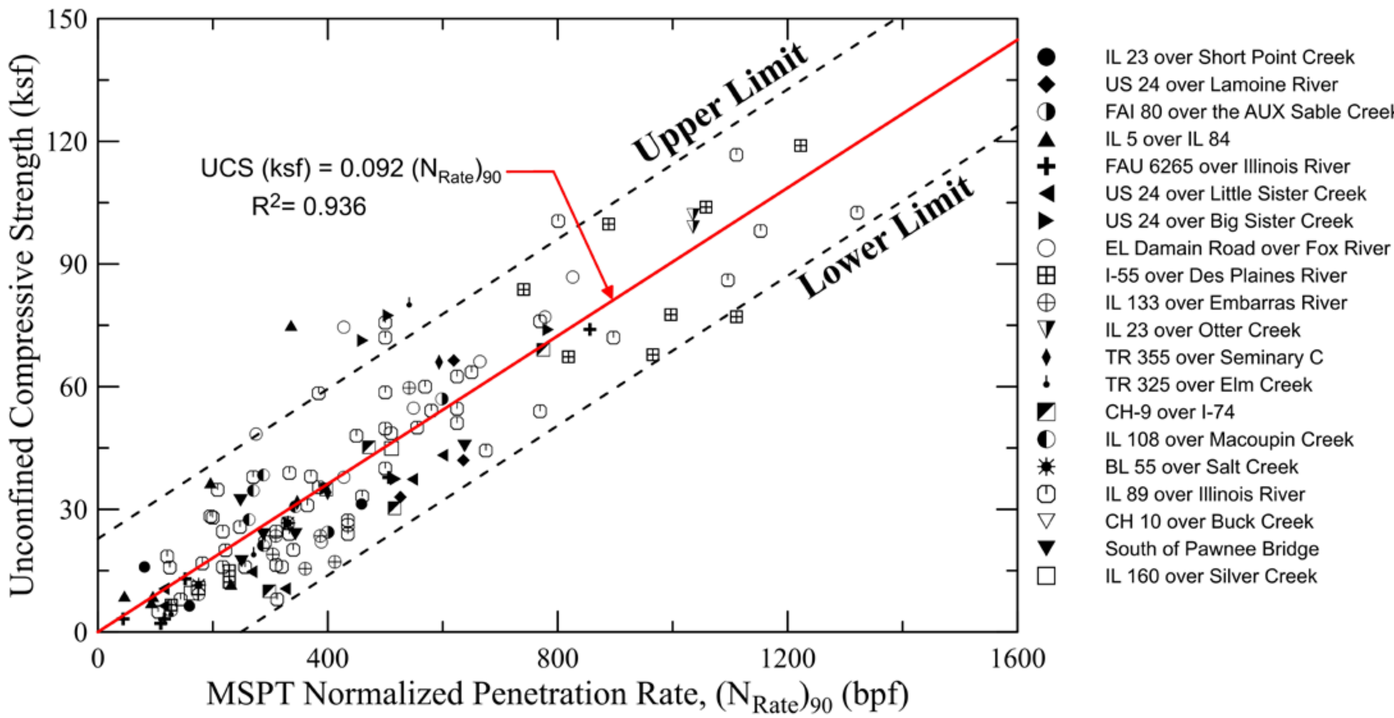

Figure 2.4. Relationship between UCS and $(N_{Rate})_{90}$ from MSPTs at 21 IDOT bridge sites.

2.6 SUMMARY

Field exploration was conducted at 16 additional IDOT bridge sites where weak shales are present. The main objective of this exploration was to develop and validate the MSPT penetration rate versus the unconfined compressive strength of weak shales relationship proposed in Phase 1 of this study and to investigate the strength and compressibility properties of weak shale in Illinois. The following is a summary of the major findings:

- Undrained Young's modulus was correlated with the in situ water content and the unconfined compressive strength of weak shales. These correlations can be used for estimating the modulus of shales for preliminary settlement analysis of bridge piers when site-specific data are not available or to evaluate site-specific data and laboratory testing.

- SPT hammer energy measurements for all operational IDOT drill rigs and the ones used for MSPT penetration rate measurements imparted an average of 90% of the theoretical maximum hammer energy. As a result, a normalized penetration rate, $(N_{Rate})_{90}$, was developed herein to improve the reliability and consistency of the proposed correlation between unconfined compressive strength and MSPT penetration rates.
- An energy-based correlation between unconfined compressive strength and normalized MSPT penetration rate was developed and validated herein for Illinois weak shales. This correlation can be used with MSPT penetration rates for drilled shaft design, especially when obtaining high-quality shale samples for triaxial compression testing is difficult or impossible. The use of MSPT penetration rates for drilled shaft design should reduce the design time and costs by reducing or eliminating shale coring and laboratory triaxial compression testing by IDOT.

CHAPTER 3: DRILLED SHAFT STATIC-LOAD TEST DATABASE

3.1 INTRODUCTION

Predictive methods for the design of drilled shafts in soils and rocks are empirical. Many of these predictive methods were developed based on databases consisting of load tests on drilled shafts in different types of rocks. In Phase 1 of this study, two load test databases for estimating the side and tip resistances of drilled shafts socketed into weak, fine-grained rocks (e.g., shales) was started. These two databases were used to evaluate the applicability of current design methods in estimating the axial capacity of drilled shafts in Illinois shales and to develop Illinois-specific design methods for the axial loaded drilled shafts in weak, fine-grained rocks.

In Phase 2, the side- and tip resistance databases were increased to include 27 additional relevant drilled shaft load tests, with a total of 155 values of side and tip resistance. These augmented databases were used to evaluate and update the Illinois-specific design equations started in Phase 1. This database is also used herein to study the load-transfer mechanism in side and tip resistance of drilled shafts in weak, fine-grained rocks.

3.2 SIDE RESISTANCE DATABASE

The updated unit side resistance database includes 93 values of side resistance from more than 65 drilled shaft load tests. The new load tests added during this phase include the two O-cell load tests conducted during this study in Illinois weak shales (see Chapter 5), three load tests conducted by Iowa DOT, and 22 load tests conducted by MoDOT on drilled shafts in Missouri shales. The updated unit side resistance database is summarized in Table R.1 in Appendix R. This drilled shaft load test database includes the following:

- Data from Osterberg load-cell tests, ring cells, and conventional top-loaded, drilled shaft load tests
- Drilled shafts embedded in weak shales, claystones, and mudstones
- Drilled shaft diameters from 13 to 78 in. (0.33 to 1.98 m)
- Most of the drilled shaft sockets were drilled normally. Only a few of them had artificially roughened socket walls that increase socket side resistance.
- *Side resistance* is defined as the maximum unit side resistance reached before load test termination.
- The ratio of drilled shaft vertical movement to diameter is less than 1.7%.

3.3 TIP RESISTANCE DATABASE

The updated unit tip resistance database includes 62 values of tip resistance from 62 drilled shaft load tests. This database is summarized in Table R.2 in Appendix R. The drilled shaft load test database includes the following:

- Data from Osterberg load-cell tests and conventional top-loaded drilled shaft load tests
- Drilled shafts embedded in weak shales, claystones, and mudstones
- Unconfined compressive strength of weak rocks, at two shaft diameters below the tip, between 10 to 100 ksf
- Drilled shaft diameters ranged from 12 to 96 in. (0.30 to 2.44 m).
- In most cases, the bottom of the drilled shaft was cleaned of loose debris before concreting.
- *Tip resistance* is defined as the maximum unit tip resistance reached before load test termination.
- Drilled shaft vertical movement at the tip elevation was 0.4 to 4.3 in. (10.2 to 109.2 mm) during the load tests.

3.4 SUMMARY

Drilled shaft load test databases for unit side and unit tip resistance started in Phase 1 of this research were augmented and are described in this chapter. These databases include only drilled shaft load tests involving weak, fine-grained rocks, not soils and stronger rocks. Drilled shaft diameters in the database range from 12 to 96 in. (0.30 to 2.44 m) for the tip resistance database and 13 to 78 in. (0.33 to 1.98 m) for the unit side resistance database.

These databases are used to in this research phase to augment and evaluate the Illinois-specific design procedure started in Phase 1. This database is also used to study the load-transfer mechanism in side and tip resistance of drilled shafts in weak, fine-grained rocks.

CHAPTER 4: EVALUATION OF PREDICTIVE METHODS

4.1 INTRODUCTION

Existing predictive methods for the side and tip resistances were reviewed in Phase 1 of this study. These methods are purely empirical and were developed using load test databases of measured side and tip resistances in different types and strengths of rock, so many of the existing correlations are not applicable to weak Illinois shales. Databases of measured side and tip resistances for drilled shafts in weak shales, claystones, and mudstones were started in Phase 1 and updated herein (see Chapter 3) to include 27 more load tests. These databases were used to evaluate the applicability of the predictive methods for drilled shafts in weak Illinois shales. The databases were also used to refine and evaluate the design correlations proposed in Phase 1.

4.2 PREDICTIVE METHODS FOR SIDE RESISTANCE

Effective stress analyses can be used to study load-transfer mechanism(s) in axially loaded drilled shafts socketed into weak shales. However, this type of analysis requires input parameters for effective stress–friction angle, cohesion intercept, and some quantitative measure of dilatancy of weak rocks. Such information is not routinely collected in field or laboratory tests (Carter and Kulhawy 1988). For this reason, available predictive methods mainly use a total-stress analysis for predicting axial capacity. These empirical total-stress methods use three general mathematical functions to correlate unconfined compressive strength of intact rock specimen to measured unit side resistance of drilled shafts: (1) linear functions, (2) power functions, and (3) piecewise functions (combination of different functions).

The database of measured side resistance of drilled shafts in weak rocks developed herein is used below to evaluate existing predictive total-stress side resistance methods.

4.2.1 Linear Functions

Reynolds and Kaderabek (1980) and Gupton and Logan (1984) recommend a linear function between undrained strength and unit side resistance for drilled shafts in rocks. Table 4.1 summarizes these methods and shows the linear design function. Table 4.1 also shows the mean and coefficient of variance (COV) of the predicted (denoted by the letter *p*) to measured (denoted by the letter *m*) unit side

resistance values, using the drilled shaft database developed herein and described in Chapter 3. In other words, the design linear functions in Table 4.1 and a q_u value were used to calculate the unit side resistance for the 87 depths at which side resistance was measured in the 74 load tests in the database. The predicted values of side resistance were then divided by the measured values at the corresponding depth to calculate the ratio of predicted (p) to measured (m) side resistance for the 87 measured values of side resistance at various depths. From these 87 ratios of predicted to measured side resistance, the mean and standard deviation were computed. Once the mean and standard deviation were computed, the coefficient of variance for each predictive method was computed by dividing the standard deviation of the predicted to measured (p to m) values by the mean of the predicted to measured values (p to m). This mean and COV are the values shown in Table 4.1.

Table 4.1. Statistics for Linear Functions for Unit Side Resistance

Design Method	Design Equation	Mean of Ratios of p to m	COV of Ratios of p to m
Reynolds and Kaderabek (1980)	$f_s(ksf) = 0.3 * q_u$	1.1	0.37
Gupton and Logan (1984)	$f_s(ksf) = 0.2 * q_u$	0.73	0.37

The side resistance method in the *Canadian Foundation Engineering Manual* (Canadian Geotechnical Society 2006) was not evaluated herein because the discontinuity spacing of weak rock for most data available is smaller than the required value of 12 in. Field exploration at 21 IDOT sites further showed that discontinuity spacing for Illinois shale is smaller than 12 in. Therefore, the method in the *Canadian Foundation Engineering Manual* (2006) is not recommended.

4.2.2 Power Functions

Rosenberg and Journeaux (1976), Horvath and Kenney (1979), Williams et al. (1980), Rowe and Armitage (1987), Toh et al. (1989), Kulhawy and Phoon (1993), O'Neil et al. (1996), Miller (2003), Kulhawy et al. (2005), and AASHTO *LRFD Bridge Design Specifications* (2006) use a power function for their predictive methods. Table 4.2 summarizes these methods, with the mean and coefficient of variance (COV) of the predicted to measured unit side resistance values for the drilled shaft database described in Chapter 3. The mean and coefficient of variance for each predictive method was computed as described above under "4.2.1 Linear Functions." The resulting mean and COV values are shown in Table 4.2.

Table 4.2. Statistics for Power Functions for Unit Side Resistance

Design Method	Design Equation	Mean of Ratios of p to m	COV of Ratios of p to m
Rosenberg and Journeaux (1976)	$f_s / P_a = 1.09 * (q_u / P_a)^{0.52}$	1.25	0.50
Horvath and Kenney (1979)	$f_s = 0.2 * \sqrt{q_u (MPa)}$	0.69	0.51
Williams et al. (1980)	$f_s / P_a = 1.84 * (q_u / P_a)^{0.37}$	1.49	0.58
Rowe and Armitage (1987)	$f_s = 0.45 * \sqrt{q_u (MPa)}$	1.54	0.51
Toh et al. (1989)	$f_s(KPa) = m * q_u$	0.92	0.65
Kulhawy and Phoon (1993)	$f_s / P_a = 2 * (q_u / 2 * P_a)^{0.5}$	1.55	0.51
O' Neil et al. (1996)	$f_s(ksf) = \alpha * q_u$	0.71	0.59
AASHTO LRFD (2006)	$f_s / P_a = \alpha_E * 0.65 * (q_u / P_a)^{0.5}$	0.71	0.58
Miller (2003)	$f_s = 0.4 * \sqrt{q_u (MPa)}$	1.37	0.51
Kulhawy et al. (2005)	$f_s / P_a = (q_u / P_a)^{0.5}$	1.1	0.51

4.2.3 Piecewise Functions

Alternatively, Meigh and Wolski (1979), Carter and Kulhawy (1988), and Abu-Hejleh and Attwooll (2005) use a piecewise function instead of a linear or power function for their proposed unit side resistance correlations. Table 4.3 summarizes these methods with the mean and coefficient of variance (COV) of predicted to measured values of unit side resistance for load tests in the drilled shaft database described in Chapter 3. The mean and coefficient of variance for each predictive method was computed as described above under "4.2.1 Linear Functions." The resulting mean and COV values are shown in Table 4.4.

Table 4.3. Statistics for Piecewise Functions for Unit Side Resistance

Method	Design Equation	Mean of Ratios of p to m	COV of Ratios of p to m
Meigh and Wolski (1979)	$f_s = 0.25 * q_u,\ 8.5 < q_u < 15$ ksf $f_s / P_a = 0.55 * (q_u / P_a)^{0.6},\ 14 < q_u < 265$ ksf	0.74	0.46
Abu-Hejleh and Attwooll (2005) "CDOT Design Method"	$f_s(\text{ksf}) = 0.075 * N = 0.3 * q_u,\ q_u < 24$ ksf and $20 < N < 100$ $f_s(\text{ksf}) = 2.05 * \sqrt{q_u},\ q_u < 100$ ksf and $N > 120$	1.13	0.42
Carter and Kulhawy (1988)	$f_s / P_a = 0.63 * (q_u / P_a)^{0.5} < 0.15 * q_u$	0.69	0.51

4.2.4 Discussion of Unit Side Resistance Results

The statistics presented in Tables 4.1, 4.2, and 4.3 for the various predictive methods for unit side resistance suggest that a linear function is better to predict the measured side resistance from load test data. Power functions give inaccurate predictions for the weaker range of IGMs (i.e., power functions commonly overestimate side resistance for values of UCS less than 40 ksf). For example, predictive methods by Miller (2003), Kulhawy et al. (2005), and Rosenberg and Journeaux (1976) show that power functions, in general, overestimate the unit side resistance when the unconfined compressive strength of the rock is less than 40 ksf and underestimate drilled shaft unit side resistance when the UCS is greater than 40 ksf. Therefore, power functions exhibit a poor representation of the observed relationship between side resistance and UCS and are not recommended.

Piecewise functions are more accurate than power functions; however, they occasionally underestimate the unit side resistance. Furthermore, the same level of accuracy can be obtained in design by using a simpler linear function as a predictive method, so a linear function is recommended. In summary, it is recommended that a linear function (e.g., a modified version of one of those shown in Table 4.1) be used to predict unit side resistance for drilled shafts constructed in weak Illinois shales.

4.3 PREDICTIVE METHODS FOR TIP RESISTANCE

Linear functions, power functions, or a combination of both are also commonly used to correlate tip resistance of drilled shafts to UCS for the design of drilled shafts in rocks. Drilled shaft load tests from the database described in Chapter 2: whose tip displacements are ≥ 3% of their tip diameter during the load test were used to evaluate the existing predictive methods. A tip displacement of ≥ 3% of the tip diameter is used to ensure all of the tip resistance predictive methods are evaluated consistently and to eliminate the influence of tip displacement on the measured capacity and the design recommendation.

4.3.1 Linear Functions

Teng (1962), Coates (1967), Rowe and Armitage (1987), and Carter and Kulhawy (1988) use linear functions for their proposed predictive methods. Table 4.4 summarizes these methods, the design equation to predict the unit tip resistance, and the mean and coefficient of variance (COV) of the predicted to measured unit tip resistance values for load test results in the drilled shaft database described in Chapter 2: The mean and coefficient of variance for each predictive method was computed as described above under "4.2.1 Linear Functions." The resulting mean and COV values are shown in Table 4.4.

Table 4.4. Statistics for Linear Functions for Unit Tip Resistance

Method	Design Equation	Mean of Ratios of p to m	COV of Ratios of p to m
Teng (1962)	$q_t = 3/5 \text{ to } 3/8 * q_u$	0.12	0.35
Coates (1967)	$q_t = 3 * q_u$	0.60	0.35
Rowe and Armitage (1987)	$q_t = 2.5 * q_u$	0.50	0.35
Carter and Kulhawy (1988)	$q_t = \left(\sqrt{s} + \sqrt{m\sqrt{s} + s}\right) * q_u$	0.01	0.40

4.3.2 Power Functions

Zhang and Einstein (1998) use a power function for their predictive method, which is summarized in Table 4.5. The mean and coefficient of variance (COV) of the predicted to measured values of unit tip resistance for the drilled shaft database described in Chapter 2: are also shown in Table 4.5. The high COV, shown in the table below, reflects the inconsistency of this method in predicting capacity. However, on average the predicted value agrees well with the measured one, as indicated by its computed mean.

Table 4.5. Statistics for Power Functions for Unit Tip Resistance

Method	Design Equation	Mean of Ratios of p to m	COV of Ratios of p to m
Zhang and Einstein (1998)	$q_t = 4.8 * \sqrt{q_u}(MPa)$	1.09	0.54

4.3.3 Piecewise Functions

ARGEMA (1992) and Abu-Hejleh and Attwooll (2005) use a combination of linear and power functions for different ranges of rock UCS for their predictive methods. The tip resistance database in Chapter 3 was used to evaluate these methods for the design of drilled shafts in weak rocks (i.e., weak Illinois shales). The values of mean and COV of the predicted to measured tip resistance values are summarized in Table 4.6. In general, piecewise functions are more accurate than the linear functions, as indicated by their means; however, the high values of COV shown in Table 4.6 are the result of great scatter in the values of the predicted to measured capacity and reflects the great uncertainty attributed to these predictive methods.

Table 4.6. Statistics for Piecewise Functions for Unit Tip Resistance

Method	Design Equation	Mean of Ratios of p to m	COV of Ratios of p to m
ARGEMA (1992)	$q_t = 4.5 * q_u < 10$ MPa	1.0	0.40
Abu-Hejleh and Attwooll (2005) "CDOT Design Method"	$q_t = 0.92 * N = 3.83 * q_u,\ 20 < N < 100$ $q_u < 24$ ksf $q_t = (1.2 + 0.48 * L/D) * q_u < 4.08 * q_u$ when $L/D > 6$ $N > 120$ and $q_u < 100$ ksf	0.89	0.40

4.3.4 Discussion of Unit Tip Resistance Results

Some of the predictive methods underestimate the tip resistance of drilled shafts, which is indicated by their low computed mean (e.g., Teng 1962; Carter and Kulhawy 1988). This would lead to a conservative design in which tip resistance is included as one of the components that contribute to total axial capacity. The underestimate of tip resistance could be up to 90%. Some other methods have high COVs (e.g., Zhang and Einstein 1998), which reflects the high uncertainty attributed to these methods or, in other words, the inconsistency of these methods in predicting the capacity. These methods would lead to conservative design because they will probably need a high factor of safety (or low LRFD [load and resistance factor design] resistance factors)

The mobilized tip resistance of drilled shafts in weak rocks is a function of allowed tip displacement, rock socket length, and UCS of the socket rock (see Figure 4.1). Figure 4.1 shows that the greater the tip displacement, the greater the tip resistance, up to a ratio of tip displacement to tip diameter of about 4.

Most of the predictive methods reviewed and evaluated herein ignore allowable displacement of the shaft tip and socket length. A new design method that implicitly accounts for these important parameters was developed herein and will be introduced in Chapter 7.

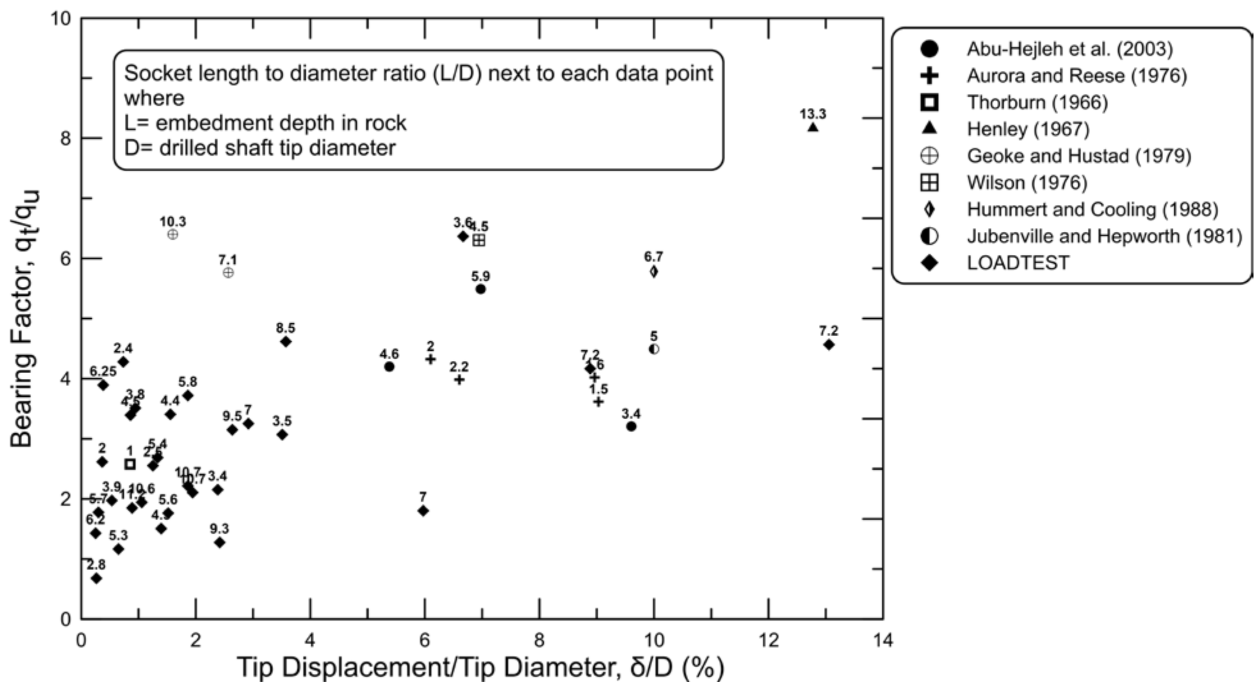

Figure 4.1. Effect of shaft tip displacement on tip resistance.

4.4 SUMMARY

Existing predictive methods for side and tip resistance were evaluated using a database of drilled shaft load tests assembled. Observations regarding the evaluation of the side resistance predictive methods are as follow:

- Power functions overestimate side resistance when UCS is less than 40 ksf and underestimate side resistance when UCS is greater than 40 ksf.
- Piecewise functions provide more accurate predictions than power functions; but they occasionally underestimate unit side resistance, which can lead to an overly conservative design.
- Linear functions, with the modifications suggested Chapter 7, are recommended for IDOT design to predict unit side resistance in weak rocks. Linear equations are simpler and easier to use than piecewise equations, represent the assembled load test data, and thus are recommended for use by IDOT to design drilled shafts in weak shales.

Observations regarding tip resistance methods are as follow:

- Tip resistance predictive methods tend to underestimate tip resistance.
- Tip resistance methods assume a predetermined tip displacement, and thus the serviceability of the drilled shafts and bridge cannot be determined. This also leads to designs in which strain compatibility does not exist between side and tip resistance.
- Many tip resistance predictive methods ignore the contribution of embedment depth to bearing capacity.
- The load test database developed herein was used to develop a design method that accounts for tip displacement, embedment depth, and UCS. This new method, presented in Chapter 7, allows the user to include allowable settlement and design shear strength to predict unit tip resistance.

CHAPTER 5: FULL-SCALE FIELD LOAD TESTS

5.1 INTRODUCTION

Two Osterberg cell (O-cell) load tests were conducted during this phase of the study on drilled shafts socketed into weak clay shales at IDOT bridge sites. These two load tests were conducted at the IL 89 over Illinois River near Spring Valley, Illinois, and IL 133 over the Embarras River near Oakland, Illinois. The results of these load tests were used to refine and calibrate the side- and tip resistance design equations proposed in Phase 1. The results of the two O-cell load tests were also used to calibrate the finite element numerical model developed for the parametric analysis to investigate the factors influencing the axial response of weak shale-socketed drilled shafts. Details of the subsurface investigation, test shaft construction, O-cell testing arrangements, and testing-results interpretations for the two load tests are presented in this section.

5.2 BRIDGE SITE AT IL 89 OVER THE ILLINOIS RIVER

Figure 5.1 shows the location of the bridge site at IL 89 over the Illinois River, located in Putnam County, just south of Spring Valley, Illinois. The eight-span bridge structure carries a two-lane highway over the Illinois River and connects Putnam and Bureau counties via IL 89. The north and south abutments of the bridge, together with Piers 1, 6, and 7 are supported on driven H-piles. Piers 2 to 5 are supported on drilled shafts socketed into the underlying sedimentary rocks.

Figure 5.1. Location of bridge site at IL 89 over the Illinois River.

As a part of the geotechnical design of the proposed bridge foundations, a full-scale O-cell load test was conducted on a test shaft socketed into the underlying weak clay shale. The main objective of this test was to measure/evaluate the mobilized unit side and tip resistances that can be used in the drilled shaft design. The O-cell load test was performed on a 5.0-ft-diameter and 71.5-ft-long test shaft adjacent to Pier 1. Figure 5.2 shows a plan view for the new bridge structure and the location of the test shaft.

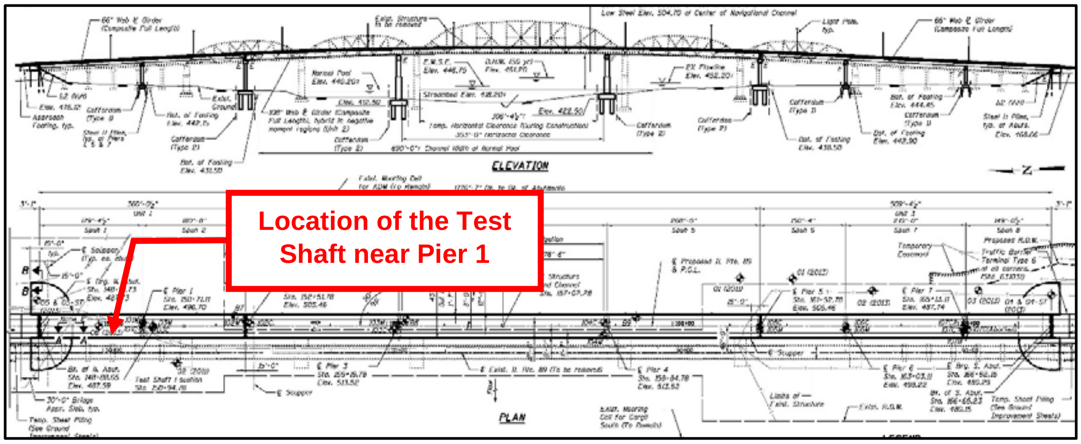

Figure 5.2. Location of test shaft of bridge site at IL 89 over the Illinois River.

Prior the test shaft construction, four borings were advanced near the test shaft. Two of the four were drilled by McCleary Engineering, and the other two by the IDOT District 3 drilling crew. The first two borings were used to obtain shale core samples. Initially, rock cores were used for determination of recovery ratio, rock quality designation (RQD) of the rock mass, and vertical spacing of joints and fractures in the shale. Afterwards, unconfined compression tests were conducted at UIUC on the retrieved weak shale specimens. The in situ moisture content of the shale specimens used in the unconfined compression tests were also measured for correlation purposes. The unconfined compression test results were also used to determine the deformability characteristics of the shale under undrained loading conditions. The other two borings were used to obtain the MSPT penetration rate at various depths in the weak shale formation. The obtained penetration rate was then used to estimate the unconfined compressive strength of the weak shales, based on the correlation developed herein. The measured and estimated values of UCS were compared to investigate the accuracy of the proposed penetration rate/UCS correlation (see Section 2.5.1).

5.2.1 Subsurface conditions

The subsurface profile at the test shaft location consists of 10 ft of silty loam and clay underlain by 25 ft of a brown, stiff, silty clay layer. Below this layer is a medium-dense sand layer 7-ft thick, underlain by another 17.5-ft-thick brown, stiff, silty clay layer. Below these strata is a gray to dark gray, thinly bedded clay–shale formation. The ground surface elevation at the test shaft is about +447.9 ft. The gray shale formation was encountered at an elevation of 390.4 ft. Figure 5.3 shows the idealized subsurface profile at the test shaft location and the unconfined compressive strength profile developed for design of the test shaft.

5.2.2 Test Shaft Construction and Instrumentation

Illini Drilled Foundations, Inc., of Danville, Illinois, completed construction of the test shaft on November 5, 2014, under the direction supervision of the project team. The 5-ft-diameter test shaft was excavated to a base elevation of +376.4 ft. The shaft was started by predrilling and installing a 72-in.-diameter temporary outer casing. Drilling of the shaft continued through an open hole under bentonite slurry until the tip of the shaft was several feet above the top of the shale. A 66-in. permanent casing was inserted and screwed into the stiff, silty clay layer above the shale. After the inner casing was screwed in, bentonite slurry was removed; and drilling continued into the clay shales. Before reaching the required tip elevation, the contractor pulled and removed the 72-in diameter temporary casing. An auger was used for drilling the shaft, and a cleanout bucket for cleaning the base of the shaft prior to placement of the reinforcing cage and concrete. After the shaft was approved for concrete placement, the reinforcing cage with the attached O-cell assembly was lowered into the excavated shaft. Concrete was then delivered to the bottom of the shaft by a pump pipe into the base of the shaft until the top of the concrete reached the ground surface elevation of +447.2 ft.

The load testing assembly consisted of a 26-in.-diameter O-cell located 2.0 ft above the tip of the shaft (i.e., at elevation = 378.4 ft). Four linear vibrating-wire displacement transducers (LVWDTs, Geokon model 4450 series) were installed between the upper and lower plates of the O-cell to measure its expansion during loading. Two vibrating-wire strain gauges (Geokon model 4911 series) were installed at four different elevations above the O-cell (see Figure 5.3), to assess the mobilized unit side resistance along the drilled shaft. Two upper compression telltale casings were attached diametrically opposite each other on the reinforcing cage and extending from the top plate of the O-cell to the ground level to measure the upper compression displacements of the shaft. The top of the shaft displacement was monitored using two automated digital-survey levels (Leica NA3000 series). A Bourdon pressure gage, voltage pressure transducer, and vibrating-wire pressure transducer were used to measure the pressure applied to the O-cell at each load interval. To evaluate the integrity of the concrete in the test shaft, four cross-hole sonic logging (CSL) tubes with a diameter of 2 in. were also installed along the full length of the test shaft and extended about 3 ft above the top of the test shaft.

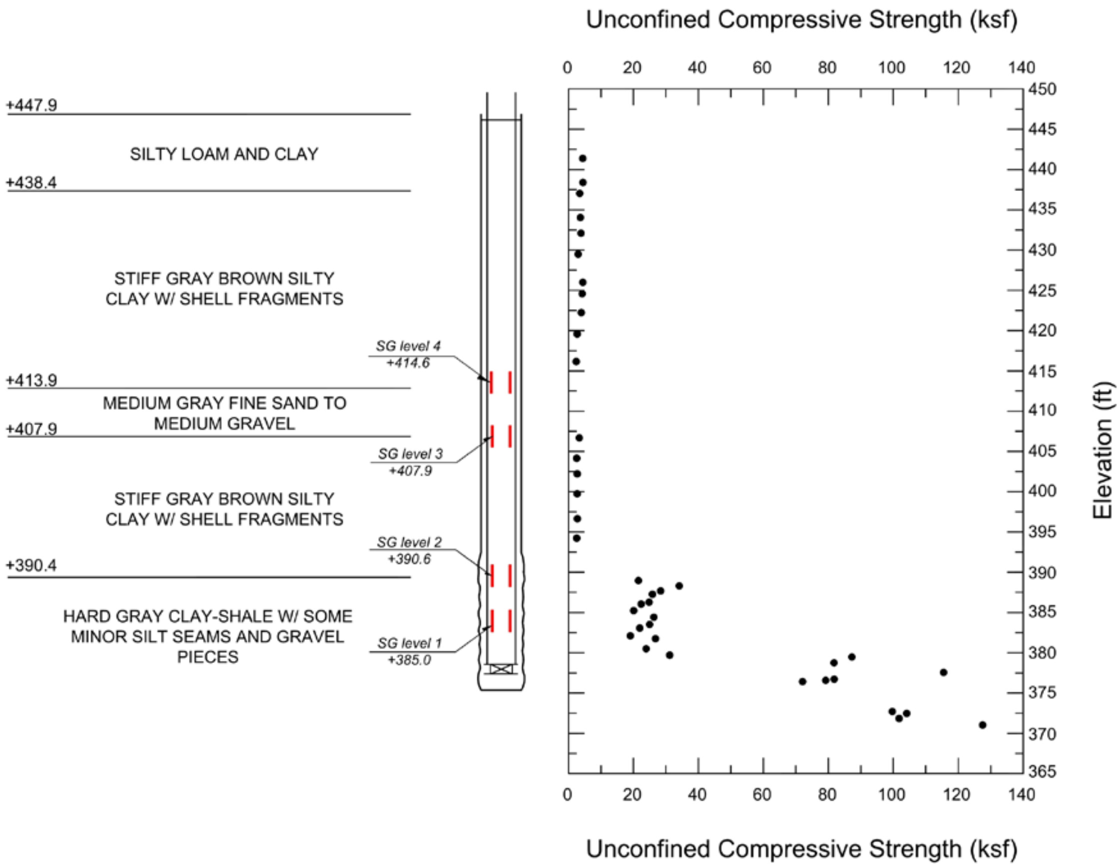

Figure 5.3. Idealized subsurface profile and the unconfined compressive strength profile in the vicinity of the bridge site at IL 89 over the Illinois River.

5.2.3 Data Acquisition and Testing Procedure

All instrumentation was connected through a data logger (Data Electronics 515 Geologger) to a laptop computer. The data logger recorded instrument readings every 30 seconds during the test. The test was initiated by pressurizing the O-Cell at the bottom of the shaft to break the tack welds that held the upper and lower plates of the O-Cell together and to form a fracture plane in the concrete surrounding the O-Cell. After the concrete break occurred, the pressure was released; and instrumentation readings were set to zero. The test shaft was then loaded using the O-Cell in a total of eight equal loading increments, resulting in a maximum sustained bi-directional load of 1,551 kips. Each load increment was held for 8 minutes. Load increments were applied using the "Quick Load Test Method" described in ASTM D1143M-07. An average of one minute was required to increase the O-cell pressure to the next load increment. Unloading of the test shaft was performed in five equal decrements.

5.2.4 Test Results and Analysis

Figure 5.4 shows the downward movement of the base plate of the O-cell and the upward movement of the top of the shaft during the bi-directional load test. The maximum sustained bi-directional load applied to the shaft was 1,551 kips. Under this load, the displacement above and below the O-cell assembly were 0.355 and 0.158 in., respectively. Further increase in the loading led to failure along the sides of the test shaft (i.e., ultimate side resistance was reached). Maximum displacements of 1.66 and 0.19 in. were measured at a maximum bi-directional load of 1,713 kips, above and below the O-cell assembly, respectively.

Figure 5.5 shows the load distribution curves along the test shaft for the eight load increments applied to the test shaft. The load distribution relationships were generated based on the recorded strain-gauge readings and the estimated drilled shaft stiffness. The elastic modulus of concrete was estimated based on the American Concrete Institute (ACI) formula, as expressed by the equation below:

$$E_c = 0.033\ (\delta_c)^{1.5}\sqrt{f'_c} \tag{5.1}$$

where:

E_c = concrete elastic modulus, in ksi

δ_c = concrete total unit weight, in pcf

f'_c = unconfined compressive strength of concrete, in psi

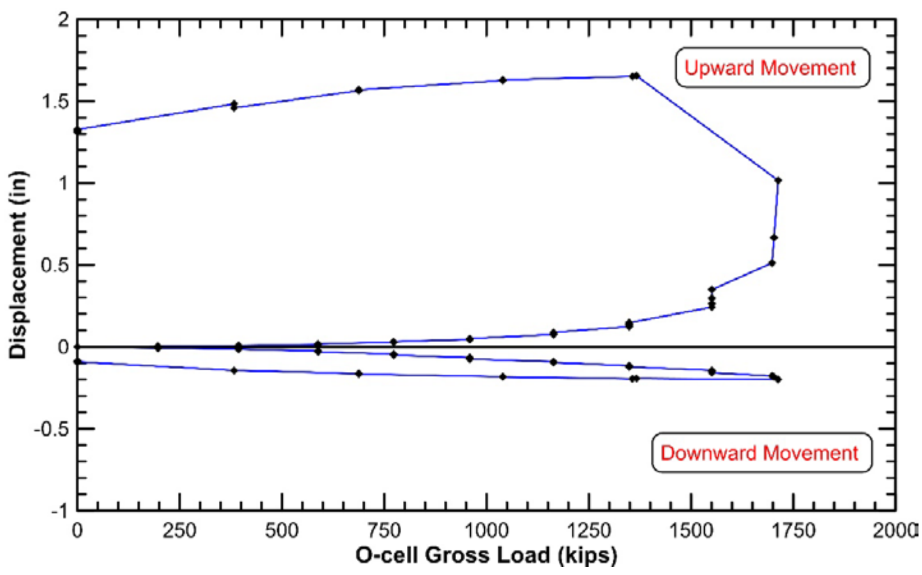

Figure 5.4. Measured load-displacement curves for downward and upward loading in the load test at the shaft tip at IL 89 over the Illinois River.

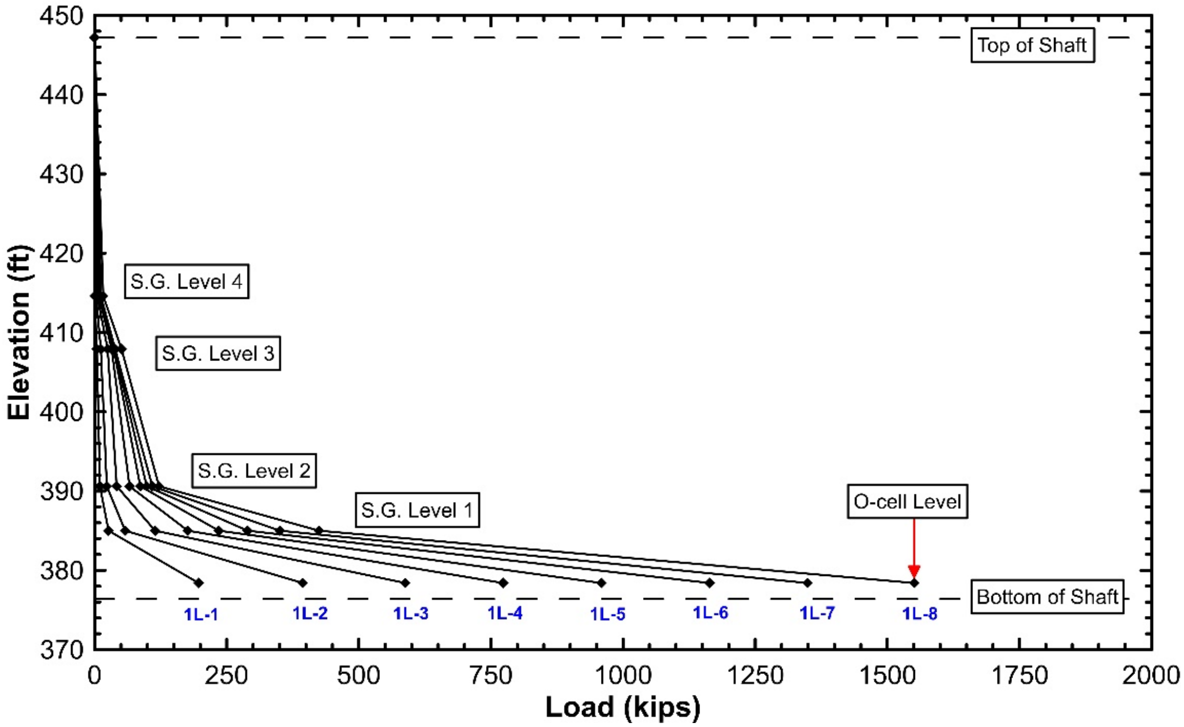

Figure 5.5. Axial load distribution curves along the test shaft during the load test at IL-89 over the Illinois River.

Concrete modulus combined with the area of reinforcing steel and nominal socket diameter provided an average shaft stiffness (EA) of 12,415,000 kips in the rock socket portion of the shaft. The magnitude of the unit side resistance mobilized for a segment of the shaft was computed as the change in the axial load over the length of the segment between adjacent strain gage (SG) measurements divided by surface area of the shaft segment. The calculated values of ultimate side resistance, assuming constant shaft stiffness and diameter, at the maximum sustained load of the O-cell, are summarized in Table 5.1. Figure 5.5 plots this data and shows about 95% of the applied load was carried by the clay–shale socket, and negligible load was transferred to the overburden soils. Mobilized net unit side resistance vs. displacement (t–z) relationships/curves based on the strain gage data along the test shaft and the estimated shaft stiffness are also presented in Figure 5.6.

Table 5.1. Average Unit Side Resistance Values for Maximum Sustained Load

Load-Transfer Zone	Unit Side Resistance (ksf)
O-cell to strain gage Level 1	10.7
Strain gage Level 1 to strain gage Level 2	3.3
Strain gage Level 2 to strain gage Level 3	0.1
Strain gage Level 3 to strain gage Level 4	0.2

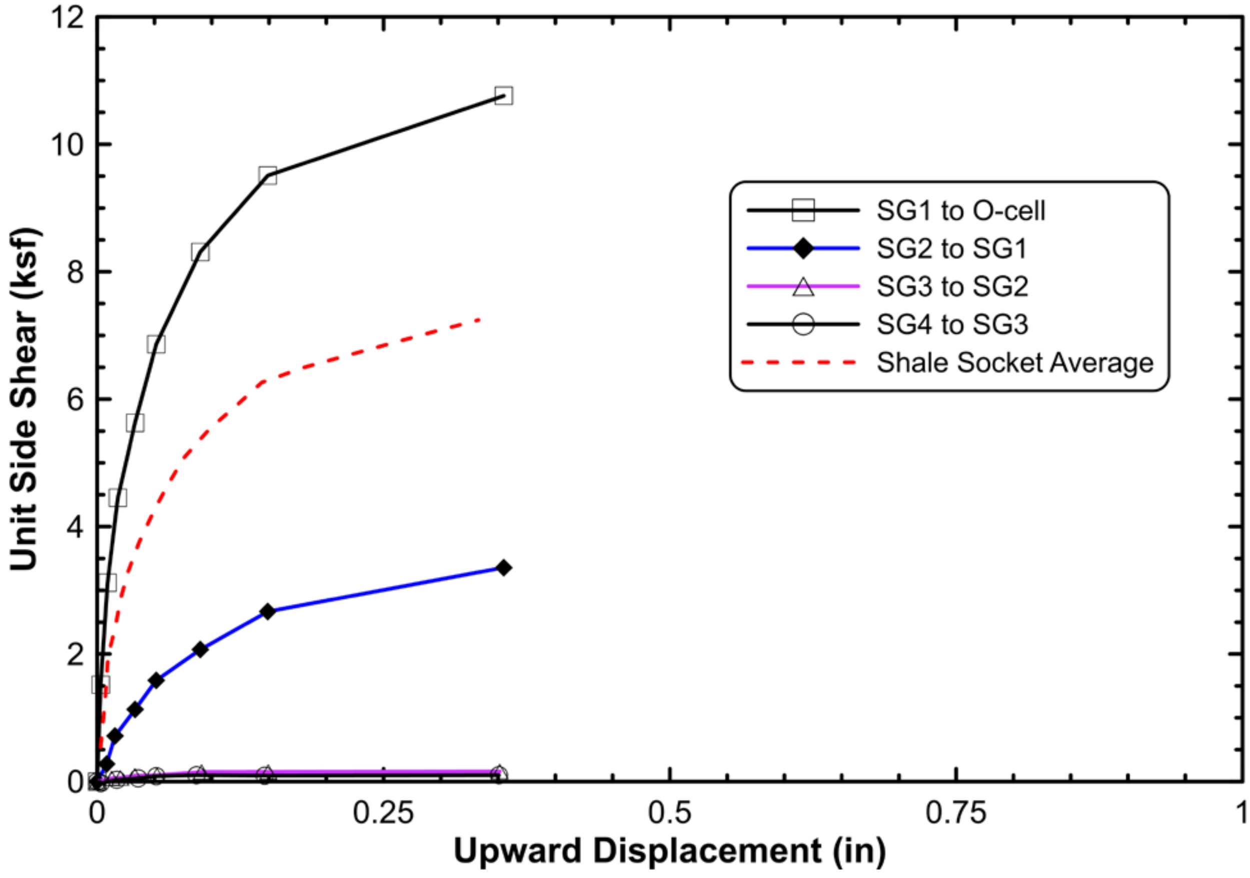

Figure 5.6. Mobilized unit side resistance along the test shaft for the load test at IL 89 over the Illinois River.

The mobilized unit tip resistance vs. displacement (q–z) relationships/curves are presented in Figure 5.7. The ultimate tip resistance was not reached during this test due to insufficient displacement being induced by the applied loading. The maximum measured tip resistance was

66.8 ksf at a relatively low displacement of 0.19 inches, which is less than 0.3 % of the drilled shaft socket diameter. Therefore, information/conclusions regarding ultimate tip resistance cannot be deduced from this load test.

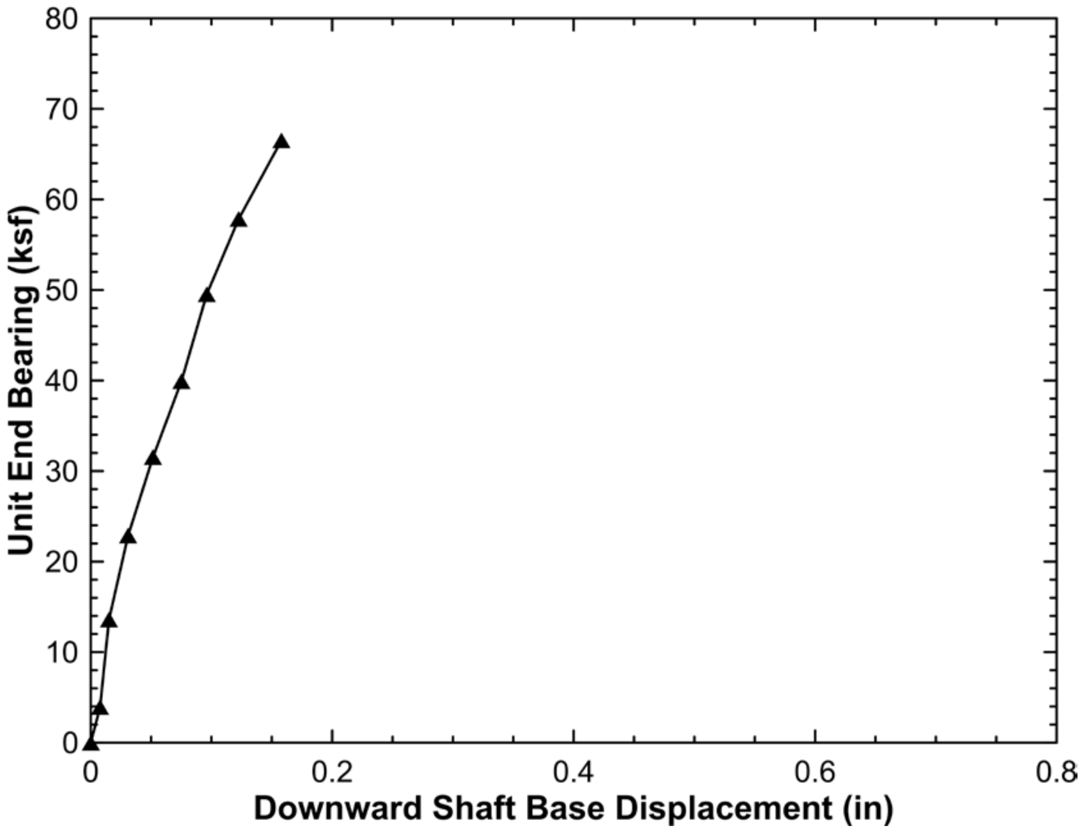

Figure 5.7. Mobilized unit tip resistance for the test shaft at IL-89 over the Illinois River.

5.3 BRIDGE SITE AT IL 133 OVER THE EMBARRAS RIVER

Figure 5.8 shows the proposed location of the bridge site at IL 133 over the Embarras River, located in Coles County just west of Oakland, Illinois. This two-span bridge structure is designed to carry a two-lane highway over the Embarras River. East and west abutments of this bridge are supported on driven H-piles foundations. The single pier is supported by drilled shaft foundations socketed into weak shales. In Phase 2 of this study, a full-scale O-cell load test was conducted on a test shaft, socketed into weak clay–shale, constructed near the existing river bridge pier (see Figure 5.9). The main objective of this load test was to measure the mobilized unit side and tip resistances along the weak shale socket and to evaluate the predictive design equations for side and tip resistance proposed in Phase 1. In addition, this load test complemented the prior Spring Valley, Illinois, load test because a drilled shaft with a shorter length and smaller diameter was going to be tested. The O-cell load test was performed on a test shaft 4.0 ft in diameter and 27.3-ft long. Figure 5.9 shows a plan view for the bridge structure and the location of the test shaft.

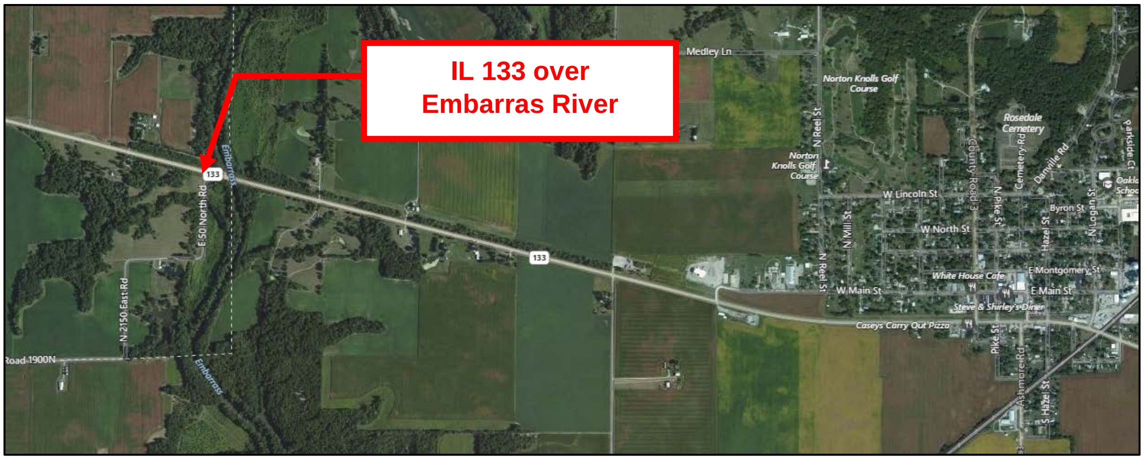

Figure 5.8. Location of the bridge at IL 133 over the Embarras River near Oakland, Illinois.

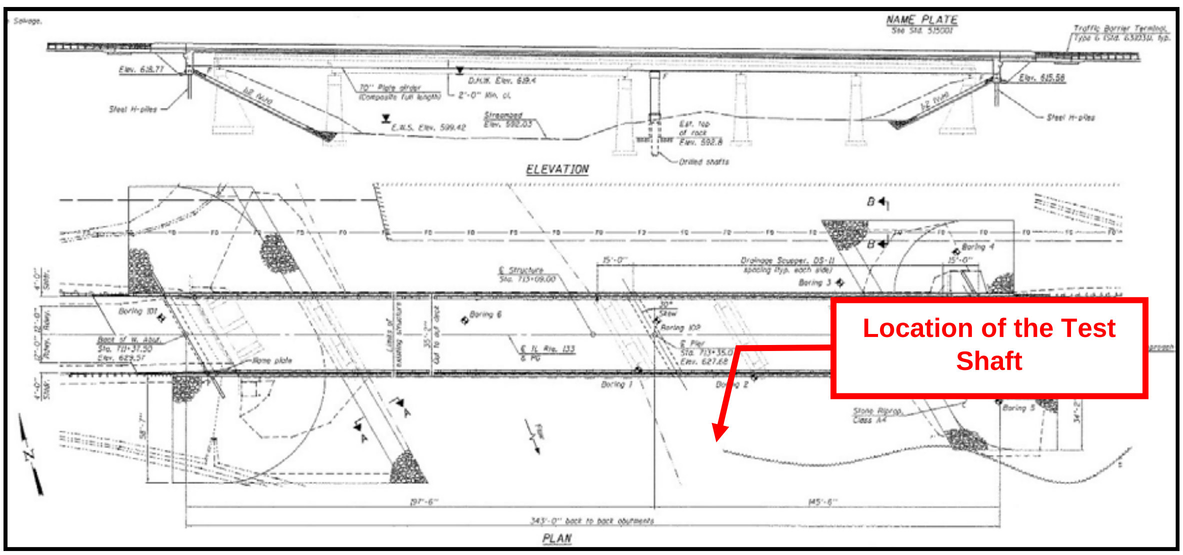

Figure 5.9. Location of test shaft of the bridge site at IL 133 over the Embarras River.

Prior to test shaft construction, four borings were advanced near the test shaft by the IDOT District 7 drilling crew and the UIUC research team. The first two borings were used to obtain shale core samples. Initially, rock cores were used for determination of recovery ratio, RQD of the rock mass, and vertical spacing of shale joints and fractures. Afterwards, unconfined compression tests were conducted on the retrieved specimen of weak shale. The in situ moisture content of the shale specimens used in the unconfined compression tests were also measured for correlation purposes. The unconfined compression test results were also used to determine the deformability characteristics of shale under undrained loading conditions (see Section 2.3.2 & 2.3.3). The other two borings were used to obtain MSPT penetration rate and blow counts at various depths in the weak shale formation. The penetration rate obtained was then used to estimate the unconfined compressive strength of the weak shales based on the correlation developed herein. The measured and estimated values of UCS were compared to investigate the accuracy of the proposed penetration rate/UCS correlation.

5.3.1 Subsurface Conditions

The subsurface profile at the test shaft location consists of 11 ft of soft to stiff, silty clay overlying the sedimentary bedrock. The ground surface elevation at the test shaft is about +600.0 ft. Weathered gray clay shale was exposed at an elevation of about +589.0 ft (11 ft below ground surface) and extending to an elevation of 564.1 ft, where the drilling was terminated. Figure 5.10 shows the idealized subsurface profile and the unconfined compressive strength profile at the test shaft location.

5.3.2 Test Shaft Construction and Instrumentation

Illini Drilled Foundations, Inc., of Danville, Illinois, completed construction of the test shaft on August 5, 2014. The 4-ft-diameter test shaft was excavated under dry conditions to a base elevation of +572.9 ft. The shaft was started by predrilling and inserting a 54-in-diameter temporary outer casing into the top of the shale bedrock. Drilling of the shaft continued into the shale layer using a 48-in.-diameter auger until the tip of the shaft was reached. After the shaft was approved for concrete placement, the reinforcing cage with the attached O-cell assembly was lowered into the excavated borehole to an elevation of +572.9 ft. Concrete was then delivered by a tremie pipe to the base of the shaft until the tip of concrete reached an elevation of +597.2 ft.

The load test assembly consisted of a 20 in.-diameter O-cell located 2.3 ft above the tip of the shaft (i.e., at elevation = +575.2 ft). Similar to the Spring Valley, Illinois, load test, four linear vibrating-wire displacement transducers (LVWDTs; Geokon model 4450 series) were installed between the upper and lower plates of the O-cell to measure its expansion during loading. Four vibrating-wire strain gauges (Geokon model 4911 series) were installed at three different elevations above the O-cell (see Figure 5.10), to assess the mobilized unit side resistance. Two upper compression telltale casings were attached diametrically opposite to the reinforcing cage and extending from the top plate of the O-cell to the ground level to measure the upper compression displacements of the drilled shaft. The displacement at the top of the drilled shaft was monitored using two automated digital-survey levels (Leica NA3000 series). A Bourdon pressure gage, voltage pressure transducer, and vibrating-wire pressure transducer were used to measure the pressure applied to the O-cell at each load interval. To evaluate the integrity of the concrete test shaft, four cross-hole sonic logging (CSL) tubes with a diameter of 2 in. were also installed along the full length of the test shaft and extending about 3 ft above the top of the test shaft.

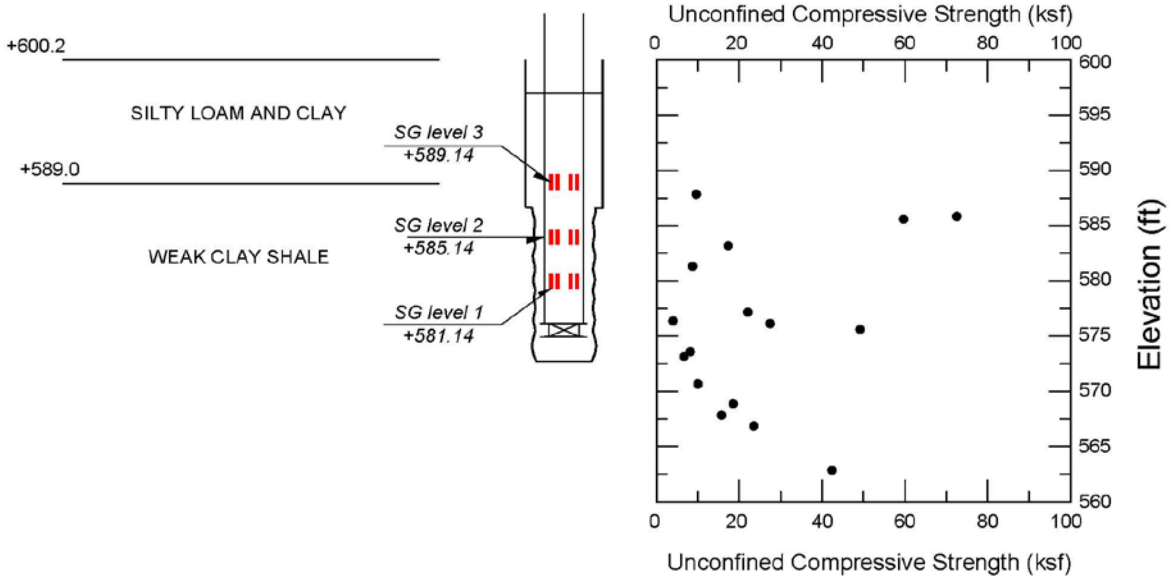

Figure 5.10. Idealized subsurface and unconfined compressive strength profiles of the bridge site at IL 133 over the Embarras River.

5.3.3 Data Acquisition and Testing Procedure

All instrumentation was connected through a data logger (Data Electronics 515 Geologger) to a laptop computer. The data logger recorded instrument readings every 30 seconds during the O-cell load test. The test was initiated by pressurizing the O-Cell to break the tack welds that held the upper and the lower plates of the O-Cell and to form a fracture plane in the concrete surrounding the O-Cell. After the concrete break occurred, the pressure was released; and instrumentation readings were set to zero. The test shaft was then loaded using the O-Cell in a total of ten equal load increments, resulting in a maximum sustained bi-directional load of 913 kips. Each load increment in the test was held for 8 minutes. Load increments were applied in accordance with the "Quick Load Test Method" (ASTM D1143M-07).

An average of one minute was required to increase the O-cell pressure to the next load increment. The loading was then increased beyond the maximum sustained load to examine the post-peak softening of the clay shales in terms of side resistance. A maximum applied load of 993 kips was reached during this stage of the test; however, this load was not sustained because the upper shaft above the O-cell started displacing rapidly. Afterwards, the test shaft was unloaded in five equal decrements.

5.3.4 Test Results and Analysis

Figure 5.11 shows the downward movement of the base plate of the O-cell and the upward movement of the top of the shaft during the bi-directional load test. The maximum sustained bi-directional load applied to the test shaft was 913 kips. Under this load, the displacements above and below the O-cell assembly were 1.282 and 1.684 in., respectively. Further increases in loading led to failure along the sides of the test shaft (i.e., ultimate side resistance was reached).

Maximum displacements of 4.155 and 1.929 in. were measured above and below the O-cell assembly. These displacements (4.155 and 1.929 in.) occurred during the first decrement of load.

Figure 5.12 shows the load distribution curves along the test shaft for the ten load increments applied to the test shaft. The load distribution is generated based on the recorded strain-gauge readings and the estimated drilled shaft stiffness. The elastic modulus of concrete was estimated using the American Concrete Institute formula. Concrete modulus (Equation 5.1), combined with the area of reinforcing steel and nominal socket diameter, provided an average shaft stiffness (EA) of 6,342,000 kips in the rock socket portion of the drilled shaft. The calculated values of ultimate side resistance, assuming constant stiffness and shaft diameter at maximum sustained load of the O-cell, are summarized in Table 5.2. Figure 5.13 shows the mobilized net unit side resistance vs. displacement (t–z) relationships, or curves, based on the strain gage data and the estimated shaft stiffness. Figure 5.13 also shows a notable post-peak-strain softening response of the clay–shale layer between the O-cell and SG-1, corresponding to a 20% decrease in unit side resistance. The other two shale layers between SG-1 to SG-2 and SG-2 to SG-3 did not exhibit strain softening but rather gained resistance with increasing shaft displacements.

Table 5.2. Average Unit Side Resistance Values for Maximum Sustained Load

Load-Transfer Zone	Unit Side Resistance (ksf)
O-cell to strain gage Level 1	6.3
Strain gage Level 1 to strain gage Level 2	7.4
Strain gage Level 2 to strain gage Level 3	2.4

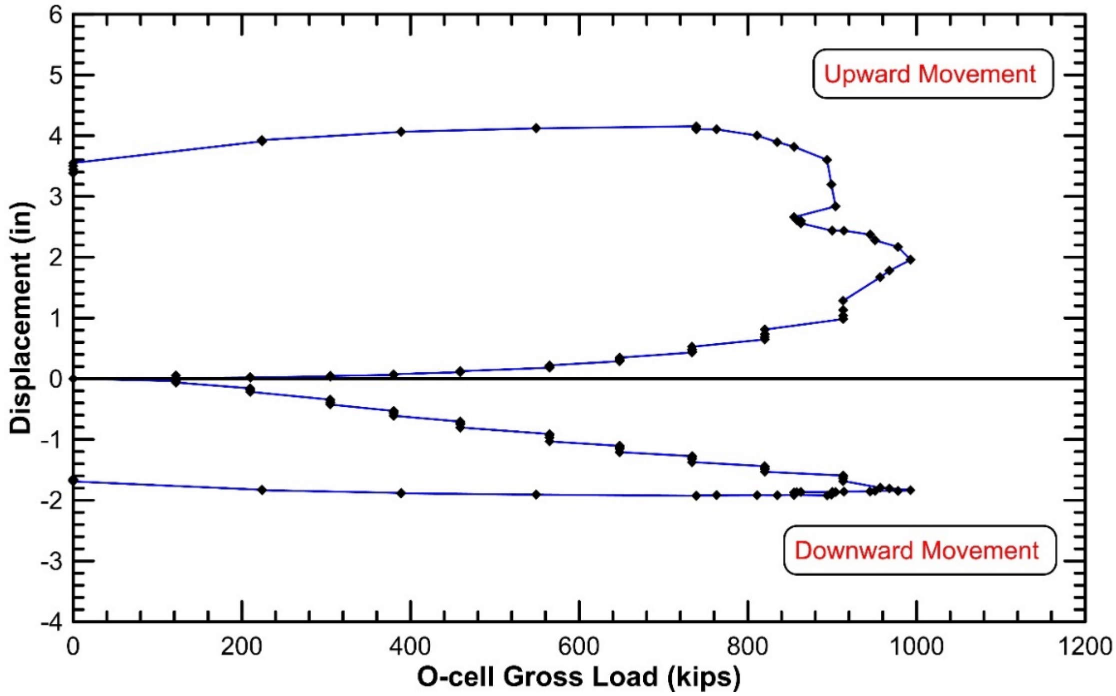

Figure 5.11. Measured load-displacement relationships for downward and upward loading of the test shaft at IL 133 over the Embarras River

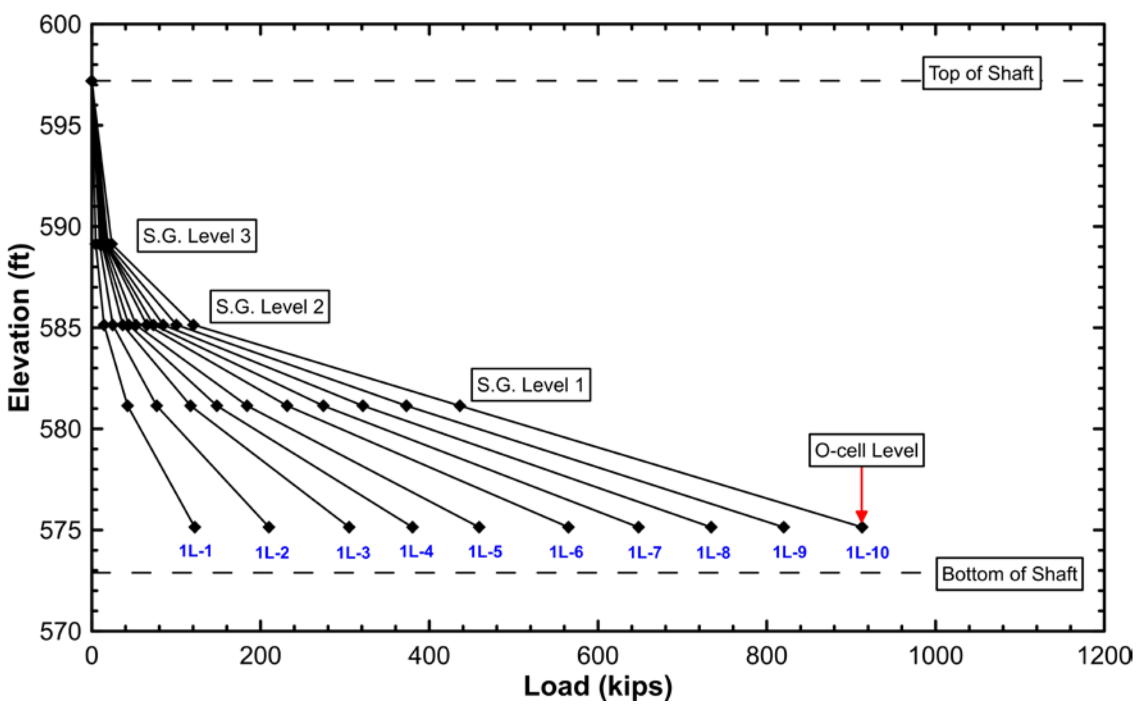

Figure 5.12. Axial load distribution relationships for the test shaft at IL 133 over the Embarras River.

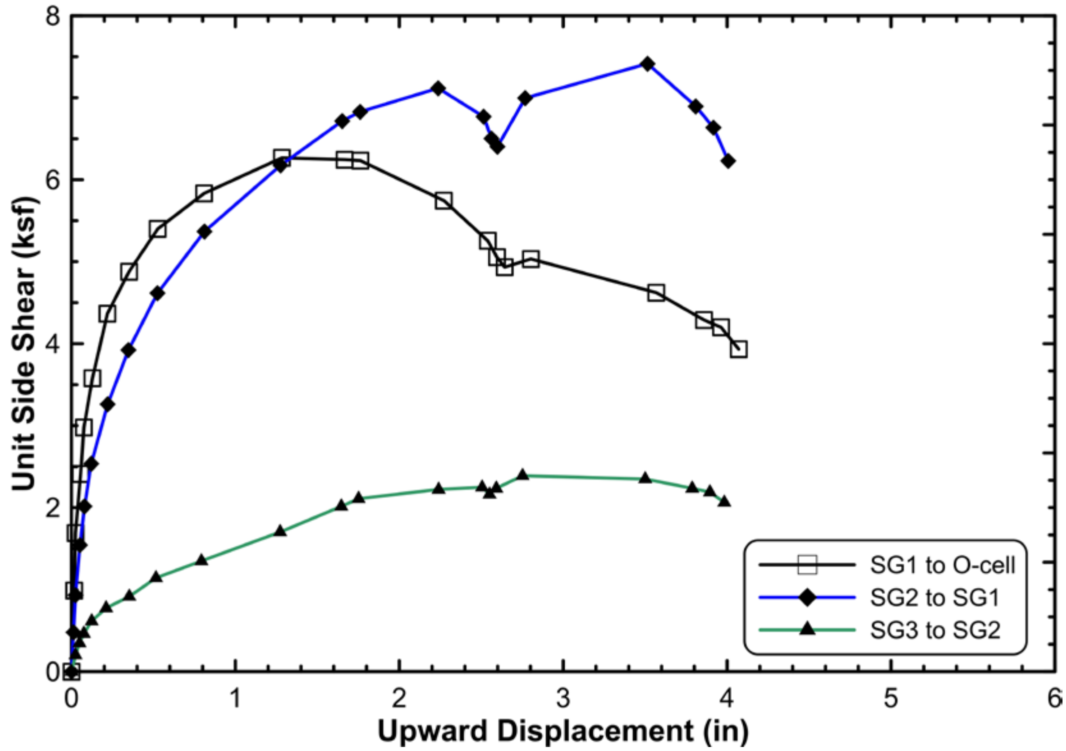

Figure 5.13. Mobilized unit side resistance for test shaft at IL 133 over the Embarras River.

The mobilized unit tip resistance vs. displacement (q–z) relationship, or curve, is shown in Figure 5.14. Ultimate tip resistance was not reached during this test, this may be due in part to insufficient cleanout of the shaft base before concrete placement, which could severely affect the unit tip resistance and settlement. Figure 5.13 and Figure 5.14 show a soft response of the unit tip resistance, which resulted in a low unit end bearing at a relatively large displacement of 1.64 in. Thus, a low bearing capacity factor (N_c = mobilized unit end bearing/unconfined compressive strength) of 3.0 was measured, which corresponds to a 40% decrease in tip resistance. This finding highlights the importance of the drilled shaft tip cleanout before placing concrete, in agreement with O'Neil and Reese (1999). If tip resistance is to be considered in design of a drilled shaft, proper techniques and inspections for doing and verifying adequate tip cleanout should be developed and followed by IDOT personnel. .

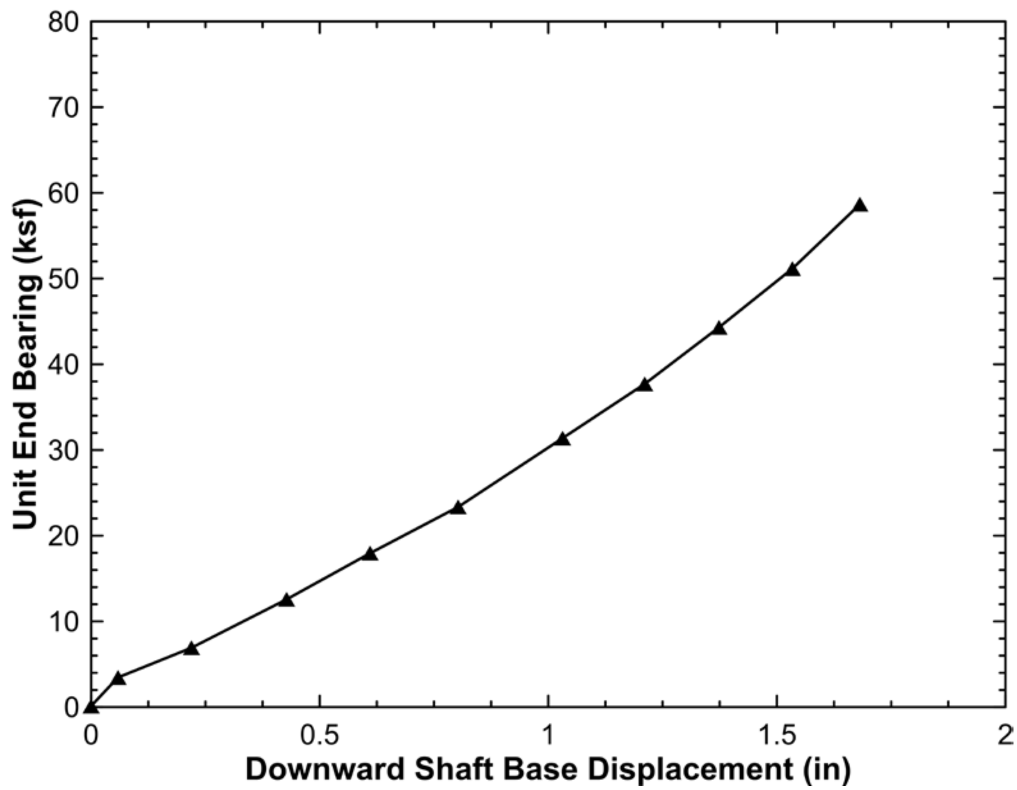

Figure 5.14. Mobilized unit tip resistance for test shaft at IL 133 over the Embarras River.

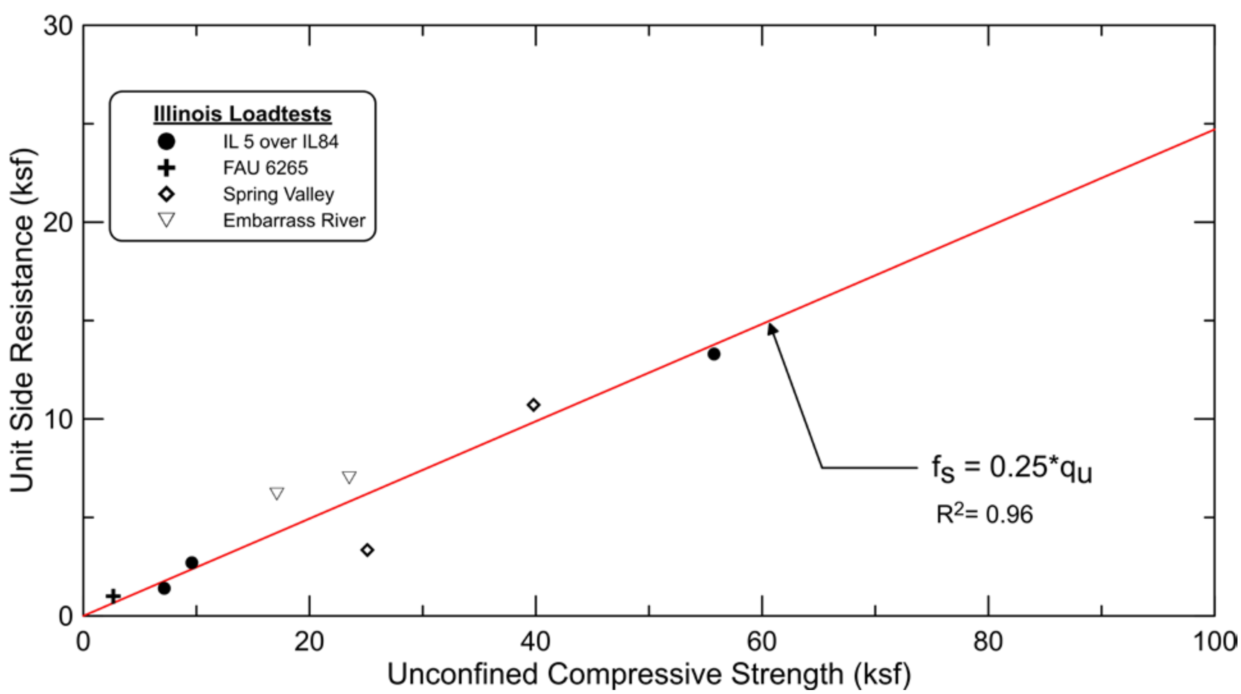

Figure 5.15. Mobilized unit side resistance for the four load tests conducted in Illinois weak shales and the line of best fit to the data.

5.4 BACK-CALCULATED ADHESION FACTORS

Measured unit side resistance of the two load tests conducted during this study were used, along with the laboratory-measured unconfined compressive strength, to back-calculate the mobilized adhesion factors (α), where it can be determined by dividing the maximum unit side resistance divided by the average unconfined compressive strength of the weak shales (i.e. $\alpha = f_{smax}/q_u$) Table 5.3 summarizes the results of the two load tests together with two load tests obtained during Phase 1 of this study. Data summarized in Table 5.3 are also used in Figure 5.15 to show the average mobilized adhesion factors of the four load tests. Data presented in Table 5.3 and Figure 5.15 show that the overall adhesion factors mobilized in these tests are slightly lower than values that the existing literature would suggest for drilled shaft load tests in weak, fine-grained rocks. However, the design procedure outlined in Chapter 7, along with the recommended LRFD resistance factors, accounts for the slight difference in the predicted to measured adhesion factors.

Table 5.3. Illinois Load Test Results for Drilled Shafts in Weak, Fine-Grained Rocks

Site	Strain-Gage Level	Average q_u (ksf)	F_{smax} (ksf)	Maximum Displacement (in.)	Adhesion Factor
IL 133 over Embarras River	SG1 to O-cell	23.5	7	1.27	0.30
IL 133 over Embarras River	SG1 to SG2	17.1	6.18	1.27	0.36
IL 89 over Illinois River	SG1 to O-cell	39.8	10.72	0.59	0.27
IL 89 over Illinois River	SG1 to SG2	25.1	3.35	0.58	0.133
John Deere Road (IL5 over IL 84)	SG1 to SG2	11.7	2.7	0.44	0.23
John Deere Road (IL5 over IL 84)	SG1 to O-cell	55.7	13.3	0.45	0.23
Illinois River Bridge replacement (FAU 6265)	SG6 to SG7	2.65	1.0	0.1	0.37

CHAPTER 6: NUMERICAL ANALYSES

6.1 INTRODUCTION

A two-dimensional (2D) finite element method (FEM) was used in this phase of the study to investigate the load-transfer mechanism of axially loaded drilled shafts socketed into weak rock, e.g., shales. The commercial finite element program, PLAXIS 2D (Brinkgreve, 2016), was used to simulate loading of a drilled shaft. A parametric study was conducted to investigate the factors that significantly affect the axial capacity of drilled shafts. Some of the factors investigated are drilled shaft socket roughness, relative stiffness between the drilled shaft and weak rock, mechanical properties of the weak rock, socket length, and socket diameter. The FEM model was calibrated and verified using an analytical solution proposed by Carter and Kulhawy (1988) and published numerical solutions by Rowe and Armitrage (1987), Pells and Turner (1979), and Hassan and O'Neill (1997). The results of the two Osterberg load tests conducted at the bridge sites at IL 89 over the Illinois River and IL 133 over the Embarras River were also used to calibrate the FEM model for predicting drilled shaft capacity in weak rocks.

6.2 FINITE ELEMENT MESH AND BOUNDARY CONDITIONS

Fifteen-node triangular axisymmetric elements (see Figure 6.1) were used in PLAXIS 2D to simulate the drilled shaft and the surrounding weak rock mass and overburden soils (see Figure 6.3). A relatively fine mesh was used in the regions where stress concentrations were anticipated, particularly along the weak rock/drilled shaft interface and at the tip of the drilled shaft. Interface elements are used to simulate the sliding of the drilled shaft along the weak rock. The loading of the shaft is simulated by applying incremental vertical displacement to the shaft head. Other boundary conditions consist of restraining both the vertical and radial displacements at the base of the model and the radial displacement on the right-hand side of the model and along the axis of symmetry. The boundary conditions used in the model are also shown in Figure 6.3. The selected model boundaries were set wide enough to eliminate significant boundary effects on load-transfer from the drilled shaft to the weak rock and overburden soils.

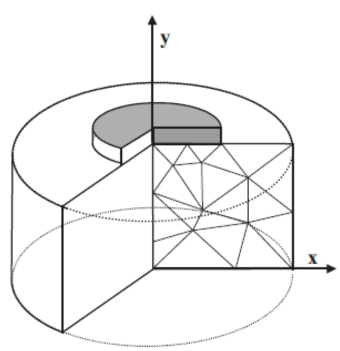

Figure 6.1. Axisymmetric FEM representation (from *PLAXIS 2D User's Manual*).

6.3 CONSTITUTIVE MODELS

The drilled shaft is assumed to be homogeneous, isotropic, and elastic with a constant Young's modulus (E_s) and Poisson's ratio (ν). The soil(s) overlying the weak rock are modeled using a Mohr-Coulomb (MC) linearly elastic, perfectly plastic constitutive model. The MC failure criteria is expressed by the equation below:

$$\tau_f = \sigma'_{nf} \tan \phi' + c' \tag{6.1}$$

where:

τ_f = shear stress at failure

σ'_{nf} = effective normal stress at failure

ϕ' = effective stress angle of internal frictional, i.e., friction angle

c' = effective stress cohesion

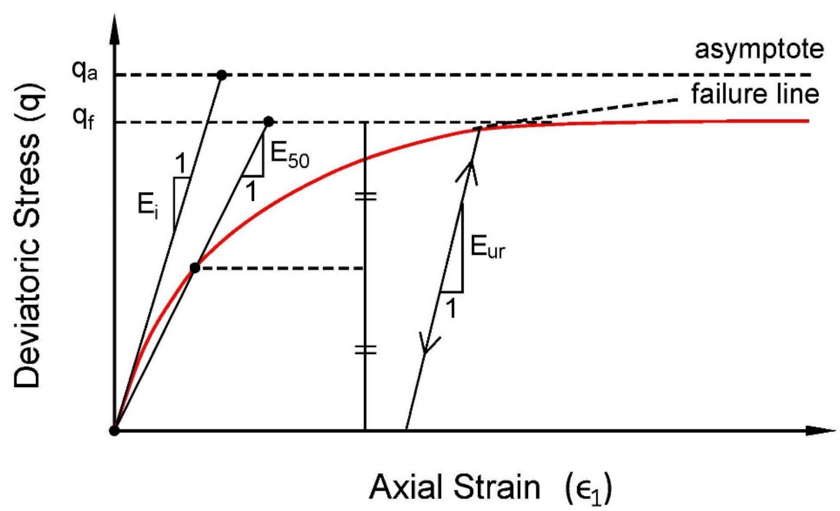

Figure 6.2. Schematic of hyperbolic stress–strain model from Schanz et al. (1998).

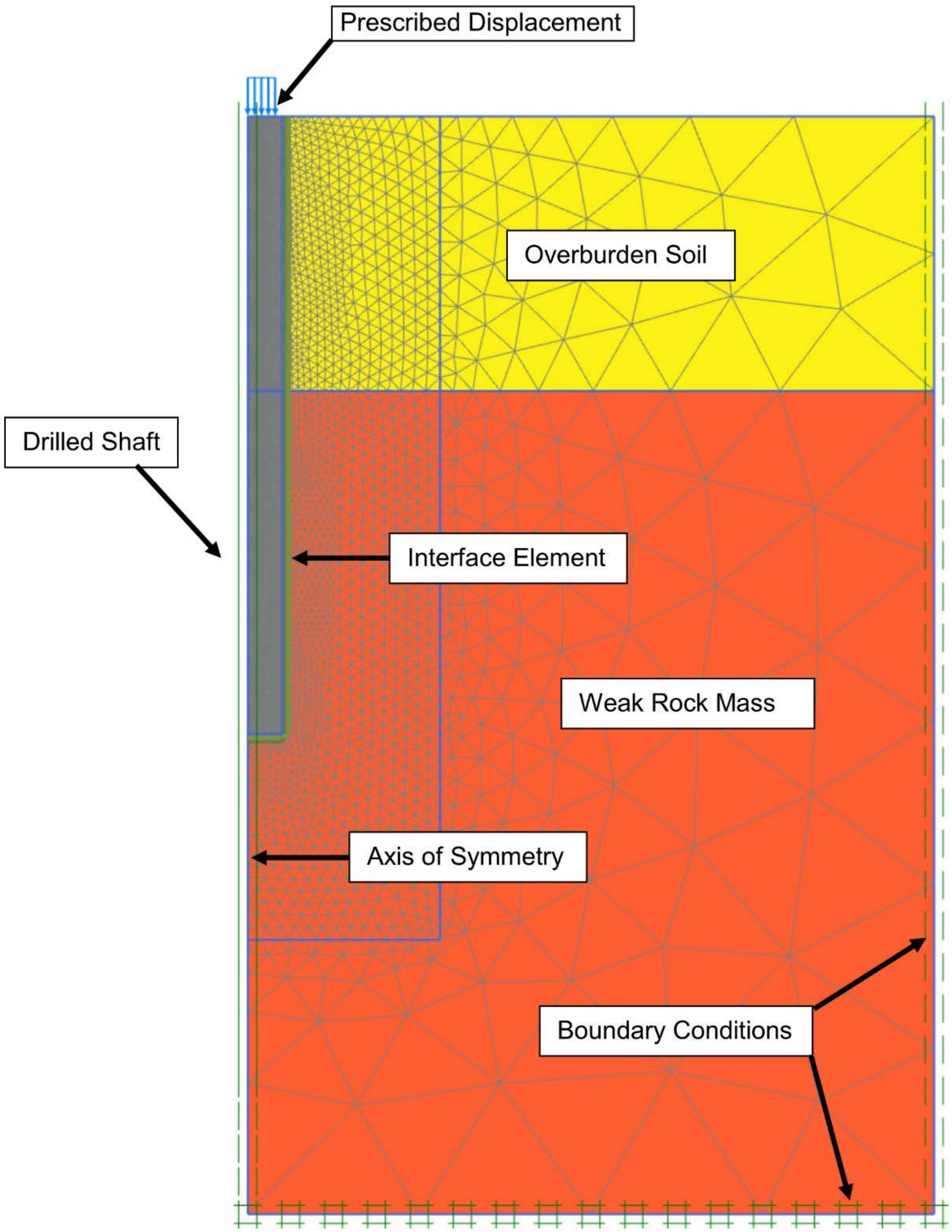

Figure 6.3. Typical finite element mesh and boundary conditions applied in drilled shaft parametric study.

The hardening soil (HS) model, developed by Schanz et al. (1998), was used to simulate the nonlinear stress–strain relationship of weak rock mass. The HS constitutive model was derived from the hyperbolic stress–strain model developed by Duncan and Chang (1970). The HS model is considered an improvement over the hyperbolic model because it utilizes the theory of plasticity rather than the theory of elasticity and includes soil dilatancy. As a result, the HS model can predict the plastic strains based on a multi-surface yield criterion. Some of the basic characteristics of the HS model are

- Failure is defined according to the MC failure criterion.
- Total strains are calculated based on stress-dependent stiffness moduli both for loading and unloading/reloading cases.
- Hardening is assumed to be isotropic, depending on both plastic shear and volumetric strain.
- The hyperbolic equation in terms of axial strain (ϵ_1) and stress difference (q) is

$$\epsilon_1 = \frac{1}{E_i} \frac{q}{1 - {}^{q}/_{q_a}} \tag{6.2}$$

where q_a is the asymptotic value of the stress difference, i.e., ultimate value of q at infinite strain, as illustrated in Figure 6.2; and E_i is the initial tangent modulus. E_i is related to the secant modulus by the modulus at 50% axial strain (E_{50}) by

$$E_i = \frac{2E_{50}}{2 - R_f} \tag{6.3}$$

where R_f is a fitting ratio that forces the hyperbolic stress–strain relationship to pass through the point of failure, i.e., ϵ_f, q_f, and can be expressed in terms of the failure stress, q_f:

$$R_f = \frac{q_f}{q_a} \tag{6.4}$$

Typical values of R_f are in the range of 0.75 to 1.0. In this study a fitting ratio of 0.9 is used, which is the default setting in PLAXIS 2D.

6.4 INTERFACE ELEMENTS

The use of continuum elements in a finite element analysis prohibits relative displacement between structure elements, e.g., a drilled shaft, and adjacent soils and rock materials. To simulate relative displacement, i.e., slippage of the side of the drilled shaft along a weak rock boundary, interface elements are introduced. Potts and Zdravkovic (2001) summarize the different methods to simulate soil-structure interaction and slippage. In the parametric study conducted herein, a zero-thickness interface formulation was used, which is proposed by Goodman et al.

(1968). To implement the interface element option, node pairs are created at the weak rock/shaft interface. As a result, one node belongs to the drilled shaft and the other node belongs to the adjacent weak rock (see Figure 6.4). The interaction between these two interface nodes involves two elastic–perfectly plastic springs to simulate slippage and gaps. Figure 6.4 shows a schematic representation of a node pair and the zero-thickness interface elements used along the drilled shaft.

Interface elements are modelled using the elastic–perfectly plastic Mohr-Coulomb strength model. The strength of the interface is defined with an interface strength-reduction factor, R_{int}. This reduction factor is similar to the adhesion factor in the total-stress analysis of axially loaded drilled shafts in cohesive soils and rock, as shown below:

$$c'_i = R_{int} \cdot c' \tag{6.5}$$

$$\tan \phi'_i = R_{int} \cdot \tan \phi' \tag{6.6}$$

$$\psi_i = 0^0 \text{ for } R_{int} < 1.0, \text{ otherwise } \psi_i = \psi \tag{6.7}$$

Where c'_i is the interface effective stress cohesion or the undrained shear strength in a total-stress analysis, ϕ'_i is the effective stress interface friction angle, and ψ_i is the interface dilation angle. Based on analysis developed herein of the drilled shaft load test database in cohesive weak rocks, the interface-reduction factor, R_{int}, was assigned a value of 0.60.

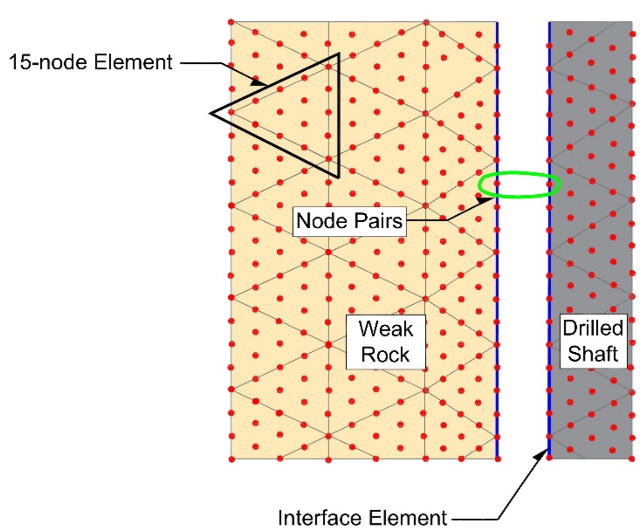

Figure 6.4. Schematic representation for the zero-thickness interface element used herein.

6.5 VALIDATION OF NUMERICAL ANALYSIS

During this study, two Osterberg cell (O-cell) load tests were conducted on drilled shafts socketed in weak rock, to validate the drilled shaft design methodology developed herein and to calibrate the FEM model for the parametric analysis. The load-displacement and load-transfer relationships measured during these two load tests were used to develop weak rock/shale-specific parameters for the drilled shaft parametric model discussed above. To calibrate the FEM model, the boundary conditions, interface elements, and load application via the O-cell at the bottom of the drilled shaft are modeled accurately for each test. These modeling features were adjusted until agreement was good between the measured and calculated drilled shaft load-deformation relationships for the measured values of UCS and Young's modulus. UCS and Young's modulus are the main input parameters for each load test site and were derived from laboratory testing performed on high-quality shale core samples. This calibrated model was then used in the subsequent parametric analysis.

6.5.1 Load Test at IL 133 over the Embarras River

An O-cell drilled shaft load test was conducted on a test drilled shaft socketed in weak "clayey shale" of the Pennsylvanian formation at the IL Route 133 bridge crossing of the Embarras River. The test shaft was 4.0 ft in diameter, with a socket length of 16.0 ft. Figure 6.5 shows an idealization of the subsurface profile and the as-built dimensions of the instrumented test drilled shaft. Four borings, two for shale coring and two for MSPTs, were conducted near the test shaft to measure the strength and compressibility parameters for the shales. Figure 6.6 shows the measured rock quality designation (RQD), total core recovery (TCR), and unconfined compression strength (UCS) for the weak shales at the vicinity of the test shaft. Details of the subsurface investigation, test shaft construction, O-cell testing arrangements, and testing-results interpretations are discussed in more detail in Chapter 5:

6.5.1.1 Numerical Model

Figure 6.7 shows the FEM model developed for the IL 133 O-cell test and the applied boundary conditions. The concrete shaft was again assumed to be an isotropic, homogeneous, and elastic with an elastic modulus (E_c) of 3,500 ksi, Poisson's ratio (ν_c) of 0.15, and a unit weight (γ_c) of 145 pcf. The HS and MC constitutive models were again used to simulate the weak shale layer and the overburden soil, respectively. The interface-reduction factor between the drilled shaft and the weak rock was assumed to be equal 0.60 as discussed above. The O-cell below the drilled shaft was simulated using a 1-ft-thick solid element. To simulate the loading induced by the load test, the O-cell was expanded upward and downward to force movement of the drilled shaft. Upon applying the bi-directional load at the O-cell location, the solid element was deactivated so the interaction between the downward and upward shaft displacement could be decoupled. This procedure is important because it allows proper simulation of the O-cell arrangement.

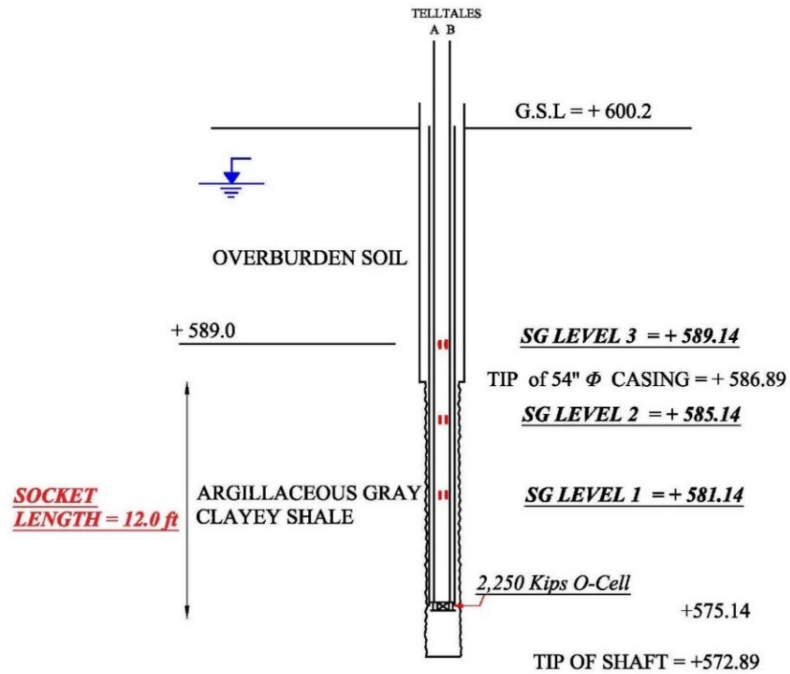

Figure 6.5. Idealized soil profile and as-built dimensions of the instrumented test shaft at IL 133 over the Embarras River.

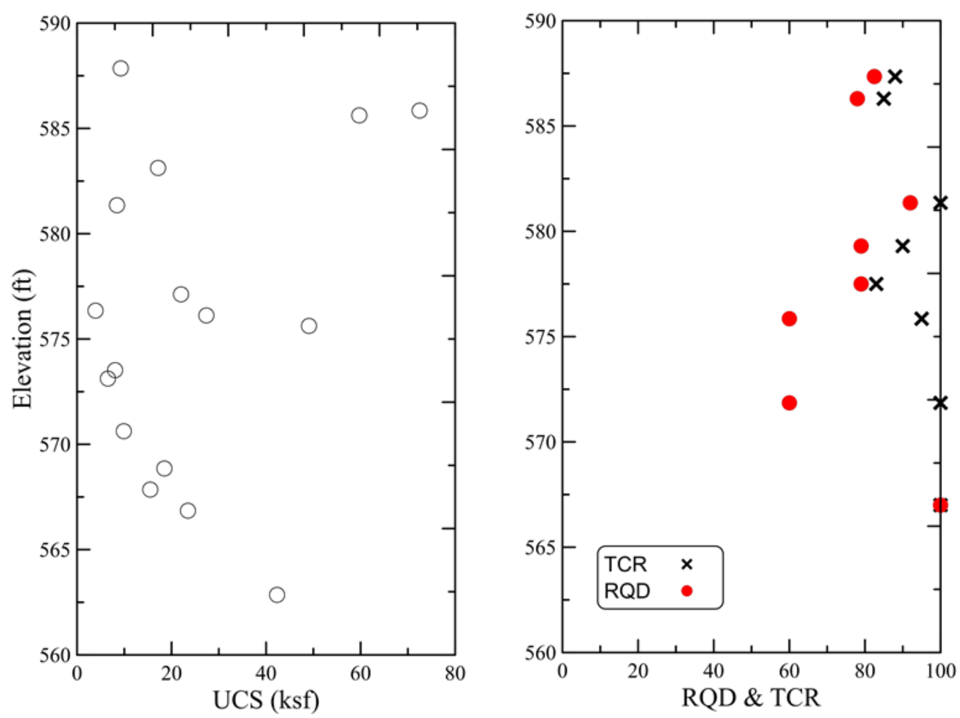

Figure 6.6. Measured UCS, RQD, and TCR versus elevation before IL 133 drilled shaft load test.

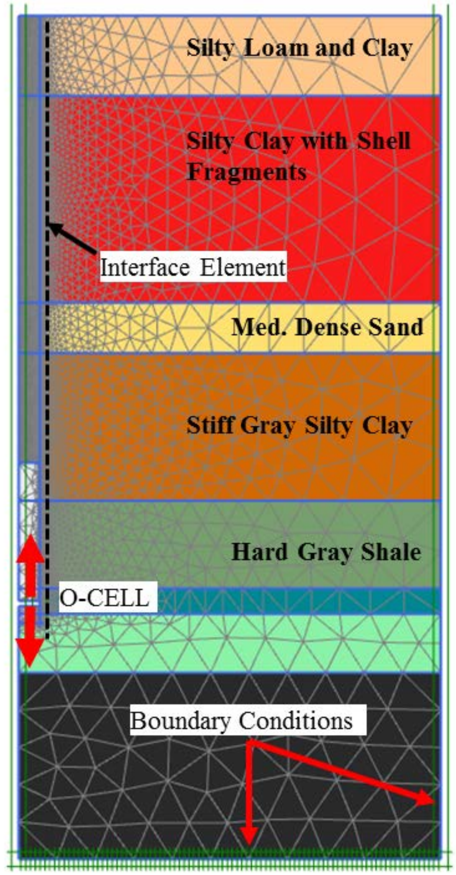

Figure 6.7. FE model and boundary conditions at IL 133 over the Embarras River.

6.5.1.2 Numerical Prediction vs. Measured

The numerically predicted load-displacement relationships for the top and bottom O-cell plates are compared to the measured values in Figure 6.8. Figure 6.8 shows good agreement between the FEM predicted and measured tip resistances. In particular, the measured tip resistance shows a soft response because the bottom of the shaft was not thoroughly cleaned before concrete was tremied in to construct the drilled shaft. As a result, to achieve a match of the measured tip resistance response, a low modulus was assigned for the weak rock directly below the shaft base. Figure 6.9 shows a comparison between the predicted and measured load-transfer relationship for this load test. Figure 6.8 and Figure 6.9 show that the numerical analysis results are in good agreement with the measured field loads and displacements. As a result, the input parameters used to calculate the load-displacement and load-transfer relationships are calibrated and can be used in the parametric study to understand the factors that significantly influence drilled shaft behavior in weak rock.

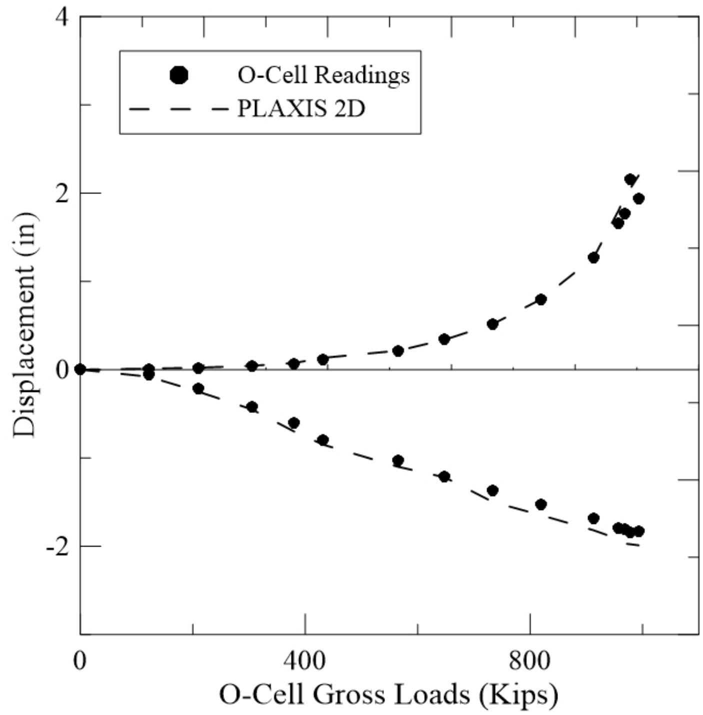

Figure 6.8. Comparison of measured and numerically predicted load-displacement relationships for the load test at IL 133 over the Embarras River.

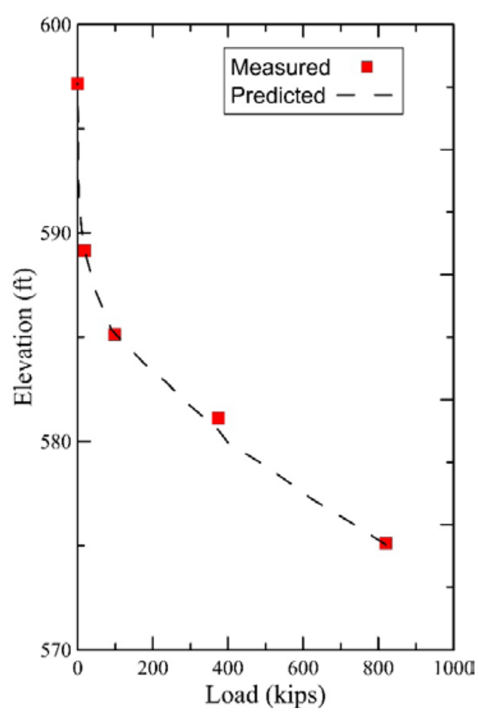

Figure 6.9. Comparison of measured and numerically predicted load-transfer relationships for last loading increment (O-cell load = 820 kips).

6.5.2 *Load Test at IL 89 over the Illinois River*

An O-cell load test was also conducted on a drilled shaft socketed in weak “clayey shale” of the Pennsylvanian formation at IL 89 over the Illinois River near Spring Valley, Illinois. The test shaft was 5.0 ft in diameter with a socket length of 12.0 ft. A numerical model using the same simulation techniques developed for the load test at IL 133 over the Embarras River was developed for this load test, too. Figure 6.11 shows an idealization of the subsurface profile and the as-built dimensions of the instrumented drilled shaft. Two borings (one for shale coring and one for MSPT) were conducted near the test shaft to measure the strength and compressibility of the shales. Figure 6.12 shows the measured RQD, TCR, and UCS for the weak shales in the vicinity of the test shaft. Additional details of the subsurface investigation, test shaft construction, O-cell testing arrangements, and interpretation of the test results are presented in Chapter 5:.

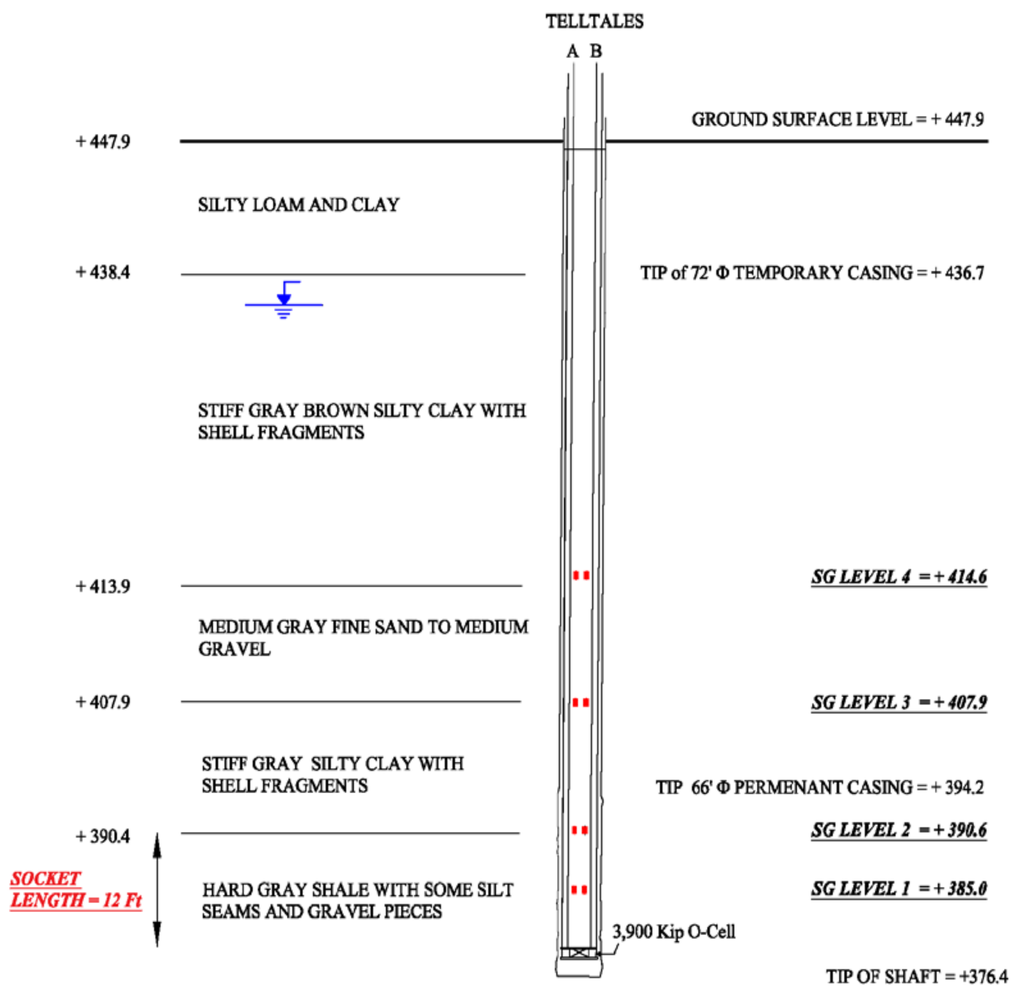

Figure 6.10. Idealized soil profile and as-built dimensions of the instrumented drilled shaft at IL 89 over the Illinois River.

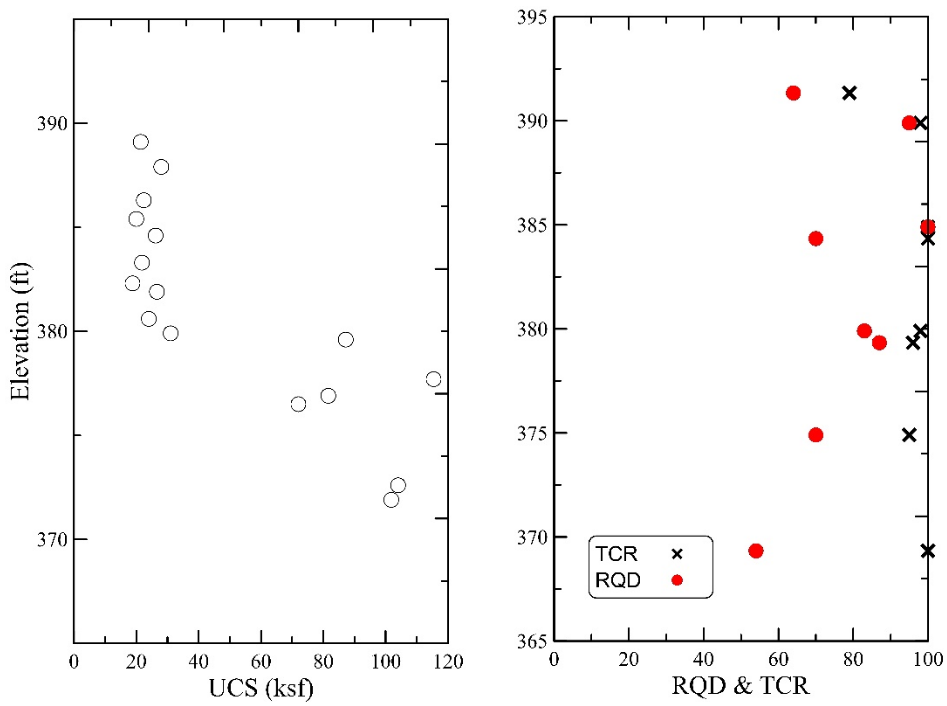

Figure 6.11. Measured UCS, RQD, and TCR versus elevation at IL 89 over the Illinois River.

6.5.2.1 Numerical Prediction vs. Measured

The numerically predicted load-displacement relationships for the top and bottom O-cell plates are compared with the measured values and are shown in Figure 6.12. This comparison shows excellent agreement between the PLAXIS 2D model and the measured load-displacement relationships. Figure 6.13 presents a comparison of the predicted and measured load-transfer relationships for the last O-cell loading increment. Review of Figure 6.12 and Figure 6.13 suggests that the numerical analysis predictions are in excellent agreement with the field-measured load-displacement and load-transfer relationships. As a result, the input parameters used to calculate the load-displacement and load-transfer relationships were considered to be calibrated and can be used in the parametric study to understand the factors that significantly influence drilled behavior in weak rock.

In summary, the 2D FEM model provided good agreement with the measured load-displacement and load-transfer relationships measured for the IL 133 and IL 89 drilled shaft load tests. As a result, the boundary conditions, interface elements, and load application via the O-cell at the bottom of the drilled shaft are modeled accurately. Thus, the 2D FEM model described above is used below to study the impact of a number of factors, e.g., UCS, shaft length to diameter, and rock socket length, in this parametric study.

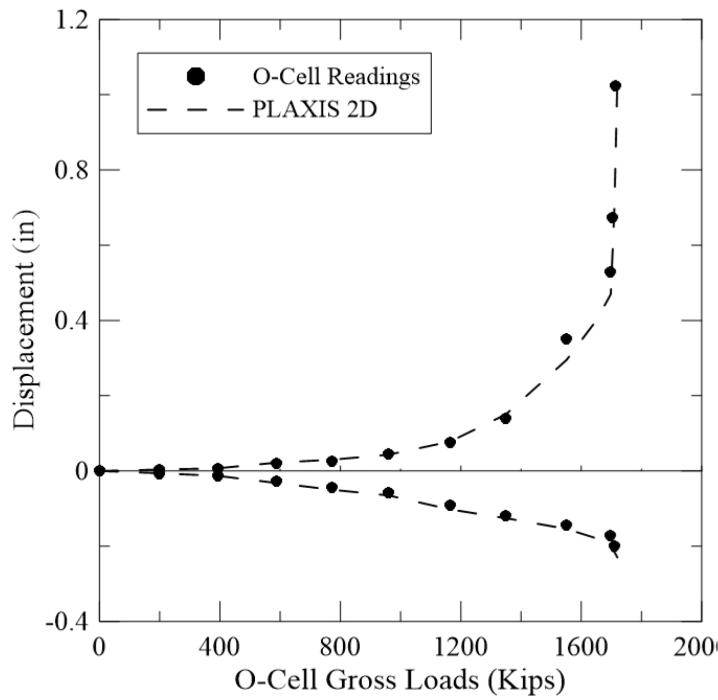

Figure 6.12. Comparison of measured and numerically predicted load-displacement relationships for drilled shear-load test at IL 89 over the Illinois River.

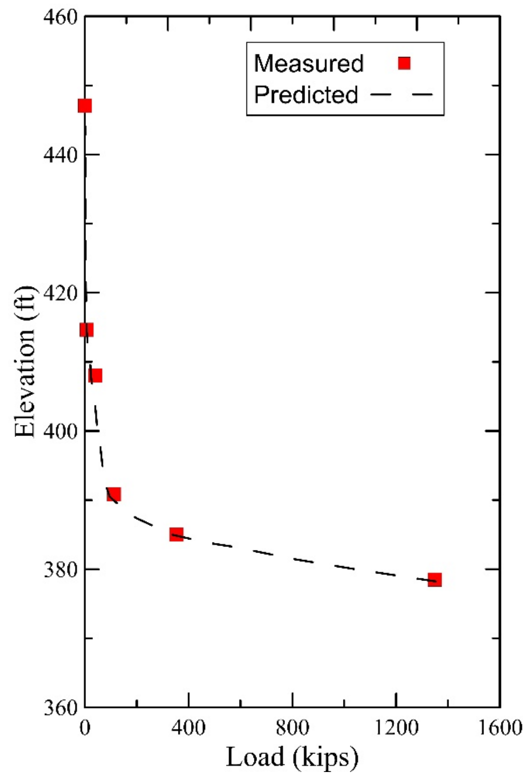

Figure 6.13. Comparison of measured and numerically predicted load-transfer relationships for last loading increment (O-cell load = 1,350 kips).

6.6 PARAMETRIC ANALYSIS

The parametric analysis described below used the load test–calibrated 2D FEM axisymmetric model. As shown above, the calibrated boundary conditions, interface elements, and load application via the O-cell at the bottom of the drilled shaft resulted in good agreement between the measured and predicted load-displacement and load-transfer relationships.

The axial response of drilled shafts socketed into weak cohesive rock is a function of the unconfined compressive strength of the weak rock, relative stiffness between the weak rock and the concrete shaft, rock socket geometry, and the weak rock/drilled shaft interface roughness. The calibrated numerical model described above was used to conduct a parametric analysis to investigate these factors. The analysis procedure consists of the following two main steps: (1) application of initial in situ stress(es) due to self-weight of overburden soils, weak rock mass, ground water and drilled shafts; and (2) application of structural loads by applying incremental vertical displacement to the shaft head.

6.6.1 Effect of Rock Socket Geometry

The effect of rock socket geometry is studied in terms of the ratio of socket length (L_s) to socket diameter (D), with a range of $1 \leq L_s/D \leq 10$. This analysis is conducted for a UCS of 20 ksf and a ratio of Young's modulus for the rock (E_r) to concrete (E_c) of 0.02. In other words, the concrete is much stiffer than the weak rock. Other pertinent parameters remained constant.

Figure 6.14 shows the percentage of ultimate axial load carried by the skin friction and tip resistance, where the ultimate load is assumed to occur at a tip displacement equal to 5% of the shaft diameter (O'Neill and Reese 1999). Figure 6.14 shows that as the L_s/D ratio increases, less load is transferred to the drilled shaft base and more load is carried by the skin friction. This implies that the axial behavior of drilled shafts with short rock sockets will be largely affected by the condition and stiffness of the weak rock at the tip of the shaft, whereas shafts with longer sockets will be less sensitive to these conditions because most of the load is carried by skin friction. Therefore, in order to rely on short-socketed drilled shafts (i.e., small L_s/D) to carry the anticipated load, proper inspection and cleanout of the tip of the drilled shaft is essential..

Figure 6.15 displays the load-transfer mechanism for different rock socket geometries. At early stages of loading, the load is predominately carried by skin friction; and a small percentage of the load is transferred to the tip of the shaft. With increasing load and displacements, the skin friction is fully mobilized; and the remaining loads will be carried by the tip resistance. This behavior is intensified for shafts with long sockets or with large ratios of socket length to diameter. However, it still applies for shorter sockets; but the tip resistance contributes more at early stages of loading.

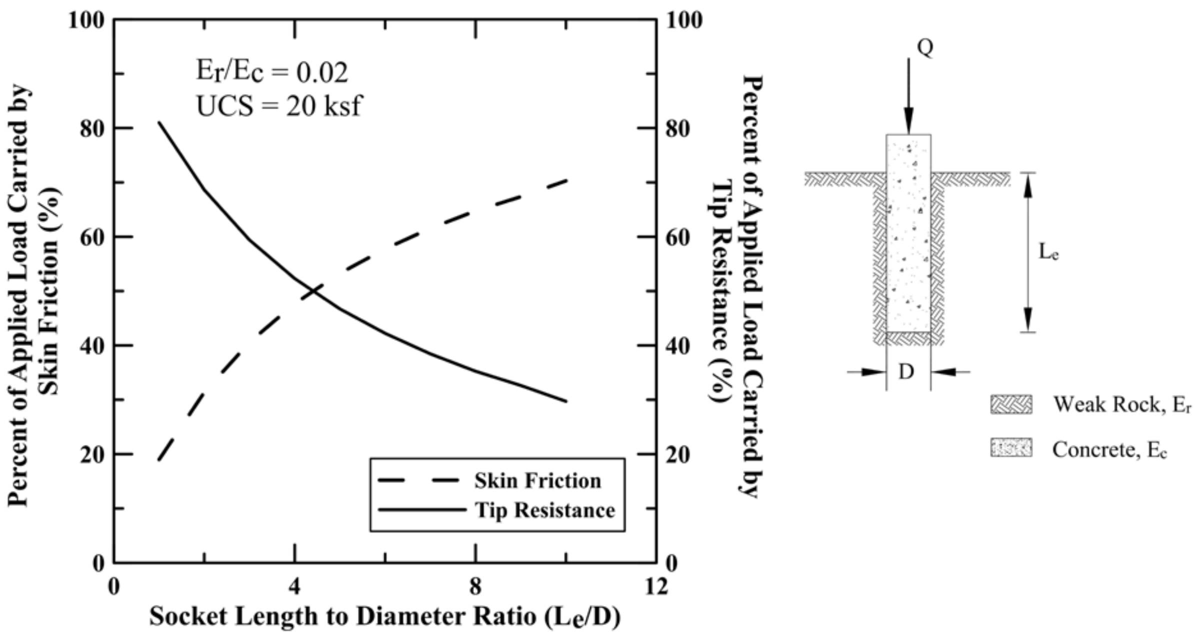

Figure 6.14. Percentage of applied load carried by skin friction and tip resistance for different socket geometries.

In summary, these results show that the portion of applied axial compressive load that is transferred to the tip of the shaft is a function of rock socket geometry, i.e., L_s/D ratios. With increasing socket lengths, the relative tip load-transfer decreases. For instance, more than 80% of the applied load is transferred to the base of the socket for L_s/D of 2. Therefore, short-socketed drilled shafts can be used only when the rock mass condition beneath the tip of shaft is relatively sound/intact and when proper inspection and cleanout of the base of the shaft is ensured. The difference in stiffness between the rock and concrete has a significant effect on the axial behavior of weak rock-socketed drilled shafts, as discussed in more detail below.

6.6.2 Effect of Relative Stiffness

The range of weak rock moduli measured during this study is between 500 to 15000 ksf. This range suggests that the relative stiffness ($n=E_r/E_c$) is low (0.005–0.04) for most of the weak cohesive rock tested herein. For this reason, understanding the influence of Young's modulus of the rock on the axial response of the drilled shaft is important. This parametric analysis was performed using a UCS of 20 ksf, a socket length of 5 ft, and a socket diameter of 15 ft.

Comparison between load-displacement relationships for different relative stiffnesses (n) is shown in Figure 6.16. Figure 6.16 shows the drilled shaft tip resistance is significantly affected by the soft response of the base, with a decrease of up to 40% of the axial load carried by the tip resistance with a soft base. Figure 6.16 also shows that skin friction is fully mobilized at greater axial displacements when the shaft is socketed in softer shales. Conversely, Figure 6.17 shows that the percent of axial load carried by skin friction for different socket geometries is only slightly influenced by rock mass modulus; and the load distribution between the side and tip resistance is mainly controlled by the ratio of the socket length to the diameter.

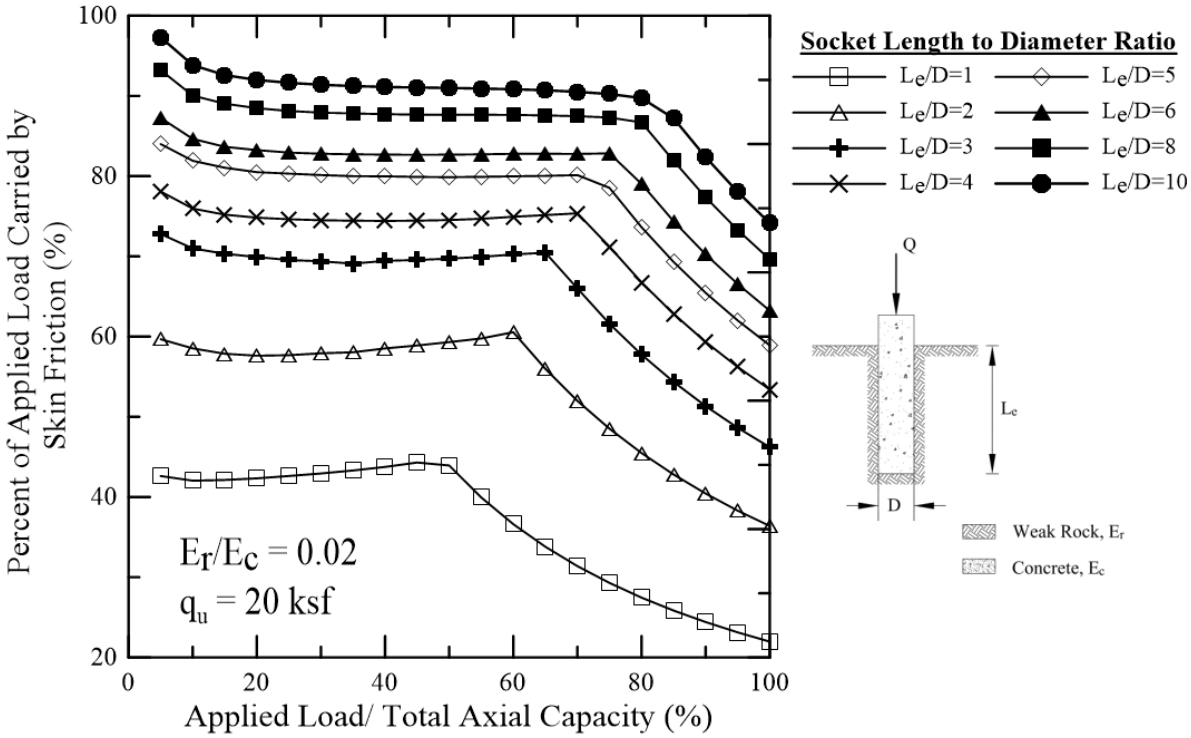

Figure 6.15. Load-transfer mechanism for weak rock-socketed drilled shafts.

In summary, these results show that tip resistance can be significantly reduced, for a given amount of serviceable displacement, when the base of the shaft is resting on soft/weathered rock or the tip is not sufficiently cleaned out prior to concrete placement. Therefore, proper inspection of the rock mass conditions beneath the tip of the shaft is necessary for the cases where tip resistance is considered to contribute in the total axial capacity of the drilled shaft. For the cases where soft/weathered rock is encountered at the base, it may be necessary to either neglect the tip resistance contribution or increase the socket length to an elevation where sound/intact rock is encountered.

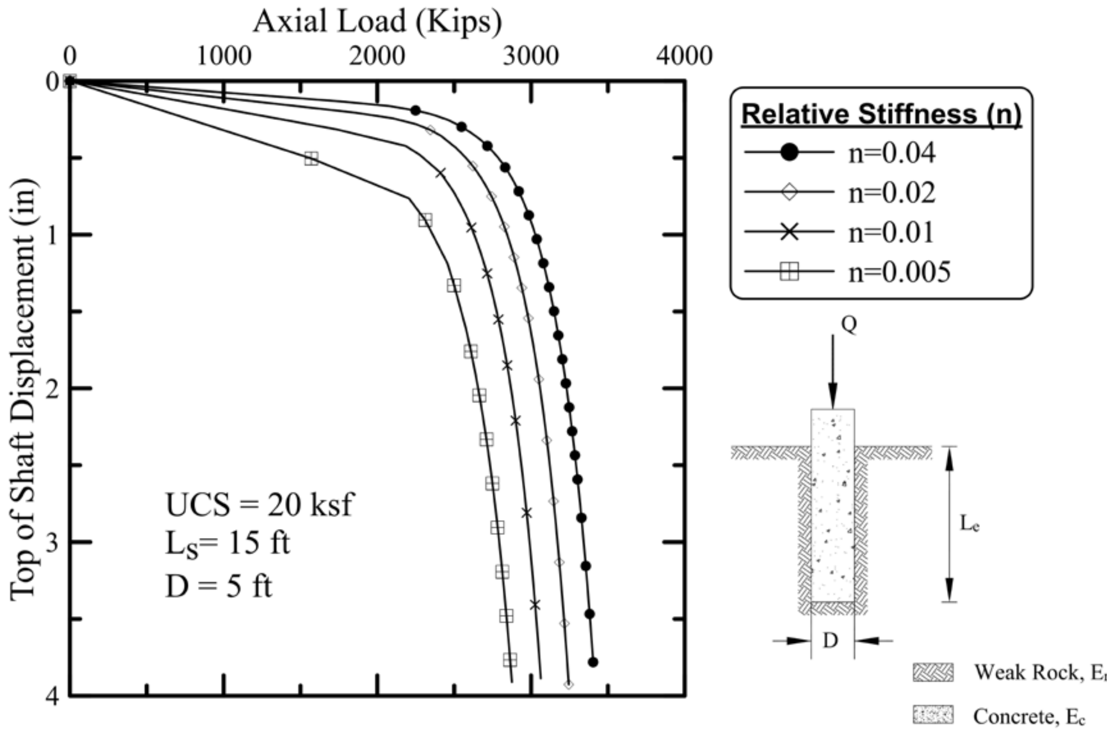

Figure 6.16. Effect of relative stiffness (n) on load-displacement response of weak rock drilled shaft sockets.

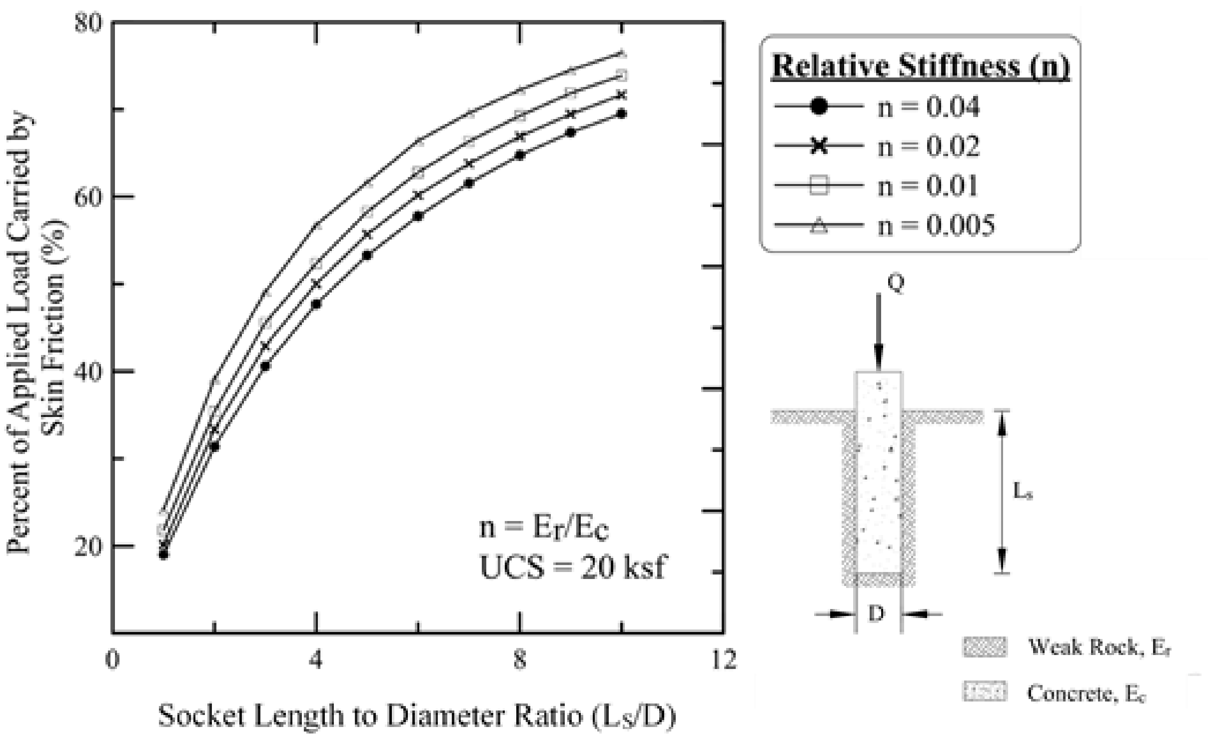

Figure 6.17. Percentage of applied load carried by skin friction for different rock socket geometries and rock stiffnesses.

6.6.3 *Effect of Socket Roughness*

The drilled shaft socket roughness also has a large influence on the mobilized side resistance (O'Neil and Reese 1999). Figure 6.18 shows the axial load-settlement response of three different socket roughness conditions, i.e., rough, normal, and smeared sockets. The interface roughness coefficients were selected based on the adhesion factors derived from the compiled load test database for unit side resistance (see Chapter 3). This analysis was also performed using a UCS of 20 ksf, a socket length of 15 ft, and socket diameter of 5 ft. Figure 6.18 indicates that the load-transfer in side resistance can be significantly improved for drilled shafts in weak rock if the rock socket or shaft walls are roughened by mechanical means, as compared to normally constructed rock sockets that exhibit smoother walls. By contrast, disintegration/smearing (i.e., formation of a soil-like material/remolded rock along the rock–socket interface) of the socket wall may compromise the unit side resistance significantly. Therefore, proper inspection of the drilled shaft side walls is needed, especially for cases where drilled shafts are constructed under bentonite slurry, which can result in formation of a bentonite layer or cake along the shaft wall.

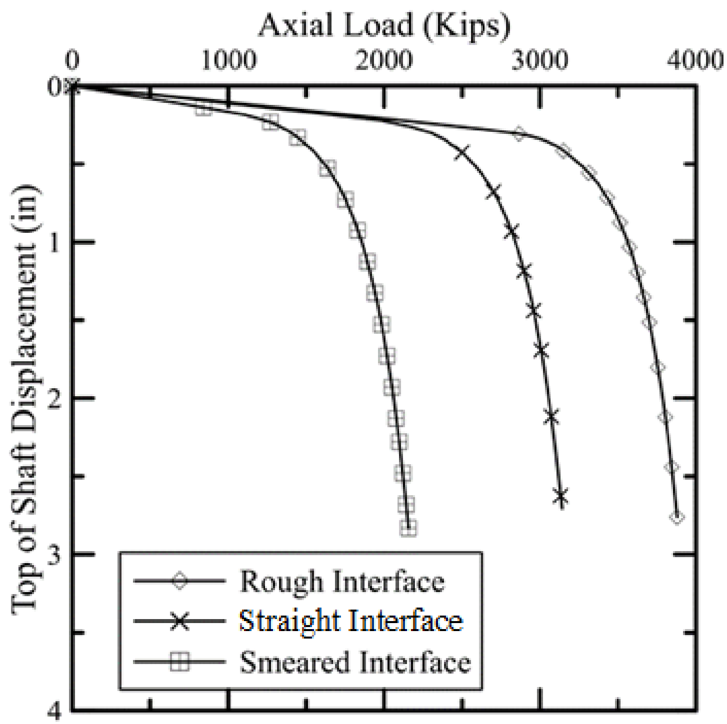

Figure 6.18. Axial load-displacement response for three different socket roughness conditions.

In summary, these results show that the axial capacity of drilled foundations is affected by the conditions at the soil/concrete interface immediately adjacent to the shaft. Artificially roughing the socket wall significantly improves the unit side resistance and thus total axial capacity at small shaft displacements. By contrast, smearing or degradation of the drilled shaft side walls can significantly reduce the drilled shaft load-carrying capacity.

6.6.4 Effect of Soil-Overburden Thickness

The effect of soil-overburden thickness on the overall load-displacement behavior was investigated next. This analysis also was performed using a UCS of 20 ksf, a socket length of 15 ft, and socket diameter of 5 ft., while changing the thickness of the soil overlying the weak rock. Figure 6.19 shows the axial load-displacement response for the different cases. Figure 6.19 indicates that the load-settlement response is not significantly affected by the overburden soil thickness because most of the load is transferred through the rock socket portion of the shaft. This conclusion is in agreement with the analysis of the drilled shaft load test database in Chapter 3:.

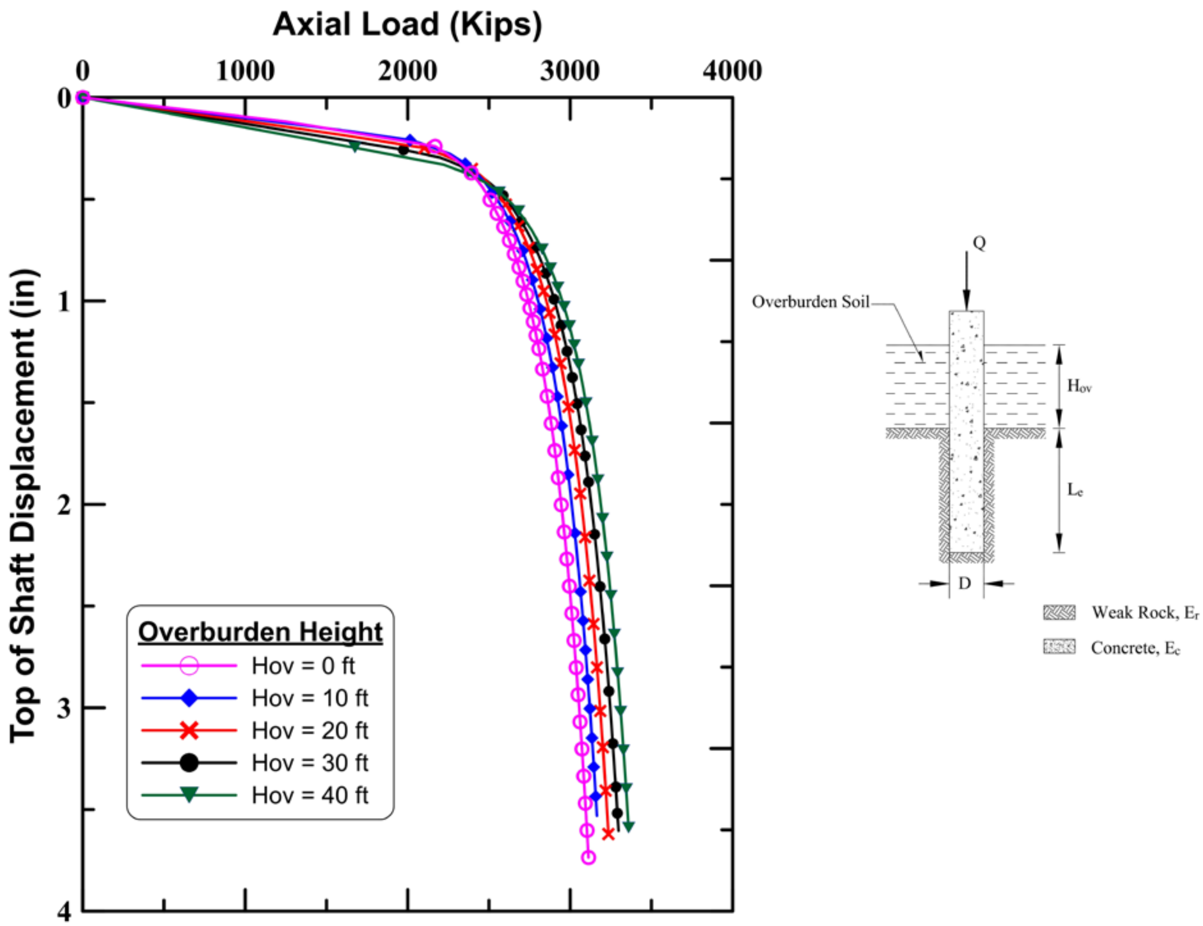

Figure 6.19. Effect of overburden height on the axial load-displacement behavior of weak rock-socketed shafts.

CHAPTER 7: ILLINOIS DESIGN METHOD FOR DRILLLED SHAFTS IN WEAK, FINE-GRAINED ROCKS

7.1 INTRODUCTION

Existing predictive methods for side and tip resistance of axially loaded drilled shafts socketed in rocks were reviewed in Phase 1 of this study and statistically evaluated, in Chapter 4: of this report, to investigate their applicability to weak, fine-grained rocks (e.g., weak shales). Drilled shafts are attractive for use in weak rock (e.g., shales); because such geomaterials are easy to excavate, drilled shafts are relatively stable, and drilled shafts provide good resistance to both axial and lateral loads. However, little attention has been given to the design of drilled shafts in weak rock. To rectify this design void, an Illinois-specific design procedure for axially loaded drilled shafts in weak, fined-grained rock was outlined in Phase 1 of this study and enhanced and verified herein (see sections below).

The enhancement and verification are based on the new load test results that include only weak, fine-grained rocks (see Chapter 3:). This chapter summarizes the new design method and the corresponding LRFD resistance factors that can be used to design drilled shaft foundations in weak Illinois shales.

7.2 PREDICTIVE METHOD FOR SIDE RESISTANCE

Undrained shear strength is the primary engineering property that controls the mobilized unit side resistance in drilled shafts socketed into weak, fine-grained rock. Analysis of the drilled shaft, full-scale load tests shows that the ultimate side resistance is not significantly affected by drilled shaft geometry (e.g., socket length and diameter) and is often fully mobilized with relatively small displacement. Analysis of the load test database also showed no significant post-peak reduction in unit side resistance with increasing shaft displacement. Review of the literature further indicates that drilled shafts in weak shales, mudstones, and claystones exhibit similar behavior in side resistance (O'Neill et al. 1996). Therefore, the proposed design method utilizes a simple first order model based solely on the unconfined compressive strength of weak, fine-grained rock to predict the unit side resistance for a drilled shaft socketed in weak, fine-grained rocks.

7.2.1 Side Resistance Predictive Method

The updated side resistance database was used to select representative and applicable load test data for developing an empirical design method for drilled shafts in weak, fine-grained rocks. Regression analyses were used to determine the line of best fit to the selected side resistance data. Figure 7.1 shows a linear function is used to correlate the measured unit side resistance and unconfined compressive strength for the design of drilled shafts in weak rocks.

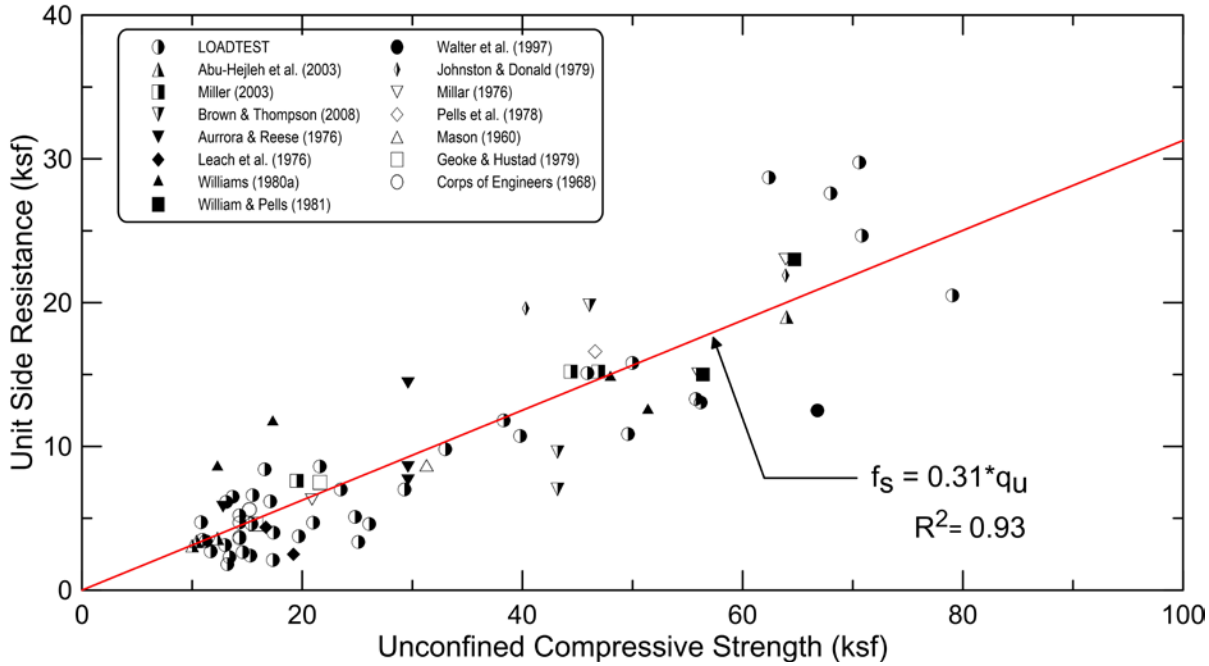

Figure 7.1. Predictive method for unit side resistance of drilled shafts in weak, fine-grained rocks.

Figure 7.1 shows that the adhesion factor did not significantly change from that proposed in Phase 1.(0.31 versus 0.30). The adhesion factor is confirmed in Phase 2 by using 34 more values of side resistance from 27 load tests in weak fine-grained rocks. As shown below, the new predictive method for side resistance, f_s, in weak Illinois shales uses an adhesion factor of 0.31 and average unconfined compressive strength, q_u, along the shaft wall:

$$f_s \text{ (ksf)} = 0.31 * q_u \leq 31 \text{ ksf} \tag{7.1}$$

where

f_s = unit side resistance of drilled shafts socketed into weak fine-grained rocks, ksf
q_u = average unconfined compressive strength of weak, fine-grained rocks along socket wall, ksf
0.31 = empirical adhesion factor, dimensionless

It is important to note that the precision of the side resistance predictive method, as reflected by the coefficient of variance, did not significantly improve (i.e. COV is approximately the same and equal to 0.43). In other words, increasing the number of load tests considered in this study confirmed the mobilized adhesion factors but did not improve the reliability of the design method.

7.3 PREDICTIVE METHOD FOR TIP RESISTANCE

Analysis of the tip resistance load test database for drilled shafts socketed into weak, fine-grained rock shows that the unit tip resistance is also a function of the unconfined compressive strength of weak rock, embedment depth in weak rock, and shaft tip displacement. The predictive method for tip resistance proposed in Phase 1 was modified herein, based on the updated load test database described in Chapter 3. The new tip resistance predictive method is also a function of the UCS of the weak rock, the embedment depth, and the shaft tip displacement.

7.3.1 Tip Resistance Predictive Method

The results of the unit tip resistance database analysis are summarized in Figure 7.2 The embedment depth of drilled shafts in weak, fine-grained rocks is normalized with the shaft diameter (see labels next to data in Figure 7.2). The line of best fit (see equation 7.2) for the load test data is shown for an embedment ratio of 2.5. Figure 7.2 shows that a bearing capacity factor (i.e., ratio between the measured unit tip resistance and unconfined compressive strength) of 4.5 can be used to predict the unit tip resistance (q_t) of shafts in weak, fine-grained rocks. This conclusion is in agreement with the common practice bearing capacity factors for drilled shafts in clays (i.e., q_t = 9*undrained shear strength (Su)).

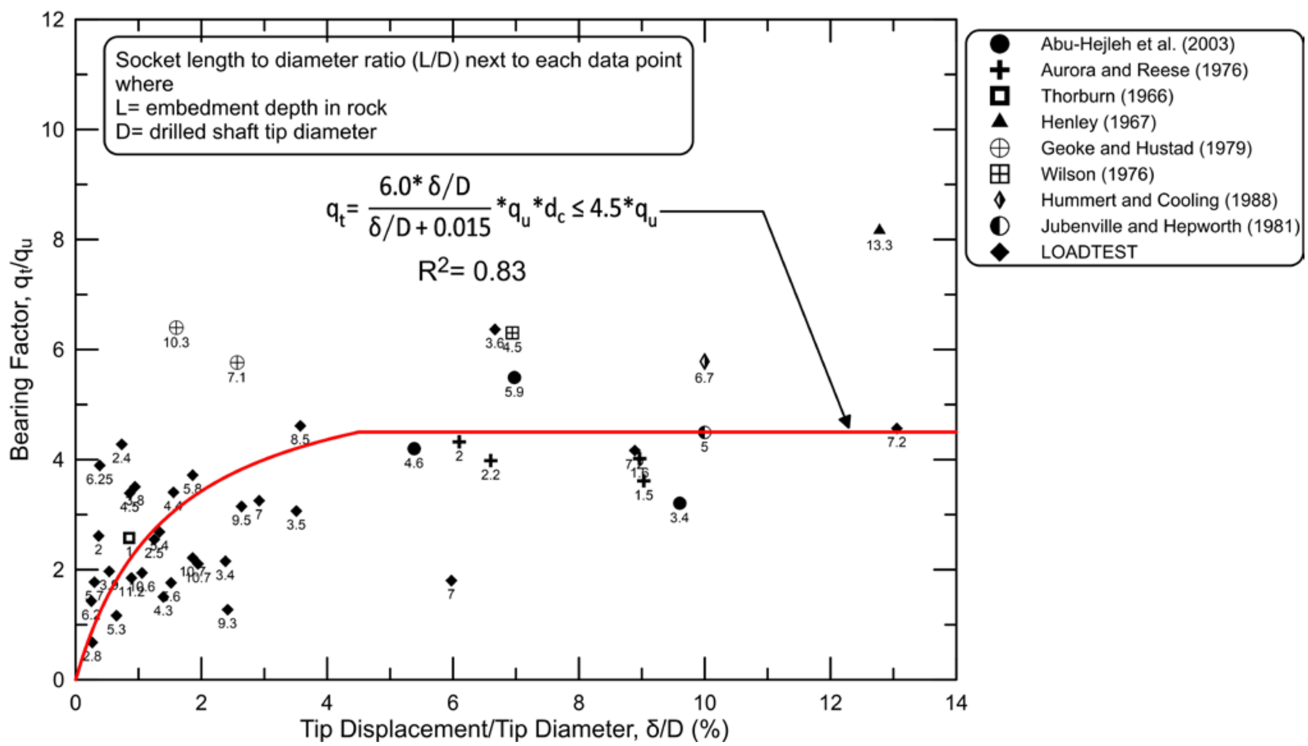

Figure 7.2. Predictive method for tip resistance of drilled shafts in weak, fine-grained rocks.

Figure 7.3 shows the effect of the embedment ratio (L/D) on the mobilized unit tip resistance for load test measurements where the maximum tip resistance was mobilized (i.e., tip displacement ≥ 3.0% of the tip diameter). Figure 7.3 suggests that the bearing capacity factor (qt/qu) increases with depth of embedment ratios less than 2.5, which agrees with the expression for the depth-correction factor proposed by Skempton (1951).

Regression analyses were used to determine the equation of best fit shown in Figure 7.2 for an embedment ratio of 2.5. The expression for the depth-correction factor proposed by Skempton (1951) was then used to back-calculate the equation for cases for which the embedment depth is zero, which is referred to as the "reference equation." The new predictive method for tip resistance in Illinois weak rocks is shown below.

$$q_t = \frac{4.0 * \delta/D}{\delta/D + 0.015} * q_u * d_c \leq 3.0 * q_u * d_c \tag{7.2}$$

where:

q_t = tip resistance, ksf
q_u = unconfined compressive strength, ksf
δ = tip movement, in.
D = tip diameter, in.
d_c = Skempton's depth-correction factor = 1.0 + 0.2 L/D ≤ 1.5
L = embedment depth in weak rock, in.

A displacement equal to 5% of the shaft diameter (O'Neil and Reese 1999) is recommended for mobilizing the ultimate tip resistance, which can be used to estimate the tip movement, δ, in the tip resistance equation above. Other serviceability-limit states (i.e., tip displacements) could be considered if a tip displacement equal to 5% of shaft diameter produces total or differential settlements that are unacceptable for the structural aspects of the design or serviceability. This can be accomplished by using a different value of δ (tip movement) in the predictive equation above.

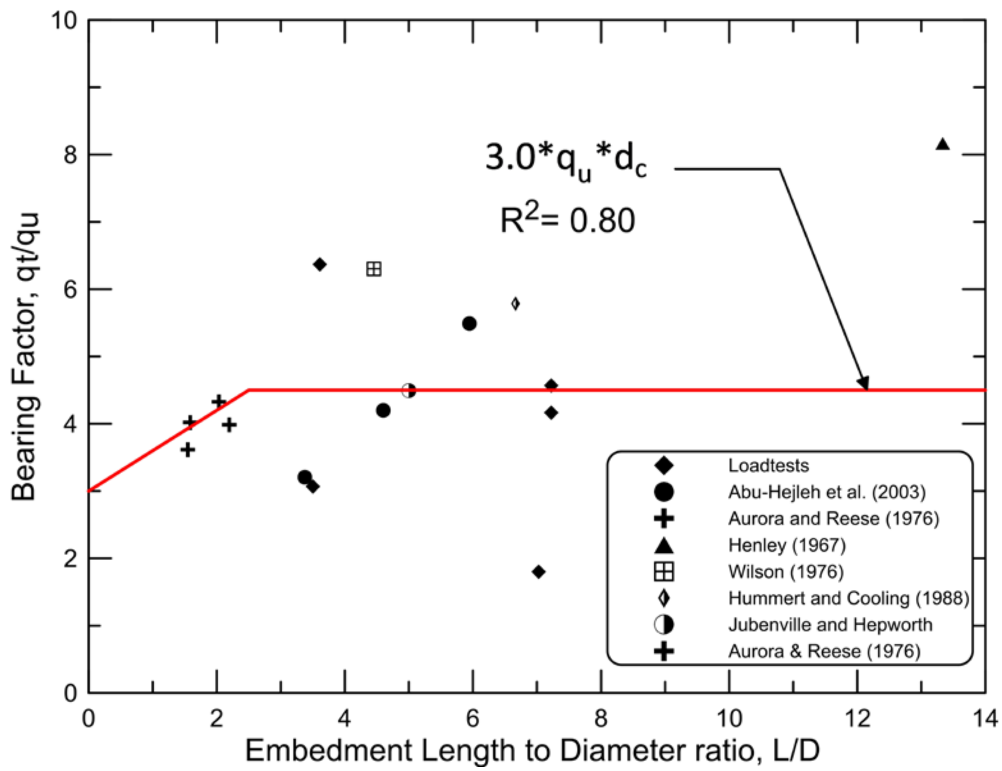

Figure 7.3. Effect of embedment ratio (L/D) on mobilized unit tip resistance of rock socketed drilled shafts.

7.4 MSPT-BASED DESIGN METHOD

An energy-based empirical correlation between normalized penetration rate $(N_{Rate})_{90}$ and unconfined compressive strength was developed herein based on the MSPT penetration rate measurements at and laboratory triaxial compression tests conducted for 21 IDOT bridge sites where weak shales were present (see Chapter 2:). This relationship can be substituted in the above drilled shaft side- and tip resistance relationships to develop an MSPT-based, drilled shaft design method. The MSPT design method proposed herein provides an economic solution for situations where the shale is highly weathered, and obtaining undisturbed/high-quality cores for laboratory testing is difficult. More importantly, it is anticipated that the MSPT-based design method will be preferred because it reduces or omits expensive and time-consuming shale-rock coring and subsequent laboratory triaxial compression testing. This will decrease the time and cost required to develop design parameters for drilled shaft design in weak Illinois shales. Furthermore, every IDOT district is equipped to measure MSPT penetration rates in weak Illinois shales, which will facilitate comparison of results and drilled shaft designs. It is anticipated future drilled shaft designs will be based, at least in part, on the proposed MSPT-based method described below:

Unit Side Resistance

$$f_s \text{ (ksf)} = 0.028*(N_{Rate})_{90} \leq 31 \text{ ksf} \tag{7.3}$$

where:

f_s = unit side resistance of drilled shafts socketed into weak, fine-grained rocks, ksf

$(N_{Rate})_{90}$ = MSPT penetration rate corrected for 90% of the theoretical energy and various field procedures.$(N_{Rate})_{90}$ is calculated based on the procedure outlined in Appendix Q

Unit Tip Resistance

$$q_t = \frac{0.368*\delta/D}{\delta/D + 0.015}*(N_{Rate})_{90}*d_c \leq 0.276*(N_{Rate})_{90}*d_c \tag{7.4}$$

where:

q_t = tip resistance, ksf

$(N_{Rate})_{90}$ = MSPT penetration rate corrected for 90% of the theoretical energy and various field procedures, bpf

δ = tip movement, in.

D = tip diameter, in.

d_c = Skempton's depth-correction factor = 1.0 + 0.2 L/D ≤ 1.5

L = embedment depth in weak rock, in.

The Limits to the unit side and tip resistance in equation 7.3 & 7.4 are set based on the measured values of these resistances in weak shales that exhibit unconfined compressive strength between 10 to 100 ksf.

7.5 NEW DESIGN PROCEDURE FOR DRILLED SHAFTS IN WEAK ROCKS

The predictive methods introduced in sections 7.2, 7.3, and 7.4 were developed for drilled shafts in weak rocks. The proposed design method for side resistance uses only the unconfined compressive strength (UCS) of the weak rock along the shaft. Tip resistance, however, is based on UCS and shaft-settlement criteria and accounts for the effect of socket length. The general Brown et al. (2010) design procedure flowchart shown in Figure 7.4 is recommended for use by IDOT with the side- and tip resistance equations presented in Equations 7.3 and 7.4 above for the design of drilled shafts in weak sedimentary rocks.

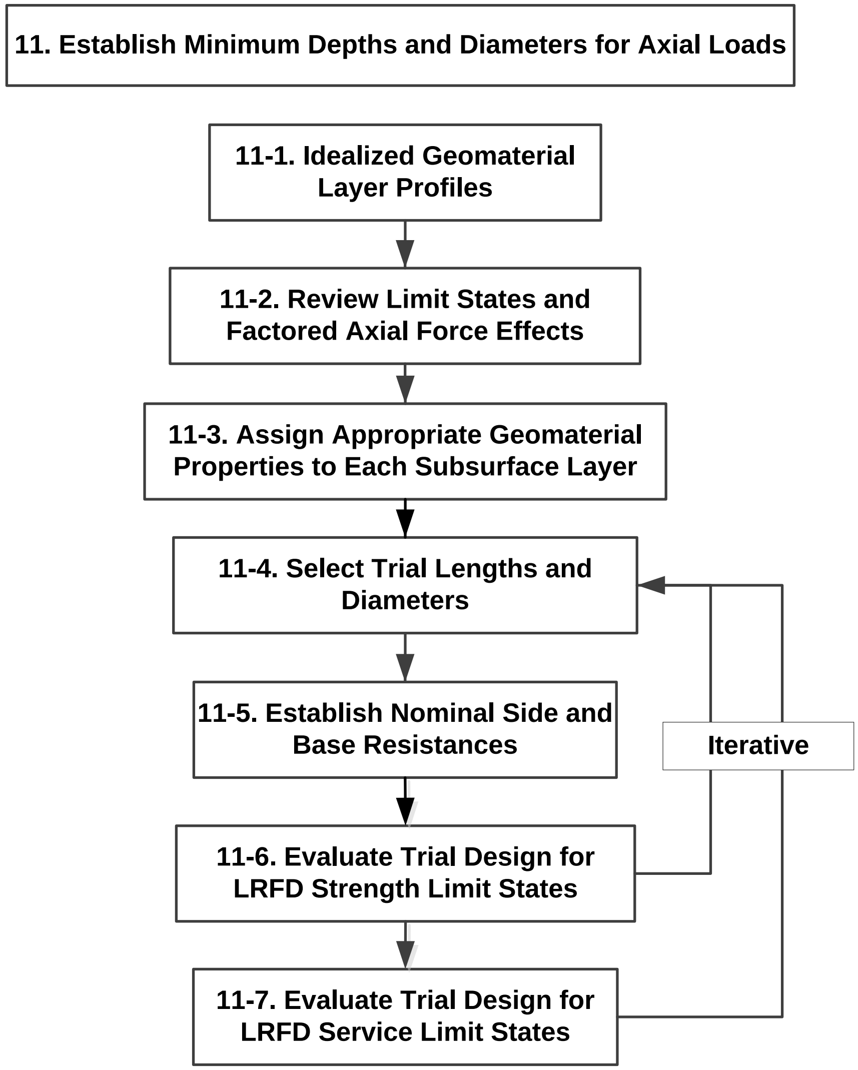

Figure 7.4. General design procedure for drilled shafts (after Brown et al. 2010).

7.6 LOAD AND RESISTANCE FACTOR DESIGN

The first order second-moment (FOSM) method as defined in NCHRP-507 (Paikowsky et al. 2004) with the modification proposed by Bloomquist et al. (2007) is used herein to calculate the load-resistance factor for the design method developed in this study. The modified FOSM approach was also checked against the first order reliability method (FORM) and both approaches yielded approximately the same resistance factors. Tables R1 and R2 provide information of the load tests considered in the resistance factor calculations. The modified FOSM formula used herein to determine the resistance factor (ϕ)

$$\varphi \geq \frac{\lambda_R \cdot \left(\gamma_D \cdot \frac{Q_D}{Q_L} + \gamma_L\right) \sqrt{\frac{\frac{\frac{Q_D{}^2}{Q_L{}^2} \cdot \lambda_{Q_D}{}^2 . COV_{Q_D}^2 + \lambda_{Q_L}{}^2 \cdot COV_{Q_L}^2}{\frac{Q_D{}^2}{Q_L{}^2} \cdot \lambda_{Q_D}{}^2 + 2\frac{Q_D}{Q_L} \cdot \lambda_{Q_D} \cdot \lambda_{Q_L} + \lambda_{Q_L}{}^2}}{\left(1+COV_R^2\right)}}}{\left(\lambda_{Q_D} \cdot \frac{Q_D}{Q_L} + \lambda_{Q_L}\right) exp\left\{\beta_t \sqrt{ln\left[\left(1+COV_R^2\right)\right]\left(\frac{\frac{Q_D{}^2}{Q_L{}^2} \cdot \lambda_{Q_D}{}^2 . COV_{Q_D}^2 + \lambda_{Q_L}{}^2 \cdot COV_{Q_L}^2}{\frac{Q_D{}^2}{Q_L{}^2} \cdot \lambda_{Q_D}{}^2 + 2\frac{Q_D}{Q_L} \cdot \lambda_{Q_D} \cdot \lambda_{Q_L} + \lambda_{Q_L}{}^2}\right)}\right\}} \tag{7.5}$$

where

λ_R = bias factor (mean value of the measured to predicted resistance (R_m/R_p) (calculated based on the analysis of the load test database)

COV_{Q_D} = coefficient of variation for dead load (0.1)

COV_{Q_L} = coefficient of variation for live load (0.2)

COV_R = coefficient of variation for resistance (calculated based on the analysis of the load test database)

β_T = target reliability index (3.0)

γ_D = load factor for dead loads (1.25)

γ_L = load factor for live loads (1.75)

Q_D/ Q_L = ratio of dead load to live load (2.0)

λ_{Q_D} = bias factor for dead load (1.05)

λ_{Q_L} = bias factor for live load (1.15)The resistance factor allows geotechnical engineers to adopt load and resistance factor design to be consistent with structural design of the bridge superstructure (Brown et al. 2010). The FOSM method requires quantifying the inherent uncertainty of the loads and resistances with a bias and coefficient of variance (COV), as well as the target reliability.

Statistical analyses were performed on two sets of drilled shaft load test data to quantify the COV and bias of the new predictive method proposed herein. *Bias* is defined as the average ratio of measured to predicted capacity and reflects how well the predicted capacity agrees with the measured one on average. Alternatively, the COV reflects the consistency of the method to predict the measured axial capacity (Long and Anderson 2012). The first set of data includes 14 load test cases where total resistance (i.e., combined side and tip resistance) is reported. The second data set includes separate measurements for side and tip resistance for 90 load tests. Analysis of these two data sets yielded a resistance factor of 0.55, which is a little higher than the 0.5 that is recommended in FHWA-NHI-10-016 for cohesive IGMs (e.g., weak shales). Because the resistance factor calculations performed herein are based on a limited number of load tests, it is recommended that a resistance factor of 0.5 be used for drilled shaft design in weak, fine-grained rocks and also to be consistent with FHWA-NHI-10-016 recommendations. This resistance factor should be applied to the total axial resistance or capacity of the drilled shaft. The resulting equation to estimate the design factored resistance of axial loaded drilled shafts is given by the following expression:

$$Q_{design} = \varphi * (f_s * P_{socket} * L_{socket} + q_t * A_{tip}) \tag{7.6}$$

where:

Q_{design} = design factored resistance, kips

φ = LRFD resistance factor = 0.50

f_s = unit side resistance, ksf

P_{socket} = rock socket perimeter, ft

L_{socket} = rock socket length, ft

q_t = unit tip resistance, ksf

A_{tip} = rock socket tip area, ft^2

7.7 SUMMARY

The predictive methods for side and tip resistances proposed in Phase 1 were revised to reflect the additional load test compiled in Phase 2 and described in Chapter 2:. The side resistance predictive method is a function of only the unconfined compressive strength of weak rock, which is similar to existing methods. Conversely, the tip resistance method is a function of unconfined compressive strength, tip displacement, and socket length. The drilled shaft design flowchart presented by Brown et al. (2010) is recommended for IDOT designs, with the modifications of sections 7.2 to 7.6 of this report for the design of drilled shafts in weak, fine-grained rocks.

CHAPTER 8: SUMMARY AND CONCLUSIONS

8.1 INTRODUCTION

The research project ICT R27-145, Modified Standard Penetration Test–based Drilled Shaft Design Method for Weak Rocks (Phase 2 study), investigated (1) load-transfer mechanisms of drilled shafts that are fully or partially embedded in weak, fine-grained rocks (e.g., weak shales) encountered in the state of Illinois; and (2) the accuracy of the method for characterizing weak shales and the design procedure developed during Phase 1 of this study (ICT- R27-99). The new design procedure developed in Phase 2 improves safety and reduces IDOT's deep-foundation costs for future bridge structures by reducing investigation and testing costs and providing a less conservative design.

The main objectives of this study were to: (1) improve the Modified Standard Penetration Test (MSPT) method developed during Phase 1 of this study; (2) improve the reliability of the empirical correlation between the unconfined compressive strength and MSPT penetration rate; (3) drill and test at 16 additional IDOT bridge sites and by including the influence of SPT hammer energy on the measured MSPT penetration rate; (4) conduct two full-scale, drilled shaft load tests to investigate the load-transfer mechanism in weak, fine-grained rocks and to evaluate the proposed predictive methods; (5) improve and verify Phase 1 drilled shaft side- and tip resistance predictive methods by including more drilled shaft load tests; (6) develop appropriate reliability-based resistance factors for drilled shaft design using the load and resistance factors design (LRFD) framework; (7) develop and calibrate a numerical model using the load test results to study the load-transfer mechanism of weak, fine-grained, socketed drilled shafts; and (8) conduct a parametric study to investigate the main factors controlling drilled shaft design. The major findings from this project are summarized below.

8.2 FIELD EXPLORATION AND LABORATORY TESTING

Field exploration was conducted at 16 additional IDOT bridge sites where weak shales are present. The main objectives of this exploration were to refine, augment, and verify the relationship proposed in Phase 1 of this study of MSPT penetration rate versus unconfined compressive strength of weak shales and to investigate the strength and compressibility properties of weak shale in Illinois. The following is a summary of the major findings of Phase 2:

- Undrained Young's modulus can be correlated with the in situ moisture content and the unconfined compressive strength of weak shales. This correlation can be used for estimating the modulus of shales for preliminary settlement analysis of bridge piers when site-specific data are not available or to evaluate site-specific data and laboratory testing.
- SPT hammer energy measurements for all IDOT drill rigs used in MSPT penetration rate measurements used herein imparted an average energy of 90% of the theoretical maximum hammer energy. A normalized penetration rate, $(N_{Rate})_{90}$, was

developed herein to improve the reliability of the proposed correlation between unconfined compressive strength and MSPT penetration rate.

- An energy-based correlation between unconfined compressive strength and normalized MSPT penetration rate was developed for Illinois weak shales, i.e., UCS (ksf) = 0.092 * $(N_{rate})_{90}$. This correlation can be used with the MSPT penetration rate for drilled shaft design, especially when obtaining high-quality shale samples for triaxial compression testing is difficult or impossible. The use of MSPT penetration rates for drilled shaft design should reduce the design time and costs by reducing or eliminating shale coring and laboratory triaxial compression testing.

8.3 IMPROVEMENTS OF ILLINOIS DRILLED SHAFT DESIGN PROCEDURE

Additional drilled shaft load test data were located in the literature and incorporated in the Phase 1 database to refine and verify the proposed side- and tip resistance design methods. This updated load test database was used for more detailed statistical analyses and development of a reliability-based load-resistance factor (LRFD) for the drilled shaft design method for weak clay-based rock developed herein. This larger database allowed identification of outlier data points in the original database. This increased the efficiency of the design correlations, reduced uncertainty in the design procedure, and was used to justify larger resistance factors for side and tip resistance developed herein.

8.3.1 Unit Side Resistance

Findings related to drilled shaft unit side resistance include the following:

- This study recommends a linear function to predict unit side resistance in weak shales—instead of the power functions commonly used to correlate rock undrained compressive strength to measured unit side resistance in a drilled shaft load test. The linear equation recommended for drilled shaft design in Illinois shales is

$$f_s(\text{ksf}) = 0.31 * q_u \leq 31 \text{ ksf}$$

- Side resistance does not change significantly with changes in shaft diameter.
- After ultimate unit side resistance is mobilized, additional drilled shaft displacement along the drilled shaft/weak rock interface does not decrease unit side resistance.

8.3.2 Unit Tip Resistance

Findings related to drilled shaft unit tip resistance include the following:

- Available predictive methods (with the exception of the methods of Abu-Hejleh et al. [2003], Abu-Hejleh and Attwooll [2005], and the *Canadian Foundation Engineering Manual,* [Canadian Geotechnical Society 2006]) correlate only the measured tip resistance in load tests to the unconfined compressive strength of weak rock.

- Analysis of load test data assembled herein indicates that mobilized tip resistance is governed not only by the undrained compressive strength of weak rock but also by drilled shaft tip movement during loading and depth of embedment of the drilled shaft in the weak rock, i.e., rock socket. Therefore, predictive methods for tip resistance should account for all of these factors, not just unconfined compressive strength.
- The load test database developed herein was used to develop a tip-capacity design method that can account for these factors. The new method uses settlement and strength criteria to predict unit tip resistance, and the recommended equation for drilled shaft tip resistance in Illinois shales is

$$q_t = \frac{4.0 * \delta/D}{\delta/D + 0.015} * q_u * d_c \leq 3.0 * q_u * d_c$$

8.4 NEW DRILLED SHAFT DESIGN PROCEDURE

New predictive methods for unit side resistance and tip resistance are presented in section 8.3 and described in detail in Chapter 7. The unit side resistance predictive method is a function of only unconfined compressive strength, while unit tip resistance is a function of unconfined compressive strength, embedment depth, and tip displacement under applied loads. The drilled shaft design flowchart proposed by Brown et al. (2010) is recommended with the use of the side and resistance equations presented in Section 8.3, for the design of drilled shafts in weak sedimentary rocks (e.g., weak shales in Illinois). Recommendations in Chapter 2 are also anticipated to be used for determining the strength and compressibility parameters.

REFERENCES

AASHTO. 2006. *LRFD highway bridge design specification*, 3rd edition. American Association of State Highway and Transportation Officials, Washington, DC. 420 pp.

Abu-Hejleh, N., and W. J. Attwooll. 2005. *Colorado's Axial Load Tests on Drilled Shafts Socketed in Weak Rocks: Synthesis and Future Needs.* Final Contract Report No. CDOT-DTD-R-2005-4. Colorado Department of Transportation, Denver, CO. 178 pp.

Abu-Hejleh, N., M. W. O'Neil, D. Hanneman, and W. J. Attwooll. 2003. *Improvement of the Geotechnical Axial Design Methodology for Colorado's Drilled Shafts Socketed in Weak Rocks*. Final Contract Report No. CDOT-DTD-R-2003-6. Colorado Department of Transportation, Denver, CO. 199 pp.

ARGEMA (Association de recherché en geotechnique marine). 1992. *Design guides for offshore structures: offshore pile design*. P. L. Tirant, ed. Paris, France: Editions Technip.

ASTM Standard D1143. 2013. *Standard Test Methods for Deep Foundations Under Static Axial Compressive Load.* ASTM International, West Conshohocken, PA.

ASTM Standard D1586-11. 2008. *Standard test method for standard penetration test (SPT) and split-barrel sampling of soils.* ASTM International, West Conshohocken, PA.

ASTM Standard D2166. 2007. *Standard test method for unconfined compressive strength of cohesive soils.* ASTM International, West Conshohocken, PA.

ASTM Standard D2216. 2010. *Standard test method for laboratory determination of water (moisture) content of soil and rock by mass.* ASTM International, West Conshohocken, PA.

ASTM Standard D6032. 2006. *Standard test method for determining rock quality designation of rock core.* ASTM International, West Conshohocken, PA.

ASTM Standard D7012. 2010. *Standard test method for compressive strength and elastic moduli of intact rock core specimens under varying states of stress and temperatures.* ASTM International, West Conshohocken, PA.

Aurora, R. P., and L. C. Reese. 1976. *Behavior of Axially Loaded Drilled Shafts in Clay–Shales.* Final Contract Report No. CFHR 3-5-72-176-4. Center for Highway Research, The University of Texas at Austin, Austin, TX. 184 pp.

Bloomquist, D., M. McVay, and Z. Hu. 2007. *Updating Florida Department of Transportation's (FDOT) Pile/Shaft Design Procedures Based on CPT & DTP Data.* BD-545, RPWO #43, UF Project #00005780. Florida Department of Transportation.

Brinkgreve, R. B. J. 2016. *PLAXIS 2D Manual.* Delft, The Netherlands.

Brown, D. A., and R. Thompson. 1994. *Drilled shaft foundation testing and design recommendation: I 65 over Mulberry of the Warrier River.* The State of Alabama Highway Department, Montgomery, Alabama. 67 pp.

Brown, D. A., J. P. Turner, and R. J. Castelli. 2010. *Drilled Shafts: Construction Procedure and*

LRFD Design Methods. Final Contract Report No. FHWA-NHI-10-016. Federal Highway Administration, Washington, DC. 970 pp.

Canadian Geotechnical Society. 2006. *Canadian Foundation Engineering Manual.* Friesens Corporation, Altona, MB. 488 pp.

Carter, J. P., and F. H. Kulhawy. 1988. *Analysis and design of drilled shaft foundations socketed into rock*. Final Contract Report No. EL-5918. Electric Power Research Institute, Palo Alto, CA. 190 pp.

Coates, D. F. 1967. *Rock Mechanics Principle.* Department of Energy, Mines, and Resources, Canada. 410 pp.

Corps of Engineers. 1968. *Investigations for Building Foundations in Expansive Clays*, vol. 1. US Army Engineer District, Fort Worth, TX.

Deere, D. U., and D. W. Deere. 1988. "The Rock Quality Designation (RQD) Index in Practice," pp. 91–101. In *Rock Classification Systems for Engineering Purposes*. ASTM STP 984. L. Kirkaldie, ed. American Society for Testing and Materials, Philadelphia, PA.

Duncan, J. M., and C.-Y. Chang. 1970. "Nonlinear analysis of stress and strain in soils." *Journal of the Soil Mechanics and Foundations Division* 96(5):1629–1653.

Geoke, P. M., and P. A. Hustad. 1979. "Instrumented Drilled Shafts in Clay–shale," pp. 149–164. In *Proceedings of Symposium on Deep Foundations*. E. M. Fuller, ed. ASCE National Convention, Atlanta.

Goodman, R.E., R. L. Taylor, and T. L. Brekke. 1968. "A model for the mechanics of jointed rock." *Journal of the Soil Mechanics and Foundation Division,* ASCE, 94(SM 3):637–659.

Gupton, C., and T. Logan. 1984. "Design guidelines for drilled shafts in weak rocks of south Florida." Proceedings of the South Florida Annual ASCE Meeting. ASCE.

Hassan, K. M., M. W. O'Neil, S. A. Sheikh, and C. D. Ealy. 1997. "Design Method for Drilled Shafts in Soft Argillaceous Rocks." *Journal of Geotechnical and Geoenvironmental Engineering* 123(3):272–280.

Hassan, K. M., and M. W. O'Neill. 1997. "Side Load-Transfer Mechanisms in Drilled Shafts in Soft Argillaceous Rock." *Journal of Geotechnical and Environmental Engineering,* ASCE, 123(2):145–152.

Henley, A. D. 1967. "Investigation of Side Shear Stress Transfer for Drilled In Foundation Shafts in Weak Rock," pp. 141–156. In *Proceedings of the Fifth Annual Symposium on Engineering Geology and Soils Engineering,* Pocatello, Idaho, April 1967.

Horvath, R. G., and T. C. Kenney. 1979. "Shaft resistance of rock socketed drilled piers," Proceedings of a Symposium on Deep Foundations, ASCE National Convention, Atlanta, Ga., Oct. 25, 1979, pp. 182-214.

Hummert, J. B., and T. L. Cooling. 1988. "Drilled pier test, Fort Collins, Colorado," pp. 1375–1382. In *Proceedings of the 2nd International on Case Histories in Geotechnical Engineering.* S. Prakash, ed.

Illinois State Geological Survey. 1996. *Bedrock Geology of Illinois.* Geologic Units: ISGS GIS Database GISDB_BEDGEO.IL_Geologic_Units_500K_1967_Py. Illinois State Geological Survey, Champaign, Illinois.

Johnston, I. W., and I. B. Donald. 1979. *Rock socket pile tests.* Final Contract Report No. 78/6/G, 703 Flinders Street–Spencer Street Overpass. Melbourne underground rail loop project, Monash University, Melbourne, Australia.

Jubenville, M. D., and R. C. Hepworth. 1981. "Drilled pier foundations in shale—Denver, Colorado, area," Drilled Piers and Caissons, Proceeding Session at the ASCE National Convention, St. Louis, Missouri. pp. 66–81.

Kulhawy, F. H., and K. K. Phoon. 1993. "Drilled shaft side resistance in clay soil to rock." In *Design and Performance of Deep Foundations: Piles and Piers in Soil and Soft Rock*. P. P. Nelson, T. D. Smith, and E. C. Clukey, eds. New York, October 24 to 28, 1993.

Kulhawy, F. H., W. A. Prakoso, and S. O. Akbas. 2005. "Evaluation of Capacity of Rock Foundation Sockets." G. Chen, S. Huang, W. Zhou, and J. Tinucci, eds. 40th U.S. Symposium on Rock Mechanics, Anchorage, Alaska, June 2005.

Leach, B. A., J. W. Medland, and H. B. Sutherland. 1976. "The ultimate bearing capacity of bored piles in weathered Keuper marl," vol. 3, pp. 507–514. 6th European Conference on Soil Mechanics and Foundation Engineering, Vienna.

Long, J. H., and A. C. Anderson. 2012. *Improved Design for Driven Piles on a Pile Load Test Program in Illinois.* Research Report FHWA-ICT-12-011, Project R27-069. Rantoul, Illinois: Illinois Center for Transportation.

Mason, R. C. 1960. "Transmission of high loads to primary foundations by large diameter shafts." Paper to the ASCE Convention, New Orleans.

Matich, M. A. J., and P. Kozicki. 1967. "Some load tests on drilled cast-in-place concrete caissons." *Canadian Geotechnical Journal* 4(4):367–375.

Meigh, A. C., and W. Wolski. 1979. "Design parameters for weak rock," pp. 59–79. 7th European Conference on Soil Mechanics and Foundation Engineering, Brighton.

Mesri, G., and R. Gibala. 1972. "Engineering Properties of Pennsylvanian Shale," pp. 59–79. E. J. Cording, ed. Thirteenth Symposium on Rock Mechanics, Illinois, August 30 to September 1, 1972.

Millar, W. R. 1976. Results of pile tests on city centre and telephone exchange sites Perth

Miller, A. D. 2003. *Prediction of Ultimate Side Shear for Drilled Shafts in Missouri Shales.* MS thesis, University of Missouri–Columbia, Missouri, MO. 393 pp.

O'Neil, M. W., and L. C. Reese. 1999. *Drilled Shafts: Construction Procedures and Design Methods*. Final Contract Report No. FHWA-IF-99-025. Federal Highway Administration, Washington, DC. 758 pp.

O'Neil, M. W., F. C. Townsend, K. H. Hassan, A. Buller, and P. S. Chan. 1996. *Load-Transfer for Drilled Shafts in Intermediate Geomaterials.* FHWA Publication No. FHWA-RD-9-172.

Department of Transportation, Federal Highway Administration, McLean, VA. 790 pp.

Paikowsky, S. G., Birgisson B., Ayyub B., Baecher G., Chernauskas L., Kuo C., McVay M.,Nguyen T., O'Malley K., O'Neill M. Stenersen K. 2004. *Load and Resistance Factor Design (LRFD) for Deep Foundations.* NCHRP Report 507. Transportation Research Board, Washington, DC.

Peck, R.B., Hanson, W.E., and Thornburn, T.H., (1974), "Foundation Engineering", John Wiley & Sons, 514 pp.

Pells, P. J. N., D. J. Douglas, B. Rodway, C. Thorne, and B. K. McMahon. 1978. *Design loading for foundations on shales and sandstone in the Sydney region.* Research Report No. R 315. The University of Sydney, Sydney.

Pells, P. J. N., and Turner R.M. Elastic Solution for the Design and Analysis of Rock – Socketed Piles, Canadian Geotechnical Journal, Vol. 1, 16, 1979, pp. 481 – 487.

Potts, D.M.,., and L. Zdravkovic. 2001 *Finite element analysis in geotechnical engineering: Application. London, Thomas Telford*

Reynolds, R. T., and T. J. Kaderbeck. 1980. "Miami limestone foundation design and construction." *Journal of the Geotechnical Engineering Division* 107(GT7):859–872.

Rosenberg, P., and N. L. Journeaux. 1976. "Friction and end bearing tests on bedrock for high capacity socket design." *Canadian Geotechnical Journal* 13(3):324–333.

Rowe, R. K., and H. H. Armitage. 1984. *Design of piles socketed into weak rocks.* GEOT-11-84. London: University of Western Ontario.

Rowe, R. K., and H. H. Armitage. 1987. "A design method for drilled piers in soft rock." *Canadian Geotechnical Journal* 24(1):126–142.

Schanz, T., P. A. Vermeer, and P. G. Bonnier. 1998. "The Hardening-Soil model: Formulation and verification," pp. 281–290. In *Beyond 2000 in Computational Geotechnics,* R. B. J. Brinkgreve, ed. Rotterdam: Balkema, 1998.

Skempton, A. W. (1951): 'The bearing capacity of clays', Building research congress, London, 1, pp. 180-189.

Stark, T. D., J. H. Long, and P. Assem. 2013. *Improvement for determining the axial capacity of drilled shafts in shale in Illinois.* Research Report No. FHWA-ICT-13-017. Illinois Center of Transportation, Springfield, IL. 136 pp.

Stroud, M.A. 1974. "The Standard Penetration Test in Insensitive Clays and Soft Rocks," pp. 367–375. European Symposium on Penetration Testing, Stockholm.

Teng, W. C. 1962. *Foundation Design.* Englewood Cliffs, NJ: Prentice-Hall.

Thorburn, S. 1966. "Large Diameter Piles Founded in Bedrock," Symposium on Large Bored Piles,. Institution of Civil Engineers., London, pp 95-103.

Toh, C. T., T. A. Ooi, H. K. Chiu, S. K. Chee, and W. H. Ting. 1989. "Design parameters for bored piles in a weathered sedimentary formation," pp. 1073–1078. 12th International

Conference on Soil Mechanics and Foundation Engineering, Rio De Janeiro, August 13 to 18, 1989.

Van Doren, L. M., S. G. Hazard, J. R. Stallings, and D. P. Schnacke. 1967. *Drilled Shaft Foundation Test Program.* Final Contract No. 35W-87-I-35W-1(58)48. State Highway Commission of Kansas. Van Doren-Hazard-Stallings-Schnacke Engineers-Architects, Topeka, KS.

Vijayvergiya, V. N., W. R. Hudson, and L. C. Reese. 1969. *Load Distribution of a Drilled Shaft in Clay Shale.* Final Contract No. 89-5. Center for Highway Research, The University of Texas at Austin, Austin, TX.

Vu, T. 2013. *Load and resistance factor design of drilled shafts at the service limit state*. PhD dissertation, University of Missouri. 382 pp.

Walter, D. J., W. J. Burwash, and R. A. Montgomry. 1997. "Design of large-diameter drilled shafts for the Northumberland Strait bridge project." *Canadian Geotechnical Journal* 34(4):580–787.

Williams, A. F. 1980a. *The design and performance of piles socketed into weak rock.* PhD dissertation, Monash University, Melbourne, Australia.

Williams, A. F., and P. J. N. Pells. 1981. "Side resistance of rock sockets in sandstone, mudstone, and shale." *Canadian Geotechnical Journal* 18(4):502–513.

Williams, A. F., I. W. Johnston, and I. B. Donald. 1980. "Design of socketed piles in weak rock," pp. 327–347. P. J. N. Pells, ed. The International Conference on Structural Foundations on Rock, Sydney, May 7 to 9, 1980. Willman, H. B., J. A. Simon, K. E. Clegg, D. H. Swann, E. Atherton, C. Collinson, J. A. Lineback, and T. C. Buschbach. 1967. *Geologic Map of Illinois.* Illinois State Geological Survey Map Series.

Wilson, L. C. 1976. "Tests of bored piles and driven piles in cretaceous mudstone at Port Elizabeth, South Africa." *Geotechnique* 26(1):5–12.

Zhang, L., and H. H. Einstein 1998. "End Bearing Capacity of Drilled Shafts in Rock." *Journal of Geotechnical and Geoenvironmental Engineering* 124(7)574–584.

APPENDIX A FIELD EXPLORATION AT CH-9 OVER I-74

A.1 BACKGROUND

Figure A.1 shows the proposed location of CH-9 over I-74 bridge site, located in Knox County, just north of Knoxville, Illinois. This three-span bridge structure is designed to carry two-lane highway over the I-74. North and South abutments of this bridge are supported on driven H-piles foundations. Piers 1 and 2, are supported by shallow foundations resting on the shallow weak shales. The weak shales near the north abutment was investigated during this study.

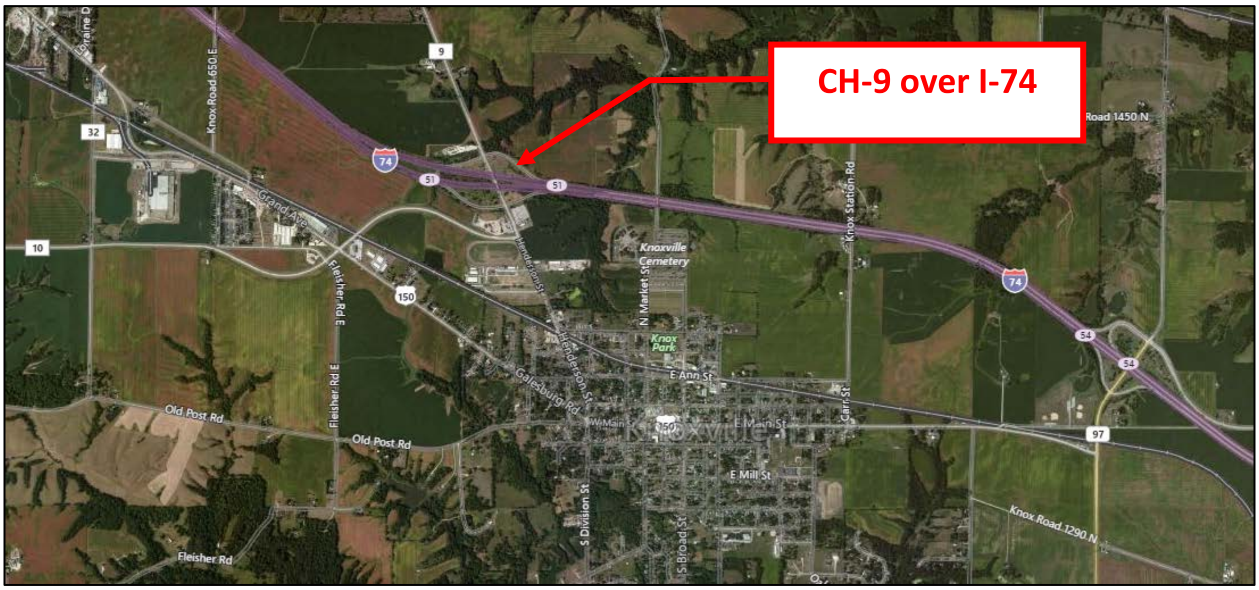

Figure A.1: Location of CH-9 over I-74 bridge near city of Knoxville.

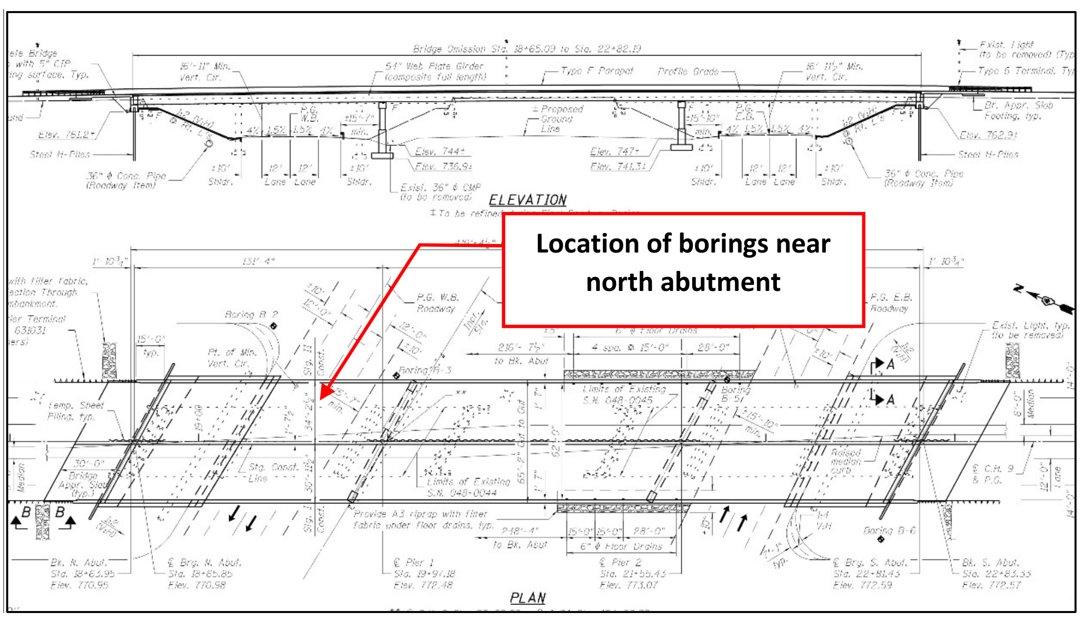

Figure A.2: Location of boring holes at CH-9 over I-74.

Figure A.2 shows a plan view of CH-9 over the I-74 bridge structure and the location of the borings drilled on March 20, 2014 by Bulldog Engineering crew and the UIUC research team. Two borings were advanced near the north abutment. These borings were drilled to the elevation of 710.0 feet.

One of the two borings drilled for each pier was used to obtain shale core. Initially rock cores were used for determination of recovery ratio, RQD of the rock mass, and vertical spacing of joints. Afterwards unconfined compression tests were conducted on the retrieved shale specimens. The in situ water content of the shale specimens used in the triaxial compression tests was also measured for correlation purposes. Triaxial test results were also used to determine the deformability characteristics of shale under undrained loading conditions.

The second boring was used to obtain MSPT blow counts at various depths. This data was used to develop a new correlation between undrained compressive strength of weak shale in Illinois and MSPT penetration rate.

The following sections discuss geology of the bridge site, MSPT test results, and laboratory test results.

A.2 SITE GEOLOGY

The geology at the bridge site consists of 10 feet of soft to stiff silty clay overlying sedimentary bedrock, e.g., shale and sandstone. The ground surface elevation at the north abutment is about 748.0 Weathered gray clay shale was exposed at an elevation of about 738 feet. Sandstone layer was exposed at elevation of 710.0 feet where the drilling was terminated. Laboratory test results are summarized in Table A.1.

A.3 MODIFIED STANDARD PENETRATION TEST RESULTS

Figure A.3 shows the Modified Standard Penetration Test results obtained in one of the two borings at CH-9 over I-74.

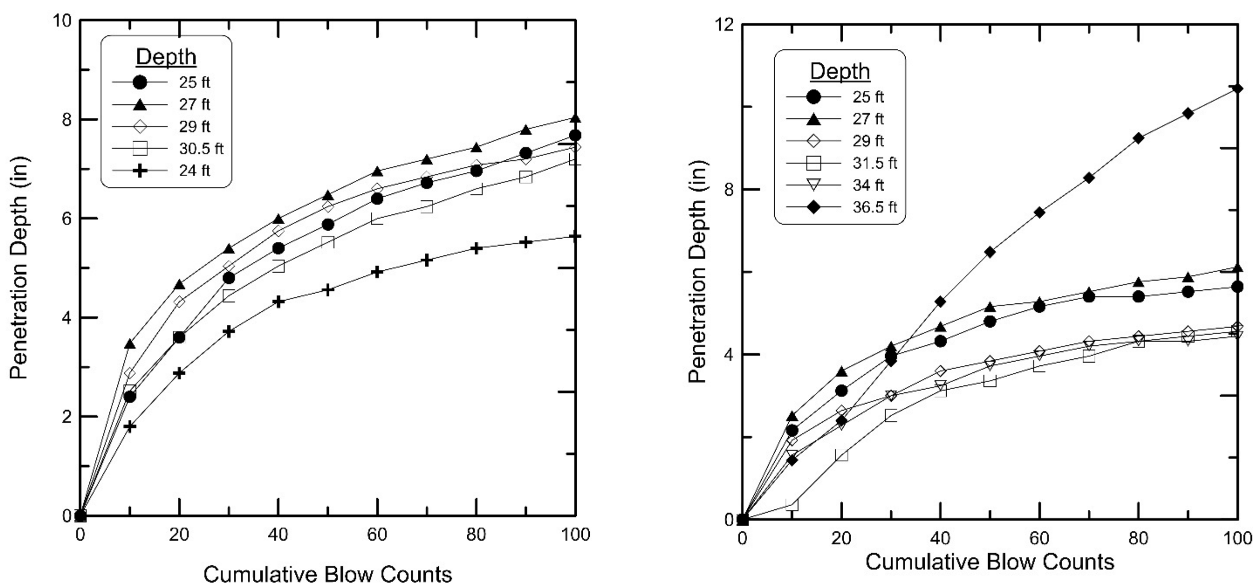

Figure A.3 Modified Standard Penetration Test results.

A.4 LABORATORY TEST RESULTS

A.4.1 Moisture Content and Total Unit Weight

Figure A.4 shows the total unit weight profile at the CH-9 over I-74 site. The total unit weight of shale was computed in accordance with ASTM D7263.

Shale specimens from unconsolidated undrained and unconfined compressive tests were used for determination of in situ water content. The resulting water content profile is shown in Figure A.5. Water content of the shale was determined in accordance with ASTM D2216.

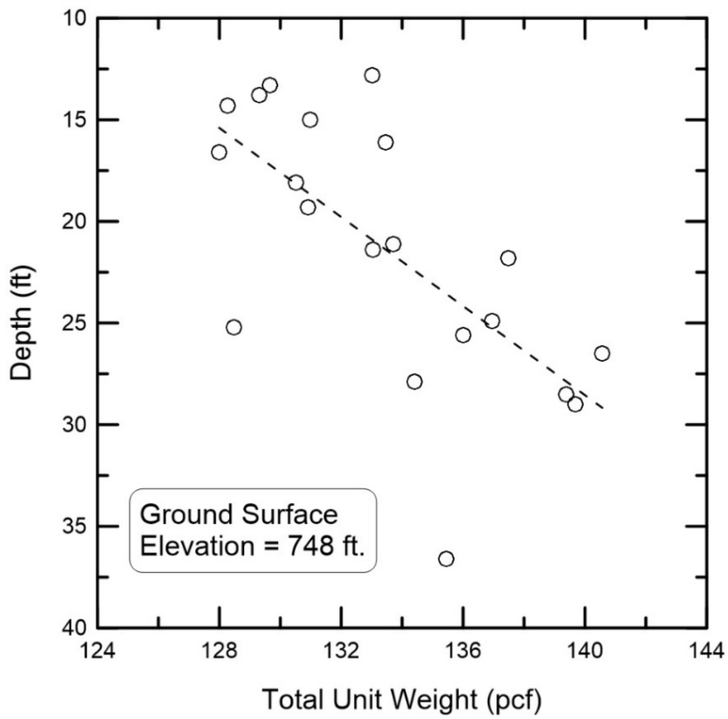

Figure A.4 Total unit weight profile.

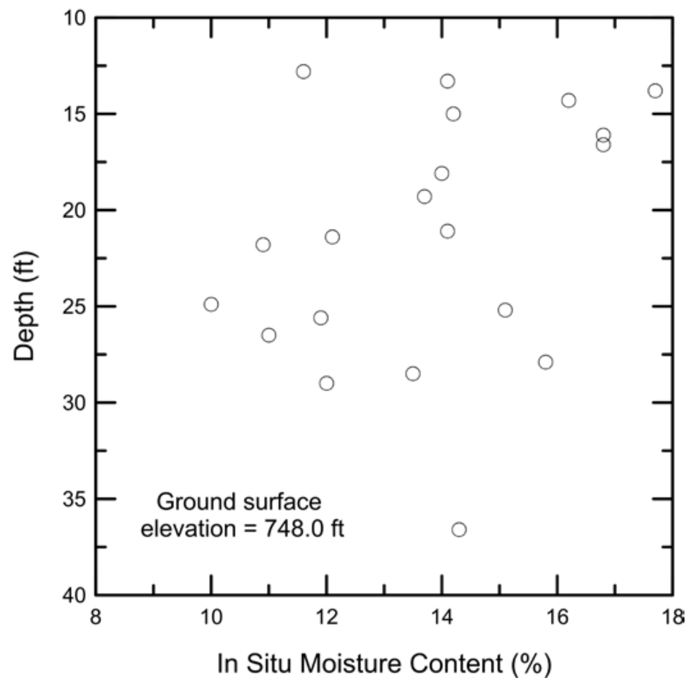

Figure A.5 In situ moisture content profile.

A.4.2 Triaxial Compression Test Results

Unconfined compression tests were performed in accordance with ASTM D7012–14 (method D). The peak deviator stress was used to calculate the undrained compressive strength for each test. The resulting undrained compressive strengths are shown in Table A.1.

A.4.3 Young's Modulus of Shale Specimen

Young's modulus was measured from results of triaxial tests in accordance to ASTM D7012–14 (method D). In short, the modulus was calculated from the slope of the stress-strain relationships that correspond to 50% of mobilized undrained compressive strength. Figure A.6 shows the relationship between Young's modulus and undrained compressive strength for the shale core tested from the CH-9 over I-74 site. This data was also used to develop a relationship between Young's modulus and shale natural water content (see Figure A.7). The unconfined compressive strength to the undrained Young's modulus ratio shown in Figure A.6 agrees well with the general trends observed in Phase 1 & 2 of this study. The site-specific relationship between undrained Young's modulus and the in situ water content is also shown in Figure A.7. Table A.1 summarizes all of the data obtained from the laboratory testing and evaluation.

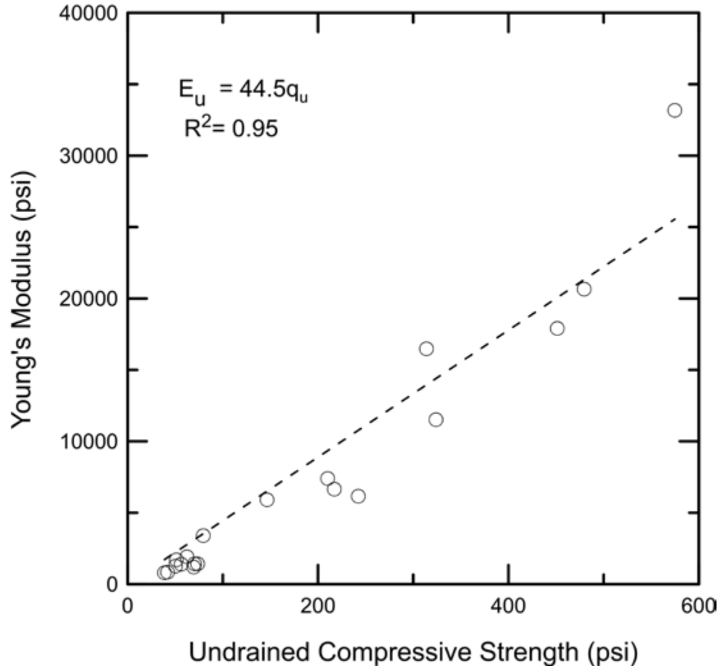

Figure A.6 Relationship between undrained compressive strength and Young's modulus.

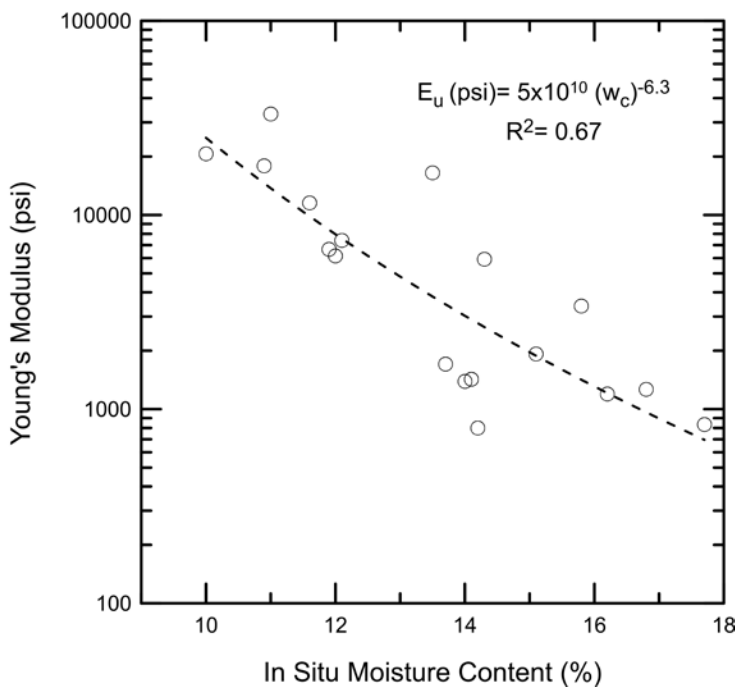

Figure A.7 Relationship between in situ moisture content and Young's modulus.

Table A.1 Laboratory Data Summary at the CH-9 over I-74

Specimen Identification	**GB-S1**	**GB-S2**	**GB-S3**
Core Run Number	1	1	1
Depth (ft.)	12.8	13.3	13.8
Initial Water Content (%)	11.6	14.1	17.7
Total Unit Weight (pcf)	133.0	129.7	129.3
Undrained Compressive Strength (ksf)	46.6	10.6	6
Strain at Peak Strength (%)	-	-	-
Young's Modulus (ksf)	1658.6	205.1	120.1
Recovery (%)	83	83	83
Rock Quality Designation (%)	50	50	50
Joint Average Vertical Spacing (in)	10	10	10
Sample Description	CLAY SHALE, Gray, Weathered	CLAY SHALE, Gray, Weathered	CLAY SHALE, Gray, Weathered

Specimen Identification	**GB-S4**	**GB-S5**	**GB-S6**
Core Run Number	**1**	**1**	**1**
Depth (ft.)	14.3	15.0	16.1
Initial Water Content (%)	16.2	14.2	16.8
Total Unit Weight (pcf)	128.3	131.0	133.45
Undrained Compressive Strength (ksf)	10	5.6	7.2
Strain at Peak Strength (%)	-	-	-
Young's Modulus (ksf)	172.3	115.1	182.1
Recovery (%)	83	83	83
Rock Quality Designation (%)	50	50	50
Joint Average Vertical Spacing (in)	10	10	10
Sample Description	CLAY SHALE, Gray, soft weathered	CLAY SHALE, Gray, soft weathered	CLAY SHALE, Gray, soft weathered

Specimen Identification	GB-S7	GB-S8	GB-S9
Core Run Number	**1**	**1**	**2**
Depth (ft.)	18.1	19.3	21.1
Initial Water Content (%)	14	13.7	14.1
Total Unit Weight (pcf)	130.5	130.9	133.7
Undrained Compressive Strength (ksf)	6.9	8.1	7.4
Strain at Peak Strength (%)	-	-	-
Young's Modulus (ksf)	200	245.6	205.1
Recovery (%)	83	83	100
Rock Quality Designation (%)	50	50	60
Joint Average Vertical Spacing (in)	10	10	12
Sample Description	CLAY SHALE, Gray, soft weathered	CLAY SHALE, Gray, soft weathered	CLAY SHALE, Gray, soft weathered

Specimen Identification	GB-S10	GB-S11	GB-S12
Core Run Number	**2**	**2**	**2**
Depth (ft.)	21.4	21.8	24.9
Initial Water Content (%)	12.1	10.9	10
Total Unit Weight (pcf)	133.0	137.5	136.9
Undrained Compressive Strength (ksf)	30.3	65	69.1
Strain at Peak Strength (%)	-	-	-
Young's Modulus (ksf)	1064.6	2577.8	2974.5
Recovery (%)	100	100	100
Rock Quality Designation (%)	60	60	60
Joint Average Vertical Spacing (in)	3-8	3-8	3-8
Sample Description	CLAY SHALE, Gray thinly bedded	CLAY SHALE, Gray thinly bedded	CLAY SHALE, Gray thinly bedded

Specimen Identification	GB-S13	GB-S14	GB-S15
Core Run Number	**2**	**2**	**3**
Depth (ft.)	25.2	25.6	26.5
Initial Water Content (%)	15.1	11.9	11.0
Total Unit Weight (pcf)	128.5	136.0	140.6
Undrained Compressive Strength (ksf)	9.0	31.2	82.8
Strain at Peak Strength (%)	-	-	-
Young's Modulus (ksf)	276.4	958.0	4776.1
Recovery (%)	100	100	100
Rock Quality Designation (%)	60	60	66
Joint Average Vertical Spacing (in)	5	5	10
Sample Description	CLAY SHALE, Gray, soft weathered	CLAY SHALE, Gray thinly bedded	CLAY SHALE, Gray Indurated

Specimen Identification	GB-S14	GB-S15	GB-S16
Core Run Number	**3**	**3**	**3**
Depth (ft.)	27.9	28.5	29.0
Initial Water Content (%)	15.1	11.9	11.0
Total Unit Weight (pcf)	128.5	136.0	140.6
Undrained Compressive Strength (ksf)	11.4	45.2	34.9
Strain at Peak Strength (%)	-	-	-
Young's Modulus (ksf)	488.9	2373.4	885.6
Recovery (%)	100	100	100
Rock Quality Designation (%)	66	66	66
Joint Average Vertical Spacing (in)	10	10	10
Sample Description	CLAY SHALE, Gray, soft weathered	CLAY SHALE, Gray thinly bedded	CLAY SHALE, Gray thinly bedded

APPENDIX B FIELD EXPLORATION AT CH-10 OVER THE BUCK CREEK

B.1 BACKGROUND

Figure B.1 shows location of CH10 over the Buck creek, located in Clay County, just North Flora, Illinois. This single span bridge structure carries a two-lane highway over the Buck creek. The weak shales near the south abutment, was investigated during this study.

Figure B.1 Location of CH10 over the Buck Creek.

Two borings were advanced near west abutment on September 18, 2014 by District 7 drilling crew. These borings were drilled to an elevation of 408.2 feet.

The first boring was used to obtain shale core samples. Initially rock cores were used for determination of recovery ratio, RQD of the rock mass, and vertical spacing of joints. Afterwards unconfined compression tests were conducted on the retrieved weak shales specimens. The in situ water content of the shale specimens used in the unconfined compression tests was also measured for correlation purposes. The unconfined compression test results were also used to determine the deformability characteristics of shale under undrained loading conditions.

The second boring was used to obtain MSPT blow counts at various depths. These data were used to improve/check the correlation between undrained compressive strength of weak shale in Illinois and MSPT penetration rates developed in Phase of this study. The following sections discuss geology of the bridge site, MSPT test results, and laboratory test results

B.2 SITE GEOLOGY

The geology at the bridge site consists of about 25 feet of soft silty clay, overlying sedimentary bedrock. The ground surface elevation at the two borings, is about 443.2.0 feet. A fairly continuous layer of thinly bedded clay shale was exposed at an elevation of 418.2 feet and extended to elevation of 408.2 feet where coring was terminated. Laboratory test results are summarized in Table B.1.

B.3 MODIFED STANDARD PENETRATION TEST RESULTS

Figure B.2 shows the Modified Standard Penetration Test results obtained in one of the borings at CH10 over the Buck Creek.

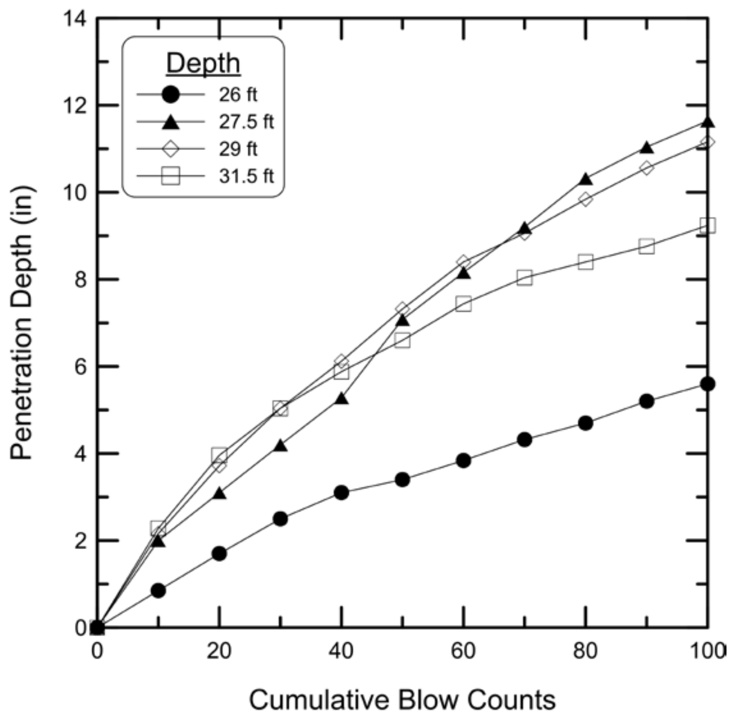

Figure B.2 Modified Standard Penetration Test results.

B.4 LABORATORY TEST RESULTS

B.4.1 Moisture Content and Total Unit Weight

Figure B.3 shows the total unit weight profile at the CH10 over the Buck Creek site. The total unit weight of the encountered shales was computed in accordance with ASTM D7263. Shale specimens from unconfined compressive tests were used for determination of in situ water content. The resulting water content profile is shown in Figure B.4. Water content of the Shales was determined in accordance with ASTM D2216.

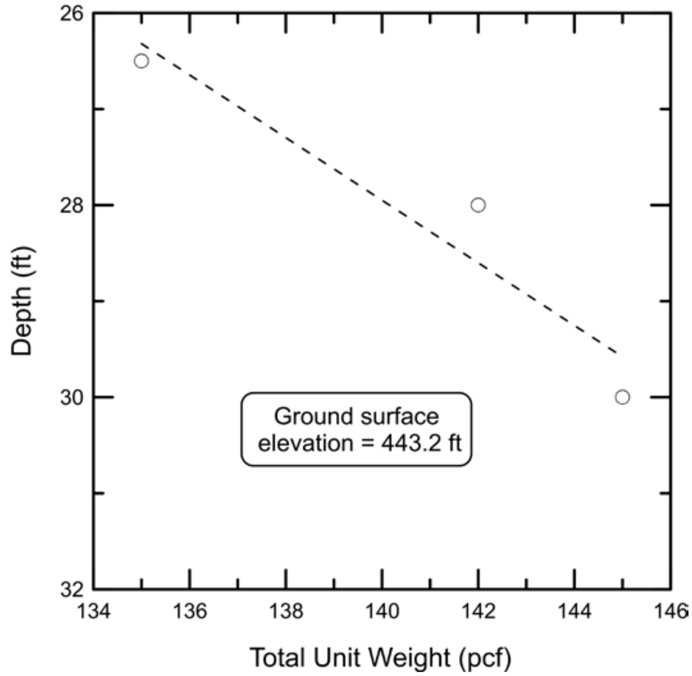

Figure B.3 Total unit weight profile.

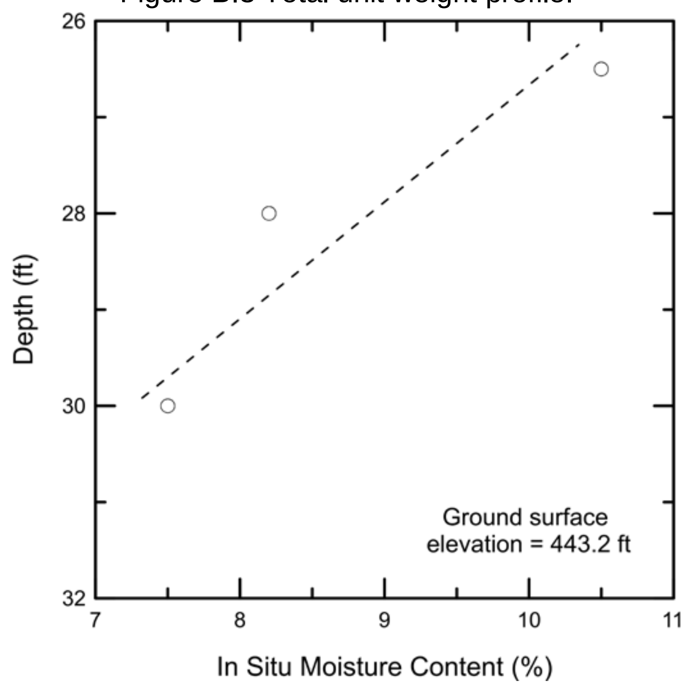

Figure B.4 In situ moisture content profile.

B.4.2 Triaxial Compression Test Results

Unconfined triaxial compression tests were performed in accordance with ASTM D7012–14 (method D). The peak deviator stress was used to calculate the undrained compressive strength for each test. The resulting undrained compressive strengths are shown in Table B.1.

B.4.3 Young's Modulus of Shale Specimen

Young's modulus was measured from results of triaxial tests in accordance to ASTM D7012–14 (method D). In short, the modulus was calculated from the slope of the stress-strain relationships that correspond to 50% of mobilized undrained compressive strength. Figure B.5 shows the relationship between Young's modulus and undrained compressive strength for the shales core tested from the CH10 over the Buck Creek site. This data was also used to develop a relationship between Young's modulus and natural water content (see Figure B.6). Table B.1 summarizes all of the data obtained from the laboratory testing and evaluation.

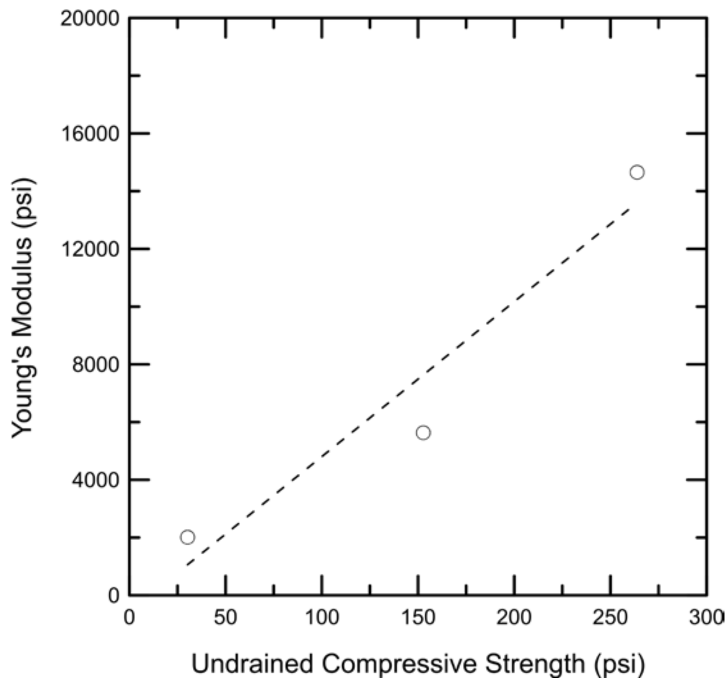

Figure B.5 Relationship between undrained compressive strength and Young's modulus.

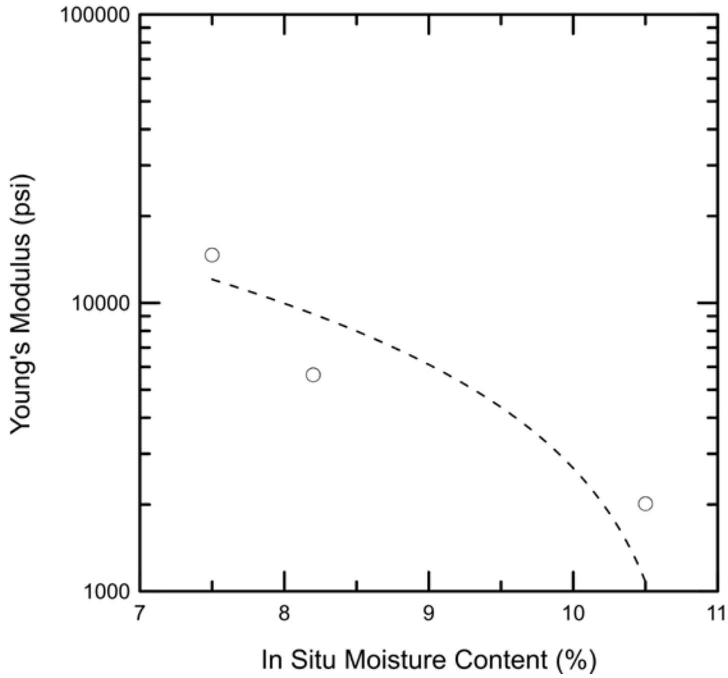

Figure B.6 Relationship between in situ moisture content and Young's modulus.

Table B.1 Laboratory Data Summary at the CH10 over the Buck Creek

Specimen Identification	**BKC-S1**	**BKC -S2**	**BKC -S3**
Core Run Number	**1**	**1**	**2**
Depth (ft.)	26.5	28.0	30
Initial Water Content (%)	10.5	8.2	7.5
Total Unit Weight (pcf)	135	142	145
Undrained Compressive Strength (ksf)	4.35	22	38.0
Strain at Peak Strength (%)	-	3.5	5.0
Young's Modulus (ksf)	290	810.5	2110.5
Recovery (%)	70	70	100
Rock Quality Designation (%)	55	55	75
Joint Average Vertical Spacing (in)	1 to 2	1 to 2	1 to 2
Sample Description	Clay Shales Tan, thinly bedded, fissile sandy	Clay Shales Gray, thinly bedded, fissile,	Clay Shales Gray, thinly bedded, fissile, with coal seams

APPENDIX C FIELD EXPLORATION AT IL 89 OVER THE ILLINOIS RIVER

C.1 BACKGROUND

Figure C.1 shows the location of IL 89 over Illinois River bridge site, located in Putnam County, just south of Spring Valley, Illinois. The eight-span bridge structure carries a two-lanes highway over Illinois River and connects Putnam and Bureau counties via IL-89. The north and south abutments of the bridge together with Piers 1,6 & 7 are supported on driven H-piles. Piers 2 to 5 are supported on drilled shafts socketed into the underlying sedimentary rocks.

Figure C.1 Location of IL 89 over Illinois River.

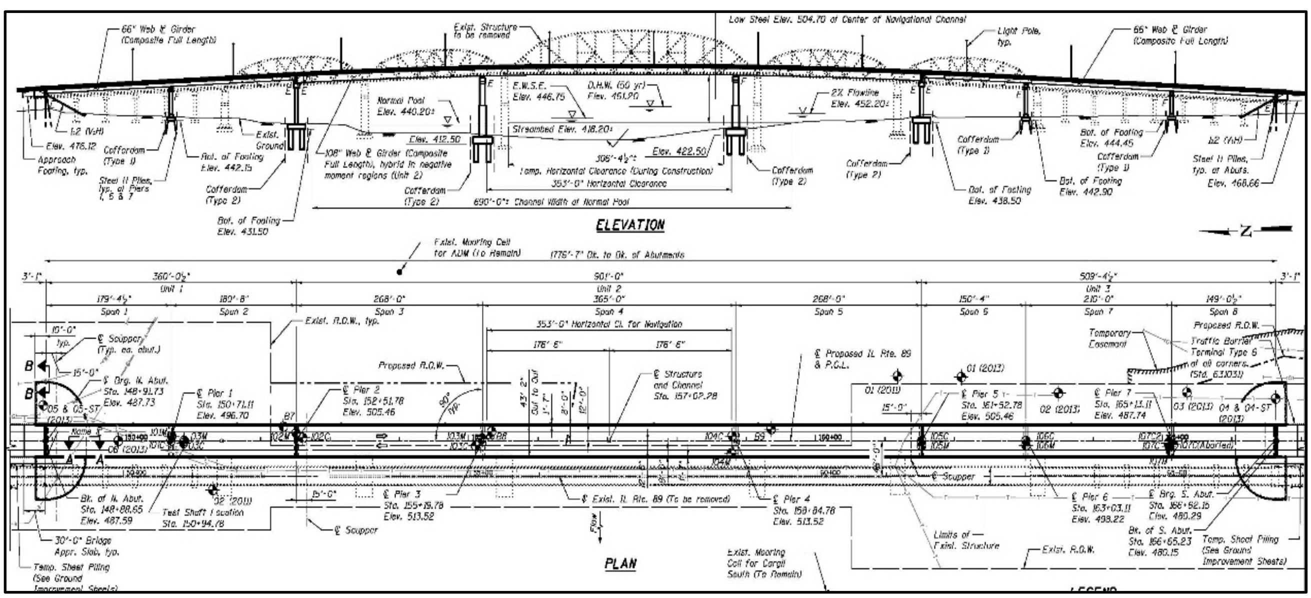

Figure C.2 Location of boring holes at IL 89 over Illinois River.

Figure C.2 shows a plan view of IL 89 over Illinois River structure and the location of the sixteen (16) borings drilled between May to October 2014 by Wang Engineering and District 3 drilling crew. The sixteen borings included two borings for each of the seven bridge piers plus another two for the test shaft near Pier 1 (see Chapter 5)

One of the two borings was used to obtain core samples. Initially rock cores were used for determination of recovery ratio, RQD of the rock mass, and vertical spacing of joints. Afterwards unconfined compression tests were conducted on the retrieved shale specimens. The in situ water content of the specimens used in the unconfined compression test was also measured for correlation purposes. The unconfined compression test results were also used to determine the deformability characteristics of the weak rock under undrained loading conditions.

The second boring was used to obtain MSPT blow counts at various depths. This data was used to check the applicability of the proposed correlation between undrained compressive strength in Illinois and MSPT penetration rate to shales. The following sections discuss geology of the bridge site, MSPT test results, and laboratory test results

C.2 SITE GEOLOGY

The geology at the site is primarily from the Quaternary and Pennsylvanian periods; the makeup of the other soils is from excavated and fill materials. The overburden at the site consists almost exclusively of materials from a number of formations in the Quaternary System. These formations range in composition from alluvial, eolian, or glacial deposits to a depth of approximately 50 ft. In terms of an engineering description, the overburden consists of largely of silts and clays with trace sand and the occasional sand and gravel lenses.

The north (Piers 1, 2, and 3) and south approaches (Piers 6, and 7), from the ground surface going downward, are underlain by excavated and fill materials, then by shales from the Bond and Mattoon Formations from the Pennsylvanian System. Willman et al, 1967 describe these formations as consisting of green to red shale, with medium gray fossililiferous limestone, medium to dark grayish green mudstone, and medium gray grainstone. Indeed shale, albeit medium to dark gray in color, was found at depths from approximately 50 to 90 ft; a coal seam with underclay was consistently encountered near depths of 85 ft. At 90 ft, the shale transitioned to light to medium gray lime mudstone and continued through 120 ft, where the majority of borings were terminated.

The piers located in the river (Piers 3 and 4), from the ground surface going downward, are underlain by sands from the Cahokia Formation in the Quarternary System, then by shales from the Bond and Mattoon Formations from the Pennsylvanian System (ISGS map). As with the north and south abutments, shale was found from depths of 50 to 90 ft with a coal seam and underclay near 85 ft. Again as with north and south abutments, the shale transitioned at 90 ft to a lime mudstone to 120 ft where the borings were terminated. Laboratory test results are summarized in Table C.1.

C.3 MODIFED STANDARD PENETRATION TEST RESULTS

Figure C3 to C10 show the Modified Standard Penetration Test results for the eight MSPTs conducted at the IL 89 over Illinois River piers and test shaft location.

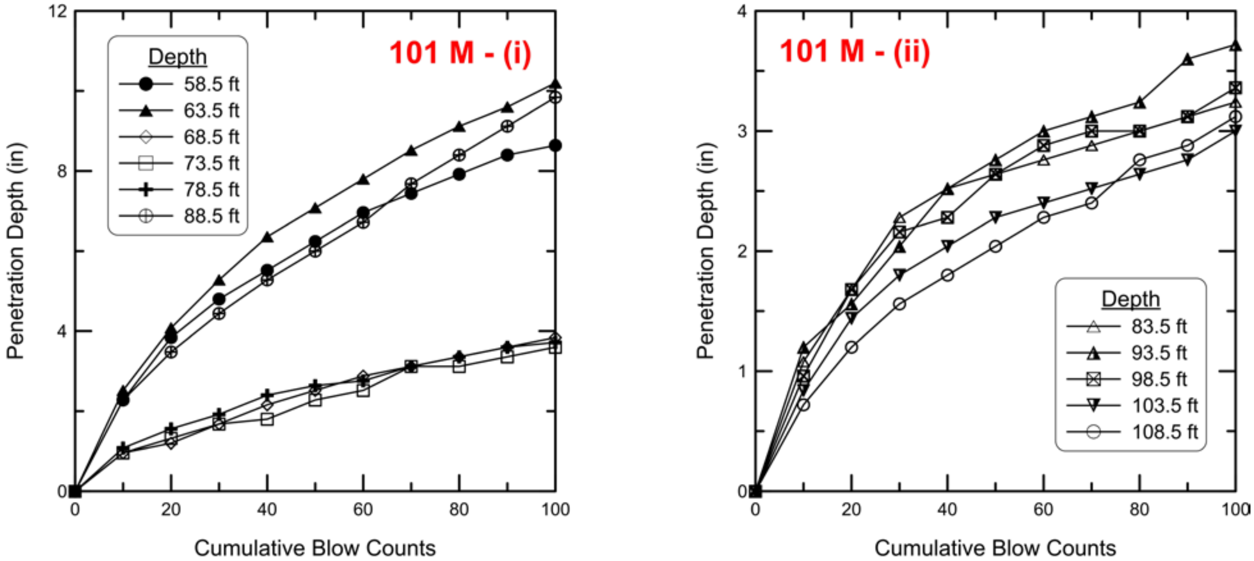

Figure C.3 Modified Standard Penetration Test results for Pier 1.

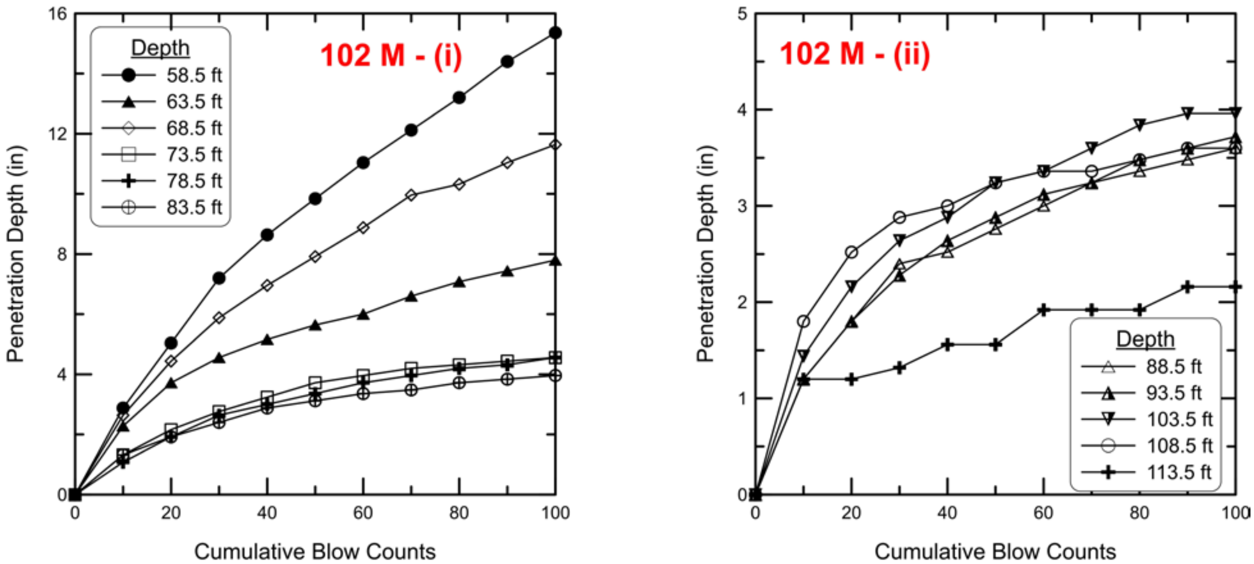

Figure C.4 Modified Standard Penetration Test results for Pier 2.

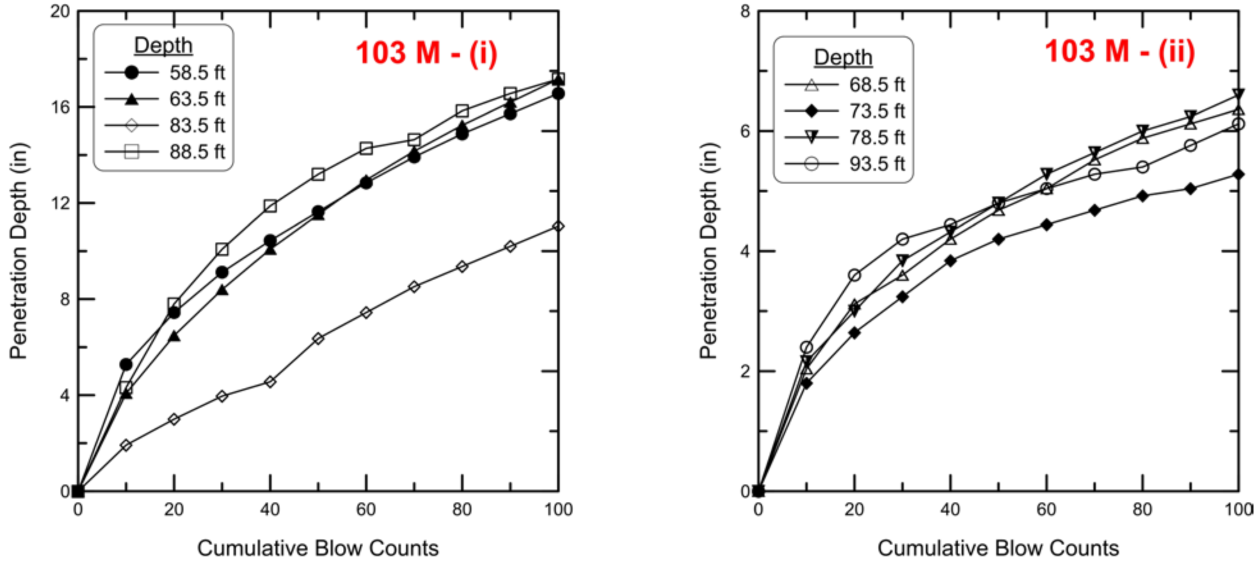

Figure C.5 Modified Standard Penetration Test results for Pier 3.

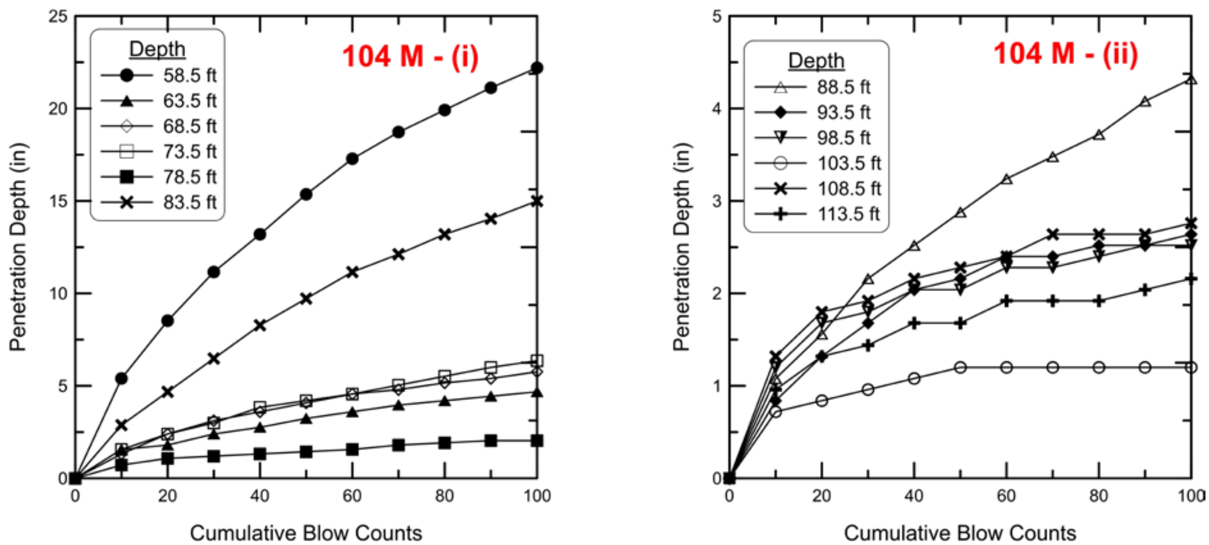

Figure C.6 Modified Standard Penetration Test results for Pier 4.

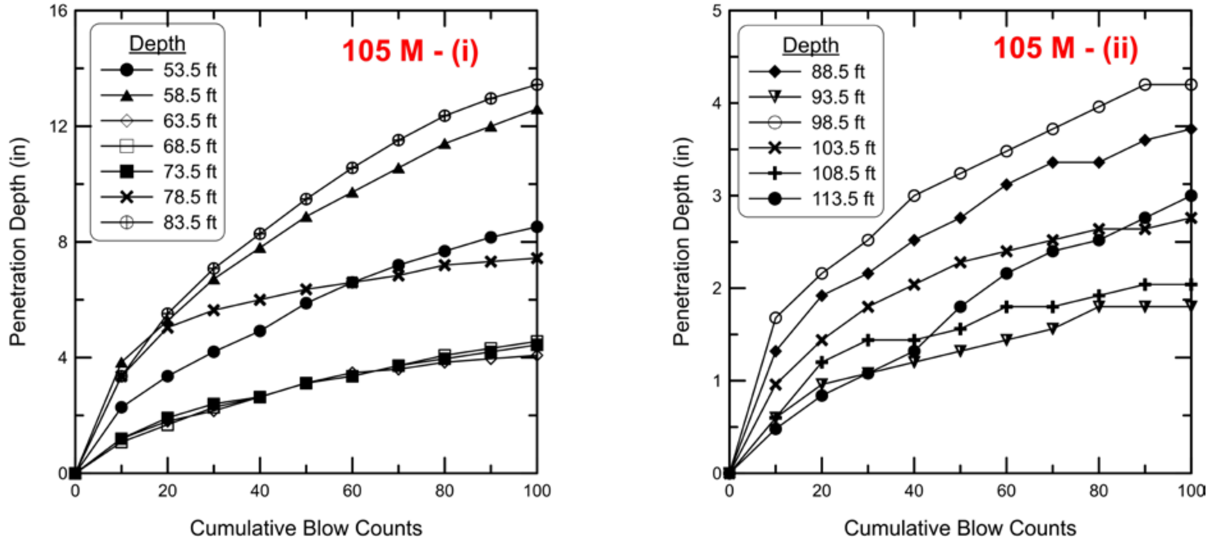

Figure C.7 Modified Standard Penetration Test results for Pier 5

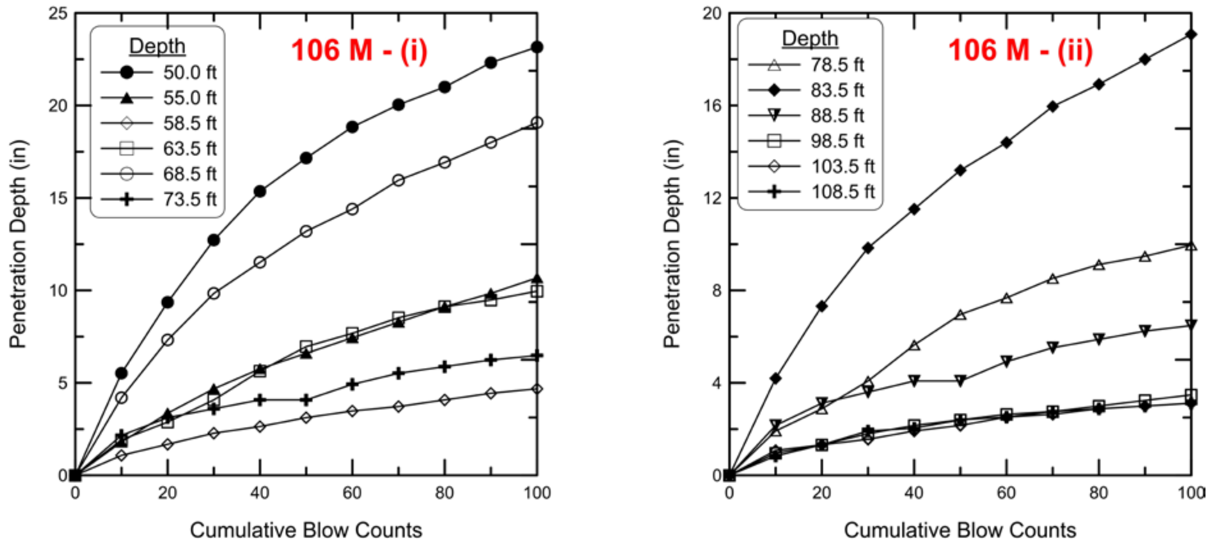

Figure C.8 Modified Standard Penetration Test results for Pier 6

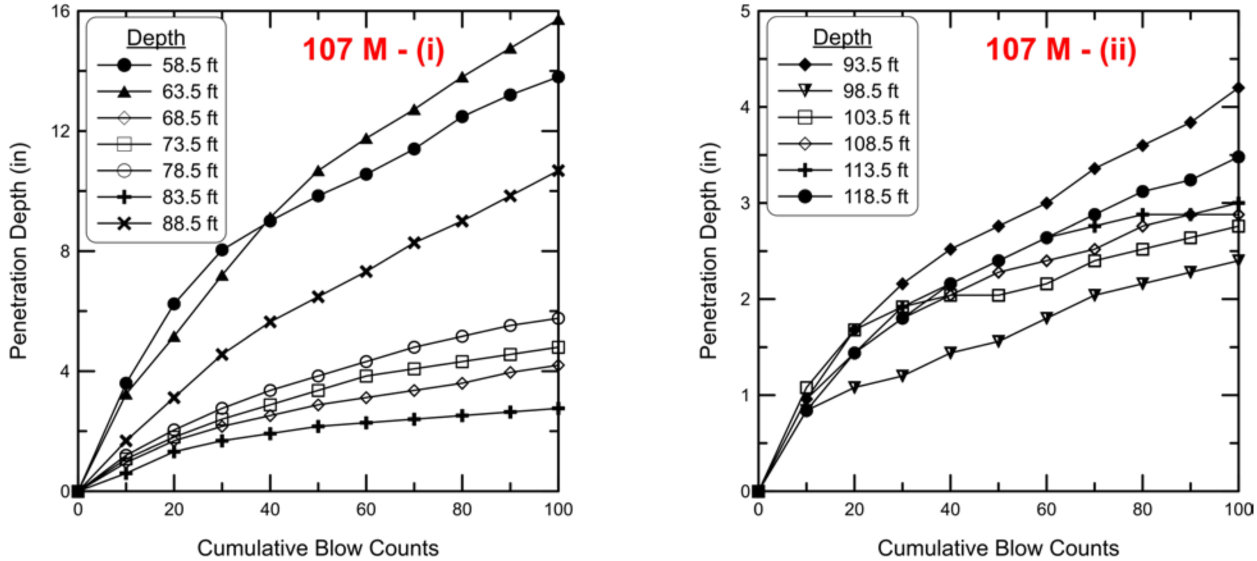

Figure C.9 Modified Standard Penetration Test results for Pier 7

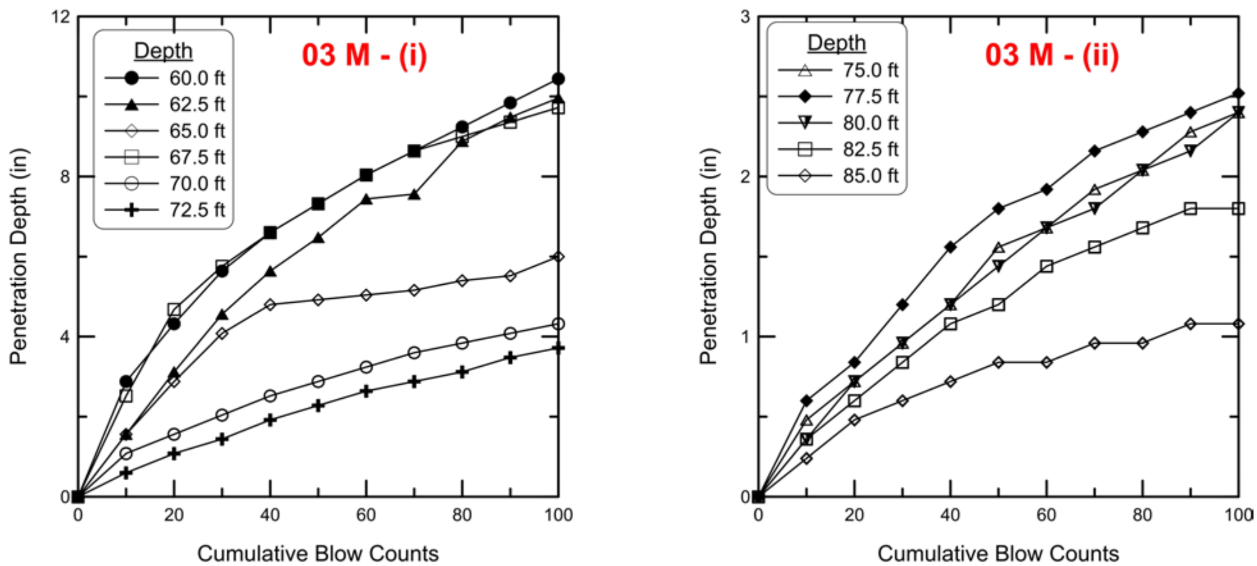

Figure C.10 Modified Standard Penetration Test results at the test shaft Location

C.4 LABORATORY TEST RESULTS

C.4.1 Moisture Content and Total Unit Weight

Figure C.11 shows the total unit weight profile at the IL89 over the Illinois River site. The total unit weight of the encountered sedimentary rock was computed in accordance with ASTM D 7263. Shale specimens from unconfined compressive tests were used for determination of in situ water content. The resulting water content profile is shown in Figure C.12. Water content of the Shales was determined in accordance with ASTM D 2216.

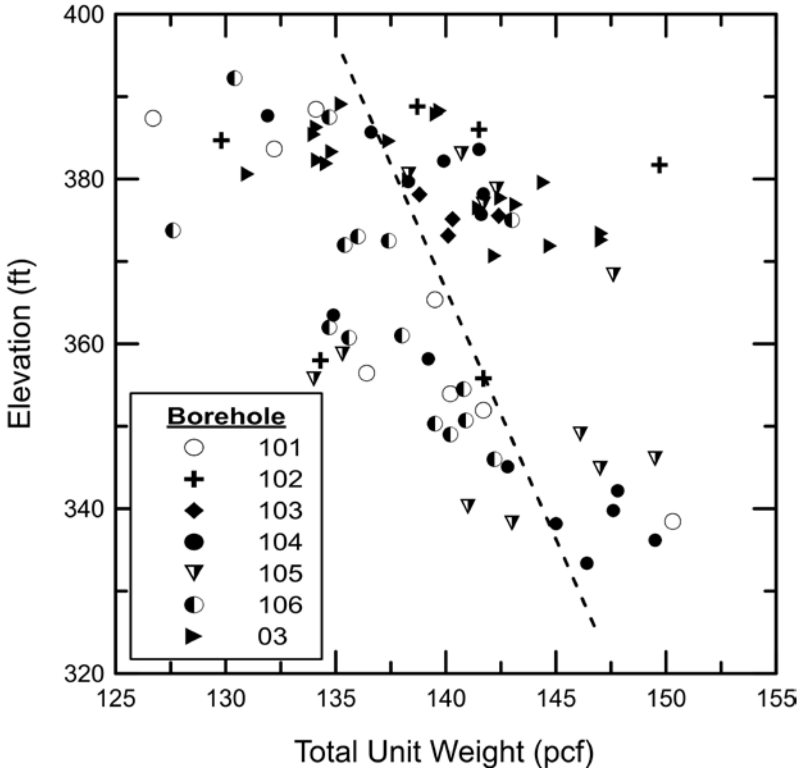

Figure C.11 Total unit weight profile.

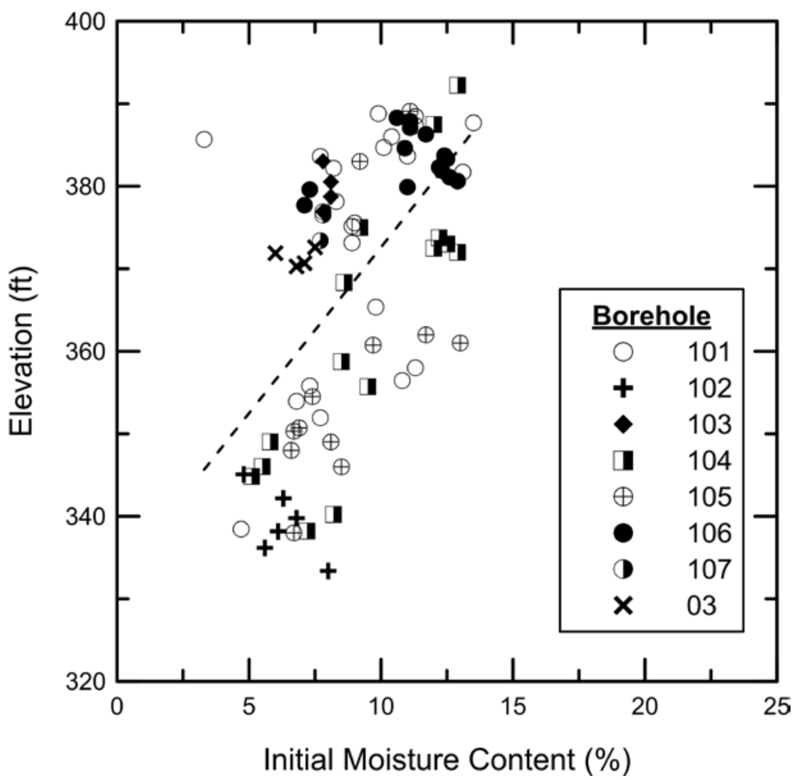

Figure C.12 In situ moisture content profile.

C.4.2 Triaxial Compression Test Results

Unconfined triaxial compression tests were performed in accordance with ASTM D7012–14 (method D). The peak deviator stress was used to calculate the undrained compressive strength for each test. The resulting undrained compressive strengths are shown in Table C.1.

C.4.3 Young's Modulus of Shale Specimen

Young's modulus was measured from results of triaxial tests in accordance to ASTM D7012–14 (method D). In short, the modulus was calculated from the slope of the stress-strain relationships that correspond to 50% of mobilized undrained compressive strength. Figure C.13 shows the relationship between Young's modulus and undrained compressive strength for the shale cores tested from the IL 89 over the Illinois River site. This data was also used to develop a relationship between Young's modulus and natural water content (see Figure C.14). The unconfined compressive strength to the undrained Young's modulus ratio shown in Figure C.13 agrees well with the general trends observed in Phase 1 & 2 of this study. The site-specific relationship between undrained Young's modulus and the in situ water content is also shown in Figure C.14. Table C.1 summarizes all of the data obtained from the laboratory testing and evaluation.

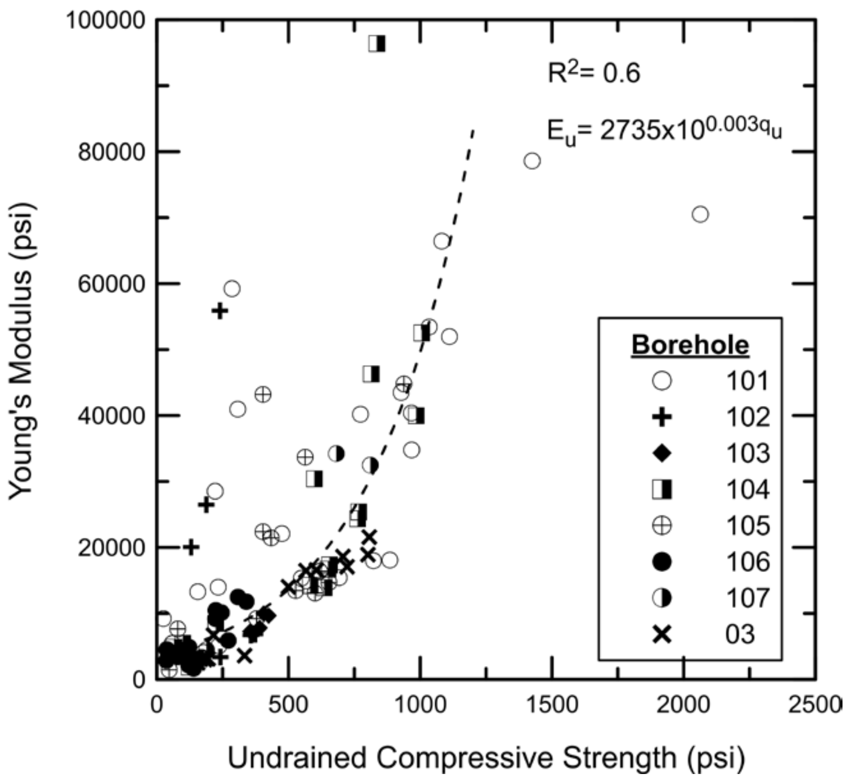

Figure C.13 Relationship between undrained compressive strength and Young's modulus.

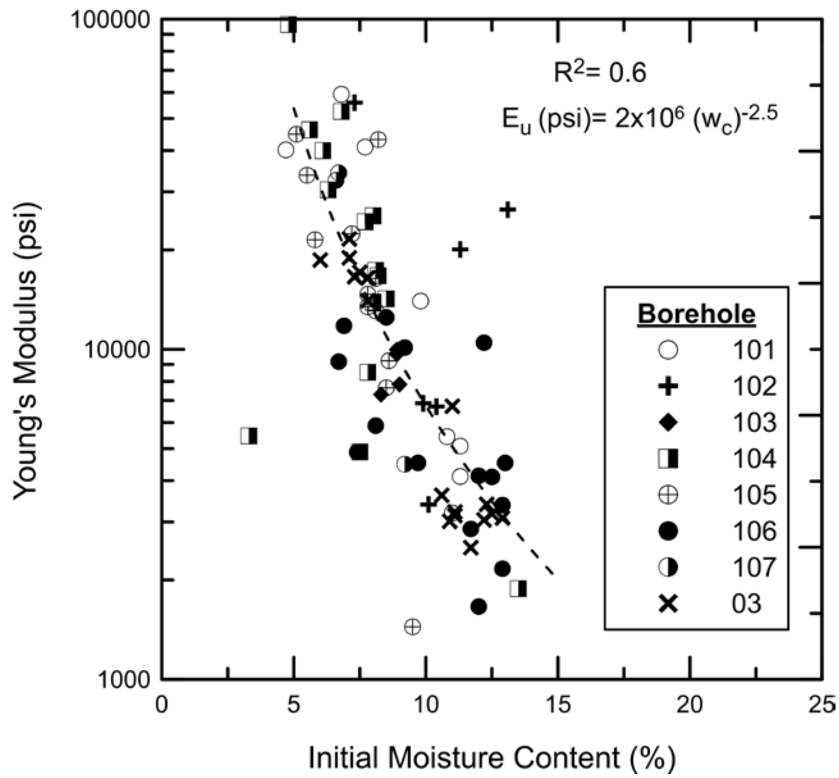

Figure C.14 Relationship between in situ moisture content and Young's modulus.

Table C.1 Laboratory Data Summary at the IL 89 over the Illinois River

Specimen Identification	**SV-101-60.8**	**SV-101-61.9**	**SV-101-62.9**
Borehole Number	**101C**	**101C**	**101C**
Core Run Number	**1**	**1**	**1**
Depth (ft.)	60.8	61.9	62.9
Initial Water Content (%)	11.3	11.3	-
Total Unit Weight (pcf)	134.1	126.7	-
Undrained Compressive Strength (ksf)	33.9	25.7	24.6
Young's Modulus (ksf)	732.2	593	477.7
Recovery (%)	79	79	79
Rock Quality Designation (%)	64	64	64
Sample Description	Very Soft Gray Very Weathered Shale	Very Soft Gray Very Weathered Shale	Very Soft Gray Very Weathered Shale

Specimen Identification	**SV-101-65.6**	**SV-101-70.5**	**SV-101-72.6**
Borehole Number	**101C**	**101C**	**101C**
Core Run Number	**1**	**3**	**3**
Depth (ft.)	65.6	70.5	72.6
Initial Water Content (%)	11	-	-
Total Unit Weight (pcf)	132.2	-	-
Undrained Compressive Strength (ksf)	24.6	81.8	79
Young's Modulus (ksf)	459.4	2146.0	2204
Recovery (%)	79	96	96
Rock Quality Designation (%)	64	87	87
Sample Description	Very Soft Gray Very Weathered Shale	Dense Gray Argillaceous Shale - Micaceous	Dense Gray Argillaceous Shale - Micaceous

Specimen Identification	**SV-101-76.5**	**SV-101-78.25**	**SV-101-80.5**
Borehole Number	**101C**	**101C**	**101C**
Core Run Number	**3**	**3**	**4**
Depth (ft.)	76.5	78.25	80.5
Initial Water Content (%)	11	-	-
Total Unit Weight (pcf)	132.2	-	-
Undrained Compressive Strength (ksf)	99.7	127.4	68.4
Young's Modulus (ksf)	2222.3	2606.6	3182.7
Recovery (%)	96	96	100
Rock Quality Designation (%)	87	87	54
Sample Description	Dense Gray Argillaceous Shale - Micaceous	Dense Gray Argillaceous Shale - Micaceous	Dense Gray Silty Shale

Specimen Identification	SV-101-82.25	SV-101-83.9	SV-101-91.25
Borehole Number	**101C**	**101C**	**101C**
Core Run Number	**4**	**4**	**5**
Depth (ft.)	82.25	83.9	91.25
Initial Water Content (%)	-	9.8	-
Total Unit Weight (pcf)	-	139.5	-
Undrained Compressive Strength (ksf)	118.4	33.6	3.6.
Young's Modulus (ksf)	2588.9	2013.6	1327.3
Recovery (%)	100	100	98
Rock Quality Designation (%)	54	54	65
Sample Description	Dense Gray Silty Shale	Dense Gray Silty Shale	Under clay

Specimen Identification	SV-101-92.8	SV-101-95.3	SV-101-97.3
Borehole Number	**101C**	**101C**	**101C**
Core Run Number	**5**	**5**	**5**
Depth (ft.)	92.8	95.3	97.3
Initial Water Content (%)	10.8	6.8	7.7
Total Unit Weight (pcf)	136.4	140.2	141.7
Undrained Compressive Strength (ksf)	8.4	41.1	44.2
Young's Modulus (ksf)	782.2	8527.7	5896.77
Recovery (%)	98	98	98
Rock Quality Designation (%)	65	65	65
Sample Description	Under clay	Under clay	Gray Argillaceous Shale with Limestone Inclusions

Specimen Identification	SV-101-99.5	SV-101-101.5	SV-101-103.5
Borehole Number	**101C**	**101C**	**101C**
Core Run Number	**5**	**6**	**6**
Depth (ft.)	99.5	101.5	103.5
Initial Water Content (%)	-	-	-
Total Unit Weight (pcf)	-	-	-
Undrained Compressive Strength (ksf)	31.9	22.4	383.7
Young's Modulus (ksf)	4106.7	1911.4	58575.1
Recovery (%)	98	100	100
Rock Quality Designation (%)	65	99	99
Sample Description	Gray Argillaceous Shale with Limestone Inclusions	Very Dense Gray Argillaceous Shale with Limestone Interclasts	Very Dense Gray Argillaceous Shale with Limestone Interclasts

Specimen Identification	SV-101-104.3	SV-101-107.5	SV-101-108.8
Borehole Number	**101C**	**101C**	**101C**
Core Run Number	**6**	**6**	**6**
Depth (ft.)	104.3	107.5	108.8
Initial Water Content (%)	-	-	-
Total Unit Weight (pcf)	-	-	-
Undrained Compressive Strength (ksf)	297.2	139.2	133.6
Young's Modulus (ksf)	10152.2	5814.5	6264.4
Recovery (%)	98	100	100
Rock Quality Designation (%)	65	99	99
Sample Description	Very Dense Gray Argillaceous Shale with Limestone Interclasts	Very Dense Gray Argillaceous Shale with Limestone Interclasts	Very Dense Gray Argillaceous Shale with Limestone Interclasts

Specimen Identification	SV-101-110.8	SV-101-111.7	SV-101-113.7
Borehole Number	**101C**	**101C**	**101C**
Core Run Number	**6**	**6**	**6**
Depth (ft.)	104.3	107.5	108.8
Initial Water Content (%)	4.7	-	-
Total Unit Weight (pcf)	150.3	-	-
Undrained Compressive Strength (ksf)	111.3	139.3	148.9
Young's Modulus (ksf)	5785.1	5007.8	7694.0
Recovery (%)	100	100	100
Rock Quality Designation (%)	99	99	99
Sample Description	Very Dense Gray Argillaceous Shale with Limestone Interclasts	Very Dense Gray Argillaceous Shale with Limestone Interclasts	Very Dense Gray Argillaceous Shale with Limestone Interclasts

Specimen Identification	SV-101-116.3	SV-101-117.6	SV-101-118.9
Borehole Number	**101C**	**101C**	**101C**
Core Run Number	**7**	**7**	**7**
Depth (ft.)	116.3	117.6	118.9
Initial Water Content (%)	-	-	-
Total Unit Weight (pcf)	-	-	-
Undrained Compressive Strength (ksf)	155.8	205.2	160
Young's Modulus (ksf)	968.0	11318.5	7480.7
Recovery (%)	100	100	100
Rock Quality Designation (%)	95	95	95
Sample Description	Very Dense Gray Sandy Shale with Limestone Stringer	Very Dense Gray Sandy Shale with Limestone Stringer	Very Dense Gray Sandy Shale with Limestone Stringer

Specimen Identification	SV-102-64.2	SV-102-67.0	SV-102-68.3
Borehole Number	**102C**	**102C**	**102C**
Core Run Number	**4**	**4**	**4**
Depth (ft.)	64.2	67.0	68.3
Initial Water Content (%)	9.9	10.4	10.1
Total Unit Weight (pcf)	138.7	141.5	129.8
Undrained Compressive Strength (ksf)	53.7	51.4	34.8
Young's Modulus (ksf)	987.7	965.5	487.8
Recovery (%)	91	91	91
Rock Quality Designation (%)	87	87	87
Sample Description	Gray Argillaceous Shale	Gray Argillaceous Shale	Gray Argillaceous Shale

Specimen Identification	SV-102-71.3	SV-102-95.0	SV-102-97.2
Borehole Number	**102C**	**102C**	**102C**
Core Run Number	**4**	**7**	**7**
Depth (ft.)	71.3	95.0	97.2
Initial Water Content (%)	13.1	11.3	7.3
Total Unit Weight (pcf)	149.7	134.3	141.7
Undrained Compressive Strength (ksf)	53.7	51.4	34.8
Young's Modulus (ksf)	987.7	965.5	487.8
Recovery (%)	91	100	100
Rock Quality Designation (%)	87	58	58
Sample Description	Gray Argillaceous Shale	Gray Under Clay	Gray Under Clay

Specimen Identification	SV-103-74.3	SV-103-76.9	SV-103-77.3
Borehole Number	**103C**	**103C**	**103C**
Core Run Number	**2**	**2**	**2**
Depth (ft.)	74.3	76.9	77.3
Initial Water Content (%)	8.3	9	8.9
Total Unit Weight (pcf)	138.8	142.4	140.3
Undrained Compressive Strength (ksf)	51.0	56.3	61.2
Young's Modulus (ksf)	1050.6	1127.8	1393.9
Recovery (%)	98	98	98
Rock Quality Designation (%)	84	84	84
Sample Description	2	2	2

Specimen Identification	SV-103-79.3	SV-104-62.5	SV-104-64.5
Borehole Number	**103C**	**104C**	**104C**
Core Run Number	**2**	**1**	**1**
Depth (ft.)	79.3	62.5	64.5
Initial Water Content (%)	8.9	13.5	3.3
Total Unit Weight (pcf)	140.1	131.9	136.6
Undrained Compressive Strength (ksf)	58.4	17.7	14.2
Young's Modulus (ksf)	1436.5	271.3	787.9
Recovery (%)	98	100	100
Rock Quality Designation (%)	84	36	36
Sample Description	Gray Argillaceous Shale	Gray Weathered Argillaceous Shale	Gray Weathered Argillaceous Shale

Specimen Identification	SV-104-66.6	SV-104-68.0	SV-104-70.5
Borehole Number	**104C**	**104C**	**104C**
Core Run Number	**2**	**2**	**2**
Depth (ft.)	66.6	68.0	70.5
Initial Water Content (%)	7.7	8.2	8.5
Total Unit Weight (pcf)	141.5	139.9	138.3
Undrained Compressive Strength (ksf)	109.8	93.6	83.6
Young's Modulus (ksf)	3506.7	2407.6	2050.4
Recovery (%)	100	100	100
Rock Quality Designation (%)	93	93	93
Sample Description	Dark Gray Weathered Argillaceous Shale	Dark Gray Weathered Argillaceous Shale	Dark Gray Argillaceous Shale

Specimen Identification	SV-104-72	SV-104-74.5	SV-104-86.7
Borehole Number	**104C**	**104C**	**104C**
Core Run Number	**2**	**2**	**4**
Depth (ft.)	72.0	74.0	86.7
Initial Water Content (%)	8.1	8.0	7.5
Total Unit Weight (pcf)	141.7	141.6	134.9
Undrained Compressive Strength (ksf)	94.4	91.5	9.4
Young's Modulus (ksf)	2496.6	2002.8	703.8
Recovery (%)	100	100	96
Rock Quality Designation (%)	93	93	70
Sample Description	Dark Gray Argillaceous Shale	Dark Gray Argillaceous Shale	Light Gray Claystone

Specimen Identification	SV-104-92	SV-104-105.1	SV-104-108.0
Borehole Number	**104C**	**104C**	**104C**
Core Run Number	**4**	**5**	**6**
Depth (ft.)	92.0	105.1	108.0
Initial Water Content (%)	7.8	4.8	6.3
Total Unit Weight (pcf)	139.2	142.8	147.8
Undrained Compressive Strength (ksf)	32.2	120.4	86.1
Young's Modulus (ksf)	1227.1	13883.4	4381.9
Recovery (%)	96	100	100
Rock Quality Designation (%)	70	77	81
Sample Description	Light Gray Sandy Shale, Micaceous	Gray Sandy Shale	Gray Sandy Shale

Specimen Identification	SV-104-110.4	SV-104-112.0	SV-104-114.0
Borehole Number	**104C**	**104C**	**104C**
Core Run Number	**6**	**6**	**6**
Depth (ft.)	110.4	112	144
Initial Water Content (%)	6.8	6.1	5.6
Total Unit Weight (pcf)	147.6	145	149.5
Undrained Compressive Strength (ksf)	144.8	141.8	117.3
Young's Modulus (ksf)	7561.8	5757.9	6664.9
Recovery (%)	100	100	100
Rock Quality Designation (%)	81	81	81
Sample Description	Gray Sandy to Silty Shale	Gray Sandy to Silty Shale	Gray Sandy to Silty Shale

Specimen Identification	SV-104-116.8	SV-105-65.5	SV-105-68.0
Borehole Number	**104C**	**105C**	**105C**
Core Run Number	**7**	**3**	**3**
Depth (ft.)	**116.8**	**65.5**	**68.0**
Initial Water Content (%)	8	7.8	8.1
Total Unit Weight (pcf)	146.4	140.7	138.3
Undrained Compressive Strength (ksf)	110.3	76.0	86.5
Young's Modulus (ksf)	3653.5	1936.6	1884.1
Recovery (%)	96	95	95
Rock Quality Designation (%)	70	91	91
Sample Description	Gray Silty Shale	Gray Shale Argillaceous with 2" thick Limestone Stringers	Gray Shale Argillaceous with 2" thick Limestone Stringers

Specimen Identification	SV-105-69.8	SV-105-71.6	SV-105-89.8
Borehole Number	**105C**	**105C**	**105C**
Core Run Number	**3**	**3**	**5**
Depth (ft.)	**69.8**	**71.6**	**89.8**
Initial Water Content (%)	8.1	7.8	8.5
Total Unit Weight (pcf)	142.3	141.7	135.3
Undrained Compressive Strength (ksf)	89.1	94.1	11.5
Young's Modulus (ksf)	2361.4	2113.1	1099.7
Recovery (%)	95	95	100
Rock Quality Designation (%)	91	91	88
Sample Description	Gray Shale Argillaceous with 2" thick Limestone Stringers	Gray Shale Argillaceous with 2" thick Limestone Stringers	Gray Claystone with Limestone Interclasts

Specimen Identification	SV-105-92.8	SV-105-99.5	SV-105-102.5
Borehole Number	**105C**	**105C**	**105C**
Core Run Number	**5**	**6**	**6**
Depth (ft.)	**92.8**	**99.5**	**102.5**
Initial Water Content (%)	9.5	5.8	5.5
Total Unit Weight (pcf)	134	146.1	149.5
Undrained Compressive Strength (ksf)	6.8	62.5	81.1
Young's Modulus (ksf)	207.6	3089.6	4849.5
Recovery (%)	100	100	100
Rock Quality Designation (%)	88	91	91
Sample Description	Gray Claystone with Limestone interclasts	Gray Shale	Gray Shale

Specimen Identification	SV-105-103.7	SV-105-108.3	SV-105-110.3
Borehole Number	105C	105C	105C
Core Run Number	6	7	7
Depth (ft.)	103.7	108.3	110.3
Initial Water Content (%)	5.1	8.2	7.5
Total Unit Weight (pcf)	147	141	143
Undrained Compressive Strength (ksf)	135.1	58	58
Young's Modulus (ksf)	6452.2	6218.6	3224.9
Recovery (%)	100	97	97
Rock Quality Designation (%)	91	59	59
Sample Description	Gray Shale	Gray Sandy Shale	Gray Sandy Shale

Specimen Identification	SV-106-58.3	SV-106-63	SV-106-75.5
Borehole Number	106C	106C	106C
Core Run Number	2	2	5
Depth (ft.)	58.3	63	75.5
Initial Water Content (%)	12.9	12	9.2
Total Unit Weight (pcf)	130.4	134.7	143
Undrained Compressive Strength (ksf)	17.4	20.1	35.4
Young's Modulus (ksf)	311.6	239.3	1456.9
Recovery (%)	83	88	89
Rock Quality Designation (%)	60	80	76
Sample Description	Gray Shale (Argillaceous)	Gray Shale (Argillaceous)	Gray Shale (Argillaceous but Slightly Sandy)

Specimen Identification	SV-106-76.8	SV-106-77.5	SV-106-78
Borehole Number	106C	106C	106C
Core Run Number	5	5	5
Depth (ft.)	76.8	77.5	78
Initial Water Content (%)	12.2	12.5	12.0
Total Unit Weight (pcf)	127.6	136	137.4
Undrained Compressive Strength (ksf)	32.3	15.9	15.9
Young's Modulus (ksf)	1508.2	590.7	595
Recovery (%)	89	89	89
Rock Quality Designation (%)	76	76	76
Sample Description	Gray Shale (Argillaceous but Slightly Sandy)	Gray Shale (Argillaceous but Slightly Sandy)	Gray Shale (Argillaceous but Slightly Sandy)

Specimen Identification	SV-106-78.5	SV-106-88.5	SV-106-89.5
Borehole Number	106C	106C	106C
Core Run Number	5	7	7
Depth (ft.)	78.5	88.5	89.5
Initial Water Content (%)	12.9	11.7	13.0
Total Unit Weight (pcf)	135.4	134.7	138
Undrained Compressive Strength (ksf)	11.4	5.3	5.6
Young's Modulus (ksf)	485.4	411.6	652.1
Recovery (%)	89	98	98
Rock Quality Designation (%)	76	74	74
Sample Description	Gray Shale (Argillaceous but Slightly Sandy)	Soft Gray Clay Shale	Soft Gray Clay Shale

Specimen Identification	SV-106-89.7	SV-106-96	SV-106-99.8
Borehole Number	106C	106C	106C
Core Run Number	7	8	8
Depth (ft.)	135.6	140.8	140.9
Initial Water Content (%)	9.7	7.4	6.7
Total Unit Weight (pcf)	135.6	140.8	140.9
Undrained Compressive Strength (ksf)	5.4	17.6	48.9
Young's Modulus (ksf)	652	703	1696
Recovery (%)	98	99	99
Rock Quality Designation (%)	74	92	92
Sample Description	Soft Gray Clay Shale	Dense Gray Sandy Silty Shale	Dense Gray Sandy Silty Shale

Specimen Identification	SV-106-100.8	SV-106-101.5	SV-106-104.5
Borehole Number	106C	106C	106C
Core Run Number	8	8	8
Depth (ft.)	100.8	101.5	104.5
Initial Water Content (%)	6.7	8.1	8.5
Total Unit Weight (pcf)	139.5	140.2	142.2
Undrained Compressive Strength (ksf)	32.1	39.1	44.4
Young's Modulus (ksf)	1319.9	845.1	1798.4
Recovery (%)	99	99	99
Rock Quality Designation (%)	92	92	92
Sample Description	Soft Gray Clay Shale	Dense Gray Sandy Silty Shale	Dense Gray Sandy Silty Shale

Specimen Identification	SV-107-68.5	SV-107-103.5	SV-107-113.5
Borehole Number	107C	107C	107C
Core Run Number	2	7	9
Depth (ft.)	68.5	103.5	113.5
Initial Water Content (%)	9.2	6.6	6.7
Total Unit Weight (pcf)	-	-	-
Undrained Compressive Strength (ksf)	27.2	116.7	98.1
Young's Modulus (ksf)	645.5	4679.4	4927.8
Recovery (%)	92	100	100
Rock Quality Designation (%)	62	100	75
Sample Description	Dark Gray Very Dense Weathered Shale	Very Dense Gray Slightly Micaceous Shale	Very Dense Gray Shale

Specimen Identification	SV-03-58.8	SV-03-59.6	SV-03-60
Borehole Number	03C	03C	03C
Core Run Number	1	1	1
Depth (ft.)	58.8	59.6	60
Initial Water Content (%)	11.1	10.6	11.1
Total Unit Weight (pcf)	135.3	139.7	139.6
Undrained Compressive Strength (ksf)	21.4	48	28
Young's Modulus (ksf)	463	520.1	451.5
Recovery (%)	98	98	98
Rock Quality Designation (%)	95	95	95
Sample Description	Gray Thinly Bedded Argillaceous Shale	Gray Thinly Bedded Argillaceous Shale	Gray Thinly Bedded Argillaceous Shale

Specimen Identification	SV-03-61.6	SV-03-62.5	SV-03-63.3
Borehole Number	03C	03C	03C
Core Run Number	1	1	2
Depth (ft.)	58.8	59.6	60
Initial Water Content (%)	11.7	-	10.9
Total Unit Weight (pcf)	134.1	134.4	137.4
Undrained Compressive Strength (ksf)	22.4	20	26.2
Young's Modulus (ksf)	361.1	293.3	434.2
Recovery (%)	98	98	100
Rock Quality Designation (%)	95	95	100
Sample Description	Gray Shale	Gray Shale	Gray Thinly Bedded Argillaceous Shale

Specimen Identification	SV-03-64.2	SV-03-64.6	SV-03-65.6
Borehole Number	03C	03C	03C
Core Run Number	2	2	2
Depth (ft.)	64.2	64.6	65.6
Initial Water Content (%)	12.4	12.5	12.2
Total Unit Weight (pcf)	-	134.8	134.2
Undrained Compressive Strength (ksf)	-	21.8	18.75
Young's Modulus (ksf)	-	457	438.1
Recovery (%)	100	100	100
Rock Quality Designation (%)	100	100	100
Sample Description	Gray Thinly Bedded Argillaceous Shale	Gray Thinly Bedded Argillaceous Shale	Gray Thinly Bedded Argillaceous Shale

Specimen Identification	SV-03-66	SV-03-66.8	SV-03-67.3
Borehole Number	03C	03C	03C
Core Run Number	2	2	2
Depth (ft.)	66.0	66.8	67.3
Initial Water Content (%)	12.3	12.6	12.9
Total Unit Weight (pcf)	134.6	-	131.0
Undrained Compressive Strength (ksf)	26.6	-	24
Young's Modulus (ksf)	488.2	-	443.9
Recovery (%)	100	100	100
Rock Quality Designation (%)	100	100	100
Sample Description	Gray Thinly Bedded Argillaceous Shale	Gray Thinly Bedded Argillaceous Shale	Gray Thinly Bedded Argillaceous Shale

Specimen Identification	SV-03-68	SV-03-68.3	SV-03-70.2
Borehole Number	03C	03C	03C
Core Run Number	2	3	3
Depth (ft.)	68	68.3	70.2
Initial Water Content (%)	11	7.3	7.1
Total Unit Weight (pcf)	138.3	144.4	142.5
Undrained Compressive Strength (ksf)	31	87.2	115.4
Young's Modulus (ksf)	968	2388.4	2725.5
Recovery (%)	100	98	98
Rock Quality Designation (%)	100	83	83
Sample Description	Gray Thinly Bedded Argillaceous Shale	Dark Gray Calcareous Shale with Minor Pyrite Inclusions	Dark Gray Calcareous Shale with Minor Pyrite Inclusions

Specimen Identification	SV-03-71	SV-03-71.4	SV-03-74.5
Borehole Number	03C	03C	03C
Core Run Number	3	3	4
Depth (ft.)	71	71.4	74.5
Initial Water Content (%)	7.8	7.8	7.7
Total Unit Weight (pcf)	143.2	141.5	147.1
Undrained Compressive Strength (ksf)	81.6	72	-
Young's Modulus (ksf)	2372.2	2021	-
Recovery (%)	98	98	95
Rock Quality Designation (%)	83	83	70
Sample Description	Gray Thinly Bedded Argillaceous Shale	Dark Gray Calcareous Shale with Minor Pyrite Inclusions	Dark Gray Calcareous Shale with Minor Pyrite Inclusions

Specimen Identification	SV-03-75.3	SV-03-76	SV-03-77.2
Borehole Number	03C	03C	03C
Core Run Number	4	4	4
Depth (ft.)	75.3	76.0	77.2
Initial Water Content (%)	7.5	6.0	7.1
Total Unit Weight (pcf)	147.1	144.7	142.2
Undrained Compressive Strength (ksf)	104	101.8	116.2
Young's Modulus (ksf)	2462.3	2682.8	3108.5
Recovery (%)	95	95	95
Rock Quality Designation (%)	70	70	70
Sample Description	Dark Gray Calcareous Shale with Minor Pyrite Inclusions	Dark Gray Calcareous Shale with Minor Pyrite Inclusions	Dark Gray Calcareous Shale with Minor Pyrite Inclusions

APPENDIX D FIELD EXPLORATION AT TR 325 OVER THE ELM CREEK

D.1 BACKGROUND

Figure D.1 shows location of TR 325 over the Elm creek, located in Clay County, just North the city of Flora, Illinois. This single span bridge structure carries a two-lane highway over the Elm creek. The weak shales near the south abutment, was investigated during this study.

Figure D.1 Location of TR 325 over the Elm creek.

Two borings were advanced near south abutment on 16 September 2014 by District 7 drilling crew. These borings were drilled to an elevation of 441.0 feet.

The first boring was used to obtain shale core samples. Initially rock cores were used for determination of recovery ratio, RQD of the rock mass, and vertical spacing of joints. Afterwards unconfined compression tests were conducted on the retrieved weak shales specimens. The in situ water content of the shale specimens used in the unconfined compression tests was also measured for correlation purposes. The unconfined compression test results were also used to determine the deformability characteristics of shale under undrained loading conditions.

The second boring was used to obtain MSPT blow counts at various depths. These data were used to improve/check the correlation between undrained compressive strength of weak shale in Illinois and MSPT penetration rates developed in Phase of this study. The following sections discuss geology of the bridge site, MSPT test results, and laboratory test results

D.2 SITE GEOLOGY

The geology at the bridge site consists of about 22 feet of soft silty clay and clay till, overlying sedimentary bedrock, e.g., shale, and sandstone. The ground surface elevation at the two borings, is about 481.0 feet. A fairly continuous layer of thinly bedded clay shale was exposed at an elevation of 459 feet and extended to elevation of 441 feet where coring was terminated. Laboratory test results are summarized in Table D.1.

D.3 MODIFED STANDARD PENETRATION TEST RESULTS

Figure D.2 shows the Modified Standard Penetration Test results obtained in one of the borings at TR 325 over the Elm creek.

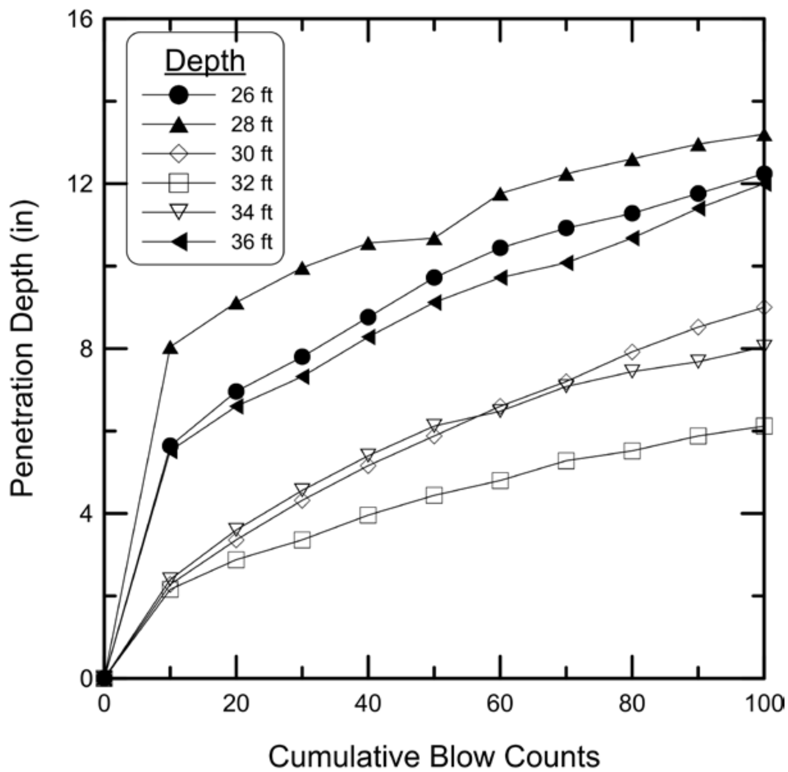

Figure D.2 Modified Standard Penetration Test results.

D.4 LABORATORY TEST RESULTS

D.4.1 Moisture Content and Total Unit Weight

Figure D.3 shows the total unit weight profile at the TR 325 over the Elm creek site. The total unit weight of the encountered shales was computed in accordance with ASTM D7263. Shale specimens from unconfined compressive tests were used for determination of in situ water content. The resulting water content profile is shown in Figure D.4. Water content of the Shales was determined in accordance with ASTM D2216.

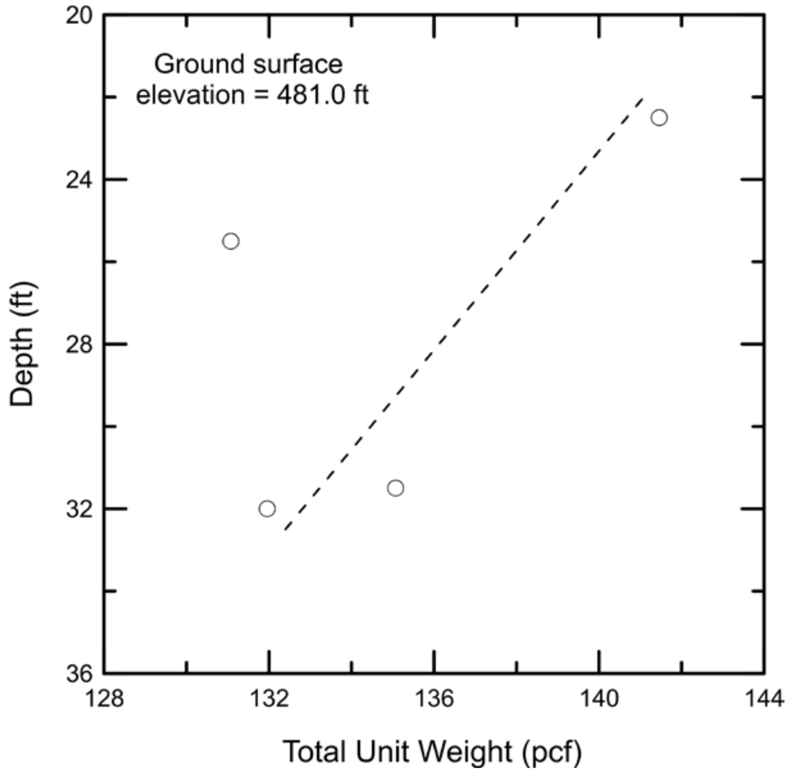

Figure D.3 Total unit weight profile.

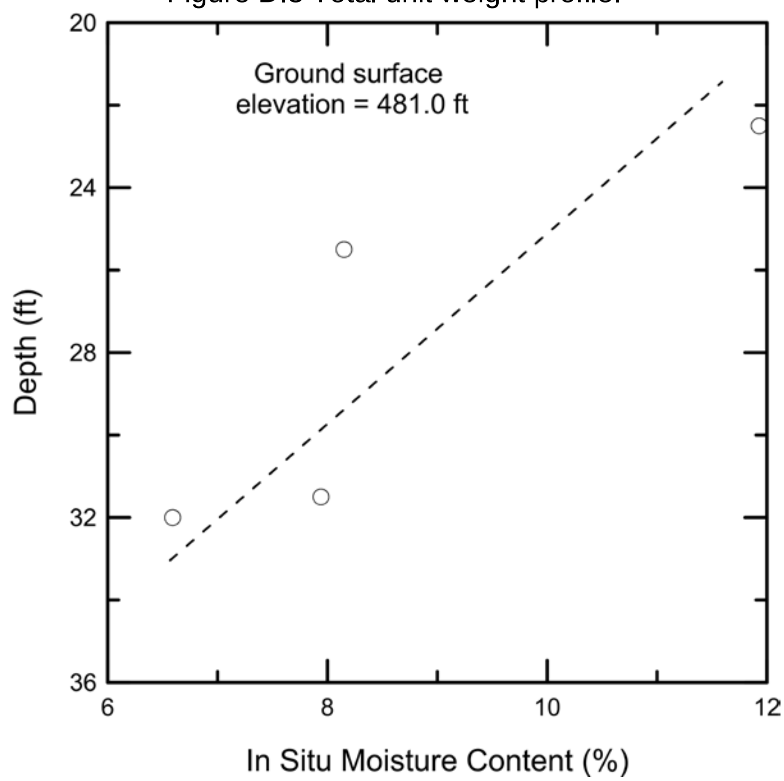

Figure D.4 In situ moisture content profile.

D.4.2 Triaxial Compression Test Results

Unconfined triaxial compression tests were performed in accordance with ASTM D7012–14 (method D). The peak deviator stress was used to calculate the undrained compressive strength for each test. The resulting undrained compressive strengths are shown in Table D.1.

D.4.3 Young's Modulus of Shale Specimen

Young's modulus was measured from results of triaxial tests in accordance to ASTM D7012–14 (method D). In short, the modulus was calculated from the slope of the stress-strain relationships that correspond to 50% of mobilized undrained compressive strength. Figure D.5 shows the relationship between Young's modulus and undrained compressive strength for the shales core tested from the TR325 over the Elm creek site. This data was also used to develop a relationship between Young's modulus and natural water content (see Figure D.6). Table D.1 summarizes all of the data obtained from the laboratory testing and evaluation.

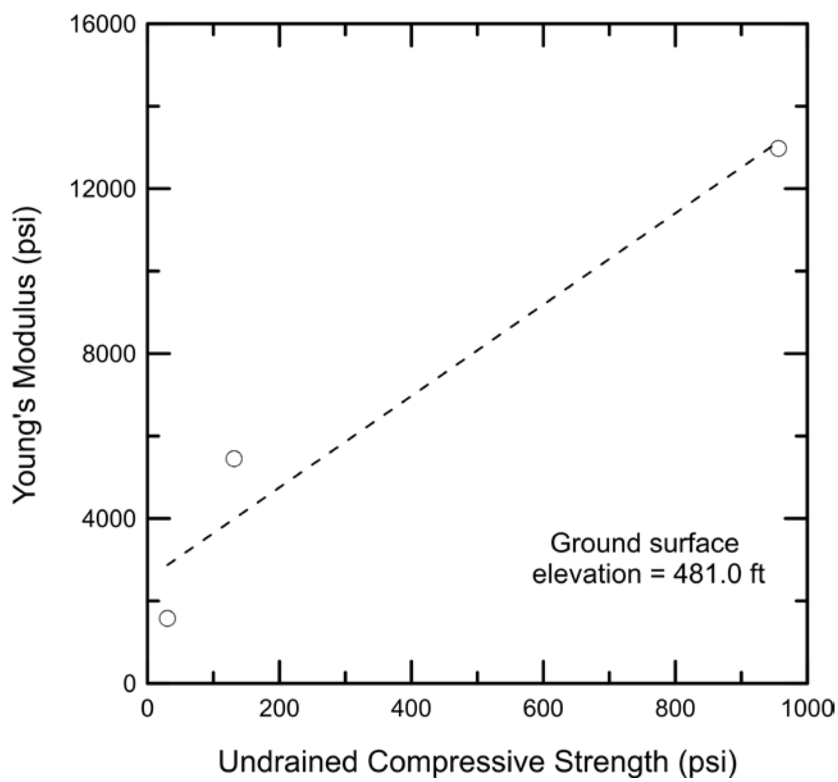

Figure D.5 Relationship between undrained compressive strength and Young's modulus.

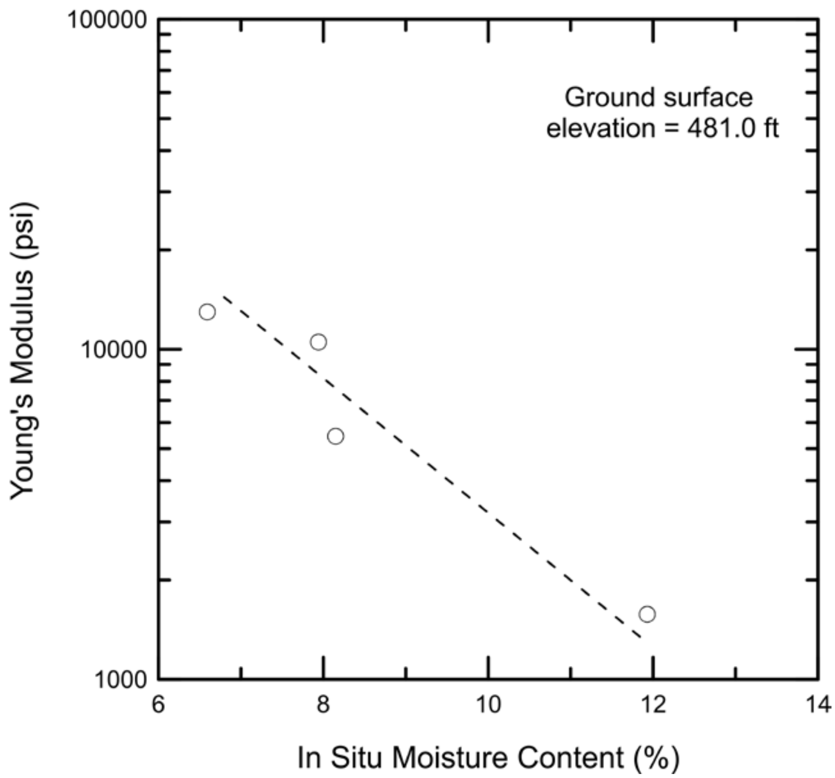

Figure D.6 Relationship between in situ moisture content and Young's modulus.

Table D.1 Laboratory Data Summary at the TR 325 over the Elm creek

Specimen Identification	EC-S1	EC -S2	EC -S3
Core Run Number	**1**	**1**	**2**
Depth (ft.)	22.5	25.5	31.5
Initial Water Content (%)	11.93	8.15	7.94
Total Unit Weight (pcf)	141.5	131.1	135.0
Undrained Compressive Strength (ksf)	4.35	18.9	137.7
Strain at Peak Strength (%)	4.84	3.35	7.94
Young's Modulus (ksf)	226.6	784.5	1514.7
Recovery (%)	68	87	100
Rock Quality Designation (%)	35	40	61
Joint Average Vertical Spacing (in)	1 to 2	1 to 2	1 to 2
Sample Description	Clay Shales Tan, thinly bedded, fissile sandy	Clay Shales Gray, thinly bedded, fissile, sandy	Clay Shales Gray, thinly bedded, fissile, sandy

Specimen Identification	EC -S4		
Core Run Number	**2**		
Depth (ft.)	32.0		
Initial Water Content (%)	6.59		
Total Unit Weight (pcf)	131.95		
Undrained Compressive Strength (ksf)	164.5		
Strain at Peak Strength (%)	4.6		
Young's Modulus (ksf)	1898.8		
Recovery (%)	100		
Rock Quality Designation (%)	61		
Joint Average Vertical Spacing (in)	1 to 2		
Sample Description	Clay Shales Gray, thinly bedded, fissile, sandy		

APPENDIX E FIELD EXPLORATION AT TR 355 OVER THE SEMINARY CREEK

E.1 BACKGROUND

Figure E.1 shows location of TR 355 over the Seminary creek, located in Clay County, just South the city of Flora, Illinois. This single span bridge structure carries a two-lane highway over the Seminary creek. The weak shales near the south abutment, was investigated during this study.

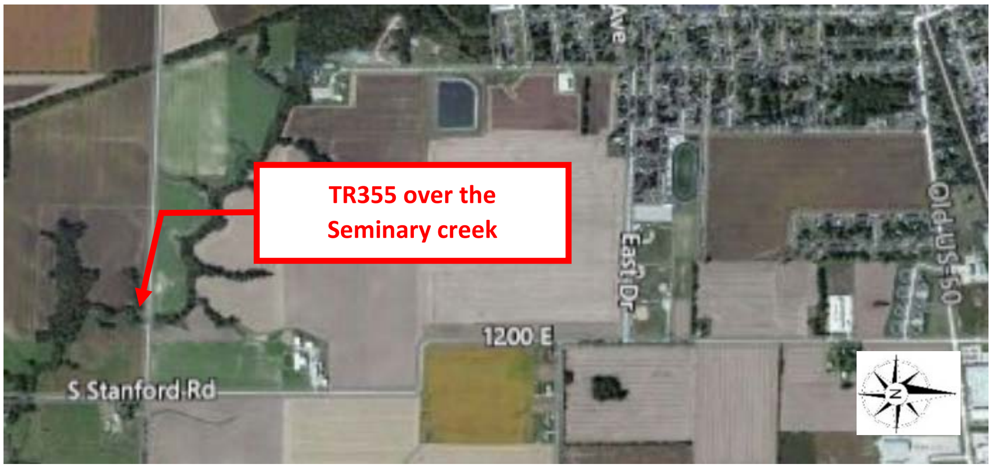

Figure E.1 Location of TR 355 over the Seminary creek.

Figure E.2 Location of boring holes at TR 355 over the Seminary creek.

Figure E.2 shows a plan view of TR 355 over the Seminary creek bridge and the location of borings drilled on September,15 2014 by District 7 drilling crew and the UIUC research team. Two borings were advanced near west abutment. These borings were drilled to an elevation of 432.0 feet.

The first boring was used to obtain shale core samples. Initially rock cores were used for determination of recovery ratio, RQD of the rock mass, and vertical spacing of joints. Afterwards unconfined compression tests were conducted on the retrieved weak shales specimens. The in situ water content of the shale specimens used in the unconfined compression tests was also measured for correlation purposes. The unconfined compression test results were also used to determine the deformability characteristics of shale under undrained loading conditions.

The second boring was used to obtain MSPT blow counts at various depths. These data were used to improve/check the correlation between undrained compressive strength of weak shale in Illinois and MSPT penetration rates developed in Phase 1 of this study. The following sections discuss geology of the bridge site, MSPT test results, and laboratory test results

E.2 SITE GEOLOGY

The geology at the bridge site consists of about 10 feet of soft silty clay loam, overlying sedimentary bedrock, e.g., shale, and sandstone. The ground surface elevation at the two borings, is about 457.0 feet. A fairly continuous layer of thinly bedded sandy clay shale was exposed at an elevation of 447 feet and extended to elevation of 434 feet. A sandstone layer underlies this layer. Coring was terminated at elevation of 432.0 feet, i.e., 2.0 feet into the sandstone. Laboratory test results are summarized in Table E.1.

E.3 MODIFED STANDARD PENETRATION TEST RESULTS

Figure E.3 shows the Modified Standard Penetration Test results obtained in one of the borings at TR 355 over the Seminary creek.

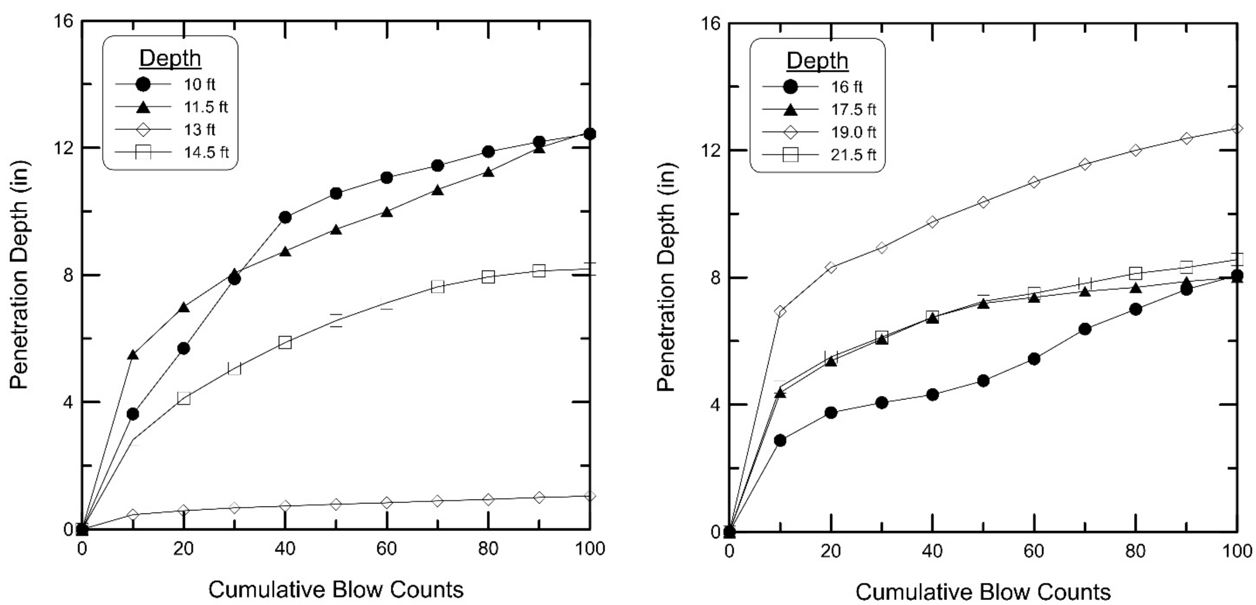

Figure E.3 Modified Standard Penetration Test results.

E.4 LABORATORY TEST RESULTS

E.4.1 Moisture Content and Total Unit Weight

Figure E.5 shows the total unit weight profile at the TR 355 over the Seminary creek site. The total unit weight of the encountered shales was computed in accordance with ASTM D7263. Shale specimens from unconfined compressive tests were used for determination of in situ water content. The resulting water content profile is shown in Figure E.6. Water content of the Shales was determined in accordance with ASTM D2216.

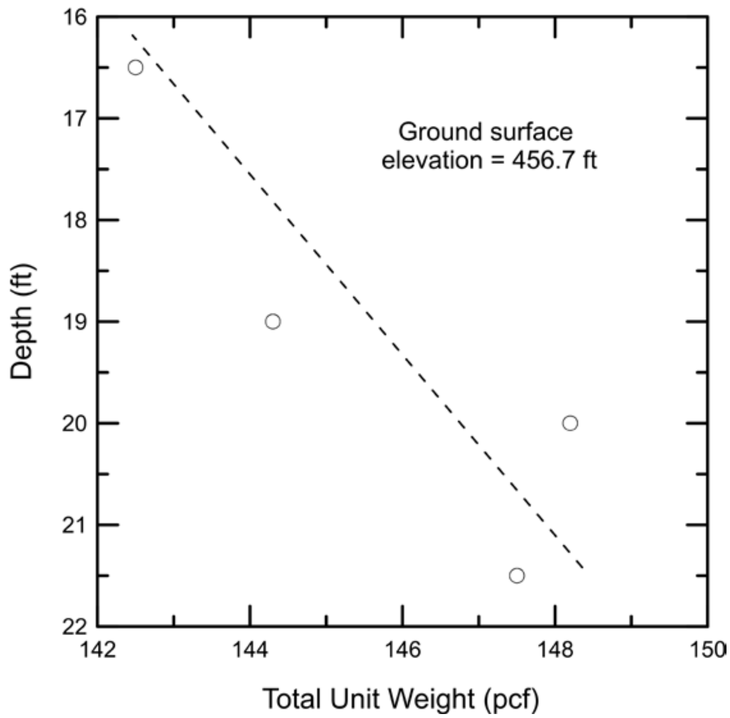

Figure E.*4 Total unit weight profile.*

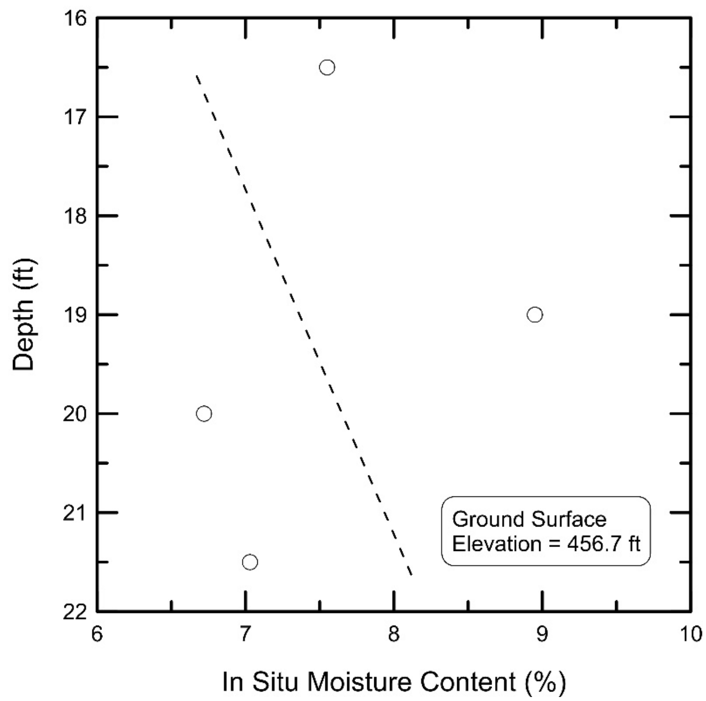

Figure E.5 In situ moisture content profile.

E.4.2 Triaxial Compression Test Results

Unconfined triaxial compression tests were performed in accordance with ASTM D7012–14 (method D). The peak deviator stress was used to calculate the undrained compressive strength for each test. The resulting undrained compressive strengths are shown in Table E.1.

E.4.3 Young's Modulus of Shale Specimen

Young's modulus was measured from results of triaxial tests in accordance to ASTM D7012–14 (method D). In short, the modulus was calculated from the slope of the stress-strain relationships that correspond to 50% of mobilized undrained compressive strength. Figure E.7 shows the relationship between Young's modulus and undrained compressive strength for the shales core tested from the TR355 over the Seminary creek site. This data was also used to develop a relationship between Young's modulus and natural water content (see Figure E.8). Table E.1 summarizes all of the data obtained from the laboratory testing and evaluation.

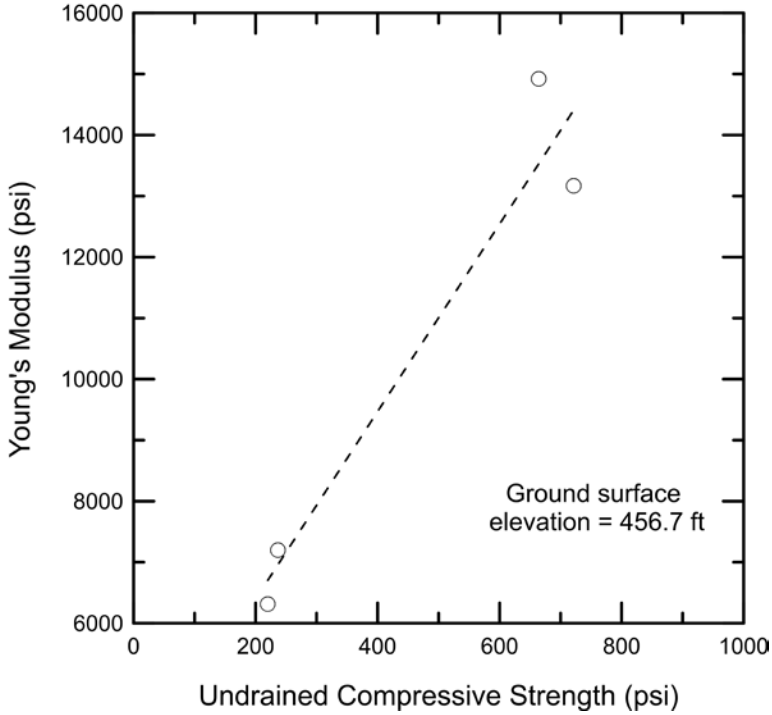

Figure E.6 Relationship between undrained compressive strength and Young's modulus.

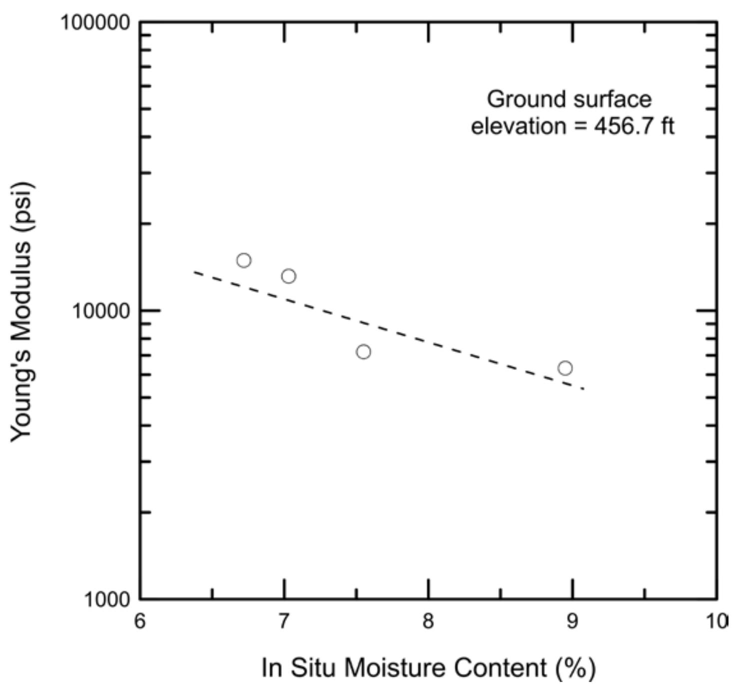

Figure E.7 Relationship between in situ moisture content and Young's modulus.

Table E.1 Laboratory Data Summary at the TR 355 over the Seminary creek

Specimen Identification	TSC-S1	TSC -S2	TSC -S3
Core Run Number	**2**	**2**	**2**
Depth (ft.)	16.5	19.0	20.0
Initial Water Content (%)	7.55	8.95	6.72
Total Unit Weight (pcf)	142.5	144.3	148.2
Undrained Compressive Strength (ksf)	34.1	31.7	95.7
Strain at Peak Strength (%)	6.59	5.48	5.07
Young's Modulus (ksf)	2957.0	966.1	2148
Recovery (%)	100	100	100
Rock Quality Designation (%)	100	100	100
Joint Average Vertical Spacing (in)	1 to 2	1 to 2	1 to 2
Sample Description	Clay Shales Tan, thinly bedded, fissile sandy	Clay Shales Gray, thinly bedded, fissile, sandy	Clay Shales Gray, thinly bedded, fissile, sandy

Specimen Identification	TSC -S4		
Core Run Number	**3**		
Depth (ft.)	21.5		
Initial Water Content (%)	7.0		
Total Unit Weight (pcf)	147.5		
Undrained Compressive Strength (ksf)	103.95		
Strain at Peak Strength (%)	5.03		
Young's Modulus (ksf)	1895.9		
Recovery (%)	100		
Rock Quality Designation (%)	98		
Joint Average Vertical Spacing (in)	1 to 2		
Sample Description	Clay Shales Gray, thinly bedded, fissile, sandy		

APPENDIX F FIELD EXPLORATION AT IL 23 OVER THE OTTER CREEK

F.1 BACKGROUND

Figure F.1 shows location of IL 23 over Otter Creek, located in LaSalle County, just north the city of Streator, Illinois. This three-span bridge structure carries a four-lane highway over the Otter Creek. North and South abutments of this bridge are supported on driven H-piles foundations. Piers 1 and 2, however, are supported by shallow foundations. The Mudstones near the south abutment, was investigated during this study.

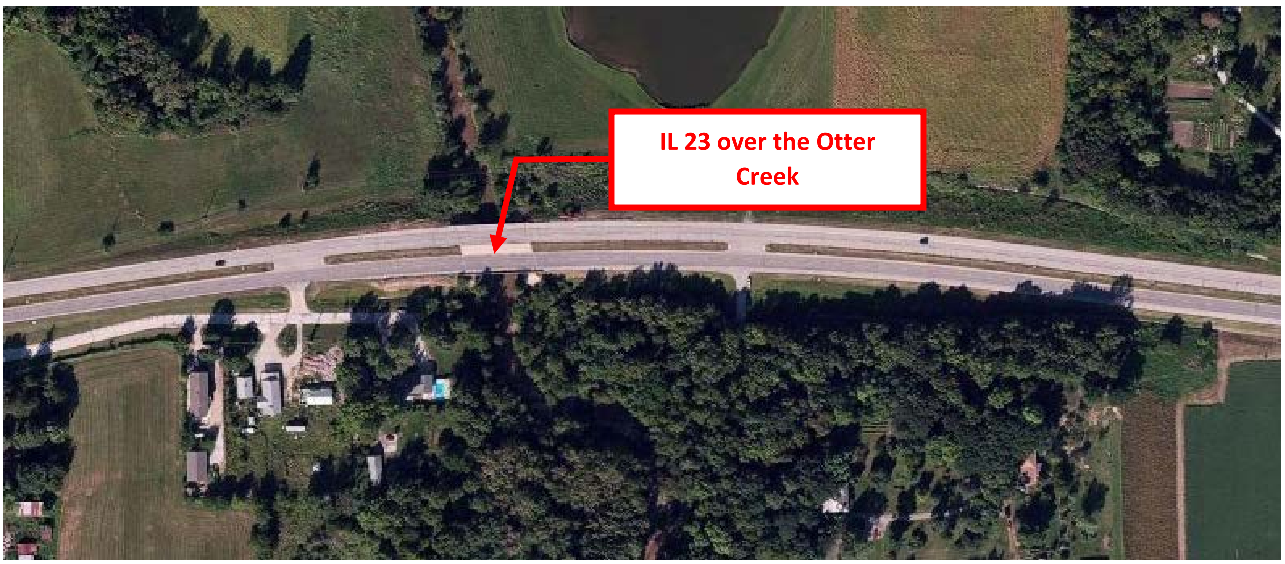

Figure F.1 Location of IL 23 over Otter Creek.

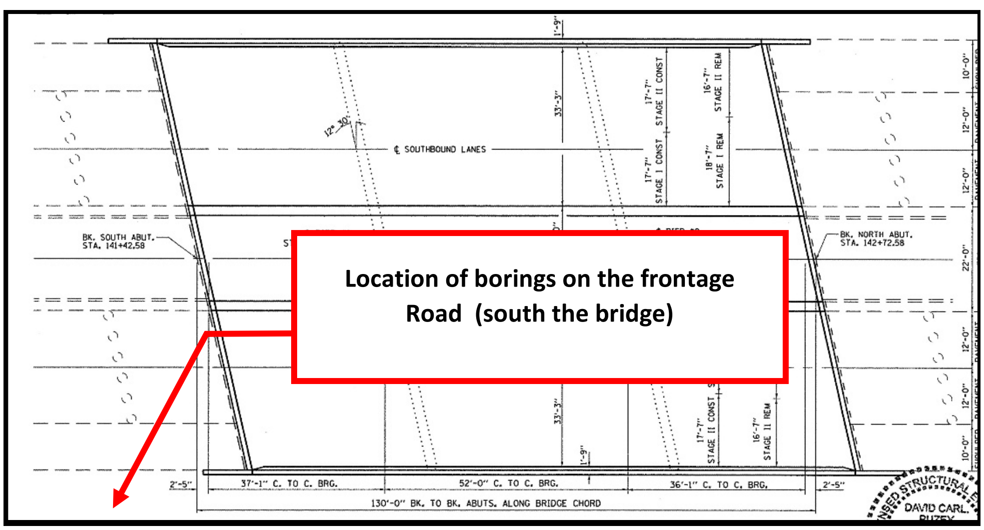

Figure F.2 Location of boring holes at IL 23 over Otter Creek.

Figure F.2 shows a plan view of IL 23 over Otter Creek structure and the location of borings drilled on October 28, 2014 by the District 3 drilling crew and the UIUC research team. Two borings were advanced on the frontage road (south the bridge). These borings were drilled to an elevation of 562.2 feet.

One of the two borings was used to obtain core samples. Initially rock cores were used for determination of recovery ratio, RQD of the rock mass, and vertical spacing of joints. Afterwards unconfined compression tests were conducted on the retrieved mudstones specimens. The in situ water content of the specimens used in the unconfined compression test was also measured for correlation purposes. The unconfined compression test results were also used to determine the deformability characteristics of the weak rock under undrained loading conditions.

The second boring was used to obtain MSPT blow counts at various depths. This data was used to check the applicability of the proposed correlation between undrained compressive strength in Illinois and MSPT penetration rate to mudstones. The following sections discuss geology of the bridge site, MSPT test results, and laboratory test results

F.2 SITE GEOLOGY

The geology at the bridge site consists of about 25 feet of weak overburden soils overlying sedimentary bedrock, e.g., mudstones and limestone. The ground surface elevation at south abutment, i.e., the two borings, is about 595.4 feet. Micaceous Mudstone was exposed at an elevation of 570.4 feet and extended till the end of the borehole. Laboratory test results are summarized in Table F.1.

F.3 MODIFED STANDARD PENETRATION TEST RESULTS

Figure F.3 shows the Modified Standard Penetration Test results obtained in one of the borings at IL 23 over the Otter Creek.

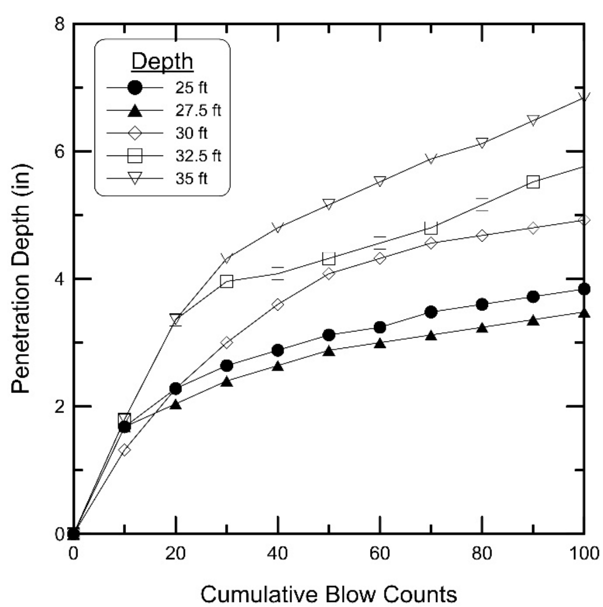

Figure F.3 Modified Standard Penetration Test results.

F.4 LABORATORY TEST RESULTS

F.4.1 Moisture Content and Total Unit Weight

Figure F.4 shows the total unit weight profile at the IL23 over the Otter Creek site. The total unit weight of the encountered sedimentary rock was computed in accordance with ASTM D7263.

Mudstone specimens from unconfined compressive tests were used for determination of in situ water content. The resulting water content profile is shown in Figure F.5. Water content of the Mudstones was determined in accordance with ASTM D2216.

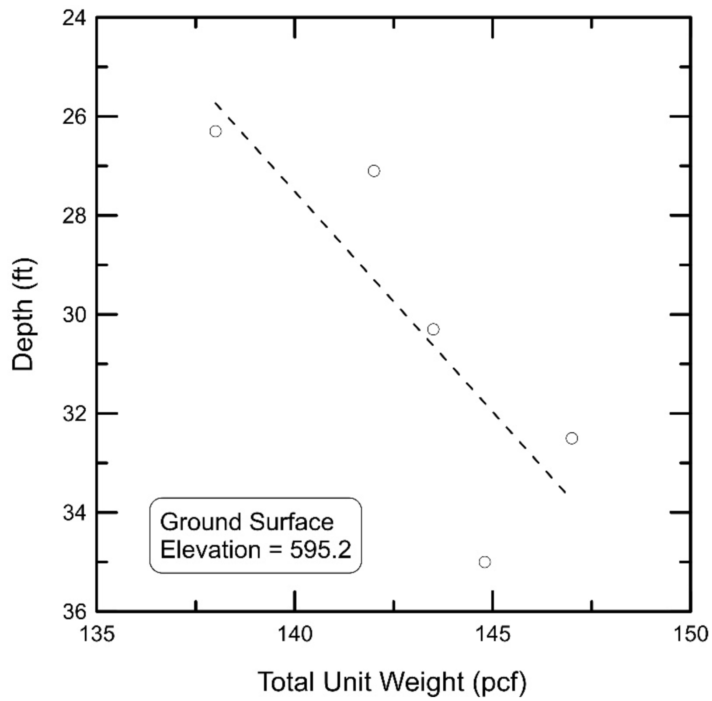

Figure F.4 Total unit weight profile.

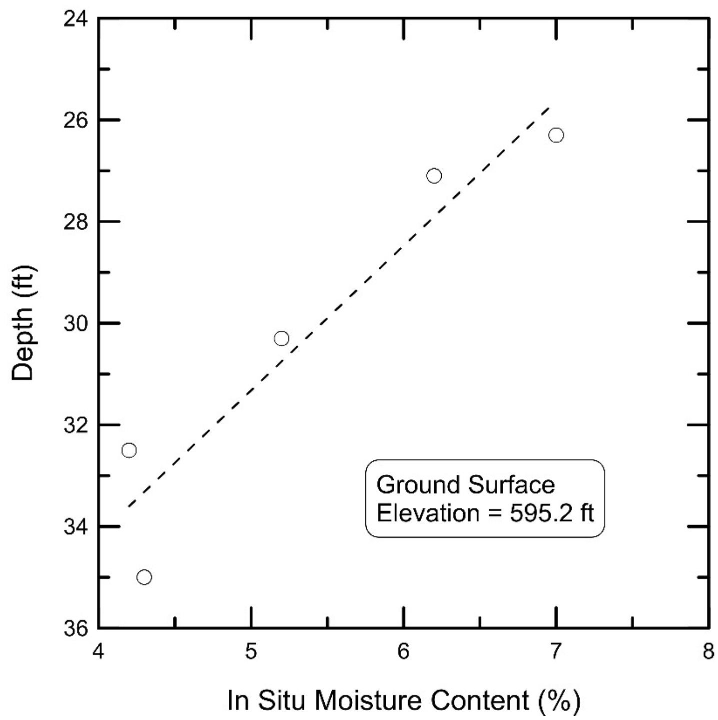

Figure F.5 In situ moisture content profile.

F.4.2 Triaxial Compression Test Results

Unconfined triaxial compression tests were performed in accordance with ASTM D7012–14 (method D). The peak deviator stress was used to calculate the undrained compressive strength for each test. The resulting undrained compressive strengths are shown in Table F.1.

F.4.3 Young's Modulus of Mudstone Specimen

Young's modulus was measured from results of triaxial tests in accordance to ASTM D7012–14 (method D). In short, the modulus was calculated from the slope of the stress-strain relationships that correspond to 50% of mobilized undrained compressive strength. Figure F.6 shows the relationship between Young's modulus and undrained compressive strength for the mudstones core tested from the IL 23 over the Otter Creek site. This data was also used to develop a relationship between Young's modulus and natural water content (see Figure F.7). Table F.1 summarizes all of the data obtained from the laboratory testing and evaluation.

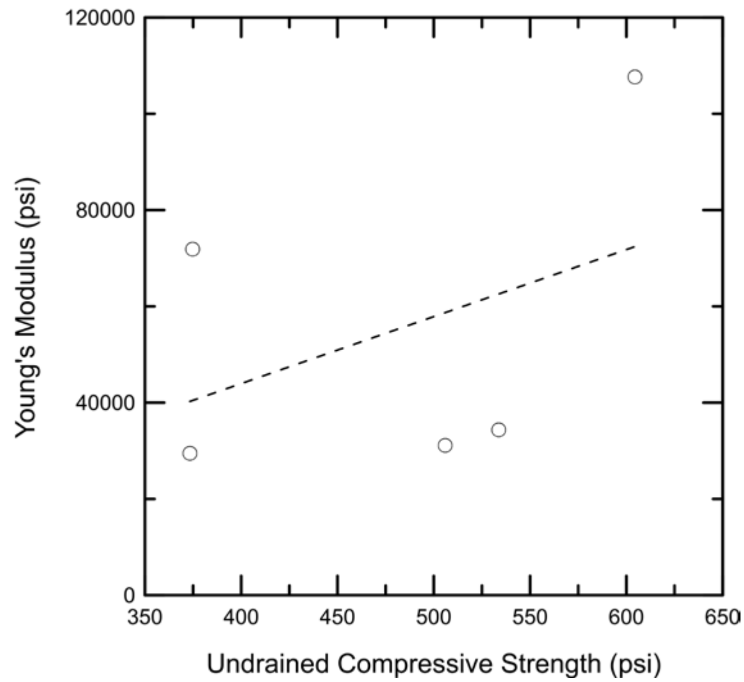

Figure F.6 Relationship between undrained compressive strength and Young's modulus.

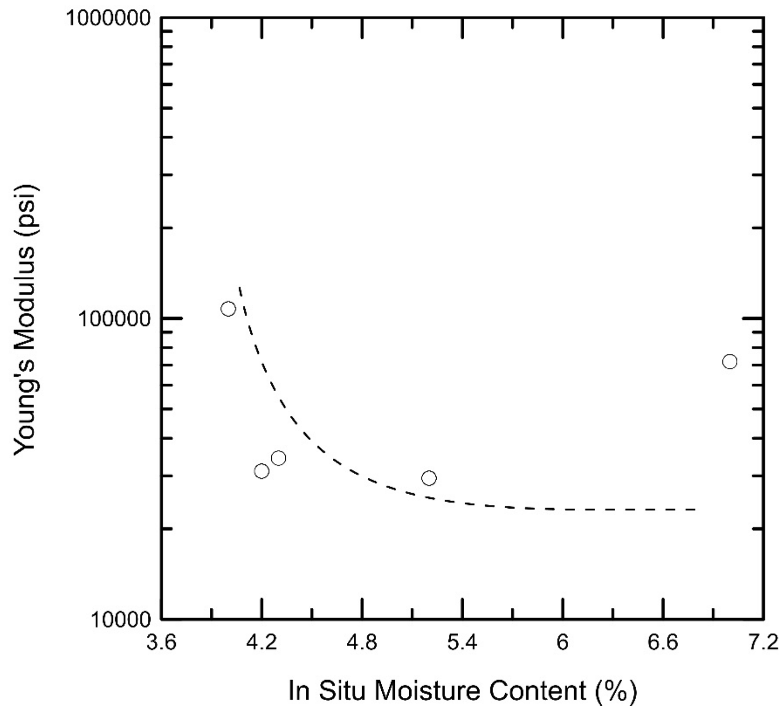

Figure F.7 Relationship between in situ moisture content and Young's modulus.

Table F.1 Laboratory Data Summary at the IL 23 over the Otter Creek

Specimen Identification	**OT-S1**	**OT-S2**	**OT-S3**
Core Run Number	**1**	**1**	**1**
Depth (ft.)	26.3	27.1	30.3
Initial Water Content (%)	7.0	4.0	5.2
Total Unit Weight (pcf)	138	142	143.5
Undrained Compressive Strength (ksf)	54.0	87.1	53.8
Strain at Peak Strength (%)	1.93	1.79	2.54
Young's Modulus (ksf)	10353.8	15509.8	4244.6
Recovery (%)	68	68	68
Rock Quality Designation (%)	57	57	57
Joint Average Vertical Spacing (in)	2 to 7	2 to 7	2 to 7
Sample Description	Gray Micaceous Mudstone with Limestone stringers	Gray Micaceous Mudstone with Limestone stringers	Gray Micaceous Mudstone with Limestone stringers

Specimen Identification	**OT-S4**	**OT-S5**	
Core Run Number	**2**	**2**	
Depth (ft.)	32.5	35.0	
Initial Water Content (%)	4.2	4.3	
Total Unit Weight (pcf)	147	144.8	
Undrained Compressive Strength (ksf)	72.9	76.9	
Strain at Peak Strength (%)	3.01	2.91	
Young's Modulus (ksf)	4480.6	4948.6	
Recovery (%)	100	100	
Rock Quality Designation (%)	72	72	
Joint Average Vertical Spacing (in)	10	10	
Sample Description	Gray Lime Mudstone with Traces of Sand and Limestone Stringers	Gray Lime Mudstone with Traces of Sand and Limestone Stringers	

APPENDIX G FIELD EXPLORATION AT IL 133 OVER THE EMBARRAS RIVER

G.1 BACKGROUND

Figure G.1 shows the proposed location of IL 133 over the Embarras River bridge site, located in Coles County, just west of Oakland, Illinois. This two-span bridge structure is designed to carry two-lane highway over the Embarras River. East and West abutments of this bridge are supported on driven H-piles foundations. The single pier is supported by drilled shaft foundations socketed into weak shales. In Phase 2 of this study, a test shaft was constructed near the pier to study the load-transfer mechanism of drilled shafts socketed into weak shales. The weak shale near the constructed test shaft was investigated during this study.

Figure G.1: Location of IL 133 over the Embarras River bridge near city of Oakland.

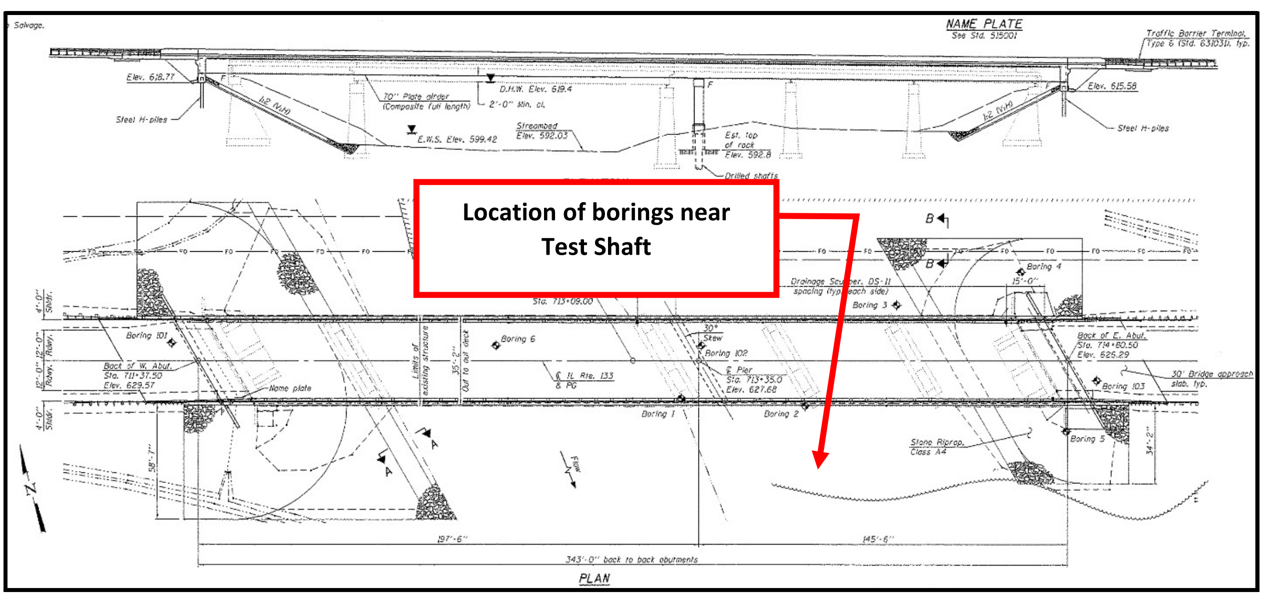

Figure G.2: Location of boring holes at IL 133 over the Embarras River.

Figure G.2 shows a plan view of IL 133 over the Embarras River bridge structure and the location of the borings drilled on May 21, 2015 and July, 22 2015 by the District 7 drilling crew and the UIUC research team. Four borings were advanced near the test shaft. The borings extended about 9.0 ft below the test shaft base (i.e. Elevation 564.1 ft).

Two of the four borings drilled were used to obtain shale core. Initially rock cores were used for determination of recovery ratio, RQD of the rock mass, and vertical spacing of joints. Afterwards unconfined compression tests were conducted on the retrieved shale specimens. The in situ water content of the shale specimens used in the triaxial compression tests was also measured for correlation purposes. Triaxial test results were also used to determine the deformability characteristics of shale under undrained loading conditions.

The other two boring were used to obtain MSPT blow counts at various depths. This data was used to improve the proposed correlation between undrained compressive strength of weak shale in Illinois and MSPT penetration rate developed in Phase 1 of this study.

The following sections discuss geology of the bridge site, MSPT test results, and laboratory test results.

G.2 SITE GEOLOGY

The geology at the bridge site consists of 11 feet of soft to stiff silty clay overlying sedimentary bedrock, e.g., shale and sandstone. The ground surface elevation at the test shaft is about 600.0 ft. Weathered gray clay shale was exposed at an elevation of about 589 feet and extend to elevation of 564.1 where the drilling was terminated. Laboratory test results are summarized in Table G.1.

G.3 MODIFIED STANDARD PENETRATION TEST RESULTS

Figure G.3 shows the Modified Standard Penetration Test results obtained in two of the four borings at IL 133 over the Embarras River.

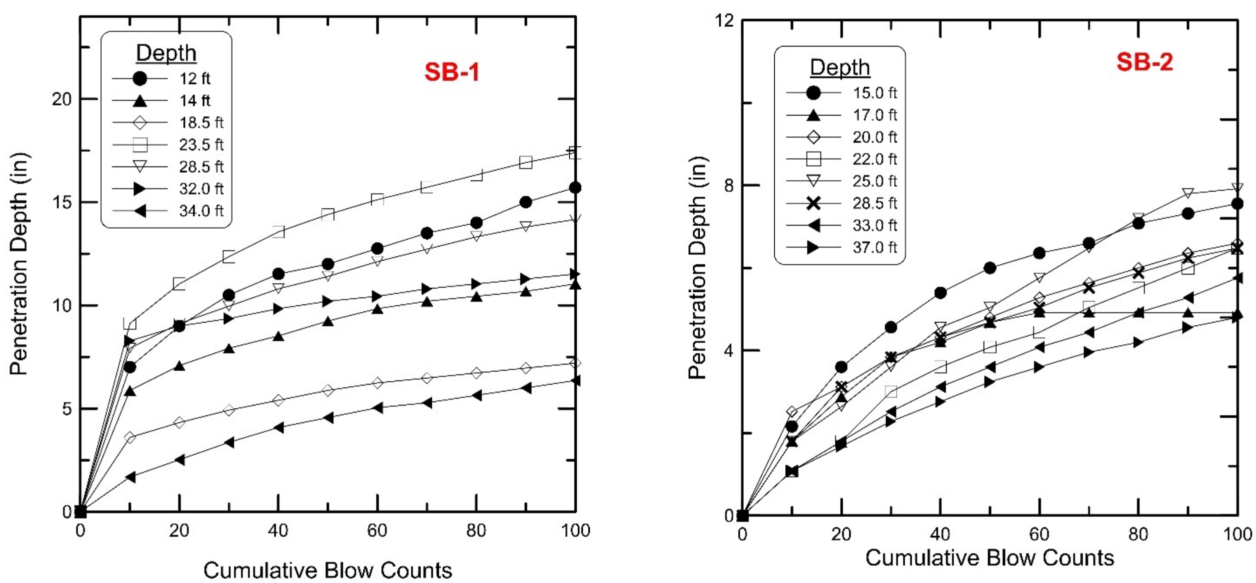

Figure G.3 Modified Standard Penetration Test results.

G.4 LABORATORY TEST RESULTS

G.4.1 Moisture Content and Total Unit Weight

Figure G.4 shows the total unit weight profile at the IL 133 over the Embarras River site. The total unit weight of shale was computed in accordance with ASTM D7263.

Shale specimens from unconsolidated undrained and unconfined compressive tests were used for determination of in situ water content. The resulting water content profile is shown in Figure G.5. Water content of the shale was determined in accordance with ASTM D2216.

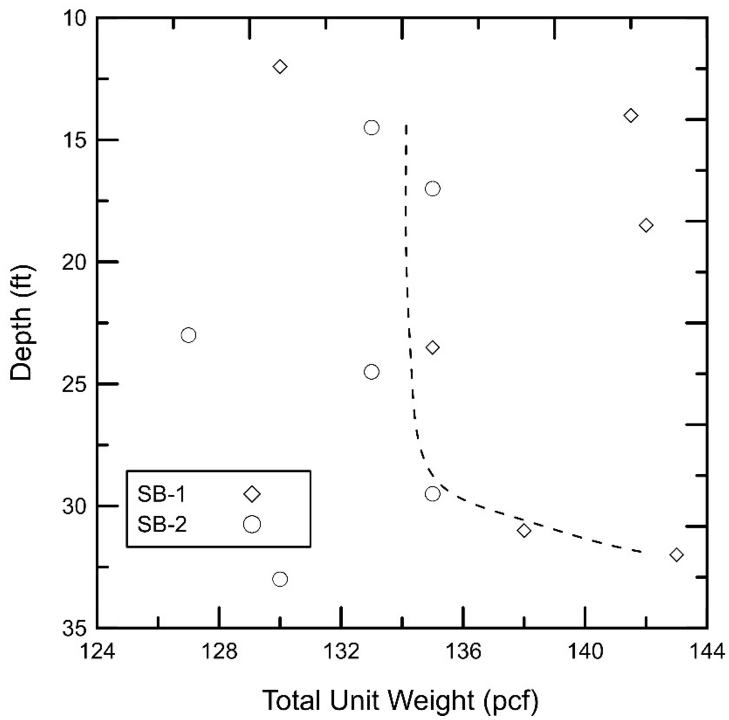

Figure G.4 Total unit weight profile.

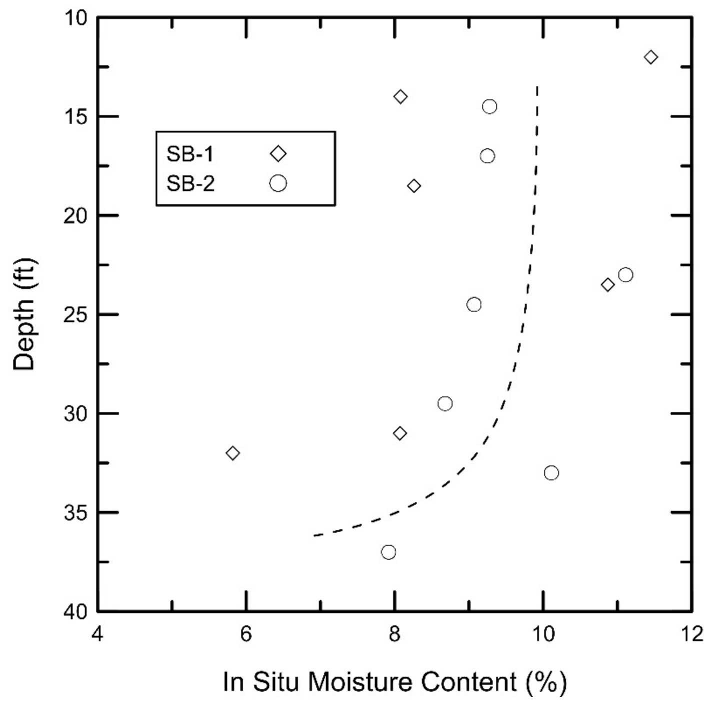

Figure G.5 In situ moisture content profile.

G.4.2 Triaxial Compression Test Results

Unconfined compression tests were performed in accordance with ASTM D7012–14 (method D). The peak deviator stress was used to calculate the undrained compressive strength for each test. The resulting undrained compressive strengths are shown in Table G.1.

G.4.3 Young's Modulus of Shale Specimen

Young's modulus was measured from results of triaxial tests in accordance to ASTM D7012–14 (method D). In short, the modulus was calculated from the slope of the stress-strain relationships that correspond to 50% of mobilized undrained compressive strength. Figure G.6 shows the relationship between Young's modulus and undrained compressive strength for the shale core tested from the IL 133 over the Embarras River site. This data was also used to develop a relationship between Young's modulus and shale natural water content (see Figure G.7). The unconfined compressive strength to the undrained Young's modulus ratio shown in Figure G.6 agrees well with the general trends observed in Phase 1 & 2 of this study. The site-specific relationship between undrained Young's modulus and the in situ water content is also shown in Figure G.7. Table G.1 summarizes all of the data obtained from the laboratory testing and evaluation.

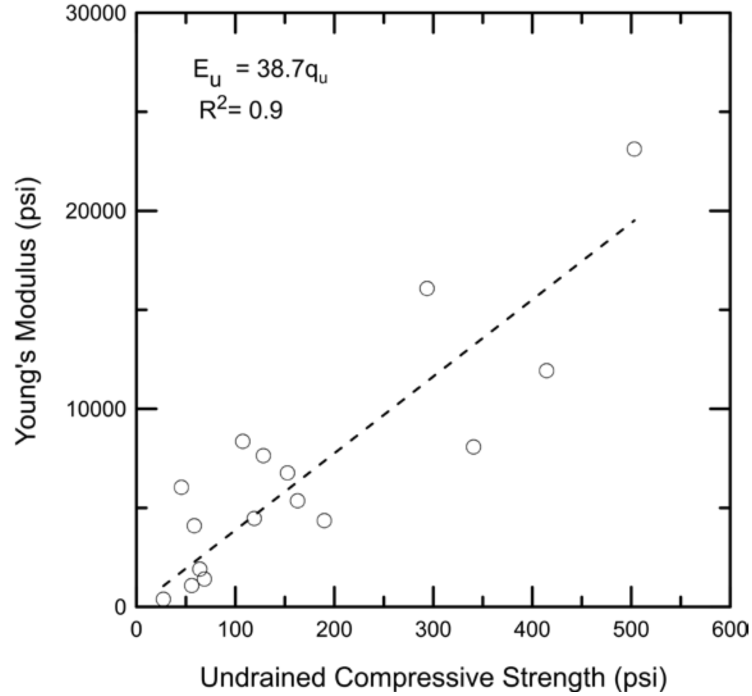

Figure G.6 Relationship between undrained compressive strength and Young's modulus.

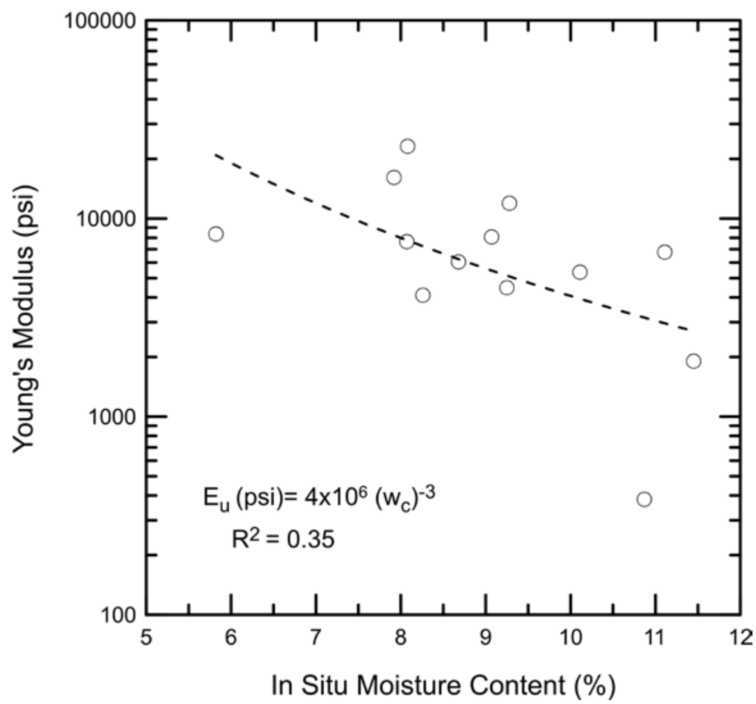

Figure G.7 Relationship between in situ moisture content and Young's modulus.

Table G.1 Laboratory Data Summary at the IL 133 over the Embarras River

Specimen Identification	**EB-B1-S1**	**EB-B1-S2**	**EB-B1-S3**
Core Run Number	**1**	**1**	**2**
Depth (ft.)	12	14	18.5
Initial Water Content (%)	11.45	8.08	8.26
Total Unit Weight (pcf)	130	141.5	142
Undrained Compressive Strength (ksf)	9.24	7.25	8.44
Strain at Peak Strength (%)	4.07	3.38	2.19
Young's Modulus (ksf)	274.3	3331.0	590.26
Recovery (%)	88.0	88.0	100
Rock Quality Designation (%)	82.5	82.5	92
Joint Average Vertical Spacing (in)	3-5	3-5	3-5
Sample Description	CLAY SHALE, Green to Gray, Weathered	CLAY SHALE, Green to Gray, Weathered	CLAY SHALE, Green to Gray, Weathered with some gravels

Specimen Identification	**EB-B1-S4**	**EB-B1-S5**	**EB-B1-S6**
Core Run Number	**3**	**4**	**5**
Depth (ft.)	23.5	31.0	32.0
Initial Water Content (%)	10.87	8.07	5.82
Total Unit Weight (pcf)	135	138	143
Undrained Compressive Strength (ksf)	3.9	18.5	15.5
Strain at Peak Strength (%)	2.66	2.57	2.57
Young's Modulus (ksf)	382.25	7639.4	8357.0
Recovery (%)	95	100	100
Rock Quality Designation (%)	60	60	100
Joint Average Vertical Spacing (in)	2	2	2
Sample Description	CLAY SHALE, Gray, sandy. Weathered and Soft	CLAY SHALE, Gray, sandy. Weathered and Soft	CLAY SHALE, Gray, sandy. Weathered and Soft

Specimen Identification	EB-B2-S1	EB-B2-S2	EB-B2-S3
Core Run Number	**1**	**1**	**2**
Depth (ft.)	14.5	17	23
Initial Water Content (%)	9.28	9.25	11.11
Total Unit Weight (pcf)	133	135	127
Undrained Compressive Strength (ksf)	59.7	17.15	22
Strain at Peak Strength (%)	4.1	2.83	3.0
Young's Modulus (ksf)	1718.2	644.2	974.7
Recovery (%)	85	85	85
Rock Quality Designation (%)	85	85	60
Joint Average Vertical Spacing (in)	2 to 5	2 to 5	2
Sample Description	CLAY SHALE, Green to Gray, Weathered	CLAY SHALE, Green to Gray, Weathered	CLAY SHALE, Green to Gray, Weathered with some gravel

Specimen Identification	EB-B2-S4	EB-B2-S5	EB-B2-S6
Core Run Number	**3**	**3**	**3**
Depth (ft.)	24.5	26.5	27.5
Initial Water Content (%)	9.07	-	-
Total Unit Weight (pcf)	133	-	-
Undrained Compressive Strength (ksf)	49.1	9.9	8.1
Strain at Peak Strength (%)	4.46	5.11	5.19
Young's Modulus (ksf)	1163.24	202.7	154.9
Recovery (%)	95	95	95
Rock Quality Designation (%)	50	50	50
Joint Average Vertical Spacing (in)	0.5 to 1	0.5 to1	0.5 to1
Sample Description	CLAY SHALE, Gray, Weathered and Soft	CLAY SHALE, Gray, Weathered and Soft	CLAY SHALE, Gray, Weathered and Soft

Specimen Identification	EB-B2-S7	EB-B2-S8	EB-B2-S9
Core Run Number	**4**	**4**	**5**
Depth (ft.)	29.5	33	37
Initial Water Content (%)	8.7	10.1	7.9
Total Unit Weight (pcf)	135	130	138
Undrained Compressive Strength (ksf)	6.5	23.5	42.3
Strain at Peak Strength (%)	3.06	4.5	3.4
Young's Modulus (ksf)	869.3	772.0	2317.2
Recovery (%)	100	100	100
Rock Quality Designation (%)	60	60	60
Joint Average Vertical Spacing (in)	2 to 5	2 to 5	2 to 8
Sample Description	CLAY SHALE, Gray, sandy. Weathered and Soft	CLAY SHALE, Gray, sandy. Weathered and Soft	CLAY SHALE, Gray, slightly weathered

APPENDIX H FIELD EXPLORATION AT I-55 OVER THE DES PLAINES RIVER

H.1 BACKGROUND

Figure H.1 shows location of I-55 over the Des Plaines River, located in Will County, just South the city of Channon, Illinois. This 7-span bridge structure carries a four-lane highway over the Des Plaines River. The abutments and the six piers of this bridge are supported shallow foundations resting on the shallow sedimentary rocks (i.e. shales, limestones). The weak shales near the Pier 2, was investigated during this study.

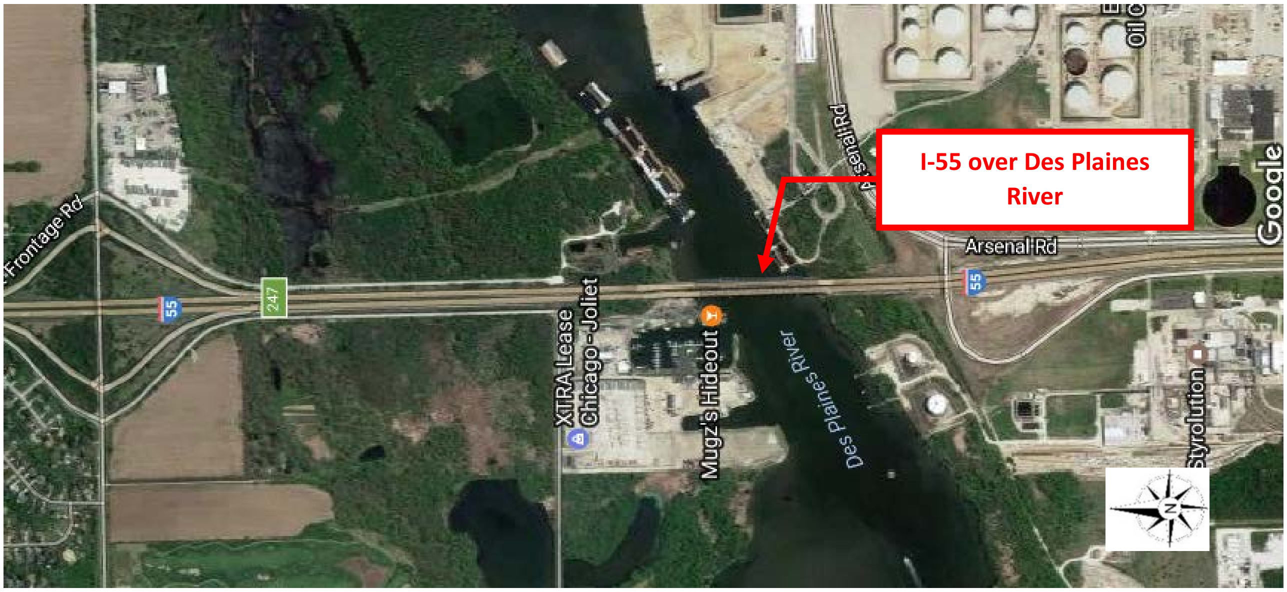

Figure H.1 Location of I-55 over the Des Plaines River.

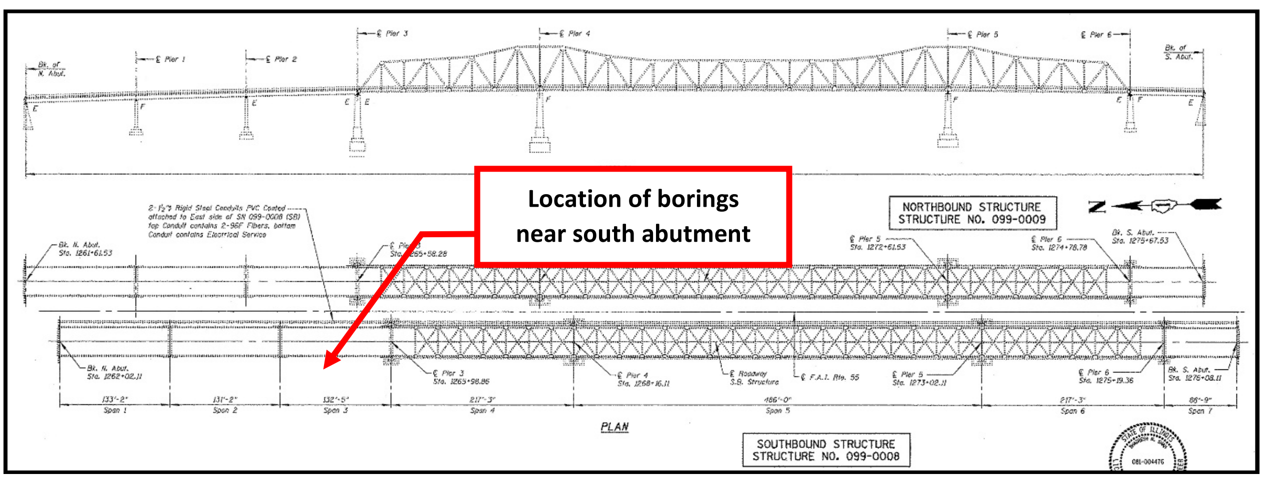

Figure H.2 Location of boring holes at I-55 over the Des Plaines River.

Figure H.2 shows a plan view of I-55 over the Des Plaines River structure and the location of borings drilled on November 19, 2015 by Wang Engineering drilling crew and the UIUC research team. Two borings were advanced near south abutment. These borings were drilled to an elevation of 445.5 feet.

The first boring was used to obtain shale core samples. Initially rock cores were used for determination of recovery ratio, RQD of the rock mass, and vertical spacing of joints. Afterwards unconfined compression tests were conducted on the retrieved weak shales specimens. The in situ water content of the shale specimens used in the unconfined compression tests was also measured for correlation purposes. The unconfined compression test results were also used to determine the deformability characteristics of shale under undrained loading conditions.

The second boring was used to obtain MSPT blow counts at various depths. These data were used to improve/check the correlation between undrained compressive strength of weak shale in Illinois and MSPT penetration rates developed in Phase of this study. The following sections discuss geology of the bridge site, MSPT test results, and laboratory test results

H.2 SITE GEOLOGY

The geology at the bridge site consists of about 30 feet of very soft to stiff brown to gray clay overlying sedimentary bedrock, e.g., shale, and limestone. The ground surface elevation at the two borings, is about 510 feet. A fairly continuous layer of clay shale was exposed at an elevation of 480 feet and extended to elevation of 445.5 feet were the coring was terminated. Laboratory test results are summarized in Table H.1.

H.3 MODIFED STANDARD PENETRATION TEST RESULTS

Figure H.3 and Figure H.4 show the Modified Standard Penetration Test results obtained in one of the borings at I-55 over the Des Plaines River.

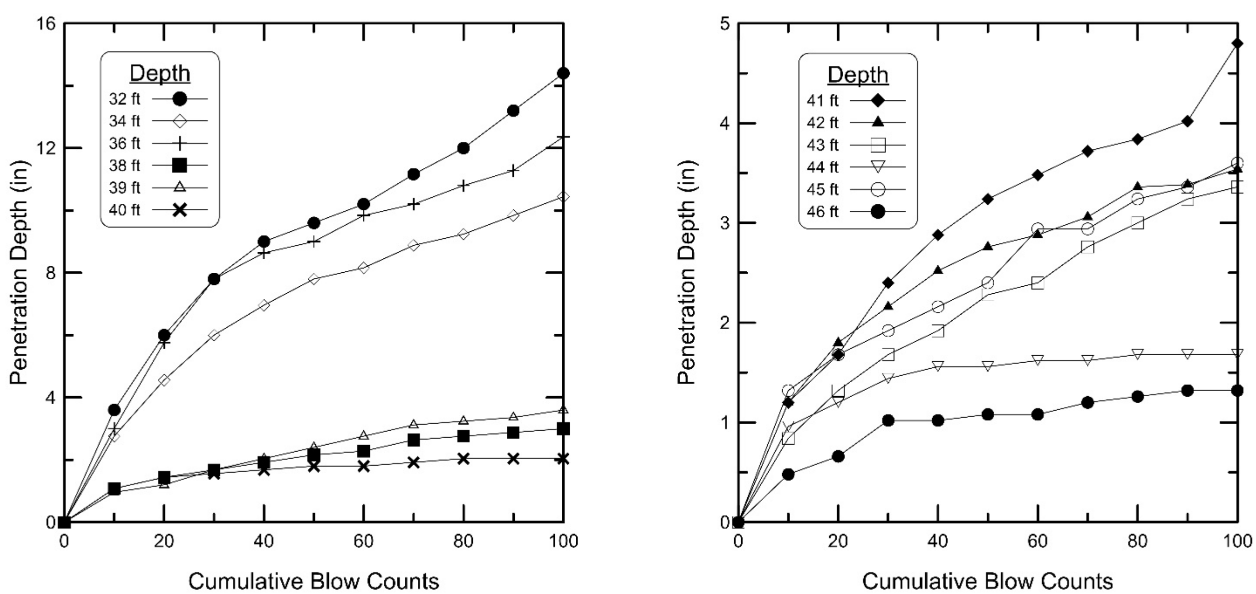

Figure H.3 Modified Standard Penetration Test results.

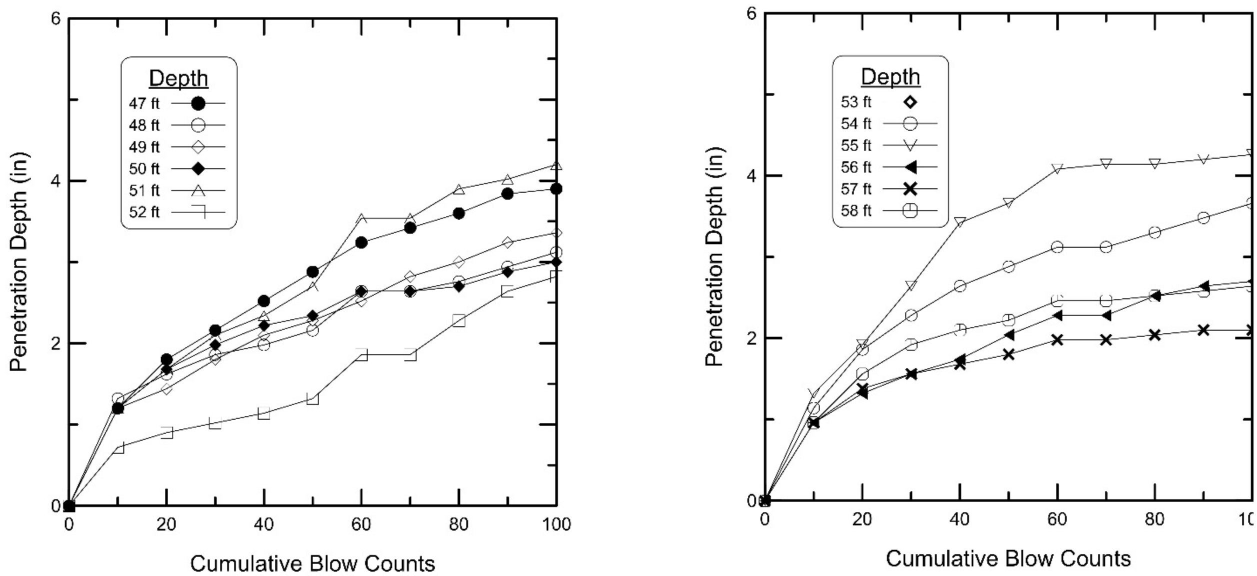

Figure H.4 Modified Standard Penetration Test results.

H.4 LABORATORY TEST RESULTS

H.4.1 Moisture Content and Total Unit Weight

Figure H.5 shows the total unit weight profile at the I-55 over the Des Plaines River site. The total unit weight of the encountered shales was computed in accordance with ASTM D7263.

Shale specimens from unconfined compressive tests were used for determination of in situ water content. The resulting water content profile is shown in Figure H.6. Water content of the Shales was determined in accordance with ASTM D2216.

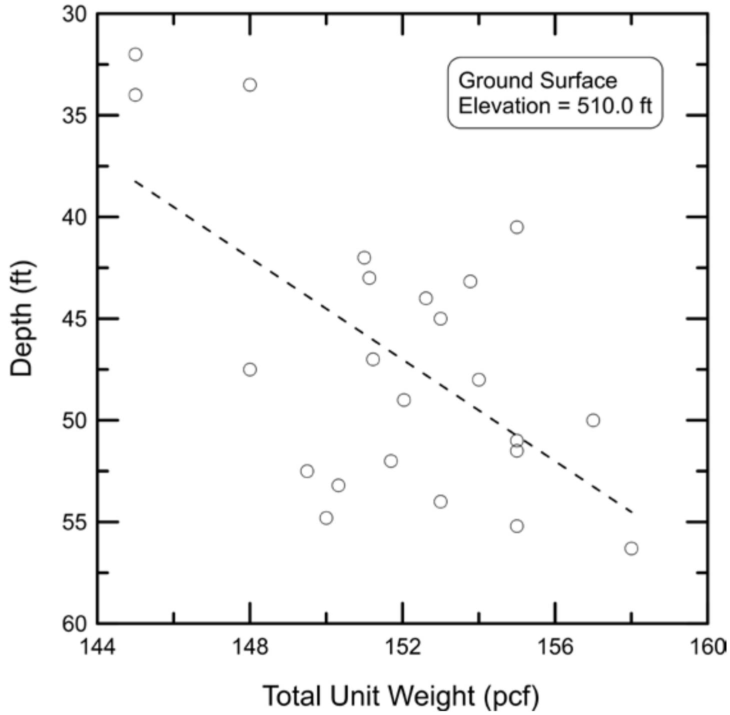

Figure H.5 Total unit weight profile.

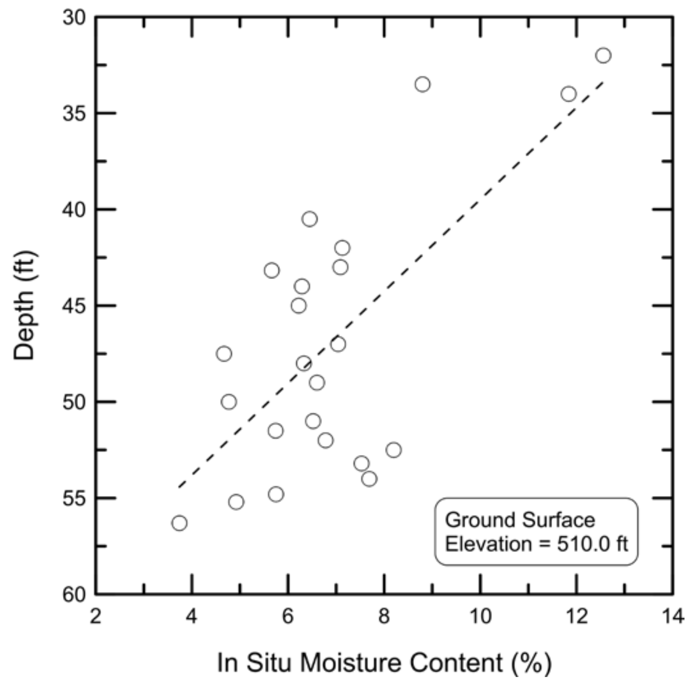

Figure H.6 In situ moisture content profile.

H.4.2 Triaxial Compression Test Results

Unconfined triaxial compression and Undrained Triaxial tests were performed in accordance with ASTM D7012–14 (method D). The peak deviator stress was used to calculate the undrained compressive strength for each test. The resulting undrained compressive strengths are shown in Table H.1.

H.4.3 Young's Modulus of Mudstone Specimen

Young's modulus was measured from results of triaxial tests in accordance to ASTM D70 ASTM D7012–14 (method D)12. In short, the modulus was calculated from the slope of the stress-strain relationships that correspond to 50% of mobilized undrained compressive strength. Figure H.7 shows the relationship between Young's modulus and undrained compressive strength for the shales core tested from the I-55 over the Des Plaines River site. This data was also used to develop a relationship between Young's modulus and natural water content (see Figure H.8). The unconfined compressive strength to the undrained Young's modulus ratio shown in Figure H.6 agrees well with the general trends observed in Phase 1 & 2 of this study. The site-specific relationship between undrained Young's modulus and the in situ water content is also shown in Figure H.7. Table H.1 summarizes all of the data obtained from the laboratory testing and evaluation.

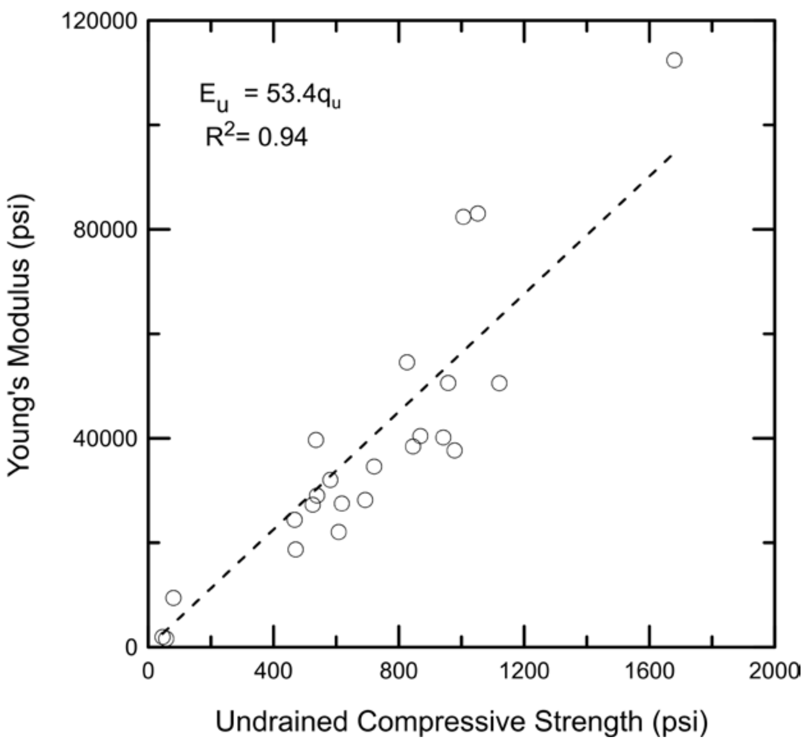

Figure H.7 Relationship between undrained compressive strength and Young's modulus.

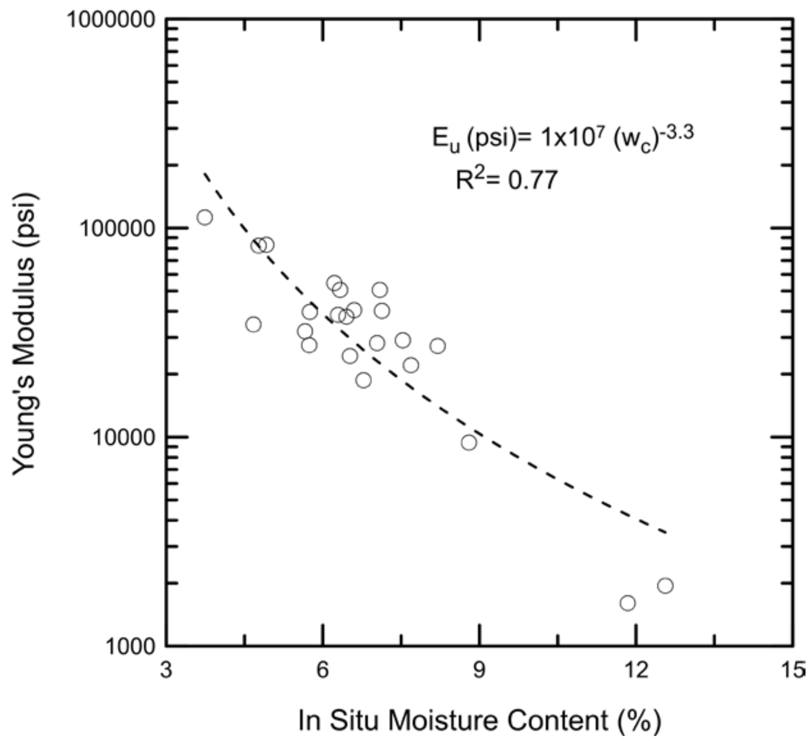

Figure H.8 Relationship between in situ moisture content and Young's modulus.

Table H.1 Laboratory Data Summary at the I-55 over the Des Plaines River

Specimen Identification	**DP-S1**	**DP-S2**	**DP-S3**
Core Run Number	**1**	**1**	**2**
Depth (ft.)	32	33.5	34
Initial Water Content (%)	12.56	8.8	11.06
Total Unit Weight (pcf)	145.0	148.1	146.2
Undrained Compressive Strength (ksf)	6.57	11.63	8.27
Strain at Peak Strength (%)	5.35	4.3	3.71
Young's Modulus (ksf)	279.8	1354.9	230.9
Recovery (%)	50	50	100
Rock Quality Designation (%)	50	50	92
Joint Average Vertical Spacing (in)	8 to 10	8 to 10	8 to 10
Sample Description	Clay Shales Gray, Weathered and Soft	Clay Shales Gray, Weathered and soft	Clay Shales Gray, Weathered

Specimen Identification	**DP-S4**	**DP-S5**	**DP-S6**
Core Run Number	**2**	**2**	**2**
Depth (ft.)	40.5	42.0	43.0
Initial Water Content (%)	6.45	7.13	7.09
Total Unit Weight (pcf)	155.0	151.0	151.1
Undrained Compressive Strength (ksf)	140.9	135.7	161.5
Strain at Peak Strength (%)	2.61	2.48	2.57
Young's Modulus (ksf)	5425.25	5784.8	7285.4
Recovery (%)	100	100	100
Rock Quality Designation (%)	92	92	92
Joint Average Vertical Spacing (in)	2 to 5	2 to 5	2 to 5
Sample Description	Clay Shales Gray, Indurated	Clay Shales Gray, Indurated	Clay Shales Gray, Indurated

Specimen Identification	**DP-S7**	**DP-S8**	**DP-S9**
Core Run Number	**2**	**2**	**2**
Depth (ft.)	43.2	44	45
Initial Water Content (%)	5.66	6.29	6.22
Total Unit Weight (pcf)	153.8	152.6	153
Undrained Compressive Strength (ksf)	83.76	121.82	118.9
Strain at Peak Strength (%)	2.72	2.48	1.94
Young's Modulus (ksf)	4613.85	5534.24	7860.7
Recovery (%)	100	100	100
Rock Quality Designation (%)	92	92	92
Joint Average Vertical Spacing (in)	4 to 8	4 to 8	4 to 8

Sample Description	Clay Shales Gray, Indurated	Clay Shales Gray, Indurated	Clay Shales Gray, Indurated

Specimen Identification	**DP-S10**	**DP-S11**	**DP-S12**
Core Run Number	**2**	**2**	**2**
Depth (ft.)	47	47.5	48
Initial Water Content (%)	7.04	4.67	6.33
Total Unit Weight (pcf)	151.2	148	154
Undrained Compressive Strength (ksf)	99.77	103.9	137.9
Strain at Peak Strength (%)	2.66	2.31	2.13
Young's Modulus (ksf)	4062.6	4981.9	7291.9
Recovery (%)	100	100	100
Rock Quality Designation (%)	92	92	92
Joint Average Vertical Spacing (in)	2 to 8	2 to 8	2 to 8
Sample Description	Clay Shales Gray, Weathered	Clay Shales Gray, Weathered	Clay Shales Gray, Weathered

Specimen Identification	**DP-S13**	**DP-S14**	**DP-S15**
Core Run Number	**2**	**3**	**3**
Depth (ft.)	49	50	51
Initial Water Content (%)	6.6	4.77	6.52
Total Unit Weight (pcf)	152	157.0	155.0
Undrained Compressive Strength (ksf)	125.2	144.95	67.32
Strain at Peak Strength (%)	2.71	1.81	2.89
Young's Modulus (ksf)	5827.4	11875.1	3514.9
Recovery (%)	100	100	100
Rock Quality Designation (%)	92	99	99
Joint Average Vertical Spacing (in)	2 to 8	2 to 8	2 to 8
Sample Description	Clay Shales Gray, Weathered	Clay Shales Gray, Weathered	Clay Shales Gray, Weathered

Specimen Identification	**DP-S16**	**DP-S17**	**DP-S18**
Core Run Number	**3**	**3**	**3**
Depth (ft.)	51.5	52.0	52.5
Initial Water Content (%)	5.74	6.78	8.2
Total Unit Weight (pcf)	155.0	151.7	149.5
Undrained Compressive Strength (ksf)	89.09	67.8	75.64
Strain at Peak Strength (%)	3.06	2.32	3.0
Young's Modulus (ksf)	27515.0	18685.8	27275.88
Recovery (%)	100	100	100
Rock Quality Designation (%)	92	99	99
Joint Average Vertical Spacing (in)	2 to 8	2 to 8	2 to 8

Sample Description	Clay Shales Gray, Indurated	Clay Shales Gray, Indurated	Clay Shales Gray, Indurated

Specimen Identification	**DP-S19**	**DP-S20**	**DP-S21**
Core Run Number	**3**	**3**	**3**
Depth (ft.)	53.2	54.0	54.8
Initial Water Content (%)	7.53	7.69	5.75
Total Unit Weight (pcf)	150.3	153.0	150.0
Undrained Compressive Strength (ksf)	77.6	87.6	77.1
Strain at Peak Strength (%)	2.96	2.81	2.49
Young's Modulus (ksf)	4181.63	3177.9	5716.5
Recovery (%)	100	100	100
Rock Quality Designation (%)	99.1	99.1	99.11
Joint Average Vertical Spacing (in)	2 to 8	2 to 8	2 to 8
Sample Description	Clay Shales Gray, Indurated	Clay Shales Gray, Indurated	Clay Shales Gray, Indurated

Specimen Identification	**DP-S22**	**DP-S23**	
Core Run Number	**3**	**3**	
Depth (ft.)	55.2	56.3	
Initial Water Content (%)	4.92	3.75	
Total Unit Weight (pcf)	155.0	158.0	
Undrained Compressive Strength (ksf)	151.60	242.05	
Strain at Peak Strength (%)	2.96	2.81	
Young's Modulus (ksf)	11964.45	16197.5	
Recovery (%)	100	100	
Rock Quality Designation (%)	99.1	99.1	
Joint Average Vertical Spacing (in)	8 to 15	8 to 15	
Sample Description	Clay Shales Gray, Indurated	Clay Shales Gray, Indurated	

APPENDIX I FIELD EXPLORATION AT US 24 OVER LITTLE SISTER CREEK

I.1 BACKGROUND

Figure I.1 shows location of US 24 over the Little Sister creek, located in Fulton County, Illinois. East and West abutments of this bridge are supported on driven H-pile foundations that likely extends to the underlying weak sedimentary rocks. The weak shale located near the east abutment, was investigated during this study.

Figure I.1 Location of US 24 over Little Sister Creek.

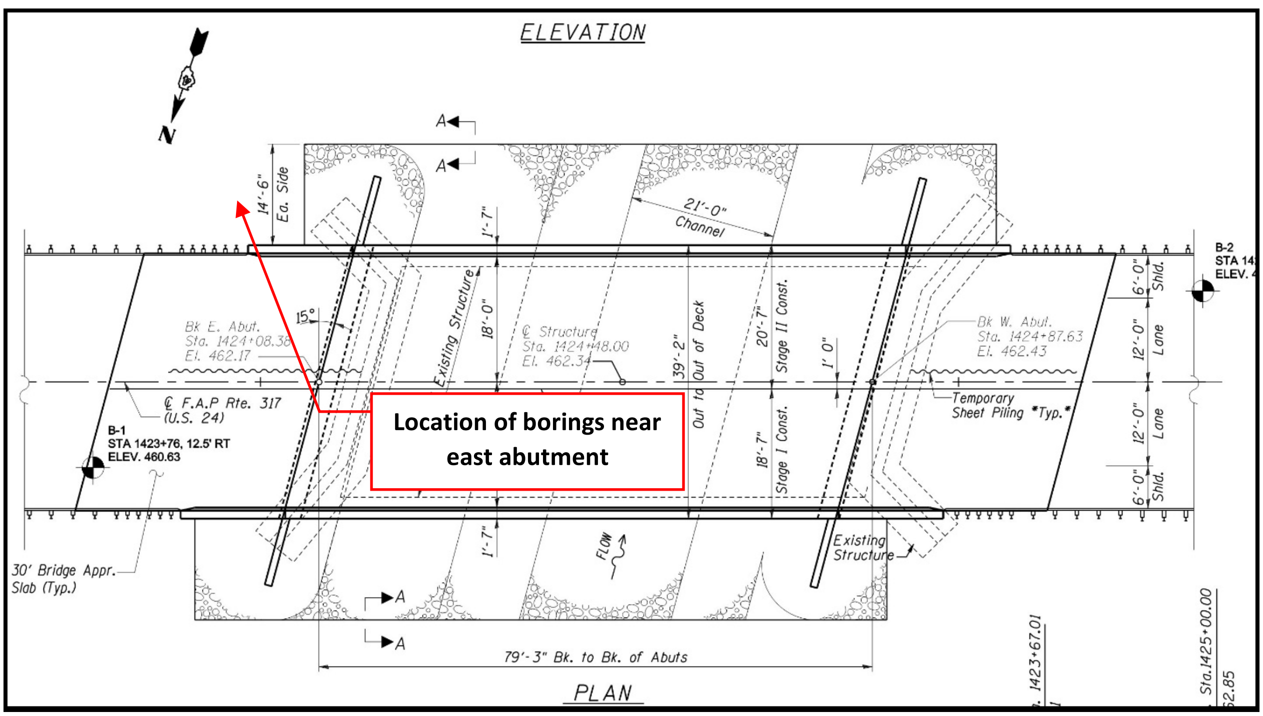

Figure I.2 Location of boring holes at US 24 over the Little Sister Creek.

Figure I.2 shows a plan view of this US 24 bridge structure over the Little sister creek and the location of borings drilled on March 1, 2016 and March 2, 2016 by Bulldog Engineering and the UIUC research team. Two borings were advanced near the south east quad of the bridge at the east abutment and in close proximity to the Little Sister Creek. These borings were drilled to the elevation of 405 feet.

The first boring was used to obtain shale core samples. Initially rock cores were used for determination of recovery ratio, RQD of the rock mass, and vertical spacing of joints. Afterwards unconfined compression tests were conducted on the retrieved weak shales specimens. The in situ water content of the shale specimens used in the unconfined compression tests was also measured for correlation purposes. The unconfined compression test results were also used to determine the deformability characteristics of shale under undrained loading conditions.

The second boring was used to obtain MSPT blow counts at various depths. These data were used to improve/check the correlation between undrained compressive strength of weak shale in Illinois and MSPT penetration rates developed in Phase of this study. The following sections discuss geology of the bridge site, MSPT test results, and laboratory test results

I.2 SITE GEOLOGY

The geology at the bridge site consists of about 18 feet of soft to medium stiff dark clay loam with traces of gravel overlying sedimentary bedrock, e.g., shale, and limestone. The ground surface elevation at the two borings, is about 453 feet. A fairly continuous layer of weak fissile clay shale was exposed at an elevation of 435 feet and extended to elevation of 405 feet were the coring was terminated. Laboratory test results are summarized in Table I.1.

I.3 MODIFIED STANDARD PENETRATION TEST RESULTS

Figure I.3 shows the Modified Standard Penetration Test results obtained in one of the borings at US 24 over the Little Sister Creek.

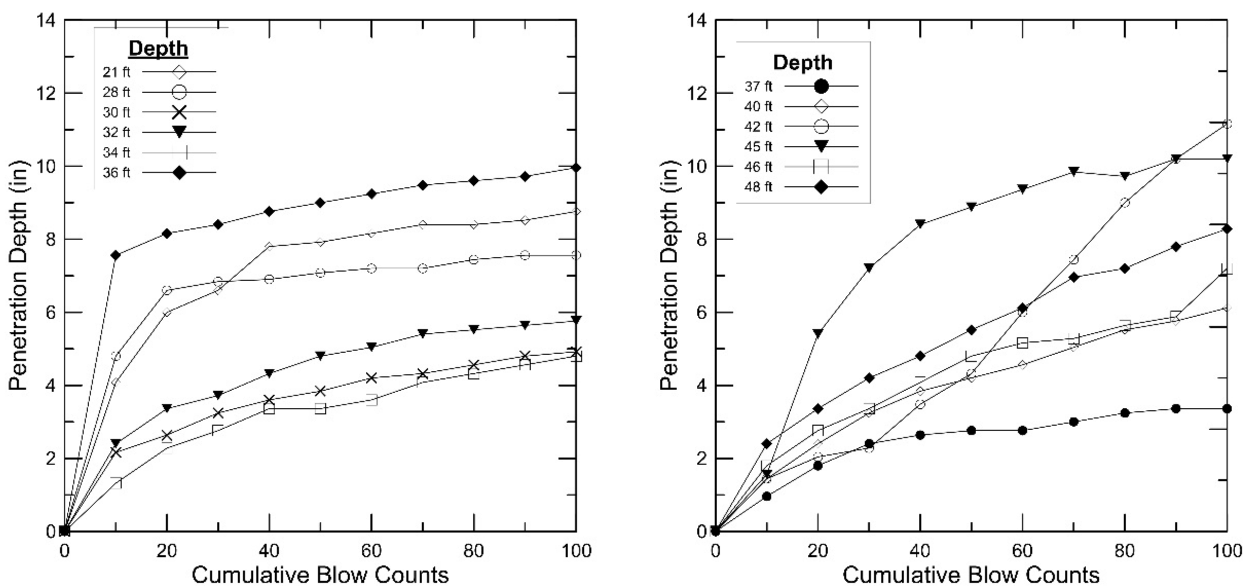

Figure I.3 Modified Standard Penetration Test results.

I.4 LABORATORY TEST RESULTS

I.4.1 Moisture Content and Total Unit Weight

Figure I.4 shows the total unit weight profile at the US 24 site. The total unit weight of shale was computed in accordance with ASTM D7263.

Shale specimens from unconsolidated undrained and unconfined compressive tests were used for determination of in situ water content. The resulting water content profile is shown in Figure I.5. Water content of the shale was determined in accordance with ASTM D2216.

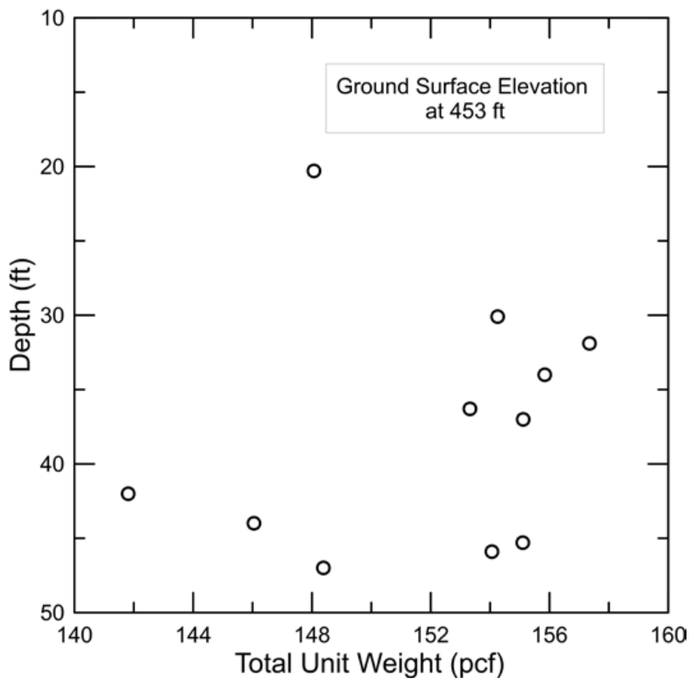

Figure I.4 Total unit weight profile.

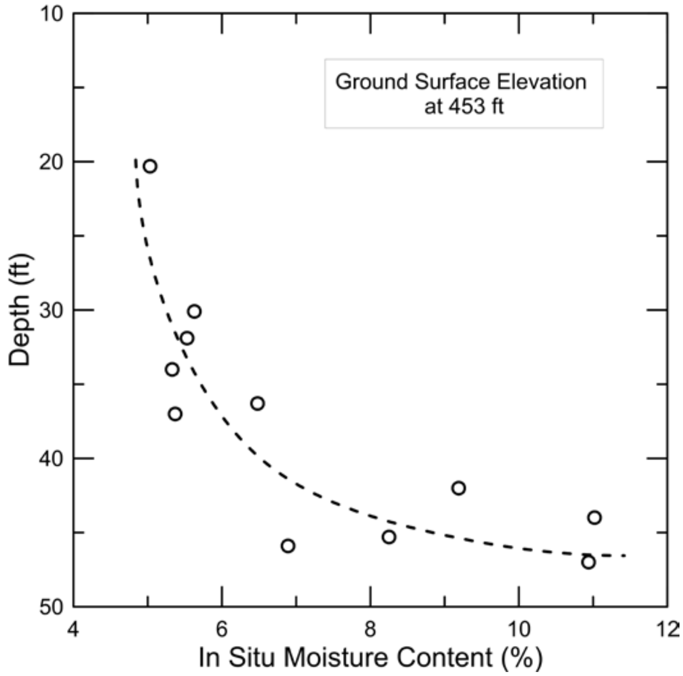

Figure I.5 In situ moisture content profile.

I.4.2 Triaxial Compression Test Results

Unconfined triaxial compression tests were performed in accordance with ASTM D7012–14 (method D). The peak deviator stress was used to calculate the undrained compressive strength for each test. The resulting undrained compressive strengths are shown in Table I.1.

I.4.3 Young's Modulus of Shale Specimen

Young's modulus was measured from results of triaxial tests in accordance to ASTM D7012–14 (method D). In short, the modulus was calculated from the slope of the stress-strain relationships that correspond to 50% of mobilized undrained compressive strength. Figure I.6 shows the relationship between Young's modulus and undrained compressive strength for the shale cores tested from the Little sister creek site. This data was also used to develop a relationship between undrained Young's modulus and shale natural water content (see Figure I.7). The unconfined compressive strength to the undrained Young's modulus ratio shown in Figure I.6 agrees well with the general trends observed in Phase 1 & 2 of this study. The site-specific relationship between undrained Young's modulus and the in situ water content is also shown in Figure I.7. The scatter shown in Figure I.7 is relatively high, as reflected by the low R-squared values. However, the correlation given in the same figure is in the acceptable range observed in this study   Table I.1 summarizes all of the data obtained from the laboratory testing and evaluation.

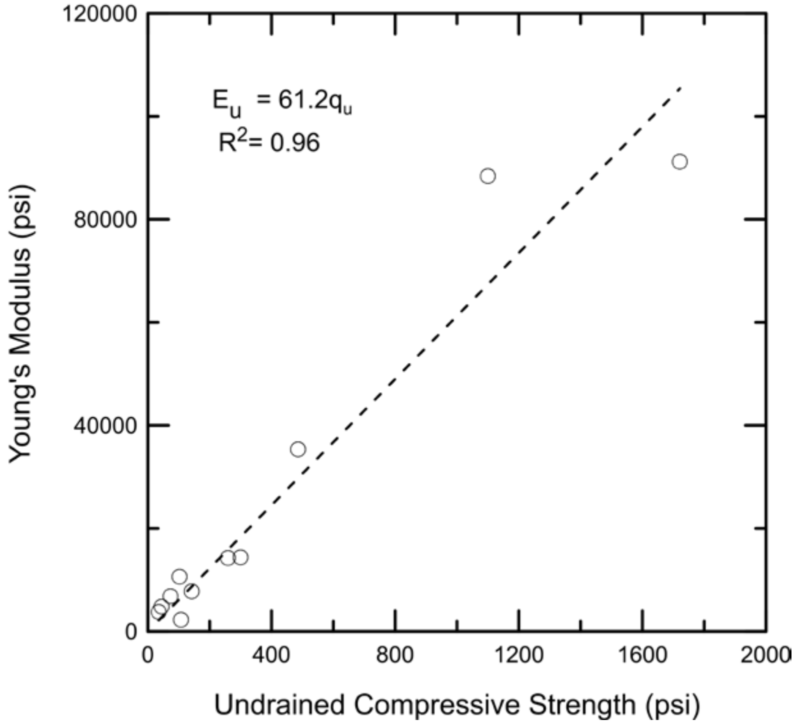

Figure I.6 Relationship between undrained compressive strength and Young's modulus.

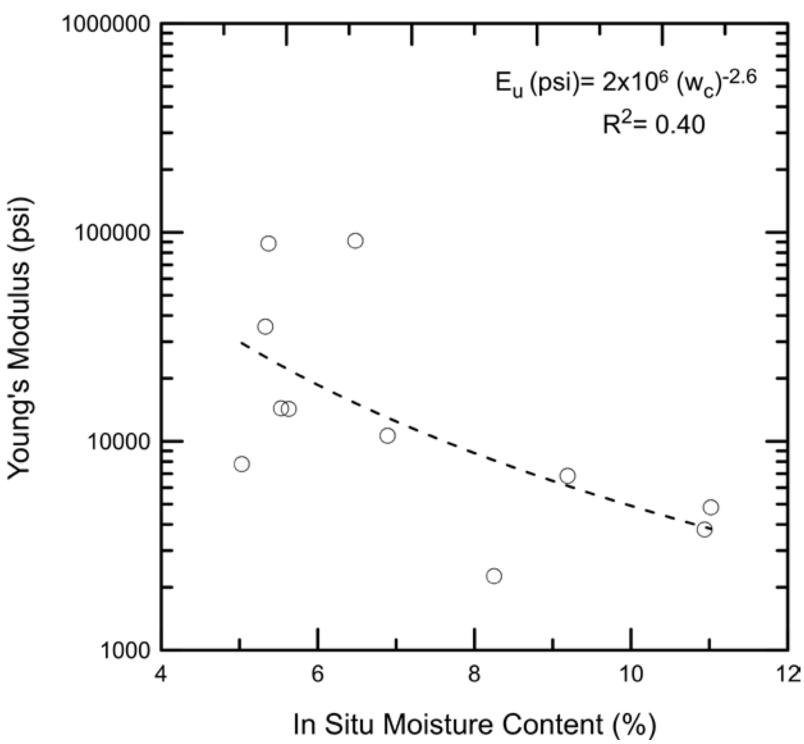

Figure I.7 Relationship between in situ moisture content and Young's modulus.

Table I.1 Laboratory Data Summary at the US 24 Over the Little Sister Creek

Specimen Identification	**LS-S1**	**LS-S2**	**LS 24-S3**
Core Run Number	**1**	**2**	**2**
Depth (ft.)	20.3	30.1	31.9
Initial Water Content (%)	5.0	5.6	5.5
Total Unit Weight (pcf)	148.0	154.3	157.3
Undrained Compressive Strength (ksf)	20.5	37.3	43.2
Strain at Peak Strength (%)	2.3	2.1	4.9
Young's Modulus (ksf)	1120	2057	2073
Recovery (%)	91	100	100
Rock Quality Designation (%)	50	80	80
Joint Average Vertical Spacing (in)	2	8	8
Sample Description	CLAY SHALE, gray and fissile weathered	CLAY SHALE, dark gray with traces of coal	CLAY SHALE, dark gray with traces of coal

Specimen Identification	**LS-S4**	**LS-S5**	**LS-S6**
Core Run Number	**2**	**2**	**2**
Depth (ft.)	34	36.3	37
Initial Water Content (%)	5.3	6.5	5.4
Total Unit Weight (pcf)	155.8	153.3	155.1
Undrained Compressive Strength (ksf)	70.1	248	158.5
Strain at Peak Strength (%)	2.9	3.5	3.6
Young's Modulus (ksf)	5093.6	13142.5	12740
Recovery (%)	100	100	100
Rock Quality Designation (%)	80	80	80
Joint Average Vertical Spacing (in)	10	12	12
Sample Description	CLAY SHALE, gray fissle	CLAY SHALE, gray Indurated	CLAY SHALE, gray, Indurated

Specimen Identification	LS-S7	LS-S8	LS-S9
Core Run Number	**3**	**3**	**3**
Depth (ft.)	42.0	44.0	45.3
Initial Water Content (%)	9.2	11	8.3
Total Unit Weight (pcf)	141.8	146	155.1
Undrained Compressive Strength (ksf)	10.6	6.4	15.4
Strain at Peak Strength (%)	2.8	2.1	3.0
Young's Modulus (ksf)	985.3	695.2	325.7
Recovery (%)	100	100	100
Rock Quality Designation (%)	80	80	80
Joint Average Vertical Spacing (in)	4	4	4
Sample Description	CLAY SHALE gray weathered fissile	CLAY SHALE gray weathered fissile	CLAY SHALE gray weathered fissile

APPENDIX J FIELD EXPLORATION AT US 24 OVER BIG SISTER CREEK

J.1 BACKGROUND

Figure J.1 shows location of US 24 over the Big Sister creek, located in Fulton County, Illinois. East and West abutments of this bridge are supported on driven H-pile foundations that likely extends to the underlying weak sedimentary rocks. The weak shale located near the east abutment, was investigated during this study.

Figure J.1 Location of US 24 over Big Sister Creek.

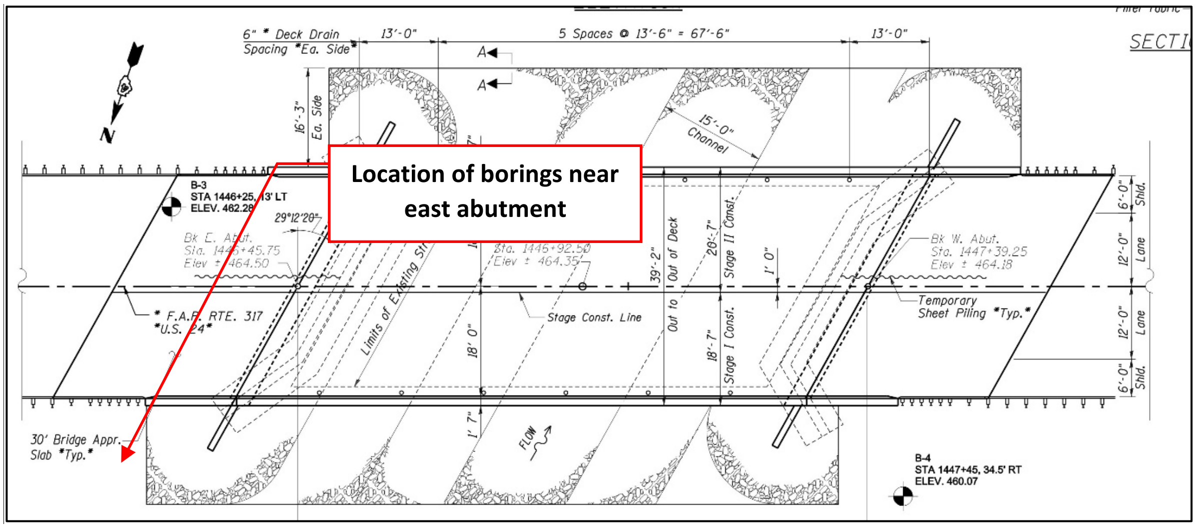

Figure J.2 Location of boring holes at US 24 over the Big Sister Creek.

Figure J.2 shows a plan view of this US 24 bridge structure over the Big sister creek and the location of borings drilled on February 29, 2016 and March 1, 2016 by Bulldog Engineering and the UIUC research team. Two borings were advanced near the north east quad of the bridge at the east abutment and in close proximity to the Big Sister Creek. These borings were drilled to the elevation of 413 feet.

The first boring was used to obtain shale core samples. Initially rock cores were used for determination of recovery ratio, RQD of the rock mass, and vertical spacing of joints. Afterwards unconfined compression tests were conducted on the retrieved weak shales specimens. The in situ water content of the shale specimens used in the unconfined compression tests was also measured for correlation purposes. The unconfined compression test results were also used to determine the deformability characteristics of shale under undrained loading conditions.

The second boring was used to obtain MSPT blow counts at various depths. These data were used to improve/check the correlation between undrained compressive strength of weak shale in Illinois and MSPT penetration rates developed in Phase of this study. The following sections discuss geology of the bridge site, MSPT test results, and laboratory test results

J.2 SITE GEOLOGY

The geology at the bridge site consists of about 20 feet of very soft to stiff brown to gray clay with thin seams of silty loam overlying sedimentary bedrock, e.g., shale, and limestone. The ground surface elevation at the two borings, is about 454 feet. A fairly continuous layer of weak fissile clay shale was exposed at an elevation of 435 feet and extended to elevation of 405 feet were the coring was terminated. Laboratory test results are summarized in Table J.1.

J.3 MODIFIED STANDARD PENETRATION TEST RESULTS

Figure J.3 shows the Modified Standard Penetration Test results obtained in one of the borings at US 24 over the Big Sister Creek.

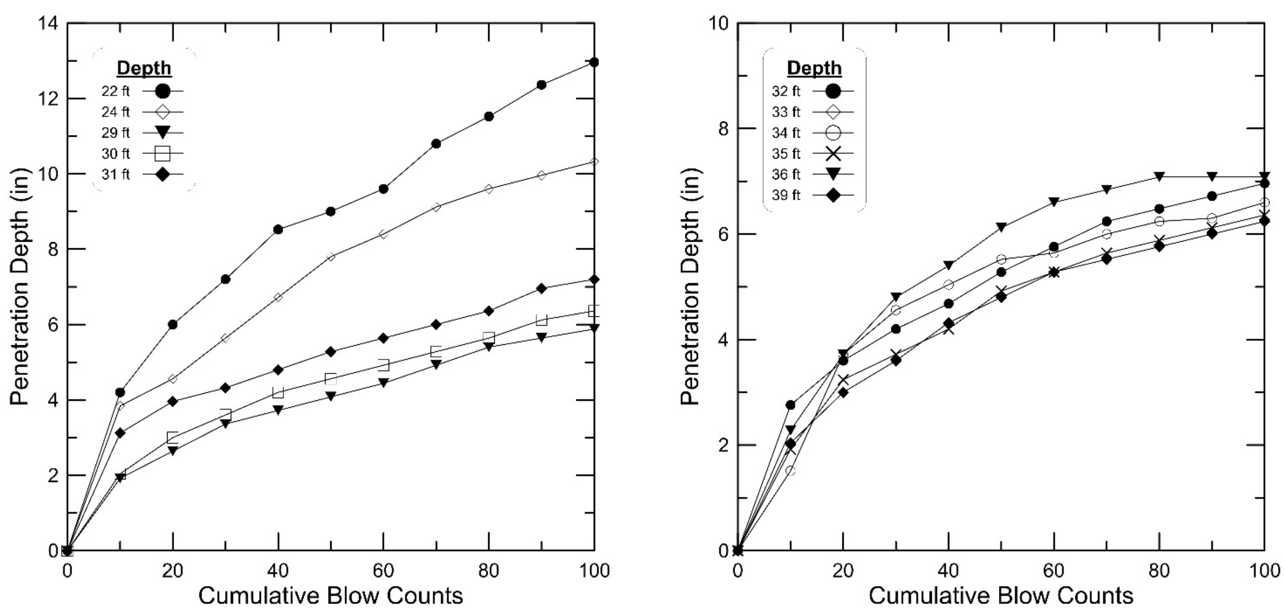

Figure J.3 Modified Standard Penetration Test results.

J.4 LABORATORY TEST RESULTS

J.4.1 Moisture Content and Total Unit Weight

Figure J.4 shows the total unit weight profile at the US 24 site. The total unit weight of shale was computed in accordance with ASTM D7263.

Shale specimens from unconsolidated undrained and unconfined compressive tests were used for determination of in situ water content. The resulting water content profile is shown in Figure J.5. Water content of the shale was determined in accordance with ASTM D2216.

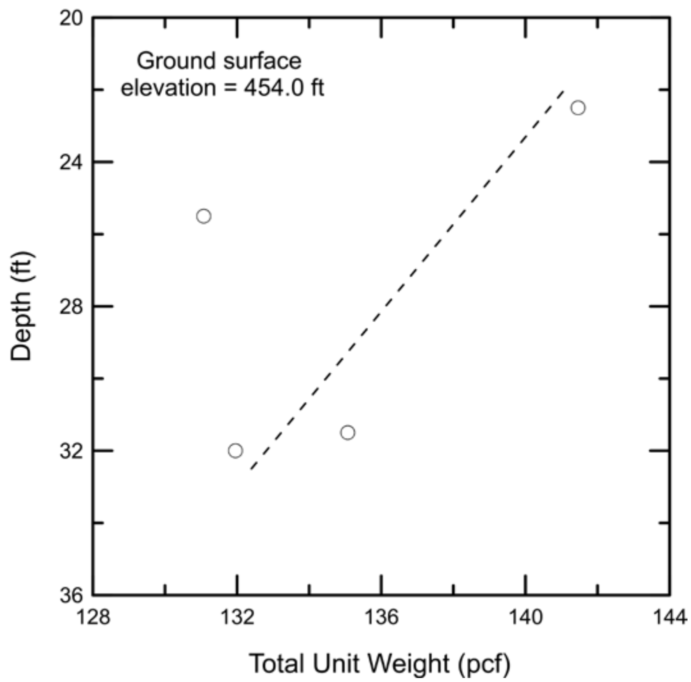

Figure J.4 Total unit weight profile.

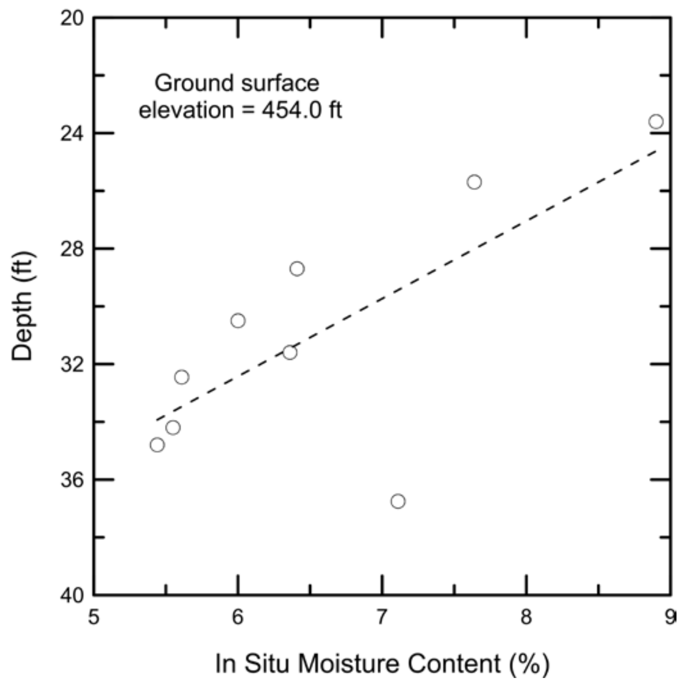

Figure J.5 In situ moisture content profile.

J.4.2 Triaxial Compression Test Results

Unconfined triaxial compression tests were performed in accordance with ASTM D7012. The peak deviator stress was used to calculate the undrained compressive strength for each test. The resulting undrained compressive strengths are shown in Table J.1.

J.4.3 Young's Modulus of Shale Specimen

Young's modulus was measured from results of triaxial tests in accordance to ASTM D7012. In short, the modulus was calculated from the slope of the stress-strain relationships that correspond to 50% of mobilized undrained compressive strength. Figure J.6 shows the relationship between Young's modulus and undrained compressive strength for the shale cores tested from the Big sister creek site. This data was also used to develop a relationship between undrained Young's modulus and shale natural water content (see Figure J.7). The unconfined compressive strength to the undrained Young's modulus ratio shown in Figure J.6 agrees well with the general trends observed in Phase 1 & 2 of this study. The site-specific relationship between undrained Young's modulus and the in situ water content is also shown in Figure J.7. The site-specific correlation in Figure J.7 yields slightly lower values for undrained Young's modulus for the range of the water contents measured in this site. Table J.1 summarizes all of the data obtained from the laboratory testing and evaluation.

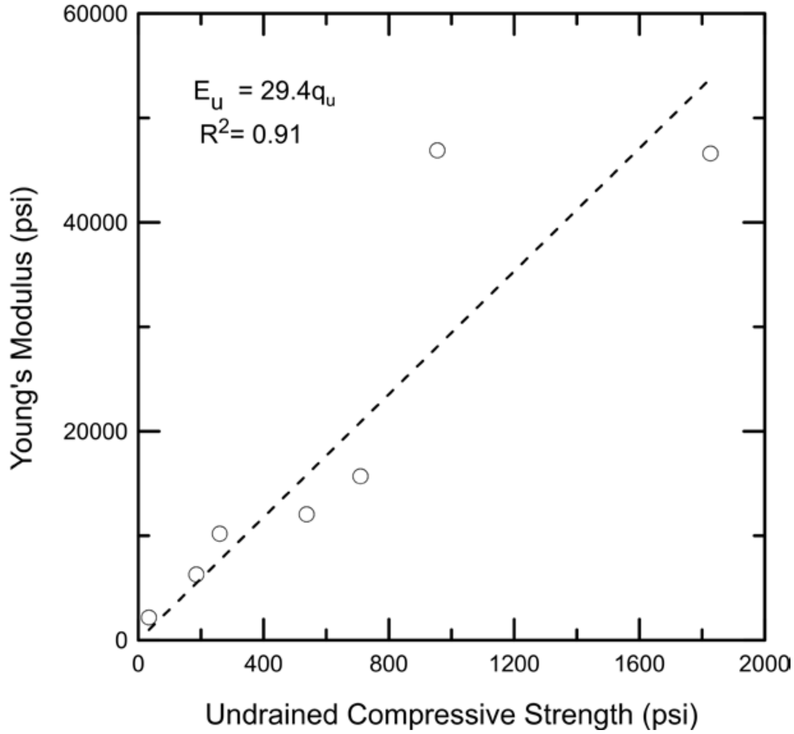

Figure J.6 Relationship between undrained compressive strength and Young's modulus.

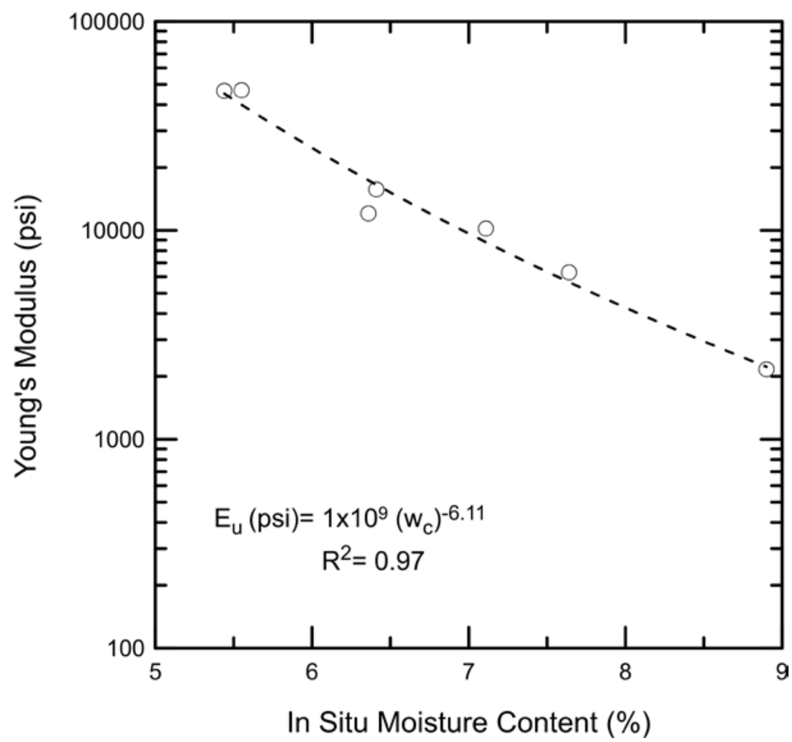

Figure J.7 Relationship between in situ moisture content and Young's modulus.

Table J.1 Laboratory Data Summary at the US 24 Over the Big Sister Creek

Specimen Identification	**BS-S1**	**BS-S2**	**BS 24-S3**
Core Run Number	**1**	**1**	**2**
Depth (ft.)	23.6	25.7	28.7
Initial Water Content (%)	8.9	7.64	6.41
Total Unit Weight (pcf)	155.1	154.6	153.3
Undrained Compressive Strength (ksf)	4.86	26.64	102.2
Strain at Peak Strength (%)			
Young's Modulus (ksf)	311.73	906.2	2261.6
Recovery (%)	91	91	100
Rock Quality Designation (%)	50	50	80
Joint Average Vertical Spacing (in)	2	2	7
Sample Description	CLAY SHALE, gray and fissile weathered	CLAY SHALE, dark gray fissile	CLAY SHALE, dark gray with traces of coal

Specimen Identification	**BS-S4**	**BS-S5**	**BS-S6**
Core Run Number	**2**	**2**	**2**
Depth (ft.)	30.5	31.6	32.45
Initial Water Content (%)	6	6.36	5.61
Total Unit Weight (pcf)	155.5	153.3	155.1
Undrained Compressive Strength (ksf)	73.96	77.4	71.28
Strain at Peak Strength (%)			
Young's Modulus (ksf)	-	1737.2	-
Recovery (%)	100	100	100
Rock Quality Designation (%)	80	80	80
Joint Average Vertical Spacing (in)	5	5	5
Sample Description	CLAY SHALE, dark gray with limestone inclusions	CLAY SHALE, dark gray with traces of coal	CLAY SHALE, dark gray with traces of coal

Specimen Identification	BS-S7	BS-S8	BS-S9
Core Run Number	**2**	**2**	**2**
Depth (ft.)	34.2	34.8	36.75
Initial Water Content (%)	5.55	5.44	7.11
Total Unit Weight (pcf)	157.4	156.6	148.5
Undrained Compressive Strength (ksf)	137.6	263.23	37.45
Strain at Peak Strength (%)			
Young's Modulus (ksf)	6756.8	6715	1469.6
Recovery (%)	100	100	100
Rock Quality Designation (%)	80	80	80
Joint Average Vertical Spacing (in)	5	5	
Sample Description	CLAY SHALE, Indurated, gray	CLAY SHALE, Indurated, gray	CLAY SHALE, dark gray with traces of coal

APPENDIX K FIELD EXPLORATION AT ELDAMAIN ROAD OVER THE FOX RIVER

K.1 BACKGROUND

Figure K.1 shows the proposed location of Eldamain road over the Fox River bridge site, located in Kendall County, just west of Yorkville, Illinois. This eight-span bridge structure is designed to carry two-lane highway over the Fox River. Pier 1 to 7 together with the north and south abutments are supported by H-piles that are embedded into the weak shales. The weak shales near Pier # 5 & 7 were investigated during this study.

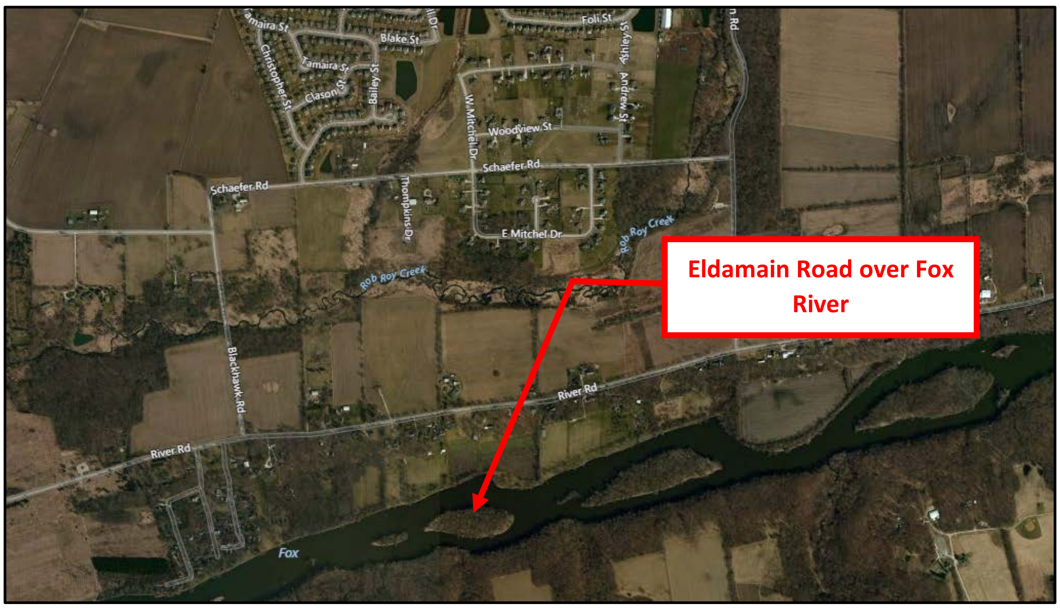

Figure K.1: Location of Eldamain Road over the Fox River near city of Yorkville.

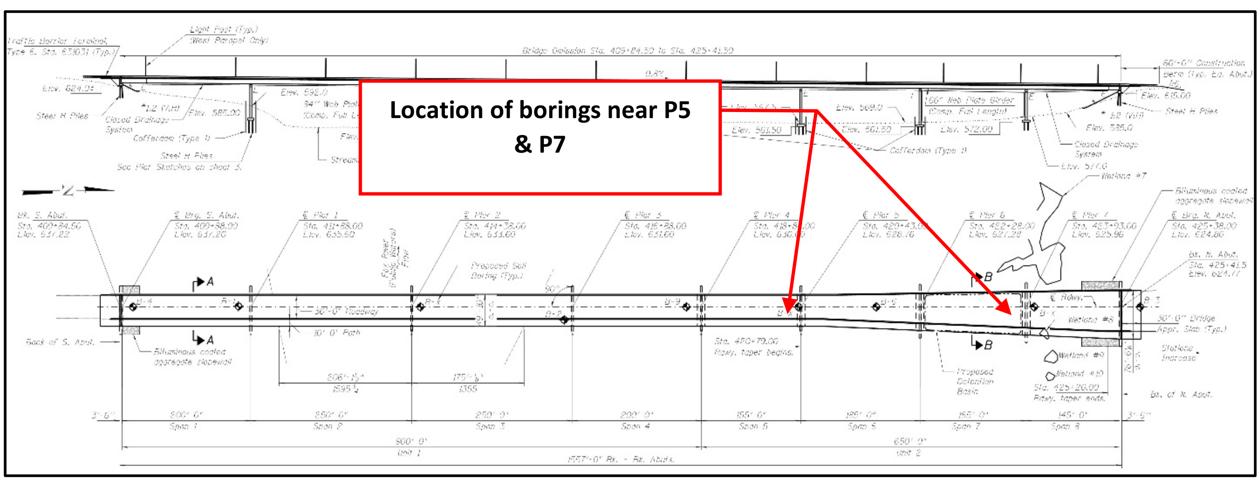

Figure K.2: Location of boring holes at Eldamain Road over the Fox River.

Figure K.2 shows a plan view of Eldamain Road over the Fox River bridge structure and the location of the borings drilled on January 21, 2016 and January 22, 2016 by Geocon

Engineering crew, McCleary Engineering and the UIUC research team. Four borings were advanced near Pier # 5 & 7 (i.e. 2 for each pier) on the north side of river. These borings were drilled to the elevation of 518 feet.

One of the two borings drilled for each pier was used to obtain shale cores. Initially rock cores were used for determination of recovery ratio, RQD of the rock mass, and vertical spacing of joints. Afterwards unconfined compression tests were conducted on the retrieved shale specimens. The in situ water content of the shale specimens used in the triaxial compression tests was also measured for correlation purposes. Triaxial test results were also used to determine the deformability characteristics of shale under undrained loading conditions.

The second boring was used to obtain MSPT blow counts at various depths. This data was used to develop a new correlation between undrained compressive strength of weak shale in Illinois and MSPT penetration rate.

The following sections discuss geology of the bridge site, MSPT test results, and laboratory test results.

K.2 SITE GEOLOGY

The geology at the bridge site consists of 25 feet of soft to stiff black silty clay overlying sedimentary bedrock, e.g., shale and limestone. The ground surface elevation at Pier # 5 & 7, is about 566.7 and 572.5 feet respectively. Weathered gray to black clay shale was exposed at an elevation of about 548 feet. Limestone layer was exposed at elevation of 531.0 feet and extended to elevation of 523.5 feet where drilling was terminated. Laboratory test results are summarized in Table K.1.

K.3 MODIFIED STANDARD PENETRATION TEST RESULTS

Figure K.3 shows the Modified Standard Penetration Test results obtained in two of the four borings at Eldamain Road over the Fox River.

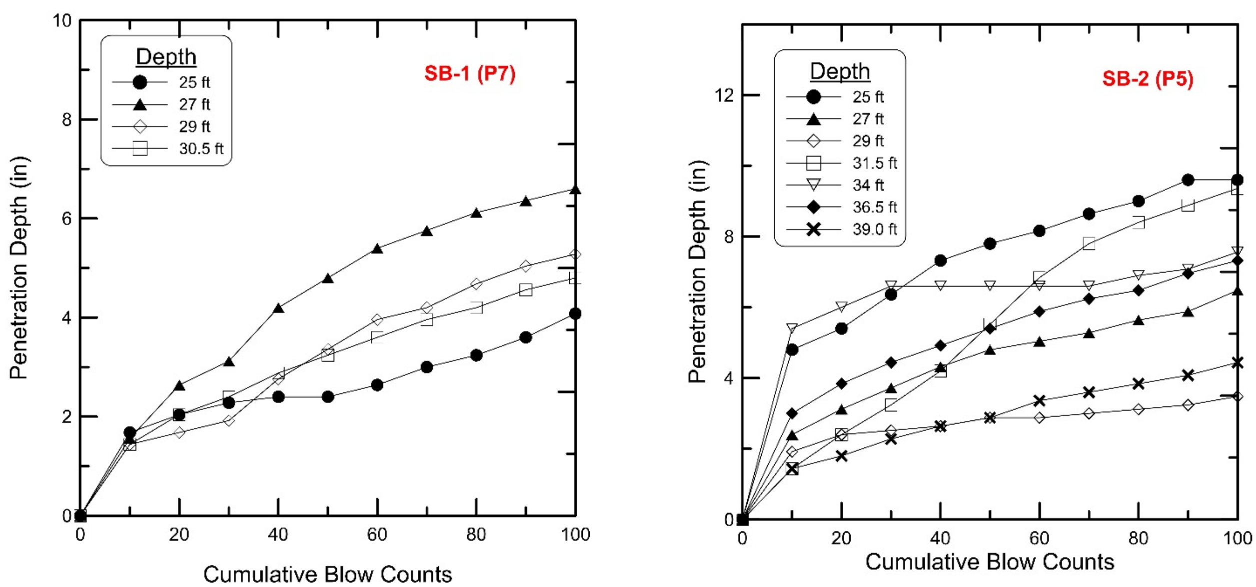

Figure K.3 Modified Standard Penetration Test results.

K.4 LABORATORY TEST RESULTS

K.4.1 Moisture Content and Total Unit Weight

Figure K.4 shows the total unit weight profile at the Eldamain Road over the Fox River. site. The total unit weight of shale was computed in accordance with ASTM D7263.

Shale specimens from unconsolidated undrained and unconfined compressive tests were used for determination of in situ water content. The resulting water content profile is shown in Figure K.5. Water content of the shale was determined in accordance with ASTM D2216.

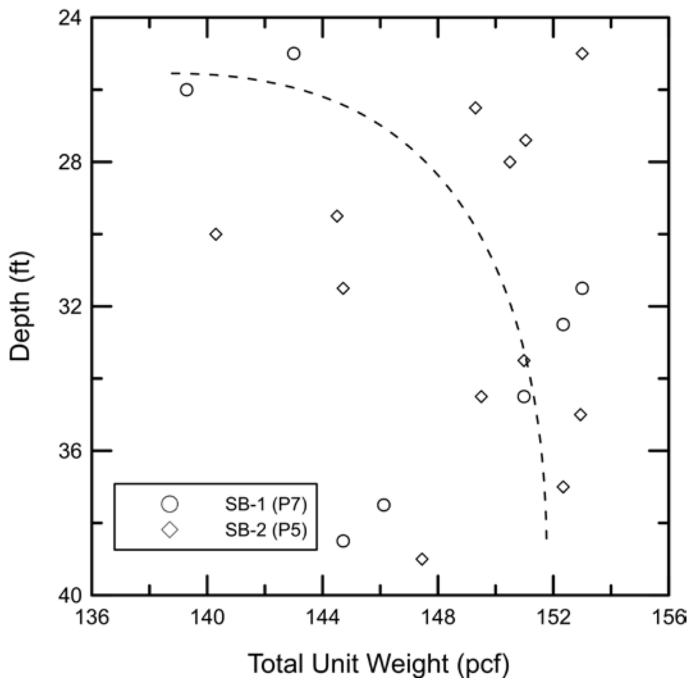

Figure K.4 Total unit weight profile.

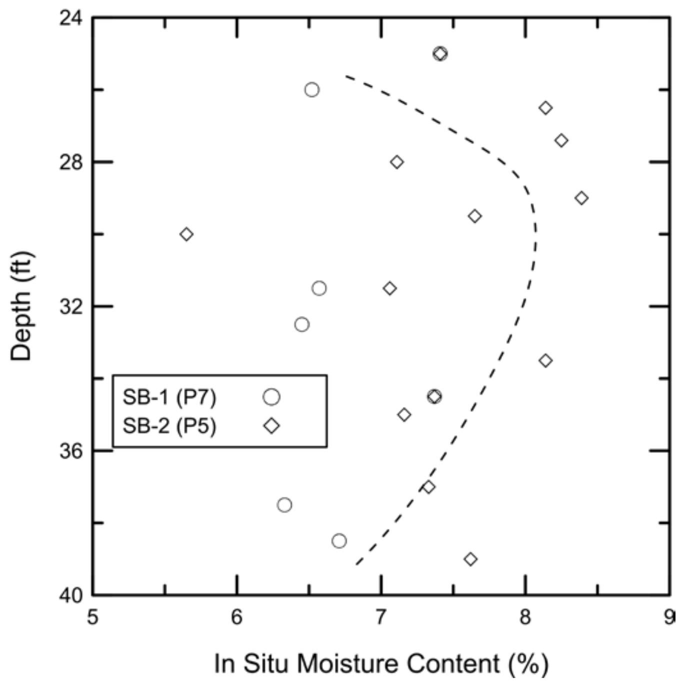

Figure K.5 In situ moisture content profile.

K.4.2 Triaxial Compression Test Results

Unconfined compression tests were performed in accordance with ASTM D7012–14 (method D). The peak deviator stress was used to calculate the undrained compressive strength for each test. The resulting undrained compressive strengths are shown in Table K.1.

K.4.3 Young's Modulus of Shale Specimen

Young's modulus was measured from results of triaxial tests in accordance to ASTM D7012–14 (method D). In short, the modulus was calculated from the slope of the stress-strain relationships that correspond to 50% of mobilized undrained compressive strength. Figure K.6 shows the relationship between Young's modulus and undrained compressive strength for the shale core tested from the Eldamain Road over the Fox River site. This data was also used to develop a relationship between Young's modulus and shale natural water content (see Figure K.7). The unconfined compressive strength to the undrained Young's modulus ratio shown in Figure K.6 agrees well with the general trends observed in Phase 1 & 2 of this study. The site-specific relationship between undrained Young's modulus and the in situ water content is also shown in Figure K.7.Table K.1 summarizes of the data obtained from the laboratory testing and evaluation.

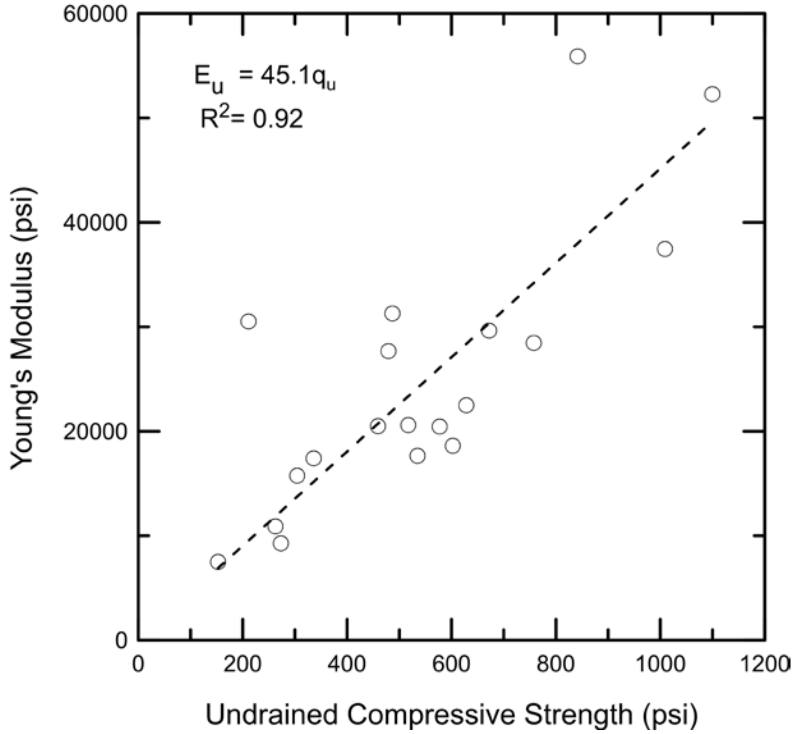

Figure K.6 Relationship between undrained compressive strength and Young's modulus.

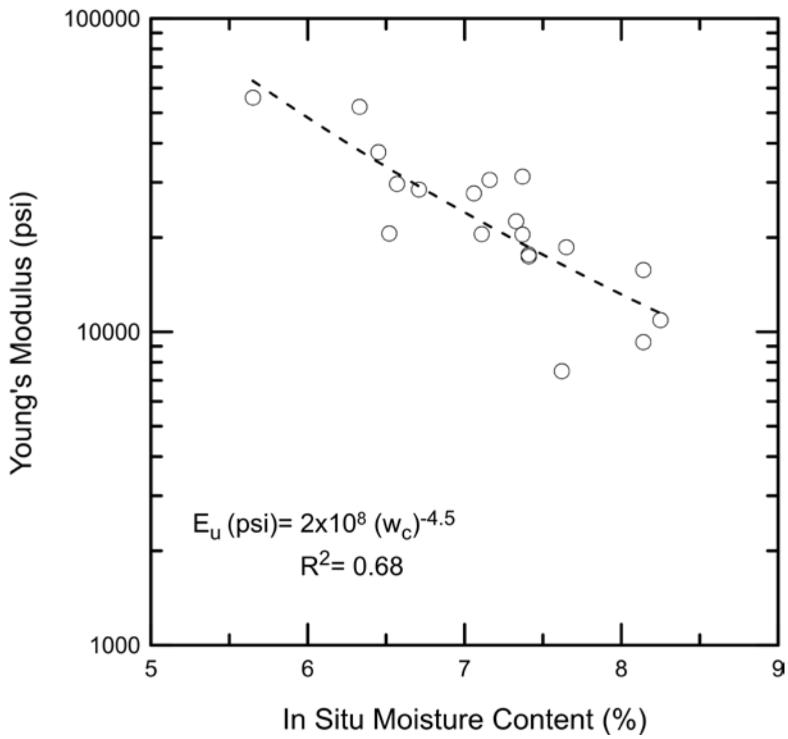

Figure K.7 Relationship between in situ moisture content and Young's modulus.

Table K.1 Laboratory Data Summary at the Eldamain road over the Fox river

Specimen Identification	**FX-B1-S1**	**FX-B1-S2**	**FX-B1.-S3**
Core Run Number	**1**	**1**	**1**
Depth (ft.)	25	26	31.5
Initial Water Content (%)	7.41	6.52	6.57
Total Unit Weight (pcf)	143.0	139.3	153
Undrained Compressive Strength (ksf)	77.06	74.54	96.82
Strain at Peak Strength (%)	3.21	2.42	2.28
Young's Modulus (ksf)	2542.34	2968.5	4270.80
Recovery (%)	98	98	98
Rock Quality Designation (%)	60	60	60
Joint Average Vertical Spacing (in)	2-12	2-12	2-12
Sample Description	CLAY SHALE, Gray, sandy	CLAY SHALE, Gray, sandy	CLAY SHALE, Gray, sandy Indurated

Specimen Identification	**FX-B1-S4**	**FX-B1-S5**	**FX-B1.-S6**
Core Run Number	**1**	**1**	**2**
Depth (ft.)	32.5	34.5	37.5
Initial Water Content (%)	6.45	7.37	6.33
Total Unit Weight (pcf)	152.3	151.0	146.1
Undrained Compressive Strength (ksf)	145.36	83.2	158.5
Strain at Peak Strength (%)	2.24	2.97	2.32
Young's Modulus (ksf)	5396.0	2946.6	7534.7
Recovery (%)	98	98	92
Rock Quality Designation (%)	60	60	75
Joint Average Vertical Spacing (in)	2-12	2-12	2-12
Sample Description	CLAY SHALE, Gray, sandy, Indurated	CLAY SHALE, Gray, sandy	CLAY SHALE, Gray, sandy Indurated

Specimen Identification	FX-B1-S7	FX-B2-S1	FX-B2.-S2
Core Run Number	**2**	**1**	**1**
Depth (ft.)	38.5	25	26.5
Initial Water Content (%)	6.71	7.4	8.1
Total Unit Weight (pcf)	150.2	153	149.3
Undrained Compressive Strength (ksf)	109.2	48.4	43.9
Strain at Peak Strength (%)	2.65	2.2	3.48
Young's Modulus (ksf)	4099.4	2507.7	2270.3
Recovery (%)	73.5	93	93
Rock Quality Designation (%)	92	100	100
Joint Average Vertical Spacing (in)	12	6-8	6-8
Sample Description	CLAY SHALE, Gray, sandy Indurated	CLAY SHALE, GRAY THINNLY BEDDEB	CLAY SHALE, GRAY THINNLY BEDDEB

Specimen Identification	FX-B2-S3	FX-B2.-S4	FX-B2.-S5
Core Run Number	**1**	**1**	**1**
Depth (ft.)	27.4	28	29.5
Initial Water Content (%)	8.25	7.11	7.65
Total Unit Weight (pcf)	151	150.5	144.5
Undrained Compressive Strength (ksf)	37.84	66.15	86.8
Strain at Peak Strength (%)	4.92	4.02	2.97
Young's Modulus (ksf)	1569.9	2954.1	2682.87
Recovery (%)	93	93	93
Rock Quality Designation (%)	100	100	100
Joint Average Vertical Spacing (in)	2-12	2-12	2-12
Sample Description	CLAY SHALE, Gray, sandy Indurated	CLAY SHALE, GRAY THINNLY BEDDEB	CLAY SHALE, GRAY THINNLY BEDDEB

Specimen Identification	FX-B2-S6	FX-B2-S7	FX-B2.-S8
Core Run Number	**1**	**1**	**1**
Depth (ft.)	30	31.5	33.5
Initial Water Content (%)	5.65	7.06	8.14
Total Unit Weight (pcf)	140.3	144.	161
Undrained Compressive Strength (ksf)	121.2	69.0	39.3
Strain at Peak Strength (%)	1.95	3.43	4.23
Young's Modulus (ksf)	8054.25	3987.25	1335.69
Recovery (%)	93	93	93
Rock Quality Designation (%)	100	100	100
Joint Average Vertical Spacing (in)	8	8	8
Sample Description	CLAY SHALE, GRAY THINNLY BEDDEB	CLAY SHALE, GRAY THINNLY BEDDEB	CLAY SHALE, GRAY THINNLY BEDDEB

Specimen Identification	FX-B2-S9	FX-B2-S10	FX-B2.-S11
Core Run Number	**1**	**2**	**2**
Depth (ft.)	34.5	35	37
Initial Water Content (%)	7.37	7.16	7.33
Total Unit Weight (pcf)	149.5	152.9	152.3
Undrained Compressive Strength (ksf)	70.14	30.4	90.5
Strain at Peak Strength (%)	2.75	3.97	4.97
Young's Modulus (ksf)	31275	305808	22502
Recovery (%)	100	100	100
Rock Quality Designation (%)	100	100	100
Joint Average Vertical Spacing (in)			
Sample Description	CLAY SHALE, GRAY THINNLY BEDDEB	CLAY SHALE, GRAY THINNLY BEDDEB	CLAY SHALE, GRAY THINNLY BEDDEB

Specimen Identification	**FX-B2-S12**		
Core Run Number	**2**		
Depth (ft.)	39		
Initial Water Content (%)	7.62		
Total Unit Weight (pcf)	152		
Undrained Compressive Strength (ksf)	22		
Strain at Peak Strength (%)	5.97		
Young's Modulus (ksf)	7494		
Recovery (%)	100		
Rock Quality Designation (%)	100		
Joint Average Vertical Spacing (in)			
Sample Description	CLAY SHALE, GRAY INDURATED		

APPENDIX L FIELD EXPLORATION AT US 150 OVER THE LITTLE VERMILLION RIVER

L.1 BACKGROUND

Figure L.1 shows location of US 150 over the Little Vermillion River, located in Vermillion County, just south Georgetown city, Illinois. This 2-span bridge structure carries a two-lane highway over the Vermillion River. The north and south abutments of this bridge are supported on driven H-piles while the pier is supported on drilled shaft foundations socketed into the underlying sedimentary rock. The weak shales near the south abutment, was investigated during this study.

Figure L.1 Location of US 150 over the Little Vermillion River.

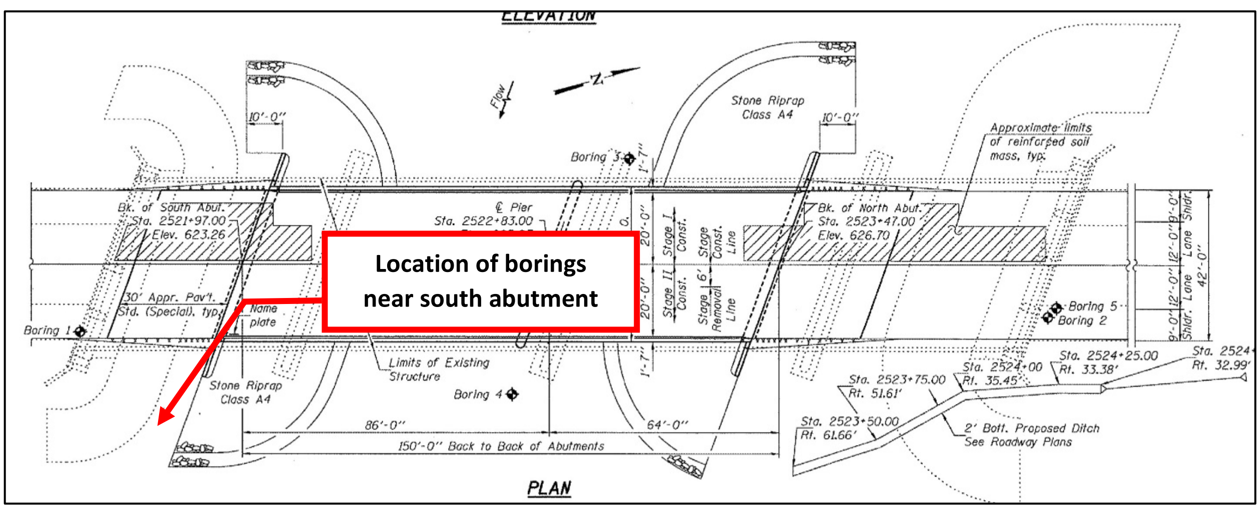

Figure L.2 Location of boring holes at US 150 over the Little Vermillion River.

Figure L.2 shows a plan view of US150 over the Little Vermillion River structure and the location of borings drilled on March, 24 2016 by Geocon drilling crew and the UIUC research team. Two borings were advanced near south abutment. These borings were drilled to an elevation of 587.0 feet.

The first boring was used to obtain shale core samples. Initially rock cores were used for determination of recovery ratio, RQD of the rock mass, and vertical spacing of joints. Afterwards unconfined compression tests were conducted on the retrieved shale specimens. The in situ water content of the shale specimens used in the unconfined compression tests was also measured for correlation purposes. The unconfined compression test results were also used to determine the deformability characteristics of shale under undrained loading conditions.

The second boring was used to obtain MSPT blow counts at various depths. These data were used to improve/check the correlation between undrained compressive strength of weak shale in Illinois and MSPT penetration rates developed in Phase 1 of this study. The following sections discuss geology of the bridge site, MSPT test results, and laboratory test results

L.2 SITE GEOLOGY

The geology at the bridge site consists of about 10.5 feet of brown/gray sandy clay loam overlying sedimentary bedrock, e.g., shale, and limestone. The ground surface elevation at the two borings, is about 622 feet. A fairly continuous layer of indurated clay shale was exposed at an elevation of 612.5 feet and extended to 587 feet were the coring was terminated. Laboratory test results are summarized in Table L.1.

L.3 MODIFED STANDARD PENETRATION TEST RESULTS

Figure L.3 shows the Modified Standard Penetration Test results obtained in one of the borings at US150 over the Little Vermillion River.

L.4 LABORATORY TEST RESULTS

L.4.1 Moisture Content and Total Unit Weight

Figure L.4 shows the total unit weight profile at the US150 over the Little Vermillion River site. The total unit weight of the encountered shales was computed in accordance with ASTM D7263.

Shale specimens from unconfined compressive tests were used for determination of in situ water content. The resulting water content profile is shown in Figure L.5. Water content of the Shales was determined in accordance with ASTM D2216.

L.4.2 Triaxial Compression Test Results

Unconfined triaxial compression tests were performed in accordance with ASTM D7012–14 (method D). The peak deviator stress was used to calculate the undrained compressive strength for each test. The resulting undrained compressive strengths are shown in Table L.1.

L.4.3 Young's Modulus of Mudstone Specimen

Young's modulus was measured from results of triaxial tests in accordance ASTM D7012–14 (method D). In short, the modulus was calculated from the slope of the stress-strain relationships that correspond to 50% of mobilized undrained compressive strengtL. Figure L.6 shows the relationship between Young's modulus and undrained compressive strength for the shales core tested from the US150 over the Little Vermillion River site. This data was also used to develop a relationship between Young's modulus and natural water content (see Figure L.7). Table L.1 summarizes all of the data obtained from the laboratory testing and evaluation.

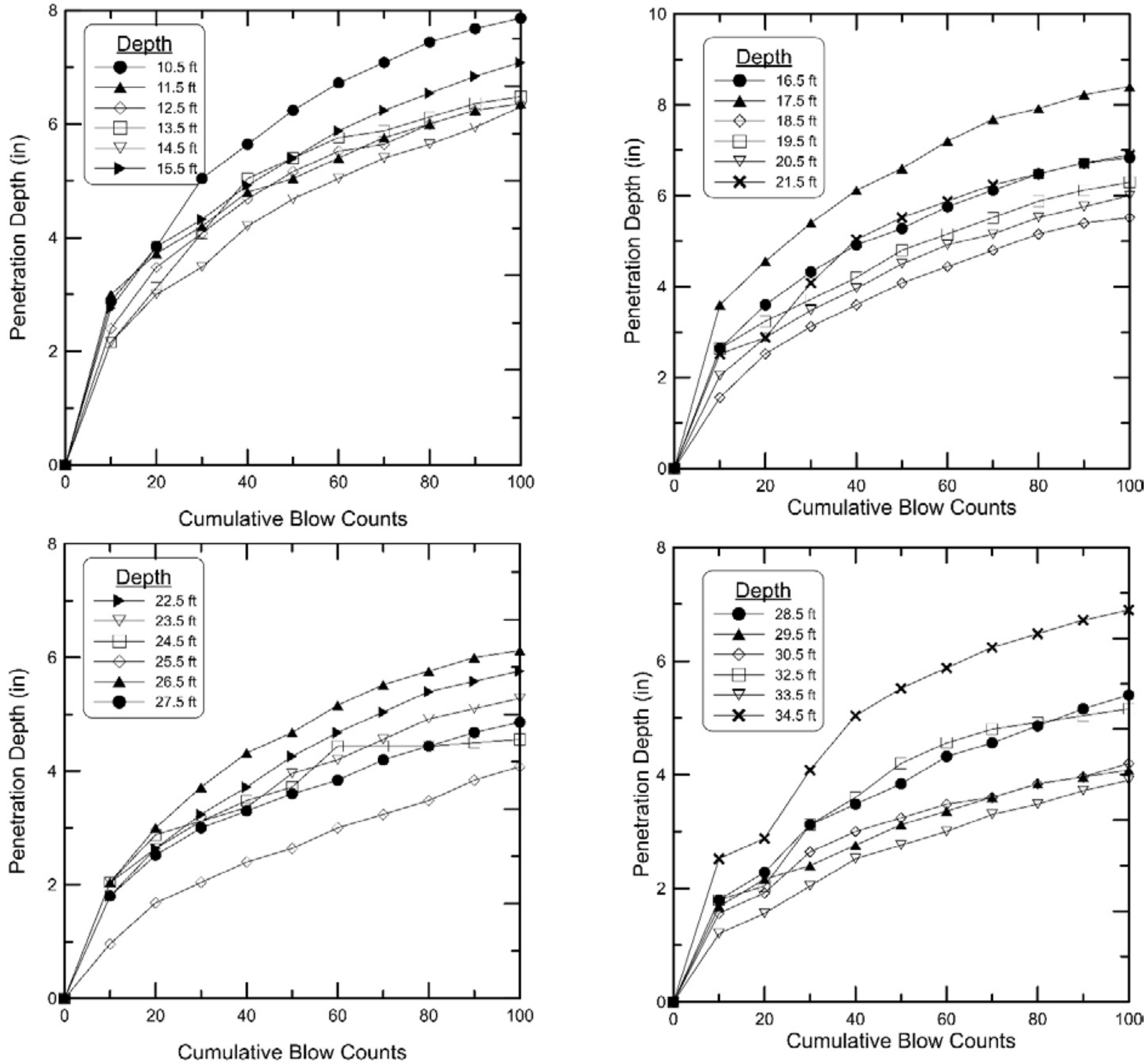

Figure L.3 Modified Standard Penetration Test results.

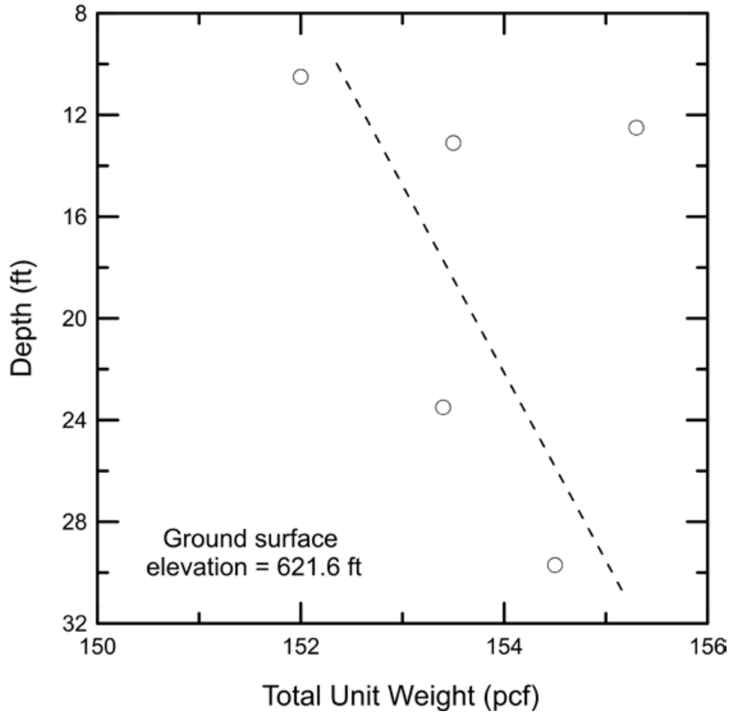

Figure L.4 Total unit weight profile.

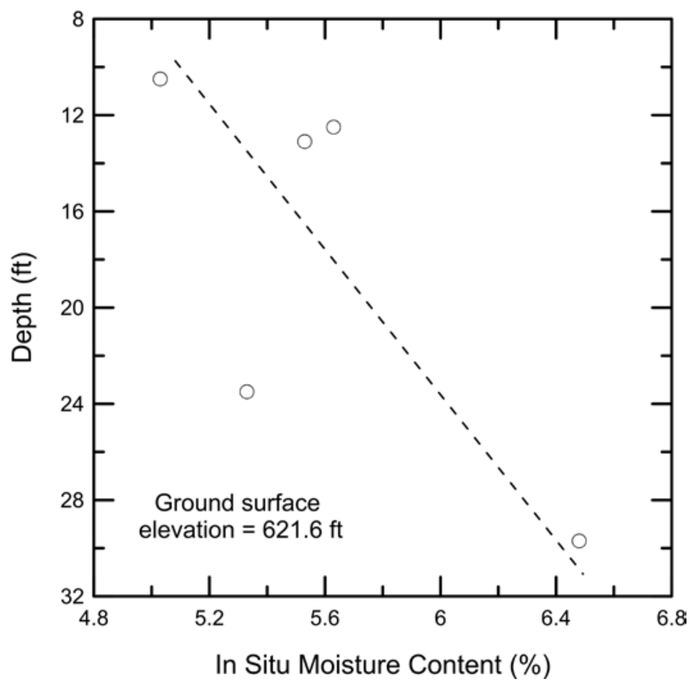

Figure L.5 In situ moisture content profile.

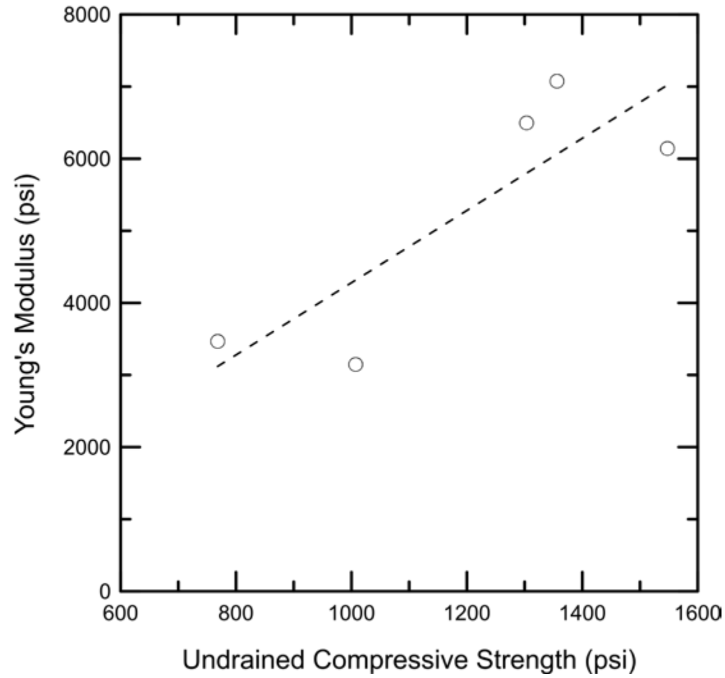

Figure L.6 Relationship between undrained compressive strength and Young's modulus.

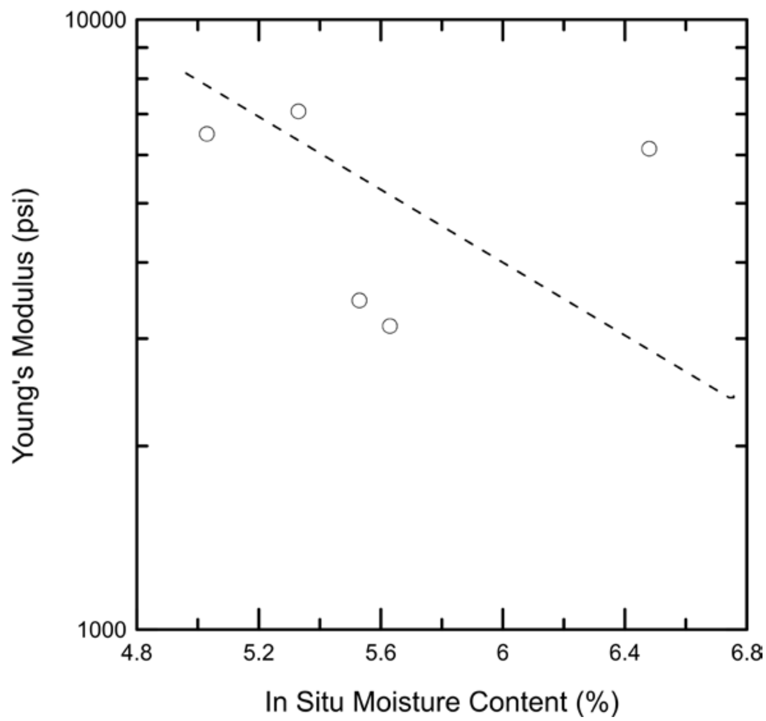

Figure L.7 Relationship between in situ moisture content and Young's modulus.

Table L.1 Laboratory Data Summary at the US 150 over the Little Vermillion River

Specimen Identification	**LV-S1**	**LV -S2**	**LV -S3**
Core Run Number	**1**	**1**	**1**
Depth (ft.)	10.5	12.5	13.1
Initial Water Content (%)	5.03	5.63	5.53
Total Unit Weight (pcf)	152	155.3	153.5
Undrained Compressive Strength (ksf)	187.8	145.1	110.7
Strain at Peak Strength (%)	4.38	5.85	5.48
Young's Modulus (ksf)	936.1	453.2	499.3
Recovery (%)	80	80	80
Rock Quality Designation (%)	65	65	65
Joint Average Vertical Spacing (in)	10	10	10
Sample Description	Gray Shales, indurated, massive	Gray Shales, indurated, massive	Gray Shales, indurated, massive

Specimen Identification	**LV-S4**	**LV-S5**	
Core Run Number	**2**	**2**	
Depth (ft.)	23.5	29.7	
Initial Water Content (%)	5.33	6.48	
Total Unit Weight (pcf)	153.4	154.5	
Undrained Compressive Strength (ksf)	195.4	223.0	
Strain at Peak Strength (%)	4.17	4.81	
Young's Modulus (ksf)	1019.3	884.8	
Recovery (%)	84	84	
Rock Quality Designation (%)	79	79	
Joint Average Vertical Spacing (in)	10	10	
Sample Description	Gray Shales, indurated, massive	Gray Shales, indurated, massive	

APPENDIX M FIELD EXPLORATION AT BL 55 OVER THE SALT CREEK

M.1 BACKGROUND

Figure M.1 shows location of BL 55 over Salt Creek, located in Logan County, just south of city of Lincolin, Illinois. This Five span bridge structure carries a four-lane highway over the Salt Creek. North and South abutments of this bridge are supported on driven H-piles foundations. Piers 1 to 4, however, are supported drilled shaft foundations that are socketed into weak shale. The weak shale near Pier 4, located near the south abutment, was investigated during this study.

Figure M.1 Location of BL 55 over Salt Creek.

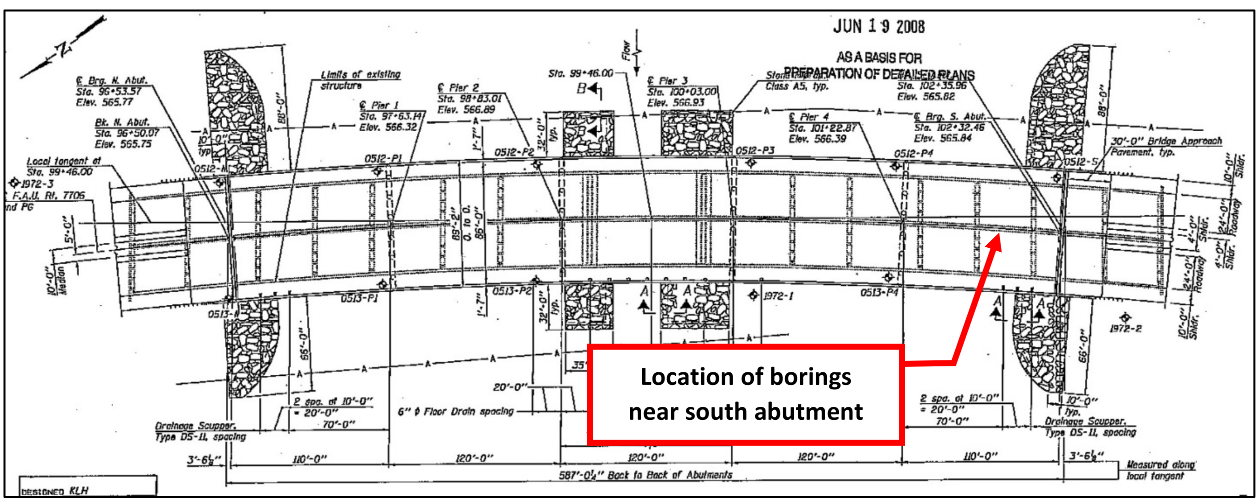

Figure M.2 Location of boring holes at BL 55 over Salt Creek.

Figure M.2 shows a plan view of BL55 over Salt Creek structure and the location of borings drilled on June 1, 2016 by the District 6 drilling crew and the UIUC research team. Two borings were advanced near south abutment and in close proximity to the Salt Creek. These borings were drilled to an elevation of 591 feet (i.e. 30 ft of shale cores were retrieved).

One of the two borings was used to obtain shale core samples. Initially rock cores were used for determination of recovery ratio, RQD of the rock mass, and vertical spacing of joints. Afterwards unconfined compression tests were conducted on the retrieved weak shales specimens. The in situ water content of the shale specimens used in the unconfined compression test was also measured for correlation purposes. The unconfined compression test results were also used to determine the deformability characteristics of shale under undrained loading conditions.

The second boring was used to obtain MSPT blow counts at various depths. This data was used to develop a new correlation between undrained compressive strength of weak shale in Illinois and MSPT penetration rate. The following sections discuss geology of the bridge site, MSPT test results, and laboratory test results

M.2 SITE GEOLOGY

The geology at the bridge site consists of about 30 feet of dark gray silt clay overlying sedimentary bedrock, e.g., shale, and limestone. The ground surface elevation at south abutment, i.e., the two borings, is about 546 feet. Gray Clay shale was exposed at an elevation of 617.5 feet. Laboratory test results are summarized in Table M.1.

M.3 MODIFED STANDARD PENETRATION TEST RESULTS

Figure M.3 shows the Modified Standard Penetration Test results obtained in one of the borings at BL55 over the Salt Creek.

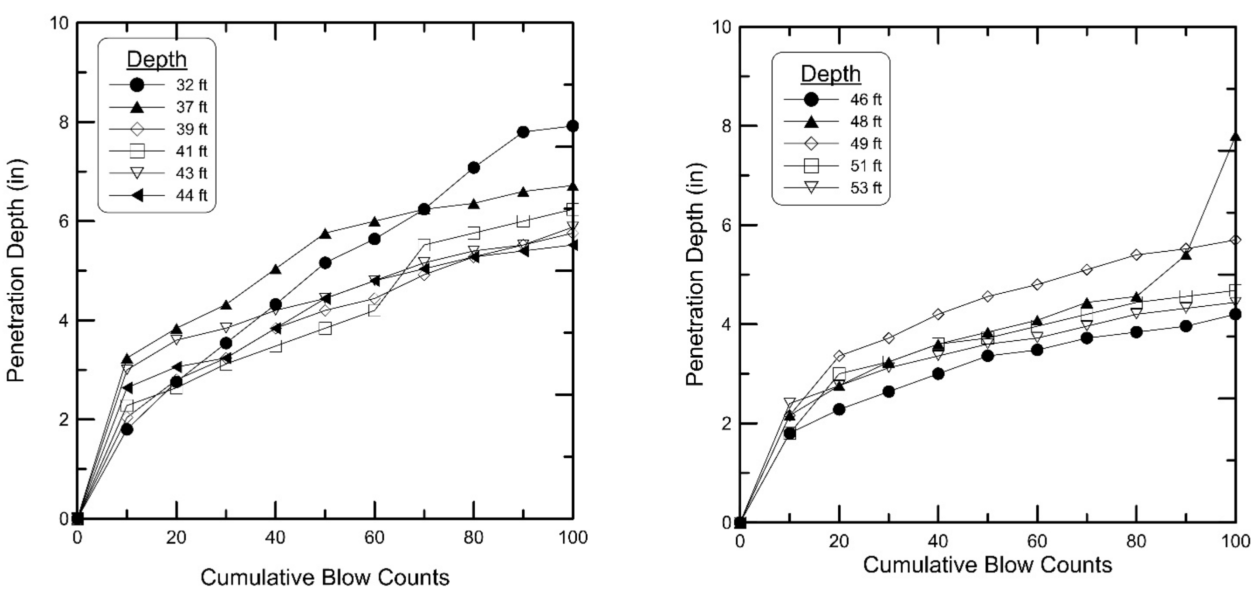

Figure M.3 Modified Standard Penetration Test results.

M.4 LABORATORY TEST RESULTS

M.4.1 Moisture Content and Total Unit Weight

Figure M.4 shows the total unit weight profile at the BL55 over the Salt Creek site. The total unit weight of shale was computed in accordance with ASTM D7263.

Shale specimens from unconsolidated undrained and unconfined compressive tests were used for determination of in situ water content. The resulting water content profile is shown in Figure M.5. Water content of the shale was determined in accordance with ASTM D2216.

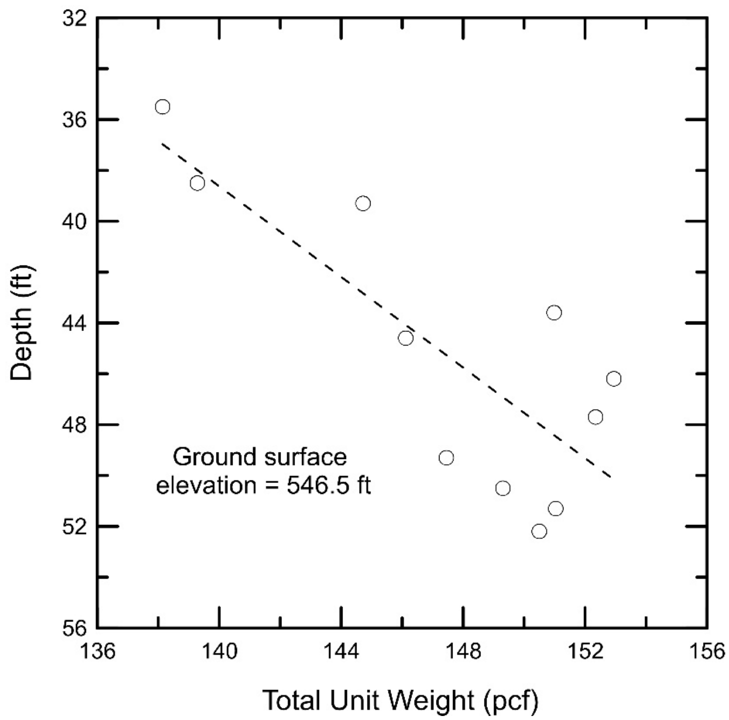

Figure M.4 Total unit weight profile.

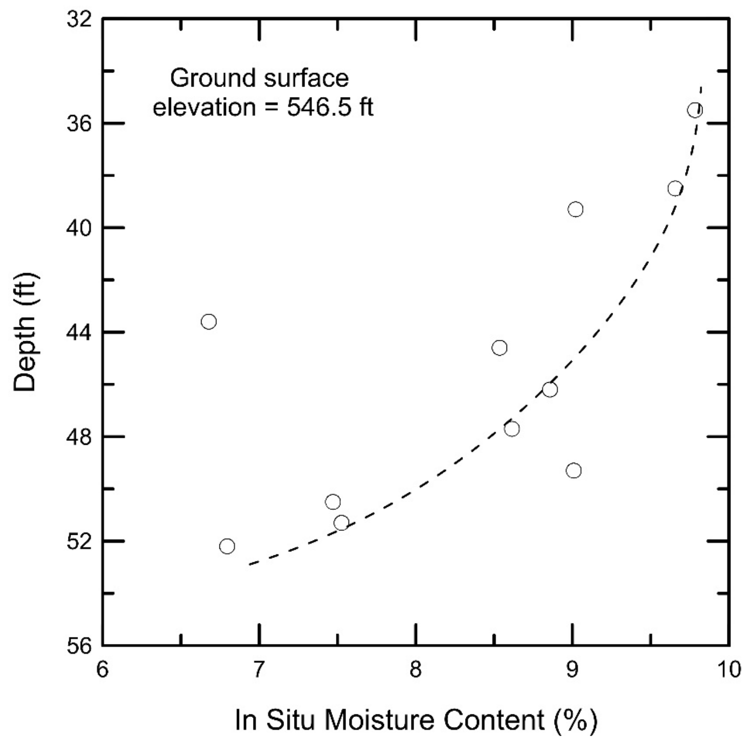

Figure M.5 In situ moisture content profile.

M.4.2 Triaxial Compression Test Results

Unconfined and confined triaxial compression tests were performed in accordance with ASTM D7012–14 (method D). The peak deviator stress was used to calculate the undrained compressive strength for each test. The resulting undrained compressive strengths are shown in Table M.1.

M.4.3 Young's Modulus of Shale Specimen

Young's modulus was measured from results of triaxial tests in accordance to ASTM D7012–14 (method D). In short, the modulus was calculated from the slope of the stress-strain relationships that correspond to 50% of mobilized undrained compressive strength. Figure M.6 shows the relationship between Young's modulus and undrained compressive strength for the shale core tested from the BL55 over the Salt Creek site. This data was also used to develop a relationship between Young's modulus and shale natural water content (see Figure M.7). The unconfined compressive strength to the undrained Young's modulus ratio shown in Figure M.6 agrees well with the general trends observed in Phase 1 & 2 of this study. The site-specific relationship between undrained Young's modulus and the in situ water content is also shown in Figure M.7. Table M.1 summarizes all of the data obtained from the laboratory testing and evaluation.

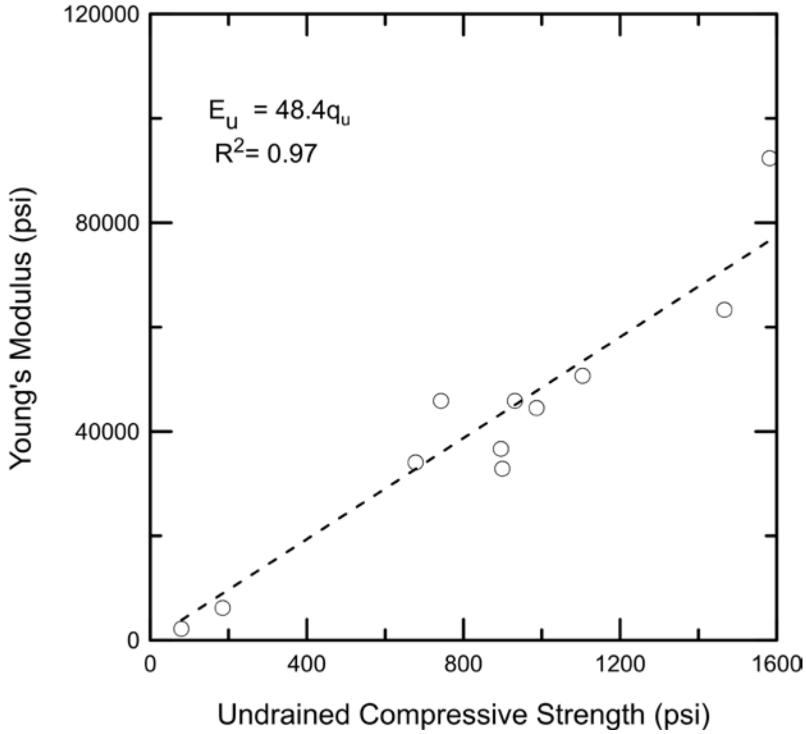

Figure M.6 Relationship between undrained compressive strength and Young's modulus.

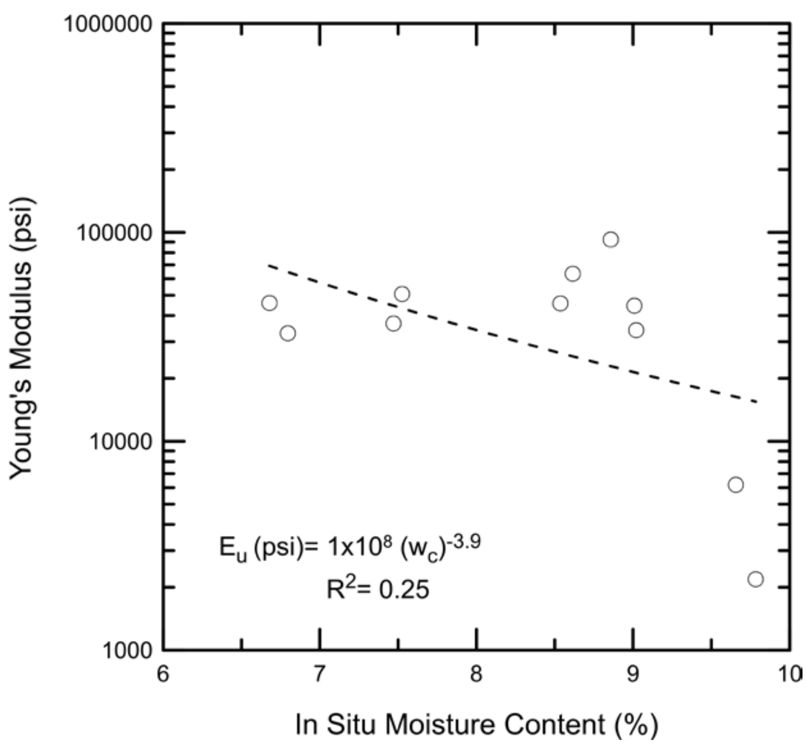

Figure M.7 Relationship between in situ moisture content and Young's modulus.

Table M.1 Laboratory Data Summary at the BL 55 over the Salt Creek site

Specimen Identification	**BL55-S1**	**BL55-S2**	**BL55-S3**
Core Run Number	**1**	**2**	**2**
Depth (ft.)	35.5	38.5	39.3
Initial Water Content (%)	9.78	9.66	9.02
Total Unit Weight (pcf)	138.1	139.3	144.7
Undrained Compressive Strength (ksf)	11.46 (UC)	26.63 (UC)	97.6 (UC)
Strain at Peak Strength (%)	5.69	4.89	3.32
Young's Modulus (ksf)	314.66	892	4903
Recovery (%)	100	100	100
Rock Quality Designation (%)	76	70	70
Joint Average Vertical Spacing (in)	2	4	12
Sample Description	CLAY SHALE, weathered, fissle, dark gray	CLAY SHALE, weathered, fissle, dark gray	CLAY SHALE, Indurated, dark gray

Specimen Identification	**BL55-S4**	**BL55-S5**	**BL55-S6**
Core Run Number	**3**	**3**	**4**
Depth (ft.)	43.6	44.6	46.2
Initial Water Content (%)	9.0	6.68	8.54
Total Unit Weight (pcf)	144.7	151	146.1
Undrained Compressive Strength (ksf)	134.2	107	228
Strain at Peak Strength (%)	3.35	2.77	3.19
Young's Modulus (ksf)	4903	6602.25	6576.57
Recovery (%)	100	100	100
Rock Quality Designation (%)	98	98	94
Joint Average Vertical Spacing (in)	12	12	12
Sample Description	CLAY SHALE, Indurated, dark gray	CLAY SHALE, Indurated, dark gray	SHALE, weathered, dark gray

Specimen Identification	BL55-S7	BL55-S8	BL55-S9
Core Run Number	**4**	**4**	**5**
Depth (ft.)	47.7	49.3	50.3
Initial Water Content (%)	8.61	9.01	7.47
Total Unit Weight (pcf)	152.3	147.45	149.3
Undrained Compressive Strength (ksf)	211.29	142.21	129
Strain at Peak Strength (%)	3.62	3.71	3.01
Young's Modulus (ksf)	9114.5	6408.07	5276.37
Recovery (%)	100	100	100
Rock Quality Designation (%)	94	94	98
Joint Average Vertical Spacing (in)	8	8	8
Sample Description	CLAY SHALE, Indurated, dark gray	CLAY SHALE, Indurated, dark gray	CLAY SHALE, Indurated, dark gray

Specimen Identification	BL55-S10	BL55-S11	
Core Run Number	**5**	**5**	
Depth (ft.)	51.3	52.2	
Initial Water Content (%)	7.53	6.8	
Total Unit Weight (pcf)	151	150	
Undrained Compressive Strength (ksf)	159.1	129.6	
Strain at Peak Strength (%)	3.06	3.26	
Young's Modulus (ksf)	7297.35	4729.94	
Recovery (%)	100	100	
Rock Quality Designation (%)	98	98	
Joint Average Vertical Spacing (in)	-	-	
Sample Description	CLAY SHALE, Indurated, dark gray	CLAY SHALE, Indurated, dark gray	

APPENDIX N FIELD EXPLORATION AT IL 108 OVER MACOUPIN CREEK

N.1 BACKGROUND

Figure N.1 shows location of the IL 108 over the Macoupin Creek, just east of the city of Carlinville, Illinois. East and west abutments of this bridge are supported on driven H-piles foundations. Piers 1, 2 and 3, however, are supported on drilled shaft foundations that are socketed. The weak shale near Pier 3, located near the east abutment, was investigated during this study.

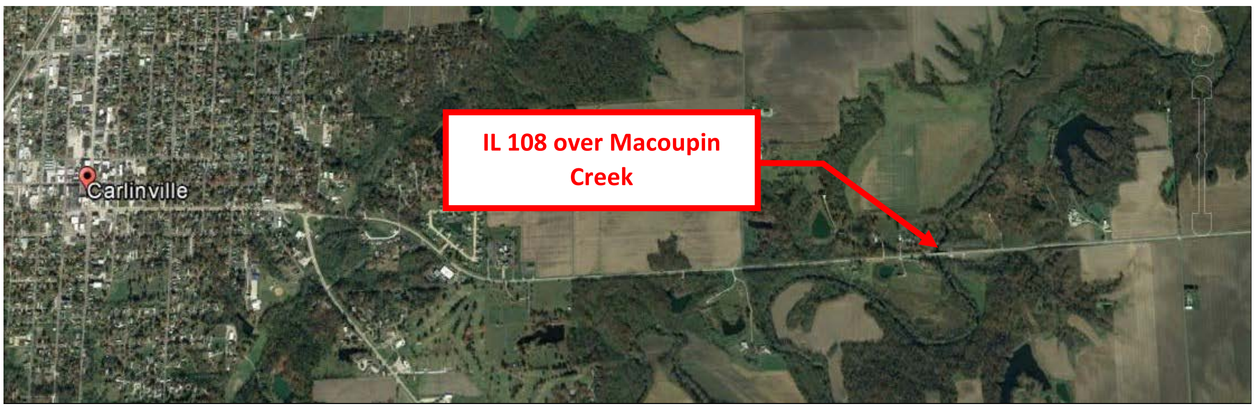

Figure N.1 Location of IL 108 over Macoupin Creek.

Figure N.2 shows a plan view of this IL 108 bridge structure over Macoupin Creek and the location of borings drilled on July 13, 2016 by the District 6 drilling crew and the UIUC research team. Two borings were advanced near the south east quad of the bridge and in close proximity to Macoupin Creek. These borings were drilled to a depth of twenty feet below the top of the weak shale layer.

Figure N.2 Location of boring holes for obtaining MSPT blow counts and shale core samples.

One of the two borings were used to obtain shale core samples. Initially rock cores were used for determination of recovery ratio, RQD of the rock mass, and vertical spacing of joints. Afterwards unconfined compression and triaxial compression tests were conducted on representative and comparable shale specimens to study effect of confining pressure on behavior of shale specimens subjected to compressive mode of shear. The in situ water content of the shale specimens used in the triaxial compression tests was also measured for correlation purposes. Triaxial test results were also used to determine the deformability characteristics of shale under undrained loading conditions.

The second boring was used to obtain MSPT blow counts at various depths. This data was used to develop a new correlation between undrained compressive strength of weak shale in Illinois and MSPT penetration rate.

The following sections discuss geology of the bridge site, MSPT test results, and laboratory test results.

N.2 SITE GEOLOGY

The geology at the bridge site consists of sandy clay loam overlying sedimentary bedrock, e.g., shale, and limestone. The ground surface elevation at the two borings is about 554.5 feet. Overburden soil at this site consists of sandy loam and silty clay loam. A relatively continuous black to gray blocky clay shale was exposed at an elevation of about 537.5 feet that extends to elevation 517.5 feet where the boring terminated.

N.3 MODIFIED STANDARD PENETRATION TEST RESULTS

Figure N.3 shows the Modified Standard Penetration Test results obtained in one of the borings at IL 108 over the Macoupin Creek.

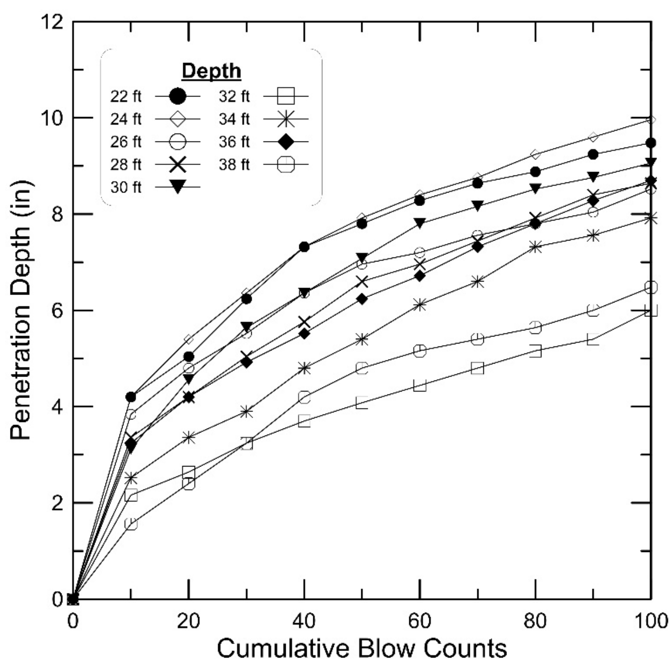

Figure N.3 Modified Standard Penetration Test results.

N.4 LABORATORY TEST RESULTS

N.4.1 Moisture Content and Total Unit Weight

Figure N.4 shows the total unit weight profile at the Macoupin Creek site. The total unit weight of shale was computed in accordance with ASTM D7263.

Shale specimens from unconfined compressive tests were used for determination of in situ water content. The resulting moisture content profile is shown in Figure N.5. Moisture content of the shale was determined in accordance with ASTM D2216.

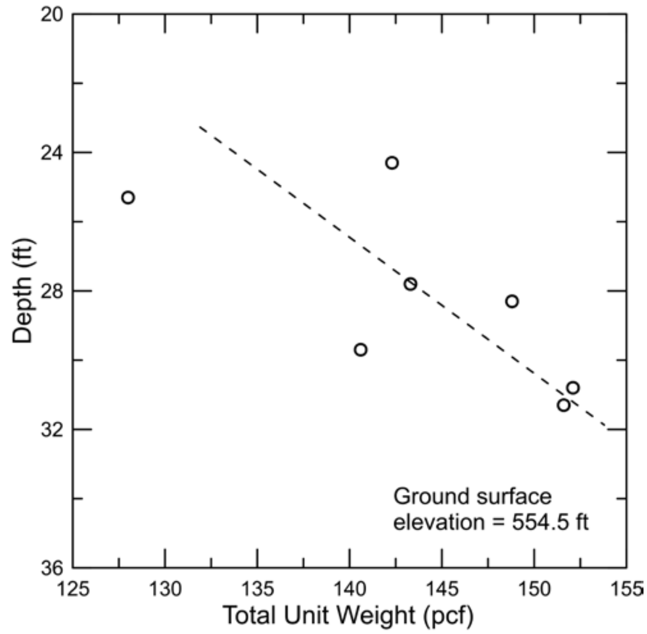

Figure N.4 Total unit weight profile.

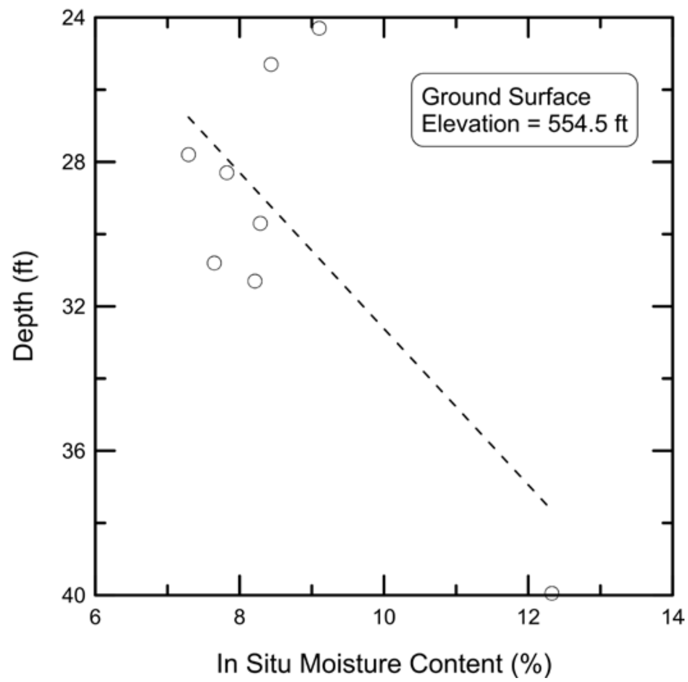

Figure N.5 In situ water content profile.

N.4.2 Triaxial Compression Test Results

Unconfined compression tests were performed in accordance with ASTM D7012–14 (method D). The peak deviator stress was used to calculate the undrained compressive strength for each test. The resulting undrained compressive strengths are shown in Table N.1.

N.4.3 Young's Modulus of Shale Specimen

Young's modulus was measured from results of triaxial tests in accordance to ASTM D7012–14 (method D). In short, the modulus was calculated from the slope of the stress-strain relationships that correspond to 50% of mobilized undrained compressive strength. Figure N.6 shows the relationship between Young's modulus and undrained compressive strength for the shale cores tested from the Macoupin Creek site. This data was also used to develop a relationship between undrained Young's modulus and shale natural water content (see Figure N.7). The unconfined compressive strength to the undrained Young's modulus ratio shown in Figure N.6 agrees well with the general trends observed in Phase 1 & 2 of this study. The site-specific relationship between undrained Young's modulus and the in situ water content is also shown in Figure N.7. Table N.1 summarizes all the data obtained from the laboratory testing and evaluation.

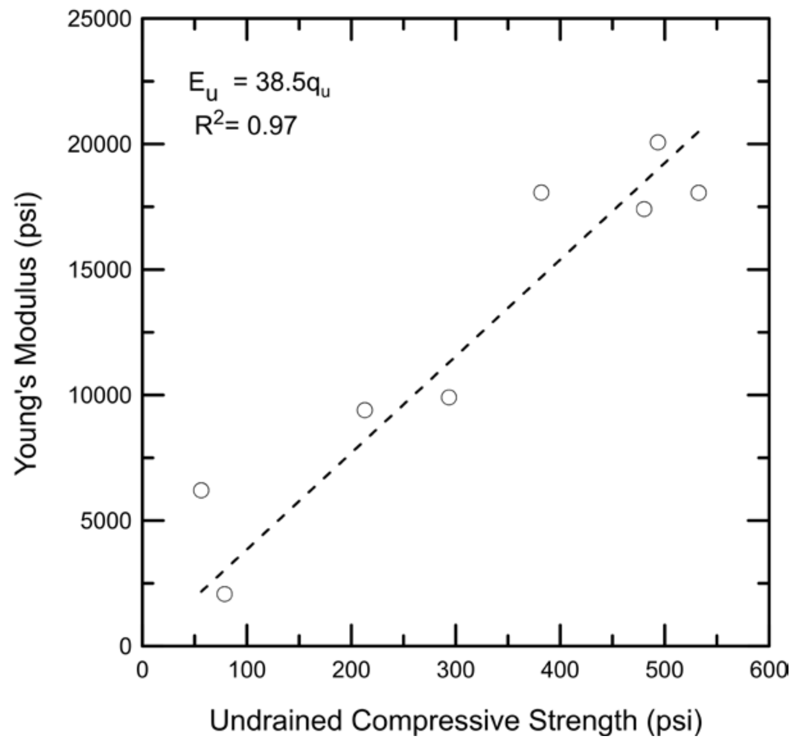

Figure N.6 Relationship between undrained compressive strength and Young's modulus.

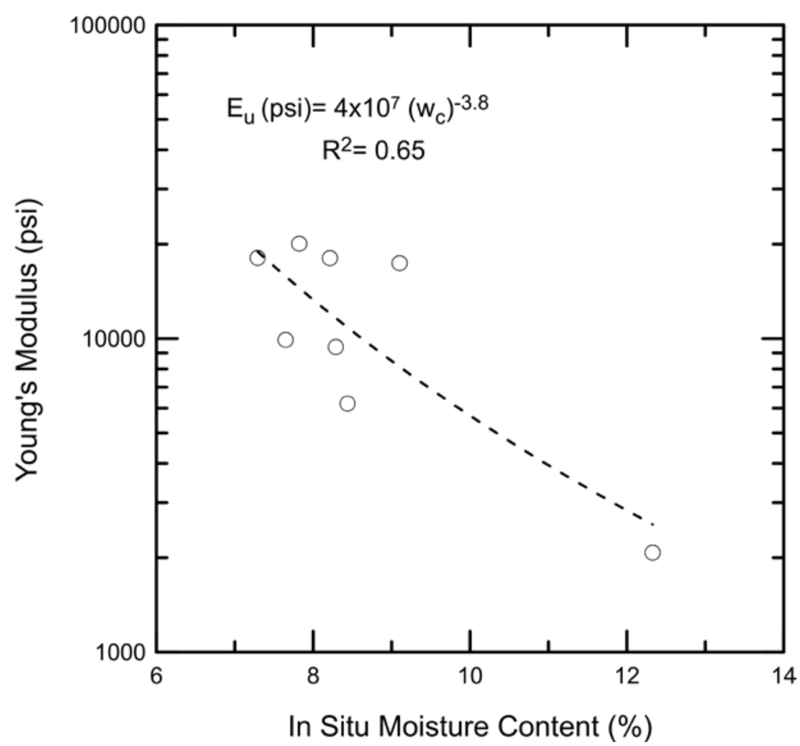

Figure N.7 Relationship between initial water content and Young's modulus.

Table N.1 Laboratory Data Summary at the IL 108 Over Macoupin Creek

Specimen Identification	**IL 108-S1**	**IL 108-S2**	**IL 108-S3**
Core Run Number	**1**	**2**	**2**
Depth (ft.)	24.3	25.3	27.8
Initial Water Content (%)	9.1	8.44	7.29
Total Unit Weight (pcf)	142.3	128.0	143.3
Undrained Compressive Strength (ksf)	69.2	8.1	55.0
Strain at Peak Strength (%)	0.7	1.76	3.41
Young's Modulus (ksf)	2507	893.5	2601
Recovery (%)	80	82	82
Rock Quality Designation (%)	65	70	70
Joint Average Vertical Spacing (in)	8	3	2
Sample Description	Gray CLAYEY SHALE	Fissle CLAYEY SHALE	CLAY SHALE, Gray and blocky

Specimen Identification	**IL 108-S4**	**IL 108-S5**	**IL 108-S6**
Core Run Number	**2**	**2**	**3**
Depth (ft.)	28.3	29.7	30.8
Initial Water Content (%)	7.82	8.29	7.65
Total Unit Weight (pcf)	148.8	140.6	152.1
Undrained Compressive Strength (ksf)	71.1	30.6	42.3
Strain at Peak Strength (%)	3.85	2.8	3.8
Young's Modulus (ksf)	2890	1352.7	1426.8
Recovery (%)	93	93	93
Rock Quality Designation (%)	82	82	82
Joint Average Vertical Spacing (in)	5	5	3
Sample Description	Gray CLAYEY SHALE	Gray CLAYEY SHALE	CLAY SHALE, Gray and

Specimen Identification	IL 108-S7	IL 108-S8
Core Run Number	**3**	**4**
Depth (ft.)	31.3	39.95
Initial Water Content (%)	8.21	5.4
Total Unit Weight (pcf)	151.6	1
Undrained Compressive Strength (ksf)	76.7	11.32
Strain at Peak Strength (%)	4.6	5.6
Young's Modulus (ksf)	2600.4	298.86
Recovery (%)	90	90
Rock Quality Designation (%)	70	70
Joint Average Vertical Spacing (in)	10	10
Sample Description	Calcareous SHALE	Gray fissle CLAYEY SHALE

APPENDIX O FIELD EXPLORATION AT CH-28 OVER THE HORSE CREEK

O.1 BACKGROUND

Figure O.1 shows location of CH28 over the Horse creek, located in Sangamon County, just South the city of Pawnee, Illinois. This 4-span bridge structure carries a two-lane highway over the Des Plaines River. The abutments and the 3 piers of this bridge are supported shallow foundations resting on the shallow sedimentary rocks (i.e. shales, limestones). The weak shales near the north abutment, was investigated during this study.

Figure O.1 Location of CH-28 over the Horse creek bridge site.

Figure O.2 Location of boring holes at CH-28 over the Horse creek.

Figure O.2 shows a plan view of CH-28 over the Horse Creek River structure and the location of borings drilled on September 1, 2016 by District 6 drilling crew and the UIUC research team.

Two borings were advanced near north abutment. These borings were drilled to an elevation of 545.0 feet.

The first boring was used to obtain shale core samples. Initially rock cores were used for determination of recovery ratio, RQD of the rock mass, and vertical spacing of joints. Afterwards unconfined compression tests were conducted on the retrieved weak shales specimens. The in situ water content of the shale specimens used in the unconfined compression tests was also measured for correlation purposes. The unconfined compression test results were also used to determine the deformability characteristics of shale under undrained loading conditions.

The second boring was used to obtain MSPT blow counts at various depths. These data were used to improve/check the correlation between undrained compressive strength of weak shale in Illinois and MSPT penetration rates developed in Phase 1 of this study. The following sections discuss geology of the bridge site, MSPT test results, and laboratory test results.

O.2 SITE GEOLOGY

The geology at the bridge site consists of about 21 feet of Medium Stiff, Dark Brown/Gray, Moist, Silty Clay, with traces of Gravel and Sand overlying sedimentary bedrock, e.g., shale, and limestone. The ground surface elevation at the two borings, is about 581 feet. A fairly continuous layer of clay shale was exposed at an elevation of 560 feet and extended to 545 feet were the coring was terminated. Laboratory test results are summarized in Table O.1.

O.3 MODIFED STANDARD PENETRATION TEST RESULTS

Figure O.3 shows the Modified Standard Penetration Test results obtained in one of the borings at CH28 over the Horse Creek River.

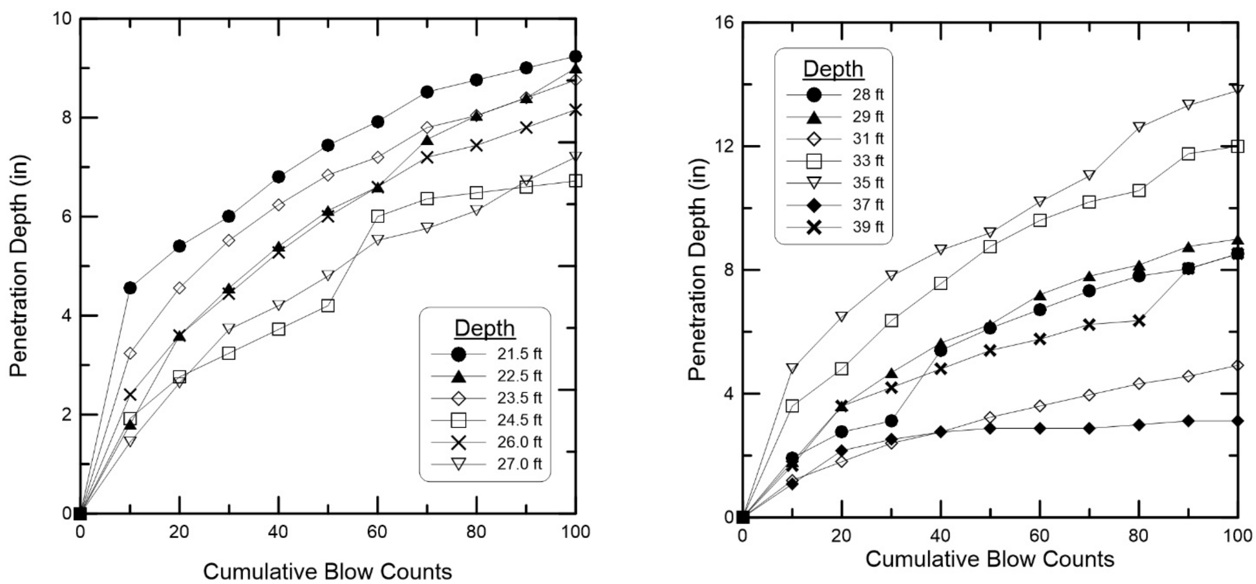

Figure O.3 Modified Standard Penetration Test results.

O.4 LABORATORY TEST RESULTS

O.4.1 Moisture Content and Total Unit Weight

Figure O.5 shows the total unit weight profile at the CH28 over the Horse creek site. The total unit weight of the encountered shales was computed in accordance with ASTM D7263.

Shale specimens from unconfined compressive tests were used for determination of in situ water content. The resulting water content profile is shown in Figure O.6. Water content of the Shales was determined in accordance with ASTM D2216.

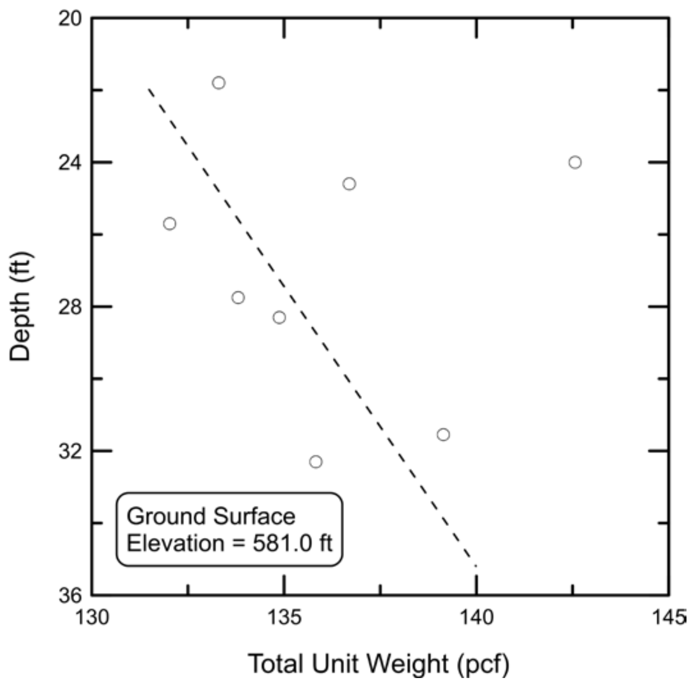

Figure O.4 Total unit weight profile.

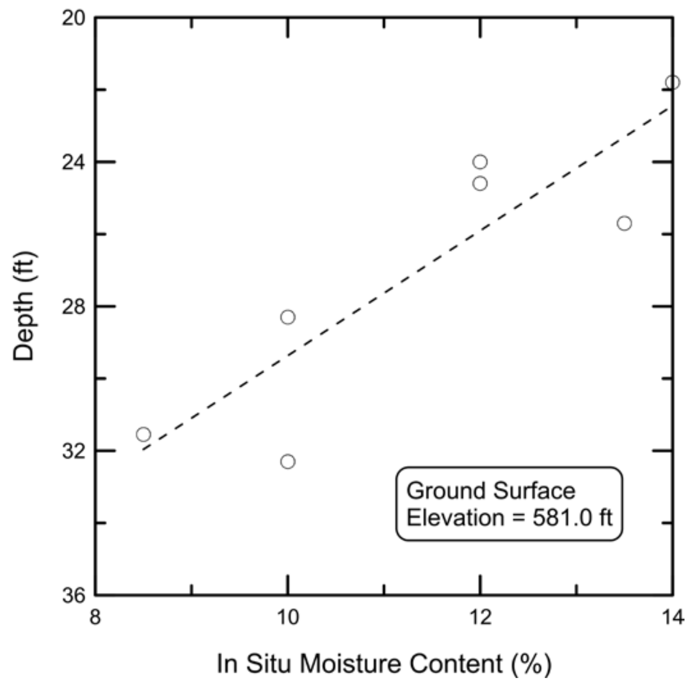

Figure O.5 In situ moisture content profile.

O.4.2 Triaxial Compression Test Results

Unconfined triaxial compression and Undrained Triaxial tests were performed in accordance with ASTM D7012–14 (method D). The peak deviator stress was used to calculate the undrained compressive strength for each test. The resulting undrained compressive strengths are shown in Table O.1.

O.4.3 Young's Modulus of Shale Specimen

Young's modulus was measured from results of triaxial tests in accordance to ASTM D7012–14 (method D). In short, the modulus was calculated from the slope of the stress-strain relationships that correspond to 50% of mobilized undrained compressive strength. Figure O.7 shows the relationship between Young's modulus and undrained compressive strength for the shales core tested from the CH28 over the Horse creek site. This data was also used to develop a relationship between Young's modulus and natural water content (see Figure O.8). Table O.1 summarizes all the data obtained from the laboratory testing and evaluation.

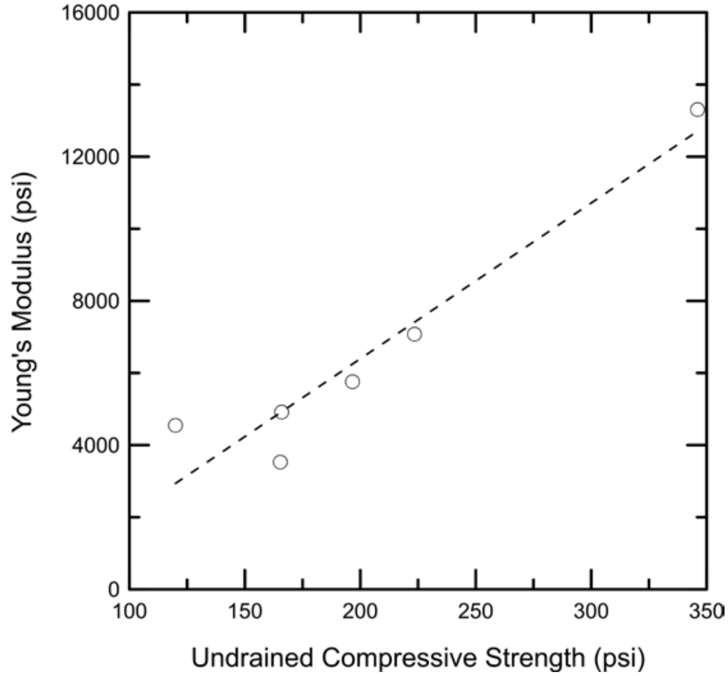

Figure O.6 Relationship between undrained compressive strength and Young's modulus.

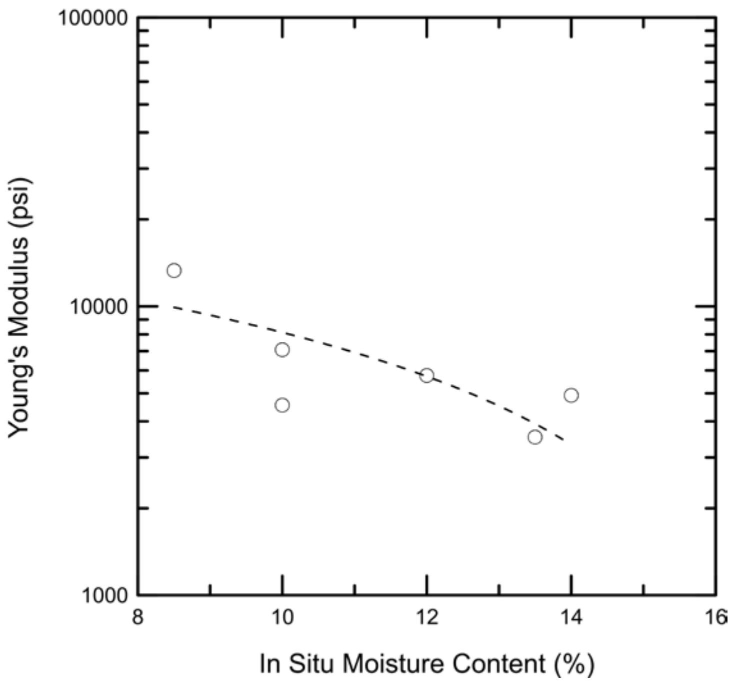

Figure O.7 Relationship between in situ moisture content and Young's modulus.

Table O.1 Laboratory Data Summary at the CH-28 over the Horse creek

Specimen Identification	**SP-S1**	**SP-S2**	**SP-S3**
Core Run Number	**1**	**1**	**1**
Depth (ft.)	21.8	24.0	24.6
Initial Water Content (%)	14	12	12
Total Unit Weight (pcf)	133.3	142.6	136.7
Undrained Compressive Strength (ksf)	23.9	28.3	45.5
Strain at Peak Strength (%)	4.29	5.85	4.7
Young's Modulus (ksf)	708.4	829.8	-
Recovery (%)	100	100	100
Rock Quality Designation (%)	100	100	100
Joint Average Vertical Spacing (in)	1 to 3	1 to 3	1 to 3
Sample Description	Clay Shales Gray, Weathered, soft	Clay Shales Gray, Weathered, soft	Clay Shales Gray, Weathered, soft

Specimen Identification	**SP-S4**	**SP-S5**	**SP-S6**
Core Run Number	**1**	**2**	**3**
Depth (ft.)	25.7	28.3	31.55
Initial Water Content (%)	13.5	10	8.5
Total Unit Weight (pcf)	132.0	134.9	133.8
Undrained Compressive Strength (ksf)	23.8	32.2	49.8
Strain at Peak Strength (%)	5.3	3.92	3.04
Young's Modulus (ksf)	508.1	1019.7	1917.1
Recovery (%)	100	68	76
Rock Quality Designation (%)	100	68	76
Joint Average Vertical Spacing (in)	2 to 7	2 to 7	2 to 7
Sample Description	Clay Shales Gray,	Clay Shales Gray,	Clay Shales Gray,

Specimen Identification	**SP-S7**		
Core Run Number	**3**		
Depth (ft.)	32.3		
Initial Water Content (%)	10		
Total Unit Weight (pcf)	135.8		
Undrained Compressive Strength (ksf)	17.28		
Strain at Peak Strength (%)	3.68		
Young's Modulus (ksf)	655.4		
Recovery (%)	76		
Rock Quality Designation (%)	76		
Joint Average Vertical Spacing (in)	2 to 7		
Sample Description	Clay Shales Gray,		

APPENDIX P FIELD EXPLORATION AT IL 160 OVER THE SILVER CREEK

P.1 BACKGROUND

Figure P.1 shows location of IL160 over the Silver Creek, located in Madison County, just south Grantfork, Illinois. This 3-span bridge structure carries a two-lane highway over the Silver Creek. The north and south abutments of this bridge are supported on driven H-piles while the piers are supported on drilled shaft foundations socketed into the underlying sedimentary rock. The weak clay shales near the north abutment, was investigated during this study.

Figure P.1 Location of IL160 over the Silver Creek.

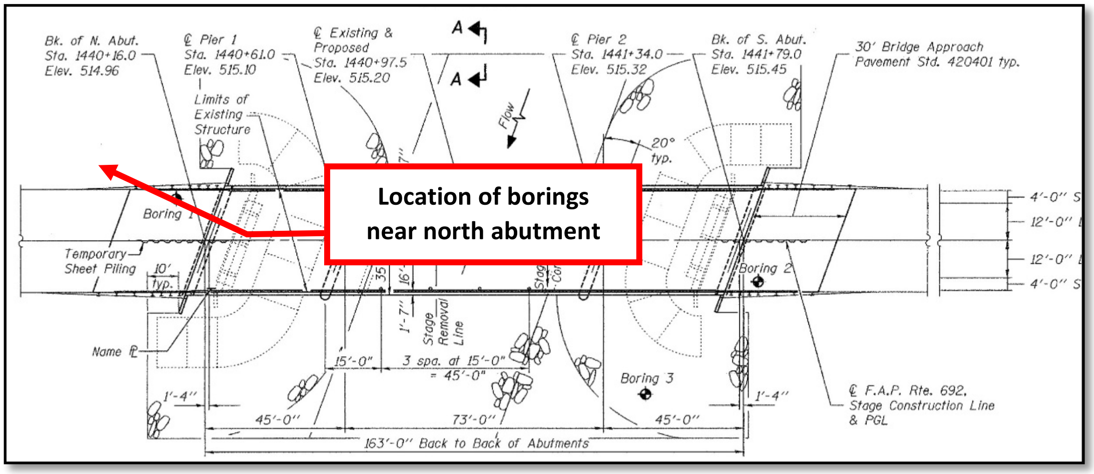

Figure P.2 Location of boring holes at IL160 over the Silver Creek.

Figure P.2 shows a plan view of IL160 over the Silver Creek structure and the location of borings drilled on March 3, 2017 by TSi Geotechnical drilling crew and the UIUC research team. Two borings were advanced near north abutment. These borings were drilled to an elevation of 487.0 feet.

The first boring was used to obtain shale core samples. Initially rock cores were used for determination of recovery ratio, RQD of the rock mass, and vertical spacing of joints. Afterwards unconfined compression tests were conducted on the retrieved shale specimens. The in situ water content of the shale specimens used in the unconfined compression tests was also measured for correlation purposes. The unconfined compression test results were also used to determine the deformability characteristics of shale under undrained loading conditions.

The second boring was used to obtain MSPT blow counts at various depths. These data were used to improve/check the correlation between undrained compressive strength of weak shale in Illinois and MSPT penetration rates developed in Phase 1 of this study. The following sections discuss geology of the bridge site, MSPT test results, and laboratory test results

P.2 SITE GEOLOGY

The geology at the bridge site consists of about 16 feet of brown/gray silty clay overlying sedimentary bedrock, e.g., limestone, and shale. The ground surface elevation at the two borings, is about 515 feet. A 2.5 feet thick gray indurated limestone layer was exposed at an elevation of 499 feet underlain by a fairly continuous layer of clay shale that extended to elevation of 487 feet were the coring was terminated. Laboratory test results are summarized in Table P.1.

P.3 MODIFED STANDARD PENETRATION TEST RESULTS

Figure P.3 shows the Modified Standard Penetration Test results obtained in one of the borings at IL160 over the Silver Creek.

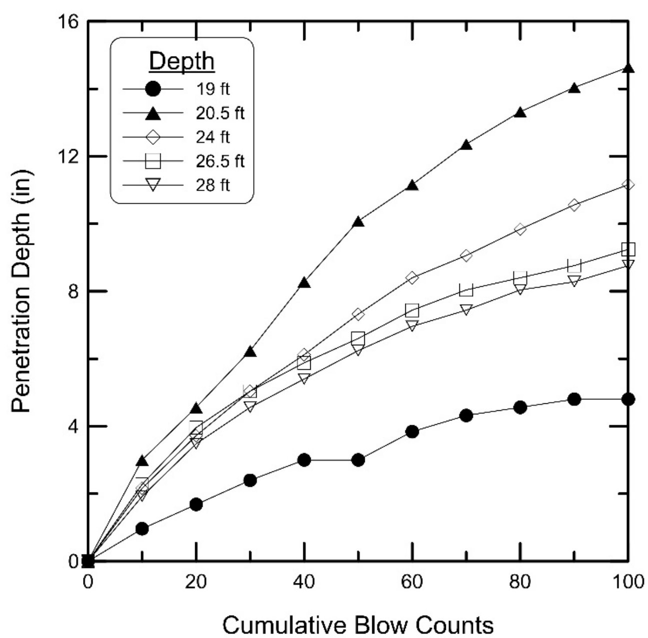

Figure P.3 Modified Standard Penetration Test results.

P.4 LABORATORY TEST RESULTS

P.4.1 Moisture Content and Total Unit Weight

Figure P.4 shows the total unit weight profile at the IL160 over the Silver Creek site. The total unit weight of the encountered shales was computed in accordance with ASTM D7263.

Shale specimens from unconfined compressive tests were used for determination of in situ water content. The resulting water content profile is shown in Figure P.5. Water content of the shales was determined in accordance with ASTM D2216.

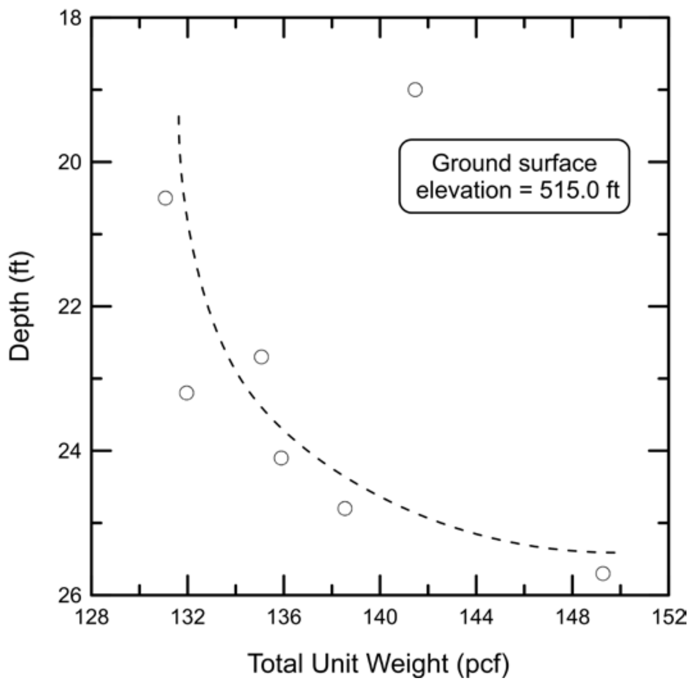

Figure P.4 Total unit weight profile.

P.4.2 Triaxial Compression Test Results

Unconfined triaxial compression tests were performed in accordance with ASTM D7012. The peak deviator stress was used to calculate the undrained compressive strength for each test. The resulting undrained compressive strengths are shown in Table P.1.

P.4.3 Young's Modulus of Shale Specimen

Young's modulus was measured from results of triaxial tests in accordance to ASTM D7012. In short, the modulus was calculated from the slope of the stress-strain relationships that correspond to 50% of mobilized undrained compressive strength. Figure P.6 shows the relationship between Young's modulus and undrained compressive strength for the shales core tested from the IL160 over Silver Creek site. This data was also used to develop a relationship between Young's modulus and natural water content (see Figure P.7). Table P.1 summarizes all the data obtained from the laboratory testing and evaluation.

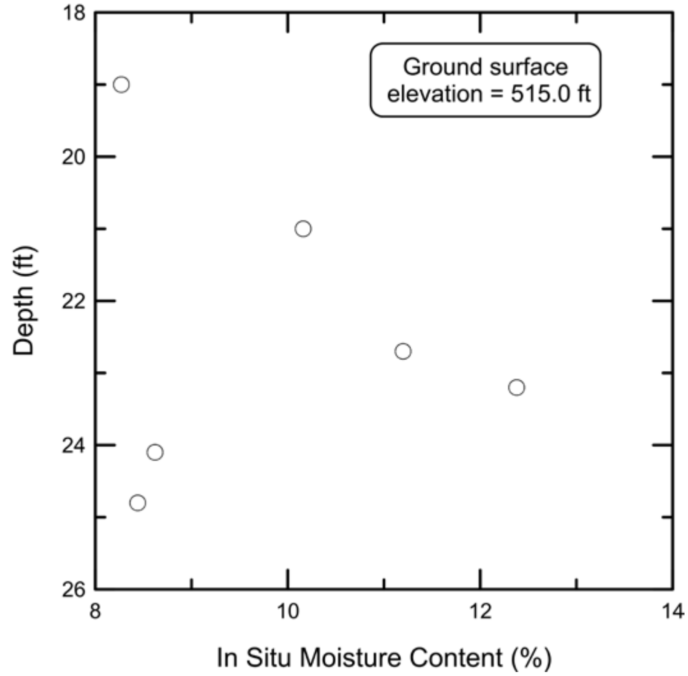

Figure P.5 In situ moisture content profile.

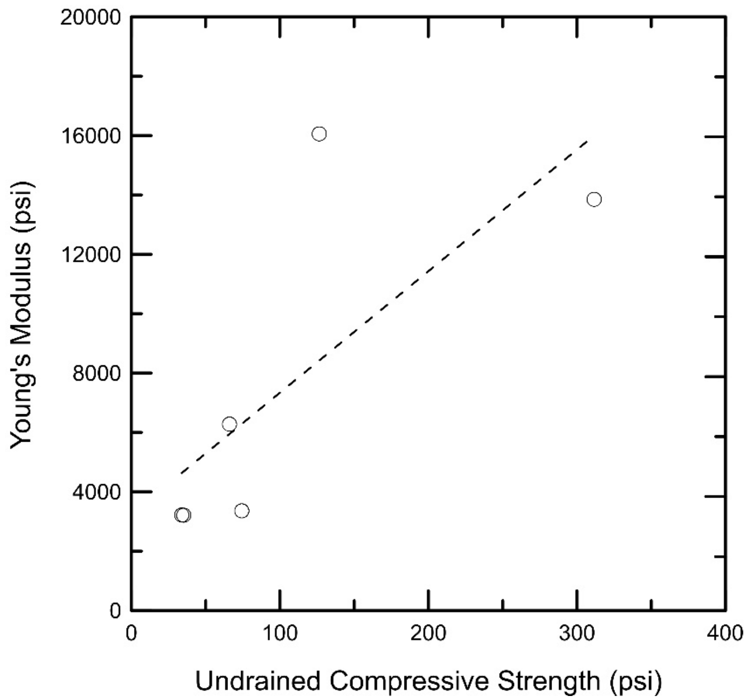

Figure P.6 Relationship between undrained compressive strength and Young's modulus.

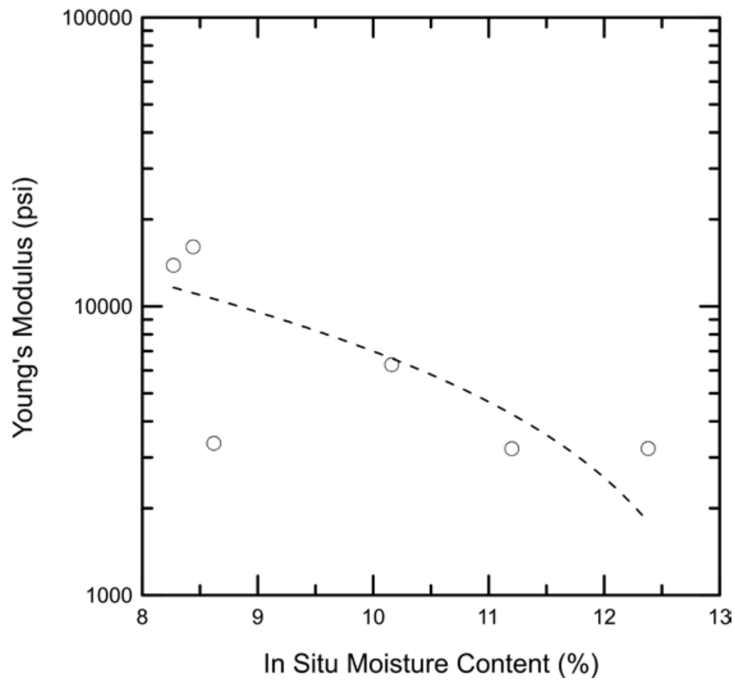

Figure P.7 Relationship between in situ moisture content and Young's modulus.

Table P.1 Laboratory Data Summary at the IL 160 over Silver Creek

Specimen Identification	**SVC-S1**	**SVC -S2**	**SVC -S3**
Core Run Number	**2**	**2**	**2**
Depth (ft.)	19	20.5	22.7
Initial Water Content (%)	8.27	10.16	11.20
Total Unit Weight (pcf)	141.5	131.1	135.1
Undrained Compressive Strength (ksf)	44.9	9.5	5.1
Strain at Peak Strength (%)	2.65	4.03	1.73
Young's Modulus (ksf)	1996.2	905	463.1
Recovery (%)	90	90	90
Rock Quality Designation (%)	55	55	55
Joint Average Vertical Spacing (in)	2 to 5	2 to 5	2 to 5
Sample Description	Dark Gray Clay Shales.	Dark Gray Clay Shales	Dark Gray Clay Shales, fissile and weathered

Specimen Identification	SVC -S4	SVC -S5	SVC -S6
Core Run Number	**2**	**3**	**3**
Depth (ft.)	23.2	24.1	24.8
Initial Water Content (%)	12.4	8.6	8.45
Total Unit Weight (pcf)	132.0	135.9	138.5
Undrained Compressive Strength (ksf)	4.89	10.7	18.22
Strain at Peak Strength (%)	1.8	3.1	2.2
Young's Modulus (ksf)	463.8	483.5	2314
Recovery (%)	90	100	100
Rock Quality Designation (%)	55	60	60
Joint Average Vertical Spacing (in)	2 to 5	8 to 12	8 to 12
Sample Description	Dark Gray Clay Shales, fissile and weathered	Gray Shales, indurated, massive	Gray Shales, indurated, massive

APPENDIX Q ILLINOIS MODIFIED STANDARD PENETRATION TEST PROCEDURE

Q.1 INTRODUCTION

The Standard Penetration Test (SPT) (ASTM D1586-11 or AASHTO T 206-09) has been used to estimate strength parameters of soils for a long time. It has also been used to estimate undrained shear strength parameters for weak rocks when it is difficult to obtain high-quality/undisturbed samples for laboratory testing. However, the full 18 inches (45 cm) of penetration required to measure an N-value (number of blows to drive split- spoon sampler the last 12 inches), can be difficult or impossible to obtain in weak rocks. To limit overstressing and damage to a split-spoon sampler, the ASTM and AASHTO test standards permit the penetration of a sampler to be halted under the following conditions:

1. A total of 50 blows have been applied during any one of the three 6 inch (0.15 m) increments,
2. A total of 100 blows have been applied, and
3. There is no observed advance of the sampler during the application of 10 successive blows

SPT data recently obtained from twenty one (21) Illinois Department of Transportation (IDOT) bridge sites underlain by weak shales typically exhibits penetrations of the split-spoon sampler of only 6 to 12 inches (15 to 30 cm) after 100 blows of an automatic trip hammer weighing 140 lbf (63.5 kg) with a drop distance of 30 inches (76 cm). This is problematic because it limits the correlated material strength to conservative values for foundation design by having less than 18 inches of penetration. Using these lower bound strengths may lead to conservative and more costly foundation designs. To expand the range of strengths interpreted from SPT results in weak fine-grained rocks (e.g. shales), the SPT procedure was modified to record penetraton data in 10 blow increments and correlate it to undrained shear strength of weak fine-grained rocks. The resulting Modified SPT (MSPT) procedure is summarized below.

Q.2 MSPT APPLICABILITY

The MSPT procedure is designed to be used in weak rocks and shales that exhibit unconfined compressive strength (UCS) between 10 and 100 ksf. The test provides a means for estimating undrained shear strength of such geomaterial as per the correlation developed by Stark et al. (2017). Geomaterial with a UCS between 10 and 100 ksf is also referred to as cohesive Intermediate Geologic Material (IGM) by O'Neill and Reese (1999).

Q.3 WHEN TO USE THE MSPT

The following two drilled shaft deisgn scenarios are envisioned for the MSPT: (1) site with prior subsurface investigation and (2) new site with no existing subsurface data. The following paragraphs describe how to use the MSPT for these two scenarios.

Prior Subsurface Investigation

If boring logs are available from a previous site investigation, determine the range of UCS from the boring logs and reported testing. If the UCS is between 10 and 100 ksf, use the MSPT for these materials and rock coring is not required if the foundation will be founded in these geomaterials. If the foundation will not be founded in these materials and the UCS exceeds 100 ksf in the other materials, rock coring of the founding materials is needed to measure the UCS for design purposes. If the foundation will not be founded in these materials and the UCS is less than 10 ksf in the other materials, traditional SPTs and soil testing of the founding materials is needed to measure the UCS for drilled shaft design purposes.

New Site with No Prior Subsurface Investigation

If investigating a new site where no previous testing or borings logs are available, a boring should be initially drilled with traditional SPTs being conducted at a reasonable depth interval, e.g., every 2.5 ft to 5 ft (0.75 to 1.5 m). Standard SPT sampling should be continued until a material with strengths typically in the range of 10 to 100 ksf, such as shale or other cohesive IGMs, are encountered, and/or the split-spoon sampler is unable to penetrate the full depth (18 inches) prior to termination. Under such conditions, the drilling crew should switch to rock coring using a double tube swivel type, split core barrel to decrease the exposure of the cored shale to the drilling fluid and maintain the strength and integrity of the shale for laboratory testing. The core barrel could have a diameter of 2.0 to 2.5 inches, e.g., NX or NQ-2 core barrel.

Shale cores should be examined to identify the geologic description of the encountered shales. Fissure Spacing, Rock Quality Designation (RQD), and Total Core Recovery (TCR) should be measured. If the extracted shale cores are highly fragmented/broken that will prevent obtaining intact specimens for laboratory UCS testing, MSPT should be conducted in a second borehole adjacent to the rock coring borehole to evaluate the UCS of that layer.

Where there are multiple borings to be drilled at a new project site, both rock coring and MSPT are recommended for the first boring to determine if the site materials are a candidate for the MSPT and to have a visual sample of the materials for contracting purposes. If the rock core or split-spoon sample exhibits an UCS between 10 and 100 ksf via visual inspection, e,.g., weak and/or highly fractured, or using a field Rimac device, proceed with MSPTs and further rock coring may not be needed at the other boring sites. MSPTs should be conducted at a reasonable depth interval, e.g., every 2.5 ft to 5 ft (0.75 to 1.5 m). At any MSPT borehole, if the measured pentration for the last 40 blows is less than 0.5 inches, the drilling crew should stop the MSPT testing and switch to rock coring because the UCS probably exceeds 100 ksf.

Q.4 MODIFIED STANDARD PENETRATION TEST

The MSPT is based on a new defined parameter termed the Penetration Rate (N_{rate}) which utilizes penetration per 10 blows instead of blows per foot. The Penetration Rate is defined as the inverse of the slope of the secondary or linear portion of a penetration versus cumulative blow counts relationship for an individual SPT (see Figure 1). The results of MSPTs conducted for twenty one (21) Illinois Department of Transportation (IDOT) bridge sites underlain by weak rocks and shales show that N_{rate} generally approaches a constant value after 40 to 60 blows and it remains constant regardless of the achieved penetration (See Note 1). Therefore, the rate of penetration can provide a means of evaluating the strength of the material beyond the current SPT procedure terminating criteria. The MSPT is stopped after 100 blows regardless of the depth of penetration.

Note 1:

This is likely due to the split-spoon sampler passing through the disturbed material at the bottom of the boring and reaching intact/undisturbed material below after 40 to 60 blows.

MSPT Procedure

The MSPT procedure is simple and similar in many respects to the SPT (ASTM D1586-11 or AASHTO T 206-09). The equipment used in the MSPT is the same as that used in SPT but the blow count and penetration data is collected differently. At each MSPT elevation or depth, the sampler penetration is measured at the end of ten (10) blows of a 140 lbf (63.5 kg) hammer falling 30 inches (76 cm) using a measuring device, such as a stick ruler. This measurement is repeated 10 times for a total of 100 blows and then the MSPT is stopped. MSPTs show a secondary/linear slope, which is often achieved after 40 to 60 blow counts for the weak fine-grained rocks tested herein with an unconfined compressive strength (UCS) of 10 to 100 ksf (0.48 to 4.8 MPa).

Figure 1 shows the penetration depth versus blow count relationship and the initial and secondary slopes of the blow count versus penetration relationship from a MSPT. The initial slope is associated with disturbed and loose material or cuttings at the bottom of the borehole and the tip of the split-spoon sampler of the MSPT. The initial slope is not representative of the UCS of the intact/undisturbed weak rock and thus is not used for the correlation between N_{rate} and UCS developed herein. The secondary slope is typically more linear and representative of the intact strength of the weak fine-grained rock. The procedure for obtaining the secondary slope and penetration rate is outlined below:

1. Drill to the desired depth of the MSPT, insert the MSPT split-spoon sampler (see Note 2) and necessary drill rod,
2. Considering the length of drill rod exposed above the casing, choose and mark a convenient point on the drill rod at which depth of penetration measurements will be taken using a measuring device, e.g., a stick ruler. This convenient point could be the bottom of the anvil or a drill rod joint.
3. Measure the initial distance of the drill rod segment between the top of the hollow stem auger or borehole casing and the point chosen in Step 2.
4. Apply 10 blows to the top of the drill rod using a 140 lbf hammer falling 30 inches, measure and record the new distance between the top of the hollow stem auger casing and the point chosen in Step 2. This can be accomplished by stopping the test or by using a stick ruler that is inserted into this length and read between the 10^{th} and 11^{th} blows of this sequence.
5. Measure and record the new distance between the top of the hollow stem auger casing and the point chosen in Step 2 before the 11^{th} blow of this sequence,
6. Repeat Steps 2 through 5 to obtain the sampler penetration for the 20-, 30-, 40-, 50-, 60-, 70-, 80-, 90-, and 100-blow count increments.
7. Obtain the SPT hammer energy rating from the driller for analyzing the MSPT results.

<u>Note 2:</u>

The split-spoon sampler and the driving shoe shall be in a good to new condition and must be replaced if it is dented or distorted. The opening of the driving shoe should be confirmed with a #11 rebar to ensure the opening is circular and 1 3/8 inches (34.9 cm) in diameter and the driving shoe reasonably sharp.

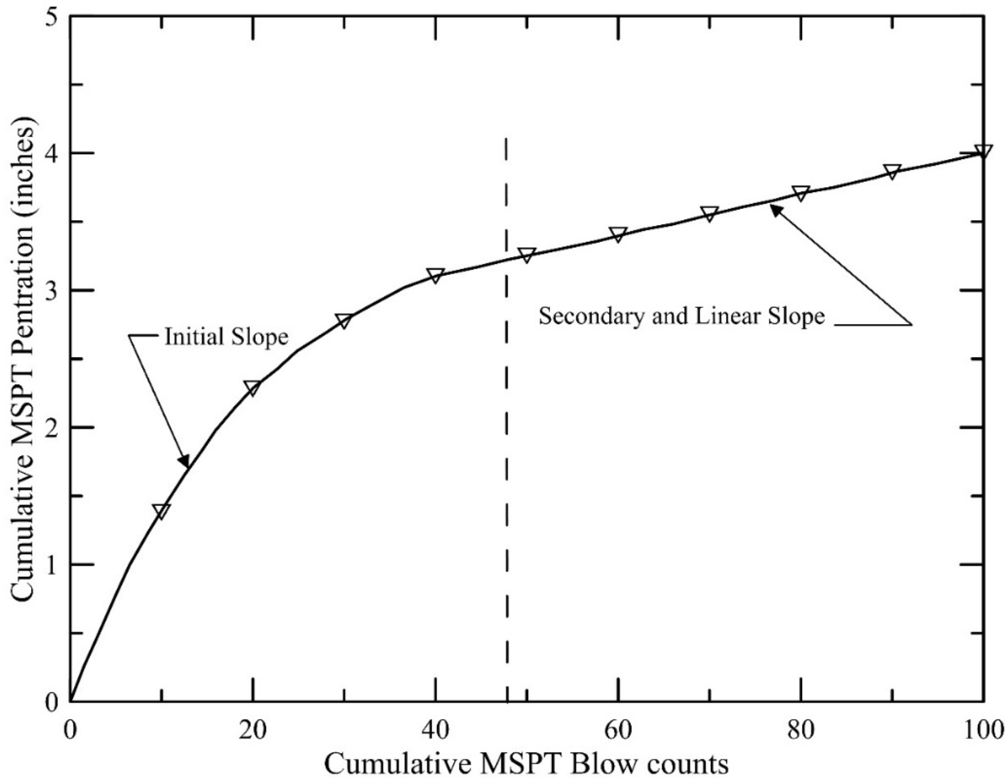

Figure 1. Typical MSPT cumulative penetration versus cumulative blow counts plot for Illinois weak shale

MSPT Analysis Procedure

The procedure for determining N_{rate} from the relationship of penetration depth versus MSPT blow counts is shown in Figure 1 and is outlined below:

1. Using the data obtained from a MSPT, plot the cumulative penetration versus cumulative blow count.
2. Determine the range of the linear portion of the resulting cumulative penetration versus cumulative MSPT blow count plot relationship.
3. Draw the best fit line through the linear portion of the cumulative penetration versus MSPT blow count plot.
4. Determine the slope of the best fit line, which is the Secondary Slope.
5. N_{rate} is the inverse of the Secondary Slope obtained in Step 3 and is defined as:

$$N_{\text{rate}} = \left(\frac{\Delta\text{Cumulative MSPT Blow count}}{\Delta\text{Cumulative Penetnration}}\right)$$

Irregular Cumulative Penetration Rates Analysis

Cumulative penetration versus cumulative blow count relationships may contain two or more linear portions (see Figure 2). Irregular plots indicate the sampler has entered a different stratigraphic layer or encountered a gravel or cobble particle. Thus, rock and/or soil material present in the split-spoon sampler from a MSPT should be carefully inspected to document any changes in material type or presence of a gravel or cobble particle, which will assist in understanding aberrant trends in the data when it is plotted. Irregular cumulative penetration versus cumulative blow count relationships can be conservatively interpreted by using the secondary slope that yields the lowest value of N_{rate} or by taking the average slope which yields an average N_{rate}.

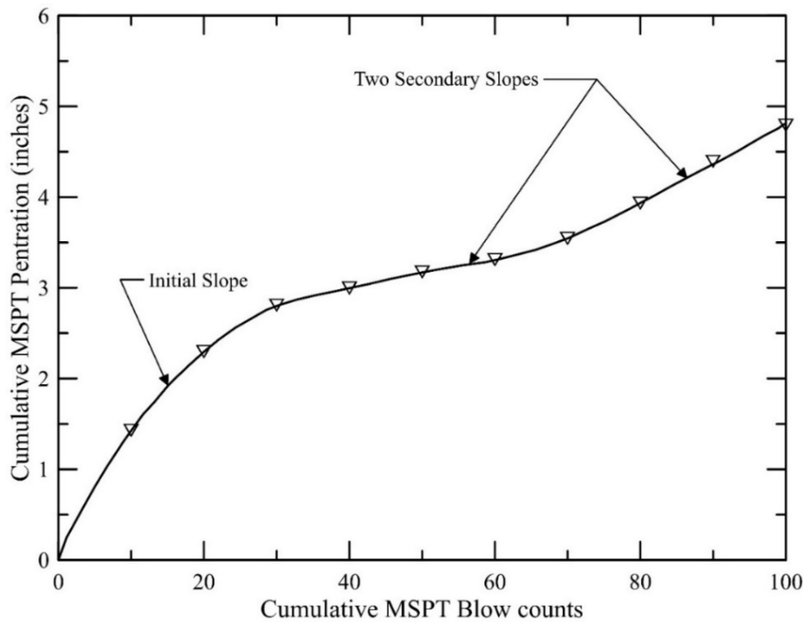

Figure 2. Irregular MSPT cumulative penetration versus cumulative penetration blow counts plot for Illinois weak shale

Q.5 MSPT Penetration Rate Correction

As with blow counts obtained from traditional SPTs, the MSPT penetration rate should be corrected for the effect of hammer energy, borehole diameter, sampler liner, and drill rod length (see Table Q.1). If the MSPT blow counts and penetration rate are obtained using an automatic trip hammer, the results from this study indicate 75% to 95% of the theoretical maximum hammer energy is delivered to the drill rod. To minimize the MSPT blow counts corrections, an energy ratio of 90% shall be used because all of the drill rigs used during this study utilized an automatic trip hammer and imparted an average of 90% of the theoretical maximum hammer energy. Thus, MSPT N_{rate} values obtained using an automatic trip hammer, which is the most commonly used hammer by IDOT, do not require significant corrections in comparison to the previously suggested energy correction factor for soils, i.e., 60% of the theoretical maximum hammer energy. A normalized penetration rate, $(N_{rate})_{90}$, was developed herein and is defined as follows for hammers that deliver 90% of theoretical maximum energy:

$$(N_{rate})_{90} = \frac{N_{rate} \times E_M \times C_B \times C_S \times C_R}{90}$$

where:

$(N_{rate})_{90}$ = N_{rate} corrected for 90% of the theoretical energy and various field procedures

E_M = hammer efficiency (i.e. average energy transfer ratio), %

C_B = borehole diameter correction

C_S = sampler correction

C_R = rod length correction, and

N_{rate} = measured penetration rate, bpf

Table Q.1 shows the recommended borehole diameter, rod length, and sampler correction factors from Skempton (1986). If the hammer does not yield 90% of the theoretical maximum hammer energy, the measured hammer energy should be inserted for E_M in the equation above to normalize the measured N_{rate} to 90% of the theoretical maximum hammer energy. The sampler correction assumes that liners will be installed in the split-spoon sampler to be consistent with Skempton (1986) even though the practice now is to not use liners.

Table Q.1: N_{rate} Correction factors after Skempton (1986)

Effect	Variable	Term	Value
Borehole diameter	2.5 – 4.5 inches 6 inches 8 inches	C_B	1.00 1.05 1.15
Sampling Spoon	Smooth sampler (or with liners) Sampler without liners	C_S	1.0 1.2
Rod Length	30 – 100 ft 20 – 30 ft 13 – 20 ft 10 – 13 ft	C_R	1.0 0.95 0.85 0.75

MSPT Data Sheets

Drilling information and MSPT data obtained at each borehole shall be recorded in the field and include the following:

1. Date,
2. Name of the Drilling Crew,
3. Type and Make of the drill rig,
4. SPT Hammer Efficiency,
5. Project/Bridge Location,
6. Boring Number and location (station and coordinates),
7. Ground Surface Elevation,
8. Ground water surface Elevation,
9. MSPT elevations and depths,
10. Description of recovered weak rock or shale, and
11. Measured penetration depth every 10 blows to the nearest 0.1 inches (2.5 mm).

Table Q.2 shows an example of a sample data sheet that could be used to record the MSPT data in the field.

Table Q.2: Sample MSPT Data Sheet

Illinois Department of Transportation

Modified SPT Log

Route: ______ Structure No.: ______ (Exist.) ______ (Prop.) Date: ______ Page: ______ of ______

Section: ______ Description: ______

County: ______ Logged by: ______ Sampler Tube Length: ______ in.

Boring No.: ______ Station: ______ Offset: ______ Latitude: ______ Longitude: ______

Drill Rig: ______ Hammer Type: ______ Hammer Efficiency (%): ______ Surface Elevation: ______

Borehole Diameter. (in.) ______ Split-barrel Sampler Description: ______

	Measured Rod Length (ft)	*Blows where exposed rod length is measured (blows)*											$N_{rate,90}$	q_u	Young's Modulus
		0	10	20	30	40	50	60	70	80	90	100	(bpf)	(ksf)	(ksi)
Test Elevation															

APPENDIX R DRILLED SHAFT LOAD TESTS DATABASE

R.1 SIDE RESISTANCE DATABASE

Table R.1 Side Resistance Database from Drilled Shaft Load Tests

Index	Reference	Geomaterial Type	fsmax (ksf)	qu (ksf)	D (in)	RQD (%)	Test Method	Remarks
1	Matich and Kozicki (1967)	Brown to gray shale and massive	> 6.5	14.4	24	—	Pull-out test	Artificially roughened
2	Corps of Engineers (1968)	Clay shale	> 5.6	15.2	—	—	—	—
3	Geoke and Hustad (1979): Shaft 1	Gray clay shale (Caddo formation)	7.5 @ 0.25 in	21.6	30	—	Compression test	Drilled with rock auger
4	Geoke and Hustad (1979): Shaft 2	Gray clay shale (Caddo formation)	4.6 @ 0.25 in	15.8	30	—	Compression test	Drilled with rock auger
5	Wilson (1976) Port Elizabeth, South Africa: West pile	Mudstone from Uitenhage series of Cretaceous system	3.76 @ 0.47 in	22.8	35.4	—	Pull-out test	Concrete defects due to water entering shaft
6	Wilson (1976) Port Elizabeth, South Africa East pile	Mudstone from Uitenhage series of Cretaceous system	2.51 @ 0.12 in	22.8	35.4	—	Pull-out test	Concrete defects due to water entering shaft
7	Mason (1960): PC25 USA	Weak shale	8.7	31.3	24	—	Compression test	—
8	Johnston and Donald (1979) Melbourne (F2)	Weathered Melbourne mudstone	19.6	40.3	47	—	Compression test	—
9	Brown and Thompson (1994)	Claystone	> 9.6 @ 0.13 in	43.2	28	—	Compression test	—
10	Brown and Thompson (1994)	Clay shale	7 @ 0.61 in	43.2	20	—	Compression test	—
11	LT-9405 IL 5 over IL 84 (2008)	Shale	1.4 @ 0.44 in	5.57	42	—	O-Cell	—
12	LT-9405 IL 5 over IL 84 (2008)	Shale	2.7 @ 0.44 in	11.7	42	—	O-Cell	—
13	LT-9405 IL 5 over IL 84 (2008)	Shale	13.3 @ 0.45 in	55.75	42	—	O-Cell	—
14	LT-8276 - FAU 6265 (1996)	Shale	1.0 @ 0.1 in	2.65	62	—	O-Cell	—

Index	Reference	Geomaterial Type	f_{smax} (ksf)	q_u (ksf)	D (in)	RQD (%)	Test Method	Remarks
15	Pells et al. (1978) PC 29	Weathered Melbourne mudstone	16.6	46.1	43	—	Compression test	—
16	Millar (1976): City Center Perth, W.A.	King Park shale	> 23 @ 1.25 in	63.9	27	—	Compression test	Drilled under bentonite
17	Millar (1976): Telephone Exchange, Perth, W.A. (TP1)	King Park shale	> 6.3 @ 1.2 in	20.9	26	—	—	—
18	Millar (1976): Telephone Exchange, Perth, W.A. (TP2)	King Park shale	15.04 @ 0.16 in	56	31	—	—	—
19	Johnston and Donald (1979) Flinders St., Melbourne (F1)	Weathered Melbourne mudstone	21.9	63.9	47.2	—	—	—
20	Walter et al. (1997)	Mudstone	12.5	66.8	35.4	—	Down-hole jack	—
21	Williams and Pells (1981)	Shale	23	64.7	27	—	—	Drilled and cast under bentonite
22	Williams and Pells (1981)	Shale	15	56.4	31	—	—	—
23	Williams (1980a): PS1 Stanley Ave., Melbourne	Weathered Melbourne mudstone	> 11.7	17.33	26	—	Compression test	Drilled normally
24	Williams (1980a): PS3 Stanley Ave., Melbourne	Weathered Melbourne mudstone	10.65	11.9	44	—	Compression test	Roughened
25	Williams (1980a): PS12 Stanley Ave., Melbourne	Weathered Melbourne mudstone	8.56	12.3	13.2	—	Compression test	Drilled with core barrel
26	Williams (1980a): PS14 Stanley Ave., Melbourne	Weathered Melbourne mudstone	10.4	12.1	15.5	—	Compression test	Roughened
27	Williams (1980a): PS15 Stanley Ave., Melbourne	Weathered Melbourne mudstone	8.6	12.5	15.5	—	Compression test	Roughened

Index	Reference	Geomaterial Type	f_{smax} (ksf)	q_u (ksf)	D (in)	RQD (%)	Test Method	Remarks
28	Williams (1980a): PS 16 Stanley Ave., Melbourne	Weathered Melbourne mudstone	> 7.5	12.1	15.5	__	__	Roughened
29	Williams (1980a): M1 Middleborough Rd. Melbourne	Weathered Melbourne mudstone	12.51	51.4	48	__	__	Drilled with bucket auger
30	Williams (1980a): M2 Middleborough Rd. Melbourne	Weathered Melbourne mudstone	13.4	48	51.2	__	__	Roughened
31	Williams (1980a): M3 Middleborough Rd. Melbourne	Weathered Melbourne mudstone	14.8	48	48.4	__	__	Drilled with bucket auger
32	Williams (1980a): M4 Middleborough Rd. Melbourne	Weathered Melbourne mudstone	12.9	48.9	53.15	__	__	Roughened
33	Williams (1980a) Pile WG303/2 Melbourne	Slightly weathered Melbourne mudstone	17.75	72.9	__	__	__	Roughened
34	Leach et al. (1976): Pile A, Kilroot, N. Ireland	Mudstone	4.38 @ 0.23 in	16.71	29.1	__	__	Drilled with auger
35	Leach et al. (1976): Pile B, Kilroot, N. Ireland	Mudstone	2.5 @ 0.55 in	19.2	29.1	__	__	Drilled with auger
36	Aurora and Reese (1976): MT1, Montopolis	Clay shale	8.56	29.6	29	__	Conventional	Drilled with auger, dry
37	Aurora and Reese (1976): MT2, Montopolis	Clay shale	7.64	29.6	31	__	Conventional	Drilled with auger, dry
38	Aurora and Reese (1976): MT3, Montopolis	Clay shale	14.4	29.6	29.5	__	Conventional	Drilled with auger, dry
39	Aurora and Reese (1976): DT1, Dallas	Clay shale	5.8 @ 0.2 in	12.8	35	__	Conventional	Drilled with auger, dry

Index	Reference	Geomaterial Type	f_{smax} (ksf)	q_u (ksf)	D (in)	RQD (%)	Test Method	Remarks
40	LT-8718-2, KS Socket (1998)	Gray to dark gray shale with limey seams	3.13 @ 0.78 in	13	72	40	O-Cell	Drilled with auger
41	LT-9048 Route 116 Over the Platte River (2004)	Gray silt shale	> 15.1 @ 0.66 in	45.9	48	—	O-Cell	Drilled with auger, dry
42	LT-8718-1 US 36 Over Republican River Socket (2001)	Dark gray shale (Graneros shale formation)	3.75 @ 1.73 in	19.7	72	49	O-Cell	Drilled with auger
43	LT-8854 I-235 Over Des Moines River Socket (2002)	Clay shale	13.05 @ 0.86 in	56.2	42	93	O-Cell	Drilled by auger and core barrel
44	LT-8816 US 281 Over Solomon River Socket (2001)	Gray to dark gray chalky shale	10.85 @ 0.72 in	49.6	42	80	O-Cell	Drilled with rock auger
45	LT-8733: Pier 1 West US 75 at 77th Street Socket (2001)	Gray shale with limestone lenses	> 8.6 @ 0.2 in	21.6	72	—	O-Cell	Drilled in dry with auger
46	Brown and Thompson (1994)	Weathered shale	19.8 @ 0.36 in	46.1	71	—	O-Cell	—
47	Miller (2003): Lexington, MO TS-1A, O-Cell to SG 2	Hard gray clay shale	15.2 @ 0.15 in	44.4	43.75	—	O-Cell	Drilled normally
48	Miller (2003): Lexington, MO TS-2, Lower to Upper O-Cell	Hard gray shale to clay shale	15.2 @ 0.48 in	46.9	46	—	O-Cell	Drilled normally
49	Miller (2003): Grandview, MO SG 5 to SG 6	Gray thinly laminated Clay shale	7.6 @ 0.65 in	19.5	77.8	—	O-Cell	Drilled normally
50	Abu-Hejleh et al. (2003): I-225	Soil-like claystone	> 2.6 @ 1.6 in	8.3	42	—	O-Cell	Slightly roughened
51	Abu-Hejleh et al. (2003): I-225	Soil-like claystone	> 3.6 @ 1.6 in	12.3	42	—	O-Cell	Slightly roughened

Index	Reference	Geomaterial Type	f_{smax} (ksf)	q_u (ksf)	D (in)	RQD (%)	Test Method	Remarks
52	Abu-Hejleh et al. (2003): I-225	Soil-like claystone	> 3.1 @ 1.6 in	10	42	__	O-Cell	Slightly roughened
53	Abu-Hejleh et al. (2003): County line	Soil-like claystone	> 3.4 @ 0.8 in	10.4	48	__	O-Cell	Slightly roughened
54	Abu-Hejleh et al. (2003): Franklin	Very hard sandy claystone	> 19 @ 0.42 in	64	42	__	O-Cell	Wet
55*	LT-1407 IL-89 Over Illinois River Socket (2014): O-Cell to SG 1	Gray Argillaceous Shale (Pennsylvanian)	10.72 @ 0.36 in	39.8	60	73	O-Cell	Drilled with auger, dry
56*	LT-1407 IL-89 Over Illinois River Socket (2014): SG 1to SG 2	Gray Argillaceous Shale (Pennsylvanian)	3.35 @ 0.36 in	25.1	60	64	O-Cell	Drilled with auger, dry
57*	LT-1425 IL-133 Over Embarras River Socket (2015): O-Cell to SG 1	Gray Argillaceous Shale (Pennsylvanian)	7.0 @ 1.28 in	23.5	48	83	O-Cell	Drilled with auger, dry
58*	LT-1425 IL-133 Over Embarras River Socket (2015): SG 1 to SG 2	Gray Argillaceous Shale (Pennsylvanian)	6.18 @ 1.28 in	17.1	48	76	O-Cell	Drilled with auger, dry
59*	LT-8998 I-235 Over UP RR Socket (2004): SG 2 to SG 3	Light Gray Clay Shale	2.64 @ 0.066 in	14.6	48	66	O-Cell	Polymer slurry
60*	LT-8998 I-235 Over UP RR Socket (2004): SG 3 to SG 4	Light Gray Clay Shale	4.14 @ 0.085 in	9.2	48	52	O-Cell	Polymer slurry
61*	LT-8756-2 I-235/28th Street Overpass Socket (2002): O-Cell to SG 1	Clay Shale	5.1 @ 0.58 in	24.8	48	-	O-Cell	Polymer slurry

Index	Reference	Geomaterial Type	f_{smax} (ksf)	q_u (ksf)	D (in)	RQD (%)	Test Method	Remarks
62*	LT-8756-2 I-235/28th Street Overpass Socket (2002): SG 1 to SG 2	Clay Shale	7.0 @ 0.58 in	29.3	48	70	O-Cell	Polymer slurry
63*	Vu (2013): Frankford, MO TS-F1, O-Cell to SG 1	Maquoketa shale	20.5 @ 0.23 in	79.05	36	-	O-Cell	Drilled with auger, dry
64*	Vu (2013): Frankford, MO TS-F2, O-Cell to SG 2	Maquoketa shale	6.13 @ 0.14 in	13.1	36	-	Rim-Cell	Drilled with auger, dry
65*	Vu (2013): Frankford, MO TS-F3, SG 1 to SG 2	Maquoketa shale	42.9 @ 0.65 in	71.7	60	-	O-Cell	Drilled with auger, dry
66*	Vu (2013): Frankford, MO TS-F3, SG 2 to SG 3	Maquoketa shale	9.8 @ 0.65 in	33.0	60	-	O-Cell	Drilled with auger, dry
67*	Vu (2013): Frankford, MO TS-F4, O-Cell to SG 2	Maquoketa shale	24.66 @ 0.33 in	70.83	36	-	O-Cell	Drilled with auger, dry
68*	Vu (2013): Frankford, MO TS-F5, O-Cell to SG 2	Maquoketa shale	29.75 @ 0.61 in	70.6	60	-	O-Cell	Drilled with auger, dry
69*	Vu (2013): Frankford, MO TS-F5, SG 2 to SG 3	Maquoketa shale	11.8 @ 0.59 in	38.3	60	-	O-Cell	Drilled with auger, dry
70*	Vu (2013): Frankford, MO TS-F6, O-Cell to SG 1	Maquoketa shale	27.6 @ 0.41 in	68	36	-	O-Cell	Drilled with auger, dry
71*	Vu (2013): Frankford, MO TS-F7, O-Cell to SG 1	Maquoketa shale	28.7 @ 0.67 in	62.4	36	-	O-Cell	Drilled with auger, dry
72*	Vu (2013): Warrensburg, MO TS-W1, O-Cell to SG 3	Sandy Shale	2.92. @ 2.4 in	8.7	36	-	O-Cell	Drilled with auger, dry
73*	Vu (2013): Warrensburg, MO TS-W2, O-Cell to SG 2	Sandy Shale	2.4 @ 1.13 in	15.3	36	-	O-Cell	Drilled with auger, dry
74*	Vu (2013): Warrensburg, MO TS-W3, O-Cell to SG 1	Hard Clay Shale	4.6 @ 3.4 in	26.1	36	-	O-Cell	Drilled with auger, dry
75*	Vu (2013): Warrensburg, MO TS-W3, SG 1 to SG 2	Soft Sandy Shale	4.7 @ 3.4 in	21.0	36	-	O-Cell	Drilled with auger, dry

Index	Reference	Geomaterial Type	f_{smax} (ksf)	q_u (ksf)	D (in)	RQD (%)	Test Method	Remarks
76*	Vu (2013): Warrensburg, MO TS-W3, SG 2 to SG 3	Sandy Shale	4.6 @ 3.4 in	15.4	36	-	O-Cell	Drilled with auger, dry
77*	Vu (2013): Warrensburg, MO TS-W4, O-Cell to SG 1	Hard Clay Shale	4.0 @ 3.4 in	17.4	36	-	O-Cell	Drilled with auger, dry
78*	Vu (2013): Warrensburg, MO TS-W4, SG 1 to SG 2	Soft Sandy Shale	6.6 @ 3.4 in	15.5	36	-	O-Cell	Drilled with auger, dry
79*	Vu (2013): Warrensburg, MO TS-W4, SG 2 to SG 3	Sandy Shale	1.8 @ 3.4 in	13.2	36	-	O-Cell	Drilled with auger, dry
80*	Vu (2013): Warrensburg, MO TS-W5, O-Cell to SG 2	Sandy Shale	1.55 @ 0.06 in	8.0	36	-	O-Cell	Drilled with auger, dry
81*	Vu (2013): Warrensburg, MO TS-W6, O-Cell to SG 2	Sandy Shale	6.5 @ 1.72 in	13.7	36	-	O-Cell	Drilled with auger, dry
82*	Vu (2013): Warrensburg, MO TS-W7, O-Cell to SG 3	Sandy Shale	2.3 @ 0.35 in	13.4	36	-	O-Cell	Drilled with auger, dry
83*	Vu (2013): Warrensburg, MO TS-W8, O-Cell to SG 1	Hard Shale	15.8 @ 2.63 in	50	36	-	O-Cell	Drilled with auger, dry
84*	Vu (2013): Warrensburg, MO TS-W8, SG1 to SG 2	Soft Shale	5.2 @ 2.63 in	14.3	36	-	O-Cell	Drilled with auger, dry
85*	Vu (2013): Warrensburg, MO TS-W8, SG2 to SG 3	Sandy Shale	4.7 @ 2.63 in	14.3	36	-	O-Cell	Drilled with auger, dry
86*	Vu (2013): Warrensburg, MO TS-W9, SG1 to SG 3	Soft Shale	3.7 @ 4.0 in	14.3	36	-	O-Cell	Drilled with auger, dry
87*	Vu (2013): Warrensburg, MO TS-W9, SG3 to SG 4	Sandy Shale	3.6 @ 4.0 in	14.3	36	-	O-Cell	Drilled with auger, dry

Index	Reference	Geomaterial Type	f_{smax} (ksf)	q_u (ksf)	D (in)	RQD (%)	Test Method	Remarks
88*	Vu (2013): Warrensburg, MO TS-W11, O-Cell to SG 1	Soft Shale	3.5 @ 0.36 in	10.95	36	-	Rim-Cell	Drilled with auger, dry
89*	Vu (2013): Warrensburg, MO TS-W11, SG1 to SG 3	Sandy Shale	2.1 @ 0.36 in	17.35	36	-	Rim-Cell	Drilled with auger, dry
90*	Vu (2013): Warrensburg, MO TS-W12, O-Cell to SG 1	Sandy Shale	8.4 @ 1.29 in	16.6	36	-	O-Cell	Drilled with auger, dry
91*	Vu (2013): Warrensburg, MO TS-W13, O-Cell to SG 3	Sandy Shale	3.4 @ 0.76 in	7.0	36	-	O-Cell	Drilled with auger, dry
92*	Vu (2013): Warrensburg, MO TS-W14, O-Cell to SG 3	Sandy Shale	3.4 @ 2.16 in	11.25	36	-	O-Cell	Drilled with auger, dry
93*	Vu (2013): Warrensburg, MO TS-W15, O-Cell to SG 3	Sandy Shale	4.72 @ 2.84 in	10.83	36	-	O-Cell	Drilled with auger, dry

***Load tests added to the database in Phase 2 of this study.**

R.2 TIP RESISTANCE DATABASE

Table R.2 Tip Resistance Database from Drilled Shaft Load Test

Index	Reference	Geomaterial Type	q_{tmax} (ksf)	q_u (ksf)	D (in.)	RQD (%)	Socket Length (in)	Tip Movement (in.)
1	LT-8718-1 US 36 Over Republican River	Geraneros Shale Formation	> 56.9	16.7	72	61	315	1.12
2	LT-8718-2 US 36 Over Republican River	Geraneros Shale Formation, dark gray shale	> 44.1	13	72	33	323	0.62
3	LT-8733: Pier 1 West US 75 at 77th Street	Severy Shale Formation	> 127	36.2	72	—	274	0.68
4	LT-8816 US 281 Over Solomon River	Gray to dark gray shale (chalky)	> 136.7	63.5	42	70	141	1.00
5	LT-8854 I 235 Over Des Moines River	Light gray and moist clay shale	> 378	81.9	42	94	356.2	1.50
6	LT-9021 US 75 Over Neosho River	Green and gray clayey shale	> 149	84.6	60	—	335	0.91
7	LT-9048 Route 116 Over Platte River	Thinly laminated silt shale, gray	> 134	52.5	48	—	120	0.60
8	LT-8415-2	Gray shale	> 140	93	96	43	413	1.34
9	Abu-Hejleh et al. (2003): County Line	Soil-like claystone	> 54	16.85	48	—	162	4.61
10	Abu-Hejleh et al. (2003): Franklin site	Blue and sandy claystone	> 254.5	46.35	42	—	249.6	2.93
11	Abu-Hejleh et al. (2003): I-225	Soil-like claystone	> 55	13.1	42	—	193.2	2.26
12	Aurora and Reese (1976): DT1	Clay shale	51	12.8	35	—	76.8	2.31
13	Vijayvergiya et al. (1969)	Clay shale	122	27.2	30	—	124.5	—
14	Thorburn (1966)	Clay shale	227	88	48	—	48	0.41
15	Thorburn (1966)	Clay shale	22.4	84	36	—	150	1.32
16	Henley (1967)	Clay shale	294	36	18	—	240	2.3

Index	Reference	Geomaterial Type	qtmax (ksf)	qu (ksf)	D (in)	RQD (%)	Socket Length (in.)	Tip Movement (in.)
17	Van Doren et al. (1967)	Clay shale	32	7.2	__	__	__	__
18	Geoke and Hustad (1979): TS 1	Caddo Formation: gray clay shale	98	17	30	__	214	0.77
19	Geoke and Hustad (1979): TS 2	Caddo and Kiamichi Formations: gray clay shale	128	20	30	__	308	0.48
20	Wilson (1976)	Mudstone, cretaceous	143.7	22.8	26.5	__	118	1.84
21	Hummert and Cooling (1988)	Shale, thinly bedded	225.6	39	18	—	120	1.8
22	Jubenville and Hepworth (1981)	Unweathered shale	76.4	17	12	__	60	1.2
23	Aurora and Reese (1976): MT1	Clay shale	119	29.6	29	__	46	2.6
24	Aurora and Reese (1976): MT2	Clay shale	107	29.6	31	—	48	2.8
25	Aurora and Reese (1976): MT3	Clay shale	128	29.6	29.5	—	60	1.8
26	Williams (1980a)	Highly weathered mudstone	133.7	13.6	12	__	__	0.75
27	Williams (1980a)	Highly weathered mudstone	146.2	14	12	__	__	0.67
28	Williams (1980a)	Moderately weathered mudstone	123.2	56	39.5	__	__	0.43
29	Williams (1980a)	Moderately weathered mudstone	137.8	51.2	39.5	__	__	0.27
30	Williams (1980a)	Moderately weathered mudstone	146.2	51.2	39.5	__	__	0.23
31	Williams (1980a)	Moderately weathered mudstone	140	56	39.5	__	__	0.27
32	Williams (1980a)	Mudstone	192	40.3	23.6			3.3
33	Williams (1980a)	Moderately weathered mudstone	148.3	29.2	39.5	__	__	4.3

Index	Reference	Geomaterial Type	q_{tmax} (ksf)	q_u (ksf)	D (in)	RQD (%)	Socket Length (in.)	Tip Movement (in.)
34*	LT-1407 IL-89 Over Illinois River Socket (2014)	Calcareous Shale	66.8	98.5	60	83	168	0.158
35*	LT-1425 IL-133 Over Embarras River Socket (2015)	Clay Shale	58.6	19.1	48	80	168	1.684
36*	LT-8998 I-235 Over UP RR Socket (2004)	Carboniferous Clay Shale	176	138	48	37	448	1.16
37*	LT-8756-2 I-235/28th Street Overpass Socket (2002)	Clay Shale	114.1	29.3	48	70	300	0.184
38*	Vu (2013): Frankford, MO TS-F1	Maquoketa Shale Formation	78.1	67	36	-	190	0.234
39*	Vu (2013): Frankford, MO TS-F2	Maquoketa Shale Formation	114.6	64.55	36	-	204	0.108
40*	Vu (2013): Frankford, MO TS-F3	Maquoketa Shale Formation	134.3	68.1	60	-	237	0.32
41*	Vu (2013): Frankford, MO TS-F4	Maquoketa Shale Formation	259.9	62.4	36	-	260	3.2
42*	Vu (2013): Frankford, MO TS-F5	Maquoketa Shale Formation	190	70.7	60	-	325	0.8
43*	Vu (2013): Frankford, MO TS-F6	Maquoketa Shale Formation	286.4	62.7	36	-	260	4.7
44*	Vu (2013): Frankford, MO TS-F7	Maquoketa Shale Formation	210.1	66.7	36	-	344	0.95
45*	Vu (2013): Frankford, MO TS-F8	Maquoketa Shale Formation	80.4	56.25	36	-	222	0.09
46*	Vu (2013): Frankford, MO TS-F9	Maquoketa Shale Formation	27.2	10.4	60	-	122	0.22

Index	Reference	Geomaterial Type	qtmax (ksf)	qu (ksf)	D (in)	RQD (%)	Socket Length (in.)	Tip Movement (in.)
47*	Vu (2013): Frankford, MO TS-F10	Maquoketa Shale Formation	44.5	10.4	60	-	144	0.44
48*	Vu (2013): Warrensburg, MO TS-W1	Soft Shale	41.5	5.8	36	-	148	0.29
49*	Vu (2013): Warrensburg, MO TS-W2	Soft Shale	60.4	5.8	36	-	210	0.52
50*	Vu (2013): Warrensburg, MO TS-W3	Hard Shale	171.4	88.3	36	-	380	0.38
51*	Vu (2013): Warrensburg, MO TS-W4	Hard Shale	131.3	71.0	36	-	404	0.32
52*	Vu (2013): Warrensburg, MO TS-W5	Sandy Shale	100.3	15.75	36	-	130	2.4
53*	Vu (2013): Warrensburg, MO TS-W6	Soft Shale	58.7	15.75	36	-	209	0.67
54*	Vu (2013): Warrensburg, MO TS-W7	Soft Shale	175.3	5.8	36	-	218	8.2
55*	Vu (2013): Warrensburg, MO TS-W8	Hard Shale	251.6	113.6	36	-	386	0.67
56*	Vu (2013): Warrensburg, MO TS-W9	Hard Shale	158.9	75.5	36	-	386	0.7
57*	Vu (2013): Warrensburg, MO TS-W10	Soft Shale	32.1	17.8	36	-	253	2.15
58*	Vu (2013): Warrensburg, MO TS-W11	Soft Shale	57.9	17.8	36	-	255	1.05
59*	Vu (2013): Warrensburg, MO TS-W12	Soft Shale	53.7	5.8	36	-	214	1.18
60*	Vu (2013): Warrensburg, MO TS-W13	Soft Shale	39.9	5.8	36	-	208	0.22
61*	Vu (2013): Warrensburg, MO TS-W14	Soft Shale	45.1	5.8	36	-	206	0.20
62*	Vu (2013): Warrensburg, MO TS-W15	Soft Shale	66.4	5.8	36	-	210	0.19

***Load tests added to the database in Phase 2 of this study.**

APPENDIX S SPT HAMMER ENERGY MEASUREMENT

Pile Dynamics, Inc.
SPT Analyzer Results

PDA-S Ver. 2016.16 - Printed: 1/21/2017

CME45C(SN302114)
TDS/AB/AB/TDS/AB

20-21.5
Test date: 11/15/2016

AR: 1.18 in^2
LE: 23.80 ft
WS: 16807.9 ft/s

SP: 0.492 k/ft3
EM: 30000 ksi

Depth: (20.00 - 21.50 ft], displaying BN: 15

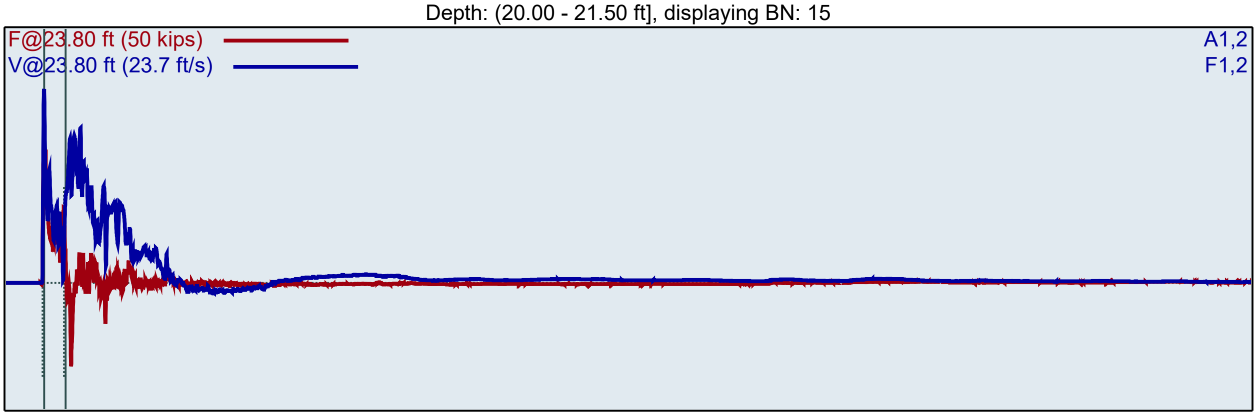

FMX: Maximum Force
VMX: Maximum Velocity
BPM: Blows/Minute

EFV: Maximum Energy
ETR: Energy Transfer Ratio - Rated

BL#	BC	FMX	VMX	BPM	EFV	ETR
	/6"	kips	ft/s	bpm	ft-lb	(%)
1	7	29	17.4	58.2	264	77.4
2	7	29	17.5	57.7	264	77.4
3	7	29	17.7	58.4	273	80.0
4	7	30	17.6	58.6	291	85.2
5	7	28	16.6	2.8	230	67.4
6	7	31	17.8	58.7	277	81.0
7	7	30	18.0	58.9	283	83.0
8	6	29	18.0	57.6	288	84.3
9	6	28	18.1	58.2	285	83.5
10	6	27	18.0	57.6	269	78.9
11	6	27	18.2	59.3	283	82.9
12	6	27	17.6	58.2	266	77.9
13	6	28	17.8	57.6	275	80.4
14	4	27	17.7	57.7	255	74.6
15	4	27	18.0	58.9	276	80.8
16	4	28	18.1	58.5	276	80.8
17	4	28	18.5	57.8	292	85.5
	Average	28	18.0	58.1	276	81.0
	Std Dev	1	0.3	0.6	11	3.1
	Maximum	29	18.5	59.3	292	85.5
	Minimum	27	17.6	57.6	255	74.6

N-value: 10

Sample Interval Time: 37.14 seconds.

CME45C(SN302114) 20-21.5
TDS/AB/AB/TDS/AB Test date: 11/15/2016

AR: 1.18 in^2 SP: 0.492 k/ft3
LE: 28.30 ft EM: 30000 ksi
WS: 16807.9 ft/s

Depth: (22.50 - 24.00 ft], displaying BN: 27

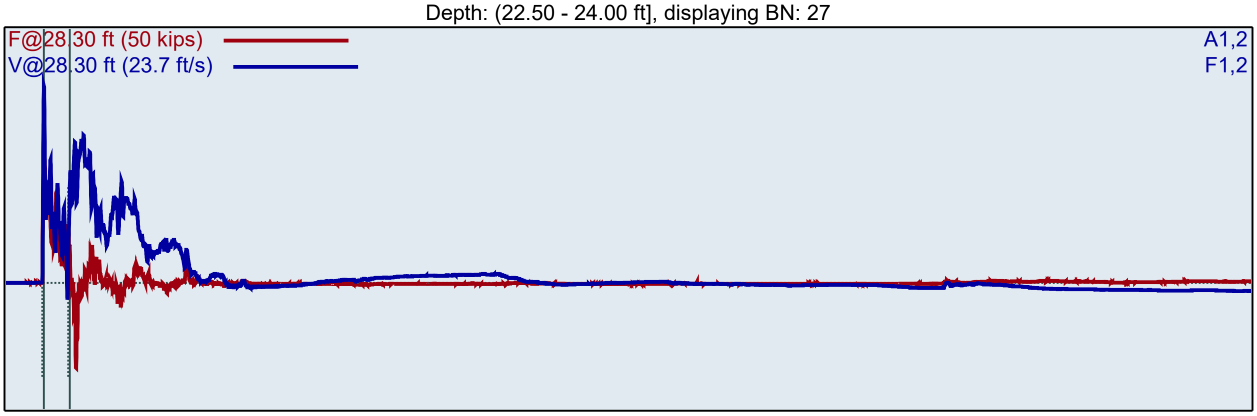

BL#	BC /6"	FMX kips	VMX ft/s	BPM bpm	EFV ft-lb	ETR (%)
18	2	31	18.5	57.9	328	96.1
19	2	30	18.3	57.7	287	84.1
20	5	31	18.5	57.2	297	87.1
21	5	30	18.2	56.5	284	83.1
22	5	31	18.4	56.8	286	83.6
23	5	30	18.0	57.3	286	83.7
24	5	31	18.2	57.4	299	87.4
25	5	30	18.6	55.5	315	92.3
26	5	30	18.3	57.4	303	88.7
27	5	31	18.3	57.5	302	88.3
28	5	31	18.2	56.8	301	88.1
29	5	30	18.0	57.2	318	93.1
	Average	31	18.3	57.0	299	87.5
	Std Dev	0	0.2	0.6	11	3.2
	Maximum	31	18.6	57.5	318	93.1
	Minimum	30	18.0	55.5	284	83.1

N-value: 10

Sample Interval Time: 11.54 seconds.

CME45C(SN302114)
TDS/AB/AB/TDS/AB

20-21.5
Test date: 11/15/2016

AR: 1.18 in^2
LE: 28.80 ft
WS: 16807.9 ft/s

SP: 0.492 k/ft3
EM: 30000 ksi

Depth: (25.00 - 26.50 ft], displaying BN: 40

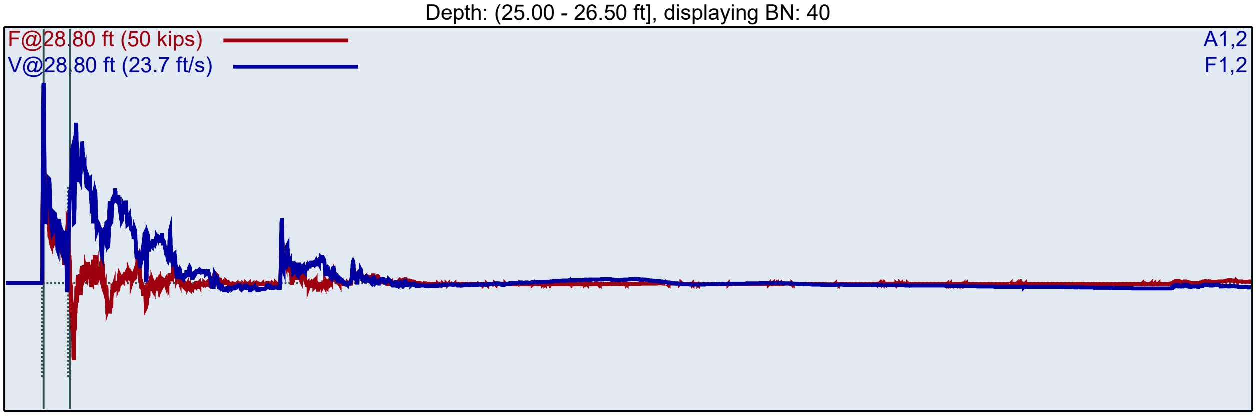

BL#	BC /6"	FMX kips	VMX ft/s	BPM bpm	EFV ft-lb	ETR (%)
30	4	32	18.8	55.6	322	94.4
31	4	30	17.8	57.0	293	85.7
32	4	31	18.1	56.6	294	86.2
33	4	31	18.0	56.4	284	83.1
34	4	30	17.8	56.9	275	80.7
35	4	30	17.7	55.5	274	80.3
36	4	31	17.9	55.4	280	82.0
37	4	30	17.8	56.2	276	80.9
38	5	30	17.6	56.8	275	80.6
39	5	28	17.7	56.9	272	79.6
40	5	29	18.6	56.3	278	81.5
41	5	29	18.8	56.7	297	87.0
42	5	29	18.8	56.6	294	86.0
	Average	29	18.1	56.4	280	82.1
	Std Dev	1	0.5	0.5	8	2.5
	Maximum	31	18.8	56.9	297	87.0
	Minimum	28	17.6	55.4	272	79.6

N-value: 9

Sample Interval Time: 12.73 seconds.

CME45C(SN302114)
TDS/AB/AB/TDS/AB

20-21.5
Test date: 11/15/2016

AR: 1.18 in^2
LE: 33.80 ft
WS: 16807.9 ft/s

SP: 0.492 k/ft3
EM: 30000 ksi

Depth: (30.00 - 31.50 ft], displaying BN: 54

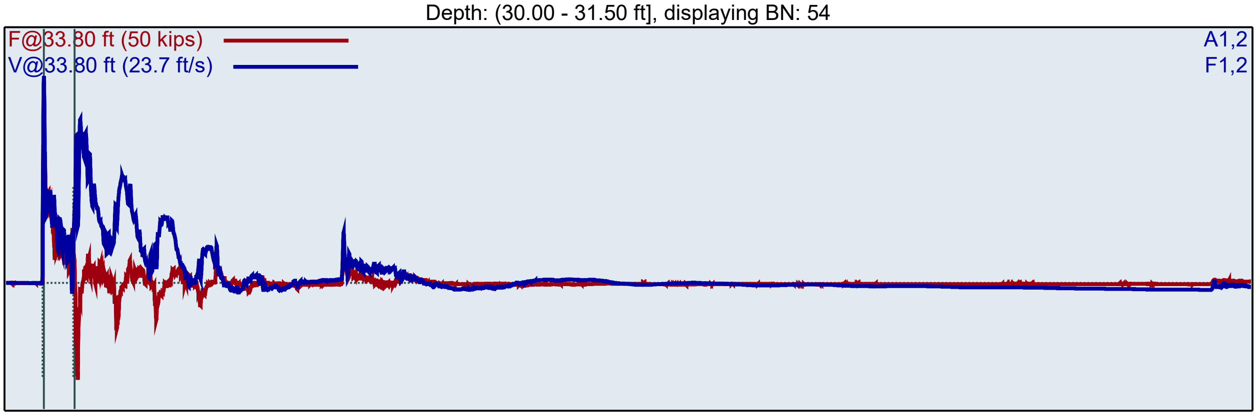

BL#	BC /6"	FMX kips	VMX ft/s	BPM bpm	EFV ft-lb	ETR (%)
43	4	29	18.9	1.9	299	87.7
44	4	31	18.7	55.2	311	91.0
45	4	31	18.6	56.3	302	88.3
46	4	30	18.5	55.7	298	87.3
47	5	30	18.8	55.8	299	87.6
48	5	30	18.6	56.7	298	87.3
49	5	31	18.6	55.8	299	87.6
50	5	30	17.5	55.4	274	80.2
51	5	31	18.6	55.5	301	88.2
52	5	30	18.8	56.0	299	87.5
53	5	31	18.6	56.1	307	89.9
54	5	31	19.2	55.7	309	90.6
55	5	31	18.9	56.0	307	89.9
56	5	31	18.7	56.2	311	91.0
	Average	31	18.6	55.9	300	88.0
	Std Dev	0	0.4	0.4	10	2.9
	Maximum	31	19.2	56.7	311	91.0
	Minimum	30	17.5	55.4	274	80.2

N-value: 10

Sample Interval Time: 13.93 seconds.

CME45C(SN302114) 20-21.5
TDS/AB/AB/TDS/AB Test date: 11/15/2016

AR: 1.18 in^2 SP: 0.492 k/ft3
LE: 38.80 ft EM: 30000 ksi
WS: 16807.9 ft/s

Depth: (35.00 - 36.50 ft], displaying BN: 71

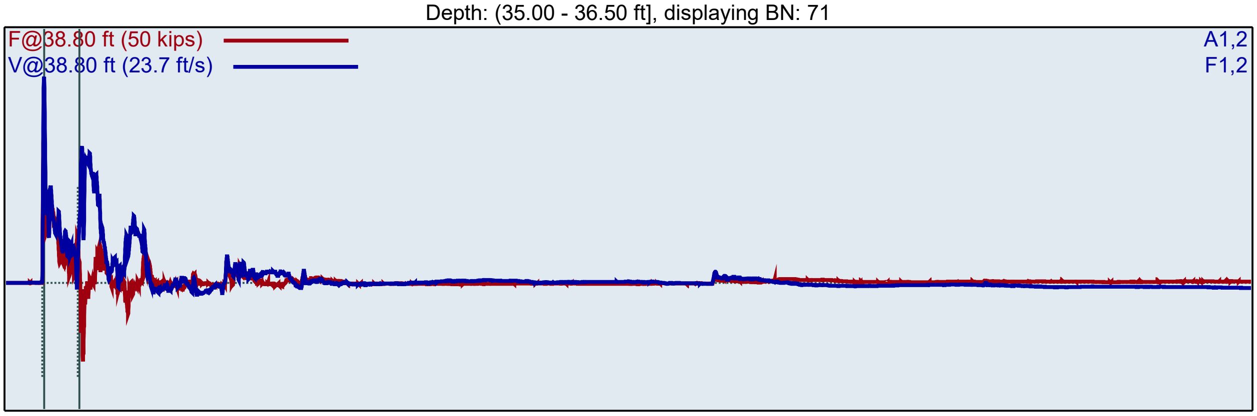

BL#	BC /6"	FMX kips	VMX ft/s	BPM bpm	EFV ft-lb	ETR (%)
57	4	31	19.4	1.9	324	95.0
58	4	31	19.3	56.6	312	91.2
59	4	30	19.3	55.0	307	89.9
60	4	29	18.3	54.7	293	85.9
61	5	29	18.6	55.6	301	88.0
62	5	29	18.9	55.6	298	87.3
63	5	30	18.7	55.3	301	88.2
64	5	29	18.6	55.2	300	88.0
65	5	29	19.3	55.5	307	90.0
66	8	29	18.7	55.8	297	86.9
67	8	30	19.1	55.4	306	89.5
68	8	30	19.3	56.1	306	89.6
69	8	30	19.3	55.7	306	89.7
70	8	30	19.2	55.5	305	89.4
71	8	30	19.2	55.5	312	91.3
72	8	30	19.1	55.6	307	89.8
73	8	30	19.2	55.7	310	90.7
	Average	30	19.0	55.6	304	89.1
	Std Dev	0	0.3	0.2	4	1.3
	Maximum	30	19.3	56.1	312	91.3
	Minimum	29	18.6	55.2	297	86.9

N-value: 13

Sample Interval Time: 17.25 seconds.

Summary of SPT Test Results

Project: CME45C(SN302114), Test Date: 11/15/2016

FMX: Maximum Force
VMX: Maximum Velocity
BPM: Blows/Minute
EFV: Maximum Energy
ETR: Energy Transfer Ratio - Rated

Instr. Length ft	Blows Applied /6"	**N Value**	**N60 Value**	Average FMX kips	Average VMX ft/s	Average BPM bpm	Average EFV ft-lb	Average ETR (%)
23.80	**7-6-4**	**10**	**14**	28	18.0	58.1	276	81.0
28.30	**2-5-5**	**10**	**14**	31	18.3	57.0	299	87.5
28.80	**4-4-5**	**9**	**12**	29	18.1	56.4	280	82.1
33.80	**4-5-5**	**10**	**14**	31	18.6	55.9	300	88.0
38.80	**4-5-8**	**13**	**18**	30	19.0	55.6	304	89.1
			Overall Average Values:	30	18.4	56.5	293	85.8
			Standard Deviation:	1	0.5	1.0	15	4.3
			Overall Maximum Value:	31	19.3	59.3	318	93.1
			Overall Minimum Value:	27	17.5	55.2	255	74.6

Summary of SPT Test Results

Project: CME75 SN350477, Test Date: 11/15/2016

FMX: Maximum Force
VMX: Maximum Velocity
BPM: Blows/Minute

EFV: Maximum Energy
ETR: Energy Transfer Ratio - Rated

Instr. Length ft	Blows Applied /6"	**N Value**	**N60 Value**	Average FMX kips	Average VMX ft/s	Average BPM bpm	Average EFV ft-lb	Average ETR (%)
23.80	**1-5-6**	**11**	**17**	30	19.0	52.1	301	88.2
28.80	**3-4-4**	**8**	**12**	31	17.4	58.2	307	90.0
33.80	**5-4-7**	**11**	**17**	31	16.6	57.5	305	89.2
38.80	**2-3-6**	**9**	**13**	32	17.1	57.1	307	90.0
43.80	**3-4-8**	**12**	**18**	30	18.6	57.1	325	95.0
48.50	**2-7-44**	**51**	**79**	31	17.0	56.6	327	95.7
			Overall Average Values:	31	17.4	56.4	318	93.2
			Standard Deviation:	1	0.8	5.4	13	3.7
			Overall Maximum Value:	32	19.5	59.6	339	99.3
			Overall Minimum Value:	28	16.0	9.5	245	71.8

CME75 SN350477
TDS/AB

20-21.5
Test date: 11/15/2016

AR: 1.18 in^2
LE: 23.80 ft
WS: 16807.9 ft/s

SP: 0.492 k/ft3
EM: 30000 ksi

Depth: (20.00 - 21.50 ft], displaying BN: 10

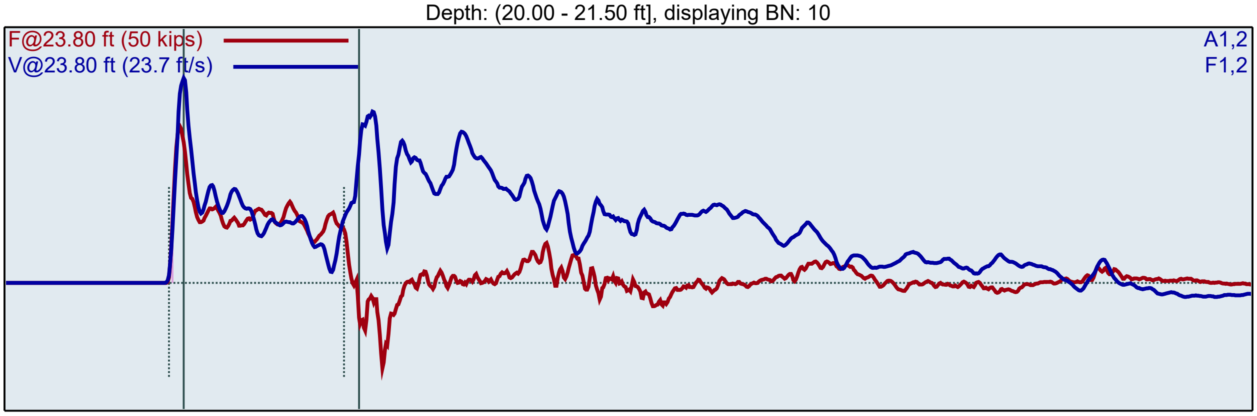

FMX: Maximum Force
VMX: Maximum Velocity
BPM: Blows/Minute

EFV: Maximum Energy
ETR: Energy Transfer Ratio - Rated

BL#	BC	FMX	VMX	BPM	EFV	ETR
	/6"	kips	ft/s	bpm	ft-lb	(%)
1	1	30	18.3	1.9	295	86.3
2	5	31	18.5	9.5	302	88.3
3	5	28	17.5	59.6	245	71.8
4	5	31	19.3	30.1	311	91.2
5	5	31	19.4	59.4	312	91.3
6	5	31	19.2	59.5	309	90.5
7	6	31	19.5	59.2	313	91.5
8	6	30	19.2	59.3	303	88.8
9	6	30	19.1	59.1	303	88.6
10	6	31	19.0	59.3	302	88.5
11	6	30	19.2	59.2	303	88.9
12	6	31	19.1	59.3	310	90.7
	Average	30	19.0	52.1	301	88.2
	Std Dev	1	0.5	15.9	18	5.3
	Maximum	31	19.5	59.6	313	91.5
	Minimum	28	17.5	9.5	245	71.8

N-value: 11

Sample Interval Time: 17.39 seconds.

CME75 SN350477 | 20-21.5
TDS/AB | Test date: 11/15/2016

AR: 1.18 in^2 | SP: 0.492 k/ft3
LE: 28.80 ft | EM: 30000 ksi
WS: 16807.9 ft/s

Depth: (25.00 - 26.50 ft], displaying BN: 21

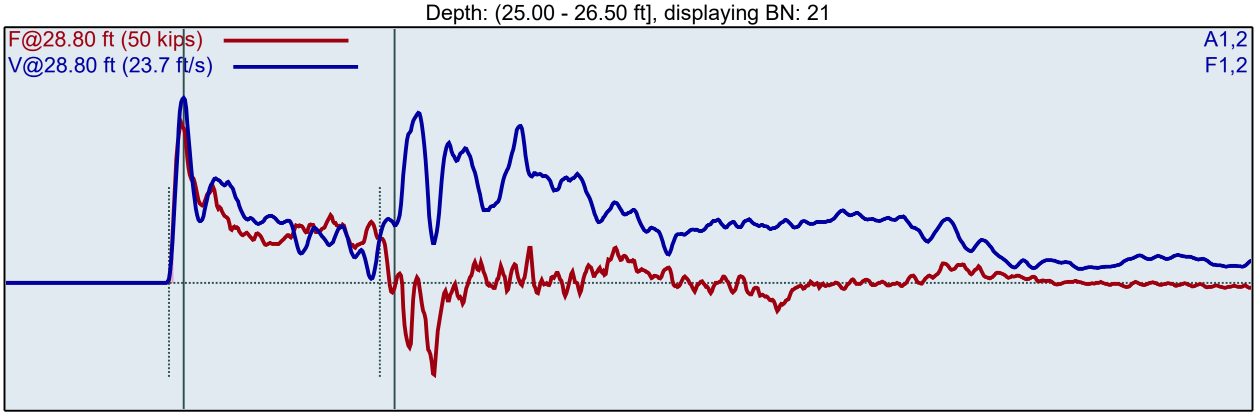

BL#	BC /6"	FMX kips	VMX ft/s	BPM bpm	EFV ft-lb	ETR (%)
13	3	32	17.6	1.9	312	91.5
14	3	32	17.9	59.4	317	92.8
15	3	32	17.6	29.7	311	91.2
16	4	32	17.5	58.2	312	91.3
17	4	32	17.7	57.9	309	90.6
18	4	32	17.5	58.2	307	90.0
19	4	32	17.5	58.1	306	89.6
20	4	31	17.6	58.3	309	90.4
21	4	31	17.2	58.2	309	90.4
22	4	31	17.1	58.4	307	89.8
23	4	31	17.2	57.9	301	88.1
	Average	31	17.4	58.2	307	90.0
	Std Dev	1	0.2	0.2	3	0.9
	Maximum	32	17.7	58.4	312	91.3
	Minimum	31	17.1	57.9	301	88.1

N-value: 8

Sample Interval Time: 11.20 seconds.

CME75 SN350477
TDS/AB

20-21.5
Test date: 11/15/2016

AR: 1.18 in^2
LE: 33.80 ft
WS: 16807.9 ft/s

SP: 0.492 k/ft3
EM: 30000 ksi

Depth: (30.00 - 31.50 ft], displaying BN: 37

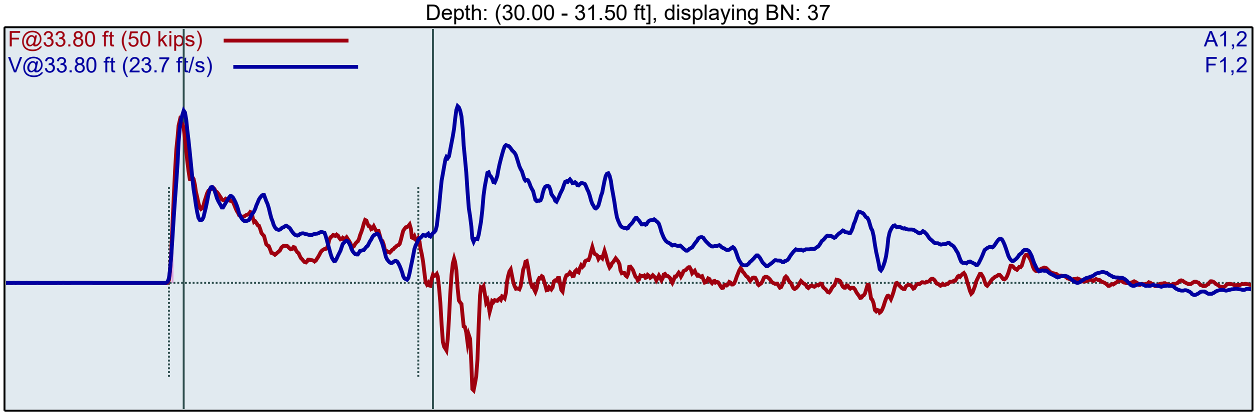

BL#	BC /6"	FMX kips	VMX ft/s	BPM bpm	EFV ft-lb	ETR (%)
24	5	32	17.2	1.9	310	90.8
25	5	32	17.6	58.4	317	92.9
26	5	32	17.6	58.9	315	92.4
27	5	32	17.7	57.7	311	91.1
28	5	32	17.4	57.6	313	91.7
29	4	32	17.1	57.3	310	90.8
30	4	30	17.1	57.4	305	89.3
31	4	30	17.1	57.6	302	88.5
32	4	31	16.5	57.5	307	89.9
33	7	31	16.5	57.4	310	90.8
34	7	31	16.4	57.7	302	88.3
35	7	31	16.7	57.5	300	87.8
36	7	31	16.3	57.5	301	88.0
37	7	32	16.4	57.4	304	89.2
38	7	31	16.0	57.5	306	89.6
39	7	31	16.4	57.6	304	89.1
	Average	31	16.6	57.5	305	89.2
	Std Dev	1	0.3	0.1	3	1.0
	Maximum	32	17.1	57.7	310	90.8
	Minimum	30	16.0	57.3	300	87.8

N-value: 11

Sample Interval Time: 15.59 seconds.

CME75 SN350477 20-21.5
TDS/AB Test date: 11/15/2016

AR: 1.18 in^2 SP: 0.492 k/ft3
LE: 38.80 ft EM: 30000 ksi
WS: 16807.9 ft/s

Depth: (35.00 - 36.50 ft], displaying BN: 48

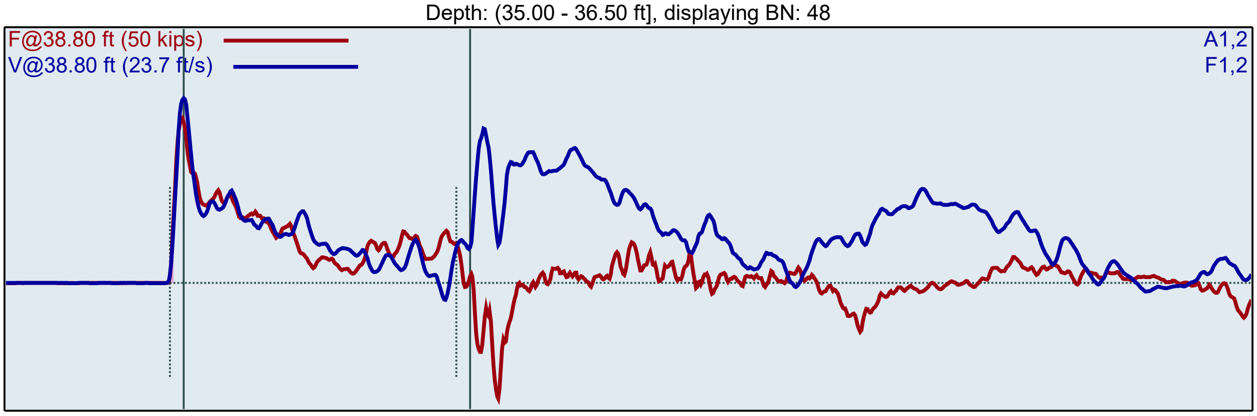

BL#	BC /6"	FMX kips	VMX ft/s	BPM bpm	EFV ft-lb	ETR (%)
40	2	32	17.4	1.9	297	87.0
41	2	32	17.4	57.9	332	97.2
42	3	32	17.1	57.9	316	92.5
43	3	32	17.3	56.9	309	90.6
44	3	32	16.9	57.2	316	92.5
45	6	32	17.0	56.7	300	87.8
46	6	32	17.0	57.1	305	89.2
47	6	32	17.0	56.9	303	88.8
48	6	32	17.2	57.1	305	89.3
49	6	32	17.1	57.1	303	88.7
50	6	32	17.3	57.1	308	90.2
	Average	32	17.1	57.1	307	90.0
	Std Dev	0	0.1	0.3	5	1.6
	Maximum	32	17.3	57.9	316	92.5
	Minimum	32	16.9	56.7	300	87.8

N-value: 9

Sample Interval Time: 10.48 seconds.

CME75 SN350477
TDS/AB

20-21.5
Test date: 11/15/2016

AR: 1.18 in^2
LE: 43.80 ft
WS: 16807.9 ft/s

SP: 0.492 k/ft3
EM: 30000 ksi

Depth: (40.00 - 41.50 ft], displaying BN: 63

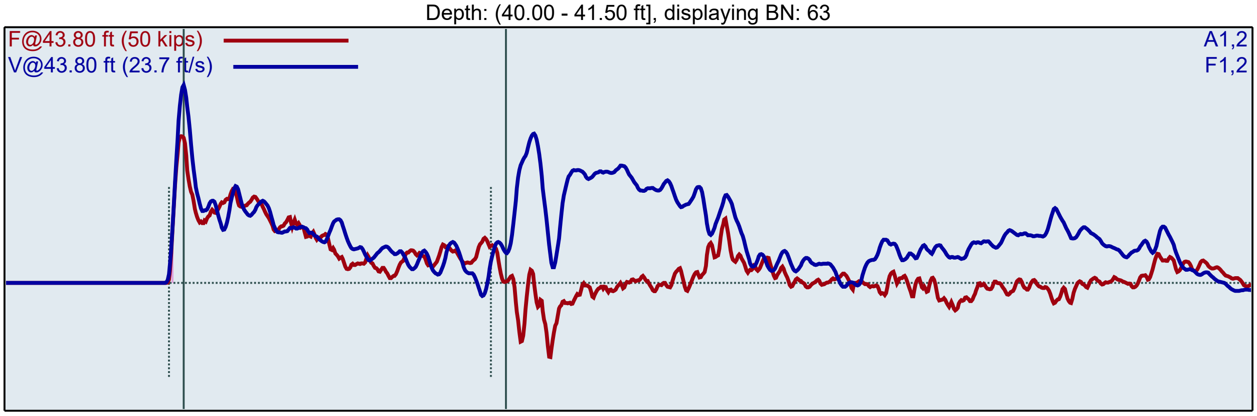

BL#	BC /6"	FMX kips	VMX ft/s	BPM bpm	EFV ft-lb	ETR (%)
51	3	31	18.7	1.9	328	96.0
52	3	31	19.0	58.9	319	93.4
53	3	31	18.7	57.7	326	95.5
54	4	30	18.7	57.1	316	92.6
55	4	30	18.9	57.1	326	95.4
56	4	30	18.3	56.9	321	94.0
57	4	31	18.5	57.1	325	95.3
58	8	29	18.6	57.3	326	95.4
59	8	30	18.9	57.0	332	97.2
60	8	29	18.6	57.3	328	96.1
61	8	29	18.4	57.0	326	95.4
62	8	29	18.4	57.1	328	96.1
63	8	29	18.4	57.1	327	95.6
64	8	29	18.7	57.0	322	94.4
65	8	30	18.5	57.4	317	92.8
	Average	30	18.6	57.1	325	95.0
	Std Dev	1	0.2	0.1	4	1.3
	Maximum	31	18.9	57.4	332	97.2
	Minimum	29	18.3	56.9	316	92.6

N-value: 12

Sample Interval Time: 14.65 seconds.

CME75 SN350477
TDS/AB

20-21.5
Test date: 11/15/2016

AR: 1.18 in^2
LE: 48.50 ft
WS: 16807.9 ft/s

SP: 0.492 k/ft3
EM: 30000 ksi

Depth: (45.00 - 46.50 ft], displaying BN: 116

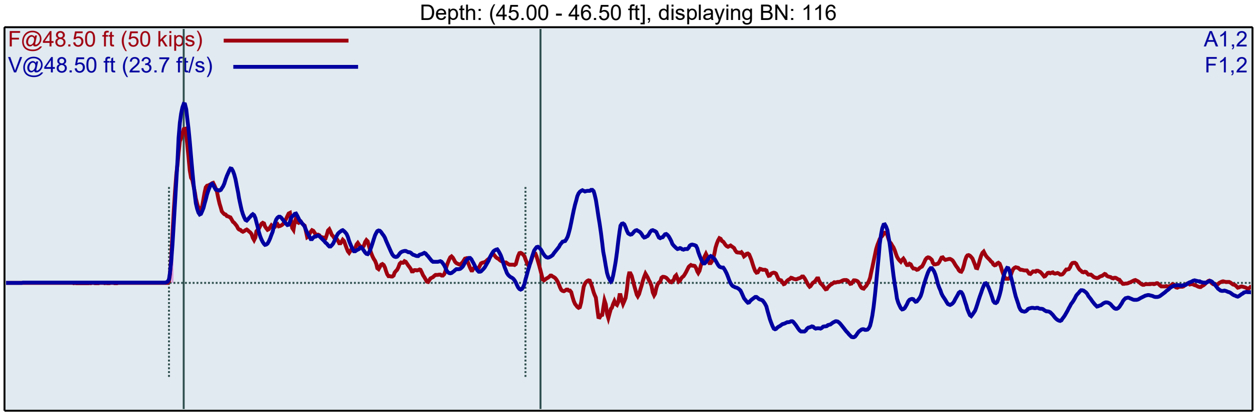

BL#	BC	FMX	VMX	BPM	EFV	ETR
	/6"	kips	ft/s	bpm	ft-lb	(%)
66	2	32	17.2	1.9	332	97.2
67	2	33	17.2	58.8	328	96.1
68	7	32	17.3	56.8	339	99.3
69	7	32	17.4	56.8	328	96.2
70	7	32	17.3	56.8	326	95.4
71	7	32	17.3	56.7	334	97.7
72	7	32	17.1	56.7	323	94.6
73	7	32	17.2	56.8	324	95.0
74	7	32	17.3	56.7	327	95.8
75	44	32	17.0	56.8	321	94.1
76	44	31	17.1	56.8	324	94.8
77	44	32	17.0	56.7	318	93.2
78	44	32	17.1	56.4	326	95.6
79	44	32	17.1	56.8	332	97.1
80	44	32	17.0	56.5	325	95.3
81	44	31	17.2	56.6	328	96.2
82	44	32	17.1	56.6	329	96.3
83	44	31	16.9	56.7	325	95.2
84	44	31	17.2	56.7	331	97.1
85	44	31	17.1	56.6	327	95.9
86	44	31	17.1	56.7	327	95.7
87	44	31	17.2	56.5	327	95.6
88	44	31	17.1	56.5	327	95.7
89	44	31	17.3	56.7	331	96.9
90	44	31	17.2	56.6	329	96.2
91	44	31	17.2	56.5	328	96.2
92	44	31	17.0	56.7	326	95.5
93	44	31	17.2	56.6	330	96.7
94	44	31	16.9	56.6	325	95.1
95	44	31	16.9	56.5	325	95.3
96	44	31	17.1	56.7	324	94.9
97	44	32	16.8	56.5	324	94.8
98	44	31	16.6	56.4	328	96.1
99	44	32	17.0	56.6	323	94.6
100	44	31	16.4	56.5	327	95.7
101	44	31	16.5	56.7	322	94.2

102	44	32	16.9	56.4	327	95.9
103	44	31	16.7	56.5	324	94.8
104	44	31	16.9	56.3	328	96.1
105	44	31	17.0	56.7	328	96.1
106	44	32	17.3	56.5	331	96.8
107	44	31	16.9	56.5	326	95.3
108	44	31	16.9	56.3	326	95.6
109	44	31	17.2	56.4	329	96.3
110	44	31	17.1	56.5	329	96.5
111	44	31	17.3	56.5	330	96.6
112	44	31	17.4	56.5	330	96.7
113	44	31	16.9	56.3	321	94.0
114	44	30	16.9	56.4	331	96.9
115	44	31	17.1	56.3	327	95.7
116	44	30	16.6	56.5	327	95.6
117	44	30	17.0	56.3	326	95.5
118	44	30	16.8	56.9	321	94.0
	Average	31	17.0	56.6	327	95.7
	Std Dev	1	0.2	0.2	4	1.0
	Maximum	32	17.4	56.9	339	99.3
	Minimum	30	16.4	56.3	318	93.2

N-value: 51

Sample Interval Time: 54.91 seconds.

Summary of SPT Test Results

Project: CME75 SN350477, Test Date: 11/15/2016

FMX: Maximum Force
VMX: Maximum Velocity
BPM: Blows/Minute

EFV: Maximum Energy
ETR: Energy Transfer Ratio - Rated

Instr. Length ft	Blows Applied /6"	**N Value**	**N60 Value**	Average FMX kips	Average VMX ft/s	Average BPM bpm	Average EFV ft-lb	Average ETR (%)
23.80	**1-5-6**	**11**	**17**	30	19.0	52.1	301	88.2
28.80	**3-4-4**	**8**	**12**	31	17.4	58.2	307	90.0
33.80	**5-4-7**	**11**	**17**	31	16.6	57.5	305	89.2
38.80	**2-3-6**	**9**	**13**	32	17.1	57.1	307	90.0
43.80	**3-4-8**	**12**	**18**	30	18.6	57.1	325	95.0
48.50	**2-7-44**	**51**	**79**	31	17.0	56.6	327	95.7
			Overall Average Values:	31	17.4	56.4	318	93.2
			Standard Deviation:	1	0.8	5.4	13	3.7
			Overall Maximum Value:	32	19.5	59.6	339	99.3
			Overall Minimum Value:	28	16.0	9.5	245	71.8

Summary of SPT Test Results

Project: CME75 (SN313927), Test Date: 10/27/2016

FMX: Maximum Force
VMX: Maximum Velocity
BPM: Blows/Minute
EFV: Maximum Energy
ETR: Energy Transfer Ratio - Rated

Instr. Length ft	Blows Applied /6"	**N Value**	**N60 Value**	Average FMX kips	Average VMX ft/s	Average BPM bpm	Average EFV ft-lb	Average ETR (%)
14.00	**4-7-11**	**18**	**27**	27	19.9	54.9	320	93.8
19.00	**3-6-9**	**15**	**22**	27	19.3	54.6	307	90.0
24.00	**3-6-17**	**23**	**34**	27	19.4	54.4	308	90.2
			Overall Average Values:	27	19.5	54.6	312	91.3
			Standard Deviation:	1	0.4	0.3	8	2.4
			Overall Maximum Value:	28	20.3	55.4	331	96.9
			Overall Minimum Value:	25	18.5	54.0	294	86.2

CME75 (SN313927)
TDS/AB

9.0-10.5 B
Test date: 10/27/2016

AR: 1.18 in^2
LE: 14.00 ft
WS: 16807.9 ft/s

SP: 0.492 k/ft3
EM: 30000 ksi

Depth: (9.00 - 10.50 ft], displaying BN: 20

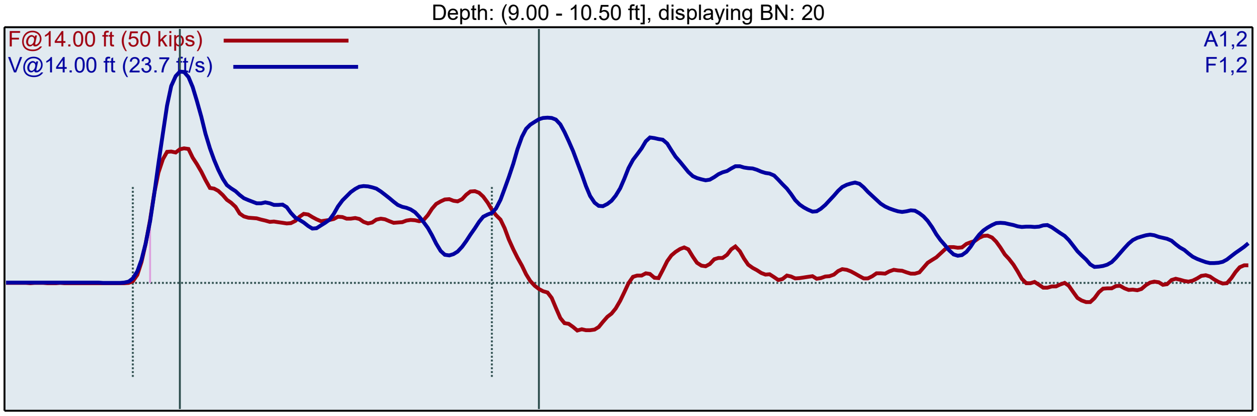

FMX: Maximum Force
VMX: Maximum Velocity
BPM: Blows/Minute

EFV: Maximum Energy
ETR: Energy Transfer Ratio - Rated

BL#	BC	FMX	VMX	BPM	EFV	ETR
	/6"	kips	ft/s	bpm	ft-lb	(%)
1	4	30	19.7	1.9	294	86.2
2	4	29	19.6	57.5	317	92.8
3	4	28	19.2	55.4	306	89.5
4	4	29	19.5	55.2	308	90.3
5	7	28	19.5	55.1	313	91.7
6	7	28	19.7	55.2	325	95.1
7	7	28	19.7	55.2	317	92.8
8	7	27	20.0	55.0	318	93.1
9	7	28	20.0	55.0	320	93.8
10	7	28	19.8	54.8	320	93.6
11	7	28	19.6	55.1	309	90.6
12	11	27	20.0	54.8	314	91.9
13	11	28	20.0	54.9	323	94.5
14	11	28	19.7	55.2	319	93.3
15	11	27	20.1	54.8	322	94.4
16	11	27	20.2	54.7	322	94.2
17	11	27	19.8	54.9	326	95.4
18	11	27	19.8	54.7	318	93.3
19	11	27	20.3	54.8	331	96.9
20	11	26	19.6	54.9	318	93.0
21	11	27	20.3	54.6	330	96.6
22	11	26	19.8	55.1	321	94.0
	Average	27	19.9	54.9	320	93.8
	Std Dev	1	0.2	0.2	5	1.6
	Maximum	28	20.3	55.2	331	96.9
	Minimum	26	19.5	54.6	309	90.6

N-value: 18

Sample Interval Time: 22.84 seconds.

CME75 (SN313927) 9.0-10.5 B
TDS/AB Test date: 10/27/2016

AR: 1.18 in^2 SP: 0.492 k/ft3
LE: 19.00 ft EM: 30000 ksi
WS: 16807.9 ft/s

Depth: (14.00 - 15.50 ft], displaying BN: 38

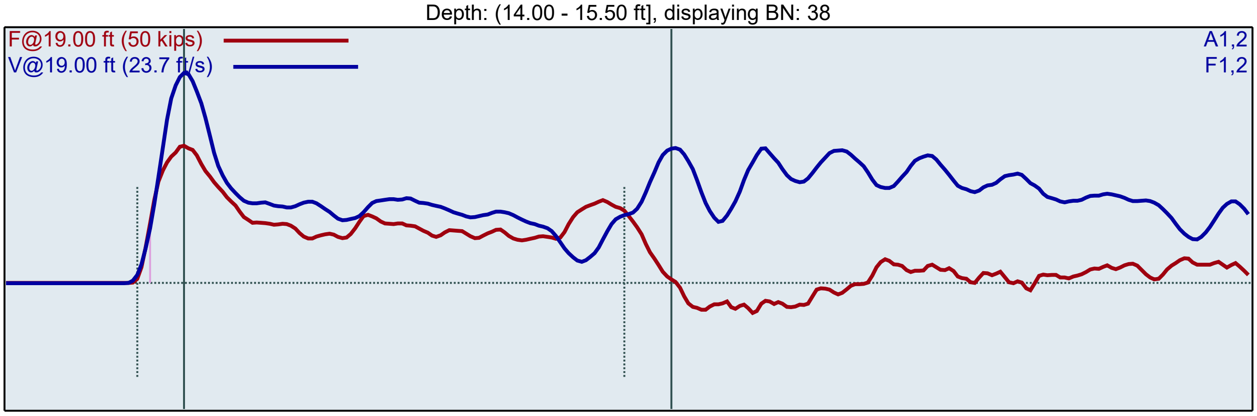

BL#	BC /6"	FMX kips	VMX ft/s	BPM bpm	EFV ft-lb	ETR (%)
24	3	28	18.7	54.7	293	85.8
25	3	28	18.7	54.9	315	92.3
26	3	28	19.1	54.8	318	93.0
27	6	27	18.8	55.4	303	88.9
28	6	27	19.1	54.3	318	93.1
29	6	27	19.0	54.9	311	91.0
30	6	27	19.0	54.7	297	86.9
31	6	27	19.3	54.7	309	90.5
32	6	27	19.3	54.6	314	92.0
33	9	27	19.7	54.7	307	89.8
34	9	27	19.4	54.5	303	88.8
35	9	27	19.3	54.4	302	88.5
36	9	27	19.4	54.6	301	88.3
37	9	27	19.3	54.3	310	90.7
38	9	27	19.5	54.6	309	90.4
39	9	27	19.3	54.4	308	90.2
40	9	26	19.3	54.4	309	90.4
	Average	27	19.3	54.6	307	90.0
	Std Dev	0	0.2	0.3	5	1.6
	Maximum	27	19.7	55.4	318	93.1
	Minimum	26	18.8	54.3	297	86.9

N-value: 14

Sample Interval Time: 17.55 seconds.

CME75 (SN313927)
TDS/AB

9.0-10.5 B
Test date: 10/27/2016

AR: 1.18 in^2
LE: 24.00 ft
WS: 16807.9 ft/s

SP: 0.492 k/ft3
EM: 30000 ksi

Depth: (19.00 - 20.50 ft], displaying BN: 64

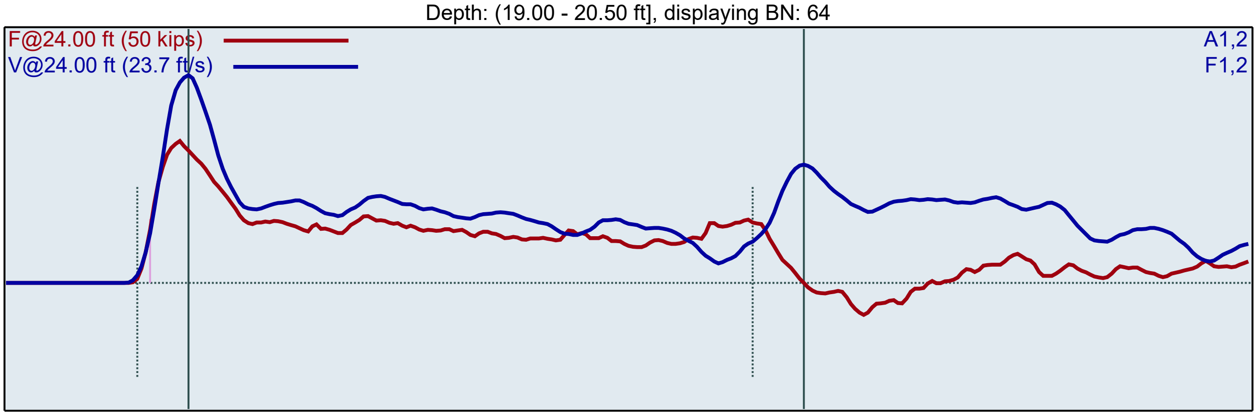

BL#	BC /6"	FMX kips	VMX ft/s	BPM bpm	EFV ft-lb	ETR (%)
41	3	29	19.3	55.3	297	86.8
42	3	29	19.7	55.0	299	87.5
43	3	28	19.0	54.9	314	91.8
44	6	28	18.7	55.0	305	89.3
45	6	28	18.5	54.4	306	89.5
46	6	27	18.5	55.0	294	86.2
47	6	27	18.9	54.8	297	87.1
48	6	27	19.2	54.5	299	87.5
49	6	27	19.3	54.6	308	90.3
50	17	27	19.8	54.3	309	90.5
51	17	27	20.1	54.9	312	91.4
52	17	26	20.0	54.4	301	88.0
53	17	26	20.2	54.3	308	90.3
54	17	27	19.6	54.2	306	89.5
55	17	27	19.5	54.8	308	90.1
56	17	27	19.1	54.2	307	89.9
57	17	27	19.2	54.3	307	89.9
58	17	25	19.6	54.0	303	88.8
59	17	28	19.4	54.2	317	92.9
60	17	26	19.6	54.2	311	91.0
61	17	27	19.5	54.2	314	91.8
62	17	27	19.5	54.1	309	90.5
63	17	28	19.5	54.3	319	93.4
64	17	28	19.3	54.0	316	92.6
65	17	27	19.3	54.1	314	91.9
66	17	26	19.7	54.3	313	91.5
	Average	27	19.4	54.4	308	90.2
	Std Dev	1	0.4	0.3	6	1.8
	Maximum	28	20.2	55.0	319	93.4
	Minimum	25	18.5	54.0	294	86.2

N-value: 23

Sample Interval Time: 27.50 seconds.

Summary of SPT Test Results

Project: CME75 (SN313927), Test Date: 10/27/2016

FMX: Maximum Force
VMX: Maximum Velocity
BPM: Blows/Minute
EFV: Maximum Energy
ETR: Energy Transfer Ratio - Rated

Instr. Length ft	Blows Applied /6"	**N Value**	**N60 Value**	Average FMX kips	Average VMX ft/s	Average BPM bpm	Average EFV ft-lb	Average ETR (%)
14.00	**4-7-11**	**18**	**27**	27	19.9	54.9	320	93.8
19.00	**3-6-9**	**15**	**22**	27	19.3	54.6	307	90.0
24.00	**3-6-17**	**23**	**34**	27	19.4	54.4	308	90.2
			Overall Average Values:	27	19.5	54.6	312	91.3
			Standard Deviation:	1	0.4	0.3	8	2.4
			Overall Maximum Value:	28	20.3	55.4	331	96.9
			Overall Minimum Value:	25	18.5	54.0	294	86.2

Summary of SPT Test Results

Project: CME 75 (SN 168457), Test Date: 8/2/2016

FMX: Maximum Force
CSX: Compression Stress Maximum
VMX: Maximum Velocity

BPM: Blows/Minute
EFV: Maximum Energy
ETR: Energy Transfer Ratio - Rated

Instr. Length ft	Blows Applied /6"	Start Depth ft	Final Depth ft	**N Value**	**N60 Value**	Average FMX kips	Average CSX ksi	Average VMX ft/s	Average BPM bpm	Average EFV ft-lb	Average ETR (%)
22.00	**9-16-31**	17.00	18.50	**47**	**75**	29	24.9	19.1	52.9	322.7	92.2
23.00	**9-23-32**	20.00	21.50	**55**	**88**	29	24.2	19.9	55.2	340.3	97.2
28.00	**6-16-26**	23.00	24.50	**42**	**67**	31	26.3	18.5	56.7	331.8	94.8
33.00	**9-24-65**	28.00	29.50	**89**	**143**	31	26.1	19.3	53.8	341.9	97.7
38.00	**6-26-42**	33.00	34.50	**68**	**109**	29	24.6	20.3	57.0	343.1	98.0
					Overall Average Values:	30	25.2	19.5	55.0	337.5	96.4
					Standard Deviation:	1	1.1	0.7	4.9	12.5	3.6
					Overall Maximum Value:	32	27.5	20.9	59.3	361.9	103.4
					Overall Minimum Value:	27	23.3	18.0	1.9	307.3	87.8

CME 75 (SN 168457)
TDS

Test date: 8/2/2016

AR: 1.18 in^2
LE: 22.00 ft
WS: 16807.9 ft/s

SP: 0.492 k/ft3
EM: 30000 ksi

Depth: (17.00 - 18.50 ft], displaying BN: 54

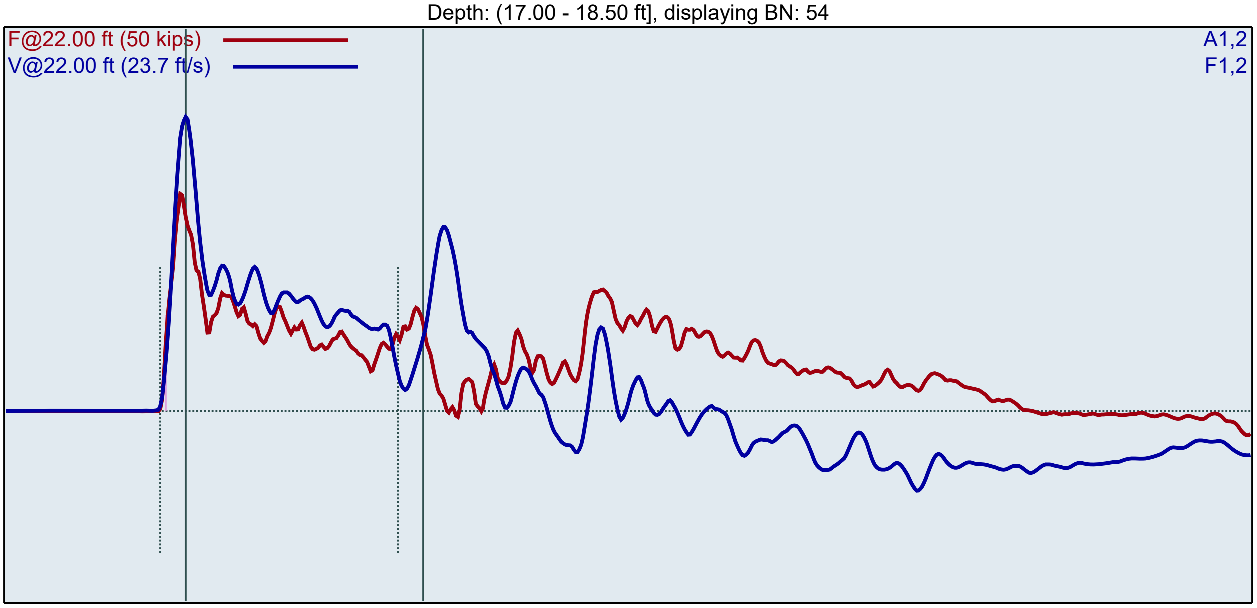

BL#	BC /6"	LP ft	FMX kips	CSX ksi	VMX ft/s	BPM bpm	EFV ft-lb	ETR (%)
1	9	17.06	28	23.9	18.8	51.7	324.4	92.7
2	9	17.11	28	24.1	18.9	52.9	334.6	95.6
3	9	17.17	29	24.3	19.0	52.6	329.4	94.1
4	9	17.22	28	24.1	18.8	52.4	322.7	92.2
5	9	17.28	28	23.9	18.7	52.7	322.7	92.2
6	9	17.33	28	24.0	19.0	52.7	325.8	93.1
7	9	17.39	29	24.5	19.0	52.7	330.3	94.4
8	9	17.44	28	24.1	18.9	52.5	323.8	92.5
9	9	17.50	29	24.6	18.9	52.7	328.3	93.8
10	16	17.53	29	24.6	18.9	52.4	321.7	91.9
11	16	17.56	29	24.4	19.0	52.5	327.6	93.6
12	16	17.59	29	24.2	19.1	52.7	322.7	92.2
13	16	17.63	28	23.9	19.1	52.9	324.0	92.6
14	16	17.66	29	24.4	19.1	52.6	329.7	94.2
15	16	17.69	29	24.9	19.3	52.9	333.5	95.3
16	16	17.72	29	24.5	19.3	52.9	331.3	94.6
17	16	17.75	29	24.7	19.2	52.7	329.2	94.1
18	16	17.78	29	24.5	19.1	52.7	327.5	93.6
19	16	17.81	28	24.1	19.1	52.6	327.3	93.5
20	16	17.84	28	24.0	19.4	52.8	329.7	94.2
21	16	17.88	29	24.3	19.3	52.4	330.8	94.5
22	16	17.91	29	24.9	19.4	52.9	330.2	94.3
23	16	17.94	29	24.6	19.1	52.5	322.8	92.2
24	16	17.97	29	24.2	19.4	52.7	323.9	92.5
25	16	18.00	29	24.5	19.3	53.0	322.1	92.0
26	31	18.02	29	24.8	19.3	52.9	325.6	93.0
27	31	18.03	29	24.4	19.5	52.8	328.2	93.8
28	31	18.05	30	25.1	19.5	52.5	330.6	94.5
29	31	18.06	29	24.8	19.5	52.9	328.2	93.8

30	31	18.08	30	25.2	19.5	53.1	328.3	93.8
31	31	18.10	29	24.9	19.6	53.0	328.3	93.8
32	31	18.11	29	24.6	19.5	52.7	330.4	94.4
33	31	18.13	30	25.1	19.5	52.7	331.3	94.7
34	31	18.15	30	25.2	19.5	52.7	324.8	92.8
35	31	18.16	30	25.4	19.5	52.5	323.0	92.3
36	31	18.18	30	25.5	19.4	52.7	320.9	91.7
37	31	18.19	30	25.8	19.5	52.8	326.8	93.4
38	31	18.21	30	25.5	19.3	53.2	315.1	90.0
39	31	18.23	30	25.6	19.2	53.0	313.1	89.5
40	31	18.24	31	26.1	19.4	52.8	320.7	91.6
41	31	18.26	30	25.7	19.3	53.2	317.7	90.8
42	31	18.27	31	26.2	19.3	53.1	319.2	91.2
43	31	18.29	31	26.2	19.3	53.4	322.5	92.1
44	31	18.31	30	25.6	18.9	53.2	314.3	89.8
45	31	18.32	30	25.7	19.1	52.8	313.4	89.6
46	31	18.34	30	25.3	19.1	53.0	316.9	90.5
47	31	18.35	30	25.5	18.8	53.0	317.3	90.6
48	31	18.37	30	25.4	18.5	53.0	316.1	90.3
49	31	18.39	30	25.2	18.4	52.9	318.3	90.9
50	31	18.40	29	24.9	18.4	53.2	318.2	90.9
51	31	18.42	29	24.8	18.4	53.4	317.1	90.6
52	31	18.44	29	24.5	18.0	52.9	314.8	89.9
53	31	18.45	29	24.4	18.0	52.9	313.2	89.5
54	31	18.47	28	23.9	18.2	53.3	313.1	89.4
55	31	18.48	29	24.3	18.3	53.1	310.7	88.8
56	31	18.50	29	24.5	18.4	52.7	314.7	89.9
		Average	29	24.9	19.1	52.9	322.7	92.2
		Std Dev	1	0.6	0.4	0.2	6.3	1.8
		Maximum	31	26.2	19.6	53.4	333.5	95.3
		Minimum	28	23.9	18.0	52.4	310.7	88.8

N-value: 47

Sample Interval Time: 62.35 seconds.

CME 75 (SN 168457)
TDS

Test date: 8/2/2016

AR: 1.18 in^2
LE: 23.00 ft
WS: 16807.9 ft/s

SP: 0.492 k/ft3
EM: 30000 ksi

Depth: (20.00 - 21.50 ft], displaying BN: 118

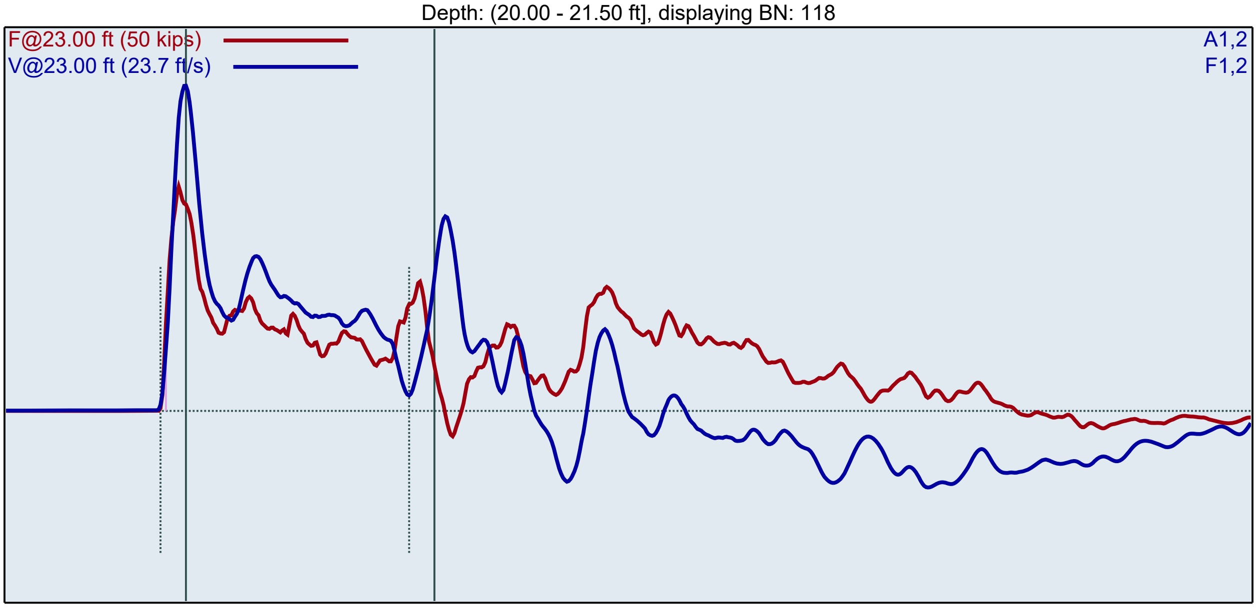

BL#	BC /6"	LP ft	FMX kips	CSX ksi	VMX ft/s	BPM bpm	EFV ft-lb	ETR (%)
57	9	20.06	28	23.4	19.1	1.9	307.5	87.9
58	9	20.11	28	23.9	19.5	51.7	337.9	96.5
59	9	20.17	28	24.1	19.7	54.6	344.4	98.4
60	9	20.22	29	24.3	19.6	55.0	346.6	99.0
61	9	20.28	28	23.9	19.5	55.1	333.9	95.4
62	9	20.33	28	23.8	19.4	54.9	341.0	97.4
63	9	20.39	28	24.0	19.7	55.1	344.8	98.5
64	9	20.44	28	24.0	19.7	54.7	339.3	96.9
65	9	20.50	28	23.8	19.6	55.4	343.2	98.1
66	23	20.52	28	23.8	19.8	55.1	344.0	98.3
67	23	20.54	28	24.0	19.8	55.1	342.0	97.7
68	23	20.57	28	24.1	19.8	55.1	340.7	97.3
69	23	20.59	28	23.9	19.7	55.0	339.8	97.1
70	23	20.61	28	23.7	19.7	55.2	336.8	96.2
71	23	20.63	28	23.6	19.6	54.9	339.6	97.0
72	23	20.65	28	23.7	19.8	55.2	348.9	99.7
73	23	20.67	28	23.8	19.8	55.1	344.5	98.4
74	23	20.70	29	24.2	19.8	55.4	341.1	97.5
75	23	20.72	28	23.8	19.7	55.2	345.2	98.6
76	23	20.74	28	24.0	19.8	55.1	342.4	97.8
77	23	20.76	29	24.2	19.9	54.7	340.4	97.2
78	23	20.78	29	24.3	20.0	55.2	346.4	99.0
79	23	20.80	28	24.0	19.9	55.2	344.5	98.4
80	23	20.83	28	23.9	19.8	55.4	344.0	98.3
81	23	20.85	28	23.9	19.8	55.3	342.9	98.0
82	23	20.87	28	23.7	19.8	55.2	346.1	98.9
83	23	20.89	28	24.1	19.8	55.2	346.2	98.9
84	23	20.91	28	24.0	19.8	55.3	347.0	99.1
85	23	20.93	28	23.9	19.8	55.4	345.0	98.6

86	23	20.96	28	23.9	19.7	55.0	339.4	97.0
87	23	20.98	28	23.9	19.8	55.1	338.7	96.8
88	23	21.00	28	23.9	19.8	54.9	338.1	96.6
89	32	21.02	28	24.1	19.8	55.2	337.4	96.4
90	32	21.03	28	24.1	19.8	55.3	337.2	96.3
91	32	21.05	29	24.2	19.8	55.3	335.2	95.8
92	32	21.06	29	24.2	19.9	55.2	340.4	97.2
93	32	21.08	29	24.2	19.9	55.3	336.4	96.1
94	32	21.09	28	24.0	19.9	55.3	338.7	96.8
95	32	21.11	29	24.3	19.9	55.1	340.0	97.1
96	32	21.13	29	24.3	19.9	55.5	341.5	97.6
97	32	21.14	29	24.5	20.0	55.4	338.9	96.8
98	32	21.16	29	24.3	19.9	54.8	340.5	97.3
99	32	21.17	29	24.2	20.0	55.3	340.9	97.4
100	32	21.19	28	24.1	19.9	55.5	340.2	97.2
101	32	21.20	29	24.4	20.0	55.2	343.1	98.0
102	32	21.22	29	24.3	20.0	55.3	341.8	97.7
103	32	21.23	29	24.2	20.0	55.3	342.0	97.7
104	32	21.25	29	24.3	20.0	55.2	341.0	97.4
105	32	21.27	29	24.2	20.0	55.0	340.8	97.4
106	32	21.28	29	24.3	20.0	55.5	340.7	97.4
107	32	21.30	29	24.2	19.9	55.3	342.0	97.7
108	32	21.31	29	24.3	20.0	55.6	339.7	97.1
109	32	21.33	29	24.2	20.0	55.0	339.0	96.9
110	32	21.34	29	24.2	20.0	55.4	338.1	96.6
111	32	21.36	29	24.2	20.0	55.1	334.7	95.6
112	32	21.38	29	24.6	20.1	55.4	333.7	95.4
113	32	21.39	29	24.7	20.1	55.5	333.6	95.3
114	32	21.41	29	24.8	20.2	55.3	332.7	95.1
115	32	21.42	29	24.9	20.2	55.5	334.8	95.6
116	32	21.44	29	24.8	20.1	55.0	336.6	96.2
117	32	21.45	29	24.5	20.0	55.5	333.6	95.3
118	32	21.47	29	24.8	20.1	55.0	339.1	96.9
119	32	21.48	29	24.7	20.0	55.2	338.8	96.8
120	32	21.50	29	24.8	20.1	55.3	337.4	96.4
		Average	29	24.2	19.9	55.2	340.3	97.2
		Std Dev	0	0.3	0.1	0.2	3.7	1.0
		Maximum	29	24.9	20.2	55.6	348.9	99.7
		Minimum	28	23.6	19.6	54.7	332.7	95.1

N-value: 55

BN: 120 9-23-32

Sample Interval Time: 68.45 seconds.

CME 75 (SN 168457)
TDS

Test date: 8/2/2016

AR: 1.18 in^2
LE: 28.00 ft
WS: 16807.9 ft/s

SP: 0.492 k/ft3
EM: 30000 ksi

Depth: (23.00 - 24.50 ft], displaying BN: 166

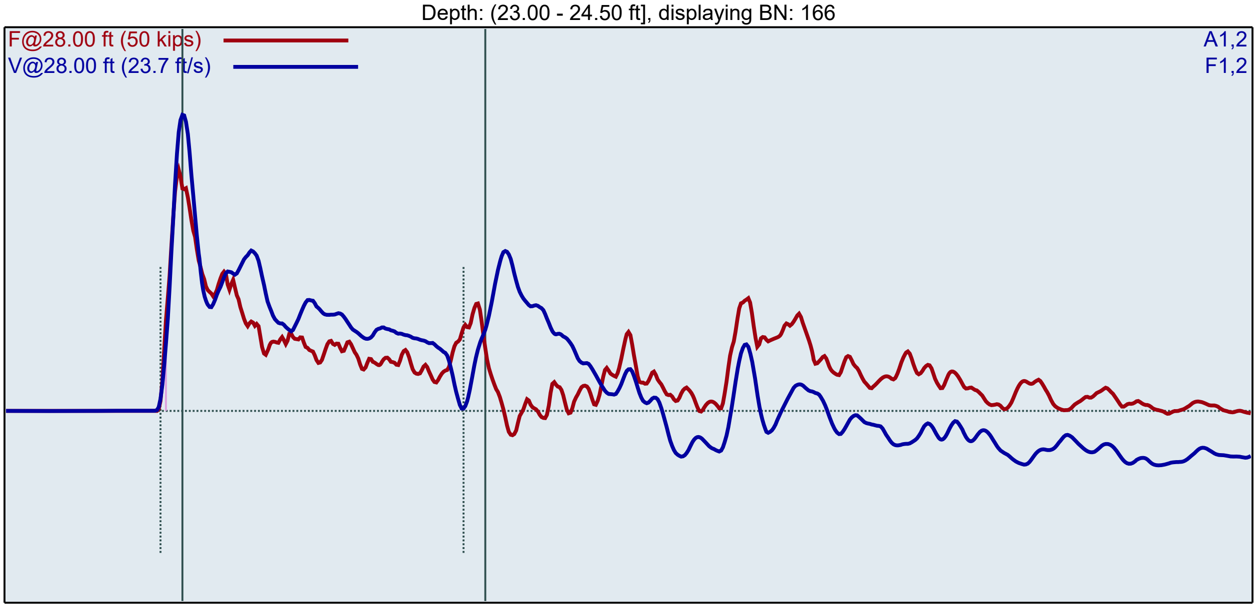

BL#	BC /6"	LP ft	FMX kips	CSX ksi	VMX ft/s	BPM bpm	EFV ft-lb	ETR (%)
121	6	23.08	30	25.3	18.2	1.9	311.2	88.9
122	6	23.17	30	25.8	18.5	54.3	325.8	93.1
123	6	23.25	30	25.8	18.3	56.4	328.1	93.7
124	6	23.33	31	26.2	18.5	56.4	342.3	97.8
125	6	23.42	31	26.1	18.5	57.1	343.1	98.0
126	6	23.50	30	25.8	18.3	56.4	336.2	96.0
127	16	23.53	30	25.8	18.3	56.8	331.3	94.7
128	16	23.56	31	26.0	18.4	57.2	335.1	95.7
129	16	23.59	31	25.9	18.4	56.8	326.9	93.4
130	16	23.63	30	25.5	18.2	57.0	322.9	92.3
131	16	23.66	30	25.8	18.5	56.6	332.0	94.9
132	16	23.69	31	25.9	18.4	56.5	325.8	93.1
133	16	23.72	31	26.2	18.5	56.6	328.1	93.7
134	16	23.75	31	25.9	18.5	57.3	332.1	94.9
135	16	23.78	31	26.1	18.4	56.4	328.6	93.9
136	16	23.81	31	26.0	18.4	57.1	329.7	94.2
137	16	23.84	31	26.1	18.4	56.6	329.6	94.2
138	16	23.88	31	26.4	18.5	56.2	331.0	94.6
139	16	23.91	31	26.4	18.6	56.4	334.0	95.4
140	16	23.94	31	26.2	18.6	57.4	335.9	96.0
141	16	23.97	31	26.5	18.6	56.3	334.4	95.5
142	16	24.00	31	26.5	18.5	56.9	328.1	93.7
143	26	24.02	31	26.3	18.5	56.4	332.9	95.1
144	26	24.04	31	26.1	18.5	57.0	332.8	95.1
145	26	24.06	31	26.0	18.5	56.8	328.9	94.0
146	26	24.08	31	26.1	18.5	57.1	327.7	93.6
147	26	24.10	31	26.5	18.6	56.6	330.5	94.4
148	26	24.12	31	26.2	18.6	56.5	334.3	95.5
149	26	24.13	31	26.5	18.6	57.1	334.1	95.5

150	26	24.15	31	26.1	18.5	56.3	335.0	95.7
151	26	24.17	31	26.2	18.5	56.8	333.4	95.3
152	26	24.19	31	26.3	18.6	56.0	334.7	95.6
153	26	24.21	31	26.2	18.5	57.1	333.4	95.3
154	26	24.23	31	26.5	18.5	56.8	337.6	96.4
155	26	24.25	31	26.4	18.5	56.2	334.5	95.6
156	26	24.27	31	26.6	18.3	56.9	332.1	94.9
157	26	24.29	31	26.4	18.5	56.8	336.5	96.2
158	26	24.31	31	26.3	18.4	56.8	333.5	95.3
159	26	24.33	31	26.3	18.2	57.1	325.1	92.9
160	26	24.35	31	26.3	18.5	56.8	334.0	95.4
161	26	24.37	31	26.6	18.4	56.6	332.6	95.0
162	26	24.38	31	26.6	18.5	56.5	334.1	95.5
163	26	24.40	31	26.6	18.5	56.6	332.7	95.1
164	26	24.42	31	26.7	18.4	57.0	333.3	95.2
165	26	24.44	32	26.8	18.5	56.7	332.9	95.1
166	26	24.46	31	26.6	18.3	57.0	327.6	93.6
167	26	24.48	31	26.5	18.5	56.5	334.6	95.6
168	26	24.50	31	26.6	18.4	57.0	330.7	94.5
		Average	31	26.3	18.5	56.7	331.8	94.8
		Std Dev	0	0.3	0.1	0.3	3.2	0.9
		Maximum	32	26.8	18.6	57.4	337.6	96.4
		Minimum	30	25.5	18.2	56.0	322.9	92.3

N-value: 42

BN: 168

Sample Interval Time: 49.69 seconds.

CME 75 (SN 168457)
TDS
Test date: 8/2/2016

AR: 1.18 in^2
LE: 33.00 ft
WS: 16807.9 ft/s
SP: 0.492 k/ft3
EM: 30000 ksi

Depth: (28.00 - 29.50 ft], displaying BN: 264

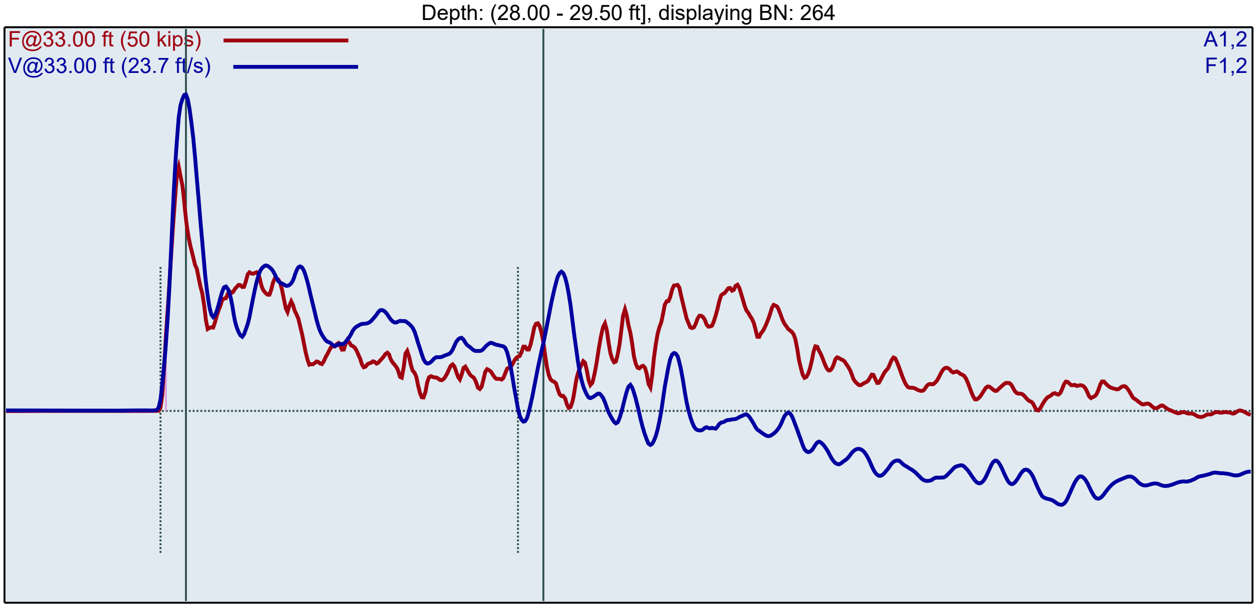

BL#	BC /6"	LP ft	FMX kips	CSX ksi	VMX ft/s	BPM bpm	EFV ft-lb	ETR (%)
169	9	28.06	29	24.9	18.4	43.1	311.5	89.0
170	9	28.11	29	24.9	18.4	43.2	316.1	90.3
171	9	28.17	29	24.7	18.5	43.2	314.6	89.9
172	9	28.22	30	25.1	18.3	43.3	312.6	89.3
173	9	28.28	30	25.1	18.3	43.3	309.8	88.5
174	9	28.33	29	24.8	18.4	43.1	311.6	89.0
175	9	28.39	29	24.6	18.4	43.1	314.5	89.9
176	9	28.44	29	24.6	18.5	43.5	314.7	89.9
177	9	28.50	29	24.9	18.5	43.0	315.7	90.2
178	24	28.52	29	24.9	18.5	43.5	311.1	88.9
179	24	28.54	29	24.8	18.5	43.4	315.2	90.1
180	24	28.56	30	25.0	18.5	42.9	313.3	89.5
181	24	28.58	29	24.6	18.5	42.8	307.3	87.8
182	24	28.60	30	25.2	18.7	43.2	314.3	89.8
183	24	28.63	30	25.2	18.7	42.9	310.4	88.7
184	24	28.65	30	25.0	18.6	43.2	312.7	89.3
185	24	28.67	30	25.1	18.5	43.1	310.1	88.6
186	24	28.69	29	24.9	18.5	43.1	308.1	88.0
187	24	28.71	29	24.6	18.9	43.1	308.6	88.2
188	24	28.73	29	24.3	18.9	43.1	310.2	88.6
189	24	28.75	28	23.9	18.8	43.0	315.3	90.1
190	24	28.77	28	23.4	19.0	43.1	315.2	90.1
191	24	28.79	28	23.4	18.9	42.9	313.8	89.6
192	24	28.81	28	23.3	19.0	42.9	317.6	90.7
193	24	28.83	27	23.3	19.0	42.8	314.4	89.8
194	24	28.85	28	23.5	18.9	42.9	311.9	89.1
195	24	28.88	28	23.4	18.7	43.1	308.5	88.1
196	24	28.90	28	23.4	18.8	42.8	312.6	89.3
197	24	28.92	28	23.3	18.7	42.9	311.7	89.0

198	24	28.94	28	23.5	18.8	43.1	311.7	89.1
199	24	28.96	28	23.4	18.7	43.0	310.8	88.8
200	24	28.98	32	27.5	19.3	1.9	359.4	102.7
201	24	29.00	28	24.0	20.0	54.2	355.2	101.5
202	65	29.01	31	26.4	19.1	58.1	347.5	99.3
203	65	29.02	31	26.5	19.2	58.0	350.9	100.2
204	65	29.02	31	26.2	19.1	58.3	350.4	100.1
205	65	29.03	31	26.6	19.2	57.9	352.5	100.7
206	65	29.04	32	26.8	19.1	58.4	349.3	99.8
207	65	29.05	31	26.6	19.1	58.1	343.4	98.1
208	65	29.05	31	26.6	19.2	58.0	346.0	98.8
209	65	29.06	31	26.4	19.1	58.4	345.3	98.7
210	65	29.07	32	26.7	19.3	58.1	350.5	100.2
211	65	29.08	31	26.5	19.4	57.7	355.9	101.7
212	65	29.08	31	26.4	19.3	58.5	353.2	100.9
213	65	29.09	31	26.3	19.4	58.3	352.3	100.6
214	65	29.10	31	26.5	19.2	58.2	347.8	99.4
215	65	29.11	32	26.7	19.1	58.1	351.4	100.4
216	65	29.12	31	26.5	19.6	57.8	356.1	101.7
217	65	29.12	32	26.9	19.2	58.8	355.5	101.6
218	65	29.13	32	27.2	19.4	58.4	356.8	101.9
219	65	29.14	32	26.8	19.5	57.9	354.6	101.3
220	65	29.15	32	26.8	19.5	57.9	355.8	101.6
221	65	29.15	31	26.7	19.6	58.5	355.7	101.6
222	65	29.16	32	26.8	19.5	58.4	352.6	100.7
223	65	29.17	32	27.2	19.5	58.2	359.8	102.8
224	65	29.18	32	27.2	19.8	58.1	361.9	103.4
225	65	29.18	32	27.3	19.5	57.9	358.5	102.4
226	65	29.19	32	27.3	19.5	58.3	353.0	100.9
227	65	29.20	32	27.1	19.5	58.1	355.6	101.6
228	65	29.21	32	27.0	19.6	58.1	355.1	101.4
229	65	29.22	32	27.3	19.8	58.0	359.7	102.8
230	65	29.22	32	27.2	19.5	58.8	352.5	100.7
231	65	29.23	32	26.8	19.8	58.2	355.8	101.7
232	65	29.24	32	27.2	19.8	58.5	351.8	100.5
233	65	29.25	32	27.1	19.7	58.5	354.7	101.3
234	65	29.25	32	27.0	19.6	57.8	350.7	100.2
235	65	29.26	30	25.3	20.3	58.3	357.0	102.0
236	65	29.27	31	25.9	20.0	58.7	354.8	101.4
237	65	29.28	31	26.3	19.7	57.7	356.0	101.7
238	65	29.28	31	26.3	19.9	58.4	353.1	100.9
239	65	29.29	31	26.3	19.5	58.5	355.5	101.6
240	65	29.30	32	27.1	19.5	57.9	353.9	101.1
241	65	29.31	32	27.0	19.4	58.8	349.4	99.8
242	65	29.32	32	26.8	19.5	58.3	349.9	100.0
243	65	29.32	32	26.9	19.5	57.8	349.5	99.9
244	65	29.33	31	26.4	19.4	58.6	347.0	99.1
245	65	29.34	31	26.4	19.2	58.3	343.2	98.0
246	65	29.35	31	26.5	19.3	58.1	346.2	98.9
247	65	29.35	31	26.6	19.4	58.0	350.8	100.2
248	65	29.36	32	26.8	19.5	58.1	354.1	101.2
249	65	29.37	32	26.8	19.5	58.2	349.6	99.9
250	65	29.38	31	26.2	19.5	59.0	347.8	99.4
251	65	29.38	32	26.9	19.5	57.6	348.6	99.6
252	65	29.39	32	26.7	19.4	58.8	346.0	98.9
253	65	29.40	32	26.7	19.6	58.4	348.2	99.5
254	65	29.41	31	26.5	19.8	58.1	353.0	100.8
255	65	29.42	31	26.5	19.7	58.4	351.3	100.4
256	65	29.42	32	26.9	19.8	58.1	354.2	101.2
257	65	29.43	31	26.3	19.6	58.9	344.6	98.5
258	65	29.44	31	26.6	19.4	58.0	343.4	98.1

259	65	29.45	32	26.7	20.0	58.5	349.7	99.9
260	65	29.45	32	26.8	19.5	58.2	348.1	99.5
261	65	29.46	32	26.9	19.7	58.1	349.1	99.7
262	65	29.47	32	26.9	19.7	58.2	346.8	99.1
263	65	29.48	32	27.0	19.8	58.2	351.5	100.4
264	65	29.48	32	26.9	19.6	58.2	349.7	99.9
265	65	29.49	32	27.1	19.7	58.1	350.0	100.0
266	65	29.50	31	26.6	19.6	58.8	344.5	98.4
		Average	31	26.1	19.3	53.8	341.9	97.7
		Std Dev	1	1.2	0.4	8.6	17.6	5.0
		Maximum	32	27.5	20.3	59.0	361.9	103.4
		Minimum	27	23.3	18.5	1.9	307.3	87.8

N-value: 89

Sample Interval Time: 169.32 seconds.

CME 75 (SN 168457)
TDS

Test date: 8/2/2016

AR: 1.18 in^2
LE: 38.00 ft
WS: 16807.9 ft/s

SP: 0.492 k/ft3
EM: 30000 ksi

Depth: (33.00 - 34.50 ft], displaying BN: 338

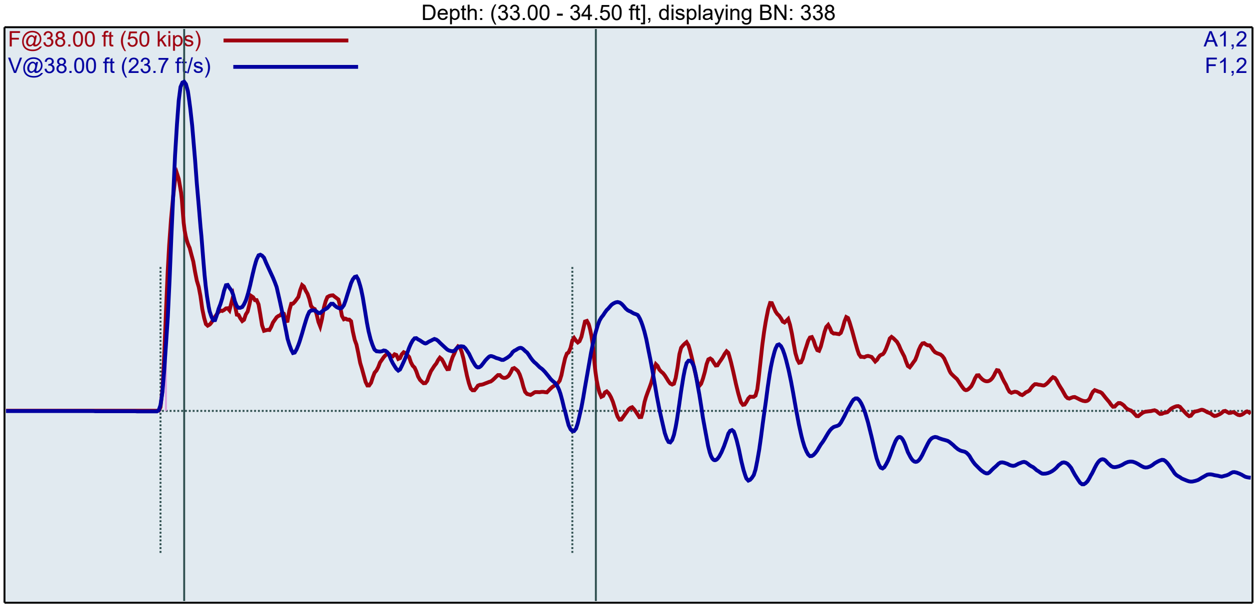

BL#	BC /6"	LP ft	FMX kips	CSX ksi	VMX ft/s	BPM bpm	EFV ft-lb	ETR (%)
267	6	33.08	28	24.0	20.1	1.9	353.5	101.0
268	6	33.17	29	24.2	20.5	57.6	362.1	103.5
269	6	33.25	28	23.8	20.3	58.3	358.9	102.5
270	6	33.33	28	23.5	20.7	58.7	367.0	104.9
271	6	33.42	28	23.6	20.6	59.1	358.1	102.3
272	6	33.50	28	23.8	20.6	58.6	354.2	101.2
273	26	33.52	28	24.1	20.7	59.0	351.8	100.5
274	26	33.54	28	24.1	20.6	58.6	346.7	99.1
275	26	33.56	28	23.8	20.6	59.2	347.1	99.2
276	26	33.58	28	23.8	20.4	58.8	346.9	99.1
277	26	33.60	29	24.4	20.2	58.9	345.9	98.8
278	26	33.62	29	24.4	20.4	58.7	345.8	98.8
279	26	33.63	29	24.3	20.2	59.3	342.5	97.9
280	26	33.65	28	23.9	20.6	58.3	343.8	98.2
281	26	33.67	28	23.9	20.2	55.5	334.1	95.5
282	26	33.69	28	23.8	20.1	53.2	339.7	97.1
283	26	33.71	28	23.3	20.5	56.0	345.5	98.7
284	26	33.73	28	23.7	20.4	57.2	341.6	97.6
285	26	33.75	28	23.8	20.5	56.9	343.2	98.1
286	26	33.77	29	24.2	20.5	56.6	345.9	98.8
287	26	33.79	28	23.9	20.5	57.3	342.0	97.7
288	26	33.81	29	24.2	20.6	56.7	346.4	99.0
289	26	33.83	28	24.0	20.5	56.4	345.0	98.6
290	26	33.85	28	23.7	20.4	56.8	343.4	98.1
291	26	33.87	28	23.8	20.2	57.2	334.3	95.5
292	26	33.88	29	24.3	19.9	56.6	338.3	96.6
293	26	33.90	29	24.6	20.0	57.2	339.6	97.0
294	26	33.92	29	24.5	20.3	56.9	339.7	97.1
295	26	33.94	29	24.4	20.5	56.5	346.1	98.9

296	26	33.96	29	24.3	20.1	57.1	341.8	97.7
297	26	33.98	28	24.1	20.1	56.6	341.1	97.5
298	26	34.00	28	23.9	20.0	57.5	338.8	96.8
299	42	34.01	29	24.4	20.3	56.4	343.5	98.1
300	42	34.02	28	24.0	20.3	56.7	343.4	98.1
301	42	34.04	29	24.5	20.2	57.1	343.6	98.2
302	42	34.05	29	24.2	20.6	56.6	348.0	99.4
303	42	34.06	29	24.3	20.3	56.9	345.0	98.6
304	42	34.07	29	24.8	20.5	56.7	344.6	98.5
305	42	34.08	29	24.9	20.0	56.6	343.9	98.3
306	42	34.10	30	25.3	20.1	57.0	345.7	98.8
307	42	34.11	30	25.3	20.2	56.8	347.6	99.3
308	42	34.12	30	25.4	20.3	56.6	345.3	98.7
309	42	34.13	30	25.0	19.9	57.1	341.8	97.6
310	42	34.14	30	25.2	20.1	56.8	340.6	97.3
311	42	34.15	29	25.0	20.0	56.9	336.5	96.1
312	42	34.17	30	25.4	20.4	56.6	344.6	98.4
313	42	34.18	30	25.2	20.4	56.5	344.0	98.3
314	42	34.19	29	24.9	20.3	56.6	346.4	99.0
315	42	34.20	30	25.5	20.3	56.6	344.9	98.5
316	42	34.21	30	25.1	20.2	56.6	344.9	98.5
317	42	34.23	29	24.3	20.6	56.8	339.9	97.1
318	42	34.24	29	24.2	20.8	57.0	339.8	97.1
319	42	34.25	29	24.4	20.9	56.3	341.1	97.5
320	42	34.26	29	24.6	20.5	57.0	338.0	96.6
321	42	34.27	30	25.3	20.3	56.6	340.5	97.3
322	42	34.29	30	25.1	20.4	57.1	343.2	98.1
323	42	34.30	30	25.3	20.4	56.7	337.9	96.5
324	42	34.31	29	24.4	20.1	56.7	344.0	98.3
325	42	34.32	28	24.1	20.3	56.2	342.2	97.8
326	42	34.33	28	23.8	20.3	56.8	338.3	96.7
327	42	34.35	29	24.2	20.2	57.3	341.8	97.7
328	42	34.36	29	25.0	20.4	56.5	348.5	99.6
329	42	34.37	30	25.1	20.1	57.1	340.1	97.2
330	42	34.38	30	25.5	20.3	56.7	349.8	99.9
331	42	34.39	30	25.3	20.2	57.1	342.4	97.8
332	42	34.40	30	25.5	20.1	57.2	338.1	96.6
333	42	34.42	30	25.2	20.2	56.3	344.9	98.5
334	42	34.43	30	25.3	20.3	56.3	344.8	98.5
335	42	34.44	30	25.6	20.3	57.0	345.7	98.8
336	42	34.45	30	25.7	20.2	56.9	344.8	98.5
337	42	34.46	31	26.1	20.2	56.9	342.6	97.9
338	42	34.48	31	26.2	20.4	56.8	346.1	98.9
339	42	34.49	31	26.0	20.2	57.4	343.1	98.0
340	42	34.50	31	25.9	20.1	56.3	341.0	97.4
		Average	29	24.6	20.3	57.0	343.1	98.0
		Std Dev	1	0.7	0.2	0.9	3.4	1.0
		Maximum	31	26.2	20.9	59.3	351.8	100.5
		Minimum	28	23.3	19.9	53.2	334.1	95.5

N-value: 68

Sample Interval Time: 76.67 seconds.

Summary of SPT Test Results

Project: CME 75 (SN 168457), Test Date: 8/2/2016

FMX: Maximum Force
CSX: Compression Stress Maximum
VMX: Maximum Velocity
BPM: Blows/Minute
EFV: Maximum Energy
ETR: Energy Transfer Ratio - Rated

Instr. Length ft	Blows Applied /6"	Start Depth ft	Final Depth ft	**N Value**	**N60 Value**	Average FMX kips	Average CSX ksi	Average VMX ft/s	Average BPM bpm	Average EFV ft-lb	Average ETR (%)
22.00	**9-16-31**	17.00	18.50	**47**	**75**	29	24.9	19.1	52.9	322.7	92.2
23.00	**9-23-32**	20.00	21.50	**55**	**88**	29	24.2	19.9	55.2	340.3	97.2
28.00	**6-16-26**	23.00	24.50	**42**	**67**	31	26.3	18.5	56.7	331.8	94.8
33.00	**9-24-65**	28.00	29.50	**89**	**143**	31	26.1	19.3	53.8	341.9	97.7
38.00	**6-26-42**	33.00	34.50	**68**	**109**	29	24.6	20.3	57.0	343.1	98.0
					Overall Average Values:	30	25.2	19.5	55.0	337.5	96.4
					Standard Deviation:	1	1.1	0.7	4.9	12.5	3.6
					Overall Maximum Value:	32	27.5	20.9	59.3	361.9	103.4
					Overall Minimum Value:	27	23.3	18.0	1.9	307.3	87.8

Summary of SPT Test Results

Project: CME550X(SN249333), Test Date: 3/10/2017

FMX: Maximum Force
VMX: Maximum Velocity
BPM: Blows/Minute

EFV: Maximum Energy
ETR: Energy Transfer Ratio - Rated

Instr. Length ft	Blows Applied /6"	**N Value**	**N60 Value**	Average FMX kips	Average VMX ft/s	Average BPM bpm	Average EFV ft-lb	Average ETR (%)
23.00	**4-14-23**	**37**	**49**	25	16.2	54.9	270	79.2
25.00	**12-18-31**	**49**	**65**	31	15.8	53.7	278	81.4
28.00	**3-10-15**	**25**	**33**	27	15.1	54.9	270	78.9
32.00	**4-15-30**	**45**	**60**	25	16.4	55.0	277	81.2
			Overall Average Values:	27	15.9	54.6	275	80.4
			Standard Deviation:	13	0.7	3.7	14	4.0
			Overall Maximum Value:	139	18.0	57.1	365	106.7
			Overall Minimum Value:	24	14.2	18.4	245	71.8

CME550X(SN249333)
TDS/AB

18.0 -19. 5FT_1
Test date: 3/10/2017

AR: 1.18 in^2
LE: 23.00 ft
WS: 16807.9 ft/s

SP: 0.492 k/ft3
EM: 30000 ksi

Depth: (18.00 - 19.50 ft], displaying BN: 39

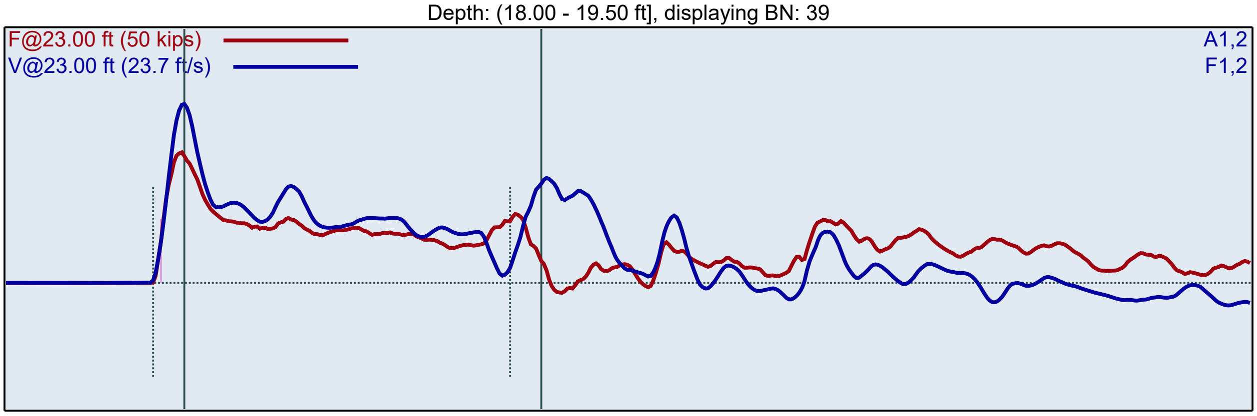

FMX: Maximum Force
VMX: Maximum Velocity
BPM: Blows/Minute

EFV: Maximum Energy
ETR: Energy Transfer Ratio - Rated

BL#	BC	FMX	VMX	BPM	EFV	ETR
	/6"	kips	ft/s	bpm	ft-lb	(%)
1	4	24	17.7	42.5	266	77.9
2	4	25	16.5	52.9	271	79.5
3	4	25	16.0	57.0	281	82.4
4	4	26	16.0	54.2	291	85.3
5	14	25	16.1	55.7	276	80.7
6	14	25	16.2	54.5	274	80.2
7	14	26	16.3	55.2	275	80.5
8	14	25	16.1	54.5	270	79.1
9	14	25	16.1	54.9	277	81.1
10	14	25	16.3	55.0	268	78.5
11	14	26	16.6	54.2	286	83.9
12	14	24	15.3	54.9	255	74.6
13	14	25	16.0	54.6	261	76.4
14	14	25	16.1	55.4	267	78.2
15	14	26	16.5	55.5	283	82.9
16	14	25	15.9	54.7	265	77.7
17	14	25	16.0	54.1	267	78.3
18	14	24	15.2	55.3	245	71.8
19	23	26	16.5	55.6	279	81.6
20	23	25	16.1	54.3	270	79.1
21	23	26	16.4	54.5	279	81.6
22	23	25	16.0	54.1	269	78.8
23	23	26	16.6	55.5	273	79.9
24	23	25	15.8	54.5	273	79.9
25	23	25	16.2	55.6	275	80.5
26	23	26	16.3	55.1	272	79.7
27	23	24	15.6	54.5	262	76.7
28	23	26	16.9	54.9	286	83.7
29	23	24	15.5	54.8	254	74.3
30	23	24	15.7	54.8	257	75.2
31	23	26	16.8	55.3	280	82.0
32	23	26	16.5	54.7	273	79.9
33	23	25	16.1	55.4	271	79.3

34	23	26	16.4	55.5	277	81.2
35	23	26	16.6	54.3	279	81.6
36	23	25	16.3	54.1	271	79.5
37	23	25	16.0	55.3	259	75.7
38	23	25	16.5	55.5	271	79.4
39	23	26	16.6	53.6	275	80.5
40	23	25	16.1	55.6	264	77.3
41	23	25	16.2	55.2	265	77.5
	Average	25	16.2	54.9	270	79.2
	Std Dev	1	0.4	0.5	9	2.6
	Maximum	26	16.9	55.7	286	83.9
	Minimum	24	15.2	53.6	245	71.8

N-value: 37

Sample Interval Time: 43.66 seconds.

CME550X(SN249333)
TDS/AB

18.0 -19. 5FT_1
Test date: 3/10/2017

AR: 1.18 in^2
LE: 25.00 ft
WS: 16807.9 ft/s

SP: 0.492 k/ft3
EM: 30000 ksi

Depth: (20.00 - 21.50 ft], displaying BN: 100

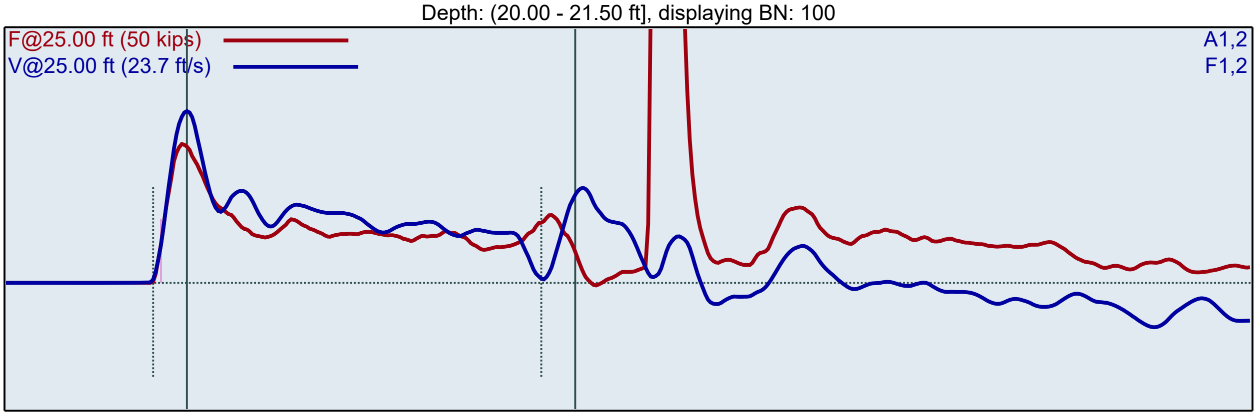

BL#	BC /6"	FMX kips	VMX ft/s	BPM bpm	EFV ft-lb	ETR (%)
42	12	27	18.3	1.9	261	76.5
43	12	28	17.7	48.4	278	81.3
44	12	28	17.5	55.4	295	86.5
45	12	27	16.4	56.3	275	80.6
46	12	27	15.8	54.2	280	81.8
47	12	28	15.9	56.0	285	83.4
48	12	27	15.7	53.5	277	81.1
49	12	28	16.1	55.3	285	83.5
50	12	27	15.6	54.4	272	79.5
51	12	27	16.0	55.6	288	84.4
52	12	27	15.9	56.2	280	81.9
53	12	27	15.7	54.0	276	80.7
54	18	25	15.0	54.2	251	73.6
55	18	28	15.9	57.1	284	83.0
56	18	27	15.7	53.9	274	80.4
57	18	25	15.0	54.8	260	76.0
58	18	27	15.8	55.4	279	81.6
59	18	26	15.3	54.7	258	75.5
60	18	27	15.8	55.7	280	81.9
61	18	25	14.9	54.4	262	76.8
62	18	27	15.7	55.6	274	80.1
63	18	26	15.7	54.3	272	79.7
64	18	27	16.0	55.3	286	83.8
65	18	27	15.8	54.7	281	82.2
66	18	27	16.0	55.7	288	84.5
67	18	27	15.7	55.1	276	80.9
68	18	27	16.1	54.4	291	85.4
69	18	27	15.7	55.0	280	82.0
70	18	26	15.8	54.7	278	81.3
71	18	27	15.9	55.6	283	83.0
72	31	27	15.8	54.3	282	82.5
73	31	26	15.8	55.2	284	83.1
74	31	26	15.6	54.8	276	80.9
75	31	27	15.8	55.4	276	80.8
76	31	26	15.7	54.6	281	82.4
77	31	26	15.7	54.9	267	78.3

78	31	27	16.0	56.2	285	83.4
79	31	25	15.1	53.9	253	74.0
80	31	26	15.5	55.3	268	78.5
81	31	26	15.8	55.5	268	78.6
82	31	27	16.0	54.6	282	82.7
83	31	25	15.2	54.9	254	74.5
84	31	27	16.3	54.8	278	81.3
85	31	27	15.9	54.8	281	82.3
86	31	26	15.7	55.5	265	77.6
87	31	27	16.4	54.9	281	82.2
88	31	27	16.0	54.7	279	81.6
89	31	27	15.7	54.9	282	82.5
90	31	26	15.4	56.0	269	78.8
91	31	27	16.1	55.0	281	82.2
92	31	27	15.9	54.5	276	80.7
93	31	26	15.5	55.0	254	74.3
94	31	26	15.6	56.0	265	77.7
95	31	26	15.9	54.2	266	77.9
96	31	27	16.0	55.7	280	81.9
97	31	26	15.7	55.1	267	78.1
98	31	27	16.3	55.1	278	81.4
99	31	27	15.8	55.3	274	80.4
100	31	139	15.9	55.5	365	106.7
101	31	139	16.0	27.5	361	105.8
102	31	27	16.3	18.4	283	82.8
	Average	31	15.8	53.7	278	81.4
	Std Dev	22	0.3	6.4	20	5.9
	Maximum	139	16.4	57.1	365	106.7
	Minimum	25	14.9	18.4	251	73.6

N-value: 49

Sample Interval Time: 68.70 seconds.

CME550X(SN249333) 18.0 -19. 5FT_1
TDS/AB Test date: 3/10/2017

AR: 1.18 in^2 SP: 0.492 k/ft3
LE: 28.00 ft EM: 30000 ksi
WS: 16807.9 ft/s

Depth: (23.50 - 25.00 ft], displaying BN: 128

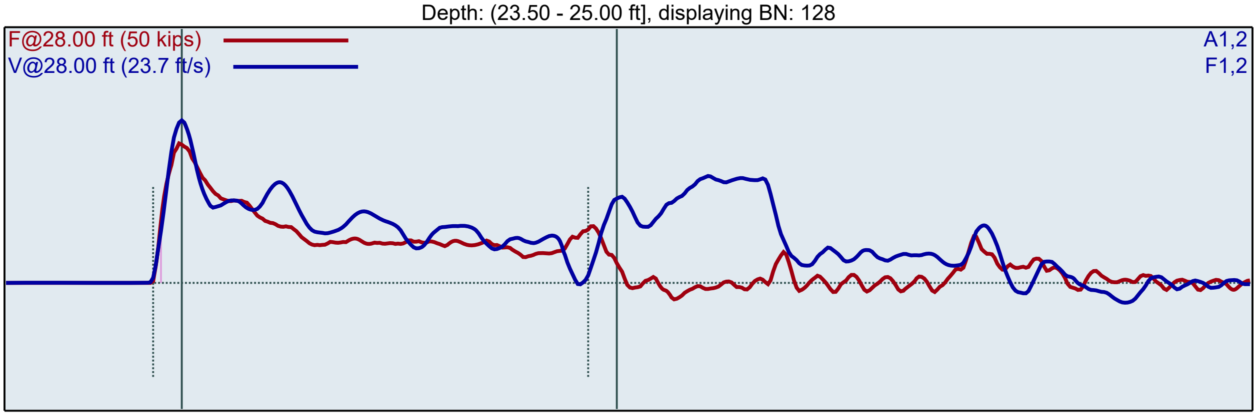

BL#	BC /6"	FMX kips	VMX ft/s	BPM bpm	EFV ft-lb	ETR (%)
103	3	26	18.7	1.9	248	72.7
104	3	28	19.0	48.3	260	76.2
105	3	27	18.7	55.4	282	82.7
106	10	27	18.0	54.6	266	77.9
107	10	27	17.1	54.7	263	77.0
108	10	27	16.9	54.5	270	79.0
109	10	27	16.7	55.7	271	79.4
110	10	27	15.0	54.1	264	77.4
111	10	27	15.0	55.5	275	80.5
112	10	27	14.9	54.7	265	77.6
113	10	27	15.2	55.6	270	79.2
114	10	27	14.9	55.5	275	80.7
115	10	26	14.6	55.7	258	75.6
116	15	26	14.2	53.8	269	78.6
117	15	27	14.5	55.5	276	80.8
118	15	27	14.3	54.9	267	78.2
119	15	28	14.9	54.8	280	82.1
120	15	27	14.5	54.7	272	79.6
121	15	27	14.5	54.8	276	80.9
122	15	27	14.4	54.9	269	78.8
123	15	27	14.9	55.8	275	80.4
124	15	27	14.6	54.4	267	78.2
125	15	27	15.0	55.1	277	81.0
126	15	27	14.9	55.6	269	78.9
127	15	27	15.0	54.5	273	79.9
128	15	27	15.1	54.6	271	79.3
129	15	26	14.6	55.5	262	76.6
130	15	26	14.6	53.9	258	75.7
	Average	27	15.1	54.9	270	78.9
	Std Dev	0	1.0	0.6	6	1.7
	Maximum	28	18.0	55.8	280	82.1
	Minimum	26	14.2	53.8	258	75.6

N-value: 25

Sample Interval Time: 29.58 seconds.

CME550X(SN249333)
TDS/AB

18.0 -19. 5FT_1
Test date: 3/10/2017

AR: 1.18 in^2
LE: 32.00 ft
WS: 16807.9 ft/s

SP: 0.492 k/ft3
EM: 30000 ksi

Depth: (28.50 - 30.00 ft], displaying BN: 177

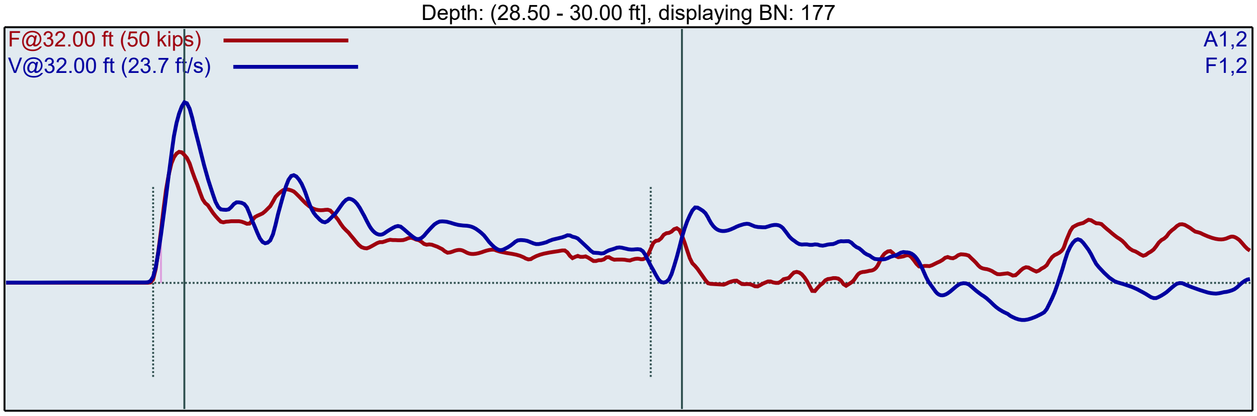

BL#	BC /6"	FMX kips	VMX ft/s	BPM bpm	EFV ft-lb	ETR (%)
131	4	25	16.7	49.1	271	79.5
132	4	26	16.2	56.0	285	83.4
133	4	25	15.7	54.8	269	78.8
134	4	26	16.2	54.7	296	86.6
135	15	25	15.9	54.9	269	78.9
136	15	26	16.2	55.5	279	81.8
137	15	25	16.0	56.2	267	78.3
138	15	26	16.0	54.3	280	81.9
139	15	24	15.7	55.7	262	76.7
140	15	25	16.1	54.8	271	79.3
141	15	26	16.3	55.5	279	81.8
142	15	25	16.3	54.9	278	81.5
143	15	25	15.7	54.9	265	77.5
144	15	25	16.2	55.5	280	82.0
145	15	25	15.9	55.7	273	80.0
146	15	26	16.5	54.2	287	84.0
147	15	25	16.2	55.2	274	80.1
148	15	25	16.1	55.4	274	80.3
149	15	24	15.5	53.7	256	75.1
150	30	26	16.4	54.8	275	80.5
151	30	25	16.4	55.6	285	83.3
152	30	24	15.9	55.2	264	77.2
153	30	26	16.4	54.4	288	84.4
154	30	26	16.4	55.3	277	81.2
155	30	26	16.2	54.7	271	79.3
156	30	26	16.2	54.7	272	79.7
157	30	25	16.5	55.0	274	80.3
158	30	26	16.7	54.8	291	85.3
159	30	25	16.4	55.1	276	80.7
160	30	25	16.4	54.4	279	81.8
161	30	26	16.4	55.2	278	81.3
162	30	25	16.2	55.6	276	80.7
163	30	26	16.8	54.8	292	85.5
164	30	25	16.6	55.2	287	83.9
165	30	26	16.6	55.0	275	80.4
166	30	25	16.5	54.9	275	80.5

167	30	25	16.6	54.8	276	80.8
168	30	25	16.5	55.3	287	84.1
169	30	25	16.9	55.3	278	81.4
170	30	25	16.7	55.3	284	83.2
171	30	25	17.0	54.6	283	83.0
172	30	26	16.4	54.4	285	83.4
173	30	26	16.8	55.3	280	82.0
174	30	24	16.6	55.0	274	80.2
175	30	25	16.9	55.6	285	83.3
176	30	24	16.8	55.0	279	81.7
177	30	26	16.8	54.1	290	84.9
178	30	25	17.1	56.4	283	83.0
179	30	24	15.8	54.2	263	77.0
	Average	25	16.4	55.0	277	81.2
	Std Dev	1	0.4	0.5	8	2.3
	Maximum	26	17.1	56.4	292	85.5
	Minimum	24	15.5	53.7	256	75.1

N-value: 45

Sample Interval Time: 52.24 seconds.

Summary of SPT Test Results

Project: CME550X(SN249333), Test Date: 3/10/2017

FMX: Maximum Force
VMX: Maximum Velocity
BPM: Blows/Minute

EFV: Maximum Energy
ETR: Energy Transfer Ratio - Rated

Instr. Length ft	Blows Applied /6"	**N Value**	**N60 Value**	Average FMX kips	Average VMX ft/s	Average BPM bpm	Average EFV ft-lb	Average ETR (%)
23.00	**4-14-23**	**37**	**49**	25	16.2	54.9	270	79.2
25.00	**12-18-31**	**49**	**65**	31	15.8	53.7	278	81.4
28.00	**3-10-15**	**25**	**33**	27	15.1	54.9	270	78.9
32.00	**4-15-30**	**45**	**60**	25	16.4	55.0	277	81.2
			Overall Average Values:	27	15.9	54.6	275	80.4
			Standard Deviation:	13	0.7	3.7	14	4.0
			Overall Maximum Value:	139	18.0	57.1	365	106.7
			Overall Minimum Value:	24	14.2	18.4	245	71.8

Summary of SPT Test Results

Project: CME55 (SN 250835), Test Date: 9/19/2016

FMX: Maximum Force
VMX: Maximum Velocity
BPM: Blows/Minute
EFV: Maximum Energy
ETR: Energy Transfer Ratio - Rated

Instr. Length ft	Blows Applied /6"	**N Value**	**N60 Value**	Average FMX kips	Average VMX ft/s	Average BPM bpm	Average EFV ft-lb	Average ETR (%)
38.86	**6-17-20**	**37**	**60**	29	16.6	59.5	328	96.2
43.86	**3-11-26**	**37**	**60**	29	17.3	59.5	339	99.3
48.86	**2-6-9**	**15**	**24**	29	16.5	59.4	332	97.1
58.86	**5-7-10**	**17**	**27**	28	16.1	56.0	334	97.9
63.86	**2-6-8**	**14**	**22**	28	16.5	59.5	328	96.1
			Overall Average Values:	29	16.7	59.0	333	97.5
			Standard Deviation:	1	0.7	5.3	8	2.4
			Overall Maximum Value:	31	18.2	59.9	352	103.0
			Overall Minimum Value:	27	15.0	1.9	313	91.5

CME55 (SN 250835) 35-36.5 FT
TDS/AB Test date: 9/19/2016

AR: 1.18 in^2 SP: 0.492 k/ft3
LE: 38.86 ft EM: 30000 ksi
WS: 16807.9 ft/s

Depth: (35.00 - 36.50 ft], displaying BN: 41

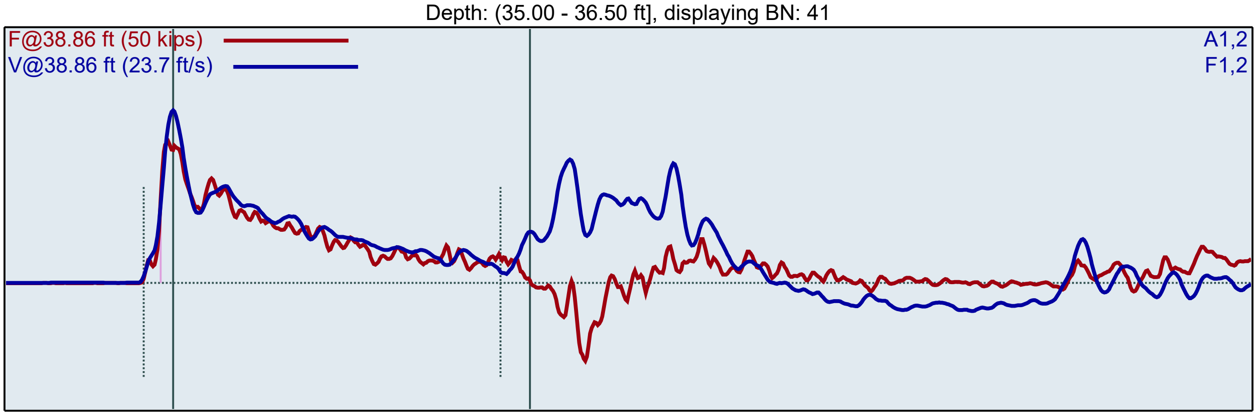

FMX: Maximum Force
VMX: Maximum Velocity
BPM: Blows/Minute
EFV: Maximum Energy
ETR: Energy Transfer Ratio - Rated

BL#	BC	FMX	VMX	BPM	EFV	ETR
	/6"	kips	ft/s	bpm	ft-lb	(%)
1	6	30	17.3	1.9	309	90.6
2	6	30	17.2	59.5	325	95.1
3	6	29	17.1	59.5	335	98.2
4	6	29	17.3	59.7	330	96.7
5	6	30	17.7	59.6	339	99.2
6	6	30	18.0	59.9	346	101.4
7	17	31	17.9	59.4	346	101.3
8	17	30	17.8	59.6	341	99.9
9	17	29	17.4	59.9	337	98.8
10	17	30	17.6	59.6	340	99.4
11	17	30	17.3	59.8	319	93.5
12	17	30	17.5	59.5	323	94.7
13	17	30	16.9	59.4	330	96.5
14	17	31	17.3	59.7	323	94.5
15	17	28	16.0	59.8	322	94.3
16	17	30	16.7	59.6	330	96.6
17	17	30	16.7	59.6	315	92.3
18	17	30	16.8	59.5	333	97.4
19	17	28	16.3	59.4	331	96.9
20	17	29	16.3	59.4	331	96.9
21	17	27	15.9	59.3	327	95.8
22	17	29	16.6	59.7	333	97.4
23	17	28	16.2	59.4	314	91.8
24	20	28	15.9	59.3	327	95.8
25	20	29	16.7	59.3	316	92.5
26	20	30	16.6	59.6	334	97.8
27	20	27	15.8	59.5	313	91.5
28	20	29	16.2	59.3	333	97.6
29	20	31	16.8	59.3	340	99.5
30	20	28	16.2	59.4	332	97.2
31	20	31	17.0	59.5	340	99.4
32	20	29	16.8	59.1	320	93.7
33	20	27	15.9	59.5	322	94.3

34	20	29	16.6	59.6	332	97.1
35	20	29	16.0	59.2	332	97.2
36	20	29	16.3	59.3	320	93.6
37	20	28	16.0	59.5	330	96.6
38	20	29	16.2	59.3	333	97.6
39	20	27	16.1	59.4	327	95.8
40	20	30	16.7	59.4	333	97.4
41	20	28	16.0	59.6	327	95.7
42	20	29	16.0	59.1	328	96.2
43	20	28	15.7	59.4	320	93.8
	Average	29	16.6	59.5	328	96.2
	Std Dev	1	0.6	0.2	8	2.3
	Maximum	31	17.9	59.9	346	101.3
	Minimum	27	15.7	59.1	313	91.5

N-value: 37

Sample Interval Time: 42.29 seconds.

CME55 (SN 250835)
TDS/AB

35-36.5 FT
Test date: 9/19/2016

AR: 1.18 in^2
LE: 43.86 ft
WS: 16807.9 ft/s

SP: 0.492 k/ft3
EM: 30000 ksi

Depth: (40.00 - 41.50 ft], displaying BN: 81

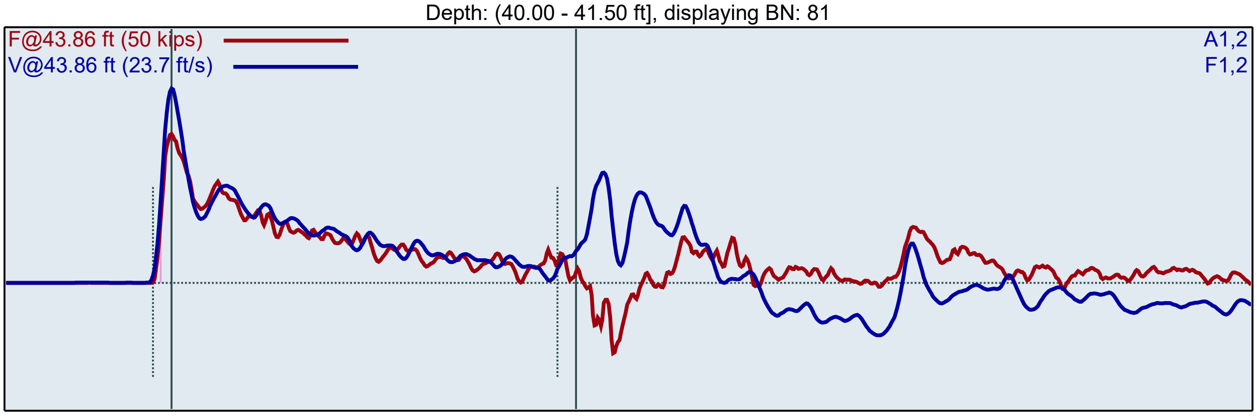

BL#	BC /6"	FMX kips	VMX ft/s	BPM bpm	EFV ft-lb	ETR (%)
44	3	31	16.9	59.9	323	94.6
45	3	28	16.2	59.3	330	96.7
46	3	28	15.3	59.3	336	98.3
47	11	28	16.4	58.9	327	95.9
48	11	28	16.5	59.5	324	95.0
49	11	27	15.6	59.1	330	96.7
50	11	29	16.7	59.4	340	99.6
51	11	29	17.3	59.3	346	101.3
52	11	29	17.5	59.6	352	103.0
53	11	29	17.5	59.6	349	102.3
54	11	30	17.2	59.4	345	101.0
55	11	29	17.1	59.6	345	100.9
56	11	30	16.9	59.3	341	99.8
57	11	29	17.0	59.5	348	102.0
58	26	30	16.3	59.3	336	98.5
59	26	29	16.6	59.5	336	98.5
60	26	29	17.0	59.5	328	95.9
61	26	29	16.2	59.6	321	94.1
62	26	29	16.8	59.5	337	98.8
63	26	29	16.9	59.6	341	99.8
64	26	29	17.1	59.5	339	99.3
65	26	29	17.1	59.6	338	99.0
66	26	28	17.5	59.4	330	96.5
67	26	28	17.8	59.5	336	98.4
68	26	28	16.7	59.6	331	97.1
69	26	28	18.1	59.5	342	100.3
70	26	28	18.1	59.3	341	100.0
71	26	28	17.4	59.5	332	97.3
72	26	28	17.9	59.4	343	100.4
73	26	29	17.8	59.7	342	100.2
74	26	29	17.9	59.6	342	100.1
75	26	28	18.1	59.6	346	101.2
76	26	28	17.9	59.7	341	100.0
77	26	29	18.0	59.4	344	100.8
78	26	29	17.6	59.5	342	100.1
79	26	29	17.6	59.7	340	99.5

80	26	29	17.8	59.4	340	99.4
81	26	29	18.0	59.1	345	101.0
82	26	29	18.1	59.5	344	100.7
83	26	29	18.2	59.4	343	100.3
	Average	29	17.3	59.5	339	99.3
	Std Dev	1	0.6	0.2	7	2.0
	Maximum	30	18.2	59.7	352	103.0
	Minimum	27	15.6	58.9	321	94.1

N-value: 37

BN: 83 3-11-26

Sample Interval Time: 39.31 seconds.

CME55 (SN 250835)
TDS/AB

35-36.5 FT
Test date: 9/19/2016

AR: 1.18 in^2
LE: 48.86 ft
WS: 16807.9 ft/s

SP: 0.492 k/ft3
EM: 30000 ksi

Depth: (45.00 - 46.50 ft], displaying BN: 98

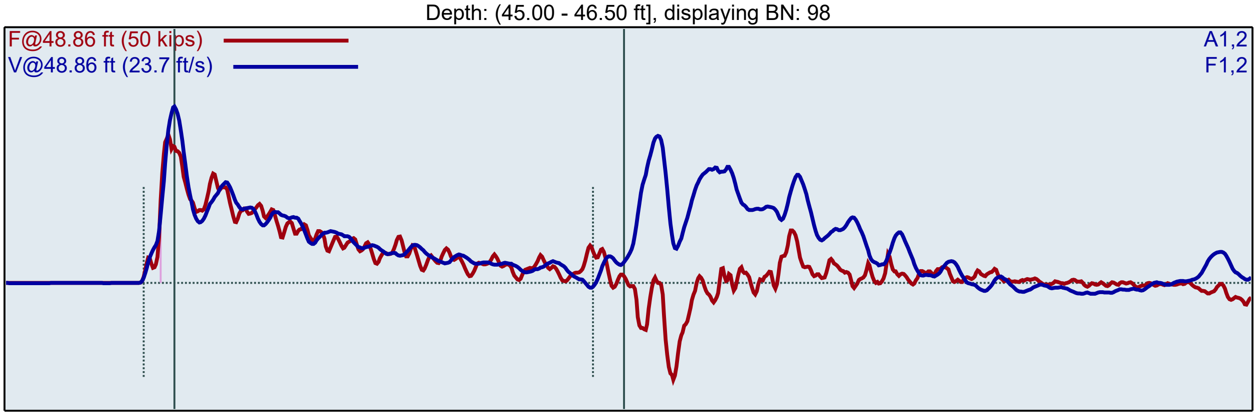

BL#	BC	FMX	VMX	BPM	EFV	ETR
	/6"	kips	ft/s	bpm	ft-lb	(%)
84	2	32	17.5	59.2	333	97.6
85	2	30	16.5	59.7	341	99.8
86	6	31	17.7	59.3	336	98.3
87	6	30	17.2	59.2	335	98.1
88	6	28	17.1	59.6	329	96.4
89	6	27	16.5	59.4	328	96.2
90	6	27	15.7	59.5	320	93.6
91	6	30	16.5	59.6	327	95.7
92	9	29	16.7	59.4	332	97.1
93	9	27	16.1	59.3	325	95.3
94	9	29	16.5	59.6	333	97.5
95	9	29	16.2	59.3	328	96.0
96	9	28	16.4	59.5	337	98.6
97	9	28	15.8	59.6	336	98.3
98	9	29	16.4	59.4	335	98.2
99	9	29	16.4	59.4	340	99.4
100	9	29	16.3	59.4	334	97.7
	Average	29	16.5	59.4	332	97.1
	Std Dev	1	0.5	0.1	5	1.5
	Maximum	31	17.7	59.6	340	99.4
	Minimum	27	15.7	59.2	320	93.6

N-value: 15

BN: 100 2-6-9

Sample Interval Time: 16.12 seconds.

CME55 (SN 250835)
TDS/AB

35-36.5 FT
Test date: 9/19/2016

AR: 1.18 in^2
LE: 58.86 ft
WS: 16807.9 ft/s

SP: 0.492 k/ft3
EM: 30000 ksi

Depth: (55.00 - 56.50 ft], displaying BN: 120

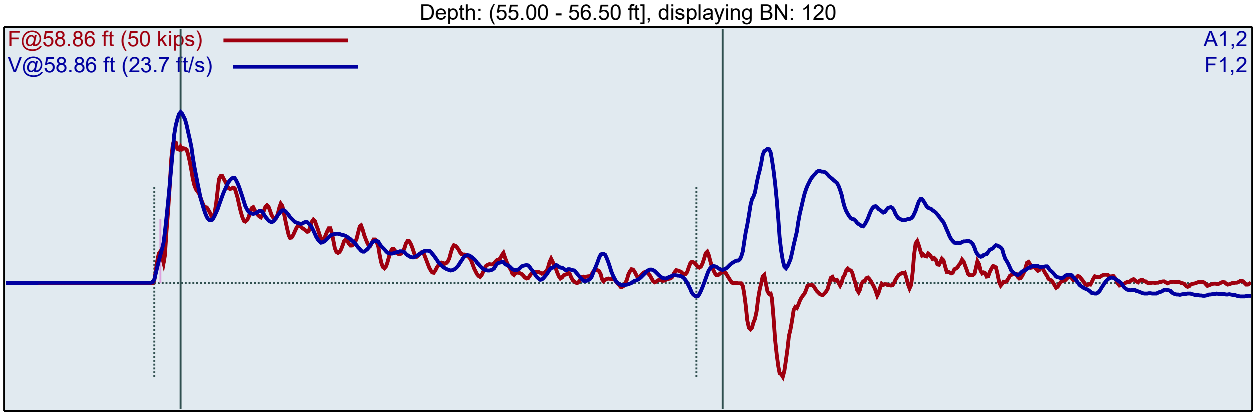

BL#	BC	FMX	VMX	BPM	EFV	ETR
	/6"	kips	ft/s	bpm	ft-lb	(%)
101	5	28	17.1	59.4	335	98.2
102	5	29	17.4	59.5	331	96.8
103	5	28	15.7	59.7	325	95.2
104	5	28	16.3	59.6	327	95.9
105	5	27	16.4	59.6	337	98.5
106	7	29	16.8	59.6	331	96.8
107	7	28	16.3	59.3	328	96.0
108	7	28	16.0	59.7	325	95.1
109	7	27	15.9	59.6	328	95.9
110	7	27	15.8	59.5	326	95.5
111	7	29	16.3	1.9	342	100.1
112	7	28	17.0	59.9	331	97.0
113	10	27	15.6	59.3	341	99.8
114	10	27	15.5	59.2	332	97.2
115	10	28	16.0	59.3	334	97.9
116	10	28	16.1	59.2	343	100.4
117	10	28	16.7	59.5	343	100.3
118	10	28	15.2	59.3	332	97.3
119	10	27	15.0	59.3	339	99.1
120	10	28	15.8	59.5	335	98.1
121	10	28	16.1	59.2	348	101.8
122	10	28	16.8	59.4	329	96.2
	Average	28	16.1	56.0	334	97.9
	Std Dev	1	0.5	13.5	7	1.9
	Maximum	29	17.0	59.9	348	101.8
	Minimum	27	15.0	1.9	325	95.1

N-value: 17

BN: 122 5-7-10

Sample Interval Time: 81.73 seconds.

CME55 (SN 250835)
TDS/AB
35-36.5 FT
Test date: 9/19/2016

AR: 1.18 in^2
LE: 63.86 ft
WS: 16807.9 ft/s
SP: 0.492 k/ft3
EM: 30000 ksi

Depth: (60.00 - 61.50 ft], displaying BN: 136

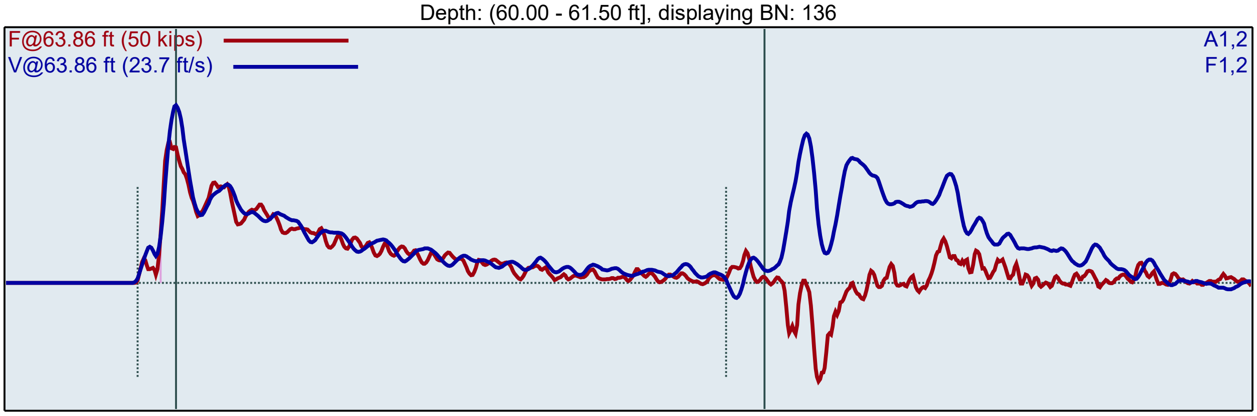

BL#	BC	FMX	VMX	BPM	EFV	ETR
	/6"	kips	ft/s	bpm	ft-lb	(%)
124	2	28	17.8	59.4	340	99.5
125	2	30	17.8	59.6	345	100.9
126	6	29	16.7	59.8	336	98.5
127	6	30	17.0	59.6	332	97.3
128	6	29	17.0	59.6	325	95.1
129	6	27	16.7	59.6	327	95.9
130	6	28	16.7	59.5	331	96.9
131	6	27	16.5	59.7	329	96.4
132	8	27	15.5	59.5	324	94.9
133	8	29	16.6	59.3	332	97.3
134	8	28	16.2	59.6	322	94.2
135	8	29	16.3	59.3	326	95.4
136	8	28	16.5	59.5	327	95.8
137	8	28	16.4	59.2	326	95.5
138	8	27	16.4	59.6	328	96.0
	Average	28	16.5	59.5	328	96.1
	Std Dev	1	0.4	0.2	4	1.1
	Maximum	30	17.0	59.8	336	98.5
	Minimum	27	15.5	59.2	322	94.2

N-value: 13

BN: 138 .2-6-8

Sample Interval Time: 14.09 seconds.

Summary of SPT Test Results

Project: CME55 (SN 250835), Test Date: 9/19/2016

FMX: Maximum Force
VMX: Maximum Velocity
BPM: Blows/Minute
EFV: Maximum Energy
ETR: Energy Transfer Ratio - Rated

Instr. Length ft	Blows Applied /6"	**N Value**	**N60 Value**	Average FMX kips	Average VMX ft/s	Average BPM bpm	Average EFV ft-lb	Average ETR (%)
38.86	**6-17-20**	**37**	**60**	29	16.6	59.5	328	96.2
43.86	**3-11-26**	**37**	**60**	29	17.3	59.5	339	99.3
48.86	**2-6-9**	**15**	**24**	29	16.5	59.4	332	97.1
58.86	**5-7-10**	**17**	**27**	28	16.1	56.0	334	97.9
63.86	**2-6-8**	**14**	**22**	28	16.5	59.5	328	96.1
			Overall Average Values:	29	16.7	59.0	333	97.5
			Standard Deviation:	1	0.7	5.3	8	2.4
			Overall Maximum Value:	31	18.2	59.9	352	103.0
			Overall Minimum Value:	27	15.0	1.9	313	91.5

APPENDIX T
Full Scale Load Test

DATA REPORT

REPORT ON DRILLED SHAFT LOAD TESTING (OSTERBERG METHOD)

TS-1 - IL-89 Over Illinois River
Bureau & Putnam Counties, IL (LT-1407)

Prepared for: Illini Drilled Foundations, Inc.
P.O. Box 1351
Danville, IL 61834

Attention: Mr. Chris Shewmaker

PROJECT NO: LT-1407, November 18, 2014

Americas
LOADTEST USA
2631-D NW 41st St
Gainesville, FL 32606, USA
Phone: +1 352 378 3717
Fax: +1 352 378 3934

Middle East
Fugro LOADTEST Middle East
P.O. Box 2863, Dubai, UAE.
Phone: +971 4 3474060
Fax: +971 4 3474069

Europe & Africa
Fugro LOADTEST
14 Scotts Avenue, Sunbury Upon Thames
Middlesex, TW16 7HZ, UK
Phone: +44 (0) 1932 784807
Fax: +44 (0) 1932 784807

Asia
Fugro LOADTEST Singapore
159 Sin Ming Road, #05-07 Amtech Building
Singapore, 575625
Phone: +65 6377 5665
Fax: +65 6377 3359

LOADTEST

DEEP FOUNDATION TESTING, EQUIPMENT & SERVICES • SPECIALIZING IN OSTERBERG CELL (O-Cell®) TECHNOLOGY
LOADTEST USA is a division of Fugro Consultants Inc.
www.loadtest.com

Issue and Revision History

Issue History

ISSUE	ISSUED TO	ISSUED BY	DATE OF ISSUE
01	Mr. Chris Shewmaker, Illini Drilled Foundations, Inc.	William G. Ryan	November 18, 2014

Revision History

Date	Rev. No.	Detailed Description of Change	Ref. Section

November 18, 2014

Illini Drilled Foundations, Inc.
P.O. Box 1351
Danville, IL 61834

Attention: Mr. Chris Shewmaker

Load Test Report: TS-1 - IL-89 Over Illinois River
Location: Bureau & Putnam Counties, IL (LT-1407)

Dear Mr. Shewmaker,

The enclosed report contains the data and analysis summary for the Osterberg Cell (O-cell) test performed on TS-1 - IL-89 Over Illinois River, on November 12, 2014. For your convenience, we have included an executive summary of the test results in addition to our standard detailed data report. Preliminary results were issued on November 14, 2014.

We would like to express our gratitude for the on-site and off-site assistance provided by your team and we look forward to working with you on future projects.

We trust that the information contained herein will suit your current project needs. If you have any questions or require further technical assistance, please do not hesitate to contact us at 352-378-3717.

Best Regards,

William G. Ryan, B.S.C.M.
Regional Manager, Loadtest USA

EXECUTIVE SUMMARY

On November 12, 2014, Loadtest USA performed an O-cell test on the nominal 60-inch diameter test shaft TS-1. Illini Drilled Foundations, Inc. completed construction of the 71.5-foot deep shaft socketed in shale on November 05, 2014. Sub-surface conditions at the test shaft location consist primarily of silty loam and clay at the surface, underlain by layers of stiff silty clay with shale fragments and fine sand. Below these strata, hard gray shale with minor silt seams and gravel pieces was encountered. Representatives of Illinois Department of Transportation (IDOT), University of Illinois and others observed construction and testing of the shaft.

The maximum sustained bi-directional load applied to the shaft was 1,551 kips. At this maximum load (1L-8), the displacements above and below the O-cell assembly were 0.355 inches and 0.158 inches, respectively. However, the maximum displacements above and below the O-cell were 1.660 inches and 0.199 inches, respectively, which occurred at load increment 1L-9. Unit side shear data calculated from strain gages indicated a maximum mobilized net side shear of 10.7 ksf between the O-cell and Strain Gage Level 1, and an average unit side shear of 7.4 ksf in the rock socket. The maximum applied unit end bearing is calculated to be 67 ksf.

Using the procedures described in the report text and in Appendix C, an equivalent top load curve for the test shaft was constructed. For a top loading of 1,250 kips, the adjusted test data indicate this shaft would displace approximately 0.11 inches. For a top loading of 2,500 kips, the adjusted test data indicate this shaft would displace approximately 0.27 inches.

LIMITATIONS OF EXECUTIVE SUMMARY

We include this executive summary to provide a very brief presentation of some of the key elements of this O-cell test. It is by no means intended to be a comprehensive or stand-alone representation of the test results. The full text of the report and the attached appendices contain important information which the engineer can use to come to more informed conclusions about the data presented herein.

TABLE OF CONTENTS

TABLES AND FIGURES

SITE CONDITIONS AND SHAFT CONSTRUCTION

Site Sub-surface Conditions: The sub-surface stratigraphy at the general location of the test shaft is reported to consist of silty loam and clay at the surface, underlain by layers of stiff silty clay with shale fragments and fine sand. Below these strata, hard gray shale with minor silt seams and gravel pieces was encountered. The generalized subsurface profile is included in Figure A and a boring log indicating conditions near the shaft is presented in Appendix E. More detailed geologic information can be obtained from IDOT.

Test Shaft Construction: Illini Drilled Foundations, Inc. completed construction of the dedicated test shaft socketed in shale on November 05, 2014. The nominal 60-inch diameter test shaft was excavated to a base elevation of +376.4 ft, The shaft was started by pre-drilling and installing a 72-inch O.D. temporary outer casing. Drilling of the shaft continued through an open hole under bentonite slurry until the tip of shaft was several feet above the socket. A 66-inch O.D. inner casing was inserted and screwed into silty clays above the shale. After screwing in the inner casing, bentonite slurry was removed and drilling continued into the rock socket. Before reaching tip, the contractor pulled and removed the 72-inch O.D. temporary casing. An auger was used for drilling the shaft and a clean-out bucket for cleaning the base. After the shaft was approved for concrete placement, the reinforcing cage with attached O-cell assembly was lowered into the excavation and held with a crane for the duration of the pour. Concrete was then delivered by tremie into the base of the shaft until the top of the concrete reached an elevation of +447.2 ft. Representatives of Illinois Department of Transportation (IDOT), University of Illinois and others observed construction of the shaft.

OSTERBERG CELL TESTING

Shaft Instrumentation: Loadtest USA assisted Illini Drilled Foundations, Inc. with the assembly and installation of test shaft instrumentation. The loading assembly consisted of one 26-inch diameter O-cell located 2.0 feet above the shaft base. The Osterberg cell was calibrated to 2,906 kips and then welded closed prior to shipping by American Equipment and Fabricating Corporation. Calibrations of the O-cell and instrumentation used for this test are included in Appendix B. Embedded O-cell testing instrumentation included the following:

- Paired upper compression telltale casings (nominal ½-inch steel pipe) attached diametrically opposed to the reinforcing cage, extending from the top of the O-cell assembly to ground level.

- Four Linear Vibrating Wire Displacement Transducers (LVWDTs, Geokon Model 4450 series) positioned between the lower and upper plates of the O-cell assembly.

- Four levels of two sister bar vibrating wire strain gages (Geokon Model 4911 Series) attached diametrically opposed to the reinforcing cage above the top of the O-cell assembly.

- Two lengths of ½-inch steel pipe, extending from the top of the shaft to the top of the bottom plate, to vent the break in the shaft formed by the expansion of the O-cell.

Details concerning the instrumentation placement appear in Table B and Figures A and B.

Test Arrangement: Throughout the load test, key elements of shaft displacement response were monitored using the equipment and instruments detailed below:

- Top of shaft displacement was monitored using a pair of automated digital survey levels (Leica NA3000 series) from an average distance of 27.5 feet (Appendix A, Page 1).

- Upper compression displacement was measured using ¼-inch telltale rods positioned inside the two casings and monitored by Linear Vibrating Wire Displacement Transducers (LVWDTs, Geokon Model 4450 series) attached to the top of the shaft (Appendix A, Page 1).

- Expansion of the O-cell assembly was measured using the four Expansion LVWDTs described under Shaft Instrumentation (Appendix A, Page 2).

A Bourdon pressure gage, voltage pressure transducer and vibrating wire pressure transducer were used to measure the pressure applied to the O-cell at each load interval. The pressure transducer was used for manually setting and maintaining loads, real time plotting and for data analysis. The Bourdon pressure gage readings were used as a real-time visual reference and as a check on the transducer. There was close agreement between the Bourdon gage and the pressure transducer.

Data Acquisition: All instrumentation were connected through a data logger (Data Electronics 515 GeoLogger) to a laptop computer allowing data to be recorded and stored automatically at 30-second intervals and displayed in real time. The same laptop computer synchronized to the data logging system was used to acquire the Leica NA3000 data.

Testing Procedures: Loadtest USA conducted the load test. Testing was begun by pressurizing the O-cell in order to break the tack welds that hold it closed (for handling and for placement in the shaft) and to form the fracture plane in the concrete surrounding the base of the O-cell. After the break occurred, the pressure was immediately released and the testing recommenced from zero pressure. Zero readings for all instrumentation were taken prior to the preliminary weld-breaking load-unload cycle, which in this case involved a maximum load of 518 kips at the O-cell.

The Osterberg cell load test was conducted as follows: The 26-inch diameter O-cell, with its base located 2.0 feet above the shaft base, was pressurized in 8 nominally equal increments, resulting in a maximum sustained bi-directional load of 1,551 kips applied to the shaft above and below the O-cell. After increment 1L-8, additional loading was attempted during 1L-9, but was halted because the upper side shear was approaching ultimate capacity and sustained loading could not be maintained. The shaft was then unloaded in five decrements and the test was concluded.

The load increments were applied using the Quick Load Test Method for Individual Piles (ASTM D1143 *Standard Test Method for Piles Under Static Axial Load*). Each successive load increment was held constant for eight minutes by manually adjusting the O-cell pressure. The data logger automatically recorded the instrument readings every 30 seconds, but herein only the 1, 2, 4 and 8 minute readings during each increment of maintained load are reported.

TEST RESULTS AND ANALYSES

General: The loads applied by the O-cell assembly act in two opposing directions, counteracted by the resistance of the shaft above and below. For the purpose of the analysis herein, it is assumed that the O-cell assembly does not impose an additional upward load until its expansion force exceeds the buoyant weight of the shaft above the O-cell assembly. Therefore, *net load*, which is defined as gross O-cell load minus the buoyant weight of the shaft above, is used to determine side shear resistance above the O-cell and to construct the equivalent top load displacement curve. For this test a shaft buoyant weight of 166 kips above the O-cell was calculated.

For the purposes of analyses herein, the maximum sustained loading at 1L-8 of 1,551 kips was used. At this maximum load (1L-8), the displacements above and below the O-cell assembly were 0.355 inches and 0.158 inches, respectively. The maximum applied load of 1,713 kips occurred at the 4-minute reading of increment 1L-9. The maximum displacements above and below the O-cell were 1.660 inches and 0.199 inches, respectively, which occurred at load increment 1L-9.

Upper Side Shear Resistance: The O-cell assembly applied a maximum ustaiend upward *net load* of 1,385 kips to the upper side shear at load interval 1L-8 (Appendix A, Page 3, Figures 1 to 3). At this loading, the upward displacement of the top of the O-cell was 0.355 inches.

Combined End Bearing and Lower Side Shear Resistance: The O-cell assembly applied a maximum sustained downward load of 1,551 kips at load interval 1L-8 (Appendix A, Page 3, Figures 1 to 3). At this loading, the average downward displacement of the O-cell base was 0.158 inches.

Strain Gage Analysis: The strain gage data appear in Appendix A, Pages 4 and 5 and the average strain measured at each level of strain gages during the test is plotted in Figure 4. On the day of the test, the unconfined compressive strength f'_c was reported to be 5,125 psi. Assuming a concrete unit weight γ_c of 145 pcf, the ACI formula (E_c=0.033 × $\gamma_c^{1.5}$ × $\sqrt{f'_c}$) was used to calculate an elastic modulus of 4,125 ksi for the concrete. Shaft stiffness estimates for each strain gage level computed from this modulus plus reinforcing steel details and nominal shaft dimensions are listed in Table B. Concrete modulus combined with the area of reinforcing steel and nominal shaft diameter, provided an average shaft stiffness (AE) of 17,448,000 kips in the upper cased shaft section, 12,415,000 kips in the uncased shaft section above the O-cell and 11,663,000 kips below the O-cell. The load distribution curves for each load increment, based on applied O-cell load and computed strain gage loads are presented in Figure 5. Mobilized net unit side shear vs. displacement (t-z) curves based on the strain gage data and estimated ACI shaft stiffness are presented in Figure 6. Shear values for loading increment 1L-8 follow in Table A:

TABLE A: Average Net Unit Side Shear Values for 1L-8

Load Transfer Zone	Displacement[1]	Net Unit Side Shear[2]
Zero Shear to Strain Gage Level 4	↑ 0.35 in	0.0 ksf
Strain Gage Level 4 to Strain Gage Level 3	↑ 0.35 in	0.2 ksf
Strain Gage Level 3 to Strain Gage Level 2	↑ 0.35 in	0.1 ksf
Strain Gage Level 2 to Strain Gage Level 1	↑ 0.35 in	3.3 ksf
Strain Gage Level 1 to O-cell	↑ 0.35 in	10.7 ksf

1 Average displacement of load transfer zone.
2 For upward-loaded shear, the buoyant weight of shaft in each zone has been subtracted from the load shed in the respective zone. Note that net unit shear values derived from the strain gages may not be ultimate values. See Figure 6 for unit shear vs. displacement (t-z) plots.

It is assumed that the unit side shear of the shaft zone below the O-cell is same as the zone immediately above at the same displacement. The load resisted by side shear in the 2.0-foot shaft section below the O-cell is calculated to be 239 kips assuming an interpolated maximum mobilized unit side shear value of 7.6 ksf at 0.158 inches displacement and a nominal shaft diameter of 60.0 inches. Then the maximum applied load to end bearing is 1,312 kips and the unit end bearing at the base of the shaft is calculated to be 66.8 ksf at the above noted O-cell downward displacement. A mobilized unit end bearing vs. displacement (q-z) curve is presented in Figure 7.

Equivalent Top Load-Displacement: Figure 8 presents the equivalent top load (ETL) curve. The procedure for calculating the curve is described in Appendix C. The curve is generated assuming the load is applied at top of shaft (+447.2 ft). A combined side shear and end-bearing resistance of 2,939 kips was mobilized during the test. For a top loading of 1,250 kips, the adjusted test data indicate this shaft would displace approximately 0.11 inches. For a top loading of 2,500 kips, the adjusted test data indicate this shaft would displace approximately 0.27 inches. For reference, Figure 8 also includes the two component curves of O-cell displacements vs. net loads, which if summed would produce a "rigid" equivalent top load. The plotted ETL curve includes the additional elastic compression of a top-loaded shaft.

Creep Limit: See Appendix D for our O-cell method for determining creep limit loading. The combined end bearing and lower side shear creep data (Appendix A, Page 3, Figure D-1) indicate that no apparent creep limit was reached at a maximum downward displacement of 0.16 inches. The upper side shear creep data (Appendix A, Page 3, Figure D-2) indicate that a creep limit of 1,160 kips was reached at an upward displacement of 0.14 inches. A top loaded shaft will not begin creep until both components begin creep displacement. This will occur at the maximum of the displacements required to reach the creep limit for each component. Due to the absence of a clearly defined combined end bearing and lower side shear creep limit, a creep limit for the equivalent top-loaded shaft cannot be estimated.

Shaft Compression Comparison: The measured maximum shaft compression, averaged from two telltales, is 0.006 inches at 1L-8 (Appendix A, Page 3). Using a weighted average shaft stiffness of 16,566,900 kips and the load distribution in Figure 5 at 1L-8, an elastic compression of 0.006 inches over the length of the compression telltales is calculated. This excellent agreement provides good evidence that the values of the estimated shaft stiffness are reasonable.

LIMITATIONS AND STANDARD OF CARE

The instrumentation, testing services and data analysis provided by Loadtest USA, outlined in this report, were performed in accordance with the accepted standards of care recognized by professionals in the drilled shaft and foundation engineering industry.

Please note that some of the information contained in this report is based on data (i.e. shaft diameter, elevations and concrete strength) provided by others. The engineer, therefore, should come to his or her own conclusions with regard to the analyses as they depend on this information. In particular, Loadtest USA typically does not observe and record drilled shaft construction details to the level of precision that the project engineer may require. In many cases, we may not be present for the entire duration of shaft construction. Since construction technique can play a significant role in determining the load bearing capacity of a drilled shaft, the engineer should pay close attention to the drilled shaft construction details that were recorded elsewhere.

We trust that this information will meet your current project needs. If you have any questions, please do not hesitate to contact us at 352-378-3717.

Prepared for Loadtest USA by

Aditya Ayithi, Ph. D.

Reviewed for Loadtest USA by

Shing K. Pang, P.E.

Brian D. Haney, P.E.

TABLE B
SUMMARY OF DIMENSIONS, ELEVATIONS & SHAFT PROPERTIES

Shaft: (TS-1 - IL-89 Over Illinois River - Bureau & Putnam Counties, IL)

Nominal shaft diameter (EL +447.2 ft to +394.2 ft)	=	66 in
Nominal shaft diameter (EL +394.2 ft to +376.4 ft)	=	60 in
O-cell: 26-9H-00075	=	26 in
Length of shaft zone above break at base of O-cell	=	68.8 ft
Length of shaft zone below break at base of O-cell	=	2.0 ft
Side shear area above O-cell base	=	1164.0 ft^2
Side shear area below O-cell base	=	31.4 ft^2
Shaft base area	=	19.6 ft^2
Buoyant weight of shaft above base of O-cell	=	163 kips
Estimated shaft stiffness, AE (EL +447.2 ft to +394.2 ft)	=	17,448,000 kips
Estimated shaft stiffness, AE (EL +394.2 ft to +378.4 ft)	=	12,415,000 kips
Estimated shaft stiffness, AE (EL +378.4 ft to +376.4 ft)	=	11,663,000 kips
Elevation of ground surface	=	+447.9 ft
Elevation of top of shaft concrete/ Design Cut-off Elevation	=	+447.2 ft
Elevation of water table	=	+437.9 ft
Elevation of base of O-cell assembly [1]	=	+378.4 ft
Elevation of shaft base	=	+376.4 ft
Casings:		
Elevation of top of outer temporary casing (72.0 in O.D., 71.0 in I.D.)	=	+446.9 ft
Elevation of bottom of outer temporary casing (72.0 in O.D., 71.0 in I.D.)	=	+436.7 ft
Elevation of top of inner permanent casing (66.0 in O.D., 65.0 in I.D.)	=	+449.9 ft
Elevation of bottom of inner permanent casing (66.0 in O.D., 65.0 in I.D.)	=	+394.2 ft
Telltale Sections:		
Elevation of top of telltale used for upper shaft compression	=	+447.9 ft
Elevation of bottom of telltale used for upper shaft compression	=	+379.8 ft
Strain Gages:		
Elevation of Strain Gage Level 4 (AE = 17,448,000 kips)	=	+414.6 ft
Elevation of Strain Gage Level 3 (AE = 17,448,000 kips)	=	+407.9 ft
Elevation of Strain Gage Level 2 (AE = 12,440,000 kips)	=	+390.6 ft
Elevation of Strain Gage Level 1 (AE = 12,440,000 kips)	=	+385.0 ft
Miscellaneous:		
Top plate diameter (2.0 inch thick)	=	52. in
Bottom plate diameter (2.0 inch thick)	=	52. in
Reinforcing cage vertical bar size (EL. +453.6 ft to +378.9, 20 No.)	=	# 11
Reinforcing cage spiral size (6 in spacing)	=	# 5
Rebar cage diameter	=	54 in
Assumed concrete unit weight	=	145 pcf
Reported 7-day unconfined compressive concrete strength	=	5,125 psi
Calculated 7-day concrete modulus	=	4,125 ksi
O-cell LVWDTs @ 0°, 90°, 180° and 270° with radius	=	20 in

[1] The break between upward and downward movement at the O-cell assembly

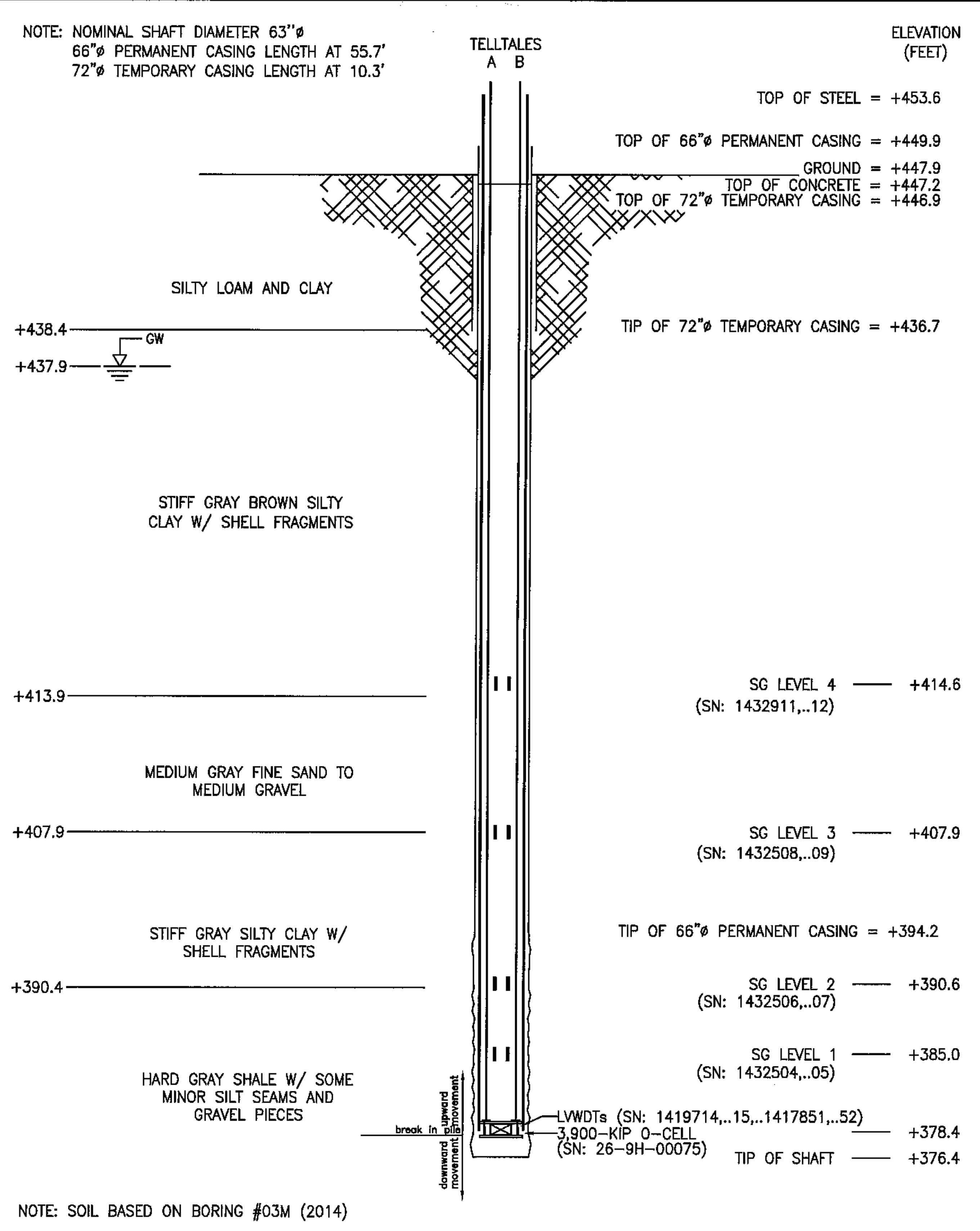

LOADTEST
www.LOADTEST.com

2631-D NW 41st St.
Gainesville, FL 32606
Phone: 800-368-1138
FAX: 352-378-3934

AS BUILT SECTION OF TEST SHAFT
ROUTE 89 OVER ILLINOIS RIVER – BUREAU & PUTNAM COUNTIES, IL

DWN BY: AJS	DATE: 12 Jun 2014	CHECKED BY: SP	LT-1407
REVISED BY: AA	DATE: 17 Nov 2014	SCALE: NTS	**FIGURE A**

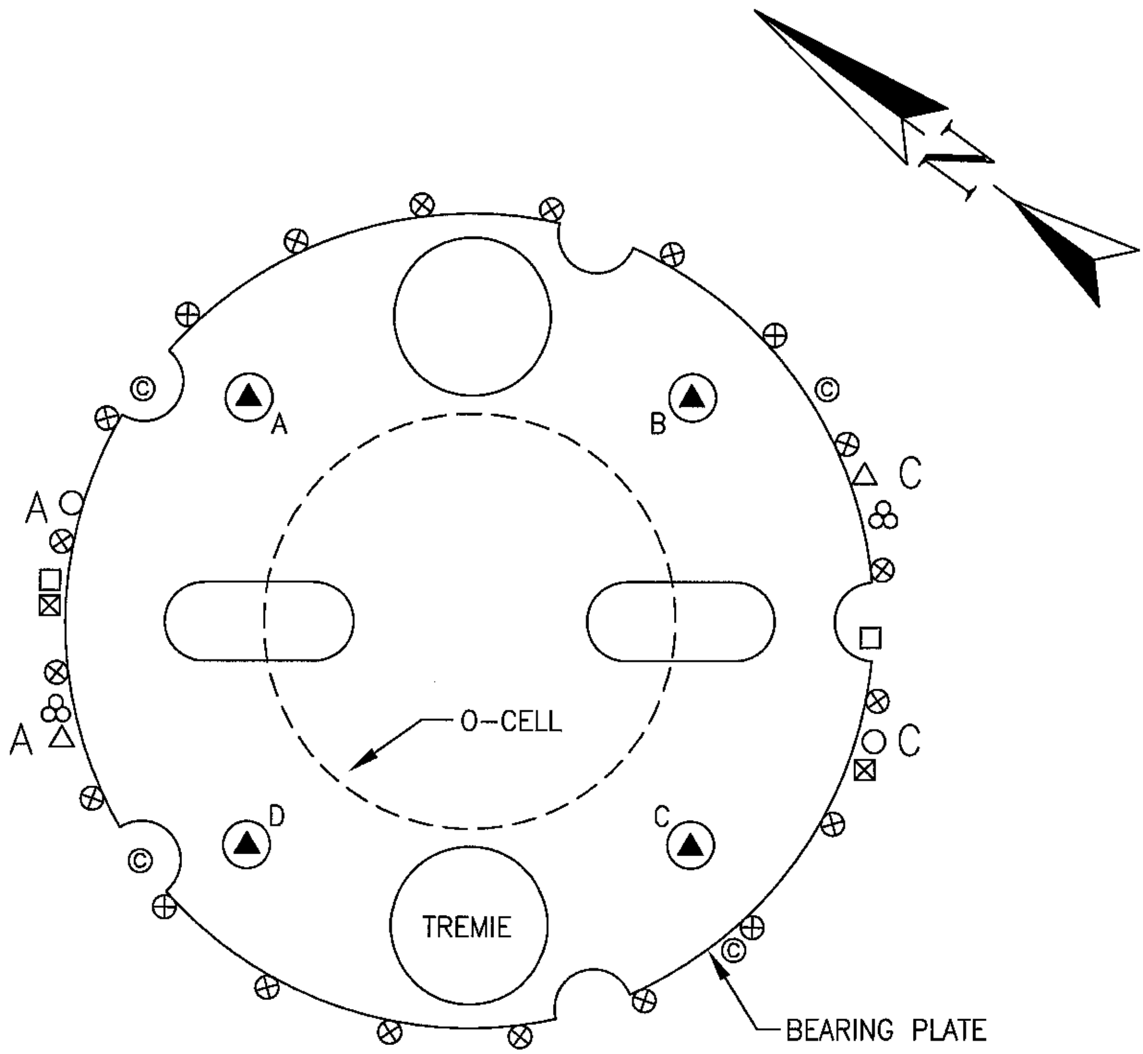

LEGEND:

STRAIN GAGE	△
LVWDT	▲
TELLTALE	○
VENT PIPE	□
HYDRAULIC HOSES	⊠
REBAR	⊗
CABLE BUNDLE	
CSL PIPE	©

LOADTEST
www.LOADTEST.com
2631-D NW 41st St.
Gainesville, FL 32606
Phone: 800-368-1138
FAX: 352-378-3934

INSTRUMENTATION LAYOUT
IL ROUTE 89 OVER ILLINOIS RIVER – BUREAU & PUTNAM COUNTIES, IL

DWN BY: AJS	DATE: 07 Nov 2014	CHECKED BY: WGR	LT-1407
REVISED BY: AJS	DATE: 13 Nov 2014	SCALE: NTS	**FIGURE B**

LOADTEST

Osterberg Cell Load-Displacement

TS-1 - IL-89 Over Illinois River - Bureau Putnam Counties, IL

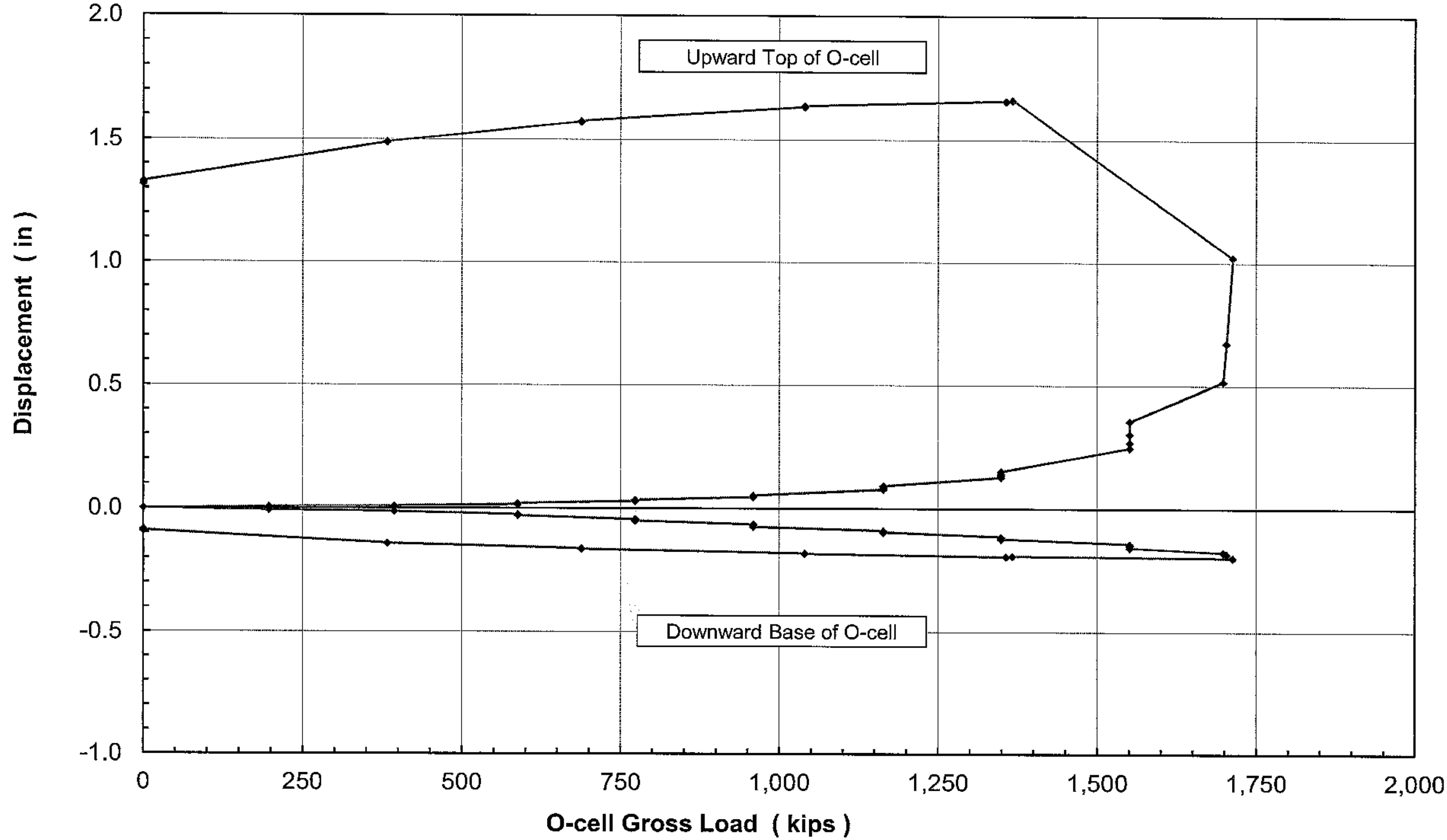

Loadtest USA Project No. LT-1407

Figure 1 of 8

Time-Osterberg Cell Load

TS-1 - IL-89 Over Illinois River - Bureau Putnam Counties, IL

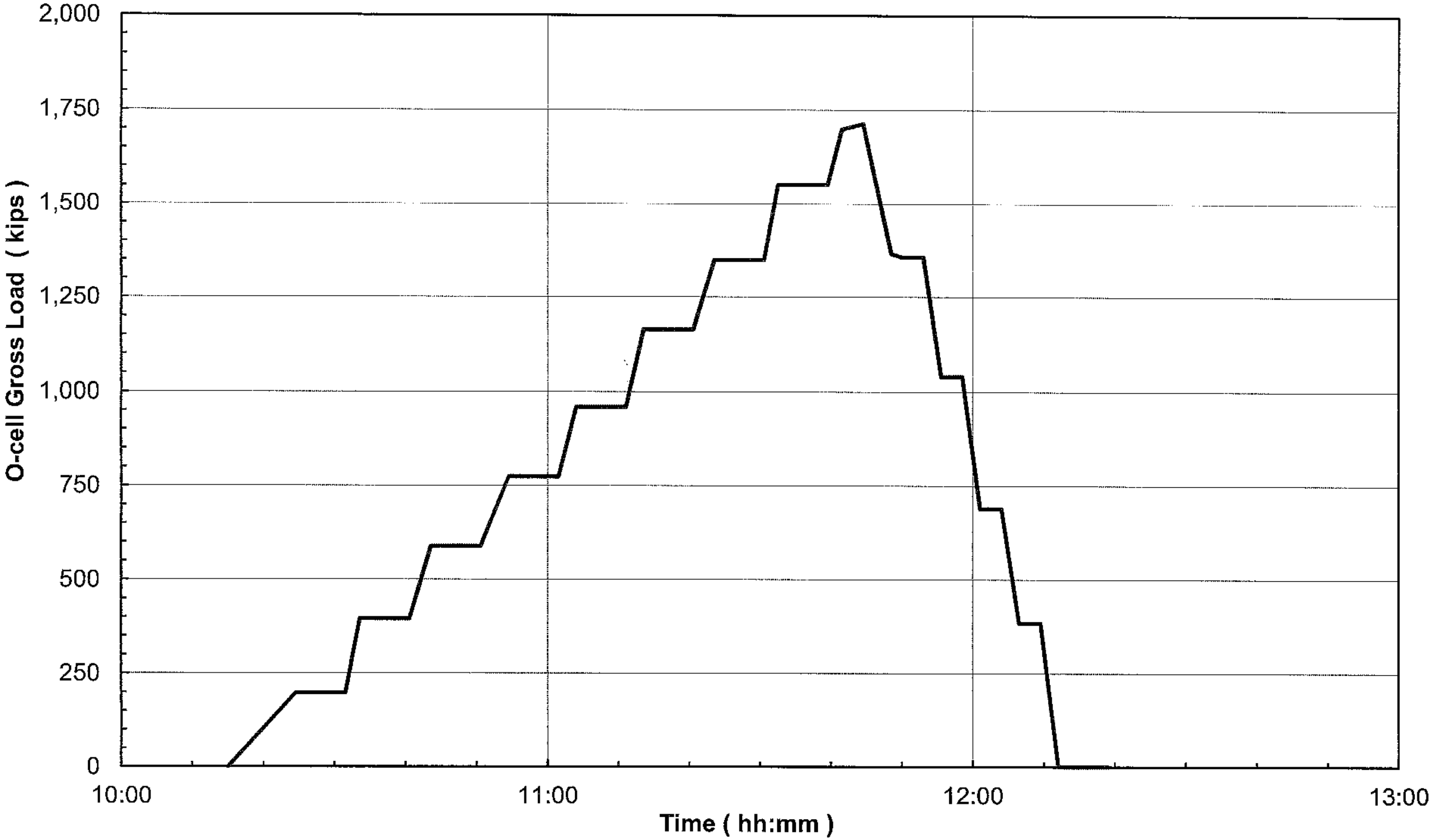

Time-Osterberg Cell Displacement

TS-1 - IL-89 Over Illinois River - Bureau Putnam Counties, IL

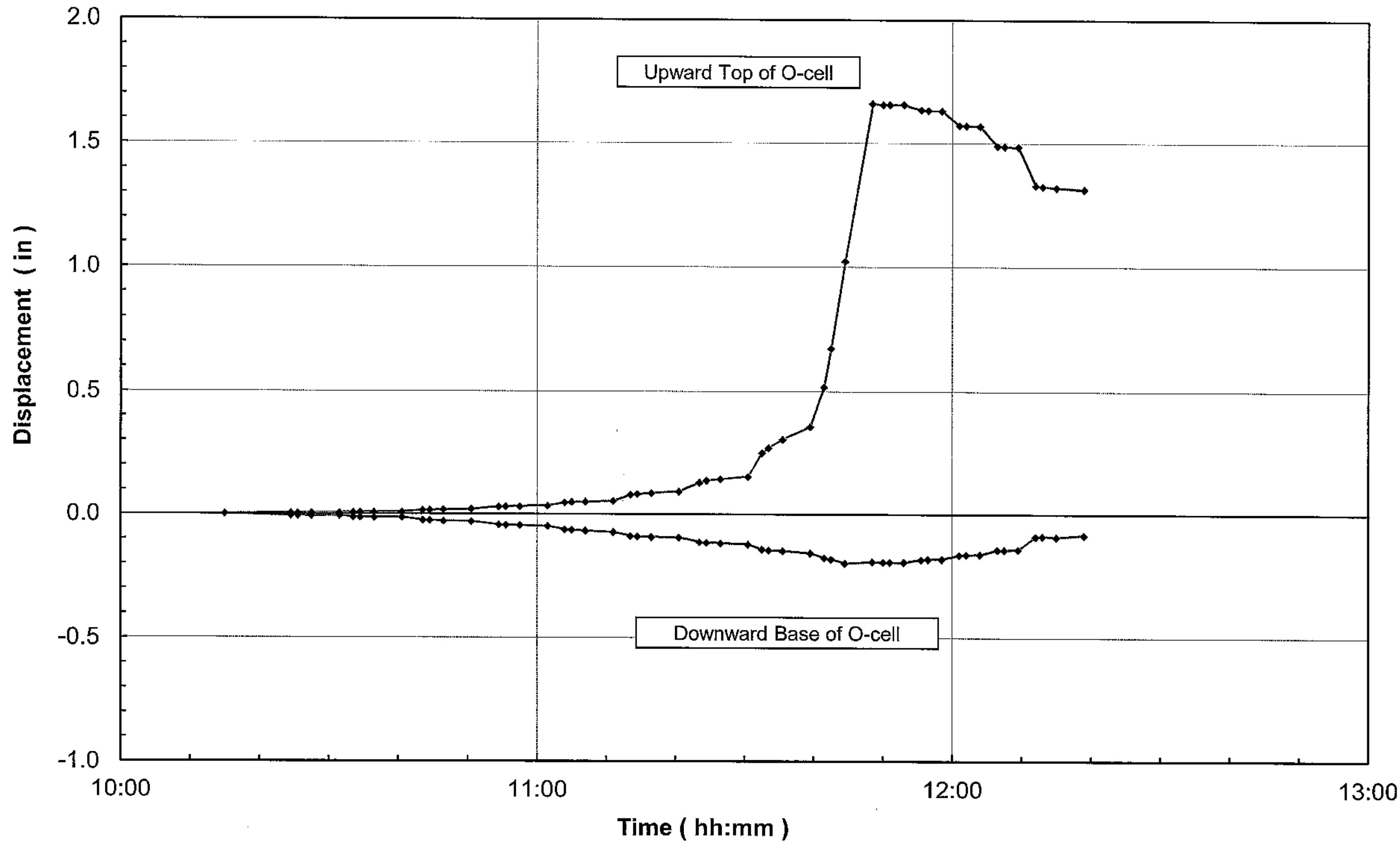

Loadtest USA Project No. LT-1407

Figure 3 of 8

LOADTEST

Osterberg Cell Load-Strain Gage Microstrain

TS-1 - IL-89 Over Illinois River - Bureau Putnam Counties, IL

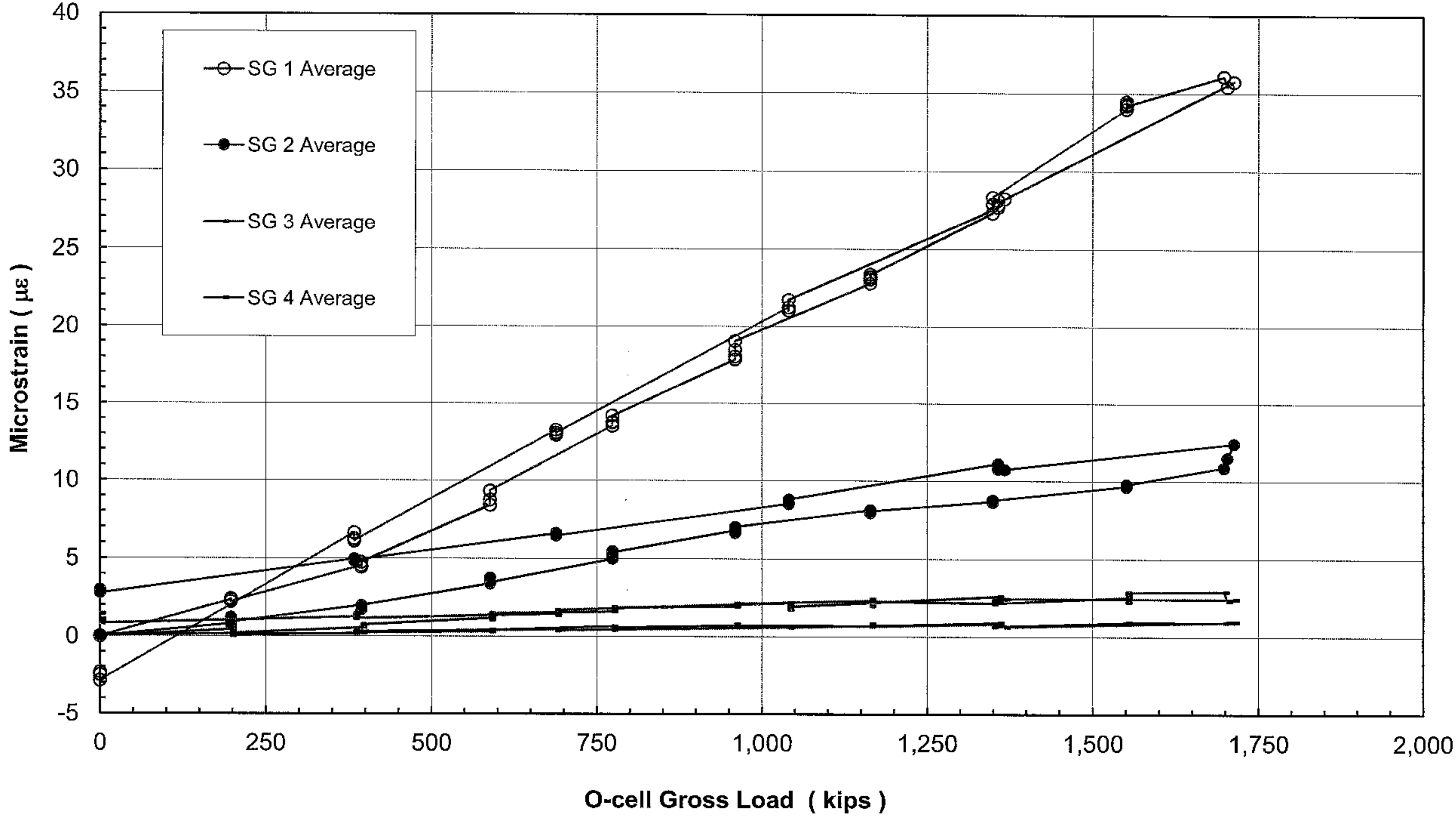

Loadtest USA Project No. LT-1407

Figure 4 of 8

LOADTEST

Strain Gage Load Distribution

TS-1 - IL-89 Over Illinois River - Bureau Putnam Counties, IL

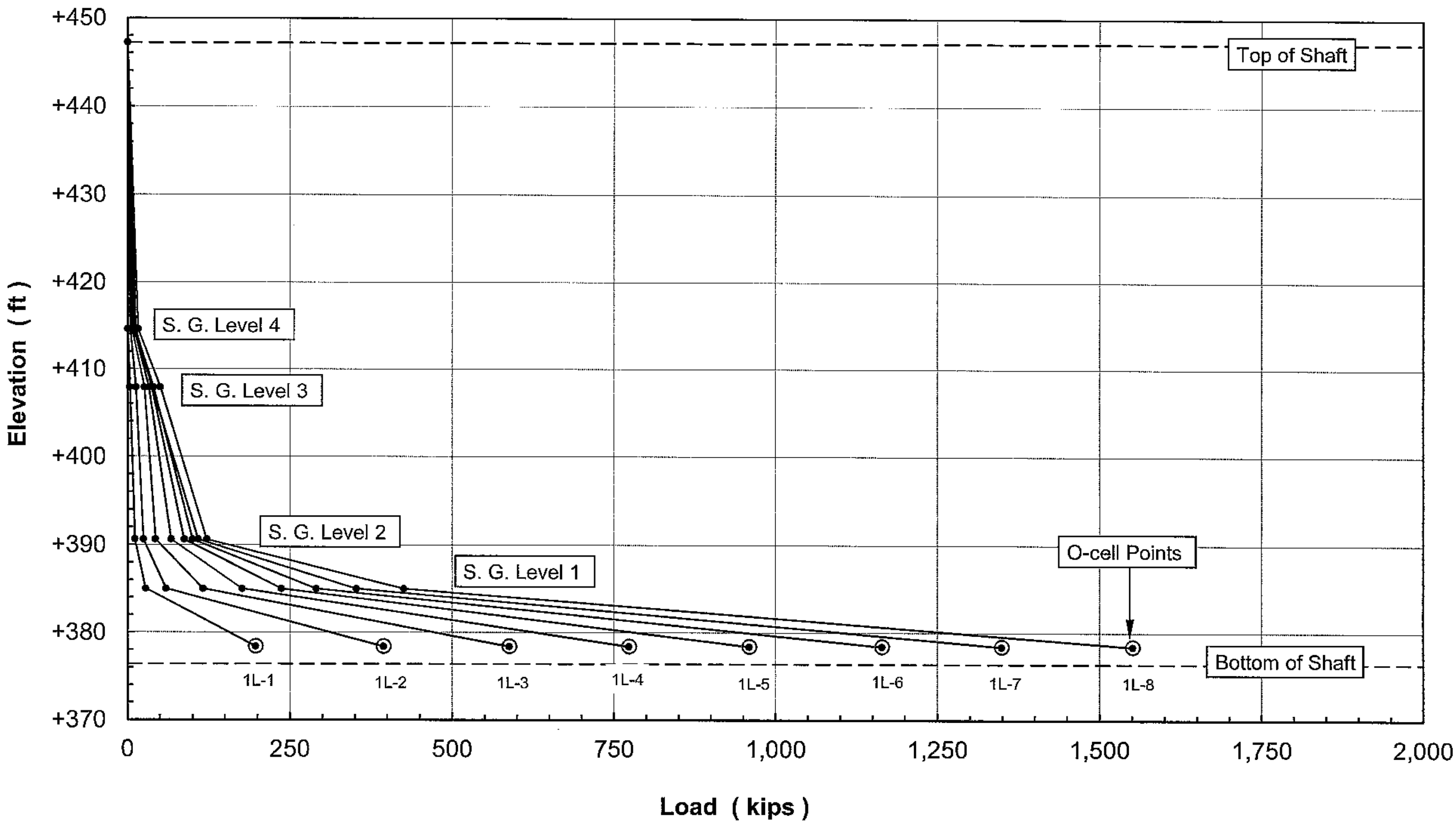

Loadtest USA Project No. LT-1407

Figure 5 of 8

LOADTEST

Mobilized Upward Net Unit Side Shear

TS-1 - IL-89 Over Illinois River - Bureau Putnam Counties, IL

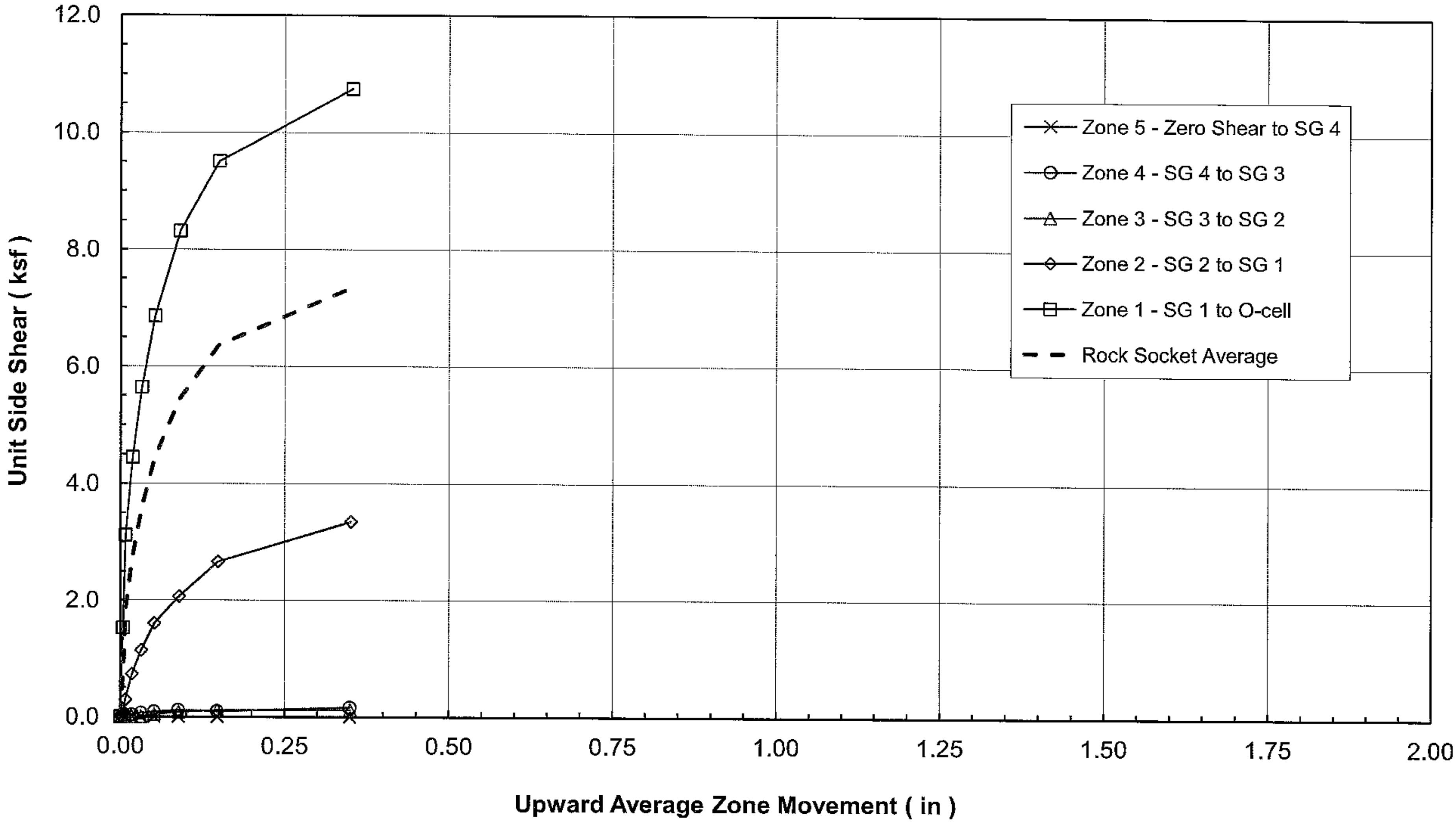

Mobilized Unit End Bearing

TS-1 - IL-89 Over Illinois River - Bureau Putnam Counties, IL

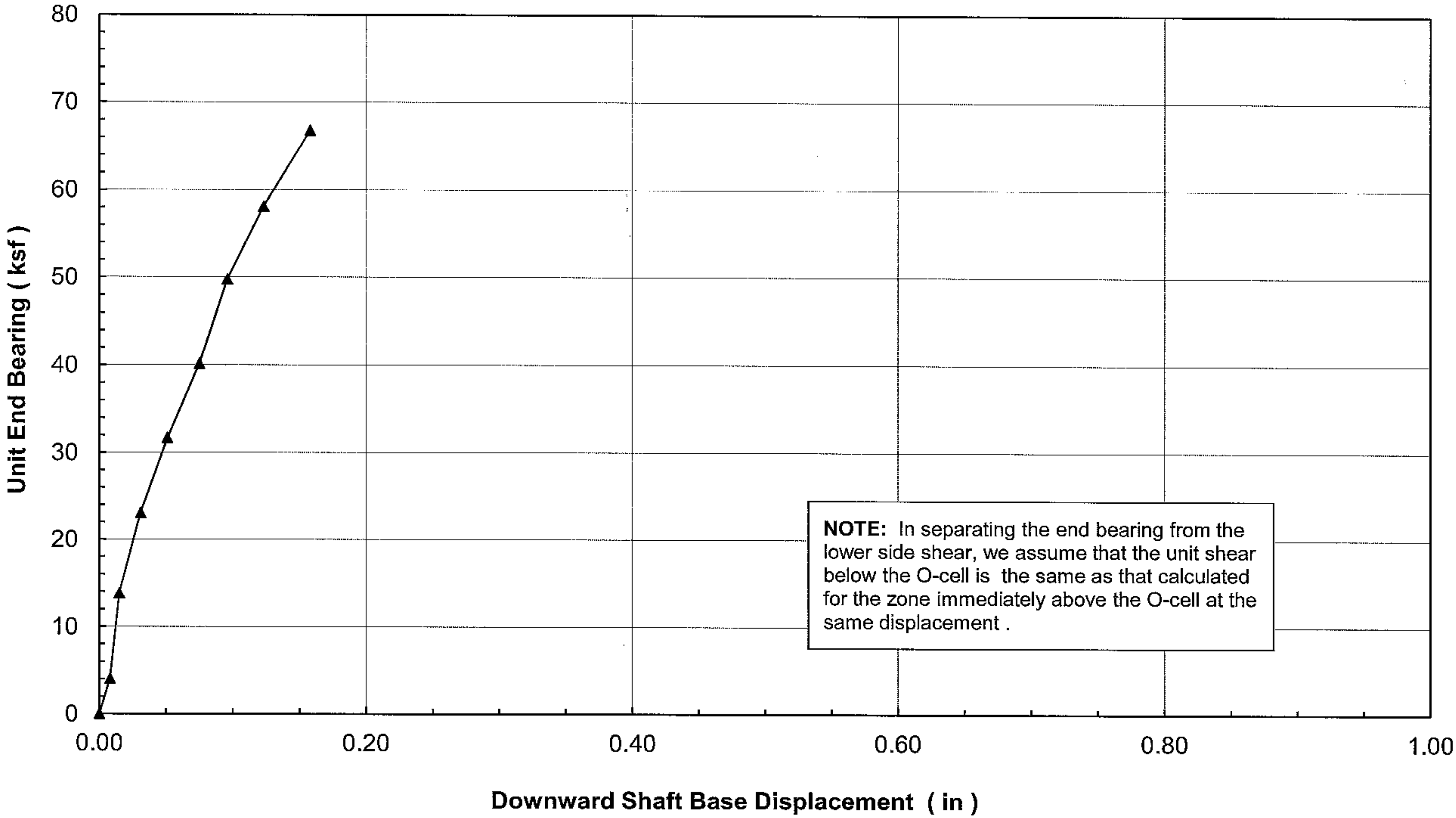

Equivalent Top Load-Displacement

TS-1 - IL-89 Over Illinois River - Bureau Putnam Counties, IL

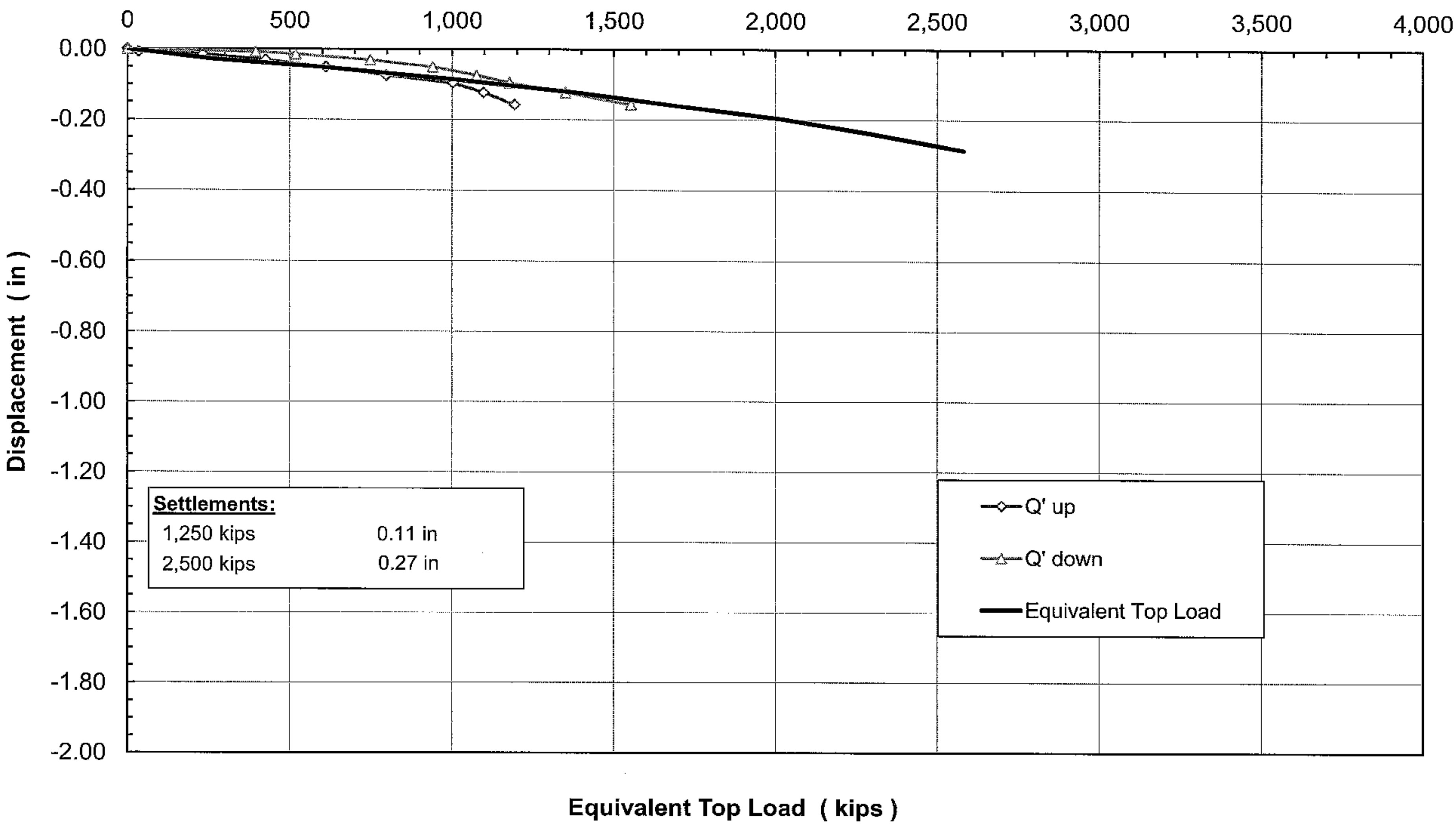

APPENDIX A

FIELD DATA AND DATA REDUCTION TABLES

Upward Top of Shaft Movement and Upper Shaft Compression
TS-1 - IL-89 Over Illinois River - Bureau & Putnam Counties, IL

Load	Hold		O-cell		Top of Shaft			Upper Compression Telltales		
Test Increment	Time (minutes)	Time (hh:mm:ss)	Pressure (psi)	Load (kips)	A-Leica (in)	B-Leica (in)	Average (in)	A-08-23839 (in)	B-08-23842 (in)	Average (in)
1 L - 0	-	10:15:00	0	0	0.000	0.000	0.000	0.000	0.000	0.000
1 L - 1	1	10:24:30	500	197	0.004	0.003	0.003	0.000	0.000	0.000
1 L - 1	2	10:25:30	500	197	0.004	0.003	0.003	0.000	0.000	0.000
1 L - 1	4	10:27:30	500	197	0.004	0.003	0.003	0.000	0.000	0.000
1 L - 1	8	10:31:30	500	197	0.004	0.004	0.004	0.000	0.000	0.000
1 L - 2	1	10:33:30	1,010	394	0.007	0.006	0.006	0.000	0.001	0.000
1 L - 2	2	10:34:30	1,010	394	0.007	0.006	0.006	0.000	0.000	0.000
1 L - 2	4	10:36:30	1,010	394	0.008	0.007	0.007	0.000	0.001	0.000
1 L - 2	8	10:40:30	1,010	394	0.008	0.007	0.007	0.000	0.001	0.001
1 L - 3	1	10:43:30	1,510	588	0.014	0.013	0.013	0.000	0.001	0.001
1 L - 3	2	10:44:30	1,510	588	0.015	0.013	0.014	0.001	0.001	0.001
1 L - 3	4	10:46:30	1,510	588	0.016	0.015	0.015	0.001	0.002	0.001
1 L - 3	8	10:50:30	1,510	588	0.018	0.016	0.017	0.001	0.002	0.002
1 L - 4	1	10:54:30	1,990	773	0.028	0.026	0.027	0.001	0.002	0.002
1 L - 4	2	10:55:30	1,990	773	0.029	0.027	0.028	0.001	0.003	0.002
1 L - 4	4	10:57:30	1,990	773	0.030	0.028	0.029	0.001	0.003	0.002
1 L - 4	8	11:01:30	1,990	773	0.032	0.029	0.031	0.001	0.003	0.002
1 L - 5	1	11:04:00	2,470	959	0.045	0.044	0.044	0.001	0.003	0.002
1 L - 5	2	11:05:00	2,470	959	0.047	0.046	0.046	0.002	0.003	0.002
1 L - 5	4	11:07:00	2,470	959	0.049	0.047	0.048	0.002	0.003	0.002
1 L - 5	8	11:11:00	2,470	959	0.052	0.051	0.051	0.002	0.003	0.002
1 L - 6	1	11:13:30	3,000	1,164	0.076	0.074	0.075	0.002	0.004	0.003
1 L - 6	2	11:14:30	3,000	1,164	0.079	0.078	0.078	0.002	0.004	0.003
1 L - 6	4	11:16:30	3,000	1,164	0.084	0.081	0.082	0.002	0.004	0.003
1 L - 6	8	11:20:30	3,000	1,164	0.089	0.087	0.088	0.002	0.005	0.004
1 L - 7	1	11:23:30	3,480	1,349	0.125	0.122	0.124	0.003	0.006	0.004
1 L - 7	2	11:24:30	3,480	1,349	0.133	0.131	0.132	0.002	0.006	0.004
1 L - 7	4	11:26:30	3,480	1,349	0.139	0.135	0.137	0.003	0.006	0.005
1 L - 7	8	11:30:30	3,480	1,349	0.148	0.145	0.147	0.003	0.006	0.005
1 L - 8	1	11:32:30	4,000	1,551	0.243	0.241	0.242	0.003	0.008	0.006
1 L - 8	2	11:33:30	4,000	1,551	0.263	0.261	0.262	0.003	0.008	0.006
1 L - 8	4	11:35:30	4,000	1,551	0.298	0.295	0.297	0.003	0.008	0.006
1 L - 8	8	11:39:30	4,000	1,551	0.350	0.347	0.349	0.003	0.009	0.006
1 L - 9	1	11:41:30	4,382	1,698	0.513	0.510	0.512	0.003	0.009	0.006
1 L - 9	2	11:42:30	4,394	1,703	0.669	0.665	0.667	0.002	0.009	0.006
1 L - 9	4	11:44:30	4,420	1,713	1.019	1.013	1.016	0.002	0.010	0.006
1 L - 9	8	11:48:30	3,527	1,367	1.657	1.652	1.655	0.002	0.009	0.005
1 U - 1	1	11:50:00	3,500	1,357	1.653	1.648	1.651	0.001	0.009	0.005
1 U - 1	2	11:51:00	3,500	1,357	1.653	1.648	1.651	0.001	0.009	0.005
1 U - 1	4	11:53:00	3,500	1,357	1.654	1.648	1.651	0.001	0.009	0.005
1 U - 2	1	11:55:30	2,680	1,040	1.632	1.628	1.630	0.001	0.008	0.005
1 U - 2	2	11:56:30	2,680	1,040	1.630	1.626	1.628	0.001	0.009	0.005
1 U - 2	4	11:58:30	2,680	1,040	1.629	1.624	1.627	0.001	0.008	0.004
1 U - 3	1	12:01:00	1,770	688	1.572	1.566	1.569	0.001	0.008	0.004
1 U - 3	2	12:02:00	1,770	688	1.570	1.565	1.568	0.001	0.007	0.004
1 U - 3	4	12:04:00	1,770	688	1.568	1.562	1.565	0.001	0.007	0.004
1 U - 4	1	12:06:30	980	383	1.488	1.484	1.486	0.001	0.006	0.003
1 U - 4	2	12:07:30	980	383	1.487	1.481	1.484	0.001	0.006	0.003
1 U - 4	4	12:09:30	980	383	1.485	1.480	1.483	0.000	0.005	0.003
1 U - 5	1	12:12:00	0	0	1.330	1.324	1.327	0.000	0.004	0.002
1 U - 5	2	12:13:00	0	0	1.325	1.320	1.323	0.001	0.004	0.002
1 U - 5	4	12:15:00	0	0	1.320	1.315	1.318	0.000	0.004	0.002
1 U - 5	8	12:19:00	0	0	1.313	1.308	1.311	0.001	0.004	0.002

LOADTEST

O-cell Expansion
TS-1 - IL-89 Over Illinois River - Bureau & Putnam Counties, IL

Load Test Increment	Hold Time (minutes)	Time (hh:mm:ss)	O-cell Pressure (psi)	O-cell Load (kips)	O-cell Expansion 1A-1419714 (in)	1B-1419715 (in)	1C-1417851 (in)	1D-1417852 (in)	Average (in)
1 L - 0	-	10:15:00	0	0	0.000	0.000	0.000	0.000	0.000
1 L - 1	1	10:24:30	500	197	0.009	0.017	0.011	0.008	0.011
1 L - 1	2	10:25:30	500	197	0.009	0.017	0.011	0.008	0.011
1 L - 1	4	10:27:30	500	197	0.010	0.018	0.012	0.008	0.012
1 L - 1	8	10:31:30	500	197	0.010	0.018	0.012	0.008	0.012
1 L - 2	1	10:33:30	1,010	394	0.017	0.029	0.020	0.014	0.020
1 L - 2	2	10:34:30	1,010	394	0.017	0.029	0.020	0.014	0.020
1 L - 2	4	10:36:30	1,010	394	0.019	0.032	0.022	0.016	0.022
1 L - 2	8	10:40:30	1,010	394	0.017	0.033	0.023	0.017	0.023
1 L - 3	1	10:43:30	1,510	588	0.036	0.053	0.038	0.031	0.040
1 L - 3	2	10:44:30	1,510	588	0.039	0.055	0.040	0.034	0.042
1 L - 3	4	10:46:30	1,510	588	0.044	0.060	0.044	0.038	0.046
1 L - 3	8	10:50:30	1,510	588	0.049	0.063	0.046	0.041	0.050
1 L - 4	1	10:54:30	1,990	773	0.073	0.091	0.068	0.063	0.074
1 L - 4	2	10:55:30	1,990	773	0.075	0.093	0.070	0.065	0.076
1 L - 4	4	10:57:30	1,990	773	0.079	0.097	0.073	0.068	0.079
1 L - 4	8	11:01:30	1,990	773	0.084	0.102	0.077	0.073	0.084
1 L - 5	1	11:04:00	2,470	959	0.113	0.132	0.101	0.098	0.111
1 L - 5	2	11:05:00	2,470	959	0.117	0.135	0.103	0.101	0.114
1 L - 5	4	11:07:00	2,470	959	0.123	0.141	0.108	0.106	0.119
1 L - 5	8	11:11:00	2,470	959	0.132	0.150	0.117	0.114	0.128
1 L - 6	1	11:13:30	3,000	1,164	0.173	0.192	0.155	0.152	0.168
1 L - 6	2	11:14:30	3,000	1,164	0.178	0.197	0.159	0.156	0.173
1 L - 6	4	11:16:30	3,000	1,164	0.185	0.204	0.165	0.162	0.179
1 L - 6	8	11:20:30	3,000	1,164	0.195	0.214	0.173	0.170	0.188
1 L - 7	1	11:23:30	3,480	1,349	0.249	0.271	0.226	0.222	0.242
1 L - 7	2	11:24:30	3,480	1,349	0.259	0.281	0.235	0.232	0.252
1 L - 7	4	11:26:30	3,480	1,349	0.268	0.291	0.243	0.240	0.260
1 L - 7	8	11:30:30	3,480	1,349	0.283	0.307	0.257	0.254	0.275
1 L - 8	1	11:32:30	4,000	1,551	0.402	0.426	0.372	0.366	0.391
1 L - 8	2	11:33:30	4,000	1,551	0.425	0.450	0.394	0.388	0.414
1 L - 8	4	11:35:30	4,000	1,551	0.460	0.491	0.432	0.426	0.452
1 L - 8	8	11:39:30	4,000	1,551	0.521	0.553	0.491	0.485	0.513
1 L - 9	1	11:41:30	4,382	1,698	0.704	0.741	0.671	0.666	0.695
1 L - 9	2	11:42:30	4,394	1,703	0.865	0.901	0.832	0.825	0.856
1 L - 9	4	11:44:30	4,420	1,713	1.229	1.270	1.199	1.185	1.221
1 L - 9	8	11:48:30	3,527	1,367	1.870	1.910	1.824	1.809	1.853
1 U - 1	1	11:50:00	3,500	1,357	1.868	1.906	1.821	1.807	1.851
1 U - 1	2	11:51:00	3,500	1,357	1.868	1.906	1.821	1.807	1.851
1 U - 1	4	11:53:00	3,500	1,357	1.870	1.906	1.822	1.808	1.851
1 U - 2	1	11:55:30	2,680	1,040	1.836	1.872	1.792	1.774	1.819
1 U - 2	2	11:56:30	2,680	1,040	1.833	1.869	1.788	1.771	1.815
1 U - 2	4	11:58:30	2,680	1,040	1.831	1.868	1.786	1.769	1.813
1 U - 3	1	12:01:00	1,770	688	1.751	1.793	1.717	1.697	1.739
1 U - 3	2	12:02:00	1,770	688	1.748	1.789	1.714	1.693	1.736
1 U - 3	4	12:04:00	1,770	688	1.746	1.786	1.708	1.690	1.732
1 U - 4	1	12:06:30	980	383	1.643	1.686	1.612	1.592	1.633
1 U - 4	2	12:07:30	980	383	1.640	1.684	1.610	1.590	1.631
1 U - 4	4	12:09:30	980	383	1.638	1.682	1.609	1.588	1.629
1 U - 5	1	12:12:00	0	0	1.425	1.459	1.409	1.384	1.420
1 U - 5	2	12:13:00	0	0	1.421	1.453	1.403	1.378	1.414
1 U - 5	4	12:15:00	0	0	1.424	1.452	1.400	1.375	1.413
1 U - 5	8	12:19:00	0	0	1.403	1.436	1.390	1.364	1.398

LOADTEST

O-cell Plate Movements and Creep (calculated)

TS-1 - IL-89 Over Illinois River - Bureau & Putnam Counties, IL

Load Test Increment	Hold Time (minutes)	Time (hh:mm:ss)	O-cell Pressure (psi)	O-cell Load (kips)	O-cell Net Load (kips)	Top of Shaft Movement (in)	Upper Comp. (in)	Upward Movement (in)	O-cell Expansion (in)	Downward Movement (in)	Creep Up Per Hold (in)	Creep Dn Per Hold (in)
1 L - 0	-	10:15:00	0	0	0	0.000	0.000	0.000	0.000	0.000		
1 L - 1	1	10:24:30	500	197	34	0.003	0.000	0.003	0.011	-0.008		
1 L - 1	2	10:25:30	500	197	34	0.003	0.000	0.003	0.011	-0.008		
1 L - 1	4	10:27:30	500	197	34	0.003	0.000	0.003	0.012	-0.009		
1 L - 1	8	10:31:30	500	197	34	0.004	0.000	0.004	0.012	-0.008	0.001	0.000
1 L - 2	1	10:33:30	1,010	394	231	0.006	0.000	0.006	0.020	-0.014		
1 L - 2	2	10:34:30	1,010	394	231	0.006	0.000	0.006	0.020	-0.014		
1 L - 2	4	10:36:30	1,010	394	231	0.007	0.000	0.007	0.022	-0.015		
1 L - 2	8	10:40:30	1,010	394	231	0.007	0.001	0.008	0.023	-0.015	0.001	0.000
1 L - 3	1	10:43:30	1,510	588	425	0.013	0.001	0.014	0.040	-0.026		
1 L - 3	2	10:44:30	1,510	588	425	0.014	0.001	0.015	0.042	-0.027		
1 L - 3	4	10:46:30	1,510	588	425	0.015	0.001	0.016	0.046	-0.030		
1 L - 3	8	10:50:30	1,510	588	425	0.017	0.002	0.019	0.050	-0.031	0.003	0.001
1 L - 4	1	10:54:30	1,990	773	610	0.027	0.002	0.029	0.074	-0.045		
1 L - 4	2	10:55:30	1,990	773	610	0.028	0.002	0.030	0.076	-0.046		
1 L - 4	4	10:57:30	1,990	773	610	0.029	0.002	0.031	0.079	-0.048		
1 L - 4	8	11:01:30	1,990	773	610	0.031	0.002	0.033	0.084	-0.051	0.002	0.003
1 L - 5	1	11:04:00	2,470	959	796	0.044	0.002	0.046	0.111	-0.065		
1 L - 5	2	11:05:00	2,470	959	796	0.046	0.002	0.048	0.114	-0.066		
1 L - 5	4	11:07:00	2,470	959	796	0.048	0.002	0.050	0.119	-0.069		
1 L - 5	8	11:11:00	2,470	959	796	0.051	0.002	0.053	0.128	-0.075	0.003	0.006
1 L - 6	1	11:13:30	3,000	1,164	1,001	0.075	0.003	0.078	0.168	-0.090		
1 L - 6	2	11:14:30	3,000	1,164	1,001	0.078	0.003	0.081	0.173	-0.092		
1 L - 6	4	11:16:30	3,000	1,164	1,001	0.082	0.003	0.085	0.179	-0.094		
1 L - 6	8	11:20:30	3,000	1,164	1,001	0.088	0.004	0.092	0.188	-0.096	0.007	0.002
1 L - 7	1	11:23:30	3,480	1,349	1,186	0.124	0.004	0.128	0.242	-0.114		
1 L - 7	2	11:24:30	3,480	1,349	1,186	0.132	0.004	0.136	0.252	-0.116		
1 L - 7	4	11:26:30	3,480	1,349	1,186	0.137	0.005	0.142	0.260	-0.118		
1 L - 7	8	11:30:30	3,480	1,349	1,186	0.147	0.005	0.152	0.275	-0.123	0.010	0.005
1 L - 8	1	11:32:30	4,000	1,551	1,388	0.242	0.006	0.248	0.391	-0.143		
1 L - 8	2	11:33:30	4,000	1,551	1,388	0.262	0.006	0.268	0.414	-0.146		
1 L - 8	4	11:35:30	4,000	1,551	1,388	0.297	0.006	0.303	0.452	-0.149		
1 L - 8	8	11:39:30	4,000	1,551	1,388	0.349	0.006	0.355	0.513	-0.158	0.052	0.009
1 L - 9	1	11:41:30	4,382	1,698	1,535	0.512	0.006	0.518	0.695	-0.177		
1 L - 9	2	11:42:30	4,394	1,703	1,540	0.667	0.006	0.673	0.856	-0.183		
1 L - 9	4	11:44:30	4,420	1,713	1,550	1.016	0.006	1.022	1.221	-0.199		
1 L - 9	8	11:48:30	3,527	1,367	1,204	1.655	0.005	1.660	1.853	-0.193		
1 U - 1	1	11:50:00	3,500	1,357	1,194	1.651	0.005	1.656	1.851	-0.195		
1 U - 1	2	11:51:00	3,500	1,357	1,194	1.651	0.005	1.656	1.851	-0.195		
1 U - 1	4	11:53:00	3,500	1,357	1,194	1.651	0.005	1.656	1.851	-0.195		
1 U - 2	1	11:55:30	2,680	1,040	877	1.630	0.005	1.635	1.819	-0.184		
1 U - 2	2	11:56:30	2,680	1,040	877	1.628	0.005	1.633	1.815	-0.182		
1 U - 2	4	11:58:30	2,680	1,040	877	1.627	0.004	1.631	1.813	-0.182		
1 U - 3	1	12:01:00	1,770	688	525	1.569	0.004	1.573	1.739	-0.166		
1 U - 3	2	12:02:00	1,770	688	525	1.568	0.004	1.572	1.736	-0.164		
1 U - 3	4	12:04:00	1,770	688	525	1.565	0.004	1.569	1.732	-0.163		
1 U - 4	1	12:06:30	980	383	220	1.486	0.003	1.489	1.633	-0.144		
1 U - 4	2	12:07:30	980	383	220	1.484	0.003	1.487	1.631	-0.144		
1 U - 4	4	12:09:30	980	383	220	1.483	0.003	1.486	1.629	-0.143		
1 U - 5	1	12:12:00	0	0	0	1.327	0.002	1.329	1.420	-0.091		
1 U - 5	2	12:13:00	0	0	0	1.323	0.002	1.325	1.414	-0.089		
1 U - 5	4	12:15:00	0	0	0	1.318	0.002	1.320	1.413	-0.093		
1 U - 5	8	12:19:00	0	0	0	1.311	0.002	1.313	1.398	-0.085		

LOADTEST

Strain Gage Readings and Loads at Levels 1 and 2
TS-1 - IL-89 Over Illinois River - Bureau & Putnam Counties, IL

Load	Hold		O-cell		Strain Gage Level 1				Strain Gage Level 2			
Test Increment	Time (minutes)	Time (hh:mm:ss)	Pressure (psi)	Load (kips)	1A-1432504 (με)	1B-1432505 (με)	Av. Strain (με)	Load (kips)	2A-1432506 (με)	2B-1432507 (με)	Av. Strain (με)	Load (kips)
1 L - 0	-	10:15:00	0	0	0.0	0.0	0.0	0	0.0	0.0	0.0	0
1 L - 1	1	10:24:30	500	197	0.6	4.1	2.3	29	0.6	1.0	0.8	10
1 L - 1	2	10:25:30	500	197	0.5	4.1	2.3	28	0.5	1.6	1.1	13
1 L - 1	4	10:27:30	500	197	0.6	4.2	2.4	30	0.6	1.7	1.2	15
1 L - 1	8	10:31:30	500	197	0.5	4.0	2.2	28	0.4	1.4	0.9	11
1 L - 2	1	10:33:30	1,010	394	1.0	8.1	4.6	57	1.3	2.7	2.0	24
1 L - 2	2	10:34:30	1,010	394	0.9	8.0	4.4	55	1.1	2.3	1.7	21
1 L - 2	4	10:36:30	1,010	394	1.0	8.1	4.5	56	1.1	2.7	1.9	24
1 L - 2	8	10:40:30	1,010	394	0.9	8.6	4.8	59	1.1	2.8	2.0	25
1 L - 3	1	10:43:30	1,510	588	2.3	14.4	8.4	104	2.2	4.6	3.4	42
1 L - 3	2	10:44:30	1,510	588	3.0	14.4	8.7	109	2.2	4.6	3.4	42
1 L - 3	4	10:46:30	1,510	588	3.3	15.3	9.3	116	2.7	4.8	3.7	47
1 L - 3	8	10:50:30	1,510	588	3.4	15.3	9.3	116	2.4	4.5	3.5	43
1 L - 4	1	10:54:30	1,990	773	5.6	21.4	13.5	168	3.0	6.9	5.0	62
1 L - 4	2	10:55:30	1,990	773	5.8	21.7	13.7	171	3.2	7.7	5.5	68
1 L - 4	4	10:57:30	1,990	773	5.9	21.7	13.8	171	3.0	7.3	5.2	64
1 L - 4	8	11:01:30	1,990	773	6.0	22.3	14.2	176	3.0	7.8	5.4	67
1 L - 5	1	11:04:00	2,470	959	7.6	28.1	17.9	222	3.7	9.9	6.8	84
1 L - 5	2	11:05:00	2,470	959	7.8	28.3	18.0	224	3.4	9.9	6.6	83
1 L - 5	4	11:07:00	2,470	959	7.9	29.0	18.5	230	3.4	10.5	6.9	86
1 L - 5	8	11:11:00	2,470	959	8.0	30.1	19.0	237	3.3	10.7	7.0	87
1 L - 6	1	11:13:30	3,000	1,164	8.9	36.6	22.8	283	2.8	13.5	8.1	101
1 L - 6	2	11:14:30	3,000	1,164	8.9	37.2	23.0	287	2.5	13.4	7.9	99
1 L - 6	4	11:16:30	3,000	1,164	8.8	37.6	23.2	289	2.5	13.4	7.9	99
1 L - 6	8	11:20:30	3,000	1,164	8.7	38.0	23.4	291	2.2	13.9	8.1	100
1 L - 7	1	11:23:30	3,480	1,349	9.2	45.4	27.3	340	0.6	16.8	8.7	108
1 L - 7	2	11:24:30	3,480	1,349	9.0	46.8	27.9	347	-0.1	17.7	8.8	109
1 L - 7	4	11:26:30	3,480	1,349	8.5	47.2	27.8	346	-0.8	18.0	8.6	107
1 L - 7	8	11:30:30	3,480	1,349	8.3	48.3	28.3	352	-1.1	18.6	8.8	109
1 L - 8	1	11:32:30	4,000	1,551	9.3	58.7	34.0	423	-5.0	24.4	9.7	120
1 L - 8	2	11:33:30	4,000	1,551	10.0	58.6	34.3	427	-5.5	24.7	9.6	120
1 L - 8	4	11:35:30	4,000	1,551	10.6	58.3	34.5	429	-5.4	24.7	9.7	120
1 L - 8	8	11:39:30	4,000	1,551	11.0	57.4	34.2	425	-5.0	24.6	9.8	122
1 L - 9	1	11:41:30	4,382	1,698	10.2	62.0	36.1	449	-5.0	26.8	10.9	136
1 L - 9	2	11:42:30	4,394	1,703	9.2	61.7	35.4	441	-3.9	26.9	11.5	143
1 L - 9	4	11:44:30	4,420	1,713	10.5	61.1	35.8	445	-5.1	29.9	12.4	155
1 L - 9	8	11:48:30	3,527	1,367	15.0	41.5	28.2	351	-1.9	23.4	10.8	134
1 U - 1	1	11:50:00	3,500	1,357	14.8	41.5	28.1	350	-1.6	23.1	10.8	134
1 U - 1	2	11:51:00	3,500	1,357	14.6	41.1	27.8	346	-1.6	23.3	10.9	135
1 U - 1	4	11:53:00	3,500	1,357	14.3	41.1	27.7	344	-0.9	23.2	11.1	138
1 U - 2	1	11:55:30	2,680	1,040	10.0	33.4	21.7	270	-2.5	20.1	8.8	109
1 U - 2	2	11:56:30	2,680	1,040	9.4	32.7	21.0	261	-2.6	19.8	8.6	107
1 U - 2	4	11:58:30	2,680	1,040	9.5	32.9	21.2	264	-2.6	19.6	8.5	106
1 U - 3	1	12:01:00	1,770	688	3.9	22.3	13.1	163	-3.1	16.0	6.4	80
1 U - 3	2	12:02:00	1,770	688	3.9	22.0	12.9	161	-3.1	16.3	6.6	82
1 U - 3	4	12:04:00	1,770	688	3.8	22.7	13.2	165	-3.0	16.2	6.6	82
1 U - 4	1	12:06:30	980	383	-0.4	12.6	6.1	76	-2.0	11.7	4.9	61
1 U - 4	2	12:07:30	980	383	-0.2	12.7	6.2	78	-1.7	11.3	4.8	60
1 U - 4	4	12:09:30	980	383	0.0	13.3	6.6	82	-1.8	11.7	5.0	62
1 U - 5	1	12:12:00	0	0	-5.0	-0.7	-2.9	-36	0.6	4.9	2.8	34
1 U - 5	2	12:13:00	0	0	-4.9	-0.1	-2.5	-31	0.9	4.6	2.8	34
1 U - 5	4	12:15:00	0	0	-4.6	0.0	-2.3	-29	1.3	4.5	2.9	36
1 U - 5	8	12:19:00	0	0	-4.9	-0.8	-2.9	-36	1.3	4.7	3.0	37

LOADTEST

Strain Gage Readings and Loads at Levels 3 and 4
TS-1 - IL-89 Over Illinois River - Bureau & Putnam Counties, IL

Load Test Increment	Hold Time (minutes)	Time (hh:mm:ss)	O-cell Pressure (psi)	O-cell Load (kips)	Strain Gage Level 3 3A-1432508 (με)	3B-1432509 (με)	Av. Strain (με)	Load (kips)	Strain Gage Level 4 4A-1432911 (με)	4B-1432912 (με)	Av. Strain (με)	Load (kips)
1 L - 0	-	10:15:00	0	0	0.0	0.0	0.0	0	0.0	0.0	0.0	0
1 L - 1	1	10:24:30	500	197	0.3	0.6	0.4	8	0.1	0.2	0.2	3
1 L - 1	2	10:25:30	500	197	0.4	0.8	0.6	10	0.2	0.1	0.1	2
1 L - 1	4	10:27:30	500	197	0.2	0.9	0.6	10	0.1	0.2	0.2	3
1 L - 1	8	10:31:30	500	197	0.6	-0.1	0.2	4	0.0	0.0	0.0	0
1 L - 2	1	10:33:30	1,010	394	0.7	0.5	0.6	10	0.2	0.2	0.2	3
1 L - 2	2	10:34:30	1,010	394	0.7	0.7	0.7	12	0.3	0.2	0.2	4
1 L - 2	4	10:36:30	1,010	394	0.6	1.0	0.8	13	0.3	0.3	0.3	5
1 L - 2	8	10:40:30	1,010	394	0.6	0.9	0.7	13	0.1	0.3	0.2	4
1 L - 3	1	10:43:30	1,510	588	1.0	1.4	1.2	21	0.2	0.4	0.3	5
1 L - 3	2	10:44:30	1,510	588	1.0	1.2	1.1	19	0.3	0.5	0.4	7
1 L - 3	4	10:46:30	1,510	588	1.0	1.5	1.2	21	0.2	0.5	0.4	6
1 L - 3	8	10:50:30	1,510	588	1.2	1.7	1.5	26	0.2	0.6	0.4	7
1 L - 4	1	10:54:30	1,990	773	1.4	1.9	1.6	28	0.5	0.8	0.6	11
1 L - 4	2	10:55:30	1,990	773	1.4	2.4	1.9	33	0.3	0.9	0.6	10
1 L - 4	4	10:57:30	1,990	773	1.7	1.7	1.7	29	0.5	0.3	0.4	7
1 L - 4	8	11:01:30	1,990	773	1.5	2.2	1.9	33	0.3	0.8	0.6	10
1 L - 5	1	11:04:00	2,470	959	1.7	2.2	2.0	34	0.6	0.8	0.7	12
1 L - 5	2	11:05:00	2,470	959	1.7	2.5	2.1	37	0.5	0.9	0.7	12
1 L - 5	4	11:07:00	2,470	959	1.6	2.4	2.0	35	0.6	0.9	0.8	14
1 L - 5	8	11:11:00	2,470	959	1.9	2.4	2.1	37	0.6	0.8	0.7	12
1 L - 6	1	11:13:30	3,000	1,164	1.8	2.8	2.3	41	0.5	0.8	0.7	12
1 L - 6	2	11:14:30	3,000	1,164	1.9	2.2	2.0	35	0.6	0.9	0.7	13
1 L - 6	4	11:16:30	3,000	1,164	2.0	2.8	2.4	42	0.8	0.9	0.8	15
1 L - 6	8	11:20:30	3,000	1,164	1.9	2.7	2.3	40	0.4	0.9	0.7	12
1 L - 7	1	11:23:30	3,480	1,349	1.8	2.6	2.2	38	0.7	0.9	0.8	14
1 L - 7	2	11:24:30	3,480	1,349	1.9	2.9	2.4	41	0.7	1.0	0.8	14
1 L - 7	4	11:26:30	3,480	1,349	1.6	3.1	2.3	41	0.5	1.1	0.8	14
1 L - 7	8	11:30:30	3,480	1,349	1.4	3.0	2.2	38	0.4	0.9	0.7	12
1 L - 8	1	11:32:30	4,000	1,551	0.7	4.4	2.6	45	0.3	1.5	0.9	16
1 L - 8	2	11:33:30	4,000	1,551	0.5	4.1	2.3	40	0.1	1.6	0.9	15
1 L - 8	4	11:35:30	4,000	1,551	0.2	5.2	2.7	48	-0.2	2.1	0.9	16
1 L - 8	8	11:39:30	4,000	1,551	-0.2	6.0	2.9	51	-0.4	2.3	0.9	16
1 L - 9	1	11:41:30	4,382	1,698	-1.6	7.4	2.9	51	-1.2	3.1	0.9	16
1 L - 9	2	11:42:30	4,394	1,703	-2.4	7.1	2.4	41	-1.6	3.5	1.0	17
1 L - 9	4	11:44:30	4,420	1,713	-4.7	9.6	2.4	43	-2.7	4.6	0.9	17
1 L - 9	8	11:48:30	3,527	1,367	-6.8	11.8	2.5	43	-4.0	5.3	0.6	11
1 U - 1	1	11:50:00	3,500	1,357	-6.6	11.4	2.4	41	-3.9	5.7	0.9	16
1 U - 1	2	11:51:00	3,500	1,357	-6.7	11.8	2.6	45	-4.0	5.6	0.8	14
1 U - 1	4	11:53:00	3,500	1,357	-6.2	11.4	2.6	46	-3.8	5.6	0.9	16
1 U - 2	1	11:55:30	2,680	1,040	-6.5	10.4	1.9	34	-4.0	5.1	0.6	10
1 U - 2	2	11:56:30	2,680	1,040	-6.5	10.1	1.8	31	-4.0	5.3	0.6	11
1 U - 2	4	11:58:30	2,680	1,040	-6.5	10.9	2.2	38	-3.9	5.2	0.6	11
1 U - 3	1	12:01:00	1,770	688	-6.2	9.6	1.7	30	-4.2	4.9	0.4	7
1 U - 3	2	12:02:00	1,770	688	-6.5	9.3	1.4	24	-4.1	5.0	0.4	7
1 U - 3	4	12:04:00	1,770	688	-5.9	8.9	1.5	26	-4.1	5.0	0.4	8
1 U - 4	1	12:06:30	980	383	-5.8	8.1	1.2	20	-3.7	4.4	0.3	5
1 U - 4	2	12:07:30	980	383	-5.6	8.6	1.5	26	-3.8	4.5	0.3	6
1 U - 4	4	12:09:30	980	383	-5.7	8.2	1.3	22	-3.9	4.2	0.2	3
1 U - 5	1	12:12:00	0	0	-4.8	6.5	0.8	15	-3.4	3.6	0.1	2
1 U - 5	2	12:13:00	0	0	-4.6	6.7	1.1	19	-3.4	3.5	0.1	1
1 U - 5	4	12:15:00	0	0	-4.6	7.5	1.4	25	-3.4	3.7	0.1	3
1 U - 5	8	12:19:00	0	0	-4.6	6.6	1.0	18	-3.3	3.5	0.1	2

APPENDIX B

O-CELL AND INSTRUMENTATION CALIBRATION SHEETS

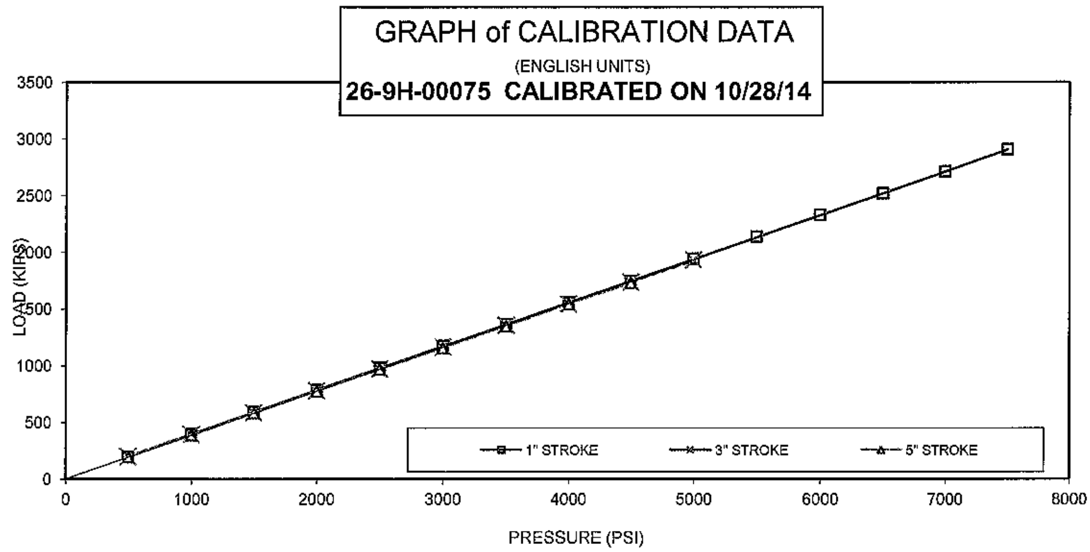

STROKE:	1 INCH	3 INCH	5 INCH
PRESSURE PSI	LOAD KIPS	LOAD KIPS	LOAD KIPS
0	0	0	0
500	195	198	196
1000	396	394	386
1500	590	584	581
2000	784	778	772
2500	978	970	967
3000	1172	1163	1157
3500	1364	1356	1349
4000	1556	1544	1542
4500	1748	1739	1731
5000	1941	1932	
5500	2136		
6000	2328		
6500	2520		
7000	2713		
7500	2906		

26" O-CELL, SERIAL # 26-9H-00075

LOAD CONVERSION FORMULA

LOAD = PRESSURE * 0.3867 + (3.71)
{KIPS} {PSI}

Regression Output:

Constant	3.7078 kips
X Coefficient	0.3867 kip / psi
R Square	0.9999
No. of Observations	34
Degrees of Freedom	32
Std Err of Y Est	5.42
Std Err of X Coeff	0.0005

CALIBRATION STANDARDS:

All data presented are derived from 6" dia. certified hydraulic pressure gauges and electronic load transducer, manufactured and calibrated by the University of Illinois at Champaign, Illinois. All calibrations and certifications are traceable through the Laboratory Master Deadweight Gauges directly to the National Institute of Standards and Technology. No specific guidelines exist for calibration of load test jacks and equipment but procedures comply with similar guidelines for calibration of gages, ANSI specifications B40.1.

* AE & FC CUSTOMER: LOADTEST INC.	* CONTRACTOR.: ILLINI DRILLED FOUNDATION
* AE & FC JOB NO: SO13199	* JOB LOCATION: DAYVILLE, IL
* CUSTOMER P.O. NO.: LT-1407-1	* DATED: 10/28/14

SERVICE ENGINEER: [signature] DATE: 10-28-14

Certificate of Calibration

Certificate Number: LT.59687.2014-10-08

Instrument: Geokon VWPX

Calibration Date: Oct 8, 2014

Model: 4500HH-10000

Temperature: 23.2 °C

Serial Number: 59687

Linear Range: 15000 psi

Reference Pressure		Gauge Readings		Linear Error		Polynomial Error	
1st Cycle (psi)	2nd Cycle (psi)	1st Cycle (digits)	2nd Cycle (digits)	1st Cycle (% FS)	2nd Cycle (% FS)	1st Cycle (% FS)	2nd Cycle (% FS)
0.	0.	8752.8	8752.9	0.30	0.29	-0.01	-0.01
3000.	3000.	7619.3	7606.5	-0.20	0.02	-0.14	0.08
6000.	6000.	6470.6	6436.0	-0.44	0.16	-0.19	0.41
9000.	9000.	5302.3	5294.4	-0.34	-0.20	-0.08	0.05
12000.	12000.	4133.8	4127.9	-0.23	-0.13	-0.16	-0.06
15000.	15000.	2936.0	2937.3	0.38	0.35	0.07	0.05

Linear Gauge Factor: **-2.58083** **psi/dig** **-0.0177942** **MPa/dig**

Polynomial Factor: **-1.031E-05** **psi/dig²** **+** **-2.460E+00** **psi/dig**

-7.110E-08 **MPa/dig²** **+** **-1.696E-02** **MPa/dig**

Logging Instrument: Datataker DT85G, Serial: 089546

Reference Instrument: SENSOTEC TJE/743-23TJA, Serial: 622335

Reference Calibrated: 2014-04-15

Reference Certificate: 1001395677

LOADTEST certifies that the above named instrument has been calibrated by comparison with standards traceable to the NIST and was found to be in tolerance in all operating ranges. Relevant documentation and certificates are available on request.

Tested by: Michael Crumpton, B.S.C.E. Signed: MZ Crumpton

Approved by: Denton A. Kort, P.E. Signed: DK

Certificate of Calibration

Instrument: Geokon LVWDT

Model: 4450-3-100

Serial Number: 08-23842

Calibration Date: May 23, 2014

Temperature: 25.5 °C

Linear Range: 100 mm

Reference Displacement		Gauge Readings		Linear Error		Polynomial Error	
1st Cycle (mm)	2nd Cycle (mm)	1st Cycle (digits)	2nd Cycle (digits)	1st Cycle (% FS)	2nd Cycle (% FS)	1st Cycle (% FS)	2nd Cycle (% FS)
0	0	2625	2621	0.00	-0.07	0.02	-0.05
20	20	3588	3583	0.06	-0.05	0.05	-0.05
40	40	4554	4545	0.17	-0.03	0.15	-0.05
60	60	5511	5502	0.08	-0.10	0.07	-0.12
80	80	6471	6462	0.06	-0.13	0.05	-0.13
100	100	7429	7430	0.00	0.02	0.02	0.04

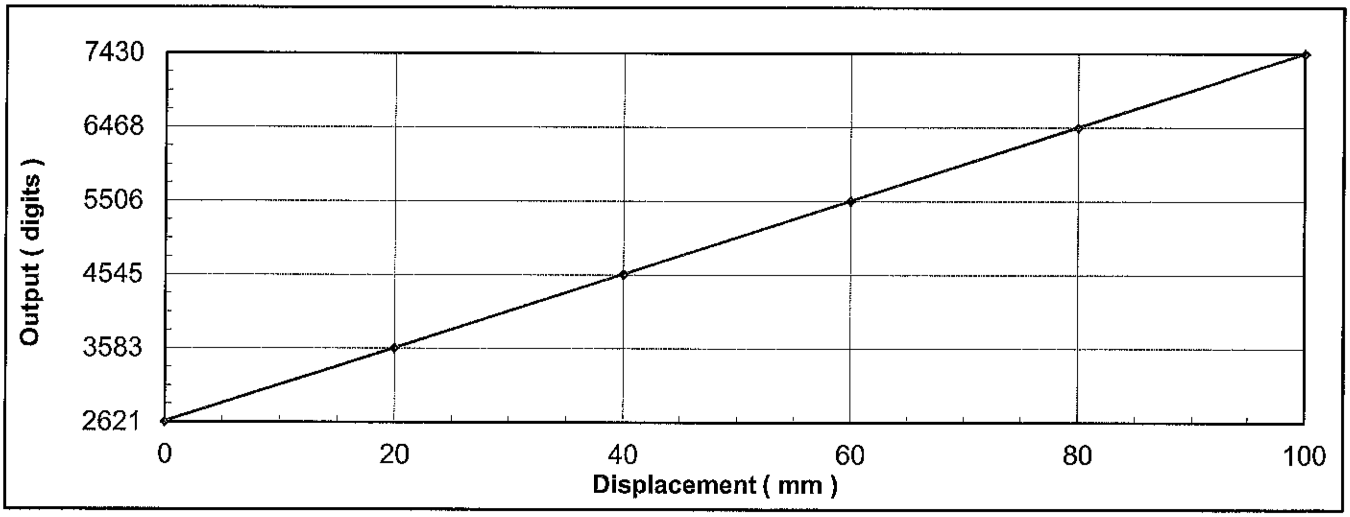

Linear Gauge Factor: **0.02081** **mm/dig** **0.0008195** **in/dig**

Polynomial Factor: **6.538E-09** **mm/dig² +** **2.075E-02** **mm/dig +** **-54.484** **mm**

Reference Instrument: Fowler Blocks, Serial: A00778
Certificate: F-47-778-1, Calibration Date: 2013-06-13

Logging Instrument: Datataker DT85G, Serial: 089546

LOADTEST certifies that the above named instrument has been calibrated by comparison with standards traceable to the NIST and was found to be in tolerance in all operating ranges. Relevant documentation and certificates are available on request.

Tested by: Michael Crumpton, B.S.C.E. Signed: MZ Crumpton

Approved by: David J. Jakstis, P.E. Signed:

Instrument Calibrated By LOADTEST, 2631-D NW 41 St, Gainesville, FL 32606

LOADTEST

DEEP FOUNDATION TESTING, EQUIPMENT & SERVICES • SPECIALIZING IN OSTERBERG CELL (O-cell®) TECHNOLOGY
O-cell® is a registered trademark.

Certificate of Calibration

Instrument: Geokon LVWDT

Model: 4450-3-100

Serial Number: 08-23839

Calibration Date: May 1, 2014

Temperature: 24.1 °C

Linear Range: 100 mm

Displacement (mm)	1st Cycle (digits)	2nd Cycle (digits)	Average (digits)	Linear Calculated (mm)	Linear Error (% FS)	Polynomial Calculated (mm)	Polynomial Error (% FS)
0	2594	2588	2591	0	-0.16	0	-0.01
20	3568	3560	3564	20	0.04	20	0.01
40	4537	4527	4532	40	0.15	40	0.03
60	5496	5489	5493	60	0.10	60	-0.02
80	6454	6448	6451	80	0.00	80	-0.03
100	7408	7407	7408	100	-0.13	100	0.02

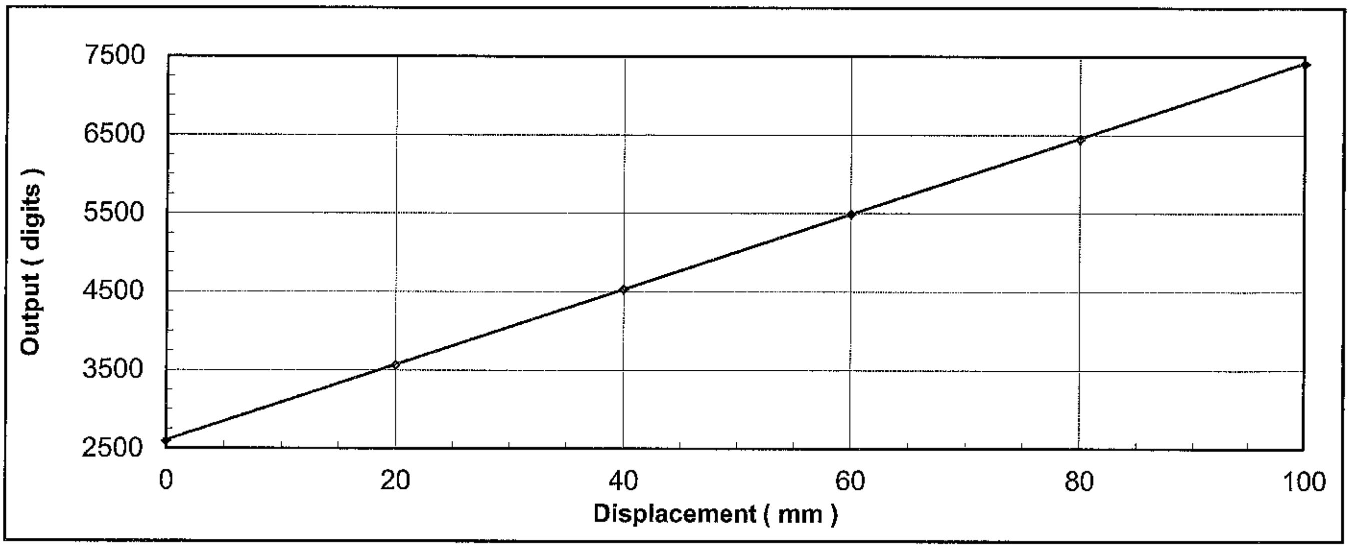

Linear Gauge Factor: **0.02077** **mm/dig** **0.0008176** **in/dig**

Polynomial Factor: **4.795E-08** **mm/dig² +** **2.029E-02** **mm/dig +** **-52.892** **mm**

Reference Instrument: Fowler Blocks, Serial: A00778, Certificate No.: F-47-778-1

Logging Instrument: Datataker DT85G, Serial: 089546

LOADTEST certifies that the above named instrument has been calibrated by comparison with standards traceable to the NIST and was found to be in tolerance in all operating ranges. Relevant documentation and certificates are available on request.

Tested by: Michael Crumpton, B.S.C.E. Signed: MZ Crumpton

Approved by: David J. Jakstis, P.E. Signed:

Instrument Calibrated By LOADTEST, 2631-D NW 41 St, Gainesville, FL 32606

LOADTEST

GEOKON 48 Spencer St. Lebanon, NH 03766 USA

Sister Bar Calibration Report

Model Number: 4911-4

Date of Calibration: October 14, 2014

This calibration has been verified/validated as of 10/27/2014

Serial Number: 1432504

Cable Length: 80 feet

Prestress: 35,000 psi

Regression Zero: 7017

Temperature: 22.6 °C

Technician:

Calibration Instruction: CI-VW Rebar

Applied Load (pounds)	Readings				Linearity % Max. Load
	Cycle #1	Cycle #2	Average	Change	
100	7063	7060	7062		
1500	7747	7743	7745	683	0.07
3000	8473	8470	8472	727	0.08
4500	9197	9195	9196	724	0.03
6000	9922	9914	9918	722	-0.11
100	7060	7054	7057		

For conversion factor, load to strain, refer to table C-2 of the Installation Manual

Gage Factor: 0.348 microstrain/ digit (GK-401 Pos. "B")

Calculated Strain = Gage Factor(Current Reading - Zero Reading)

Note: The above calibration uses the linear regression method.

Users are advised to establish their own zero conditions.

Linearity: ((Calculated Load - Applied Load)/Max. Applied Load) X 100 percent

The above instrument was found to be in tolerance in all operating ranges.
The above named instrument has been calibrated by comparison with standards traceable to the NIST, in compliance with ANSI Z540-1.

GEOKON 48 Spencer St. Lebanon, NH 03766 USA

Sister Bar Calibration Report

Model Number: 4911-4

Date of Calibration: October 14, 2014

This calibration has been verified/validated as of 10/27/2014

Serial Number: 1432505

Cable Length: 80 feet

Prestress: 35,000 psi

Regression Zero: 7216

Temperature: 22.6 °C

Technician:

Calibration Instruction: CI-VW Rebar

Applied Load (pounds)	Readings				Linearity % Max. Load
	Cycle #1	Cycle #2	Average	Change	
100	7265	7265	7265		
1500	7943	7942	7943	678	0.08
3000	8658	8658	8658	715	-0.21
4500	9389	9388	9389	731	0.01
6000	10114	10114	10114	725	0.06
100	7265	7265	7265		

For conversion factor, load to strain, refer to table C-2 of the Installation Manual

Gage Factor: 0.349 microstrain/ digit (GK-401 Pos. "B")

Calculated Strain = Gage Factor(Current Reading - Zero Reading)

Note: The above calibration uses the linear regression method.

Users are advised to establish their own zero conditions.

Linearity: ((Calculated Load - Applied Load)/Max. Applied Load) X 100 percent

The above instrument was found to be in tolerance in all operating ranges.
The above named instrument has been calibrated by comparison with standards traceable to the NIST, in compliance with ANSI Z540-1.

GEOKON 48 Spencer St. Lebanon, NH 03766 USA

Sister Bar Calibration Report

Model Number: 4911-4

Date of Calibration: October 14, 2014

This calibration has been verified/validated as of 10/27/2014

Serial Number: 1432506

Cable Length: 75 feet

Prestress: 35,000 psi

Regression Zero: 7038

Temperature: 22.6 °C

Technician:

Calibration Instruction: CI-VW Rebar

Applied Load (pounds)	Readings				Linearity % Max. Load
	Cycle #1	Cycle #2	Average	Change	
100	7089	7091	7090		
1500	7779	7780	7780	690	-0.05
3000	8522	8523	8523	743	-0.06
4500	9269	9271	9270	747	0.09
6000	10011	10010	10011	741	0.01
100	7091	7091	7091		

For conversion factor, load to strain, refer to table C-2 of the Installation Manual

Gage Factor: 0.342 microstrain/ digit (GK-401 Pos. "B")

Calculated Strain = Gage Factor(Current Reading - Zero Reading)

Note: The above calibration uses the linear regression method.

Users are advised to establish their own zero conditions.

Linearity: ((Calculated Load - Applied Load)/Max. Applied Load) X 100 percent

The above instrument was found to be in tolerance in all operating ranges.
The above named instrument has been calibrated by comparison with standards traceable to the NIST, in compliance with ANSI Z540-1.

GEOKON 48 Spencer St. Lebanon, NH 03766 USA

Sister Bar Calibration Report

Model Number: 4911-4

Date of Calibration: October 14, 2014

This calibration has been verified/validated as of 10/27/2014

Serial Number: 1432507

Cable Length: 75 feet

Prestress: 35,000 psi

Regression Zero: 7233

Temperature: 22.6 °C

Technician:

Calibration Instruction: CI-VW Rebar

Applied Load (pounds)	Readings				Linearity % Max. Load
	Cycle #1	Cycle #2	Average	Change	
100	7283	7279	7281		
1500	7969	7960	7965	684	0.03
3000	8695	8695	8695	730	0.03
4500	9427	9425	9426	731	0.04
6000	10155	10154	10155	729	-0.03
100	7279	7277	7278		

For conversion factor, load to strain, refer to table C-2 of the Installation Manual

Gage Factor: 0.347 microstrain/ digit (GK-401 Pos. "B")

Calculated Strain = Gage Factor(Current Reading - Zero Reading)

Note: The above calibration uses the linear regression method.

Users are advised to establish their own zero conditions.

Linearity: ((Calculated Load - Applied Load)/Max. Applied Load) X 100 percent

The above instrument was found to be in tolerance in all operating ranges.
The above named instrument has been calibrated by comparison with standards traceable to the NIST, in compliance with ANSI Z540-1.

GEOKON 48 Spencer St. Lebanon, NH 03766 USA

Sister Bar Calibration Report

Model Number: 4911-4

Date of Calibration: October 14, 2014

This calibration has been verified/validated as of 10/27/2014

Serial Number: 1432508

Cable Length: 70 feet

Prestress: 35,000 psi

Regression Zero: 7339

Temperature: 22.6 °C

Technician:

Calibration Instruction: CI-VW Rebar

Applied Load (pounds)	Readings				Linearity % Max. Load
	Cycle #1	Cycle #2	Average	Change	
100	7391	7395	7393		
1500	8064	8066	8065	672	-0.11
3000	8792	8794	8793	728	-0.15
4500	9529	9527	9528	735	0.05
6000	10257	10260	10259	731	0.10
100	7395	7397	7396		

For conversion factor, load to strain, refer to table C-2 of the Installation Manual

Gage Factor: 0.347 microstrain/ digit (GK-401 Pos. "B")

Calculated Strain = Gage Factor(Current Reading - Zero Reading)

Note: The above calibration uses the linear regression method.

Users are advised to establish their own zero conditions.

Linearity: ((Calculated Load - Applied Load)/Max. Applied Load) X 100 percent

The above instrument was found to be in tolerance in all operating ranges.
The above named instrument has been calibrated by comparison with standards traceable to the NIST, in compliance with ANSI Z540-1.

GEOKON 48 Spencer St. Lebanon, NH 03766 USA

Sister Bar Calibration Report

Model Number:	4911-4	Date of Calibration:	October 14, 2014
			This calibration has been verified/validated as of 10/27/2014
Serial Number:	1432509	Cable Length:	70 feet
Prestress:	35,000 psi	Regression Zero:	7178
Temperature:	22.6 °C	Technician:	
Calibration Instruction:	CI-VW Rebar		

Applied Load (pounds)	Readings				Linearity % Max. Load
	Cycle #1	Cycle #2	Average	Change	
100	7235	7232	7234		
1500	7901	7899	7900	666	-0.25
3000	8638	8632	8635	735	-0.05
4500	9369	9364	9367	732	0.03
6000	10103	10092	10098	731	0.09
100	7232	7228	7230		

For conversion factor, load to strain, refer to table C-2 of the Installation Manual

Gage Factor: 0.347 microstrain/ digit (GK-401 Pos. "B")

Calculated Strain = Gage Factor(Current Reading - Zero Reading)

Note: The above calibration uses the linear regression method.

<u>Users are advised to establish their own zero conditions.</u>

Linearity: ((Calculated Load - Applied Load)/Max. Applied Load) X 100 percent

The above instrument was found to be in tolerance in all operating ranges.
The above named instrument has been calibrated by comparison with standards traceable to the NIST, in compliance with ANSI Z540-1.

GEOKON 48 Spencer St. Lebanon, NH 03766 USA

Sister Bar Calibration Report

Model Number: 4911-4

Date of Calibration: October 22, 2014

This calibration has been verified/validated as of 10/27/2014

Serial Number: 1432911

Cable Length: 65 feet

Prestress: 35,000 psi

Regression Zero: 6900

Temperature: 23.2 °C

Technician:

Calibration Instruction: CI-VW Rebar

Applied Load (pounds)	Readings				Linearity % Max. Load
	Cycle #1	Cycle #2	Average	Change	
100	6957	6956	6957		
1500	7628	7626	7627	670	-0.23
3000	8363	8360	8362	735	-0.20
4500	9106	9101	9104	742	0.08
6000	9840	9835	9838	734	0.09
100	6955	6953	6954		

For conversion factor, load to strain, refer to table C-2 of the Installation Manual

Gage Factor: 0.346 microstrain/ digit (GK-401 Pos. "B")

Calculated Strain = Gage Factor(Current Reading - Zero Reading)

Note: The above calibration uses the linear regression method.

Users are advised to establish their own zero conditions.

Linearity: ((Calculated Load - Applied Load)/Max. Applied Load) X 100 percent

The above instrument was found to be in tolerance in all operating ranges.
The above named instrument has been calibrated by comparison with standards traceable to the NIST, in compliance with ANSI Z540-1.

GEOKON 48 Spencer St. Lebanon, NH 03766 USA

Sister Bar Calibration Report

Model Number: 4911-4

Date of Calibration: October 22, 2014

This calibration has been verified/validated as of 10/27/2014

Serial Number: 1432912

Cable Length: 65 feet

Prestress: 35,000 psi

Regression Zero: 7173

Temperature: 23.2 °C

Technician:

Calibration Instruction: CI-VW Rebar

Applied Load (pounds)	Readings				Linearity % Max. Load
	Cycle #1	Cycle #2	Average	Change	
100	7231	7228	7230		
1500	7896	7894	7895	665	-0.20
3000	8623	8622	8623	728	-0.21
4500	9355	9357	9356	733	-0.01
6000	10091	10087	10089	733	0.17
100	7228	7227	7228		

For conversion factor, load to strain, refer to table C-2 of the Installation Manual

Gage Factor: 0.348 microstrain/ digit (GK-401 Pos. "B")

Calculated Strain = Gage Factor(Current Reading - Zero Reading)

Note: The above calibration uses the linear regression method.

Users are advised to establish their own zero conditions.

Linearity: ((Calculated Load - Applied Load)/Max. Applied Load) X 100 percent

The above instrument was found to be in tolerance in all operating ranges.
The above named instrument has been calibrated by comparison with standards traceable to the NIST, in compliance with ANSI Z540-1.

GEOKON 48 Spencer St. Lebanon, NH 03766 USA

Vibrating Wire Displacement Transducer Calibration Report

Range: 150 mm

Serial Number: 1417851

Calibration Instruction: CI-4400

Cable Length: 90 feet

Calibration Date: June 05, 2014

This calibration has been verified/validated as of 10/27/2014

Temperature: 23.4 °C

Technician:

GK-401 Reading Position B

Actual Displacement (mm)	Gage Reading 1st Cycle	Gage Reading 2nd Cycle	Average Gage Reading	Calculated Displacement Linear	Error Linear (%FS)	Calculated Displacement Polynomial	Error Polynomial (%FS)
0.0	2581	2578	2580	-0.41	-0.27	-0.04	-0.03
30.0	3586	3581	3584	30.12	0.08	30.05	0.03
60.0	4578	4576	4577	60.32	0.21	60.05	0.03
90.0	5561	5559	5560	90.21	0.14	89.94	-0.04
120.0	6541	6540	6541	120.02	0.01	119.97	-0.02
150.0	7516	7515	7516	149.66	-0.22	150.03	0.02

(mm) Linear Gage Factor (G): 0.03040 (mm/ digit) **Regression Zero: 2593**

Polynomial Gage Factors: A: 1.0987E-07 B: 0.02929 C: ______

Calculate C by setting D = 0 and R_1 = initial field zero reading into the polynomial equation

(inches) Linear Gage Factor (G): 0.001197 (inches/digit)

Polynomial Gage Factors: A: 4.3254E-09 B: 0.001153 C: ______

Calculate C by setting D = 0 and R_1 = initial field zero reading into the polynomial equation

Calculated Displacement: **Linear, $D = G(R_1 - R_0)$**

Polynomial, $D = AR_1^2 + BR_1 + C$

Refer to manual for temperature correction information.

The above instrument was found to be in tolerance in all operating ranges.
The above named instrument has been calibrated by comparison with standards traceable to the NIST, in compliance with ANSI Z540-1.

GEOKON 48 Spencer St. Lebanon, NH 03766 USA

Vibrating Wire Displacement Transducer Calibration Report

Range: 150 mm

Serial Number: 1417852

Calibration Instruction: CI-4400

Cable Length: 90 feet

Calibration Date: June 05, 2014

This calibration has been verified/validated as of 10/27/2014

Temperature: 23.4 °C

Technician:

GK-401 Reading Position B

Actual Displacement (mm)	Gage Reading 1st Cycle	Gage Reading 2nd Cycle	Average Gage Reading	Calculated Displacement Linear	Error Linear (%FS)	Calculated Displacement Polynomial	Error Polynomial (%FS)
0.0	2534	2533	2534	-0.29	-0.19	-0.03	-0.02
30.0	3529	3528	3529	30.13	0.09	30.07	0.05
60.0	4513	4512	4513	60.21	0.14	60.00	0.00
90.0	5493	5491	5492	90.16	0.11	89.94	-0.04
120.0	6470	6471	6471	120.08	0.05	120.02	0.01
150.0	7442	7440	7441	149.75	-0.17	150.00	0.00

(mm) Linear Gage Factor (G): 0.03057 (mm/ digit) **Regression Zero: 2543**

Polynomial Gage Factors: A: 8.1951E-08 B: 0.02976 C: ______

Calculate C by setting D = 0 and R_1 = initial field zero reading into the polynomial equation

(inches) Linear Gage Factor (G): 0.001204 (inches/digit)

Polynomial Gage Factors: A: 3.2264E-09 B: 0.001171 C: ______

Calculate C by setting D = 0 and R_1 = initial field zero reading into the polynomial equation

Calculated Displacement: **Linear, $D = G(R_1 - R_0)$**

Polynomial, $D = AR_1^2 + BR_1 + C$

Refer to manual for temperature correction information.

The above instrument was found to be in tolerance in all operating ranges.
The above named instrument has been calibrated by comparison with standards traceable to the NIST, in compliance with ANSI Z540-1.

GEOKON 48 Spencer St. Lebanon, NH 03766 USA

Vibrating Wire Displacement Transducer Calibration Report

Range: 150 mm

Calibration Date: July 25, 2014

This calibration has been verified/validated as of 10/27/2014

Serial Number: 1419714

Temperature: 23.5 °C

Calibration Instruction: CI-4400

Technician:

Cable Length: 90 feet

GK-401 Reading Position B

Actual Displacement (mm)	Gage Reading 1st Cycle	Gage Reading 2nd Cycle	Average Gage Reading	Calculated Displacement Linear	Error Linear (%FS)	Calculated Displacement Polynomial	Error Polynomial (%FS)
0.0	2720	2720	2720	-0.24	-0.16	-0.06	-0.04
30.0	3712	3711	3712	30.11	0.07	30.08	0.05
60.0	4696	4695	4696	60.24	0.16	60.10	0.07
90.0	5671	5664	5668	89.99	0.00	89.86	-0.09
120.0	6647	6649	6648	120.01	0.01	119.98	-0.01
150.0	7624	7622	7623	149.86	-0.09	150.04	0.03

(mm) Linear Gage Factor (G): 0.03062 (mm/ digit) **Regression Zero: 2728**

Polynomial Gage Factors: A: 5.4959E-08 B: 0.03005 C: ________

Calculate C by setting $D = 0$ and R_1 = initial field zero reading into the polynomial equation

(inches) Linear Gage Factor (G): 0.001205 (inches/digit)

Polynomial Gage Factors: A: 2.1638E-09 B: 0.001183 C: ________

Calculate C by setting $D = 0$ and R_1 = initial field zero reading into the polynomial equation

Calculated Displacement: **Linear, $D = G(R_1 - R_0)$**

Polynomial, $D = AR_1^2 + BR_1 + C$

Refer to manual for temperature correction information.

The above instrument was found to be in tolerance in all operating ranges.
The above named instrument has been calibrated by comparison with standards traceable to the NIST, in compliance with ANSI Z540-1.

GEOKON 48 Spencer St. Lebanon, NH 03766 USA

Vibrating Wire Displacement Transducer Calibration Report

Range: 150 mm

Serial Number: 1419715

Calibration Instruction: CI-4400

Cable Length: 90 feet

Calibration Date: July 25, 2014

This calibration has been verified/validated as of 10/27/2014

Temperature: 23.5 °C

Technician:

GK-401 Reading Position B

Actual Displacement (mm)	Gage Reading 1st Cycle	Gage Reading 2nd Cycle	Average Gage Reading	Calculated Displacement Linear	Error Linear (%FS)	Calculated Displacement Polynomial	Error Polynomial (%FS)
0.0	2758	2756	2757	-0.31	-0.21	-0.04	-0.03
30.0	3747	3745	3746	30.11	0.07	30.06	0.04
60.0	4726	4724	4725	60.22	0.14	60.01	0.00
90.0	5699	5703	5701	90.23	0.15	90.03	0.02
120.0	6666	6668	6667	119.94	-0.04	119.89	-0.07
150.0	7638	7637	7638	149.79	-0.14	150.06	0.04

(mm) Linear Gage Factor (G): 0.03075 (mm/ digit) **Regression Zero: 2767**

Polynomial Gage Factors: A: 8.3365E-08 B: 0.02989 C: ________

Calculate C by setting D = 0 and R_1 = initial field zero reading into the polynomial equation

(inches) Linear Gage Factor (G): 0.001211 (inches/digit)

Polynomial Gage Factors: A: 3.2821E-09 B: 0.001177 C: ________

Calculate C by setting D = 0 and R_1 = initial field zero reading into the polynomial equation

Calculated Displacement: **Linear, $D = G(R_1 - R_0)$**

Polynomial, $D = AR_1^2 + BR_1 + C$

Refer to manual for temperature correction information.

The above instrument was found to be in tolerance in all operating ranges.
The above named instrument has been calibrated by comparison with standards traceable to the NIST, in compliance with ANSI Z540-1.

APPENDIX C

CONSTRUCTION OF THE EQUIVALENT TOP LOAD-DISPLACEMENT CURVE

CONSTRUCTION OF THE EQUIVALENT TOP-LOADED LOAD-SETTLEMENT CURVE FROM THE RESULTS OF AN O-CELL TEST (August, 2000)

Introduction: Some engineers find it useful to see the results of an O-cell load test in the form of a curve showing the load versus settlement of a top-loaded driven or bored pile (drilled shaft). We believe that an O-cell test can provide a good estimate of this curve when using the method described herein.

Assumptions: We make the following assumptions, which we consider both reasonable and usually conservative:

1. The end bearing load-movement curve in a top-loaded shaft has the same loads for a given movement as the net (subtract buoyant weight of pile above O-cell) end bearing load-movement curve developed by the bottom of the O-cell when placed at or near the bottom of the shaft.

2. The side shear load-movement curve in a top-loaded shaft has the same net shear, multiplied by an adjustment factor 'F', for a given downward movement as occurred in the O-cell test for that same movement at the top of the cell in the upward direction. The same applies to the upward movement in a top-loaded tension test. Unless noted otherwise, we use the following adjustment factors:
(a) F = 1.00 in all rock sockets and for primarily cohesive soils in compression
(b) F = 0.95 in primarily cohesionless soils
(c) F = 0.80 for all soils in top load tension tests.

3. We initially assume the pile behaves as a rigid body, but include the elastic compressions that are part of the movement data obtained from an O-cell test (OLT). Using this assumption, we construct an equivalent top-load test (TLT) movement curve by the method described below in Procedure Part I. We then use the following Procedure Part II to correct for the effects of the additional elastic compressions in a TLT.

4. Consider the case with the O-cell, or the bottom O-cell of more than one level of cells, placed some distance above the bottom of the shaft. We assume the part of the shaft below the cell, now top-loaded, has the same load-movement behavior as when top-loading the entire shaft. For this case the subsequent "end bearing movement curve" refers to the movement of the entire length of shaft below the cell.

Procedure Part I: Please refer to the attached Figure A showing O-cell test results and to Figure B, the constructed equivalent top loaded settlement curve. Note that each of the curves shown has points numbered from 1 to 12 such that the same point number on each curve has the same magnitude of movement. For example, point 4 has an upward and downward movement of 0.40 inches in Figure A and the same 0.40 inches downward in Figure B.

Note: This report shows the O-cell movement data in a Figure similar to Fig. A, but uses the gross loads as obtained in the field. Fig. A uses net loads to make it easier for the reader to convert Fig. A into Fig. B without the complication of first converting gross to net loads. For conservative reconstruction of the top loaded settlement curve we first convert both of the O-cell components to net load.

Using the above assumptions, construct the equivalent curve as follows: Select an arbitrary movement such as the 0.40 inches to give point 4 on the shaft side shear load movement curve in Figure A and record the 2,090 ton load in shear at that movement. Because we have initially assumed a rigid pile, the top of pile moves downward the same as the bottom. Therefore, find point 4 with 0.40 inches of upward movement on the end bearing load movement curve and record the corresponding load of 1,060 tons. Adding these two loads will give the total load of 3,150 tons due to side shear plus end bearing at the same movement and thus gives point 4 on the Figure B load settlement curve for an equivalent top-loaded test.

One can use the above procedure to obtain all the points in Figure B up to the component that moved the least at the end of the test, in this case point 5 in side shear. To take advantage of the fact that the test produced end bearing movement data up to point 12, we need to make an extrapolation of the side shear curve. We usually use a convenient and suitable hyperbolic curve fitting technique for this extrapolation. Deciding on the maximum number of data points to provide a good fit (a high r^2 correlation coefficient) requires some judgment. In this case we omitted point 1 to give an $r^2 = 0.999$ (including point 1 gave an $r^2 = 0.966$) with the result shown as points 6 to 12 on the dotted extension of the measured side shear curve. Using the same movement matching procedure described earlier we can then extend the equivalent curve to points 6 to 12. The results, shown in Figure B as a dashed line, signify that this part of the equivalent curve depends partly on extrapolated data.

Sometimes, if the data warrants, we will use extrapolations of both side shear and end bearing to extend the equivalent curve to a greater movement than the maximum measured (point 12). An appendix in this report gives the details of the extrapolation(s) used with the present O-cell test and shows the fit with the actual data.

Procedure Part II: The elastic compression in the equivalent top load test always exceeds that in the O-cell test. It not only produces more top movement, but also additional side shear movement, which then generates more side shear, which produces more compression, etc . . . An exact solution of this load transfer problem requires knowing the side shear vs. vertical movement (t-y) curves for a large number of pile length increments and solving the resulting set of simultaneous equations or using finite element or finite difference simulations to obtain an approximate solution for these equations. We usually do not have the data to obtain the many accurate t-y curves required. Fortunately, the approximate solution described below usually suffices.

The attached analysis p. 6 gives the equations for the elastic compressions that occur in the OLT with one or two levels of O-cells. Analysis p. 7 gives the equations for the elastic compressions that occur in the equivalent TLT. Both sets of equations do not include the elastic compression below the O-cell because the same compression takes place in both the OLT and the TLT. This is equivalent to taking $L_3 = 0$. Subtracting the OLT from the TLT compression gives the desired additional elastic compression at the top of the TLT. We then add the additional elastic compression to the 'rigid' equivalent curve obtained from Part I to obtain the final, corrected equivalent load-settlement curve for the TLT on the same pile as the actual OLT.

Note that the above pp. 6 and 7 give equations for each of three assumed patterns of developed side shear stress along the pile. The pattern shown in the center of the three applies to any approximately determined side shear distribution. Experience has shown the initial solution for the additional elastic compression, as described above, gives an adequate and slightly conservative (high) estimate of the additional compression versus more sophisticated load-transfer analyses as described in the first paragraph of this Part II.

The analysis p. 8 provides an example of calculated results in English units on a hypothetical 1-stage, single level OLT using the simplified method in Part II with the centroid of the side shear distribution 44.1% above the base of the O-cell. Figure C compares the corrected with the rigid curve of Figure B. Page 9 contains an example equivalent to that above in SI units.

The final analysis p. 10 provides an example of calculated results in English units on a hypothetical 3-stage, multi level OLT using the simplified method in Part II with the centroid of the combined upper and middle side shear distribution 44.1% above the base of the bottom O-cell. The individual centroids of the upper and middle side shear distributions lie 39.6% and 57.9% above and below the middle O-cell, respectively. Figure E compares the corrected with the rigid curve. Page 11 contains an example equivalent to that above in SI units.

Other Tests: The example illustrated in Figure A has the maximum component movement in end bearing. The procedures remain the same if the maximum test movement occurred in side shear. Then we would have extrapolated end bearing to produce the dashed-line part of the reconstructed top-load settlement curve.

The example illustrated also assumes a pile top-loaded in compression. For a pile top-loaded in tension we would, based on Assumptions 2. and 3., use the upward side shear load curve in Figure A, multiplied by the F = 0.80 noted in Assumption 2., for the equivalent top-loaded displacement curve.

Expected Accuracy: We know of only five series of tests that provide the data needed to make a direct comparison between actual, full scale, top-loaded pile movement behavior and the equivalent behavior obtained from an O-cell test by the method described herein. These involve three sites in Japan and one in Singapore, in a variety of soils, with three compression tests on bored piles (drilled shafts), one compression test on a driven pile and one tension test on a bored pile. The largest bored pile had a 1.2-m diameter and a 37-m length. The driven pile had a 1-m increment modular construction and a 9-m length. The largest top loading = 28 MN (3,150 tons).

The following references detail the aforementioned Japanese tests and the results therefrom:

Kishida H. et al., 1992, "Pile Loading Tests at Osaka Amenity Park Project," Paper by Mitsubishi Co., also briefly described in Schmertmann (1993, see bibliography). Compares one drilled shaft in tension and another in compression.

Ogura, H. et al., 1995, "Application of Pile Toe Load Test to Cast-in-place

Concrete Pile and Precast Pile," special volume 'Tsuchi-to-Kiso' on Pile Loading Test, Japanese Geotechnical Society, Vol. 3, No. 5, Ser. No. 448. Original in Japanese. Translated by M. B. Karkee, GEOTOP Corporation. Compares one drilled shaft and one driven pile, both in compression.

We compared the predicted equivalent and measured top load at three top movements in each of the above four Japanese comparisons. The top movements ranged from ¼ inch (6 mm) to 40 mm, depending on the data available. The (equiv./meas.) ratios of the top load averaged 1.03 in the 15 comparisons with a coefficient of variation of less than 10%. We believe that these available comparisons help support the practical validity of the equivalent top load method described herein.

L. S. Peng, A. M. Koon, R. Page and C. W. Lee report the results of a class-A prediction by others of the TLT curve from an Osterberg cell test on a 1.2 m diameter, 37.2 m long bored pile in Singapore, compared to an adjacent pile with the same dimensions actually top-loaded by kentledge. They report about a 4% difference in ultimate capacity and less than 8% difference in settlements over the 1.0 to 1.5 times working load range -- comparable to the accuracy noted above. Their paper has the title "OSTERBERG CELL TESTING OF PILES", and was published in March 1999 in the Proceedings of the International Conference on Rail Transit, held in Singapore and published by the Association of Consulting Engineers Singapore.

B. H. Fellenius has made several finite element method (FEM) studies of an OLT in which he adjusted the parameters to produce good load-deflection matches with the OLT up and down load-deflection curves. He then used the same parameters to predict the TLT deflection curve. We compared the FEM-predicted curve with the equivalent load-deflection predicted by the previously described Part I and II procedures, with the results again comparable to the accuracy noted above. The ASCE has published a paper by Fellenius et. al. titled "O-Cell Testing and FE Analysis of 28-m-Deep Barrette in Manila, Philippines" in the Journal of Geotechnical and Geoenvironmental Engineering, Vol. 125, No. 7, July 1999, p. 566. It details one of his comparison studies.

Limitations: The engineer using these results should judge the conservatism, or lack thereof, of the aforementioned assumptions and extrapolation(s) before utilizing the results for design purposes. For example, brittle failure behavior may produce movement curves with abrupt changes in curvature (not hyperbolic). However, we believe the hyperbolic fit method and our assumptions used usually produce reasonable equivalent top load settlement curves.

August, 2000

Example of the Construction of an Equivalent Top-Loaded Settlement Curve (Figure B) From Osterberg Cell Test Results (Figure A)

Figure A

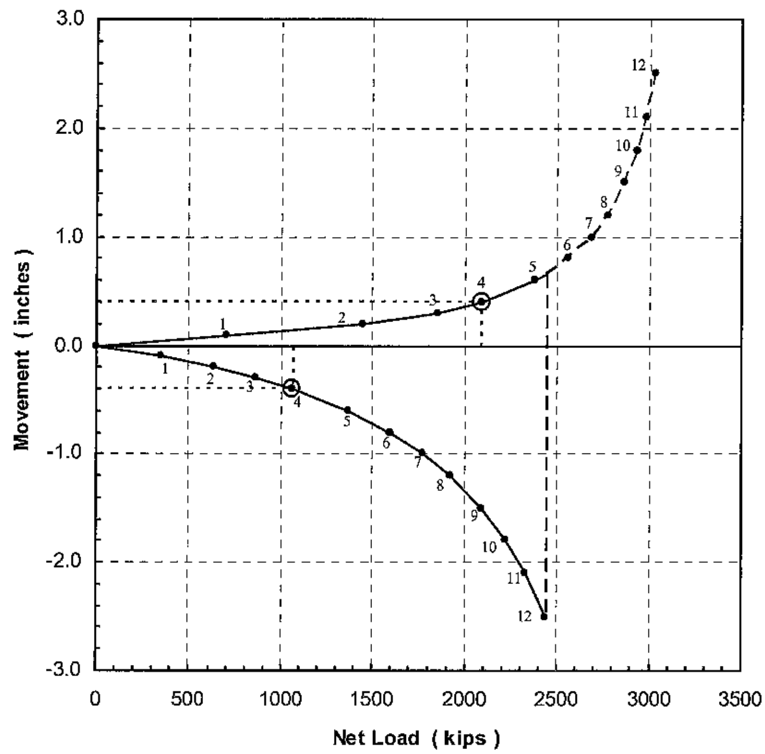

Figure B

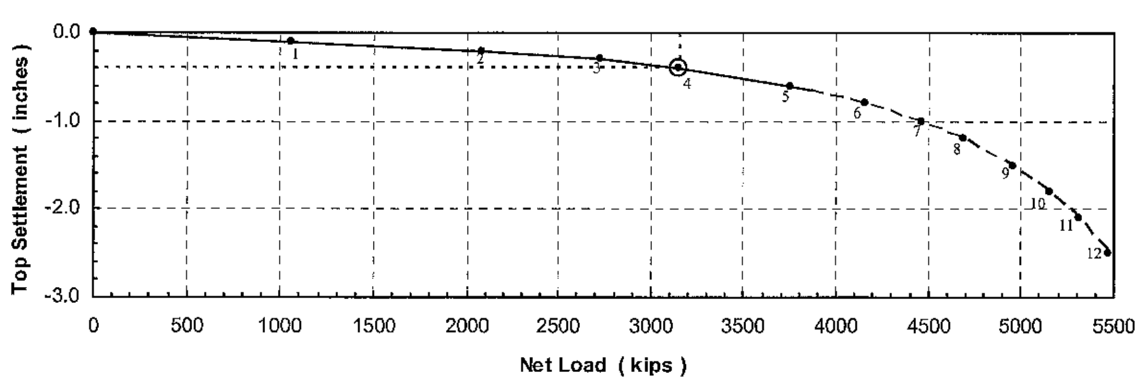

Theoretical Elastic Compression in O-cell Test
Based on Pattern of Developed Side Shear Stress

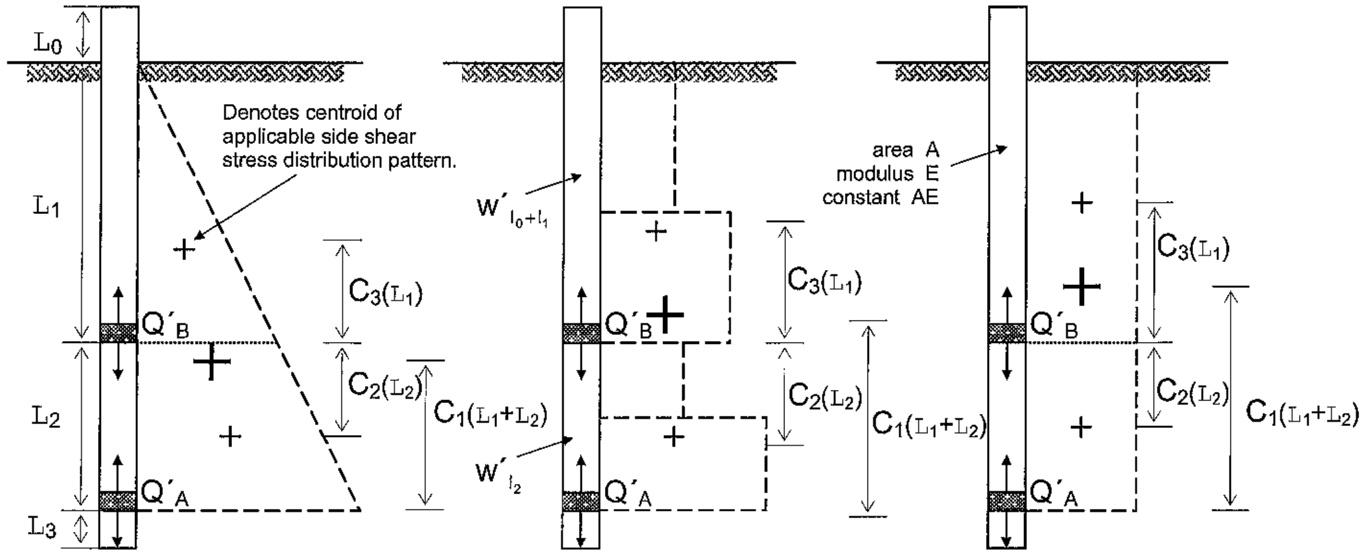

1-Stage Single Level Test (Q'_A only):

$$\delta_{OLT} = \delta_{\uparrow(l_1+l_2)}$$

$C_1 = \frac{1}{3}$	Centroid Factor $= C_1$	$C_1 = \frac{1}{2}$
$\delta_{\uparrow(l_1+l_2)} = \frac{1}{3}\frac{Q'_{\uparrow A}(l_1+l_2)}{AE}$	$\delta_{\uparrow(l_1+l_2)} = C_1\frac{Q'_{\uparrow A}(l_1+l_2)}{AE}$	$\delta_{\uparrow(l_1+l_2)} = \frac{1}{2}\frac{Q'_{\uparrow A}(l_1+l_2)}{AE}$

3-Stage Multi Level Test (Q'_A and Q'_B): $\delta_{OLT} = \delta_{\uparrow l_1} + \delta_{\downarrow l_2}$

$C_3 = \frac{1}{3}$	Centroid Factor $= C_3$	$C_3 = \frac{1}{2}$
$\delta_{\uparrow l_1} = \frac{1}{3}\frac{Q'_{\uparrow B} l_1}{AE}$	$\delta_{\uparrow l_1} = C_3\frac{Q'_{\uparrow B} l_1}{AE}$	$\delta_{\uparrow l_1} = \frac{1}{3}\frac{Q'_{\uparrow B} l_1}{AE}$
$C_2 = \frac{1}{3}\left(\frac{3l_1+2l_2}{2l_1+l_2}\right)$	Centroid Factor $= C_2$	$C_2 = \frac{1}{2}$
$\delta_{\downarrow l_2} = \frac{1}{3}\left(\frac{3l_1+2l_2}{2l_1+l_2}\right)\frac{Q'_{\downarrow B} l_2}{AE}$	$\delta_{\downarrow l_2} = C_2\frac{Q'_{\downarrow B} l_2}{AE}$	$\delta_{\downarrow l_2} = \frac{1}{2}\frac{Q'_{\downarrow B} l_2}{AE}$

Net Loads:

$Q'_{\uparrow A} = Q_{\uparrow A} - W'_{l_0+l_1+l_2}$ $\qquad Q'_{\uparrow B} = Q_{\uparrow B} - W'_{l_0+l_1}$ $\qquad Q'_{\downarrow B} = Q'_{\downarrow B} + W'_{l_2}$

W' = pile weight, buoyant where below water table

Theoretical Elastic Compression in Top Loaded Test Based on Pattern of Developed Side Shear Stress

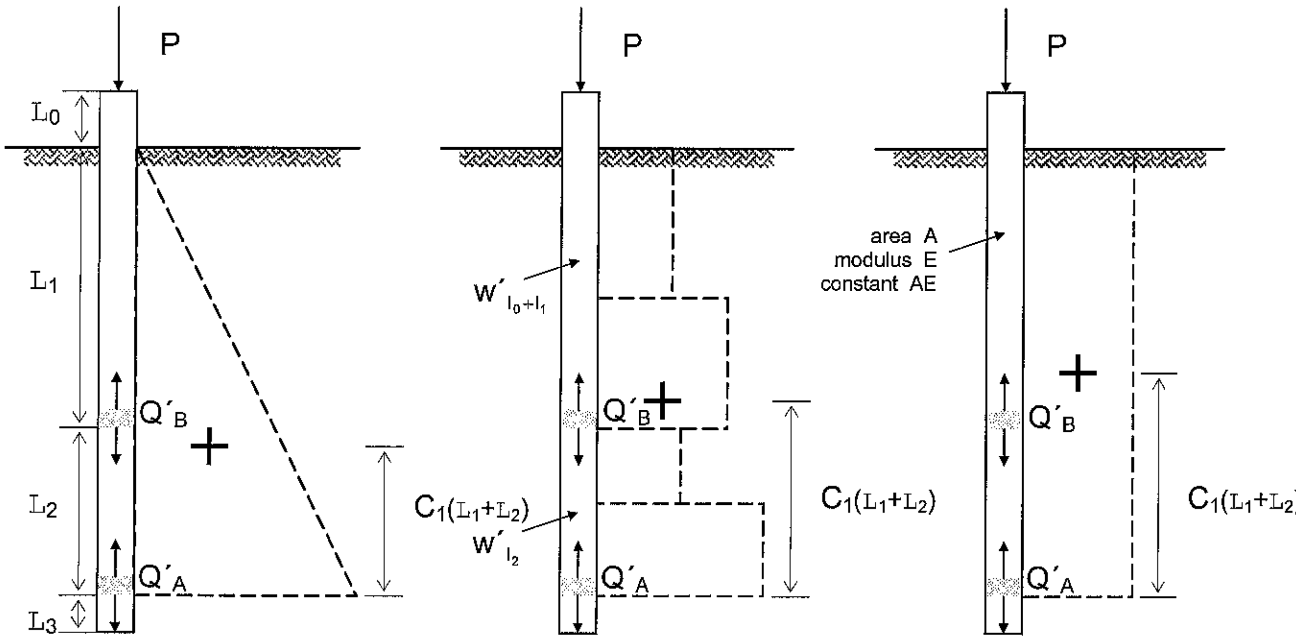

Top Loaded Test: $\delta_{TLT} = \delta_{\downarrow l_0} + \delta_{\downarrow l_1+l_2}$

$\delta_{\downarrow l_0} = \frac{Pl_0}{AE}$	$\delta_{\downarrow l_0} = \frac{Pl_0}{AE}$	$\delta_{\downarrow l_0} = \frac{Pl_0}{AE}$
$C_1 = \frac{1}{3}$	Centroid Factor $= C_1$	$C_1 = \frac{1}{2}$
$\delta_{\downarrow l_1+l_2} = \frac{(Q'_{\downarrow A}+2P)}{3}\frac{(l_2+l_2)}{AE}$	$\delta_{\downarrow l_1+l_2} = [(C_1)Q'_{\downarrow A}+(1-C_1)P]\frac{(l_1+l_2)}{AE}$	$\delta_{\downarrow l_1+l_2} = \frac{(Q'_{\downarrow A}+P)}{2}\frac{(l_1+l_2)}{AE}$

Net and Equivalent Loads:

$Q'_{\downarrow A} = Q_{\downarrow A} - W'_{l_0+l_1+l_2}$ $\quad P_{single} = Q'_{\downarrow A} + Q'_{\uparrow A}$ $\quad P_{multi} = Q'_{\downarrow A} + Q'_{\uparrow B} + Q'_{\downarrow B}$

Component loads Q selected at the same (±) Δ_{OLT}.

Example Calculation for the Additional Elastic Compression Correction For Single Level Test (English Units)

Given:

C_1	=	0.441	
AE	=	3,820,000	kips (assumed constant throughout test)
I_0	=	5.9	ft
I_1	=	30.0	ft (embedded length of shaft above O-cell)
I_2	=	0.00	ft
I_3	=	0.0	ft
Shear reduction factor	=	1.00	(cohesive soil)

Δ_{OLT} (in)	$Q'_{\downarrow A}$ (kips)	$Q'_{\uparrow A}$ (kips)	P (kips)	δ_{TLT} (in)	δ_{OLT} (in)	Δ_δ (in)	$\Delta_{OLT} + \Delta_\delta$ (in)
0.000	0	0	0	0.000	0.000	0.000	0.000
0.100	352	706	1058	0.133	0.047	0.086	0.186
0.200	635	1445	2080	0.257	0.096	0.160	0.360
0.300	867	1858	2725	0.339	0.124	0.215	0.515
0.400	1061	2088	3149	0.396	0.139	0.256	0.656
0.600	1367	2382	3749	0.478	0.159	0.319	0.919
0.800	1597	2563	4160	0.536	0.171	0.365	1.165
1.000	1777	2685	4462	0.579	0.179	0.400	1.400
1.200	1921	2773	4694	0.613	0.185	0.427	1.627
1.500	2091	2867	4958	0.651	0.191	0.460	1.960
1.800	2221	2933	5155	0.680	0.196	0.484	2.284
2.100	2325	2983	5308	0.703	0.199	0.504	2.604
2.500	2434	3032	5466	0.726	0.202	0.524	3.024

Figure C

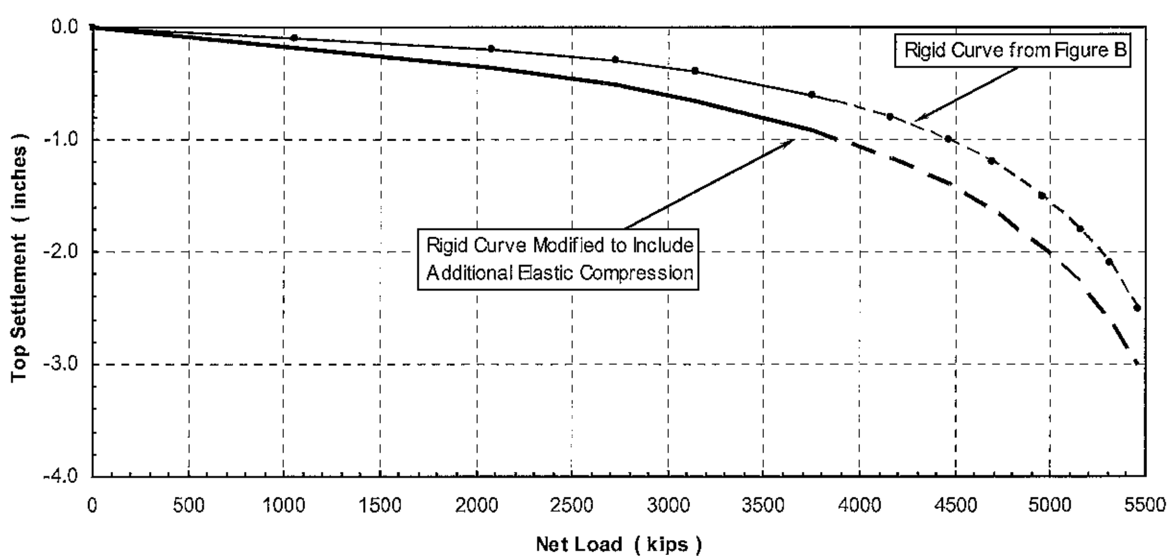

Example Calculation for the Additional Elastic Compression Correction For Single Level Test (SI Units)

Given:

C_1	=	0.441	
AE	=	17,000	MN (assumed constant throughout test)
I_0	=	1.80	m
I_1	=	14.69	m (embedded length of shaft above mid-cell)
I_2	=	0.00	m
I_3	=	0.0	m
Shear reduction factor	=	1.00	(cohesive soil)

Δ_{OLT} (mm)	$Q'_{\downarrow A}$ (MN)	$Q'_{\uparrow A}$ (mm)	P (MN)	δ_{TLT} (mm)	δ_{OLT} (mm)	Δ_δ (mm)	$\Delta_{OLT} + \Delta_\delta$ (mm)
0.00	0.00	0.00	0.00	0.00	0.00	0.00	0.00
2.54	1.57	3.14	4.71	3.37	1.20	2.17	4.71
5.08	2.82	6.43	9.25	6.52	2.45	4.07	9.15
7.62	3.86	8.27	12.12	8.61	3.15	5.46	13.08
10.16	4.72	9.29	14.01	10.05	3.54	6.51	16.67
15.24	6.08	10.60	16.68	12.14	4.04	8.10	23.34
20.32	7.11	11.40	18.50	13.60	4.34	9.26	29.58
25.40	7.90	11.94	19.85	14.70	4.55	10.15	35.55
30.48	8.55	12.33	20.88	15.55	4.70	10.85	41.33
38.10	9.30	12.75	22.05	16.53	4.86	11.67	49.77
45.72	9.88	13.05	22.93	17.27	4.97	12.29	58.01
53.34	10.34	13.27	23.61	17.84	5.06	12.79	66.13
63.50	10.83	13.48	24.31	18.44	5.14	13.30	76.80

Figure D

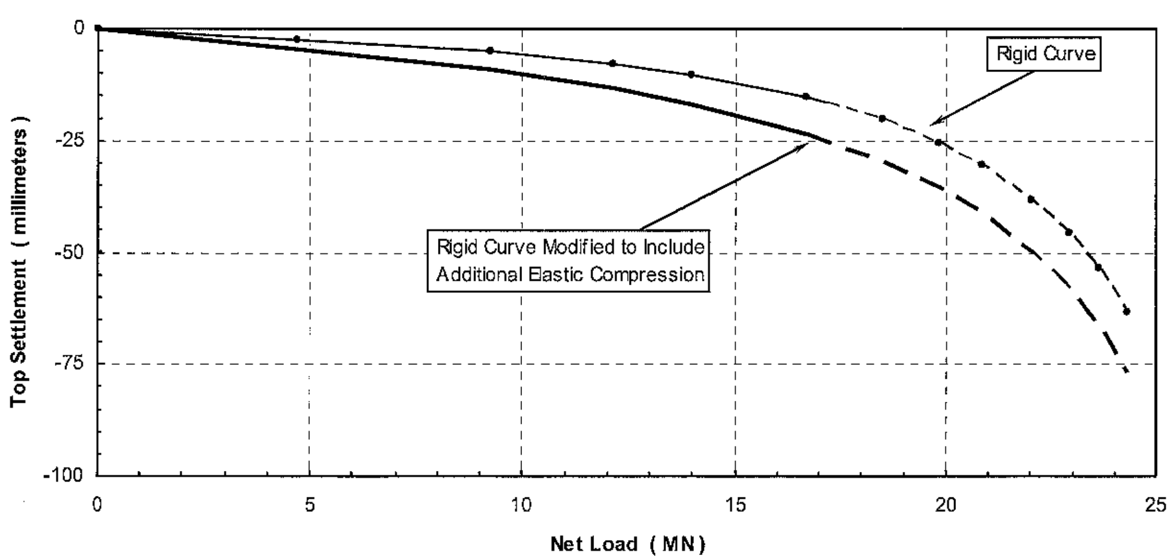

Example Calculation for the Additional Elastic Compression Correction For Multi Level Test (English Units)

Given:

C_1	=	0.441	
C_2	=	0.579	
C_3	=	0.396	
AE	=	3,820,000	kips (assumed constant throughout test)
I_0	=	5.9	ft
I_1	=	30.0	ft (embedded length of shaft above mid-cell)
I_2	=	18.2	ft (embedded length of shaft between O-cells)
I_3	=	0.0	ft
Shear reduction factor	=	1.00	(cohesive soil)

Δ_{OLT} (in)	$Q'_{\downarrow A}$ (kips)	$Q'_{\downarrow B}$ (kips)	$Q'_{\uparrow A}$ (kips)	P (kips)	δ_{TLT} (in)	δ_{OLT} (in)	Δ_δ (in)	$\Delta_{OLT} + \Delta_\delta$ (in)
0.000	0	0	0	0	0.000	0.000	0.000	0.000
0.100	352	247	459	1058	0.133	0.025	0.107	0.207
0.200	635	506	939	2080	0.257	0.052	0.205	0.405
0.300	867	650	1208	2725	0.339	0.067	0.272	0.572
0.400	1061	731	1357	3149	0.396	0.075	0.321	0.721
0.600	1367	834	1548	3749	0.478	0.085	0.393	0.993
0.800	1597	897	1666	4160	0.536	0.092	0.444	1.244
1.000	1777	940	1745	4462	0.579	0.096	0.483	1.483
1.200	1921	971	1802	4694	0.613	0.099	0.513	1.713
1.500	2091	1003	1864	4958	0.651	0.103	0.548	2.048
1.800	2221	1027	1907	5155	0.680	0.105	0.575	2.375
2.100	2325	1044	1939	5308	0.703	0.107	0.596	2.696
2.500	2434	1061	1971	5466	0.726	0.109	0.618	3.118

Figure E

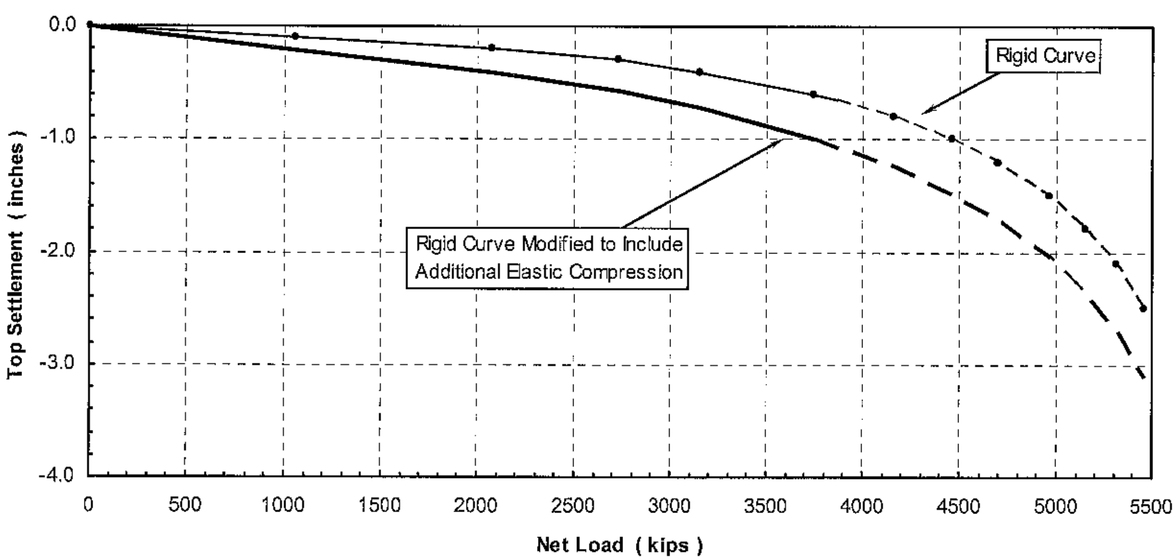

Example Calculation for the Additional Elastic Compression Correction For Multi Level Test (SI Units)

Given:

C_1	=	0.441	
C_2	=	0.579	
C_3	=	0.396	
AE	=	17,000	MN (assumed constant throughout test)
I_0	=	1.80	m
I_1	=	9.14	m (embedded length of shaft above mid-cell)
I_2	=	5.55	m (embedded length of shaft between O-cells)
I_3	=	0.00	m
Shear reduction factor	=	1.00	(cohesive soil)

Δ_{OLT} (mm)	$Q'_{\downarrow A}$ (MN)	$Q'_{\downarrow B}$ (MN)	$Q'_{\uparrow B}$ (mm)	P (MN)	δ_{TLT} (mm)	δ_{OLT} (mm)	Δ_δ (mm)	$\Delta_{OLT} + \Delta_\delta$ (mm)
0.00	0.00	0.00	0.00	0.00	0.00	0.00	0.00	0.00
2.54	1.57	1.10	2.04	4.71	3.37	0.64	2.73	5.27
5.08	2.82	2.25	4.18	9.25	6.52	1.31	5.21	10.29
7.62	3.86	2.89	5.37	12.12	8.61	1.69	6.92	14.54
10.16	4.72	3.25	6.04	14.01	10.05	1.90	8.15	18.31
15.24	6.08	3.71	6.89	16.68	12.14	2.17	9.97	25.21
20.32	7.11	3.99	7.41	18.50	13.60	2.33	11.27	31.59
25.40	7.90	4.18	7.76	19.85	14.70	2.44	12.26	37.66
30.48	8.55	4.32	8.02	20.88	15.55	2.52	13.03	43.51
38.10	9.30	4.46	8.29	22.05	16.53	2.61	13.92	52.02
45.72	9.88	4.57	8.48	22.93	17.27	2.67	14.60	60.32
53.34	10.34	4.64	8.62	23.61	17.84	2.71	15.13	68.47
63.50	10.83	4.72	8.76	24.31	18.44	2.76	15.68	79.18

Figure F

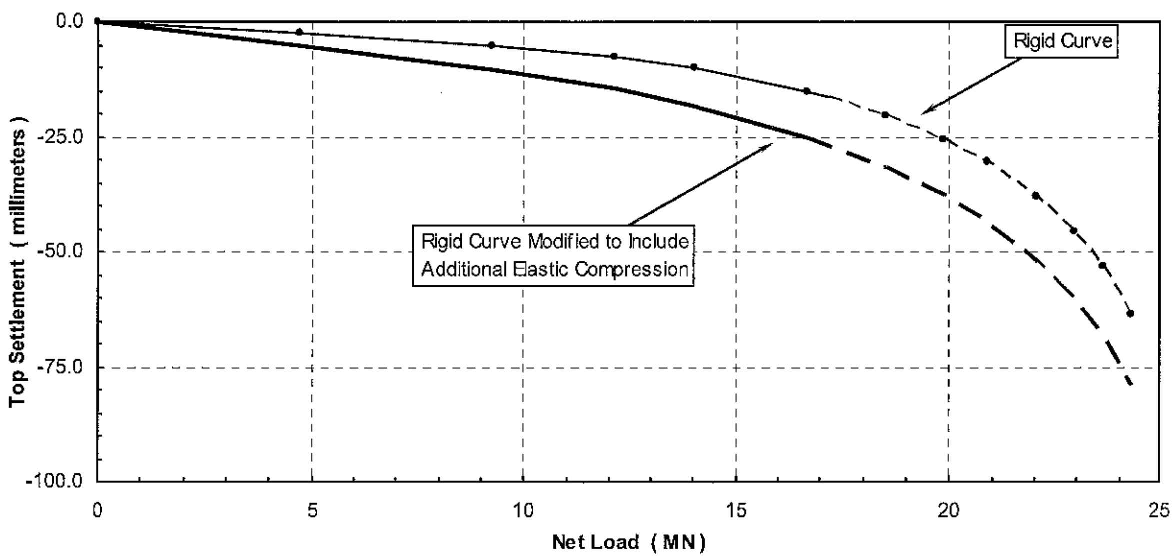

APPENDIX D

O-CELL METHOD FOR DETERMINING CREEP LIMIT LOADING

O-CELL METHOD FOR DETERMINING A CREEP LIMIT LOADING ON THE EQUIVALENT TOP-LOADED SHAFT (September, 2000)

Background: O-cell testing provides a sometimes useful method for evaluating that load beyond which a top-loaded drilled shaft might experience significant unwanted creep behavior. We refer to this load as the "creep limit," also sometimes known as the "yield limit" or "yield load".

To our knowledge, Housel (1959) first proposed the method described below for determining the creep limit. Stoll (1961), Bourges and Levillian (1988), and Fellenius (1996) provide additional references. This method also follows from long experience with the pressuremeter test (PMT). Figure 8 and section 9.4 from ASTM D4719-94, reproduced below, show and describe the creep curve routinely determined from the PMT. The creep curve shows how the movement or strain obtained over a fixed time interval, 30 to 60 seconds, changes versus the applied pressure. One can often detect a distinct break in the curve at the pressure P_e in Figure 8. Plastic deformations may become significant beyond this break loading and progressively more severe creep can occur.

Definition: Similarly with O-cell testing using the ASTM Quick Method, one can conveniently measure the additional movement occurring over the final time interval at each constant load step, typically 2 to 4 minutes. A break in the curve of load vs. movement (as at P_e with the PMT) indicates the creep limit.

We usually indicate such a creep limit in the O-cell test for either one, or both, of the side shear and end bearing components, and herein designate the corresponding movements as M_{CL1} and M_{CL2}. We then combine the creep limit data to predict a creep limit load for the equivalent top loaded shaft.

Procedure if both M_{CL1} and M_{CL2} available: Creep cannot begin until the shaft movement exceeds the M_{CL} values. A conservative approach would assume that creep begins when movements exceed the lesser of the M_{CL} values. However, creep can occur freely only when the shaft has moved the greater of the two M_{CL} values. Although less conservative, we believe the latter to match behavior better and therefore set the creep limit as that load on the equivalent top-loaded movement curve that matches the greater M_{CL}.

Procedure if only M_{CL1} available: If we cannot determine a creep limit in the second component before it reaches its maximum movement M_x, we treat M_x as M_{CL2}. From the above method one can say that the creep limit load exceeds, by some unknown amount, that obtained when using $M_{CL2} = M_x$.

Procedure if no creep limit observed: Then, according to the above, the creep limit for the equivalent top-loaded shaft will exceed, again by some unknown amount, that load on the equivalent curve that matches the movement of the component with the maximum movement.

Limitations: The accuracy in estimating creep limits depends, in part, on the scatter of the data in the creep limit plots. The more scatter, the more difficult to define a limit. The user should make his or her own interpretation if he or she intends to make important use of the creep limit interpretations. Sometimes we obtain excessive scatter of the data and do not attempt an interpretation for a creep limit and will indicate this in the report.

Excerpts from ASTM D4719
"Standard Test Method for Pressuremeter Testing in Soils"

9.4 For Procedure A, plot the volume increase readings (V_{60}) between the 30 s and 60 s reading on a separate graph. Generally, a part of the same graph is used, see Fig. 8. For Procedure B, plot the pressure decrease reading between the 30 s and 60 s reading on a separate graph. The test curve shows an almost straight line section within the range of either low volume increase readings (V_{60}) for Procedure A or low pressure decrease for Procedure B. In this range, a constant soil deformation modulus can be measured. Past the so-called creep pressure, plastic deformations become prevalent.

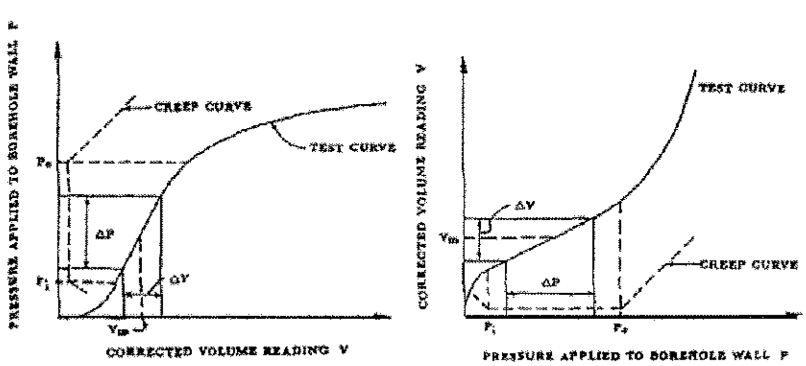

FIG. 8 Pressuremeter Test Curves for Procedure A

References

Housel, W.S. (1959), "Dynamic & Static Resistance of Cohesive Soils", ASTM STP 254, pp. 22-23.

Stoll, M.U.W. (1961, Discussion, Proc. 5th ICSMFE, Paris, Vol. III, pp. 279-281.

Bourges, F. and Levillian, J-P (1988), "force portante des rideaux plans metalliques charges verticalmement," Bull. No. 158, Nov.-Dec., des laboratoires des ponts et chaussees, p. 24.

Fellenius, Bengt H. (1996), Basics of Foundation Design, BiTech Publishers Ltd., p.79.

LOADTEST

Combined End Bearing and Lower Side Shear Creep Limit

TS-1 - IL-89 Over Illinois River - Bureau Putnam Counties, IL

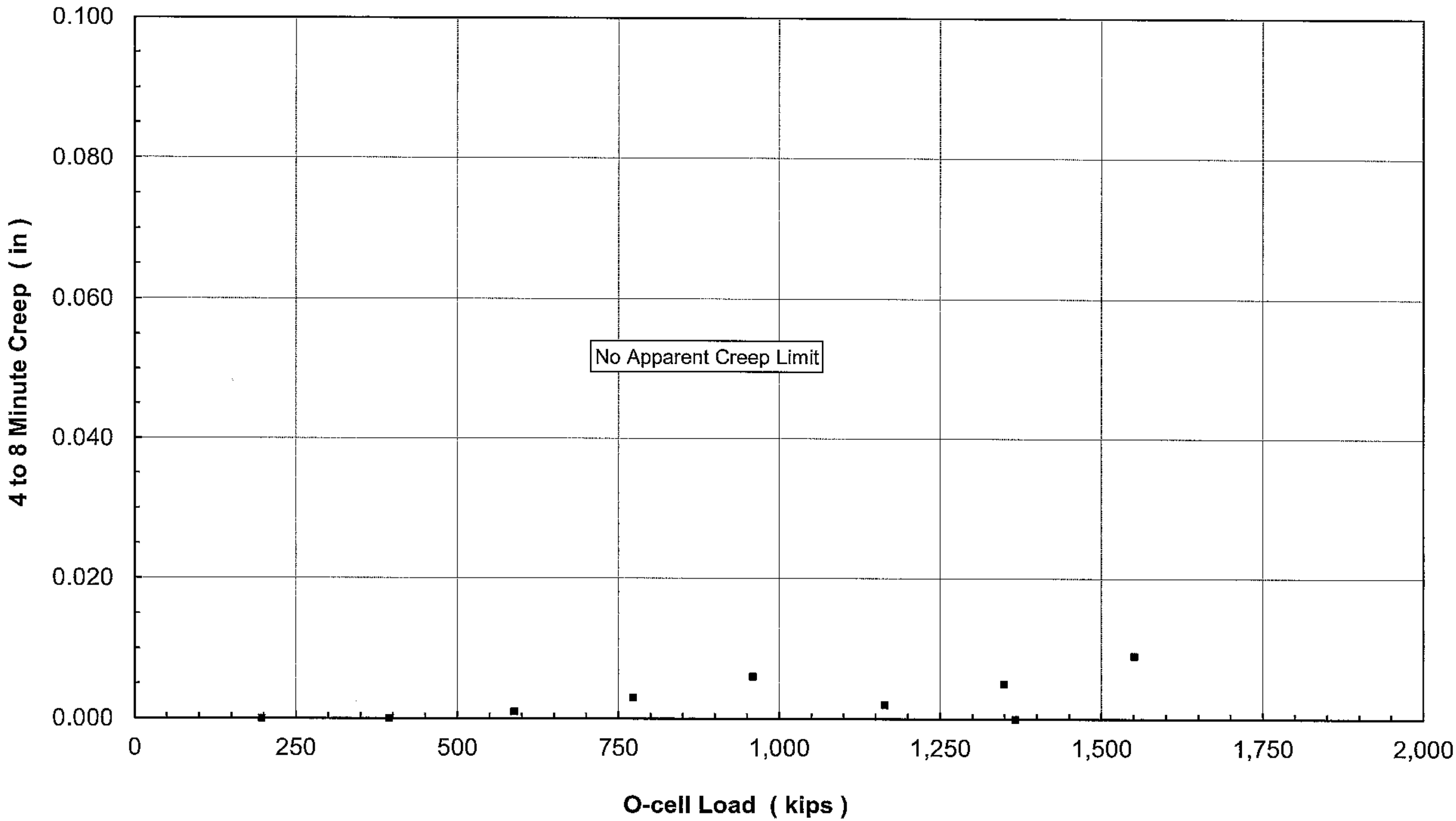

Figure D-1

Upper Side Shear Creep Limit

TS-1 - IL-89 Over Illinois River - Bureau Putnam Counties, IL

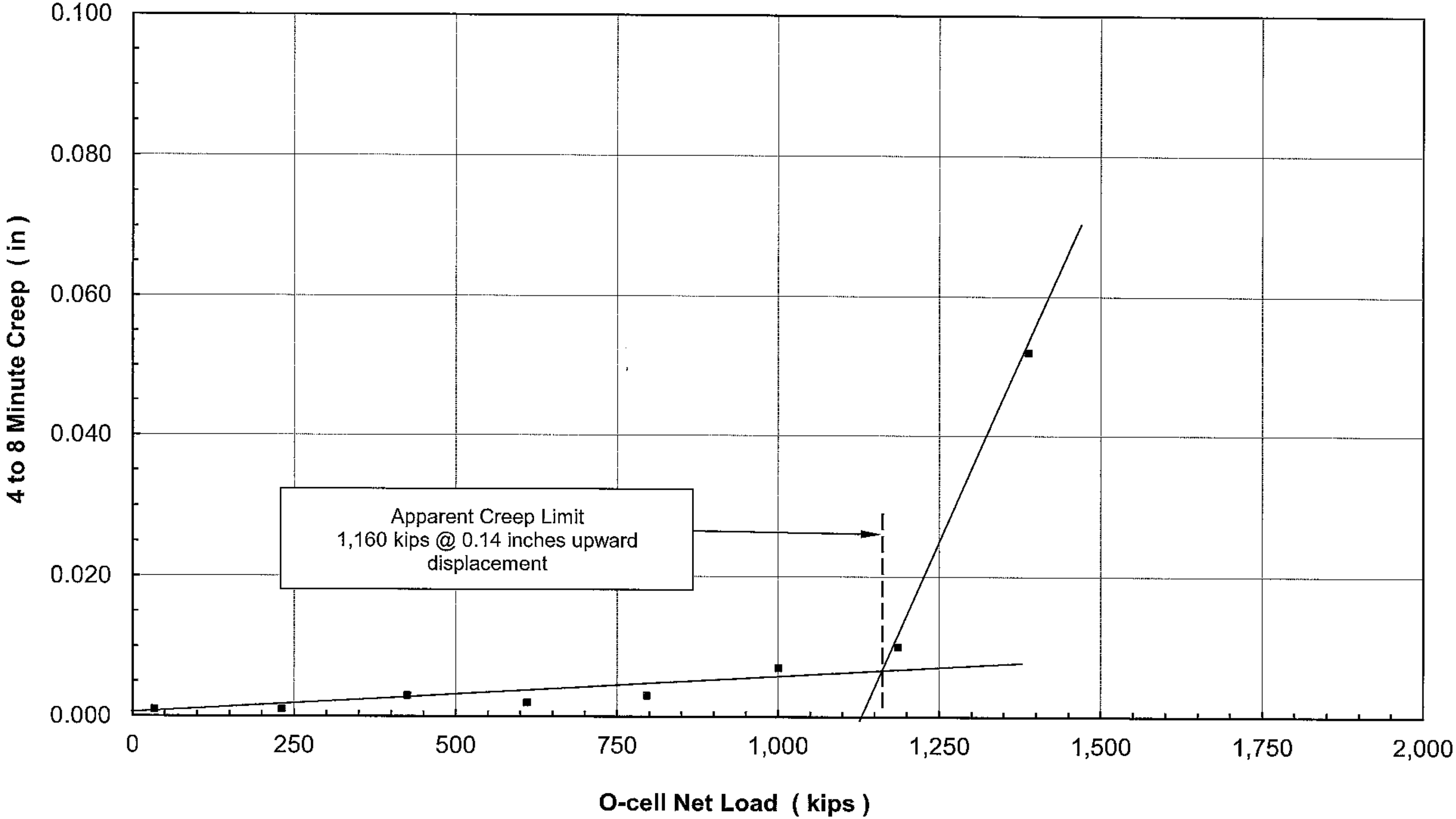

Loadtest USA Project No. LT-1407

Figure D-2

APPENDIX E

SOIL BORING LOG

Illinois Department of Transportation
Division of Highways
IDOT

SOIL BORING LOG

Date 5/21/14

ROUTE IL 89 (FAP 698) DESCRIPTION IL 89 over Illinois River at Spring Valley LOGGED BY TLM

SECTION (1)BR LOCATION SE 1/4, **SEC.** 3, **TWP.** 15N, **RNG.** 11E, 4th **PM**, **Latitude** 41.3125453, **Longitude** -89.1996188

COUNTY Putnam, Bureau DRILLING METHOD Mud Rotary HAMMER TYPE Automatic

STRUCT. NO. 078-0047 (Prop.) 078-0006 (Exist.)
Station 57+32 (Exist.)

BORING NO. 103M (Pier #3)
Station 155+19.38
Offset 3.0 ft Lt.
Ground Surface Elev. 453.15 ft

Surface Water Elev. 448.35 ft
Stream Bed Elev. 423.15 ft

Groundwater Elev.:
First Encounter ____ ft
Upon Completion ____ ft
After ____ Hrs. ____ ft

	DEPTH (ft)	BLOWS (/6")	UCS Qu (tsf)	MOIST (%)
Barge Deck Ground Surface Elevation = Barge Deck Elevation				
River Water 448.35	-5			
	-10			
	-15			
	-20			

	DEPTH (ft)	BLOWS (/6")	UCS Qu (tsf)	MOIST (%)
	-25			
Stream Bed 423.15	-30			
Soft Gray Sandy Clay with Shells				
	-35			
	-40			

DRAFT

The Unconfined Compressive Strength (UCS) Failure Mode is indicated by (B-Bulge, S-Shear, P-Penetrometer)
The SPT (N value) is the sum of the last two blow values in each sampling zone (AASHTO T206)

Illinois Department of Transportation
Division of Highways
IDOT

SOIL BORING LOG

Date 5/21/14

ROUTE IL 89 (FAP 698) **DESCRIPTION** IL 89 over Illinois River at Spring Valley **LOGGED BY** TLM

SECTION (1)BR **LOCATION** SE 1/4, **SEC.** 3, **TWP.** 15N, **RNG.** 11E, 4th **PM**, **Latitude** 41.3125453, **Longitude** -89.1996188

COUNTY Putnam, Bureau **DRILLING METHOD** Mud Rotary **HAMMER TYPE** Automatic

STRUCT. NO. 078-0047 (Prop.) 078-0006 (Exist.)
Station 57+32 (Exist.)

BORING NO. 103M (Pier #3)
Station 155+19.38
Offset 3.0 ft Lt.
Ground Surface Elev. 453.15 ft

Surface Water Elev. 448.35 ft
Stream Bed Elev. 423.15 ft

Groundwater Elev.:
First Encounter ft
Upon Completion ft
After Hrs. ft

Description	Depth (ft)	Blows (/6")	UCS Qu (tsf)	Moist (%)
Soft Gray Sandy Clay with Shells *(continued)*				
	-45			
	-50			
		WH		41
	-55			
Top of Shale 395.65				
				18
	-60			

Description	Depth (ft)	Blows (/6")	UCS Qu (tsf)	Moist (%)
Gray Argillaceous Shale (Pennsylvanian) Modified Standard Penetration Test used from 58.5 ft to end of boring. Results are on a separate log sheet. *(continued)*				
	-65		5.1 S	20
386.15				
Dark Gray Argillaceous Shale (Pennsylvanian)				
	-70		5.5 S	15
	-75		6.6 S	15
				13
	-80			

DRAFT

The Unconfined Compressive Strength (UCS) Failure Mode is indicated by (B-Bulge, S-Shear, P-Penetrometer)
The SPT (N value) is the sum of the last two blow values in each sampling zone (AASHTO T206)

BBS, form 137 (Rev. 8-99)

Illinois Department of Transportation
Division of Highways
IDOT

SOIL BORING LOG

Date 5/21/14

ROUTE IL 89 (FAP 698) **DESCRIPTION** IL 89 over Illinois River at Spring Valley **LOGGED BY** TLM

SECTION (1)BR **LOCATION** SE 1/4, **SEC.** 3, **TWP.** 15N, **RNG.** 11E, 4th **PM**, **Latitude** 41.3125453, **Longitude** -89.1996188

COUNTY Putnam, Bureau **DRILLING METHOD** Mud Rotary **HAMMER TYPE** Automatic

STRUCT. NO. 078-0047 (Prop.) 078-0006 (Exist.)
Station 57+32 (Exist.)

BORING NO. 103M (Pier #3)
Station 155+19.38
Offset 3.0 ft Lt.
Ground Surface Elev. 453.15 ft

Surface Water Elev. 448.35 ft
Stream Bed Elev. 423.15 ft

Groundwater Elev.:
First Encounter ft
Upon Completion ft
After Hrs. ft

Description	DEPTH (ft)	BLOWS (/6")	UCS Qu (tsf)	MOIST (%)
Dark Gray Argillaceous Shale (Pennsylvanian) *(continued)*				
	-85		>11.5 S	14
+/- 1" thick layer of Black Shale, Possibly Coal				20
	-90			
361.65				
Gray Silty Clayey Shale Note: Casing broke with the movement of the barge. Sand filled the bottom 15 ft to 20 ft of borehole. Stopped boring at 95 ft.				16
358.15	-95			
End of Boring				
	-100			

The Unconfined Compressive Strength (UCS) Failure Mode is indicated by (B-Bulge, S-Shear, P-Penetrometer)
The SPT (N value) is the sum of the last two blow values in each sampling zone (AASHTO T206)

DATA REPORT

REPORT ON DRILLED SHAFT LOAD TESTING (OSTERBERG METHOD)

TS-1 - IL-133 Over Embarras River
Oakland, IL (LT-1425)

Prepared for: **The Board of Trustees of University of Illinois**
205 North Mathews
Urbana, IL 61801

Attention: **Mr. James Long**

PROJECT NO: **LT-1425, August 21, 2015**

Americas
LOADTEST USA
2631-D NW 41st St
Gainesville, FL 32606, USA
Phone: +1 352 378 3717
Fax: +1 352 378 3934

Middle East
Fugro LOADTEST Middle East
P.O. Box 2863, Dubai, UAE.
Phone: +971 4 3474060
Fax: +971 4 3474069

Europe & Africa
Fugro LOADTEST
14 Scotts Avenue, Sunbury Upon Thames
Middlesex, TW16 7HZ, UK
Phone: +44 (0) 1932 784807
Fax: +44 (0) 1932 784807

Asia
Fugro LOADTEST Singapore
159 Sin Ming Road, #05-07 Amtech Building
Singapore, 575625
Phone: +65 6377 5665
Fax: +65 6377 3359

LOADTEST

Issue and Revision History

Issue History

ISSUE	ISSUED TO	ISSUED BY	DATE OF ISSUE
Prelim	Mr. James Long, The Board of Trustees of University of Illinois	William G. Ryan	August 18, 2015
01	Mr. James Long, The Board of Trustees of University of Illinois	William G. Ryan	August 21, 2015

Revision History

Date	Rev. No.	Detailed Description of Change	Ref. Section

August 21, 2015

The Board of Trustees of University of Illinois
205 North Mathews Ave
Urbana, IL 61801

Attention: Mr. James Long

Load Test Report: TS-1 - IL-133 Over Embarras River
Location: Oakland, IL (LT-1425)

Dear Mr. Long,

The enclosed report contains the data and analysis summary for the Osterberg Cell (O-cell) test performed on TS-1 - IL-133 Over Embarras River, on August 17, 2015. For your convenience, we have included an executive summary of the test results in addition to our standard detailed data report. Preliminary results were issued on August 18, 2015.

We would like to express our gratitude for the on-site and off-site assistance provided by your team and we look forward to working with you on future projects.

We trust that the information contained herein will suit your current project needs. If you have any questions or require further technical assistance, please do not hesitate to contact us at 352-378-3717.

Best Regards,

William G. Ryan, B.S.C.M.
Regional Manager, Loadtest USA

EXECUTIVE SUMMARY

On August 17, 2015, Loadtest USA performed an O-cell test on a nominal 48-inch diameter test shaft TS-1. Illini Drilled Foundations, Inc. completed construction of the 27.3-foot deep shaft socketed in shale on August 05, 2015. Sub-surface conditions at the test shaft location consist primarily of clay overburden underlain by clay shale. Representatives of University of Illinois, Illinois Department of Transportation (IDOT) and others observed construction and testing of the shaft.

The maximum sustained bi-directional load applied to the shaft was 913 kips. At this load, the displacements above and below the O-cell assembly were 1.282 inches and 1.684 inches, respectively. Unit side shear data calculated from strain gages indicated an average mobilized net side shear of 6.2 ksf between O-cell and Strain Gage Level 2, in the rock socket. The maximum applied unit end bearing is calculated to be 58.6 ksf. Unit values correspond to the above respective displacements.

Using the procedures described in the report text and in Appendix C, an equivalent top load curve for the test shaft was constructed. For a top loading of 750 kips, the adjusted test data indicate this shaft would displace approximately 0.26 inches. For a top loading of 1,500 kips, the adjusted test data indicate this shaft would displace approximately 1.25 inches.

LIMITATIONS OF EXECUTIVE SUMMARY

We include this executive summary to provide a very brief presentation of some of the key elements of this O-cell test. It is by no means intended to be a comprehensive or stand-alone representation of the test results. The full text of the report and the attached appendices contain important information which the engineer can use to come to more informed conclusions about the data presented herein.

TABLE OF CONTENTS

TABLES AND FIGURES

SITE CONDITIONS AND SHAFT CONSTRUCTION

Site Sub-surface Conditions: The sub-surface stratigraphy at the general location of the test shaft is reported to consist of clay overburden at the surface underlain by clay shale. The generalized subsurface profile is included in Figure A and a boring log indicating conditions near the shaft is presented in Appendix E. More detailed geologic information can be obtained from IDOT.

Test Shaft Construction: Illini Drilled Foundations, Inc. completed construction of the dedicated test shaft socketed in shale on August 05, 2015. The nominal 48-inch diameter test shaft was excavated dry to a base elevation of +572.9 ft. The shaft was started by drilling with a 54-inch auger, followed by inserting a 54-inch O.D. casing into top of the shale strata. Then drilling continued into shale with a 48-inch auger until the shaft reached the base. After the shaft was approved for concrete placement, the reinforcing cage with attached O-cell assembly was inserted into the excavation and temporarily supported from the crane. Concrete was then delivered by tremie into the base of the shaft until the top of the concrete reached an elevation of +597.2 ft. The contractor removed the casing immediately after concrete placement. Representatives of University of Illinois, IDOT and others observed construction of the shaft.

OSTERBERG CELL TESTING

Shaft Instrumentation: Loadtest USA assisted University of Illinois with the assembly and installation of test shaft instrumentation. The loading assembly consisted of one 20-inch diameter O-cell, located 2.3 feet above the shaft base. The Osterberg cell was calibrated to 2,943 kips and then welded closed prior to shipping by American Equipment and Fabricating Corporation. Calibrations of the O-cell and instrumentation used for this test are included in Appendix B. Embedded O-cell testing instrumentation included the following:

- Paired upper compression telltale casings (nominal ½-inch steel pipe) attached diametrically opposed to the reinforcing cage, extending from the top of the O-cell assembly to ground level.
- Four Linear Vibrating Wire Displacement Transducers (LVWDTs, Geokon Model 4450 series) positioned between the lower and upper plates of the O-cell assembly.
- Three levels of four sister bar vibrating wire strain gages (Geokon Model 4911 Series) attached at 90° spacing to the reinforcing cage above the top of the O-cell assembly.

- Two lengths of ½-inch steel pipe, extending from the top of the shaft to the top of the bottom plate, to vent the break in the shaft formed by the expansion of the O-cells.

Details concerning the instrumentation placement appear in Table B and Figure A.

Test Arrangement: Throughout the load test, key elements of shaft displacement response were monitored using the equipment and instruments detailed below:

- Top of shaft displacement was monitored using a pair of automated digital survey levels (Leica NA3000 series) from an average distance of 30 feet (Appendix A, Page 1).

- Upper compression displacement was measured using ¼-inch telltale rods positioned inside the two casings and monitored by Linear Vibrating Wire Displacement Transducers (LVWDTs, Geokon Model 4450 series) attached to the top of the shaft (Appendix A, Page 1).

- Expansion of the O-cell assembly was measured using the four Expansion LVWDTs described under Shaft Instrumentation (Appendix A, Page 2).

A Bourdon pressure gage, a voltage and a vibrating wire pressure transducers were used to measure the pressure applied to the O-cell at each load interval. The voltage pressure transducer was used for automatically setting and maintaining loads and vibrating pressure transducer was used for real time plotting and for data analysis. The Bourdon pressure gage readings were used as a real-time visual reference and as a check on the transducer. There was a close agreement between the Bourdon gage and the pressure transducer.

Data Acquisition: All instrumentation were connected through a data logger (Data Electronics 515 GeoLogger) to a laptop computer allowing data to be recorded and stored automatically at 30-second intervals and displayed in real time. The laptop computer synchronized to the data logging system was used to acquire the Leica NA3000 data.

Testing Procedures: Loadtest USA conducted the load test. Testing was begun by pressurizing the O-cell in order to break the tack welds that hold it closed (for handling and for placement in the shaft) and to form the fracture plane in the concrete surrounding the base of the O-cell. After the break occurred, the pressure was immediately released and the testing recommenced from zero pressure. Zero readings for all instrumentation were taken prior to the preliminary weld-breaking load-unload cycle, which in this case involved a maximum load of 204 kips at the O-cell.

The Osterberg cell load test was conducted as follows: The 20-inch diameter O-cell, with its base located 2.3 feet above the shaft base, was pressurized in 10 nominally equal increments, resulting in a maximum bi-directional load of 913 kips applied to the shaft above and below the O-cell. After 1L-10, the loading was continued as per the Engineer's requirements and then halted because the upper shaft above the O-cell started displacing rapidly. The shaft was then unloaded in five decrements and the test was concluded.

The load increments were applied using the Quick Load Test Method for Individual Piles (ASTM D1143 *Standard Test Method for Piles Under Static Axial Load*). Each successive load increment was held constant for eight minutes by automatically adjusting the O-cell pressure. Approximately one minute was used to move between increments. The data logger automatically recorded the instrument readings every 30 seconds, but herein only the 1, 2, 4 and 8 minute readings during each increment of maintained load up to 1L-10 are reported. After 1L-10, selected readings only are reported as per the Engineer's requirements.

TEST RESULTS AND ANALYSES

General: The loads applied by the O-cell assembly act in two opposing directions, counteracted by the resistance of the shaft above and below. For the purpose of the analysis herein, it is assumed that the O-cell assembly does not impose an additional upward load until its expansion force exceeds the buoyant weight of the shaft above the O-cell assembly. Therefore, *net load*, which is defined as gross O-cell load minus the buoyant weight of the shaft above, is used to determine side shear resistance above the O-cell and to construct the equivalent top load displacement curve. For this test a shaft buoyant weight of 27 kips above the O-cell was calculated.

For the purposes of analyses herein, the maximum sustained loading at 1L-10 of 913 kips was used. The maximum applied load of 993 kips occurred at the third minute reading of increment 1X-11, at which point the displacements above and below the O-cell were 1.957 inches and 1.833 inches, respectively. The maximum displacements of 4.155 inches above the O-cell and 1.926 inches below the O-cell were occurred at fourth minute reading of increment 1U-1.

Upper Side Shear Resistance: The O-cell assembly applied a maximum upward *net load* of 886 kips to the upper side shear at load interval 1L-10 (Appendix A, Page 3, Figures 1 to 3). At this loading, the upward displacement of the top of the O-cell was 1.282 inches.

Combined End Bearing and Lower Side Shear Resistance: The O-cell assembly applied a maximum downward load of 913 kips at load interval 1L-10 (Appendix A, Page 3, Figures 1 to 3). At this loading, the average downward displacement of the O-cell base was 1.684 inches.

Strain Gage Analysis: The strain gage data appear in Appendix A, Pages 4 through 6 and the average strain measured at each level of strain gages during the test is plotted in Figure 4. On the day of the test, the unconfined compressive strength f'_c was reported to be 3,080 psi. Assuming a concrete unit weight γ_c of 145 pcf, the ACI formula ($E_c = 0.033 \times \gamma_c^{1.5} \times \sqrt{f'_c}$) was used to calculate an elastic modulus of 3,198 ksi for the concrete. This, combined with the area of reinforcing steel and nominal shaft diameter, provided an average shaft stiffness (AE) of 7,879,000 kips in the upper cased shaft section, 6,342,000 kips in the uncased shaft section above the O-cell and 5,829,000 kips below the O-cell. The load distribution curves for each load increment based on applied O-cell load and computed strain gage loads, are presented in Figure 5. Mobilized net unit side shear vs. displacement (t-z) curves based on the strain gage data and estimated ACI shaft stiffness are presented in Figures 6 & 6a. Note that Figure 6 presents the unit side shear curves for increments up to 1L-10 and Figure 6a presents unit side shear curves up to increment 1X-14. Shear values for loading increment 1L-10 follow in Table A:

TABLE A: Average Net Unit Side Shear Values for 1L-10

Load Transfer Zone	Displacement[1]	Net Unit Side Shear[2]
Zero Shear to Strain Gage Level 3	↑ 1.27 in	0.1 ksf
Strain Gage Level 3 to Strain Gage Level 2	↑ 1.27 in	1.7 ksf
Strain Gage Level 2 to Strain Gage Level 1	↑ 1.27 in	6.2 ksf
Strain Gage Level 1 to O-cell	↑ 1.28 in	6.3 ksf

1 Average displacement of load transfer zone.
2 For upward-loaded shear, the buoyant weight of shaft in each zone has been subtracted from the load shed in the respective zone. Note that net unit shear values derived from the strain gages may not be ultimate values. See Figures 6 & 6a for unit shear vs. displacement (t-z) plots.

It is assumed that the unit side shear of the 2.3-foot shaft section below the O-cell behaves the same as the shaft zone immediately above. The load resisted by side shear in the 2.3-foot shaft section below the O-cell is calculated to be 177 kips assuming an unit side shear value of 6.3 ksf and a nominal shaft diameter of 48.0 inches. The maximum applied load to end bearing is 736 kips and the unit end bearing at the base of the shaft is calculated to be 58.6 ksf at a displacement of 1.684 inches. A mobilized unit end bearing vs. displacement (q-z) curve is presented in Figure 7.

Equivalent Top Load-Displacement: Figure 8 presents the equivalent top load (ETL) curve. The procedure for calculating the curve is described in Appendix C. The curve is generated assuming the load is applied at top of shaft (+597.2 ft). A combined side shear and end-bearing resistance of 1,799 kips was mobilized during the test. For a top loading of 750 kips, the adjusted test data indicate this shaft would displace approximately 0.26 inches. For a top loading of 1,500 kips, the adjusted test data indicate this shaft would displace approximately 1.25 inches. For reference, Figure 8 also includes the two component curves of O-cell displacements vs. net loads, which if summed would produce a "rigid" equivalent top load. The plotted ETL curve includes the additional elastic compression of a top-loaded shaft.

Note that the equivalent top load curve applies to incremental loading durations of eight minutes. Creep effects will reduce the ultimate resistance of both components and increase shaft top displacement for a given loading over longer times. The Engineer can estimate such additional creep effects by suitable extrapolation of time effects using the creep data presented herein.

Creep Limit: See Appendix D for our O-cell method for determining creep limit loading. The combined end bearing and lower side shear creep data (Appendix A, Page 3, Figure D-1) indicate indeterminate creep limit. The upper side shear creep data (Appendix A, Page 3, Figure D-2) indicate that a creep limit of 525 kips was reached at a displacement of 0.21 inches. A top loaded shaft will not begin creep until both components begin creep displacement. This will occur at the maximum of the displacements required to reach the creep limit for each component. Due to the absence of a clearly defined combined end bearing and lower side shear creep limit, a creep limit for the equivalent top-loaded shaft cannot be estimated.

Shaft Compression Comparison: The measured maximum shaft compression, averaged from two telltales, is 0.012 inches at 1L-10 (Appendix A, Page 2). Using a weighted average shaft stiffness of 7,060,700 kips and the load distribution in Figure 5 at 1L-10, an elastic compression of 0.008 inches over the length of the compression telltales is calculated.

LIMITATIONS AND STANDARD OF CARE

The instrumentation, testing services and data analysis provided by Loadtest USA, outlined in this report, were performed in accordance with the accepted standards of care recognized by professionals in the drilled shaft and foundation engineering industry.

Please note that some of the information contained in this report is based on data (i.e. shaft diameter, elevations and concrete strength) provided by others. The engineer, therefore, should come to his or her own conclusions with regard to the analyses as they depend on this information. In particular, Loadtest USA typically does not observe and record drilled shaft construction details to the level of precision that the project engineer may require. In many cases, we may not be present for the entire duration of shaft construction. Since construction technique can play a significant role in determining the load bearing capacity of a drilled shaft, the engineer should pay close attention to the drilled shaft construction details that were recorded elsewhere.

We trust that this information will meet your current project needs. If you have any questions, please do not hesitate to contact us at 352-378-3717.

Prepared for Loadtest USA by

Aditya Ayithi, Ph. D.

Reviewed for Loadtest USA by

Shing K. Pang, M.S.

Abraham Alende, B.S.C.E.

TABLE B
SUMMARY OF DIMENSIONS, ELEVATIONS & SHAFT PROPERTIES

Shaft: (TS-1 - IL-133 Over Embarras River - Oakland, IL)		
Nominal shaft diameter (EL +597.2 ft to +586.9 ft)	=	54 in
Nominal shaft diameter (EL +586.9 ft to +572.9 ft)	=	48 in
O-cell: 20-9H-00141	=	20 in
Length of shaft zone above break at base of O-cell	=	22.1 ft
Length of shaft zone below break at base of O-cell	=	2.3 ft
Side shear area above O-cell base	=	293.4 ft^2
Side shear area below O-cell base	=	28.3 ft^2
Shaft base area	=	12.6 ft^2
Buoyant weight of shaft above base of O-cell	=	27 kips
Estimated shaft stiffness, AE (EL +597.2 ft to +586.9 ft)	=	7,879,000 kips
Estimated shaft stiffness, AE (EL +586.9 ft to +575.1 ft)	=	6,342,000 kips
Estimated shaft stiffness, AE (EL +575.1 ft to +572.9 ft)	=	5,829,000 kips
Elevation of ground surface	=	+600.2 ft
Elevation of top of shaft concrete	=	+597.2 ft
Elevation of water table	=	+597.2 ft
Elevation of base of O-cell assembly [1]	=	+575.1 ft
Elevation of shaft base	=	+572.9 ft
Casings:		
Elevation of top of temporary casing (54.0 in O.D., 53.3 in I.D.)	=	+601.2 ft
Elevation of bottom of temporary casing (54.0 in O.D., 53.3 in I.D.)	=	+586.9 ft
Telltale Sections:		
Elevation of top of telltale used for upper shaft compression	=	+600.2 ft
Elevation of bottom of telltale used for upper shaft compression	=	+576.6 ft
Strain Gages:		
Elevation of Strain Gage Level 3 (AE = 7,879,000 kips)	=	+589.1 ft
Elevation of Strain Gage Level 2 (AE = 6,342,000 kips)	=	+585.1 ft
Elevation of Strain Gage Level 1 (AE = 6,342,000 kips)	=	+581.1 ft
Miscellaneous:		
Top plate diameter (2.0 inch thick)	=	40.0 in
Bottom plate diameter (2.0 inch thick)	=	40.0 in
Reinforcing cage vertical bar size (EL. +600.14 ft to +574.97, 17 No.)	=	# 10
Reinforcing cage spiral size (5 in spacing)	=	# 6
Rebar cage diameter	=	42 in
Assumed concrete unit weight	=	145 pcf
Estimated 12-day unconfined compressive concrete strength	=	3,080 psi
Calculated 12-day concrete modulus	=	3,198 ksi
O-cell LVWDTs @ 0°, 90°, 180° and 270° with radius	=	19.5 in

[1] The break between upward and downward movement at the O-cell assembly

NOTE: NOMINAL SHAFT DIAMETER 48"ø
TOP EL. OF 54"ø TEMP. CASING = +601.22'

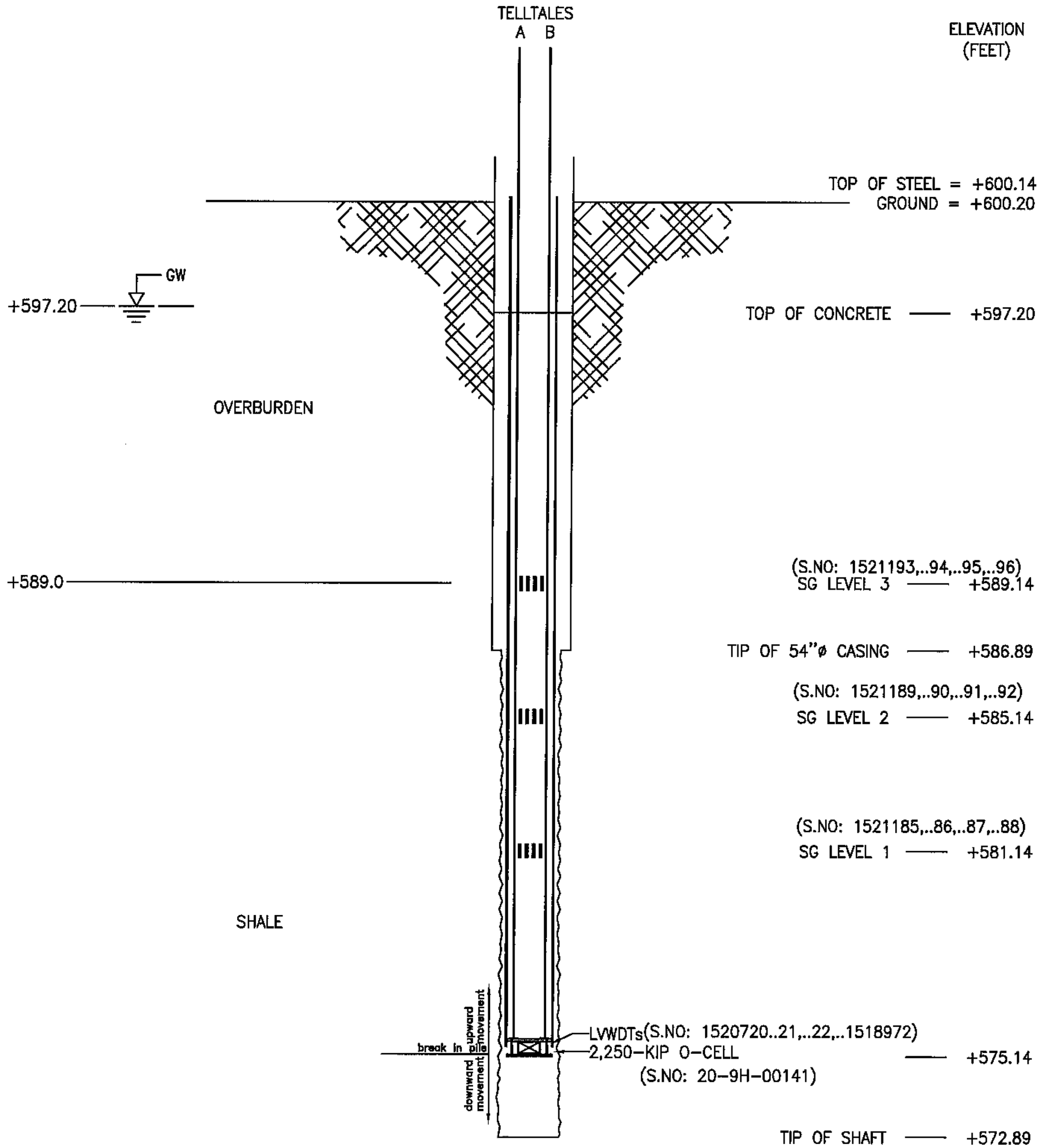

LOADTEST
www.LOADTEST.com
2631-D NW 41st St.
Gainesville, FL 32606
Phone: 800-368-1138
FAX: 352-378-3934

SCHEMATIC SECTION OF AS-BUILT TEST SHAFT

IL 133 OVER EMBARRAS RIVER - COLES COUNTY, IL

DWN BY: ZKB	DATE: 8 Aug 2015	CHECKED BY:	LT-1425
REVISED BY: AA	DATE: 21 Aug 2015	SCALE: NTS	**FIGURE A**

Osterberg Cell Load-Displacement

TS-1 - IL-133 Over Embarras River - Oakland, IL

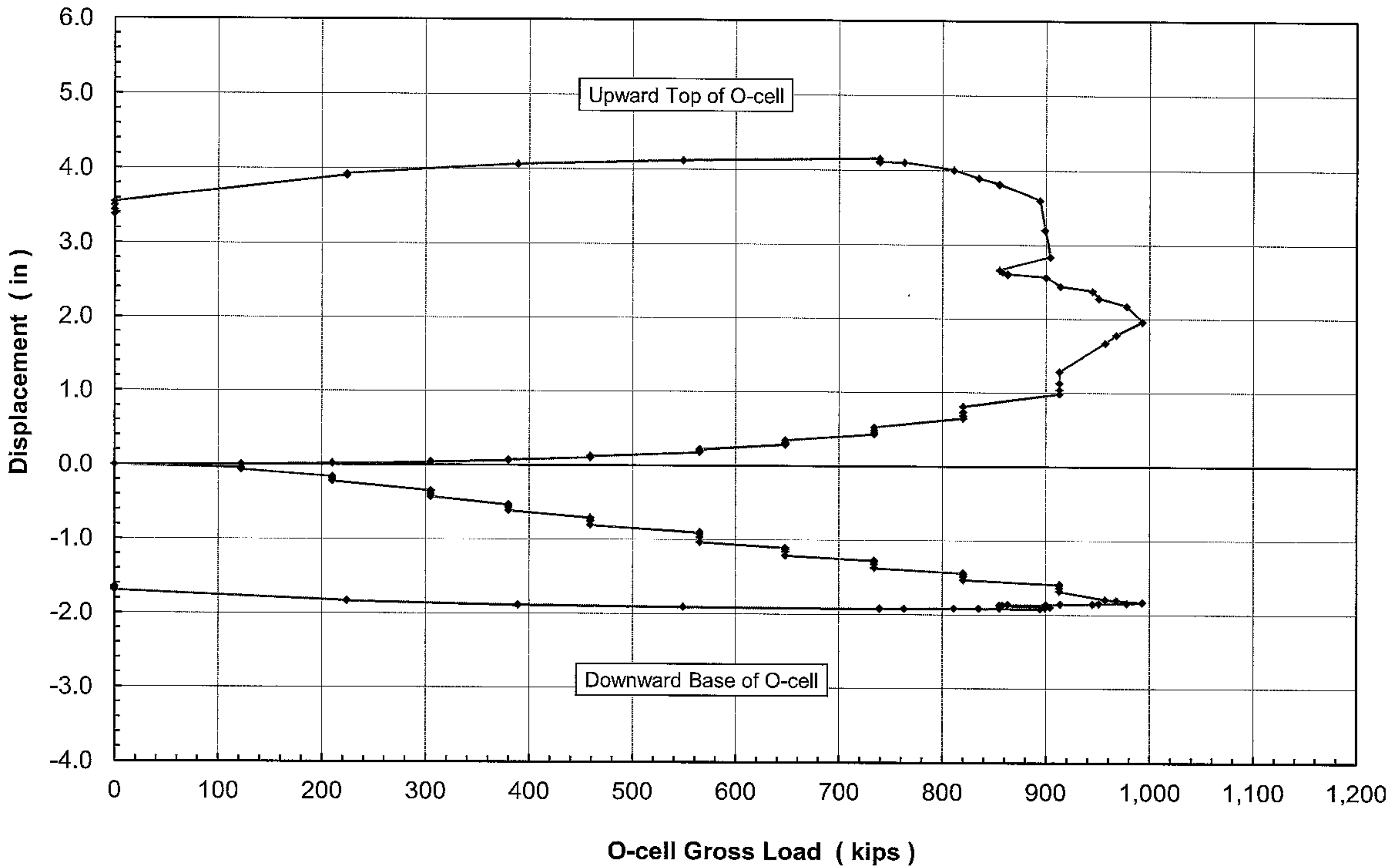

Loadtest USA Project No. LT-1425

Figure 1 of 8

Time-Osterberg Cell Load

TS-1 - IL-133 Over Embarras River - Oakland, IL

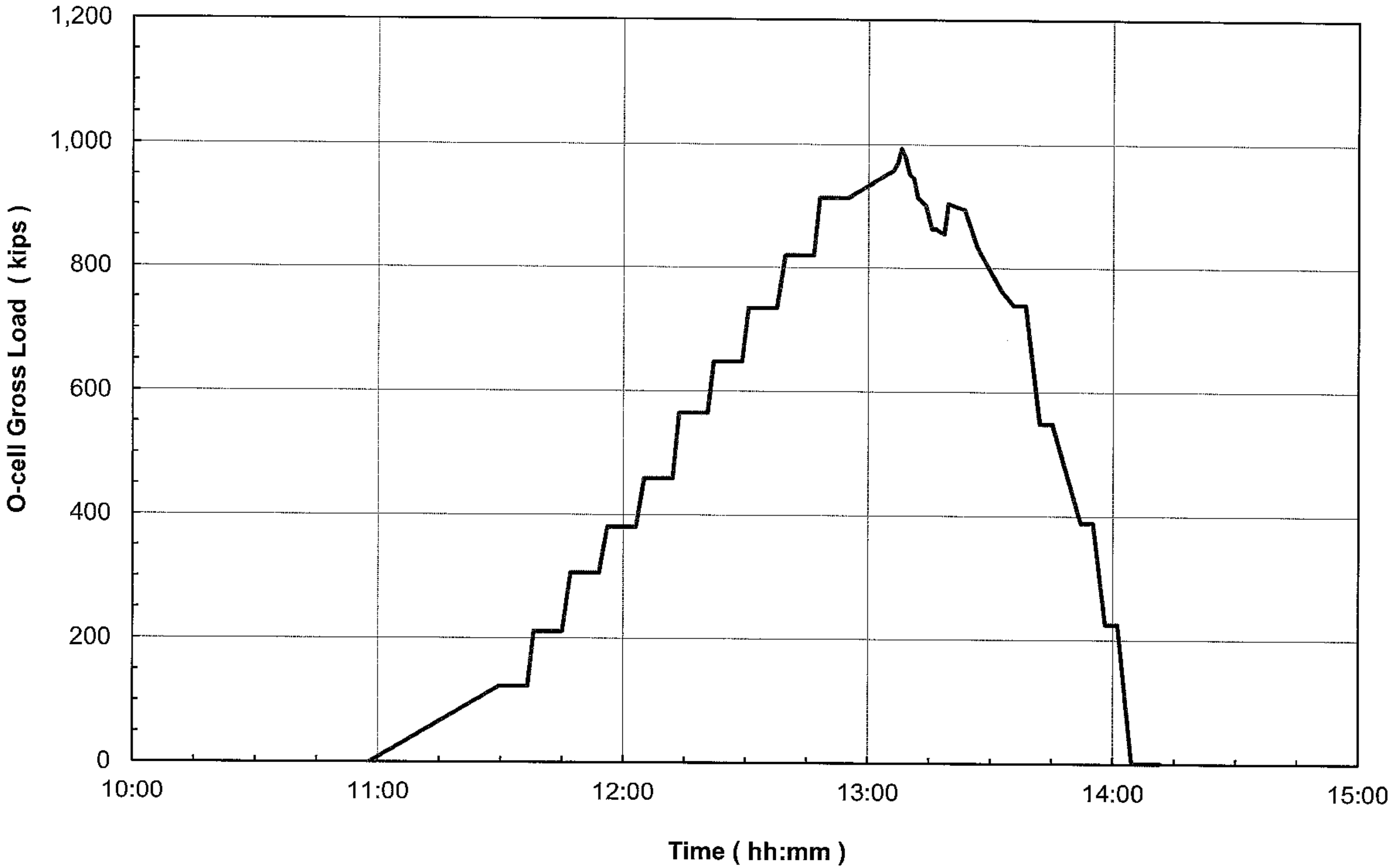

LOADTEST

Time-Osterberg Cell Displacement

TS-1 - IL-133 Over Embarras River - Oakland, IL

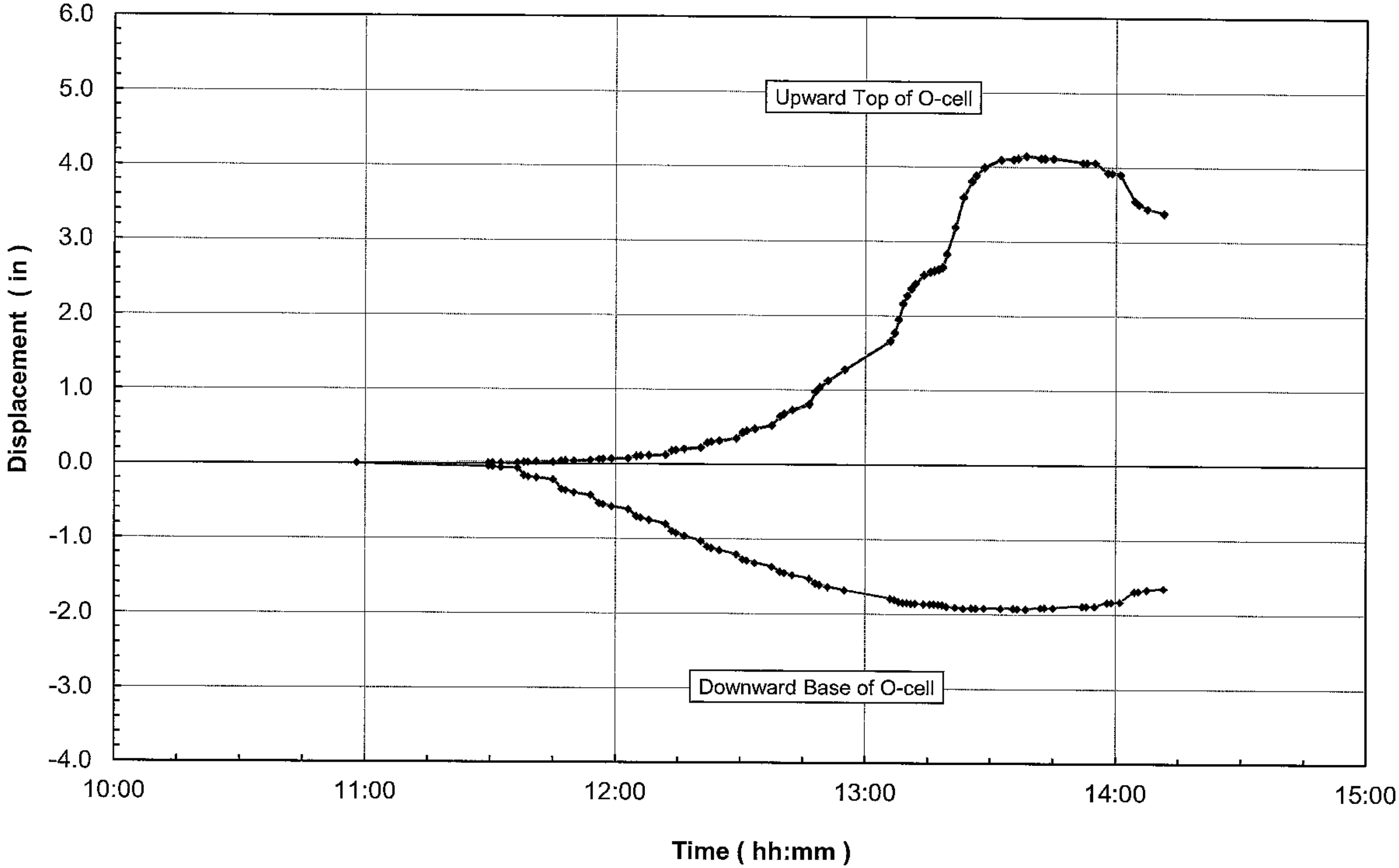

Osterberg Cell Load-Strain Gage Microstrain

TS-1 - IL-133 Over Embarras River - Oakland, IL

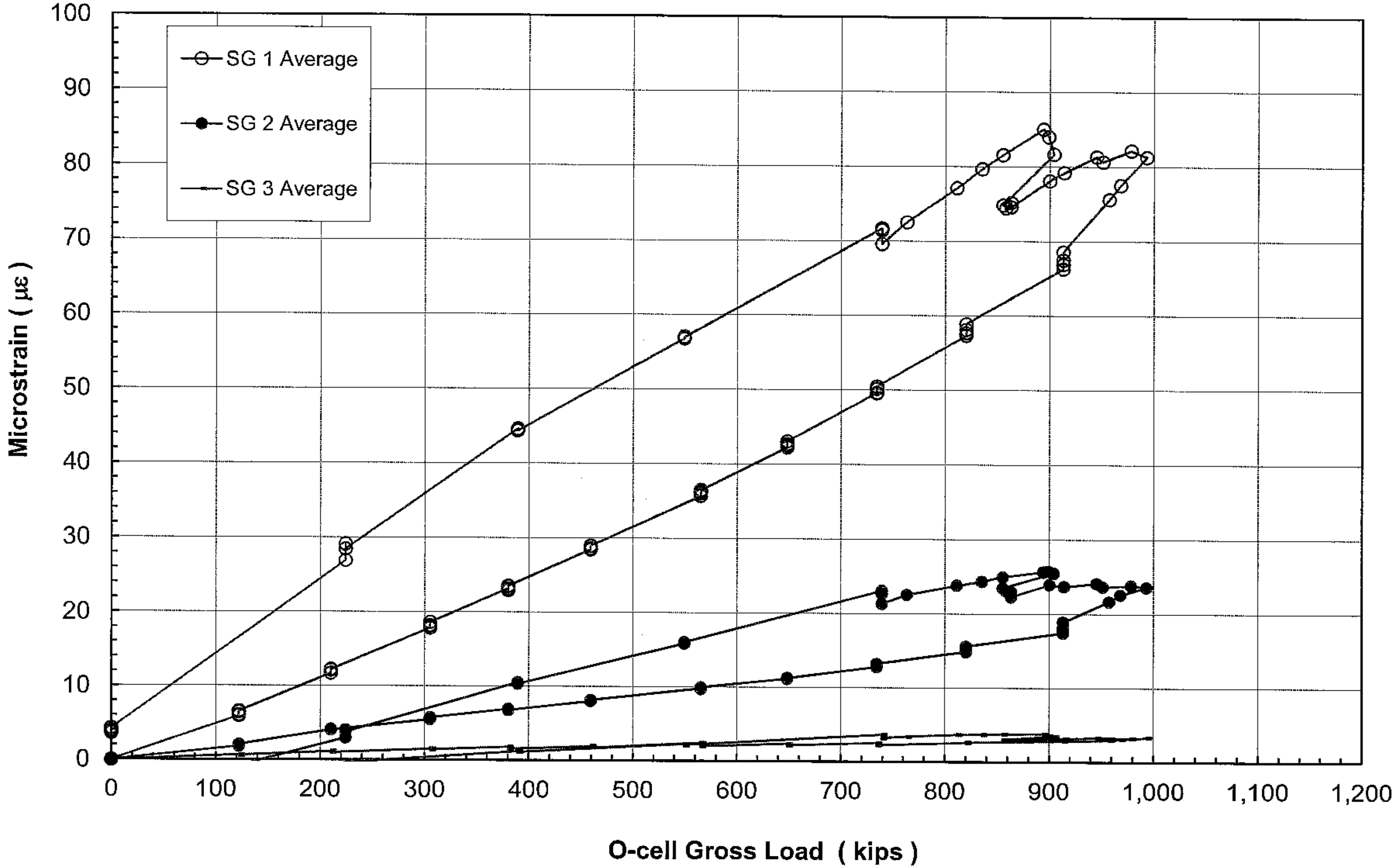

Loadtest USA Project No. LT-1425

Figure 4 of 8

Strain Gage Load Distribution

TS-1 - IL-133 Over Embarras River - Oakland, IL

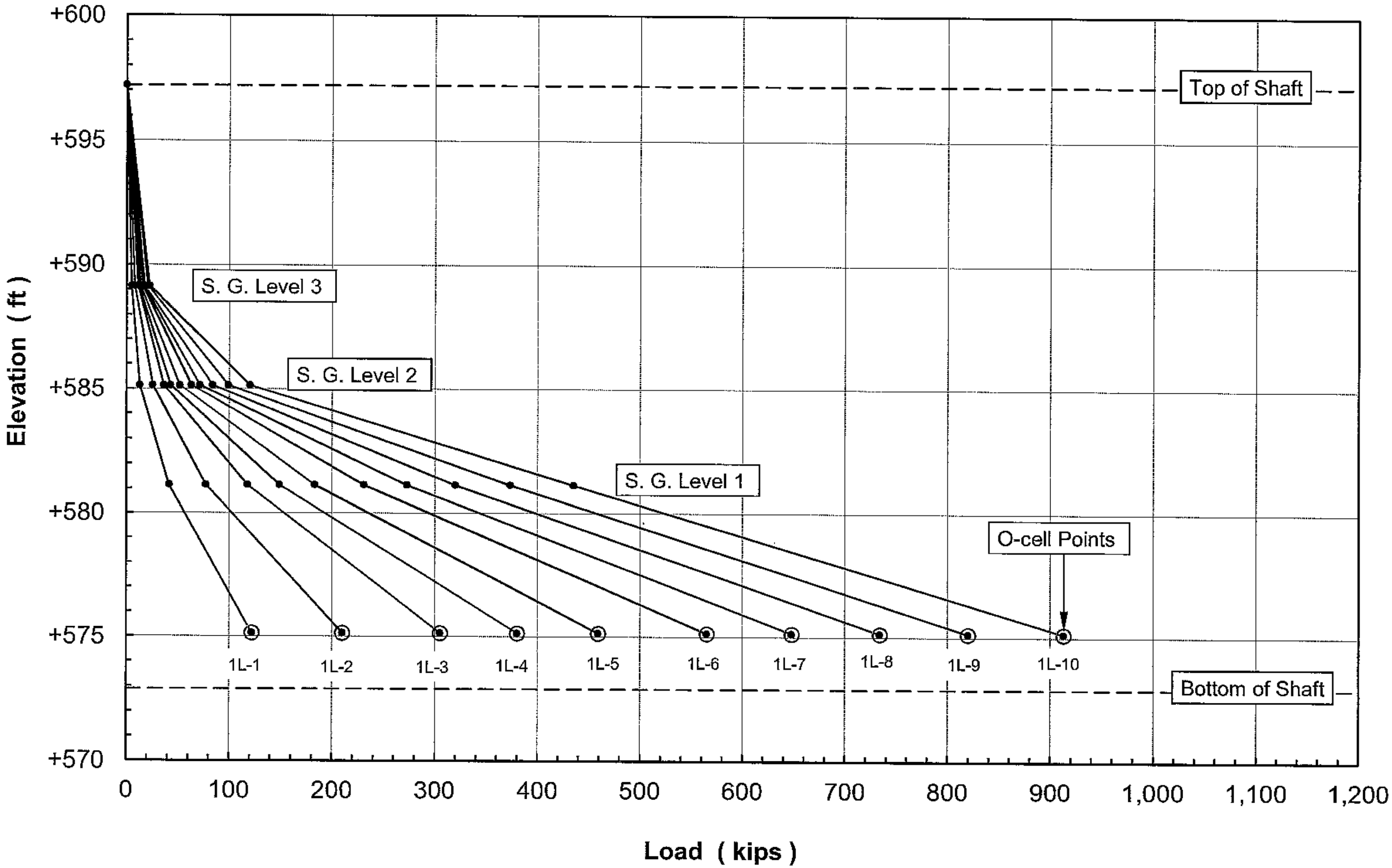

Mobilized Upward Net Unit Side Shear

TS-1 - IL-133 Over Embarras River - Oakland, IL

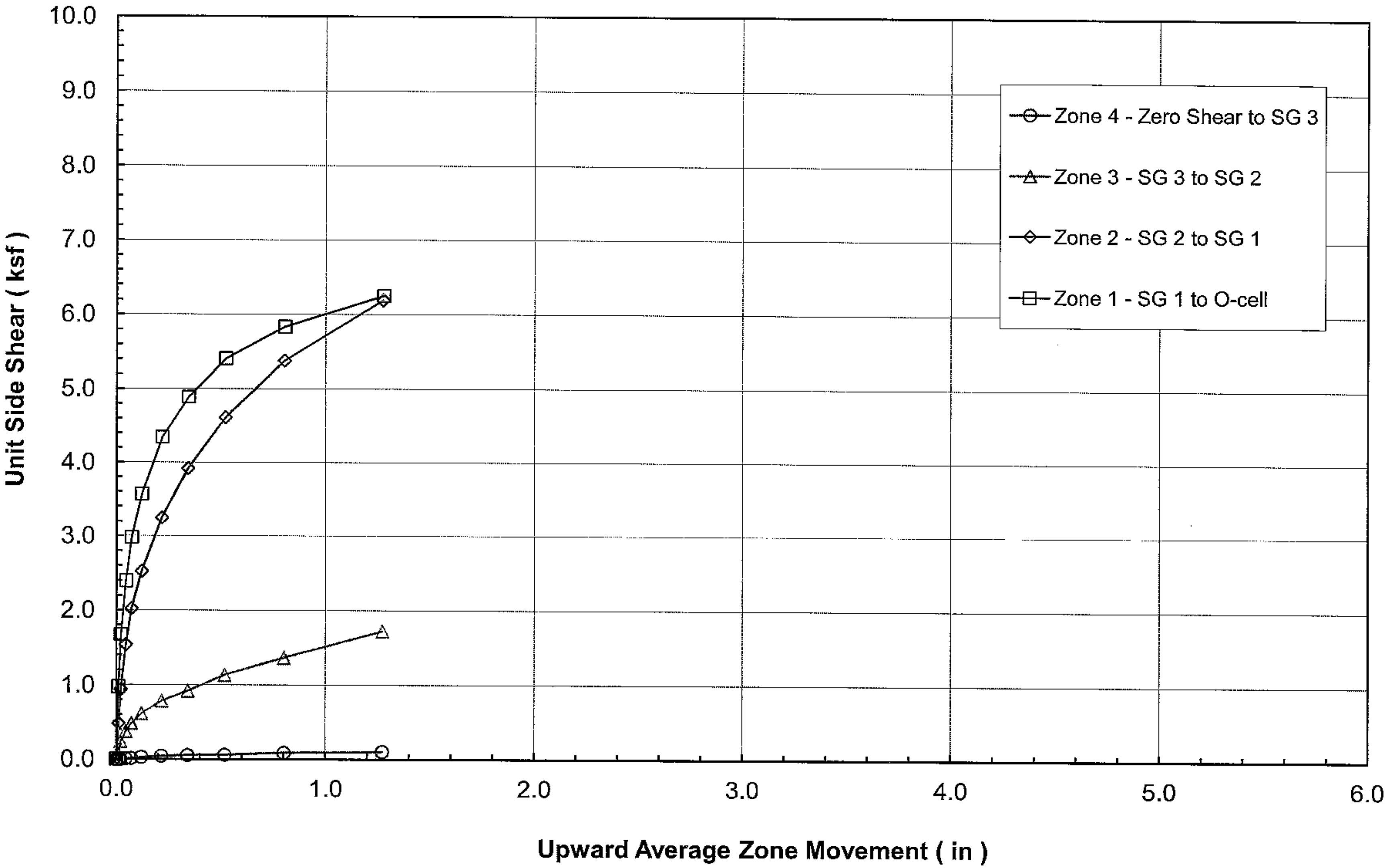

Loadtest USA Project No. LT-1425

Figure 6 of 8

Mobilized Upward Net Unit Side Shear

TS-1 - IL-133 Over Embarras River - Oakland, IL

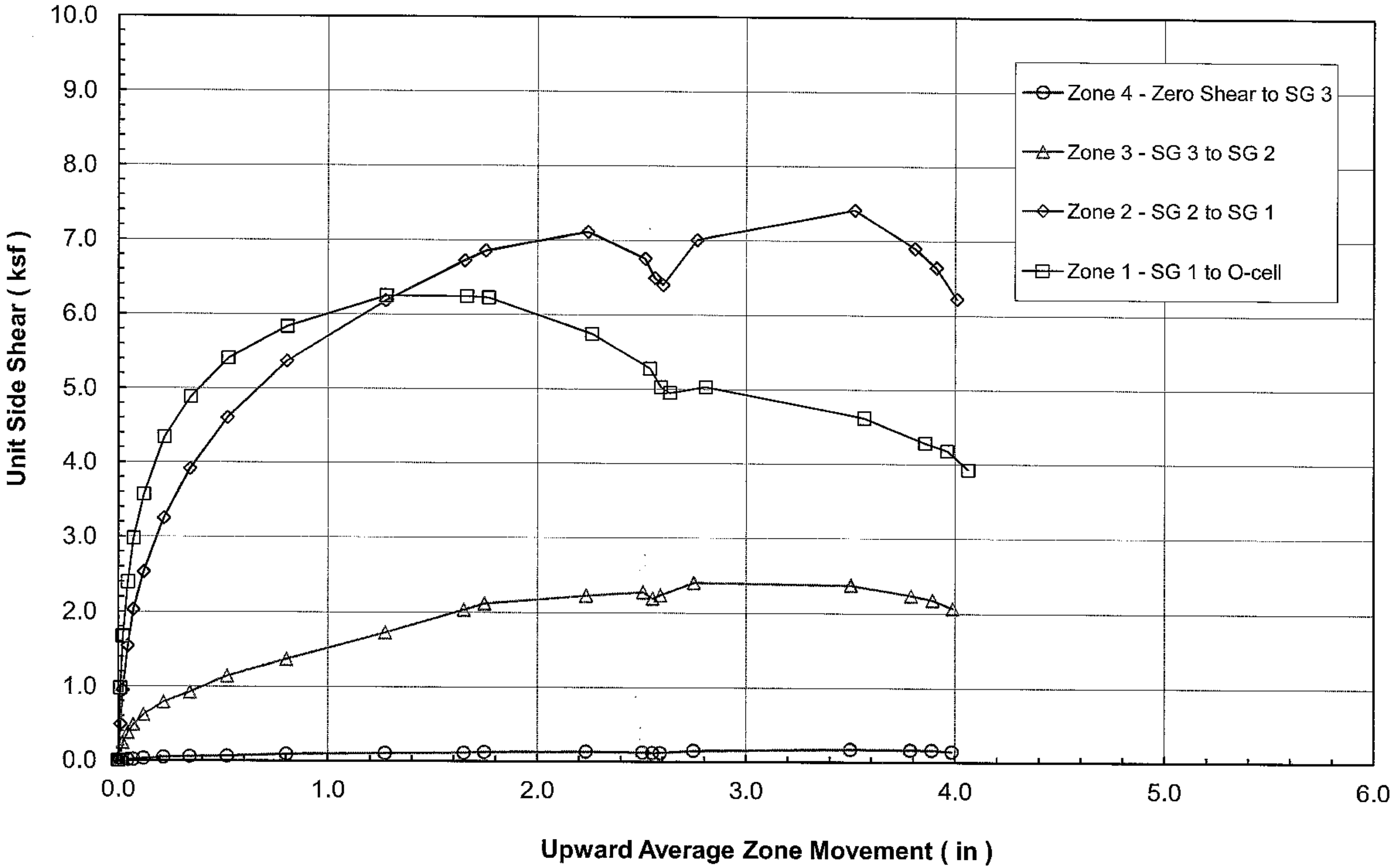

Loadtest USA Project No. LT-1425

Figure 6a of 8

Mobilized Unit End Bearing

TS-1 - IL-133 Over Embarras River - Oakland, IL

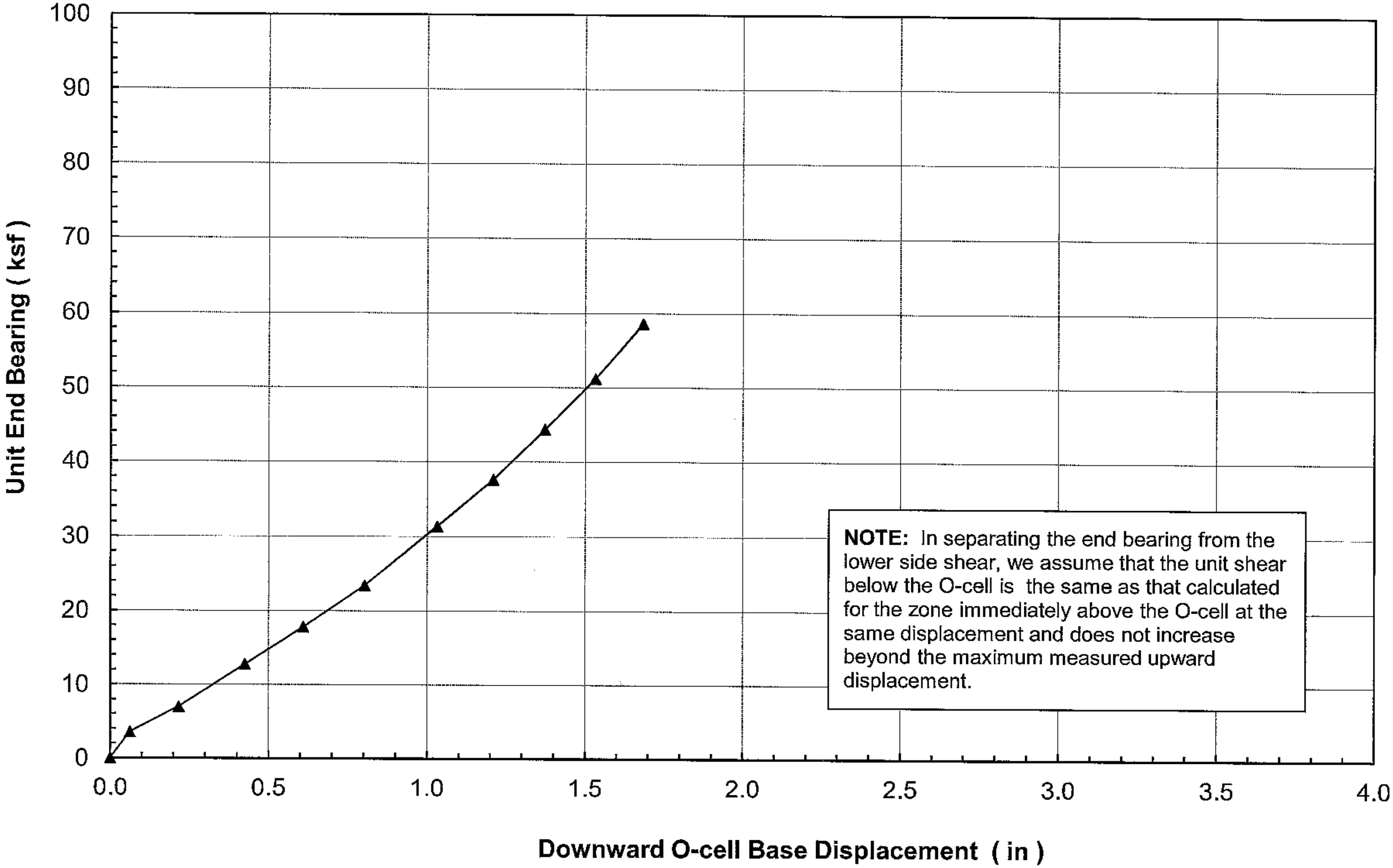

Equivalent Top Load-Displacement

TS-1 - IL-133 Over Embarras River - Oakland, IL

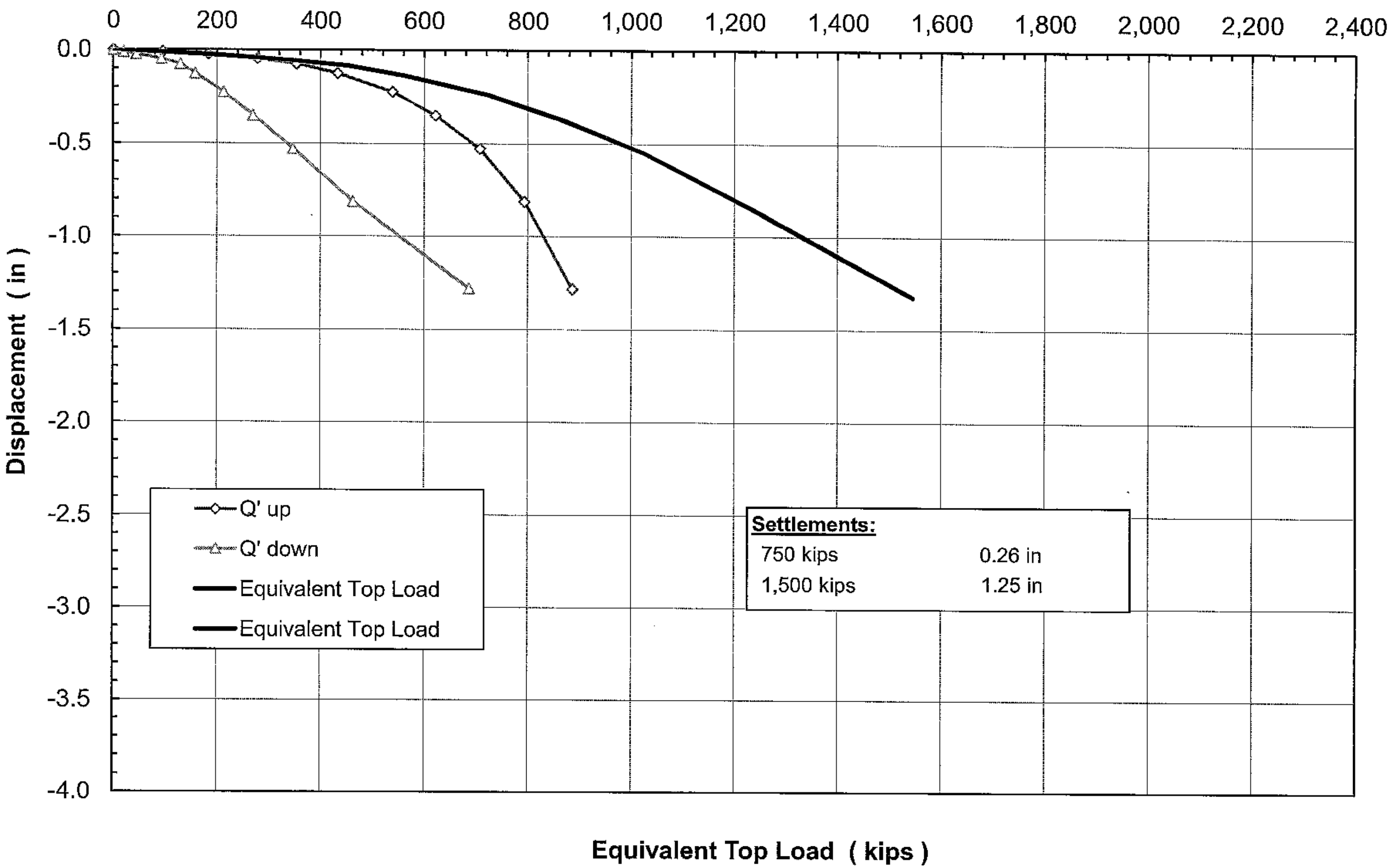

Loadtest USA Project No. LT-1425

Figure 8 of 8

APPENDIX A

FIELD DATA AND DATA REDUCTION TABLES

LOADTEST

Upward Top of Shaft Movement and Upper Shaft Compression
TS-1 - IL-133 Over Embarras River - Oakland, IL

Load	Hold		O-cell		Top of Shaft			Upper Compression Telltales		
Test Increment	Time (minutes)	Time (hh:mm:ss)	Pressure (psi)	Load (kips)	A-Leica (in)	B-Leica (in)	Average (in)	A-08-23840 (in)	B-1424656 (in)	Average (in)
1 L - 0	-	10:58:00	0	0	0.000	0.000	0.000	0.000	0.000	0.000
1 L - 1	1	11:29:30	490	122	0.007	0.004	0.005	0.003	0.002	0.002
1 L - 1	2	11:30:30	490	122	0.006	0.007	0.006	0.003	0.002	0.002
1 L - 1	4	11:32:30	490	122	0.006	0.008	0.007	0.002	0.001	0.001
1 L - 1	8	11:36:30	490	122	0.008	0.010	0.009	0.003	0.001	0.001
1 L - 2	1	11:38:00	880	210	0.016	0.018	0.017	0.004	0.002	0.002
1 L - 2	2	11:39:00	880	210	0.016	0.018	0.017	0.005	0.002	0.002
1 L - 2	4	11:41:00	880	210	0.017	0.030	0.023	0.005	0.003	0.003
1 L - 2	8	11:45:00	880	210	0.018	0.021	0.019	0.005	0.003	0.003
1 L - 3	1	11:47:00	1,300	305	0.033	0.036	0.034	0.005	0.003	0.003
1 L - 3	2	11:48:00	1,300	305	0.033	0.046	0.039	0.005	0.003	0.003
1 L - 3	4	11:50:00	1,300	305	0.035	0.033	0.034	0.006	0.003	0.003
1 L - 3	8	11:54:00	1,300	305	0.038	0.051	0.044	0.006	0.003	0.003
1 L - 4	1	11:56:00	1,630	380	0.058	0.059	0.058	0.007	0.004	0.004
1 L - 4	2	11:57:00	1,630	380	0.060	0.063	0.061	0.007	0.003	0.003
1 L - 4	4	11:59:00	1,630	380	0.062	0.065	0.063	0.007	0.004	0.004
1 L - 4	8	12:03:00	1,630	380	0.067	0.070	0.069	0.007	0.005	0.005
1 L - 5	1	12:05:00	1,980	459	0.101	0.102	0.102	0.008	0.005	0.005
1 L - 5	2	12:06:00	1,980	459	0.104	0.108	0.106	0.007	0.004	0.004
1 L - 5	4	12:08:00	1,980	459	0.111	0.113	0.112	0.007	0.005	0.005
1 L - 5	8	12:12:00	1,980	459	0.119	0.119	0.119	0.008	0.005	0.005
1 L - 6	1	12:13:30	2,450	565	0.176	0.173	0.174	0.009	0.007	0.007
1 L - 6	2	12:14:30	2,450	565	0.182	0.179	0.180	0.008	0.007	0.007
1 L - 6	4	12:16:30	2,450	565	0.197	0.200	0.198	0.008	0.007	0.007
1 L - 6	8	12:20:30	2,450	565	0.214	0.217	0.215	0.008	0.006	0.006
1 L - 7	1	12:22:00	2,820	648	0.279	0.283	0.281	0.010	0.006	0.006
1 L - 7	2	12:23:00	2,820	648	0.295	0.298	0.296	0.009	0.006	0.006
1 L - 7	4	12:25:00	2,820	648	0.310	0.311	0.310	0.009	0.007	0.007
1 L - 7	8	12:29:00	2,820	648	0.338	0.341	0.339	0.009	0.008	0.008
1 L - 8	1	12:30:30	3,200	734	0.422	0.424	0.423	0.010	0.009	0.009
1 L - 8	2	12:31:30	3,200	734	0.444	0.446	0.445	0.010	0.008	0.008
1 L - 8	4	12:33:30	3,200	734	0.473	0.473	0.473	0.010	0.009	0.009
1 L - 8	8	12:37:30	3,200	734	0.517	0.519	0.518	0.010	0.008	0.008
1 L - 9	1	12:39:30	3,580	820	0.636	0.639	0.637	0.011	0.009	0.009
1 L - 9	2	12:40:30	3,580	820	0.671	0.674	0.672	0.011	0.010	0.010
1 L - 9	4	12:42:30	3,580	820	0.722	0.724	0.723	0.011	0.010	0.010
1 L - 9	8	12:46:30	3,580	820	0.799	0.800	0.799	0.012	0.010	0.010
1 L - 10	1	12:48:00	3,990	913	0.971	0.972	0.971	0.013	0.011	0.011
1 L - 10	2	12:49:00	3,990	913	1.028	1.031	1.030	0.012	0.011	0.011
1 L - 10	4	12:51:00	3,990	913	1.120	1.120	1.120	0.012	0.011	0.011
1 L - 10	8	12:55:00	3,990	913	1.269	1.271	1.270	0.012	0.012	0.012
1 X - 11	1	13:06:00	4,186	957	1.655	1.654	1.655	0.013	0.014	0.014
1 X - 11	2	13:07:00	4,237	968	1.766	1.763	1.765	0.014	0.014	0.014
1 X - 11	3	13:08:00	4,348	993	1.943	1.942	1.943	0.014	0.014	0.014
1 X - 11	4	13:09:00	4,281	978	2.155	2.152	2.154	0.014	0.015	0.015
1 X - 11	5	13:10:00	4,161	951	2.264	2.260	2.262	0.014	0.015	0.015
1 X - 11	6	13:11:00	4,133	945	2.359	2.357	2.358	0.014	0.015	0.015
1 X - 11	7	13:12:00	3,996	914	2.424	2.420	2.422	0.013	0.015	0.015
1 X - 11	9	13:14:00	3,934	900	2.545	2.541	2.543	0.013	0.015	0.015
1 X - 12	1	13:15:30	3,771	863	2.586	2.578	2.582	0.013	0.016	0.016
1 X - 12	2	13:16:30	3,769	863	2.601	2.593	2.597	0.013	0.016	0.016
1 X - 12	3	13:17:30	3,749	858	2.620	2.614	2.617	0.013	0.015	0.015
1 X - 12	4	13:18:30	3,734	855	2.649	2.641	2.645	0.013	0.015	0.015
1 X - 13	1	13:19:30	3,952	904	2.825	2.817	2.821	0.013	0.016	0.016
1 X - 13	3	13:21:30	3,929	899	3.187	3.176	3.182	0.014	0.017	0.017
1 X - 13	5	13:23:30	3,908	894	3.591	3.579	3.585	0.013	0.017	0.017
1 X - 14	1	13:25:30	3,734	855	3.806	3.793	3.800	0.013	0.017	0.017
1 X - 14	2	13:26:30	3,648	835	3.884	3.872	3.878	0.013	0.016	0.016
1 X - 14	4	13:28:30	3,540	811	3.994	3.980	3.987	0.012	0.016	0.016
1 X - 14	8	13:32:30	3,327	763	4.096	4.082	4.089	0.012	0.015	0.015
1 U - 1	1	13:35:30	3,220	739	4.100	4.085	4.093	0.012	0.013	0.013
1 U - 1	2	13:36:30	3,220	739	4.116	4.102	4.109	0.011	0.013	0.013
1 U - 1	4	13:38:30	3,220	739	4.149	4.134	4.142	0.010	0.013	0.013
1 U - 2	1	13:42:00	2,380	549	4.117	4.103	4.110	0.010	0.011	0.011
1 U - 2	2	13:43:00	2,380	549	4.117	4.104	4.111	0.010	0.012	0.012
1 U - 2	4	13:45:00	2,380	549	4.117	4.103	4.110	0.010	0.011	0.011
1 U - 3	1	13:52:00	1,670	389	4.061	4.048	4.055	0.008	0.010	0.010
1 U - 3	2	13:53:00	1,670	389	4.061	4.046	4.054	0.008	0.011	0.011
1 U - 3	4	13:55:00	1,670	389	4.060	4.046	4.053	0.009	0.010	0.010
1 U - 4	1	13:58:00	940	224	3.926	3.913	3.920	0.007	0.009	0.009
1 U - 4	2	13:59:00	940	224	3.924	3.913	3.919	0.008	0.009	0.009
1 U - 4	4	14:01:00	940	224	3.905	3.893	3.899	0.007	0.009	0.009
1 U - 5	1	14:04:30	0	0	3.546	3.541	3.544	0.006	0.007	0.007
1 U - 5	2	14:05:30	0	0	3.498	3.493	3.496	0.006	0.008	0.008
1 U - 5	4	14:07:30	0	0	3.438	3.433	3.436	0.006	0.007	0.007
1 U - 5	8	14:11:30	0	0	3.378	3.375	3.377	0.006	0.008	0.008

LOADTEST

O-cell Expansion

TS-1 - IL-133 Over Embarras River - Oakland, IL

Load Test Increment	Hold Time (minutes)	Time (hh:mm:ss)	O-cell Pressure (psi)	O-cell Load (kips)	O-cell Expansion A-1520720 (in)	B-1520721 (in)	C-1520722 (in)	D-1518972 (in)	Average (in)
1 L - 0	-	10:58:00	0	0	0.000	0.000	0.000	0.000	0.000
1 L - 1	1	11:29:30	490	122	0.046	0.035	0.042	0.054	0.045
1 L - 1	2	11:30:30	490	122	0.054	0.042	0.049	0.062	0.052
1 L - 1	4	11:32:30	490	122	0.063	0.051	0.058	0.072	0.061
1 L - 1	8	11:36:30	490	122	0.074	0.061	0.069	0.084	0.072
1 L - 2	1	11:38:00	880	210	0.178	0.161	0.174	0.196	0.177
1 L - 2	2	11:39:00	880	210	0.195	0.176	0.192	0.213	0.194
1 L - 2	4	11:41:00	880	210	0.215	0.197	0.213	0.235	0.215
1 L - 2	8	11:45:00	880	210	0.238	0.220	0.237	0.258	0.238
1 L - 3	1	11:47:00	1,300	305	0.377	0.357	0.382	0.406	0.381
1 L - 3	2	11:48:00	1,300	305	0.394	0.374	0.400	0.423	0.398
1 L - 3	4	11:50:00	1,300	305	0.423	0.405	0.431	0.454	0.428
1 L - 3	8	11:54:00	1,300	305	0.467	0.447	0.475	0.498	0.472
1 L - 4	1	11:56:00	1,630	380	0.586	0.563	0.598	0.622	0.592
1 L - 4	2	11:57:00	1,630	380	0.602	0.579	0.615	0.639	0.609
1 L - 4	4	11:59:00	1,630	380	0.632	0.609	0.646	0.671	0.640
1 L - 4	8	12:03:00	1,630	380	0.675	0.652	0.691	0.715	0.683
1 L - 5	1	12:05:00	1,980	459	0.801	0.778	0.822	0.847	0.812
1 L - 5	2	12:06:00	1,980	459	0.821	0.797	0.842	0.867	0.832
1 L - 5	4	12:08:00	1,980	459	0.855	0.832	0.878	0.903	0.867
1 L - 5	8	12:12:00	1,980	459	0.913	0.892	0.940	0.964	0.927
1 L - 6	1	12:13:30	2,450	565	1.064	1.041	1.097	1.124	1.081
1 L - 6	2	12:14:30	2,450	565	1.096	1.073	1.129	1.156	1.113
1 L - 6	4	12:16:30	2,450	565	1.152	1.130	1.188	1.213	1.171
1 L - 6	8	12:20:30	2,450	565	1.233	1.212	1.271	1.295	1.253
1 L - 7	1	12:22:00	2,820	648	1.368	1.346	1.413	1.440	1.392
1 L - 7	2	12:23:00	2,820	648	1.404	1.381	1.450	1.477	1.428
1 L - 7	4	12:25:00	2,820	648	1.447	1.424	1.495	1.521	1.472
1 L - 7	8	12:29:00	2,820	648	1.530	1.507	1.581	1.607	1.556
1 L - 8	1	12:30:30	3,200	734	1.676	1.650	1.734	1.765	1.706
1 L - 8	2	12:31:30	3,200	734	1.716	1.688	1.774	1.806	1.746
1 L - 8	4	12:33:30	3,200	734	1.775	1.747	1.836	1.867	1.806
1 L - 8	8	12:37:30	3,200	734	1.866	1.836	1.929	1.963	1.899
1 L - 9	1	12:39:30	3,580	820	2.049	2.016	2.120	2.159	2.086
1 L - 9	2	12:40:30	3,580	820	2.103	2.069	2.174	2.211	2.139
1 L - 9	4	12:42:30	3,580	820	2.186	2.149	2.251	2.288	2.219
1 L - 9	8	12:46:30	3,580	820	2.306	2.269	2.372	2.414	2.341
1 L - 10	1	12:48:00	3,990	913	2.542	2.497	2.607	2.655	2.575
1 L - 10	2	12:49:00	3,990	913	2.618	2.570	2.680	2.735	2.651
1 L - 10	4	12:51:00	3,990	913	2.740	2.688	2.801	2.861	2.772
1 L - 10	8	12:55:00	3,990	913	2.933	2.877	2.997	3.060	2.966
1 X - 11	1	13:06:00	4,186	957	3.422	3.354	3.497	3.578	3.462
1 X - 11	2	13:07:00	4,237	968	3.544	3.474	3.622	3.707	3.587
1 X - 11	3	13:08:00	4,348	993	3.745	3.669	3.827	3.920	3.790
1 X - 11	4	13:09:00	4,281	978	3.969	3.887	4.052	4.151	4.015
1 X - 11	5	13:10:00	4,161	951	4.079	3.994	4.162	4.264	4.125
1 X - 11	6	13:11:00	4,133	945	4.181	4.095	4.268	4.372	4.229
1 X - 11	7	13:12:00	3,996	914	4.246	4.158	4.334	4.439	4.294
1 X - 11	9	13:14:00	3,934	900	4.373	4.283	4.463	4.571	4.422
1 X - 12	1	13:15:30	3,771	863	4.412	4.321	4.501	4.613	4.462
1 X - 12	2	13:16:30	3,769	863	4.428	4.337	4.520	4.628	4.478
1 X - 12	3	13:17:30	3,749	858	4.454	4.361	4.545	4.652	4.503
1 X - 12	4	13:18:30	3,734	855	4.483	4.391	4.576	4.685	4.534
1 X - 13	1	13:19:30	3,952	904	4.676	4.582	4.776	4.893	4.732
1 X - 13	3	13:21:30	3,929	899	5.047	4.949	5.155	5.277	5.107
1 X - 13	5	13:23:30	3,908	894	5.458	5.357	5.574	5.699	5.522
1 X - 14	1	13:25:30	3,734	855	5.667	5.564	5.785	5.907	5.731
1 X - 14	2	13:26:30	3,648	835	5.745	5.642	5.865	5.991	5.811
1 X - 14	4	13:28:30	3,540	811	5.852	5.748	5.974	6.101	5.919
1 X - 14	8	13:32:30	3,327	763	5.955	5.849	6.078	6.208	6.023
1 U - 1	1	13:35:30	3,220	739	5.958	5.853	6.083	6.210	6.026
1 U - 1	2	13:36:30	3,220	739	5.977	5.872	6.103	6.231	6.046
1 U - 1	4	13:38:30	3,220	739	6.013	5.908	6.140	6.266	6.081
1 U - 2	1	13:42:00	2,380	549	5.962	5.857	6.088	6.214	6.030
1 U - 2	2	13:43:00	2,380	549	5.962	5.857	6.088	6.214	6.030
1 U - 2	4	13:45:00	2,380	549	5.962	5.857	6.088	6.214	6.030
1 U - 3	1	13:52:00	1,670	389	5.883	5.780	6.008	6.135	5.951
1 U - 3	2	13:53:00	1,670	389	5.883	5.779	6.008	6.134	5.951
1 U - 3	4	13:55:00	1,670	389	5.883	5.779	6.008	6.135	5.951
1 U - 4	1	13:58:00	940	224	5.700	5.600	5.818	5.936	5.764
1 U - 4	2	13:59:00	940	224	5.699	5.599	5.817	5.935	5.762
1 U - 4	4	14:01:00	940	224	5.673	5.573	5.790	5.907	5.736
1 U - 5	1	14:04:30	0	0	5.195	5.107	5.284	5.384	5.242
1 U - 5	2	14:05:30	0	0	5.140	5.053	5.226	5.332	5.187
1 U - 5	4	14:07:30	0	0	5.066	4.981	5.151	5.243	5.110
1 U - 5	8	14:11:30	0	0	4.993	4.910	5.074	5.163	5.035

O-cell Plate Movements and Creep (calculated)
TS-1 - IL-133 Over Embarras River - Oakland, IL

Load Test Increment	Hold Time (minutes)	Time (hh:mm:ss)	O-cell Pressure (psi)	O-cell Load (kips)	O-cell Net Load (kips)	Top of Shaft Movement (in)	Upper Comp. (in)	Upward Movement (in)	O-cell Expansion (in)	Downward Movement (in)	Creep Up Per 8 Min. (in)	Creep Dn Per 8 Min. (in)
1 L - 0	-	10:58:00	0	0	0	0.000	0.000	0.000	0.000	0.000		
1 L - 1	1	11:29:30	490	122	95	0.005	0.002	0.007	0.045	-0.038		
1 L - 1	2	11:30:30	490	122	95	0.006	0.002	0.008	0.052	-0.044		
1 L - 1	4	11:32:30	490	122	95	0.007	0.001	0.008	0.061	-0.053		
1 L - 1	8	11:36:30	490	122	95	0.009	0.001	0.010	0.072	-0.062	0.004	0.018
1 L - 2	1	11:38:00	880	210	183	0.017	0.002	0.019	0.177	-0.158		
1 L - 2	2	11:39:00	880	210	183	0.017	0.002	0.019	0.194	-0.175		
1 L - 2	4	11:41:00	880	210	183	0.023	0.003	0.026	0.215	-0.189		
1 L - 2	8	11:45:00	880	210	183	0.019	0.003	0.022	0.238	-0.216	0.000	0.054
1 L - 3	1	11:47:00	1,300	305	278	0.034	0.003	0.037	0.381	-0.344		
1 L - 3	2	11:48:00	1,300	305	278	0.039	0.003	0.042	0.398	-0.356		
1 L - 3	4	11:50:00	1,300	305	278	0.034	0.003	0.037	0.428	-0.391		
1 L - 3	8	11:54:00	1,300	305	278	0.044	0.003	0.047	0.472	-0.425	0.020	0.068
1 L - 4	1	11:56:00	1,630	380	353	0.058	0.004	0.062	0.592	-0.530		
1 L - 4	2	11:57:00	1,630	380	353	0.061	0.003	0.064	0.609	-0.545		
1 L - 4	4	11:59:00	1,630	380	353	0.063	0.004	0.067	0.640	-0.573		
1 L - 4	8	12:03:00	1,630	380	353	0.069	0.005	0.074	0.683	-0.609	0.014	0.072
1 L - 5	1	12:05:00	1,980	459	432	0.102	0.005	0.107	0.812	-0.705		
1 L - 5	2	12:06:00	1,980	459	432	0.106	0.004	0.110	0.832	-0.722		
1 L - 5	4	12:08:00	1,980	459	432	0.112	0.005	0.117	0.867	-0.750		
1 L - 5	8	12:12:00	1,980	459	432	0.119	0.005	0.124	0.927	-0.803	0.014	0.106
1 L - 6	1	12:13:30	2,450	565	538	0.174	0.007	0.181	1.081	-0.900		
1 L - 6	2	12:14:30	2,450	565	538	0.180	0.007	0.187	1.113	-0.926		
1 L - 6	4	12:16:30	2,450	565	538	0.198	0.007	0.205	1.171	-0.966		
1 L - 6	8	12:20:30	2,450	565	538	0.215	0.006	0.221	1.253	-1.032	0.032	0.132
1 L - 7	1	12:22:00	2,820	648	621	0.281	0.006	0.287	1.392	-1.105		
1 L - 7	2	12:23:00	2,820	648	621	0.296	0.006	0.302	1.428	-1.126		
1 L - 7	4	12:25:00	2,820	648	621	0.310	0.007	0.317	1.472	-1.155		
1 L - 7	8	12:29:00	2,820	648	621	0.339	0.008	0.347	1.556	-1.209	0.060	0.108
1 L - 8	1	12:30:30	3,200	734	707	0.423	0.009	0.432	1.706	-1.274		
1 L - 8	2	12:31:30	3,200	734	707	0.445	0.008	0.453	1.746	-1.293		
1 L - 8	4	12:33:30	3,200	734	707	0.473	0.009	0.482	1.806	-1.324		
1 L - 8	8	12:37:30	3,200	734	707	0.518	0.008	0.526	1.899	-1.373	0.088	0.098
1 L - 9	1	12:39:30	3,580	820	793	0.637	0.009	0.646	2.086	-1.440		
1 L - 9	2	12:40:30	3,580	820	793	0.672	0.010	0.682	2.139	-1.457		
1 L - 9	4	12:42:30	3,580	820	793	0.723	0.010	0.733	2.219	-1.486		
1 L - 9	8	12:46:30	3,580	820	793	0.799	0.010	0.809	2.341	-1.532	0.152	0.092
1 L - 10	1	12:48:00	3,990	913	886	0.971	0.011	0.982	2.575	-1.593		
1 L - 10	2	12:49:00	3,990	913	886	1.030	0.011	1.041	2.651	-1.610		
1 L - 10	4	12:51:00	3,990	913	886	1.120	0.011	1.131	2.772	-1.641		
1 L - 10	8	12:55:00	3,990	913	886	1.270	0.012	1.282	2.966	-1.684	0.302	0.086
1 X - 11	1	13:06:00	4,186	957	930	1.655	0.014	1.669	3.462	-1.793		
1 X - 11	2	13:07:00	4,237	968	941	1.765	0.014	1.779	3.587	-1.808		
1 X - 11	3	13:08:00	4,348	993	966	1.943	0.014	1.957	3.790	-1.833		
1 X - 11	4	13:09:00	4,281	978	951	2.154	0.015	2.169	4.015	-1.846		
1 X - 11	5	13:10:00	4,161	951	924	2.262	0.015	2.277	4.125	-1.848		
1 X - 11	6	13:11:00	4,133	945	918	2.358	0.015	2.373	4.229	-1.856		
1 X - 11	7	13:12:00	3,996	914	887	2.422	0.015	2.437	4.294	-1.857		
1 X - 11	9	13:14:00	3,934	900	873	2.543	0.015	2.558	4.422	-1.864		
1 X - 12	1	13:15:30	3,771	863	836	2.582	0.016	2.598	4.462	-1.864		
1 X - 12	2	13:16:30	3,769	863	836	2.597	0.016	2.613	4.478	-1.865		
1 X - 12	3	13:17:30	3,749	858	831	2.617	0.015	2.632	4.503	-1.871		
1 X - 12	4	13:18:30	3,734	855	828	2.645	0.015	2.660	4.534	-1.874		
1 X - 13	1	13:19:30	3,952	904	877	2.821	0.016	2.837	4.732	-1.895		
1 X - 13	3	13:21:30	3,929	899	872	3.182	0.017	3.199	5.107	-1.908		
1 X - 13	5	13:23:30	3,908	894	867	3.585	0.017	3.602	5.522	-1.920		
1 X - 14	1	13:25:30	3,734	855	828	3.800	0.017	3.817	5.731	-1.914		
1 X - 14	2	13:26:30	3,648	835	808	3.878	0.016	3.894	5.811	-1.917		
1 X - 14	4	13:28:30	3,540	811	784	3.987	0.016	4.003	5.919	-1.916		
1 X - 14	8	13:32:30	3,327	763	736	4.089	0.015	4.104	6.023	-1.919		
1 U - 1	1	13:35:30	3,220	739	712	4.093	0.013	4.106	6.026	-1.920		
1 U - 1	2	13:36:30	3,220	739	712	4.109	0.013	4.122	6.046	-1.924		
1 U - 1	4	13:38:30	3,220	739	712	4.142	0.013	4.155	6.081	-1.926		
1 U - 2	1	13:42:00	2,380	549	522	4.110	0.011	4.121	6.030	-1.909		
1 U - 2	2	13:43:00	2,380	549	522	4.111	0.012	4.123	6.030	-1.907		
1 U - 2	4	13:45:00	2,380	549	522	4.110	0.011	4.121	6.030	-1.909		
1 U - 3	1	13:52:00	1,670	389	362	4.055	0.010	4.065	5.951	-1.886		
1 U - 3	2	13:53:00	1,670	389	362	4.054	0.011	4.065	5.951	-1.886		
1 U - 3	4	13:55:00	1,670	389	362	4.053	0.010	4.063	5.951	-1.888		
1 U - 4	1	13:58:00	940	224	197	3.920	0.009	3.929	5.764	-1.835		
1 U - 4	2	13:59:00	940	224	197	3.919	0.009	3.928	5.762	-1.834		
1 U - 4	4	14:01:00	940	224	197	3.899	0.009	3.908	5.736	-1.828		
1 U - 5	1	14:04:30	0	0	0	3.544	0.007	3.551	5.242	-1.691		
1 U - 5	2	14:05:30	0	0	0	3.496	0.008	3.504	5.187	-1.683		
1 U - 5	4	14:07:30	0	0	0	3.436	0.007	3.443	5.110	-1.667		
1 U - 5	8	14:11:30	0	0	0	3.377	0.008	3.385	5.035	-1.650		

LOADTEST

Strain Gage Readings and Loads at Level 1
TS-1 - IL-133 Over Embarras River - Oakland, IL

Load Test Increment	Hold Time (minutes)	Time (hh:mm:ss)	O-cell Pressure (psi)	O-cell Load (kips)	Strain Gage Level 1 1A-1521185 (με)	1B-1521186 (με)	1C-1521187 (με)	1D-1521188 (με)	Av. Strain (με)	Load (kips)
1L-0	-	10:58:00	0	0	0.0	0.0	0.0	0.0	0.0	0
1L-1	1	11:29:30	490	122	8.8	1.9	1.2	11.8	5.9	38
1L-1	2	11:30:30	490	122	9.1	2.3	1.2	11.6	6.0	38
1L-1	4	11:32:30	490	122	9.3	2.6	1.8	12.1	6.4	41
1L-1	8	11:36:30	490	122	9.3	2.9	2.0	12.0	6.6	42
1L-2	1	11:38:00	880	210	15.4	5.0	5.5	20.7	11.7	74
1L-2	2	11:39:00	880	210	15.8	5.8	5.6	21.2	12.1	77
1L-2	4	11:41:00	880	210	16.4	6.0	5.4	21.1	12.2	77
1L-2	8	11:45:00	880	210	16.6	5.6	5.4	21.1	12.2	77
1L-3	1	11:47:00	1,300	305	22.6	8.6	9.9	30.2	17.8	113
1L-3	2	11:48:00	1,300	305	22.9	8.6	10.3	30.8	18.2	115
1L-3	4	11:50:00	1,300	305	23.0	8.7	9.9	30.8	18.1	115
1L-3	8	11:54:00	1,300	305	23.3	8.7	10.6	31.8	18.6	118
1L-4	1	11:56:00	1,630	380	27.1	10.4	15.1	39.9	23.1	147
1L-4	2	11:57:00	1,630	380	26.8	9.8	15.3	39.8	22.9	145
1L-4	4	11:59:00	1,630	380	27.2	10.3	16.0	40.3	23.4	149
1L-4	8	12:03:00	1,630	380	27.0	10.4	16.3	40.3	23.5	149
1L-5	1	12:05:00	1,980	459	30.9	12.2	21.8	48.7	28.4	180
1L-5	2	12:06:00	1,980	459	30.9	12.4	21.9	49.0	28.6	181
1L-5	4	12:08:00	1,980	459	30.9	12.7	22.6	49.4	28.9	183
1L-5	8	12:12:00	1,980	459	30.5	12.0	23.1	50.0	28.9	183
1L-6	1	12:13:30	2,450	565	35.5	14.3	31.1	61.7	35.6	226
1L-6	2	12:14:30	2,450	565	35.5	14.7	31.6	62.0	36.0	228
1L-6	4	12:16:30	2,450	565	35.4	14.5	32.3	62.7	36.2	230
1L-6	8	12:20:30	2,450	565	35.1	14.3	33.0	63.3	36.4	231
1L-7	1	12:22:00	2,820	648	38.6	16.0	40.4	73.9	42.2	268
1L-7	2	12:23:00	2,820	648	38.9	16.0	40.9	74.8	42.6	270
1L-7	4	12:25:00	2,820	648	38.1	15.7	41.0	74.8	42.4	269
1L-7	8	12:29:00	2,820	648	37.8	15.2	42.5	76.5	43.0	273
1L-8	1	12:30:30	3,200	734	41.8	15.4	50.8	90.0	49.5	314
1L-8	2	12:31:30	3,200	734	41.6	15.2	50.9	90.5	49.6	314
1L-8	4	12:33:30	3,200	734	41.4	15.0	52.0	91.9	50.1	318
1L-8	8	12:37:30	3,200	734	40.6	14.3	53.5	93.4	50.4	320
1L-9	1	12:39:30	3,580	820	44.9	15.9	62.2	106.4	57.3	364
1L-9	2	12:40:30	3,580	820	45.0	15.4	63.1	107.3	57.7	366
1L-9	4	12:42:30	3,580	820	45.9	16.1	63.2	107.2	58.1	368
1L-9	8	12:46:30	3,580	820	45.9	16.6	64.3	108.8	58.9	374
1L-10	1	12:48:00	3,990	913	51.3	19.0	73.4	121.5	66.3	420
1L-10	2	12:49:00	3,990	913	51.0	19.4	74.5	122.9	66.9	425
1L-10	4	12:51:00	3,990	913	50.7	19.0	76.0	124.5	67.5	428
1L-10	8	12:55:00	3,990	913	50.4	18.8	79.1	126.2	68.6	435
1X-11	1	13:06:00	4,186	957	51.1	20.6	92.5	138.4	75.6	480
1X-11	2	13:07:00	4,237	968	51.4	21.2	96.4	141.3	77.6	492
1X-11	3	13:08:00	4,348	993	51.8	22.4	103.2	147.8	81.3	516
1X-11	4	13:09:00	4,281	978	49.6	23.0	107.3	148.7	82.2	521
1X-11	5	13:10:00	4,161	951	47.6	22.5	106.8	145.8	80.7	512
1X-11	6	13:11:00	4,133	945	47.1	23.4	108.8	146.1	81.4	516
1X-11	7	13:12:00	3,996	914	44.7	22.4	107.3	142.5	79.2	503
1X-11	9	13:14:00	3,934	900	42.5	22.1	107.9	140.1	78.1	496
1X-12	1	13:15:30	3,771	863	39.5	20.0	104.0	135.1	74.7	473
1X-12	2	13:16:30	3,769	863	39.4	20.4	105.1	136.0	75.2	477
1X-12	3	13:17:30	3,749	858	38.9	19.3	104.8	135.2	74.5	473
1X-12	4	13:18:30	3,734	855	38.6	20.3	105.4	135.4	74.9	475
1X-13	1	13:19:30	3,952	904	42.2	26.1	116.1	142.3	81.7	518
1X-13	3	13:21:30	3,929	899	42.3	32.8	121.9	138.9	84.0	533
1X-13	5	13:23:30	3,908	894	42.8	38.8	125.7	132.7	85.0	539
1X-14	1	13:25:30	3,734	855	40.9	38.5	121.9	124.9	81.6	517
1X-14	2	13:26:30	3,648	835	39.8	37.8	119.4	121.8	79.7	505
1X-14	4	13:28:30	3,540	811	38.8	36.4	116.2	117.2	77.1	489
1X-14	8	13:32:30	3,327	763	35.5	33.4	110.1	111.2	72.6	460
1U-1	1	13:35:30	3,220	739	33.3	31.2	106.2	107.8	69.6	442
1U-1	2	13:36:30	3,220	739	34.6	32.8	108.9	109.4	71.5	453
1U-1	4	13:38:30	3,220	739	34.8	33.5	109.3	109.2	71.7	455
1U-2	1	13:42:00	2,380	549	23.9	20.3	90.1	93.4	56.9	361
1U-2	2	13:43:00	2,380	549	23.8	20.6	90.2	93.4	57.0	362
1U-2	4	13:45:00	2,380	549	23.7	20.3	90.0	93.2	56.8	360
1U-3	1	13:52:00	1,670	389	14.4	11.1	74.2	77.5	44.3	281
1U-3	2	13:53:00	1,670	389	14.6	11.0	74.4	78.1	44.5	282
1U-3	4	13:55:00	1,670	389	14.6	11.4	74.5	77.9	44.6	283
1U-4	1	13:58:00	940	224	5.6	4.8	51.7	51.6	28.4	180
1U-4	2	13:59:00	940	224	6.1	5.2	52.4	52.7	29.1	185
1U-4	4	14:01:00	940	224	4.8	4.3	49.3	49.0	26.9	170
1U-5	1	14:04:30	0	0	-2.4	3.7	12.1	3.7	4.3	27
1U-5	2	14:05:30	0	0	-2.0	4.0	11.0	2.8	4.0	25
1U-5	4	14:07:30	0	0	-1.4	5.0	10.0	1.5	3.8	24
1U-5	8	14:11:30	0	0	-0.7	5.9	8.7	0.3	3.6	23

LOADTEST

Strain Gage Readings and Loads at Level 2
TS-1 - IL-133 Over Embarras River - Oakland, IL

Load Test Increment	Hold Time (minutes)	Time (hh:mm:ss)	O-cell Pressure (psi)	O-cell Load (kips)	Strain Gage Level 2 2A-1521189 (με)	2B-1521190 (με)	2C-1521191 (με)	2D-1521192 (με)	Av. Strain (με)	Load (kips)
1L-0	-	10:58:00	0	0	0.0	0.0	0.0	0.0	0.0	0
1L-1	1	11:29:30	490	122	3.4	0.8	-0.1	3.1	1.8	11
1L-1	2	11:30:30	490	122	3.7	0.7	-0.3	3.4	1.9	12
1L-1	4	11:32:30	490	122	4.1	0.8	-0.3	3.5	2.0	13
1L-1	8	11:36:30	490	122	4.2	0.9	-0.3	3.5	2.1	13
1L-2	1	11:38:00	880	210	8.0	2.1	-0.6	6.6	4.0	26
1L-2	2	11:39:00	880	210	8.2	1.9	-0.7	6.8	4.0	26
1L-2	4	11:41:00	880	210	8.5	2.1	-0.8	6.8	4.2	26
1L-2	8	11:45:00	880	210	8.3	2.0	-1.0	6.8	4.0	26
1L-3	1	11:47:00	1,300	305	10.5	3.0	-0.3	8.8	5.5	35
1L-3	2	11:48:00	1,300	305	10.9	3.3	-0.2	9.0	5.8	36
1L-3	4	11:50:00	1,300	305	10.6	3.0	-0.3	9.0	5.6	35
1L-3	8	11:54:00	1,300	305	10.8	3.5	0.0	8.7	5.7	36
1L-4	1	11:56:00	1,630	380	12.0	3.8	1.4	10.5	6.9	44
1L-4	2	11:57:00	1,630	380	11.8	3.7	1.3	10.3	6.8	43
1L-4	4	11:59:00	1,630	380	11.7	3.7	1.4	10.3	6.8	43
1L-4	8	12:03:00	1,630	380	11.4	3.9	1.7	10.0	6.8	43
1L-5	1	12:05:00	1,980	459	12.2	4.6	3.8	11.6	8.0	51
1L-5	2	12:06:00	1,980	459	12.1	4.6	4.0	11.6	8.1	51
1L-5	4	12:08:00	1,980	459	11.8	4.8	4.1	11.6	8.1	51
1L-5	8	12:12:00	1,980	459	11.7	4.9	4.5	11.6	8.2	52
1L-6	1	12:13:30	2,450	565	12.9	5.4	6.9	14.0	9.8	62
1L-6	2	12:14:30	2,450	565	12.4	5.5	7.0	13.9	9.7	62
1L-6	4	12:16:30	2,450	565	12.2	5.6	7.5	14.1	9.8	62
1L-6	8	12:20:30	2,450	565	12.2	5.6	8.1	14.0	10.0	63
1L-7	1	12:22:00	2,820	648	12.6	5.6	10.2	16.2	11.1	71
1L-7	2	12:23:00	2,820	648	12.6	5.6	10.3	16.5	11.3	71
1L-7	4	12:25:00	2,820	648	12.1	5.7	10.5	16.5	11.2	71
1L-7	8	12:29:00	2,820	648	11.9	5.6	10.9	16.7	11.3	71
1L-8	1	12:30:30	3,200	734	12.6	5.3	13.6	19.7	12.8	81
1L-8	2	12:31:30	3,200	734	12.4	5.3	14.0	20.0	12.9	82
1L-8	4	12:33:30	3,200	734	12.3	5.2	14.3	20.3	13.0	83
1L-8	8	12:37:30	3,200	734	12.2	5.1	14.7	20.8	13.2	84
1L-9	1	12:39:30	3,580	820	12.6	5.4	17.6	24.0	14.9	94
1L-9	2	12:40:30	3,580	820	12.4	5.2	17.4	24.4	14.9	94
1L-9	4	12:42:30	3,580	820	12.8	5.8	17.8	24.6	15.3	97
1L-9	8	12:46:30	3,580	820	13.0	6.0	18.3	25.2	15.6	99
1L-10	1	12:48:00	3,990	913	14.3	6.7	20.5	28.4	17.5	111
1L-10	2	12:49:00	3,990	913	14.6	6.6	20.4	29.3	17.7	112
1L-10	4	12:51:00	3,990	913	14.6	6.8	21.2	30.0	18.1	115
1L-10	8	12:55:00	3,990	913	15.2	7.5	21.9	31.1	18.9	120
1X-11	1	13:06:00	4,186	957	16.3	8.3	26.5	35.6	21.7	138
1X-11	2	13:07:00	4,237	968	16.7	8.7	27.6	37.3	22.6	143
1X-11	3	13:08:00	4,348	993	16.3	8.9	30.1	39.0	23.6	150
1X-11	4	13:09:00	4,281	978	15.3	8.9	32.0	39.1	23.8	151
1X-11	5	13:10:00	4,161	951	14.7	9.2	32.2	38.5	23.6	150
1X-11	6	13:11:00	4,133	945	14.6	9.8	33.3	38.7	24.1	153
1X-11	7	13:12:00	3,996	914	13.9	9.8	33.1	37.9	23.7	150
1X-11	9	13:14:00	3,934	900	13.8	10.3	34.0	37.6	23.9	152
1X-12	1	13:15:30	3,771	863	11.8	9.5	32.6	35.2	22.3	141
1X-12	2	13:16:30	3,769	863	12.5	10.1	33.5	36.2	23.0	146
1X-12	3	13:17:30	3,749	858	12.4	10.1	34.0	36.1	23.1	147
1X-12	4	13:18:30	3,734	855	12.6	10.6	34.3	36.5	23.5	149
1X-13	1	13:19:30	3,952	904	14.1	11.9	37.2	38.6	25.5	161
1X-13	3	13:21:30	3,929	899	14.4	13.1	37.5	37.9	25.7	163
1X-13	5	13:23:30	3,908	894	15.0	12.8	36.1	38.5	25.6	162
1X-14	1	13:25:30	3,734	855	15.1	11.6	33.9	39.2	24.9	158
1X-14	2	13:26:30	3,648	835	14.7	11.0	32.4	39.3	24.3	154
1X-14	4	13:28:30	3,540	811	14.7	9.9	30.8	39.8	23.8	151
1X-14	8	13:32:30	3,327	763	13.8	8.6	28.5	39.2	22.5	143
1U-1	1	13:35:30	3,220	739	12.3	7.7	27.9	37.4	21.3	135
1U-1	2	13:36:30	3,220	739	13.9	8.7	28.8	39.2	22.6	144
1U-1	4	13:38:30	3,220	739	14.4	9.0	29.0	39.8	23.1	146
1U-2	1	13:42:00	2,380	549	7.5	2.2	21.5	32.9	16.0	102
1U-2	2	13:43:00	2,380	549	7.4	2.2	21.7	32.5	16.0	101
1U-2	4	13:45:00	2,380	549	7.5	2.0	21.3	32.5	15.8	100
1U-3	1	13:52:00	1,670	389	2.1	-2.3	15.8	25.8	10.3	66
1U-3	2	13:53:00	1,670	389	2.2	-2.3	16.0	26.1	10.5	67
1U-3	4	13:55:00	1,670	389	2.3	-2.2	16.0	26.0	10.5	67
1U-4	1	13:58:00	940	224	-2.8	-4.3	8.1	14.2	3.8	24
1U-4	2	13:59:00	940	224	-2.5	-4.1	8.6	14.3	4.1	26
1U-4	4	14:01:00	940	224	-3.7	-4.6	7.4	12.7	3.0	19
1U-5	1	14:04:30	0	0	-7.6	-3.8	-3.7	-6.1	-5.3	-34
1U-5	2	14:05:30	0	0	-7.4	-3.6	-4.2	-6.6	-5.5	-35
1U-5	4	14:07:30	0	0	-7.1	-3.1	-4.9	-7.1	-5.6	-35
1U-5	8	14:11:30	0	0	-6.8	-2.7	-5.3	-7.7	-5.6	-36

LOADTEST

Strain Gage Readings and Loads at Level 3
TS-1 - IL-133 Over Embarras River - Oakland, IL

Load Test Increment	Hold Time (minutes)	Time (hh:mm:ss)	O-cell Pressure (psi)	O-cell Load (kips)	Strain Gage Level 3 3A-1521193 (με)	3B-1521194 (με)	3C-1521195 (με)	3D-1521196 (με)	Av. Strain (με)	Load (kips)
1 L - 0	-	10:58:00	0	0	0.0	0.0	0.0	0.0	0.0	0
1 L - 1	1	11:29:30	490	122	0.1	1.1	0.1	1.4	0.7	5
1 L - 1	2	11:30:30	490	122	0.0	0.9	0.1	1.3	0.6	4
1 L - 1	4	11:32:30	490	122	0.0	1.1	0.1	1.1	0.6	4
1 L - 1	8	11:36:30	490	122	0.3	1.1	0.1	1.1	0.6	5
1 L - 2	1	11:38:00	880	210	0.5	2.2	-0.3	2.2	1.2	9
1 L - 2	2	11:39:00	880	210	0.4	2.4	-0.1	2.1	1.2	9
1 L - 2	4	11:41:00	880	210	0.4	2.3	-0.6	2.2	1.1	8
1 L - 2	8	11:45:00	880	210	0.5	2.3	-0.6	1.9	1.0	8
1 L - 3	1	11:47:00	1,300	305	0.7	3.1	-0.4	2.7	1.5	12
1 L - 3	2	11:48:00	1,300	305	0.9	3.0	-0.4	2.8	1.5	12
1 L - 3	4	11:50:00	1,300	305	0.7	2.7	-0.4	2.6	1.4	11
1 L - 3	8	11:54:00	1,300	305	0.8	3.0	-0.4	2.5	1.4	11
1 L - 4	1	11:56:00	1,630	380	1.2	3.3	-0.1	2.9	1.8	14
1 L - 4	2	11:57:00	1,630	380	0.7	3.3	0.0	2.8	1.7	13
1 L - 4	4	11:59:00	1,630	380	1.2	3.0	0.1	2.7	1.7	14
1 L - 4	8	12:03:00	1,630	380	1.1	3.0	-0.1	2.2	1.5	12
1 L - 5	1	12:05:00	1,980	459	1.4	3.3	0.5	2.5	1.9	15
1 L - 5	2	12:06:00	1,980	459	1.6	3.4	0.5	2.5	2.0	16
1 L - 5	4	12:08:00	1,980	459	1.4	3.1	0.6	2.4	1.9	15
1 L - 5	8	12:12:00	1,980	459	1.5	3.1	0.5	1.9	1.7	14
1 L - 6	1	12:13:30	2,450	565	2.4	3.5	1.4	2.6	2.5	19
1 L - 6	2	12:14:30	2,450	565	2.1	3.1	1.1	2.3	2.1	17
1 L - 6	4	12:16:30	2,450	565	2.0	3.2	1.3	2.1	2.2	17
1 L - 6	8	12:20:30	2,450	565	2.0	3.0	1.3	1.8	2.0	16
1 L - 7	1	12:22:00	2,820	648	2.2	3.2	1.9	2.2	2.4	19
1 L - 7	2	12:23:00	2,820	648	2.5	3.0	1.8	2.2	2.4	19
1 L - 7	4	12:25:00	2,820	648	2.3	3.0	1.7	1.7	2.2	17
1 L - 7	8	12:29:00	2,820	648	2.3	2.7	2.0	1.7	2.2	17
1 L - 8	1	12:30:30	3,200	734	2.6	3.0	2.5	2.1	2.5	20
1 L - 8	2	12:31:30	3,200	734	2.5	2.8	2.5	2.0	2.5	19
1 L - 8	4	12:33:30	3,200	734	2.4	2.5	2.4	2.0	2.3	18
1 L - 8	8	12:37:30	3,200	734	2.2	2.5	2.5	1.8	2.2	18
1 L - 9	1	12:39:30	3,580	820	2.9	2.6	2.9	2.0	2.6	20
1 L - 9	2	12:40:30	3,580	820	2.7	2.7	2.8	2.3	2.6	21
1 L - 9	4	12:42:30	3,580	820	3.1	2.8	3.0	1.7	2.6	21
1 L - 9	8	12:46:30	3,580	820	3.1	2.7	3.3	1.6	2.6	21
1 L - 10	1	12:48:00	3,990	913	3.2	2.8	3.6	1.7	2.9	22
1 L - 10	2	12:49:00	3,990	913	3.2	2.6	3.8	2.0	2.9	23
1 L - 10	4	12:51:00	3,990	913	3.2	2.4	3.8	1.9	2.8	22
1 L - 10	8	12:55:00	3,990	913	3.1	2.3	3.8	2.2	2.8	22
1 X - 11	1	13:06:00	4,186	957	3.0	2.0	4.5	2.3	3.0	23
1 X - 11	2	13:07:00	4,237	968	3.1	2.2	4.6	2.6	3.1	25
1 X - 11	3	13:08:00	4,348	993	3.0	2.0	5.1	3.1	3.3	26
1 X - 11	4	13:09:00	4,281	978	2.6	1.7	5.3	3.2	3.2	25
1 X - 11	5	13:10:00	4,161	951	2.7	1.8	5.4	3.1	3.2	25
1 X - 11	6	13:11:00	4,133	945	3.0	1.3	5.7	3.2	3.3	26
1 X - 11	7	13:12:00	3,996	914	2.8	1.2	5.9	2.7	3.1	25
1 X - 11	9	13:14:00	3,934	900	2.7	1.0	6.1	2.7	3.1	25
1 X - 12	1	13:15:30	3,771	863	2.5	1.0	5.8	2.6	3.0	23
1 X - 12	2	13:16:30	3,769	863	2.4	0.8	6.1	2.7	3.0	24
1 X - 12	3	13:17:30	3,749	858	2.6	0.6	6.1	2.7	3.0	24
1 X - 12	4	13:18:30	3,734	855	2.7	0.8	6.0	2.7	3.0	24
1 X - 13	1	13:19:30	3,952	904	2.9	0.8	7.1	3.2	3.5	27
1 X - 13	3	13:21:30	3,929	899	2.8	0.7	7.7	3.1	3.6	28
1 X - 13	5	13:23:30	3,908	894	2.9	0.7	7.9	3.6	3.8	30
1 X - 14	1	13:25:30	3,734	855	2.5	0.7	8.0	3.8	3.8	30
1 X - 14	2	13:26:30	3,648	835	2.6	0.5	8.1	3.6	3.7	29
1 X - 14	4	13:28:30	3,540	811	2.5	0.6	8.0	3.5	3.7	29
1 X - 14	8	13:32:30	3,327	763	2.1	0.2	7.9	3.4	3.4	27
1 U - 1	1	13:35:30	3,220	739	2.1	0.1	7.5	3.0	3.2	25
1 U - 1	2	13:36:30	3,220	739	2.3	0.2	7.7	3.3	3.4	27
1 U - 1	4	13:38:30	3,220	739	2.5	0.4	8.1	3.5	3.6	29
1 U - 2	1	13:42:00	2,380	549	0.7	-0.9	6.1	2.8	2.2	17
1 U - 2	2	13:43:00	2,380	549	0.7	-0.9	6.0	2.6	2.1	17
1 U - 2	4	13:45:00	2,380	549	1.0	-0.8	6.1	2.7	2.3	18
1 U - 3	1	13:52:00	1,670	389	-0.4	-1.5	4.7	1.9	1.2	9
1 U - 3	2	13:53:00	1,670	389	-0.4	-1.6	4.7	2.0	1.2	9
1 U - 3	4	13:55:00	1,670	389	-0.2	-1.5	4.7	2.0	1.2	10
1 U - 4	1	13:58:00	940	224	-1.3	-2.7	2.8	-0.2	-0.3	-3
1 U - 4	2	13:59:00	940	224	-1.2	-2.5	3.0	-0.2	-0.2	-2
1 U - 4	4	14:01:00	940	224	-1.5	-2.6	2.7	-0.1	-0.4	-3
1 U - 5	1	14:04:30	0	0	-1.3	-3.6	-0.1	-4.2	-2.3	-18
1 U - 5	2	14:05:30	0	0	-1.3	-3.9	-0.1	-4.8	-2.5	-20
1 U - 5	4	14:07:30	0	0	-1.3	-3.7	-0.1	-4.6	-2.4	-19
1 U - 5	8	14:11:30	0	0	-1.0	-3.5	-0.3	-4.4	-2.3	-18

APPENDIX B

O-CELL AND INSTRUMENTATION CALIBRATION SHEETS

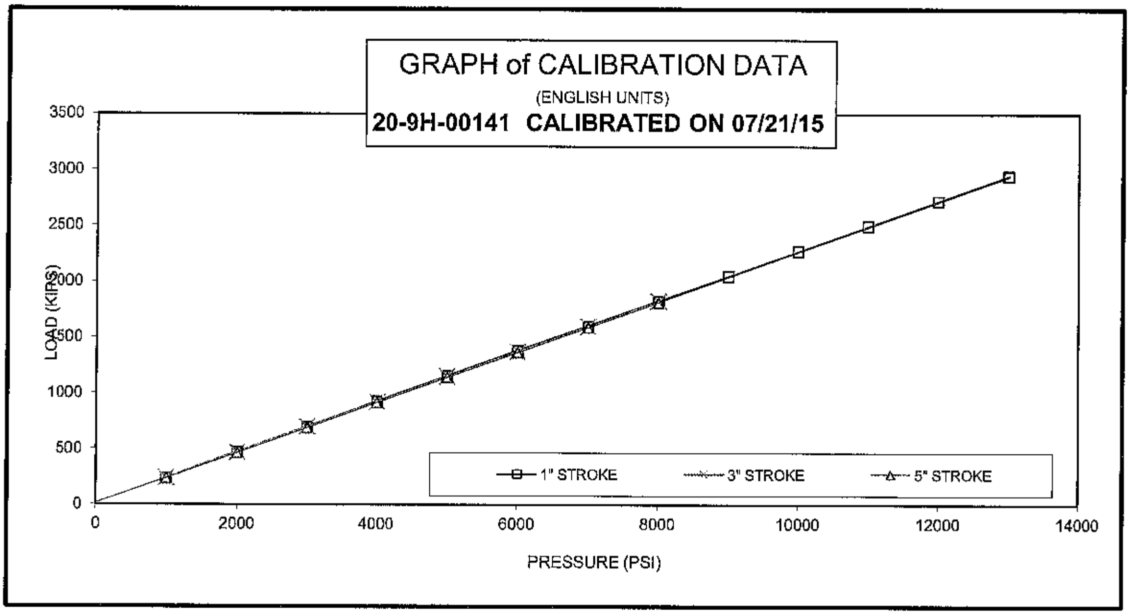

STROKE:	1 INCH	3 INCH	5 INCH
PRESSURE PSI	LOAD KIPS	LOAD KIPS	LOAD KIPS
0	0	0	0
1000	232	232	231
2000	463	463	460
3000	693	691	687
4000	921	919	913
5000	1147	1146	1138
6000	1376	1369	1363
7000	1598	1595	1587
8000	1822	1820	1810
9000	2046		
10000	2269		
11000	2494		
12000	2719		
13000	2943		

20" O-CELL, SERIAL # 20-9H-00141

LOAD CONVERSION FORMULA

LOAD = PRESSURE * 0.2258 + (11.72)
{KIPS} {PSI}

Regression Output:

Constant	11.7224 kips
X Coefficient	0.2258 kip / psi
R Square	1.0000
No. of Observations	29
Degrees of Freedom	27
Std Err of Y Est	4.57
Std Err of X Coeff	0.0003

CALIBRATION STANDARDS:

All data presented are derived from 6" dia. certified hydraulic pressure gauges and electronic load transducer, manufactured and calibrated by the University of Illinois at Champaign, Illinois. All calibrations and certifications are traceable through the Laboratory Master Deadweight Gauges directly to the National Institute of Standards and Technology. No specific guidelines exist for calibration of load test jacks and equipment but procedures comply with similar guidelines for calibration of gages, ANSI specifications B40.1.

* AE & FC CUSTOMER: FUGRO CONSULTANTS, INC.	* CONTRACTOR.: AJ WALKER CONSTRUCTION
* AE & FC JOB NO: SOLP00042	* JOB LOCATION: MATTOON, IL
* CUSTOMER P.O. NO.: LT-1425-1	* DATED: 07/21/15

SERVICE ENGINEER: ______ DATE: 7-21-15

GEOKON 48 Spencer St. Lebanon, NH 03766 USA

Sister Bar Calibration Report

Model Number: 4911-4

Date of Calibration: July 06, 2015

This calibration has been verified/validated as of 07/20/2015

Serial Number: 1521185

Cable Length: 35 feet

Prestress: 35,000 psi

Regression Zero: 6999

Temperature: 23.4 °C

Technician:

Calibration Instruction: CI-VW Rebar

Applied Load (pounds)	Readings				Linearity % Max. Load
	Cycle #1	Cycle #2	Average	Change	
100	7056	7053	7055		
1500	7732	7734	7733	678	-0.25
3000	8480	8482	8481	748	-0.02
4500	9226	9222	9224	743	0.03
6000	9965	9967	9966	742	0.06
100	7054	7054	7054		

For conversion factor, load to strain, refer to table C-2 of the Installation Manual

Gage Factor: 0.343 microstrain/ digit (GK-401 Pos. "B")

Calculated Strain = Gage Factor(Current Reading - Zero Reading)

Note: The above calibration uses the linear regression method.

Users are advised to establish their own zero conditions.

Linearity: ((Calculated Load - Applied Load)/Max. Applied Load) X 100 percent

The above instrument was found to be in tolerance in all operating ranges.
The above named instrument has been calibrated by comparison with standards traceable to the NIST, in compliance with ANSI Z540-1.

GEOKON 48 Spencer St. Lebanon, NH 03766 USA

Sister Bar Calibration Report

Model Number: 4911-4

Date of Calibration: July 06, 2015

This calibration has been verified/validated as of 07/20/2015

Serial Number: 1521186

Cable Length: 35 feet

Prestress: 35,000 psi

Regression Zero: 7074

Temperature: 23.4 °C

Technician:

Calibration Instruction: CI-VW Rebar

Applied Load (pounds)	Readings				Linearity % Max. Load
	Cycle #1	Cycle #2	Average	Change	
100	7128	7128	7128		
1500	7808	7808	7808	680	-0.13
3000	8543	8546	8545	737	-0.17
4500	9291	9291	9291	746	0.12
6000	10027	10025	10026	735	0.03
100	7129	7129	7129		

For conversion factor, load to strain, refer to table C-2 of the Installation Manual

Gage Factor: 0.344 microstrain/ digit (GK-401 Pos. "B")

Calculated Strain = Gage Factor(Current Reading - Zero Reading)

Note: The above calibration uses the linear regression method.

Users are advised to establish their own zero conditions.

Linearity: ((Calculated Load - Applied Load)/Max. Applied Load) X 100 percent

The above instrument was found to be in tolerance in all operating ranges.
The above named instrument has been calibrated by comparison with standards traceable to the NIST, in compliance with ANSI Z540-1.

GEOKON 48 Spencer St. Lebanon, NH 03766 USA

Sister Bar Calibration Report

Model Number: 4911-4

Date of Calibration: July 06, 2015

This calibration has been verified/validated as of 07/20/2015

Serial Number: 1521187

Cable Length: 35 feet

Prestress: 35,000 psi

Regression Zero: 7078

Temperature: 23.4 °C

Technician:

Calibration Instruction: CI-VW Rebar

Applied Load (pounds)	Readings				Linearity % Max. Load
	Cycle #1	Cycle #2	Average	Change	
100	7128	7132	7130		
1500	7811	7813	7812	682	-0.18
3000	8558	8558	8558	746	0.04
4500	9301	9299	9300	742	0.13
6000	10034	10033	10034	734	-0.07
100	7132	7134	7133		

For conversion factor, load to strain, refer to table C-2 of the Installation Manual

Gage Factor: 0.344 microstrain/ digit (GK-401 Pos. "B")

Calculated Strain = Gage Factor(Current Reading - Zero Reading)

Note: The above calibration uses the linear regression method.

<u>Users are advised to establish their own zero conditions.</u>

Linearity: ((Calculated Load - Applied Load)/Max. Applied Load) X 100 percent

The above instrument was found to be in tolerance in all operating ranges.
The above named instrument has been calibrated by comparison with standards traceable to the NIST, in compliance with ANSI Z540-1.

GEOKON 48 Spencer St. Lebanon, NH 03766 USA

Sister Bar Calibration Report

Model Number: 4911-4

Date of Calibration: July 06, 2015

This calibration has been verified/validated as of 07/20/2015

Serial Number: 1521188

Cable Length: 35 feet

Prestress: 35,000 psi

Regression Zero: 7176

Temperature: 23.4 °C

Technician:

Calibration Instruction: CI-VW Rebar

Applied Load (pounds)	Readings				Linearity % Max. Load
	Cycle #1	Cycle #2	Average	Change	
100	7237	7236	7237		
1500	7918	7919	7919	682	-0.37
3000	8675	8675	8675	756	-0.27
4500	9441	9441	9441	766	0.14
6000	10193	10192	10193	752	0.07
100	7237	7238	7238		

For conversion factor, load to strain, refer to table C-2 of the Installation Manual

Gage Factor: 0.339 microstrain/ digit (GK-401 Pos. "B")

Calculated Strain = Gage Factor(Current Reading - Zero Reading)

Note: The above calibration uses the linear regression method.

Users are advised to establish their own zero conditions.

Linearity: ((Calculated Load - Applied Load)/Max. Applied Load) X 100 percent

The above instrument was found to be in tolerance in all operating ranges.
The above named instrument has been calibrated by comparison with standards traceable to the NIST, in compliance with ANSI Z540-1.

48 Spencer St. Lebanon, NH 03766 USA

Sister Bar Calibration Report

Model Number: 4911-4

Date of Calibration: July 06, 2015

This calibration has been verified/validated as of 07/20/2015

Serial Number: 1521189

Cable Length: 30 feet

Prestress: 35,000 psi

Regression Zero: 7177

Temperature: 23.4 °C

Technician:

Calibration Instruction: CI-VW Rebar

Applied Load (pounds)	Readings				Linearity % Max. Load
	Cycle #1	Cycle #2	Average	Change	
100	7232	7230	7231		
1500	7914	7914	7914	683	-0.08
3000	8651	8653	8652	738	-0.13
4500	9396	9396	9396	744	0.03
6000	10140	10135	10138	742	0.10
100	7231	7231	7231		

For conversion factor, load to strain, refer to table C-2 of the Installation Manual

Gage Factor: 0.344 microstrain/ digit (GK-401 Pos. "B")

Calculated Strain = Gage Factor(Current Reading - Zero Reading)

Note: The above calibration uses the linear regression method.

Users are advised to establish their own zero conditions.

Linearity: ((Calculated Load - Applied Load)/Max. Applied Load) X 100 percent

The above instrument was found to be in tolerance in all operating ranges.
The above named instrument has been calibrated by comparison with standards traceable to the NIST, in compliance with ANSI Z540-1.

GEOKON 48 Spencer St. Lebanon, NH 03766 USA

Sister Bar Calibration Report

Model Number: 4911-4

Date of Calibration: July 06, 2015

This calibration has been verified/validated as of 07/20/2015

Serial Number: 1521190

Cable Length: 30 feet

Prestress: 35,000 psi

Regression Zero: 7030

Temperature: 23.4 °C

Technician:

Calibration Instruction: CI-VW Rebar

Applied Load (pounds)	Readings				Linearity % Max. Load
	Cycle #1	Cycle #2	Average	Change	
100	7079	7079	7079		
1500	7765	7767	7766	687	-0.02
3000	8500	8506	8503	737	0.00
4500	9239	9242	9241	738	0.04
6000	9975	9975	9975	734	-0.03
100	7079	7080	7080		

For conversion factor, load to strain, refer to table C-2 of the Installation Manual

Gage Factor: 0.345 microstrain/ digit (GK-401 Pos. "B")

Calculated Strain = Gage Factor(Current Reading - Zero Reading)

Note: The above calibration uses the linear regression method.

Users are advised to establish their own zero conditions.

Linearity: ((Calculated Load - Applied Load)/Max. Applied Load) X 100 percent

The above instrument was found to be in tolerance in all operating ranges.
The above named instrument has been calibrated by comparison with standards traceable to the NIST, in compliance with ANSI Z540-1.

GEOKON 48 Spencer St. Lebanon, NH 03766 USA

Sister Bar Calibration Report

Model Number: 4911-4

Date of Calibration: July 06, 2015

This calibration has been verified/validated as of 07/20/2015

Serial Number: 1521191

Cable Length: 30 feet

Prestress: 35,000 psi

Regression Zero: 7089

Temperature: 23.4 °C

Technician:

Calibration Instruction: CI-VW Rebar

Applied Load (pounds)	Readings				Linearity % Max. Load
	Cycle #1	Cycle #2	Average	Change	
100	7142	7144	7143		
1500	7823	7828	7826	683	-0.14
3000	8564	8568	8566	740	-0.15
4500	9314	9314	9314	748	0.10
6000	10054	10051	10053	739	0.03
100	7145	7147	7146		

For conversion factor, load to strain, refer to table C-2 of the Installation Manual

Gage Factor: 0.343 microstrain/ digit (GK-401 Pos. "B")

Calculated Strain = Gage Factor(Current Reading - Zero Reading)

Note: The above calibration uses the linear regression method.

Users are advised to establish their own zero conditions.

Linearity: ((Calculated Load - Applied Load)/Max. Applied Load) X 100 percent

The above instrument was found to be in tolerance in all operating ranges.
The above named instrument has been calibrated by comparison with standards traceable to the NIST, in compliance with ANSI Z540-1.

GEOKON 48 Spencer St. Lebanon, NH 03766 USA

Sister Bar Calibration Report

Model Number: 4911-4

Date of Calibration: July 06, 2015

This calibration has been verified/validated as of 07/20/2015

Serial Number: 1521192

Cable Length: 30 feet

Prestress: 35,000 psi

Regression Zero: 7211

Temperature: 23.4 °C

Technician:

Calibration Instruction: CI-VW Rebar

Applied Load (pounds)	Readings				Linearity % Max. Load
	Cycle #1	Cycle #2	Average	Change	
100	7263	7260	7262		
1500	7934	7932	7933	671	-0.03
3000	8654	8652	8653	720	-0.13
4500	9388	9383	9386	733	0.20
6000	10103	10100	10102	716	-0.04
100	7261	7258	7260		

For conversion factor, load to strain, refer to table C-2 of the Installation Manual

Gage Factor: 0.349 microstrain/ digit (GK-401 Pos. "B")

Calculated Strain = Gage Factor(Current Reading - Zero Reading)

Note: The above calibration uses the linear regression method.

Users are advised to establish their own zero conditions.

Linearity: ((Calculated Load - Applied Load)/Max. Applied Load) X 100 percent

The above instrument was found to be in tolerance in all operating ranges.
The above named instrument has been calibrated by comparison with standards traceable to the NIST, in compliance with ANSI Z540-1.

GEOKON 48 Spencer St. Lebanon, NH 03766 USA

Sister Bar Calibration Report

Model Number: 4911-4

Date of Calibration: July 06, 2015

This calibration has been verified/validated as of 07/20/2015

Serial Number: 1521193

Cable Length: 30 feet

Prestress: 35,000 psi

Regression Zero: 6950

Temperature: 23.4 °C

Technician:

Calibration Instruction: CI-VW Rebar

Applied Load (pounds)	Readings				Linearity % Max. Load
	Cycle #1	Cycle #2	Average	Change	
100	7009	7002	7006		
1500	7692	7688	7690	684	-0.16
3000	8435	8430	8433	743	-0.24
4500	9194	9188	9191	758	0.21
6000	9933	9926	9930	739	0.00
100	7003	6997	7000		

For conversion factor, load to strain, refer to table C-2 of the Installation Manual

Gage Factor: 0.342 microstrain/ digit (GK-401 Pos. "B")

Calculated Strain = Gage Factor(Current Reading - Zero Reading)

Note: The above calibration uses the linear regression method.

Users are advised to establish their own zero conditions.

Linearity: ((Calculated Load - Applied Load)/Max. Applied Load) X 100 percent

The above instrument was found to be in tolerance in all operating ranges.
The above named instrument has been calibrated by comparison with standards traceable to the NIST, in compliance with ANSI Z540-1.

GEOKON 48 Spencer St. Lebanon, NH 03766 USA

Sister Bar Calibration Report

Model Number: 4911-4

Date of Calibration: July 06, 2015

This calibration has been verified/validated as of 07/20/2015

Serial Number: 1521194

Cable Length: 30 feet

Prestress: 35,000 psi

Regression Zero: 7168

Temperature: 23.4 °C

Technician:

Calibration Instruction: CI-VW Rebar

Applied Load (pounds)	Readings				Linearity % Max. Load
	Cycle #1	Cycle #2	Average	Change	
100	7219	7220	7220		
1500	7914	7914	7914	694	-0.10
3000	8665	8666	8666	752	-0.02
4500	9417	9416	9417	751	0.04
6000	10165	10162	10164	747	-0.02
100	7221	7220	7221		

For conversion factor, load to strain, refer to table C-2 of the Installation Manual

Gage Factor: 0.340 microstrain/ digit (GK-401 Pos. "B")

Calculated Strain = Gage Factor(Current Reading - Zero Reading)

Note: The above calibration uses the linear regression method.

Users are advised to establish their own zero conditions.

Linearity: ((Calculated Load - Applied Load)/Max. Applied Load) X 100 percent

The above instrument was found to be in tolerance in all operating ranges.
The above named instrument has been calibrated by comparison with standards traceable to the NIST, in compliance with ANSI Z540-1.

GEOKON 48 Spencer St. Lebanon, NH 03766 USA

Sister Bar Calibration Report

Model Number: 4911-4

Date of Calibration: July 06, 2015

This calibration has been verified/validated as of 07/20/2015

Serial Number: 1521195

Cable Length: 30 feet

Prestress: 35,000 psi

Regression Zero: 7201

Temperature: 23.4 °C

Technician:

Calibration Instruction: CI-VW Rebar

Applied Load (pounds)	Readings				Linearity % Max. Load
	Cycle #1	Cycle #2	Average	Change	
100	7258	7254	7256		
1500	7947	7943	7945	689	-0.09
3000	8689	8685	8687	742	-0.25
4500	9446	9447	9447	760	0.18
6000	10192	10186	10189	742	0.03
100	7254	7249	7252		

For conversion factor, load to strain, refer to table C-2 of the Installation Manual

Gage Factor: 0.341 microstrain/ digit (GK-401 Pos. "B")

Calculated Strain = Gage Factor(Current Reading - Zero Reading)

Note: The above calibration uses the linear regression method.

Users are advised to establish their own zero conditions.

Linearity: ((Calculated Load - Applied Load)/Max. Applied Load) X 100 percent

The above instrument was found to be in tolerance in all operating ranges.
The above named instrument has been calibrated by comparison with standards traceable to the NIST, in compliance with ANSI Z540-1.

GEOKON 48 Spencer St. Lebanon, NH 03766 USA

Sister Bar Calibration Report

Model Number: 4911-4

Date of Calibration: July 06, 2015

This calibration has been verified/validated as of 07/20/2015

Serial Number: 1521196

Cable Length: 30 feet

Prestress: 35,000 psi

Regression Zero: 7294

Temperature: 23.4 °C

Technician:

Calibration Instruction: CI-VW Rebar

Applied Load (pounds)	Readings				Linearity % Max. Load
	Cycle #1	Cycle #2	Average	Change	
100	7348	7351	7350		
1500	8037	8040	8039	689	-0.23
3000	8795	8797	8796	757	-0.02
4500	9550	9549	9550	754	0.06
6000	10299	10301	10300	750	0.03
100	7352	7352	7352		

For conversion factor, load to strain, refer to table C-2 of the Installation Manual

Gage Factor: 0.340 microstrain/ digit (GK-401 Pos. "B")

Calculated Strain = Gage Factor(Current Reading - Zero Reading)

Note: The above calibration uses the linear regression method.

Users are advised to establish their own zero conditions.

Linearity: ((Calculated Load - Applied Load)/Max. Applied Load) X 100 percent

The above instrument was found to be in tolerance in all operating ranges.
The above named instrument has been calibrated by comparison with standards traceable to the NIST, in compliance with ANSI Z540-1.

GEOKON 48 Spencer St. Lebanon, NH 03766 USA

Vibrating Wire Displacement Transducer Calibration Report

Range: 230 mm

Calibration Date: June 30, 2015

This calibration has been verified/validated as of 07/20/2015

Serial Number: 1518972

Temperature: 23.2 °C

Calibration Instruction: CI-4400

Technician:

Cable Length: 40 feet

GK-401 Reading Position B

Actual Displacement (mm)	Gage Reading 1st Cycle	Gage Reading 2nd Cycle	Average Gage Reading	Calculated Displacement Linear	Error Linear (%FS)	Calculated Displacement Polynomial	Error Polynomial (%FS)
0.0	2514	2514	2514	-0.38	-0.16	-0.01	-0.01
46.0	3496	3496	3496	46.09	0.04	46.02	0.01
92.0	4472	4473	4473	92.31	0.13	92.02	0.01
138.0	5443	5442	5443	138.21	0.09	137.93	-0.03
184.0	6413	6412	6413	184.12	0.05	184.05	0.02
230.0	7374	7374	7374	229.62	-0.16	229.99	-0.01

(mm) Linear Gage Factor (G): 0.04733 (mm/ digit) **Regression Zero: 2522**

Polynomial Gage Factors: A: 1.1494E-07 B: 0.04619 C: ________

Calculate C by setting D = 0 and R_1 = initial field zero reading into the polynomial equation

(inches) Linear Gage Factor (G): 0.001863 (inches/digit)

Polynomial Gage Factors: A: 4.525E-09 B: 0.001818 C: ________

Calculate C by setting D = 0 and R_1 = initial field zero reading into the polynomial equation

Calculated Displacement: **Linear, $D = G(R_1 - R_0)$**

Polynomial, $D = AR_1^2 + BR_1 + C$

Refer to manual for temperature correction information.

The above instrument was found to be in tolerance in all operating ranges.
The above named instrument has been calibrated by comparison with standards traceable to the NIST, in compliance with ANSI Z540-1.

GEOKON 48 Spencer St. Lebanon, NH 03766 USA

Vibrating Wire Displacement Transducer Calibration Report

Range: 230 mm

Serial Number: 1520720

Calibration Instruction: CI-4400

Cable Length: 40 feet

Calibration Date: July 06, 2015

This calibration has been verified/validated as of 07/20/2015

Temperature: 23.3 °C

Technician: [signature]

GK-401 Reading Position B

Actual Displacement (mm)	Gage Reading 1st Cycle	Gage Reading 2nd Cycle	Average Gage Reading	Calculated Displacement Linear	Error Linear (%FS)	Calculated Displacement Polynomial	Error Polynomial (%FS)
0.0	2570	2570	2570	-0.42	-0.18	-0.06	-0.02
46.0	3561	3562	3562	46.14	0.06	46.08	0.03
92.0	4546	4544	4545	92.32	0.14	92.06	0.02
138.0	5521	5522	5522	138.18	0.08	137.92	-0.04
184.0	6496	6499	6498	184.01	0.00	183.96	-0.02
230.0	7471	7469	7470	229.68	-0.14	230.04	0.02

(mm) Linear Gage Factor (G): 0.04696 (mm/ digit) **Regression Zero: 2579**

Polynomial Gage Factors: A: 1.0925E-07 B: 0.04586 C: ______

Calculate C by setting D = 0 and R_1 = initial field zero reading into the polynomial equation

(inches) Linear Gage Factor (G): 0.001849 (inches/digit)

Polynomial Gage Factors: A: 4.3012E-09 B: 0.001806 C: ______

Calculate C by setting D = 0 and R_1 = initial field zero reading into the polynomial equation

Calculated Displacement: **Linear, $D = G(R_1 - R_0)$**

Polynomial, $D = AR_1^2 + BR_1 + C$

Refer to manual for temperature correction information.

The above instrument was found to be in tolerance in all operating ranges.
The above named instrument has been calibrated by comparison with standards traceable to the NIST, in compliance with ANSI Z540-1.

GEOKON 48 Spencer St. Lebanon, NH 03766 USA

Vibrating Wire Displacement Transducer Calibration Report

Range: 230 mm

Serial Number: 1520721

Calibration Instruction: CI-4400

Cable Length: 40 feet

Calibration Date: July 06, 2015

This calibration has been verified/validated as of 07/20/2015

Temperature: 23.3 °C

Technician: [signature]

GK-401 Reading Position B

Actual Displacement (mm)	Gage Reading 1st Cycle	Gage Reading 2nd Cycle	Average Gage Reading	Calculated Displacement Linear	Error Linear (%FS)	Calculated Displacement Polynomial	Error Polynomial (%FS)
0.0	2549	2547	2548	-0.38	-0.16	0.04	0.02
46.0	3536	3535	3536	46.07	0.03	45.97	-0.01
92.0	4518	4517	4518	92.25	0.11	91.91	-0.04
138.0	5499	5500	5500	138.43	0.19	138.09	0.04
184.0	6471	6471	6471	184.12	0.05	184.03	0.01
230.0	7437	7437	7437	229.55	-0.20	229.96	-0.02

(mm) Linear Gage Factor (G): 0.04703 (mm/ digit) **Regression Zero: 2556**

Polynomial Gage Factors: A: 1.3123E-07 B: 0.04572 C: ______

Calculate C by setting D = 0 and R_1 = initial field zero reading into the polynomial equation

(inches) Linear Gage Factor (G): 0.001852 (inches/digit)

Polynomial Gage Factors: A: 5.1667E-09 B: 0.001800 C: ______

Calculate C by setting D = 0 and R_1 = initial field zero reading into the polynomial equation

Calculated Displacement: **Linear, $D = G(R_1 - R_0)$**

Polynomial, $D = AR_1^2 + BR_1 + C$

Refer to manual for temperature correction information.

The above instrument was found to be in tolerance in all operating ranges.
The above named instrument has been calibrated by comparison with standards traceable to the NIST, in compliance with ANSI Z540-1.

GEOKON 48 Spencer St. Lebanon, NH 03766 USA

Vibrating Wire Displacement Transducer Calibration Report

Range: 230 mm

Serial Number: 1520722

Calibration Instruction: CI-4400

Cable Length: 40 feet

Calibration Date: July 06, 2015

This calibration has been verified/validated as of 07/20/2015

Temperature: 23.3 °C

Technician: [signature]

GK-401 Reading Position B

Actual Displacement (mm)	Gage Reading 1st Cycle	Gage Reading 2nd Cycle	Average Gage Reading	Calculated Displacement Linear	Error Linear (%FS)	Calculated Displacement Polynomial	Error Polynomial (%FS)
0.0	2653	2653	2653	-0.33	-0.14	-0.03	-0.01
46.0	3631	3632	3632	46.12	0.05	46.03	0.01
92.0	4604	4605	4605	92.32	0.14	92.03	0.01
138.0	5572	5573	5573	138.27	0.12	137.99	0.00
184.0	6536	6536	6536	184.02	0.01	183.93	-0.03
230.0	7499	7499	7499	229.74	-0.11	230.04	0.02

(mm) Linear Gage Factor (G): 0.04748 (mm/ digit) **Regression Zero: 2660**

Polynomial Gage Factors: A: 1.043E-07 B: 0.04642 C: ______

Calculate C by setting D = 0 and R_1 = initial field zero reading into the polynomial equation

(inches) Linear Gage Factor (G): 0.001869 (inches/digit)

Polynomial Gage Factors: A: 4.1062E-09 B: 0.001827 C: ______

Calculate C by setting D = 0 and R_1 = initial field zero reading into the polynomial equation

Calculated Displacement: **Linear, $D = G(R_1 - R_0)$**

Polynomial, $D = AR_1^2 + BR_1 + C$

Refer to manual for temperature correction information.

The above instrument was found to be in tolerance in all operating ranges.
The above named instrument has been calibrated by comparison with standards traceable to the NIST, in compliance with ANSI Z540-1.

Certificate of Calibration

Certificate Number: LT.59685.2015-01-07

Instrument: Geokon VWPX

Calibration Date: Jan 7, 2015

Model: 4500HH-10000

Temperature: 19.0 °C

Serial Number: 59685

Linear Range: 15000 psi

Reference Pressure		Gauge Readings		Linear Error		Polynomial Error	
1st Cycle (psi)	2nd Cycle (psi)	1st Cycle (digits)	2nd Cycle (digits)	1st Cycle (% FS)	2nd Cycle (% FS)	1st Cycle (% FS)	2nd Cycle (% FS)
0.	0.	8972.2	8970.2	0.21	0.24	-0.01	0.03
3000.	3000.	7836.5	7783.3	-0.51	0.40	-0.46	0.45
6000.	6000.	6663.2	6618.1	-0.58	0.18	-0.40	0.36
9000.	9000.	5477.8	5438.6	-0.45	0.21	-0.27	0.39
12000.	12000.	4288.6	4271.1	-0.26	0.04	-0.21	0.09
15000.	15000.	3083.2	3080.0	0.21	0.26	-0.01	0.04

Linear Gauge Factor: **-2.54704** **psi/dig** **-0.0175612** **MPa/dig**

Polynomial Factor: **-7.163E-06** **psi/dig²** + **-2.461E+00** **psi/dig**

-4.939E-08 **MPa/dig²** + **-1.697E-02** **MPa/dig**

Logging Instrument: Datataker DT85G, Serial: 085637

Reference Instrument: SENSOTEC TJE/743-23TJA, Serial: 622335

Reference Calibrated: 2014-04-15

Reference Certificate: 1001395677

LOADTEST certifies that the above named instrument has been calibrated by comparison with standards traceable to the NIST and was found to be in tolerance in all operating ranges. Relevant documentation and certificates are available on request.

Tested by: Michael Crumpton, B.S.C.E. Signed: MZ Crumpton

Approved by: David J. Jakstis, P.E. Signed:

GEOKON 48 Spencer St. Lebanon, NH 03766 USA

Vibrating Wire Displacement Transducer Calibration Report

Range: 100 mm

Serial Number: 1424656

Calibration Instruction: CI-4400

Cable Length: 25 feet

Calibration Date: September 22, 2014

This calibration has been verified/validated as of 11/19/2014

Temperature: 23.6 °C

Technician:

GK-401 Reading Position B

Actual Displacement (mm)	Gage Reading 1st Cycle	Gage Reading 2nd Cycle	Average Gage Reading	Calculated Displacement Linear	Error Linear (%FS)	Calculated Displacement Polynomial	Error Polynomial (%FS)
0.0	2514	2511	2513	-0.22	-0.22	0.00	0.00
20.0	3496	3494	3495	20.07	0.07	20.03	0.03
40.0	4463	4463	4463	40.06	0.06	39.89	-0.11
60.0	5441	5440	5441	60.25	0.25	60.08	0.08
80.0	6400	6398	6399	80.04	0.04	80.01	0.01
100.0	7354	7354	7354	99.76	-0.24	99.98	-0.02

(mm) Linear Gage Factor (G): 0.02065 (mm/ digit) **Regression Zero: 2523**

Polynomial Gage Factors: A: 6.9004E-08 B: 0.01997 C: ________

Calculate C by setting D = 0 and R_1 = initial field zero reading into the polynomial equation

(inches) Linear Gage Factor (G): 0.0008130 (inches/digit)

Polynomial Gage Factors: A: 2.7167E-09 B: 0.0007862 C: ________

Calculate C by setting D = 0 and R_1 = initial field zero reading into the polynomial equation

Calculated Displacement: **Linear, $D = G(R_1 - R_0)$**

Polynomial, $D = AR_1^2 + BR_1 + C$

Refer to manual for temperature correction information.

The above instrument was found to be in tolerance in all operating ranges.
The above named instrument has been calibrated by comparison with standards traceable to the NIST, in compliance with ANSI Z540-1.

Certificate of Calibration

Certificate Number: LT.08-23840.2014-11-06

Instrument: Geokon LVWDT
Calibration Date: Nov 6, 2014

Model: 4450-3-100
Temperature: 23.0 °C

Serial Number: 08-23840
Linear Range: 100 mm

Reference Displacement		Gauge Readings		Linear Error		Polynomial Error	
1st Cycle (mm)	2nd Cycle (mm)	1st Cycle (digits)	2nd Cycle (digits)	1st Cycle (% FS)	2nd Cycle (% FS)	1st Cycle (% FS)	2nd Cycle (% FS)
0.00	0.00	2646.9	2643.5	-0.12	-0.19	0.03	-0.04
20.00	20.00	3621.4	3616.2	0.08	-0.03	0.05	-0.06
40.00	40.00	4593.8	4585.5	0.24	0.06	0.11	-0.06
60.00	60.00	5555.8	5548.5	0.18	0.02	0.06	-0.10
80.00	80.00	6515.6	6510.6	0.07	-0.03	0.04	-0.06
100.00	100.00	7468.5	7471.6	-0.18	-0.11	-0.03	0.04

Linear Gauge Factor: **0.02073** **mm/dig** **0.0008161** **in/dig**

Polynomial Factor: **4.892E-08** **mm/dig²** + **2.023E-02** **mm/dig**

1.926E-09 **in/dig²** + **7.966E-04** **in/dig**

Logging Instrument: Datataker DT80G, Serial: 93385

Reference Instrument: Fowler Blocks, Serial: 060572

Reference Calibrated: 2014-05-10

Reference Certificate: 1001568996

LOADTEST certifies that the above named instrument has been calibrated by comparison with standards traceable to the NIST and was found to be in tolerance in all operating ranges. Relevant documentation and certificates are available on request.

Tested by: Michael Crumpton, B.S.C.E. Signed: MZ Crumpton

Approved by: David J. Jakstis, P.E. Signed:

APPENDIX C

CONSTRUCTION OF THE EQUIVALENT TOP LOAD-DISPLACEMENT CURVE

CONSTRUCTION OF THE EQUIVALENT TOP-LOADED LOAD-SETTLEMENT CURVE FROM THE RESULTS OF AN O-CELL™ TEST (October, 2001)

Introduction: Some engineers find it useful to see the results of an O-cell™ load test in the form of a curve showing the load versus settlement of a top-loaded driven or bored pile (drilled shaft). We believe that an O-cell™ test can provide a good estimate of this curve when using the method described herein.

Assumptions: We make the following assumptions, which we consider both reasonable and usually conservative:

1. The end bearing load-movement curve in a top-loaded pile has the same loads for a given movement as the net (subtract buoyant weight of pile above the O-cell™) end bearing load-movement curve developed by the bottom of the O-cell™ when placed at or near the bottom of the pile.

2. The side shear load-movement curve in a top-loaded pile has the same net shear, multiplied by an adjustment factor 'F', for a given downward movement as occurred in the O-cell™ test for that same movement at the top of the cell in the upward direction. The same applies to the upward movement in a top-loaded tension test. Unless noted otherwise, we use the following adjustment factors:
(a) F = 1.00 in all rock sockets and for primarily cohesive soils in compression
(b) F = 0.95 in primarily cohesionless soils
(c) F = 0.80 for all soils in top load tension tests.

3. We initially assume the pile behaves as a rigid body, but include the elastic compressions that are part of the movement data obtained from an O-cell™ test (OLT). Using this assumption, we construct an equivalent top-load test (TLT) movement curve by the method described below in Procedure Part I. We then use the following Procedure Part II to correct for the effects of the additional elastic compressions in a TLT.

4. Consider the case with the O-cell™, or the lower O-cell™ of more than one level of cells, placed some distance above the bottom of the pile. We assume the part of the pile below the cell, now top-loaded, has the same load-movement behavior as when top-loading the entire pile. For this case the subsequent "end bearing movement curve" refers to the movement of the entire length of pile below the cell

Procedure Part I: Please refer to the attached Figure A showing O-cell™ test results and to Figure B, the constructed equivalent top load-settlement curve. Note that each of the curves shown has points numbered from 1 to 12 such that the same point number on each curve has the same magnitude of movement. For example, point 4 has an upward and downward movement of 10.2 mm in Figure A and the same 10.2 mm downward in Figure B.

Note: This report shows the O-cell movement data in a Figure similar to Fig. A, but uses the gross loads as obtained in the field. Fig. A uses net loads to make it easier for the reader to convert Fig. A into Fig. B without the complication of the first converting gross to net loads. For our conservative reconstruction of the top loaded settlement curve we first convert both of the O-cell components to net loads.

Using the above assumptions, construct the equivalent curve as follows: Select an arbitrary movement such as the 10.2 mm to give point 4 on the pile side shear load movement curve in Figure A and record the 18.6 MN load in shear at that movement. Because we have initially assumed a rigid pile, the top of pile moves downward the same as the bottom. Therefore, find point 4 with 10.2 mm of downward movement on the end bearing load movement curve and record the corresponding load of 9.4 MN. Adding these two loads will give the total load of 28.0 MN due to side shear plus end bearing at the same movement and thus gives point 4 on the Figure B load settlement curve for an equivalent top-loaded test.

One can use the above procedure to obtain all the points in Figure B up to the component that moved the least at the end of the test, in this case point 5 in side shear. To take advantage of the fact that the test produced end bearing movement data up to point 12, we need to make an extrapolation of the side shear curve. We usually use a convenient and suitable hyperbolic curve fitting technique for this extrapolation. Deciding on the maximum number of data points to provide a good fit (a high r^2 correlation coefficient) requires some judgment. In this case we omitted point 1 to give an $r^2 = 0.999$ (including point 1 gave an $r^2 = 0.966$) with the result shown as points 6 to 12 on the dotted extension of the measured side shear curve. Using the same movement matching procedure described earlier we can then extend the equivalent curve to points 6 to 12. The results, shown in Figure B as a dashed line, signify that this part of the equivalent curve depends partly on extrapolated data.

Sometimes, if the data warrants, we will use extrapolations of both side shear and end bearing to extend the equivalent curve to a greater movement than the maximum measured (point 12). An appendix in this report gives the details of the extrapolation(s) used with the present O-cell™ test and shows the fit with the actual data.

Procedure Part II: The elastic compression in the equivalent top load test always exceeds that in the O-cell™ test. It not only produces more top movement, but also additional side shear movement, which then generates more side shear, which produces more compression, etc . . . An exact solution of this load transfer problem requires knowing the side shear vs. vertical movement (t-y) curves for a large number of pile length increments and solving the resulting set of simultaneous equations or using finite element or finite difference simulations to obtain an approximate solution for these equations. We usually do not have the data to obtain the many accurate t-y curves required. Fortunately, the approximate solution described below usually suffices.

The attached analysis p. 6 gives the equations for the elastic compressions that occur in the OLT with one or two levels of O-cells™. Analysis p. 7 gives the equations for the elastic compressions that occur in the equivalent TLT. Both sets of equations do not include the elastic compression below the O-cell™ because the same compression takes place in both the OLT and the TLT. This is equivalent to taking $L_3 = 0$. Subtracting the OLT from the TLT compression gives the desired additional elastic compression at the top of the TLT. We then add the additional elastic compression to the 'rigid' equivalent curve obtained from Part I to obtain the final, corrected equivalent load-settlement curve for the TLT on the same pile as the actual OLT.

Note that the above pp. 6 and 7 give equations for each of three assumed patterns of developed side shear stress along the pile. The pattern shown in the center of the three applies to any approximately determined side shear distribution. Experience has shown the initial solution for the additional elastic compression, as described above, gives an adequate and slightly conservative (high) estimate of the additional compression versus more sophisticated load-transfer analyses as described in the first paragraph of this Part II.

The analysis p. 8 provides an example of calculated results on a hypothetical 1-stage, single level OLT using the simplified method in Part II with the centriod of the side shear distribution 44.1% above the base of the O-cell™. Figure C compares the corrected with the rigid curve of Figure B.

The final analysis p. 9 provides an example of calculated results on a hypothetical 3-stage, multi level OLT using the simplified method in Part II with the centroid of the combined upper and middle side shear distribution 44.1% above the base of the lower O-cell™. The individual centroids of the upper and middle side shear distributions lie 39.6% and 57.9% above and below the upper O-cell™, respectively. Figure D compares the corrected with the rigid curve.

Other Tests: The example illustrated in Figure A has the maximum component movement in end bearing. The procedures remain the same if the maximum test movement occurred in side shear. Then we would have extrapolated end bearing to produce the dashed-line part of the reconstructed top-load settlement curve.

The example illustrated also assumes a pile top-loaded in compression. For a pile top-loaded in tension we would, based on Assumptions 2. and 3., use the upward side shear load curve in Figure A, multiplied by the F = 0.80 noted in Assumption 2., for the equivalent top-loaded displacement curve.

Expected Accuracy: We know of only five series of tests that provide the data needed to make a direct comparison between actual, full scale, top-loaded pile movement behavior and the equivalent behavior obtained from an O-cell™ test by the method described herein. These involve three sites in Japan and one in Singapore, in a variety of soils, with three compression tests on bored piles (drilled shafts), one compression test on a driven pile and one tension test on a bored pile. The largest bored pile had a 1.2 m diameter and a 37 m length. The driven pile had a 1-m increment modular construction and a 9 m length. The largest top loading equaled 28 MN.

The following references detail the aforementioned Japanese tests and the results therefrom:

> Kishida H. et al., 1992, "Pile Loading Tests at Osaka Amenity Park Project," Paper by Mitsubishi Co., also briefly described in Schmertmann (1993, see bibliography). Compares one drilled shaft in tension and another in compression.
>
> Ogura, H. et al., 1995, "Application of Pile Toe Load Test to Cast-in-place Concrete Pile and Precast Pile," special volume 'Tsuchi-to-Kiso' on Pile Loading Test, Japanese Geotechnical Society, Vol. 3, No. 5, Ser. No. 448. Original in Japanese. Translated by M. B. Karkee, GEOTOP Corporation. Compares one drilled shaft and one driven pile, both in compression.

We compared the predicted equivalent and measured top load at three top movements in each of the above four Japanese comparisons. The top movements ranged from 6 mm to 40 mm, depending on the data available. The (equiv./meas.) ratios of the top load averaged 1.03 in the 15 comparisons with a coefficient of variation of less than 10%. We believe that these available comparisons help support the practical validity of the equivalent top load method described herein.

L. S. Peng, A. M. Koon, R. Page and C. W. Lee report the results of a class-A prediction by others of the TLT curve from an Osterberg cell test on a 1.2 m diameter, 37.2 m long bored pile in Singapore, compared to an adjacent pile with the same dimensions actually top-loaded by kentledge. They report about a 4% difference in ultimate capacity and less than 8% difference in settlements over the 1.0 to 1.5 times working load range -- comparable to the accuracy noted above. Their paper has the title "OSTERBERG CELL TESTING OF PILES", and was published in March 1999 in the Proceedings of the International Conference on Rail Transit, held in Singapore and published by the Association of Consulting Engineers Singapore.

B. H. Fellenius has made several finite element method (FEM) studies of an OLT in which he adjusted the parameters to produce good load-deflection matches with the OLT up and down load-deflection curves. He then used the same parameters to predict the TLT deflection curve. We compared the FEM-predicted curve with the equivalent load-deflection predicted by the previously described Part I and II procedures, with the results again comparable to the accuracy noted above. The ASCE has published a paper by Fellenius et. al. titled "O-Cell Testing and FE Analysis of 28-m-Deep Barrette in Manila, Philippines" in the Journal of Geotechnical and Geoenvironmental Engineering, Vol. 125, No. 7, July 1999, p. 566. It details one of his comparison studies.

Limitations: The engineer using these results should judge the conservatism, or lack thereof, of the aforementioned assumptions and extrapolation(s) before utilizing the results for design purposes. For example, brittle failure behavior may produce movement curves with abrupt changes in curvature (not hyperbolic). However, we believe the hyperbolic fit method and our assumptions used usually produce reasonable equivalent top load settlement curves.

October, 2001

Example of the Construction of an Equivalent Top-Loaded Settlement Curve (Figure B) From Osterberg Cell Test Results (Figure A)

Figure A

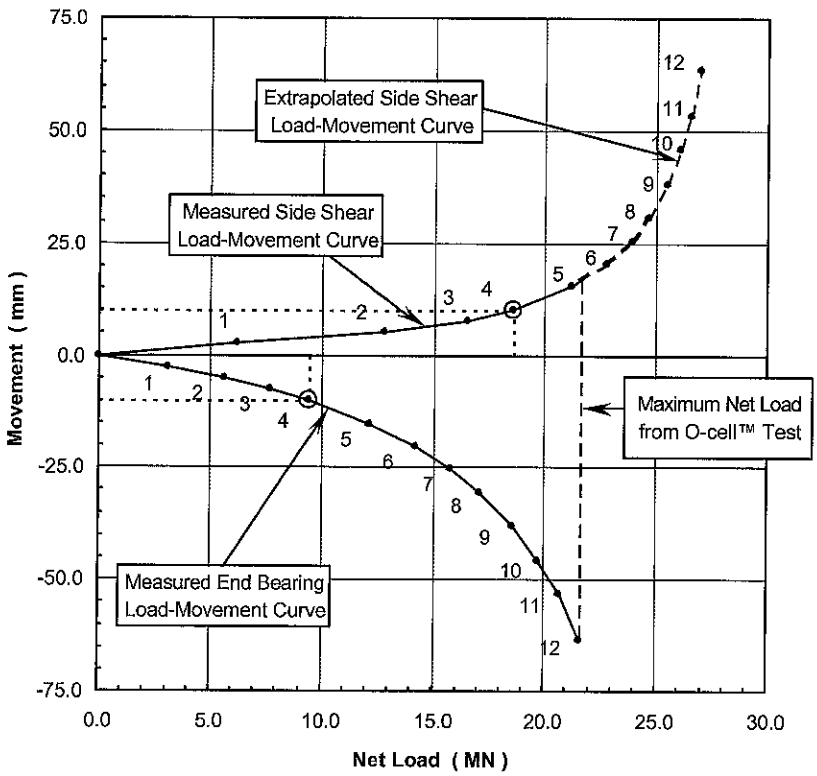

Figure B

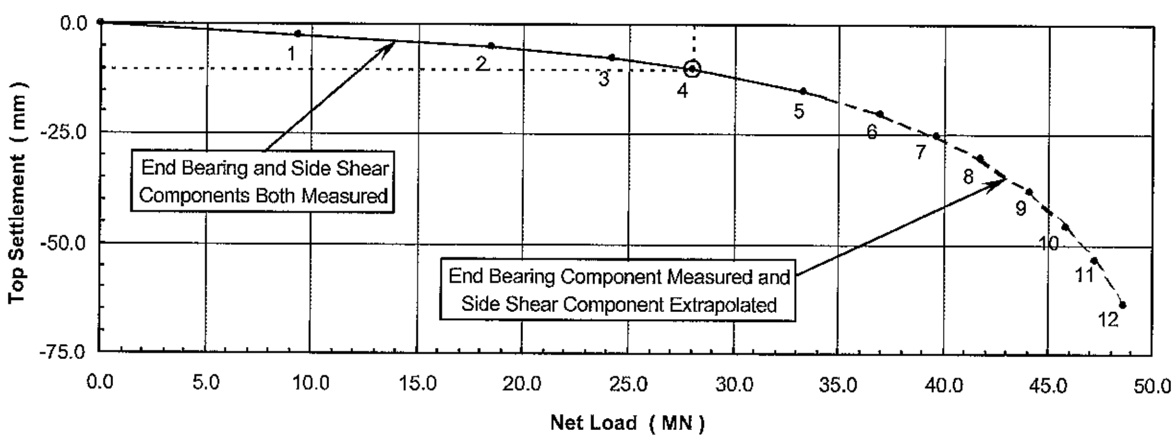

Theoretical Elastic Compression in O-cell™ Test Based on Pattern of Developed Side Shear Stress

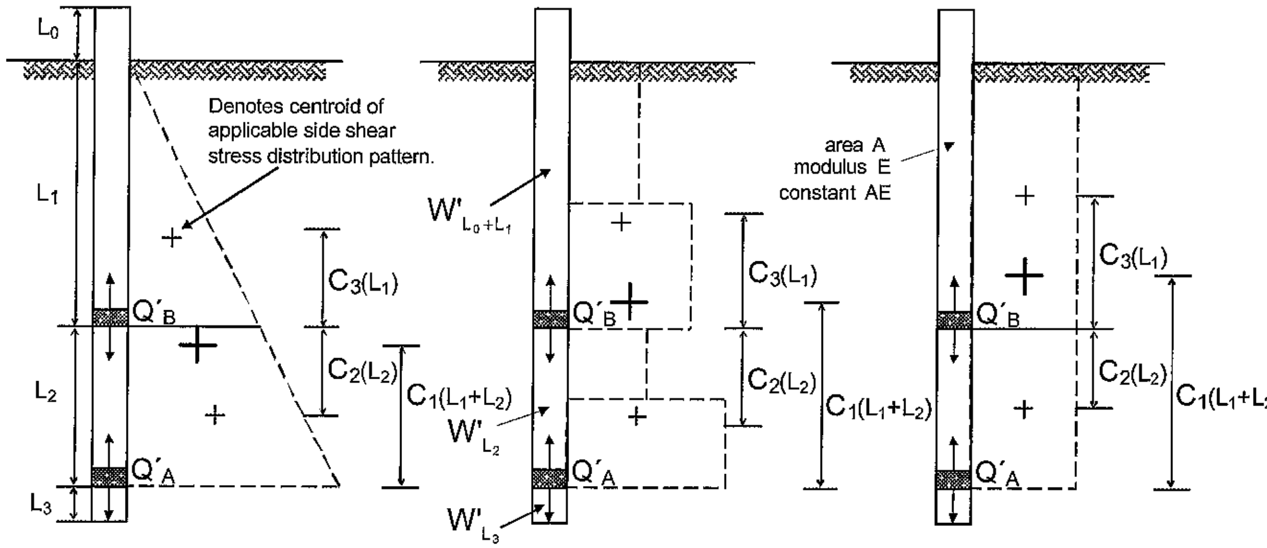

1-Stage Single Level Test (Q´A only): $\delta_{OLT} = \delta_{\uparrow(L_1+L_2)}$

$C_1 = \frac{1}{3}$	Centroid Factor $= C_1$	$C_1 = \frac{1}{2}$
$\delta_{\uparrow(L_1+L_2)} = \frac{1}{3}\frac{Q'_{\uparrow A}(L_1+L_2)}{AE}$	$\delta_{\uparrow(L_1+L_2)} = C_1\frac{Q'_{\uparrow A}(L_1+L_2)}{AE}$	$\delta_{\uparrow(L_1+L_2)} = \frac{1}{2}\frac{Q'_{\uparrow A}(L_1+L_2)}{AE}$

3-Stage Multi Level Test (Q´A and Q´B): $\delta_{OLT} = \delta_{\uparrow L_1} + \delta_{\downarrow L_2}$

$C_3 = \frac{1}{3}$	Centroid Factor $= C_3$	$C_3 = \frac{1}{2}$
$\delta_{\uparrow L_1} = \frac{1}{3}\frac{Q'_{\uparrow B} L_1}{AE}$	$\delta_{\uparrow L_1} = C_1\frac{Q'_{\uparrow B} L_1}{AE}$	$\delta_{\uparrow L_1} = \frac{1}{2}\frac{Q'_{\uparrow B} L_1}{AE}$
$C_2 = \frac{1}{3}\left(\frac{3L_1+2L_2}{2L_1+L_2}\right)$	Centroid Factor $= C_2$	$C_2 = \frac{1}{2}$
$\delta_{\downarrow L_2} = \frac{1}{3}\left(\frac{3L_1+2L_2}{2L_1+L_2}\right)\frac{Q'_{\downarrow B} L_2}{AE}$	$\delta_{\downarrow L_2} = C_2\frac{Q'_{\downarrow B} L_2}{AE}$	$\delta_{\downarrow L_2} = \frac{1}{2}\frac{Q'_{\downarrow B} L_2}{AE}$

Net Loads:

$Q'_{\uparrow A} = Q_{\uparrow A} - W'_{L_0+L_1+L_2}$ $\quad$ $Q'_{\uparrow B} = Q_{\uparrow B} - W'_{L_0+L_1}$ $\quad$ $Q'_{\downarrow B} = Q_{\downarrow B} + W'_{L_2}$

W' = pile weight, buoyant where below water table

Theoretical Elastic Compression in Top Loaded Test Based on Pattern of Developed Side Shear Stress

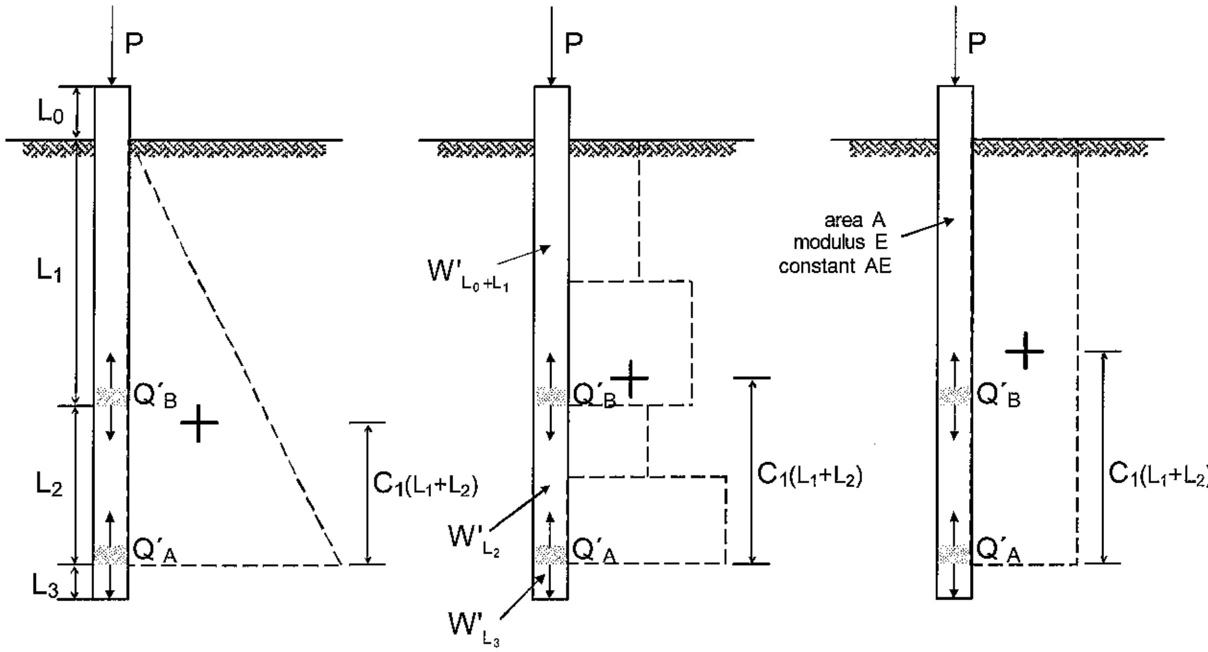

Top Loaded Test: $\delta_{TLT} = \delta_{\downarrow L_0} + \delta_{\downarrow L_1+L_2}$

$\delta_{\downarrow L_0} = \dfrac{PL_0}{AE}$	$\delta_{\downarrow L_0} = \dfrac{PL_0}{AE}$	$\delta_{\downarrow L_0} = \dfrac{PL_0}{AE}$
$C_1 = \dfrac{1}{3}$	Centroid Factor $= C_1$	$C_1 = \dfrac{1}{2}$
$\delta_{\downarrow L_1+L_2} = \dfrac{(Q'_{\downarrow A}+2P)}{3}\dfrac{(L_1+L_2)}{AE}$	$\delta_{\downarrow L_1+L_2} = [(C_1)Q'_{\downarrow A}+(1-C_1)P]\dfrac{(L_1+L_2)}{AE}$	$\delta_{\downarrow L_1+L_2} = \dfrac{(Q'_{\downarrow A}+P)}{2}\dfrac{(L_1+L_2)}{AE}$

Net and Equivalent Loads:

$Q'_{\downarrow A} = Q_{\downarrow A} + W'_{L_3}$

$P_{single} = Q'_{\downarrow A} + Q'_{\uparrow A}$ $\qquad$ $P_{multi} = Q'_{\downarrow A} + Q'_{\uparrow B} + Q'_{\downarrow B}$ $\qquad$ $P_{equivalent} = P - W'_{L_0+L_1+L_2+L_3}$

Component loads Q selected at the same (±) Δ_{OLT}.

Example Calcuation for the Additional Elastic Compression Correction for Single Level Test

Given:

C_1 = 0.441
AE = 17000 **MN** (assumed constant throughout test)
L_0 = 1.80 **m**
L_1 = 14.69 **m** (embedded pile length above O-cell™)
L_2 = 0.00 **m**
L_3 = 0.00 **m**
W' = 0.90 **MN**
Shear reduction factor = 1.00 (cohesive soil)

Δ_{OLT} (mm)	$Q'_{\downarrow A}$ (MN)	$Q'_{\uparrow A}$ (MN)	P (MN)	$P_{equivalent}$ (MN)	δ_{TLT} (mm)	δ_{OLT} (mm)	Δ_{δ} (mm)	$\Delta_{OLT} + \Delta_{\delta}$ (mm)
0.00	0.00	0.00	0.00	0.00	0.00	0.00	0.00	0.00
2.54	1.57	3.14	4.71	3.81	3.37	1.20	2.17	4.71
5.08	2.82	6.43	9.25	8.35	6.52	2.45	4.07	9.15
7.62	3.86	8.27	12.12	11.22	8.61	3.15	5.46	13.08
10.16	4.72	9.29	14.01	13.11	10.05	3.54	6.51	16.67
15.24	6.08	10.60	16.68	15.78	12.14	4.04	8.10	23.34
20.32	7.11	11.40	18.50	17.60	13.60	4.34	9.26	29.58
25.40	7.90	11.94	19.85	18.95	14.70	4.55	10.15	35.55
30.48	8.55	12.33	20.88	19.98	15.55	4.70	10.85	41.33
38.10	9.30	12.75	22.05	21.15	16.53	4.86	11.67	49.77
45.72	9.88	13.05	22.93	22.03	17.27	4.97	12.29	58.01
53.34	10.34	13.27	23.61	22.71	17.84	5.06	12.79	66.13
63.50	10.83	13.48	24.31	23.41	18.44	5.14	13.30	76.80

Figure C

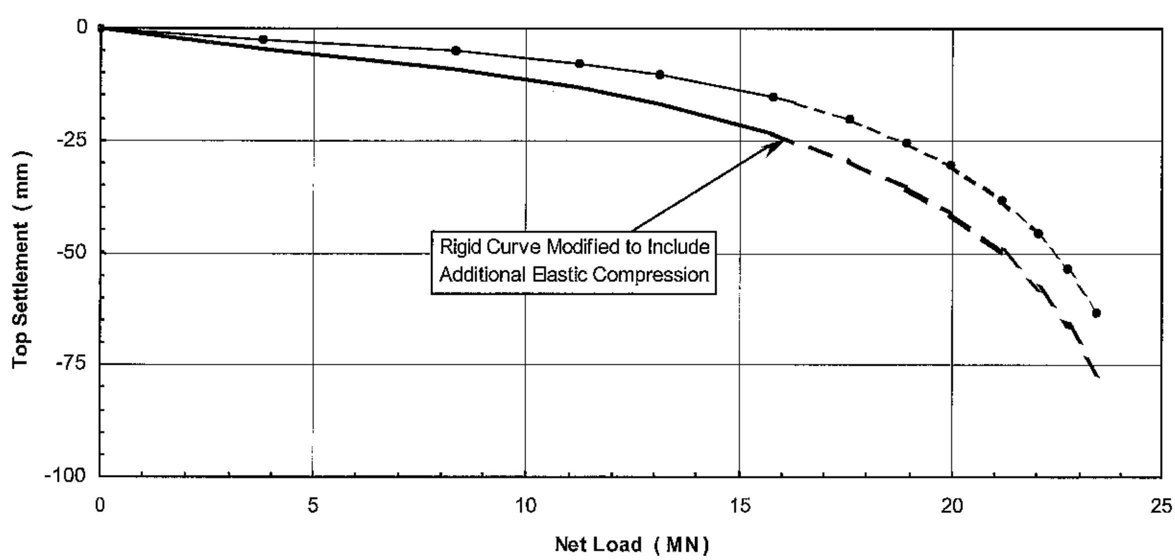

Example Calcuation for the Additional Elastic Compression Correction for Multi Level Test

Given:

C_1 =	0.441	
C_2 =	0.579	
C_3 =	0.396	
AE =	17000	**MN** (assumed constant throughout test)
L_0 =	1.80	m
L_1 =	9.14	m (embedded pile length above upper O-cell™)
L_2 =	5.55	m (embedded pile length between O-cells™)
L_3 =	0.00	m
W' =	0.90	**MN**
Shear reduction factor =	1.00 (cohesive soil)	

Δ_{OLT} (mm)	$Q'_{\downarrow A}$ (MN)	$Q'_{\downarrow B}$ (MN)	$Q'_{\uparrow B}$ (MN)	P (MN)	$P_{equivalent}$ (MN)	δ_{TLT} (mm)	δ_{OLT} (mm)	Δ_{δ} (mm)	$\Delta_{OLT} + \Delta_{\delta}$ (mm)
0.00	0.00	0.00	0.00	0.00	0.00	0.00	0.00	0.00	0.00
2.54	1.57	1.10	2.04	4.71	3.81	3.37	0.64	2.73	5.27
5.08	2.82	2.25	4.18	9.25	8.35	6.52	1.31	5.21	10.29
7.62	3.86	2.89	5.37	12.12	11.22	8.61	1.69	6.92	14.54
10.16	4.72	3.25	6.04	14.01	13.11	10.05	1.90	8.15	18.31
15.24	6.08	3.71	6.89	16.68	15.78	12.14	2.17	9.97	25.21
20.32	7.11	3.99	7.41	18.50	17.60	13.60	2.33	11.27	31.59
25.40	7.90	4.18	7.76	19.85	18.95	14.70	2.44	12.26	37.66
30.48	8.55	4.32	8.02	20.88	19.98	15.55	2.52	13.03	43.51
38.10	9.30	4.46	8.29	22.05	21.15	16.53	2.61	13.92	52.02
45.72	9.88	4.57	8.48	22.93	22.03	17.27	2.67	14.60	60.32
53.34	10.34	4.64	8.62	23.61	22.71	17.84	2.71	15.13	68.47
63.50	10.83	4.72	8.76	24.31	23.41	18.44	2.76	15.68	79.18

Figure D

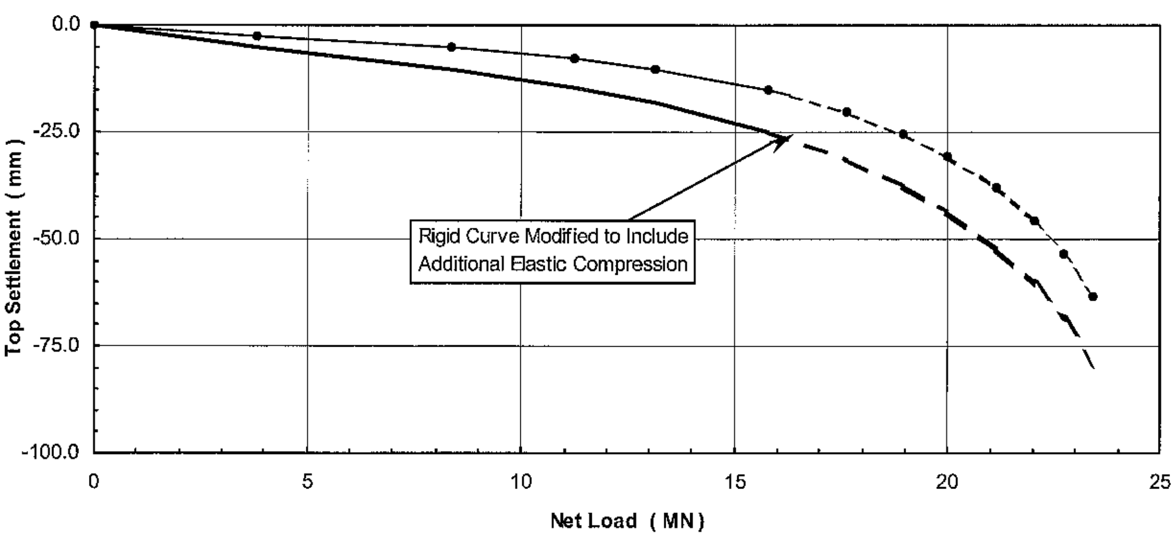

APPENDIX D

O-CELL METHOD FOR DETERMINING CREEP LIMIT LOADING

O-CELL METHOD FOR DETERMINING A CREEP LIMIT LOADING ON THE EQUIVALENT TOP-LOADED SHAFT (September, 2000)

Background: O-cell testing provides a sometimes useful method for evaluating that load beyond which a top-loaded drilled shaft might experience significant unwanted creep behavior. We refer to this load as the "creep limit," also sometimes known as the "yield limit" or "yield load".

To our knowledge, Housel (1959) first proposed the method described below for determining the creep limit. Stoll (1961), Bourges and Levillian (1988), and Fellenius (1996) provide additional references. This method also follows from long experience with the pressuremeter test (PMT). Figure 8 and section 9.4 from ASTM D4719-94, reproduced below, show and describe the creep curve routinely determined from the PMT. The creep curve shows how the movement or strain obtained over a fixed time interval, 30 to 60 seconds, changes versus the applied pressure. One can often detect a distinct break in the curve at the pressure P_e in Figure 8. Plastic deformations may become significant beyond this break loading and progressively more severe creep can occur.

Definition: Similarly with O-cell testing using the ASTM Quick Method, one can conveniently measure the additional movement occurring over the final time interval at each constant load step, typically 2 to 4 minutes. A break in the curve of load vs. movement (as at P_e with the PMT) indicates the creep limit.

We usually indicate such a creep limit in the O-cell test for either one, or both, of the side shear and end bearing components, and herein designate the corresponding movements as M_{CL1} and M_{CL2}. We then combine the creep limit data to predict a creep limit load for the equivalent top loaded shaft.

Procedure if both M_{CL1} and M_{CL2} available: Creep cannot begin until the shaft movement exceeds the M_{CL} values. A conservative approach would assume that creep begins when movements exceed the lesser of the M_{CL} values. However, creep can occur freely only when the shaft has moved the greater of the two M_{CL} values. Although less conservative, we believe the latter to match behavior better and therefore set the creep limit as that load on the equivalent top-loaded movement curve that matches the greater M_{CL}.

Procedure if only M_{CL1} available: If we cannot determine a creep limit in the second component before it reaches its maximum movement M_x, we treat M_x as M_{CL2}. From the above method one can say that the creep limit load exceeds, by some unknown amount, that obtained when using $M_{CL2} = M_x$.

Procedure if no creep limit observed: Then, according to the above, the creep limit for the equivalent top-loaded shaft will exceed, again by some unknown amount, that load on the equivalent curve that matches the movement of the component with the maximum movement.

Limitations: The accuracy in estimating creep limits depends, in part, on the scatter of the data in the creep limit plots. The more scatter, the more difficult to define a limit. The user should make his or her own interpretation if he or she intends to make important use of the creep limit interpretations. Sometimes we obtain excessive scatter of the data and do not attempt an interpretation for a creep limit and will indicate this in the report.

Excerpts from ASTM D4719
"Standard Test Method for Pressuremeter Testing in Soils"

9.4 For Procedure A, plot the volume increase readings (V_{60}) between the 30 s and 60 s reading on a separate graph. Generally, a part of the same graph is used, see Fig. 8. For Procedure B, plot the pressure decrease reading between the 30 s and 60 s reading on a separate graph. The test curve shows an almost straight line section within the range of either low volume increase readings (V_{60}) for Procedure A or low pressure decrease for Procedure B. In this range, a constant soil deformation modulus can be measured. Past the so-called creep pressure, plastic deformations become prevalent.

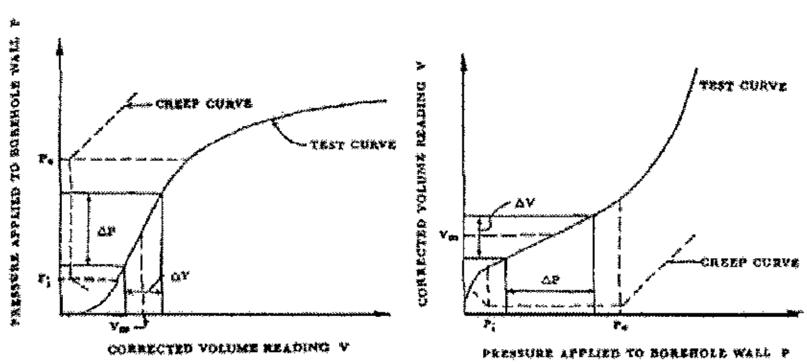

FIG. 8 Pressuremeter Test Curves for Procedure A

References

Housel, W.S. (1959), "Dynamic & Static Resistance of Cohesive Soils", ASTM STP 254, pp. 22-23.

Stoll, M.U.W. (1961, Discussion, Proc. 5th ICSMFE, Paris, Vol. III, pp. 279-281.

Bourges, F. and Levillian, J-P (1988), "force portante des rideaux plans metalliques charges verticalmement," Bull. No. 158, Nov.-Dec., des laboratoires des ponts et chaussees, p. 24.

Fellenius, Bengt H. (1996), Basics of Foundation Design, BiTech Publishers Ltd., p.79.

LOADTEST

Combined End Bearing and Lower Side Shear Creep Limit

TS-1 - IL-133 Over Embarras River - Oakland, IL

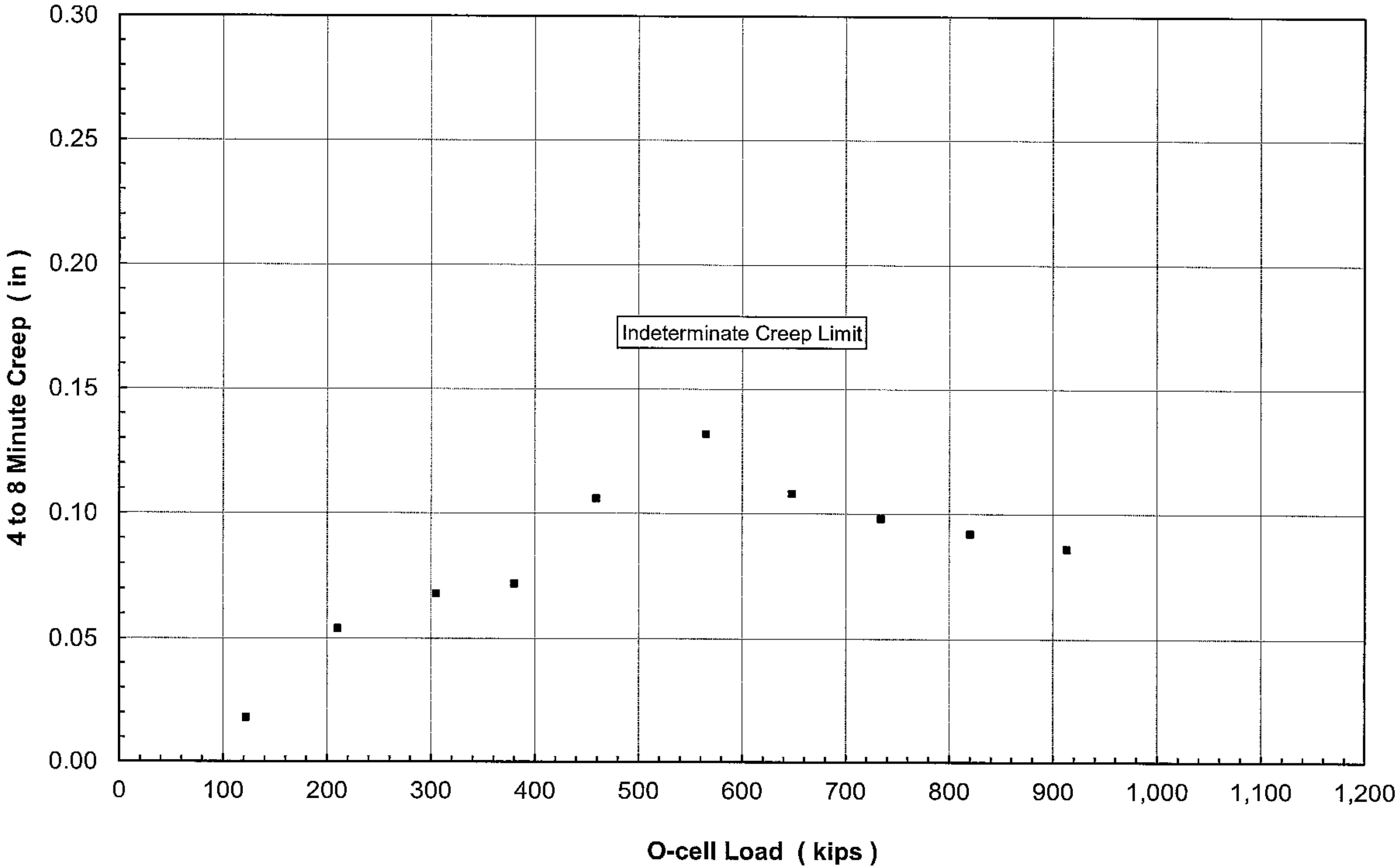

Loadtest USA Project No. LT-1425

Figure D-1

LOADTEST

Upper Side Shear Creep Limit

TS-1 - IL-133 Over Embarras River - Oakland, IL

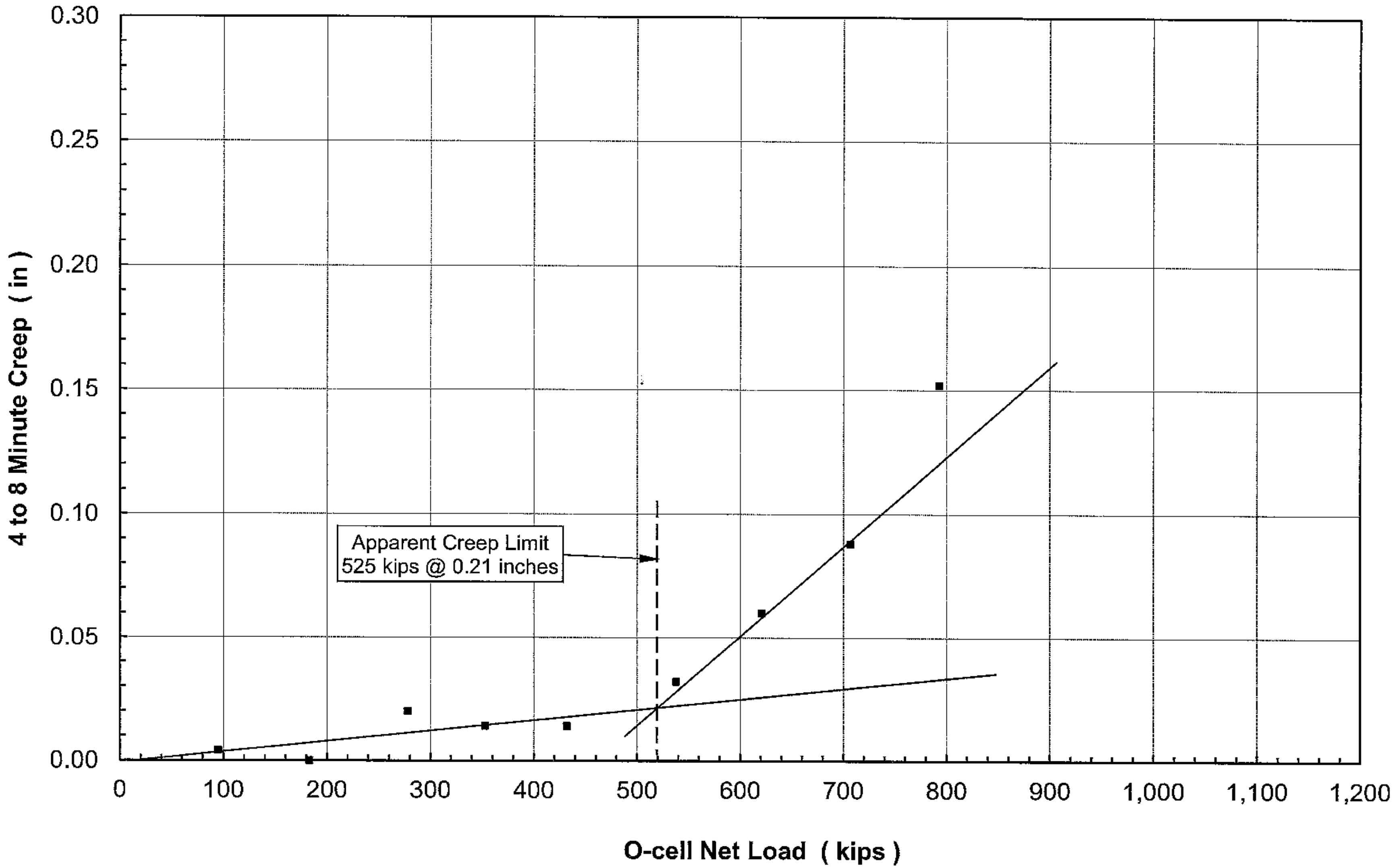

Loadtest USA Project No. LT-1425

Figure D-2

APPENDIX E

SOIL BORING LOG

Illinois Department of Transportation
Division of Highways
Illinois Department of Transportation

SOIL BORING LOG

Date 5/10/10

ROUTE FAP 749 (IL 133) **DESCRIPTION** Embarras River **LOGGED BY** E. Sandschafer

SECTION (122BR)B-1 **LOCATION** W 1/2 - Sec 14, E 1/2 - Sec 15, **SEC.**, **TWP.** 14 N, **RNG.** 10 E, 3 PM

COUNTY Coles **DRILLING METHOD** Hollow stem auger & split spoon **HAMMER TYPE** Auto 140#

STRUCT. NO. 015-0030
Station 713+10

BORING NO. 102 (2010)
Station 713+36
Offset 6.00ft Lt
Ground Surface Elev. 623.83 ft

Surface Water Elev. 596.00 ft
Stream Bed Elev. 593.00 ft

Groundwater Elev.:
First Encounter 594.3 ft
Upon Completion 596.8 ft
After 24 **Hrs.** 598.8 ft

Description	Elev.	DEPTH (ft)	BLOWS (/6")	UCS Qu (tsf)	MOIST (%)
1 1/2" asphalt on 7" bridge deck.	623.13				
Air.		-5			
		-10			
		-15			
		-20			

Description	Elev.	DEPTH (ft)	BLOWS (/6")	UCS Qu (tsf)	MOIST (%)
Air. *(continued)*	598.83	-25			
Soft, very damp, dark gray, SILTY LOAM w/ wood chunk.			0		
			0	0.3	32
	594.33		0	B	
Medium, wet, gray, fine grained, SAND. *3% passing #200 sieve.*		-30	1		
			7		22
	592.83		7		
Gray, SANDSTONE.	589.33				
Very dense, moist, brown, SANDY CLAY SHALE.	588.83	-35	50/5"		6
Borehole continued with rock coring.			50/2"		
			50/2"		
		-40			

Latitude W 88 deg 03.775 min, Longitude N 39 deg 39.541 min, Map Datum WGS 84

The Unconfined Compressive Strength (UCS) Failure Mode is indicated by (B-Bulge, S-Shear, P-Penetrometer)
The SPT (N value) is the sum of the last two blow values in each sampling zone (AASHTO T206)

Illinois Department of Transportation
Division of Highways
Illinois Department of Transportation

ROCK CORE LOG

Date 5/10/10

ROUTE FAP 749 (IL 133) **DESCRIPTION** Embarras River **LOGGED BY** E. Sandschafer

SECTION (122BR)B-1 **LOCATION** W 1/2 - Sec 14, E 1/2 - Sec 15, **SEC.**, **TWP.** 14 N, **RNG.** 10 E, 3 **PM**

COUNTY Coles **CORING METHOD** Rotary, surf set diamond bit

STRUCT. NO. 015-0030
Station 713+10

CORING BARREL TYPE & SIZE NW, conv split inner bbl

Core Diameter 2.06 in
Top of Rock Elev. 592.83 ft
Begin Core Elev. 588.83 ft

BORING NO. 102 (2010)
Station 713+36
Offset 6.00ft Lt
Ground Surface Elev. 623.83 ft

Description	Elev.	DEPTH (ft)	CORE (#)	RECOVERY (%)	R.Q.D. (%)	CORE TIME (min/ft)	STRENGTH (tsf)
Gray, slightly weathered, SANDY CLAY SHALE.	588.83		B102C1	78	78	1.4	
Rock core B102C1 from 37.0' to 37.5' depth = 35.3 tsf.		-40	B102C2	98	79	1	
	583.03						
Gray, moderately weathered, SANDY CLAY SHALE.	582.43						
Gray, slightly weathered, SANDY CLAY SHALE. *Rock core B102C2 from 44.5' to 45.0' depth = 23.3 tsf.*	578.83	-45					
Gray, weathered, SANDY CLAY SHALE. *Rock core B102C3 from 46.1' to 46.5' depth = 1.6 tsf. This core exhibited a slickensided diagonal shear plane failure.*	573.83	-50	B102C3	100	79	1.2	
Extent of exploration. Benchmark: Chiseled square on SE wingwall of existing structure, BM 1624 714+78.5, 18.5' Rt, Elev = 622.32'.		-55					

Color pictures of the cores Available upon request
Cores will be stored for examination until 05/10/15
The "Strength" column represents the uniaxial compressive strength of the core sample (ASTM D-2938)

Illinois Department of Transportation

ILLINOIS